Lessons learnt from implementing intelligent metering and energy monitoring devices in a new housing development

D.M. Whaley, W.Y. Saman, E. Halawa, L.T. Mudge

Sustainable Energy Centre
University of South Australia
Mawson Lakes
South Australia 5095
david.whaley@unisa.edu.au

ABSTRACT

This paper describes the lessons learnt from monitoring energy and water usage of houses in a leading Eco-friendly housing development. The various issues faced during the installation and commissioning of the monitoring systems are discussed, along with recommendations to prevent such problems. The paper also shows some examples of results, discusses resident's feedback regarding the use of in-home monitoring systems, and gives examples of both positive and negative experiences using such equipment.

Keywords – EcoVision, energy monitoring, in-home display, water monitoring, zero energy home

INTRODUCTION

Currently, residential buildings represent approximately 20% of Australia's greenhouse gas emissions, with 30-40% of this figure being attributed to heating and cooling **(**Wilkenfeld *et al.* 2002, ABS 2010). As the number of dwellings, and their average area continue to increase, it is anticipated that heating and cooling requirements will also increase. This will further escalate the peak electrical demand, which is already largely caused by residential buildings (Koomey & Brown 2002, EES 2004, TEPCO 2004).

With this in mind, along with the South Australian State Government's vision for sustainable living, the Land Management Corporation (LMC), has developed the Lochiel Park Green Village. The village is a 106-dwelling demonstration residential development, which exemplifies *South Australia's Strategic Plan* objective 'Attaining Sustainability' (LMC 2009). The residents in Lochiel Park will be highly energy efficient as each house is designed to maximise benefits from environmental elements and reduce energy consumption. LMC have established the following targets:

- 78% saving of drinking water,
- 87% of all water used in the development will be from recycled water,
- 66% reduction in energy use, and
- 74% reduction of greenhouse gas emissions.

Location and Site Summary

Lochiel Park Green Village is a leading eco-friendly new housing development situated in Council district of Campbelltown, South Australia. The village is situated along the Torrens River, approximately 8km North East of the Adelaide CBD, as shown in Fig. 1. The figure also shows the 14.7Ha development area, of which 4.2Ha is designated for 106 residential properties, whilst the remaining 10.5Ha is open space, which includes wetlands, ovals, community gardens and a water recycling plant.

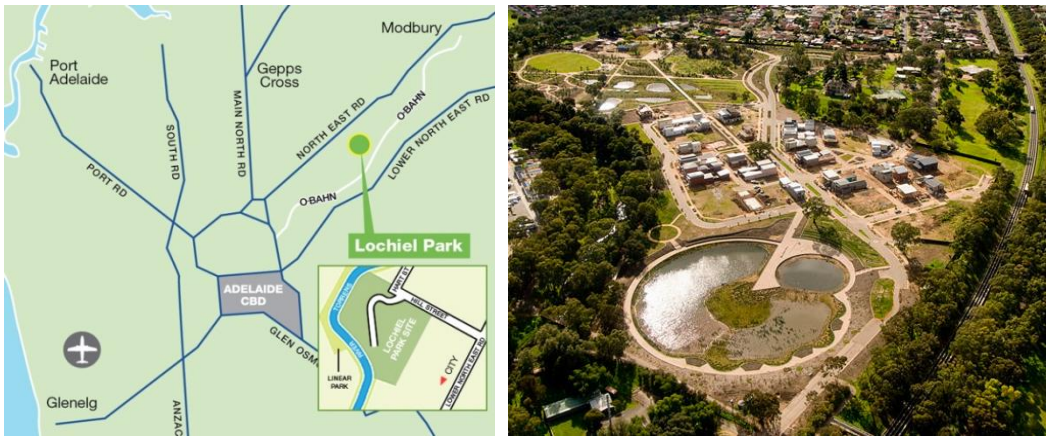

Fig. 1: Lochiel Park Green Village (left) location, relative to the Adelaide CBD, and (right) aerial photograph (LMC 2009**)**.

Zero Net Energy Design of Houses

The houses within the Lochiel Park housing development are designed to be net zero energy homes, with a minimum 7.5 energy star rating. This is achieved by appropriately orientating and designing the houses, ensuring residents use energy efficient appliances, and by utilising roof-mounted photovoltaic panels (1kW/100m^2 of liveable area) and gas-boosted solar hot water systems (Saman & Halawa, 2009). Each house also uses its collected rain water, and will make use of recycled storm water, once the water recycling / treatment plant construction is complete.

OVERVIEW OF HOME MONITORING SYSTEMS

Each of the 106 houses incorporates a touch screen computer and an in-home display, a programmable logic controller (PLC), and an array of intelligent meters and sensors, which comprehensively measure and display general electricity, water and gas usage, in real-time. Furthermore, each property has a fully customisable load management system installed, which allows devices to be deactivated during periods of peak electricity demand. In addition, 10 houses are monitored in detail. Indoor air temperature / relative humidity, individual appliance electricity usage and rain water tank levels are also monitored. A summary of the measured and calculated parameters for both the *general* and *detailed* systems, along with each sensor type, is shown in Tab. 1.

Note that several monitoring systems / options were explored. The EcoVision system was selected as it offers a simple, robust, reliable and cost-effective monitoring system. Despite recent technological advances, hard-wired sensors were selected for this project, as they were deemed simple to install and configure, compared to wireless alternatives. An outline of the EcoVision system is shown on the EcoVision website (EV, 2010).

Tab.1: EcoVision measured and calculated* parameters for the general and detailed monitoring systems. Note that (D) indicates digital, whilst (A) represents analogue.

	Electricity (kWh)						Water (L)					Tank Level (%)	Gas (L)		GHG (kg)	Temp / RH
System	Solar (D)	Import (D)	Export (D)	Total*	Net*	Individual appliances (D)	Mains (D)	Recycled (D)	Hot Usage (D)	Mains Hot (D)	Rain*	Volume (A)	Mains (D)	Hot Water (D)	Greenhouse Gas Emissions*	Living , Lounge, Bed rooms (6 A)
General	✓	✓	✓	✓	✓	×	✓	✓	✓	✓	✓	×	✓	×	✓	×
Detailed	✓	✓	✓	✓	✓	✓	✓	✓	✓	✓	✓	✓	✓	✓	✓	✓

Monitoring System Outline

An overview of the detailed monitoring system schematic is shown in Fig. 2. The figure identifies the EcoVision touch screen, the programmable logic controller (PLC), the optical network terminal (ONT), the contactors, the interconnecting cables, and the various analogue and digital sensors. Note that an overview of the general monitoring system can also be seen in the figure, due to the common components; i.e. the 8 digital sensors surrounded by the dashed box are the only sensors used in this system.

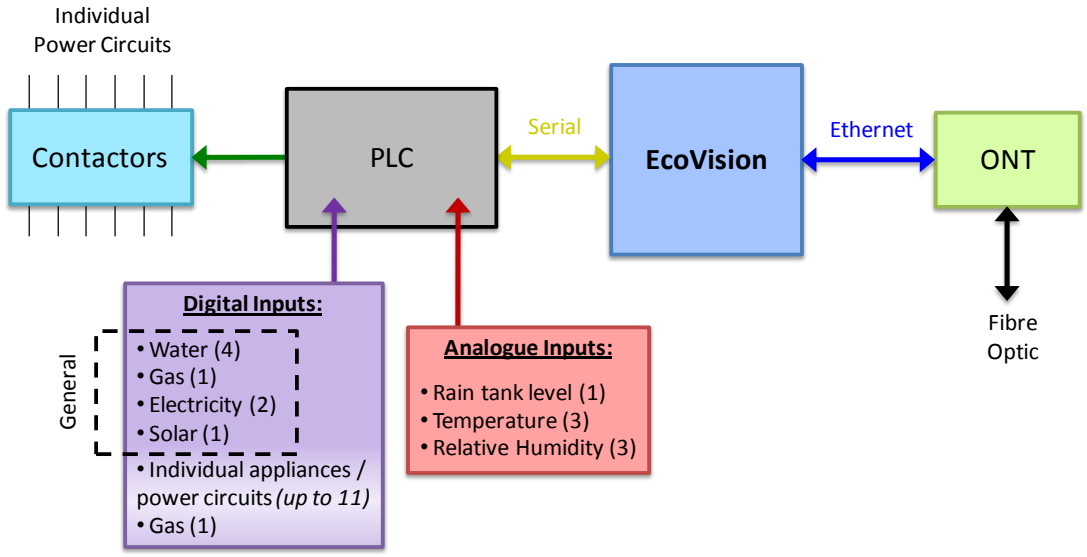

Fig. 2: Overview of the detailed monitoring systems, showing various components. Note that the dashed box represents the sensors used in the general monitoring system.

The figure shows that the various sensors (which are identified in the figure and Tab. 1, depending on which system is considered) are directly connected to the PLC. The PLC communicates back and forth with the EcoVision via a Serial cable, which allows the EcoVision to display and store the measured data. The stored data is transferred from the EcoVision to the Lochiel Park sever via the ONT and the Virtual Private Network, using Ethernet and Fibre Optic cables, respectively. This arrangement also allows the local weather data to be displayed on each system.

Load Management System

The Load Management system effectively interrupts power to up to 6 individual power circuits or appliances, and is controlled by the EcoVision and executed by the PLC. Up to 6 contactors (seen in Fig. 2) are installed, which are typically wired in the refrigerated air conditioner, pool / spa pump, laundry, kitchen, oven and dishwasher power circuits. Note that the majority of residents do not have swimming pools or spas installed and have hence customised their load management system such that additional appliances, such as a second oven, second air conditioner, or an induction cooker can be controlled by load management system.

The load management system is activated (if enabled) once the average electricity power usage exceeds a predefined limit of 3, 4 or 5kW. In this case, up to 6 power circuits, which have an adjustable hierarchal order, will have their power interrupted. This effectively shuts down nominated appliances, until the average electricity usage falls below the predefined limit. Once interrupted, power to that circuit / appliance, will not automatically restart due to safety reasons, i.e. the resident must disable the load management system to re-energise any interrupted loads. Note that this feature is completely voluntary, and that in the past one electricity provider offered financial incentives to residents who maintained a 3kW limit at all times.

EcoVision System

In-Home Display

The EcoVision computer not only records and stores data, it acts as the in-home display. The touch screen allows users to select i) the type of measured data shown on the screen, e.g. electricity, water, gas, etc. and ii) the time scale, i.e. month, week, day or hour. Fig. 3 below shows various EcoVision screens for random Lochiel Park houses.

Fig. 3: EcoVision screens, showing (left) electricity and (right) gas usage, for 1 day.

Data Storage

The EcoVision continuously samples the PLC and updates a locally-stored CSV data file with information regarding digital input pulses (and analogue values, for applicable detailed monitoring systems) each minute. These files are appropriately identified by lot number, month and year, and are automatically copied to the central Lochiel Park server each night. The CSV files are copied to a local computer (and analysed) by establishing a remote desktop connection to the Lochiel Park server. The typical file size of a general and detailed monitored house, for one month, is 6.1 and 13.1MB, respectively.

ISSUES ENCOUNTERED

Many issues have been faced during the installation and commissioning stages for the first 25 houses. While some initial teething problems were anticipated during the commissioning stage, a number of unexpected issues have also surfaced. These issues, which mainly cause the EcoVision to collect invalid data, or cause significant delays commissioning the systems, are further discussed below.

Hardware Issues

Sensors

- A small number of water and gas sensors were nonoperational when installed.
- Some sensors, e.g. gas, rain tank level, temperature are not readily available.
- Some sensors, such as Wattmeters, temperature and rain level sensors are not correctly labelled, installed and or configured.

Wiring

- Some cables connecting sensors to PLCs have been unintentionally severed by people, whilst some are cut short, requiring extensions or re-cabling.
- Some cables, i.e. Ethernet and serial, were not correctly terminated.
- Some EcoVision power supplies required replacing, and were not correctly installed.

Metering

- Incorrect gas, water and electricity meters have been installed on some properties. These are incompatible with their respective sensors and must be replaced by utility personnel. Meter replacement, in some instances, has taken several months.
- About half the electricity billing meters, which are fitted with sensor equipment, were incorrectly configured when installed. This can only be corrected by utility personnel, who have taken some months to carry this out.
- The rain water tanks of some properties are fitted with only one rain water tank water meter, instead of the required two. Other properties have one of these rain tank meters installed in the incorrect direction or in the incorrect location.

Appliance Installation

- The grid-connected inverter of one property was not installed, whilst the solar hot water system of another had its water and gas inlets incorrectly connected.
- One faulty ONT was installed, whilst some are not correctly configured.

EcoVision

- Some screens crash / freeze.
- Some systems do not automatically restart following a power outage (black out).

Residents

- Some residents cannot provide access to properties during business hours, or restrict access to billing meters.
- Some residents shut down their EcoVision screen, or did not wish to restart it following a power outage.

PRELIMINARY RESULTS AND ECOVISION EXPERIENCES

This section briefly shows some measured data from a select few houses equipped with the detailed monitoring systems, despite many houses currently operating correctly. The sample data shown is not exhaustive, however, it should give a general indication of the types of data analyses possible, as a result of using the EcoVision systems.

Sample Data

Power and Temperature Profile

Fig. 4 shows the total electricity and air conditioner consumption, dining and bed room temperatures for one house, for 15-18th March 2010. As in many instances, the peak electrical demand is attributed to the operation of air conditioner on hot days. Observing the temperature profiles and the air conditioner load profiles, one can see that the occupants switched the air conditioner on during the afternoon and evening where outside air is still at its peak or near peak value. During the night time, the temperatures in the rooms dropped down to comfort levels without the need for air conditioning.

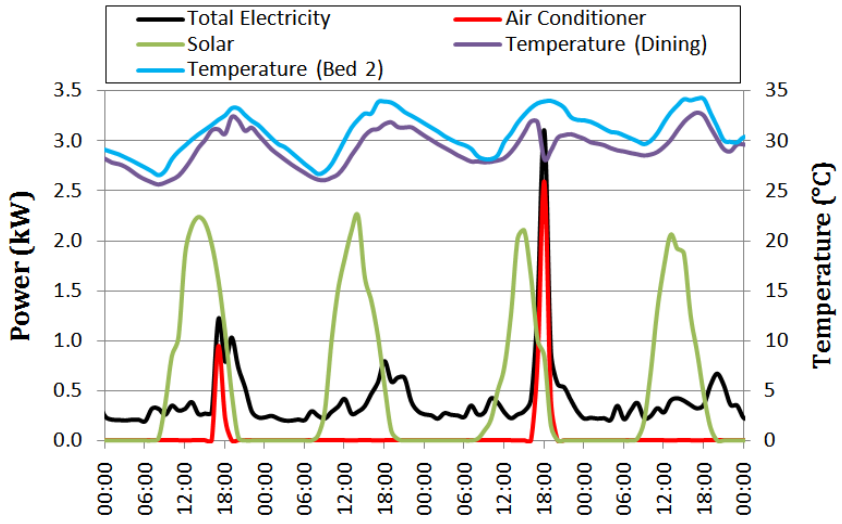

Fig. 4: Total electricity, solar and air conditioner load, and temperature profile of one house. The peak temperatures for 15-18 March 2010 were 32.1, 34.9, 36.0 and 35.6°C.

Average Energy Consumption / Generation

Fig. 5 summarises the monthly average total consumed, generated and net electricity for 2010. The average solar generated energy is shown to peak in January and steadily decrease each month, reaching its trough in June, as expected due to seasonal changes. The average total consumed energy decreases from its summer peaks (January and February), reaching its trough in April. The average total electricity usage then increases in May and peaks in July. Interestingly, the average winter electricity usage peak is

about 30% higher than its summer equivalent. For these reasons, the average net energy (supplied from the grid), is steady between summer and autumn and then sharply increases as winter approaches; it reaches its peak in June.

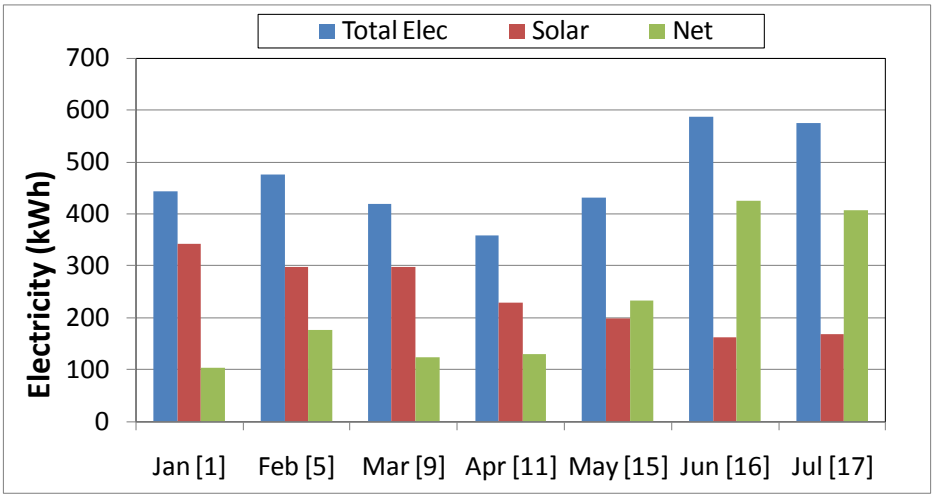

Fig. 5: Average monthly consumed (total), generated (solar) and the net electricity for [the number of lived-in] Lochiel Park houses for 2010.

Note that the number of houses sampled each month varies as houses and EcoVision systems are continuously built and commissioned, respectively. Also note that the data shown has not been fully scrutinised. Therefore a full interpretation of the Fig. 5 should not be made at this stage. Despite this, thus far it appears that the average Lochiel Park house relies on about 210kWh of electricity from the grid each month. This is significantly lower than typical Adelaide houses (of a similar size) monitored in 2002-2003 (Saman & Mudge 2003), which consumed over 600kWh per month.

The average data also indicates that approximately 53% of the energy consumed was generated on the roof tops of the monitored houses, which significantly reduces the greenhouse gas emissions for the housing development. In addition, the use of solar hot water systems, the data of which is not discussed in this paper, further reduces the housing development's greenhouse gas emissions.

Example of Positive Outcomes

To date, the EcoVision system has alerted residents to four known leaks at three separate properties. Each leak was detected by observing higher than expected water and gas usage rates of each respective screen. This is explained with the aid of Fig. 6, which shows the water screen of one house with a water leak. The bottom time-varying graph shows an average water usage rate of about 0.5L/min during the early hours of the morning, when there should ideally be zero water usage. The leak was located between the billing meter and the house, and was fixed by a plumber. Despite this, it is estimated that the leak wasted about 41,000L of potable water, as the leak was not detected until several months after the EcoVision system was commissioned.

The water screen of EcoVision system also alerted residents of two other water leaks. The first was caused by a leaking garden tap, whilst the second was caused by a leaking hot water tap. Both leaks were detected by observing unusual water usage rates during the early hours of the morning or late at night, and it is estimated that each leak wasted less than 200L. The property with the leaking hot water tap also had a gas leak. This

was detected by the gas fitter when the resident was demonstrating their EcoVision system. The fitter noticed that gas was being consumed by the only gas appliance, i.e. an instantaneous gas booster which forms part of the solar water system, despite not using hot water. After a brief investigation the fitter found the leak at the gas inlet of the gas booster unit and fixed the leak.

Fig. 6: EcoVision screen showing water usage page. Two sections are zoomed showing the water flow rates before (red) and after (green) a major water leak was fixed.

Negative Outcomes

Thus far, two residents have reported negative experiences with the EcoVsision system; both relate to the Load Management features. Although all residents are briefed about the load management system and are made aware of the voluntary use of such a system, many do not understand the need for such a load shedding system and vow not to use it, as they would prefer to be comfortable. One resident, whose air conditioner was tripped during a hot summer's day, felt that the system should have automatically re-energised their air conditioner, and when they discovered that this does not occur for safety reasons, they decided to deactivate this feature.

Another resident had a negative experience using the load management system, when they unintentionally activated the system and did not realise that their dishwasher and laundry appliances had their power interrupted. The resident called in the services of their preferred electrician who did not receive specialised training and was hence was unaware of the in-home monitoring system. This electrician took two days to determine the cause of the problem, which could have been solved by a phone call to either the developers, the people monitoring data, or to one of the project's preferred electricians.

Resident's Feedback

Despite the above negative experiences, the majority of residents are thrilled to be able to monitor their water, electricity and gas usage using their EcoVision system. The real-time display allows residents to determine energy usage profiles of their appliances. This, along with knowledge of the electricity feed-in tariff, allows residents to optimise their appliance usage and solar credits by using energy intensive appliances after sunset. Many residents have mentioned that they use the EcoVision display to determine total

daily water, gas and electricity usage. They then challenge themselves to consume less water and energy the following day until they find a comfortable level. Note that the net feed-in tariff offered to South Australians was $0.44 / kWh, at the time of publication.

In contrast, there are some residents that do not use their EcoVision systems to reflect upon their water, gas or electricity usage. Although they understand the reasons behind the system, they are determined to continue living the lifestyle they want, and do not wish to change their behaviour, regardless of their energy and water usage patterns.

In addition, despite residents receiving an overview of the EcoVision system and its Load Management features, during the commissioning stage and also in one of two 'after hours' training sessions, a small number of residents have expressed concern over lack of documentation. These residents have requested a detailed instruction manual, which covers the EcoVision system, including its Load Management features. Such a manual does not yet exist, however, EcoVision staff are currently addressing this.

SUMMARY, RECOMMENDATIONS AND CONCLUSIONS

This paper has described the Lochiel Park housing development, given an overview of the intelligent monitoring equipment, discussed problems associated with developing, installing and commissioning such a new evaluation and monitoring system. The paper has also shown some preliminary data, and has discussed resident's experiences and feedback regarding the use of the EcoVision home monitoring system.

Recommendations

To prevent the reoccurrence of the delay causing problems mentioned above, it is highly recommended that all trades-people involved in such a large project, are appropriately trained, and are judged competent to install and commission intelligent monitoring equipment. It is critical that tradespeople are aware of the need for long cables between the sensors and the PLC, and that they work diligently to avoid damaging these.

It is also recommended that utility personnel are appropriately trained, such that they i) provide the correct types of billing meters, and ii) appropriately configure and verify correct operation of these billing meters.

To further prevent resident associated delays, training sessions should be periodically run that explain the function of the EcoVision system, especially the load management system features. These should also explain the need for access to properties and meter boxes to verify correct operation of the systems.

Conclusions

The main conclusions from this paper are:

- Although preliminary, the data for the limited period of monitoring suggests that the average Lochiel Park houses consume less electrical energy than typical average Adelaide houses of a similar size.
- The roof-mounted PV systems generate about half the total development's electrical energy consumption.

- The majority of residents are delighted with their in-home monitoring systems, they regularly review their data and some attempt to modify their lifestyles to reduce their water, and energy usage.

REFERENCES

ABS, (2010), *Energy in Focus; Energy Efficiency in Australian Homes,* Australian Bureau of Statistics.

EES, 2004: *Electrical Peak Load Analysis – Victoria 1999* – 2003, Energy Efficient Strategies, prepared for VENCORP.

EV, 2010, EcoVision Systems website (accessed 10 February 2010): http://www.ecovisionsolutions.com.au/

Koomey, J. & Brown, R.E., 2002: *The role of building technologies in reducing and controlling peak electricity demand*, Energy Analysis Dept. – Environmental Energy. Technologies Division – Ernest Orlando Lawrence Berkeley National Laboratory – University of California – Berkeley, CA 94720, September – available online at http://enduse.lbl.gov/Info/LBNL-49947.pdf

LMC, 2009, *LMC Projects: Lochiel Park–Adelaide's Green* Village, Land Management Corporation website (accessed 30 July 2010):

http://www.lmc.sa.gov.au/home/inner.asp?pageid=292&mainid=20&subid=46

Saman, W. & Halawa, E., (2009), *The impact of passive design and solar energy use in a housing development on the electrical grid*, presented and published in Proceedings ISES Solar Word Congress October, 2009, Johannesburg, South Africa.

Saman, W. & Mudge, L.T. 2003, Development, Implementation and Promotion of a Scoresheet for Household Greenhouse Gas Reduction in South Australia: Final Report, Sustainable Energy Centre, University of South Australia, Mawson Lakes, Adelaide.

TEPCO, 2004: Electricity Market in Japan – Tokyo Electric Power Company website: http://www.tepco.co.jp/en/news/presen/pdf-1/0406-e.pdf - accessed 27 March 2009

Wilkenfeld, G. and Associates (2002), *Australia's National Greenhouse Gas Inventory, 1990, 1995 And 1999, End Use Allocation*, Department of Climate Change, Canberra.

ACKNOWLEDGEMENTS

The authors wish to acknowledge the funding and support provided by the CSIRO's Intelligent Grid Cluster. They would also like to thank the support and information provided by LMC, in particular Andrew Bishop and Phil Donaldson.

BRIEF BIOGRAPHY OF PRESENTER

David Whaley is a Research Engineer for the Sustainable Energy Centre, at the University of South Australia. He obtained his PhD in Electrical and Electronic Engineering, from The University of Adelaide in 2009, and is a member of Engineers Australia and the IEEE. His research interests include renewable energy technologies.

Wind Power Forecasting for Improved Maintenance Scheduling

Iain Pople[1] and Andrea Bunting[2]
[1]Acciona Energy:
Lvl 1/ 95 Coventry St
South Melbourne VIC 3205
IPople@accionaenergy.com.au
[2]School of Aerospace, Mechanical and Manufacturing Engineering
RMIT University
GPO Box 2476, Melbourne VIC 3001
andrea.bunting@rmit.edu.au

ABSTRACT

As the penetration of wind power in Australia increases, the variability of wind power is expected to impact on both the supply-demand balance of the electricity system and the stability of weak grids. The system operator now requires forecasts of wind farm output to aid effective scheduling of generation. However, wind power forecasting may also benefit the wind farm operator. One beneficial area is maintenance scheduling: wind farm operators may be able to schedule downtime to coincide with periods when low power output is forecast. There are a number of regular maintenance tasks that must be undertaken, involving different numbers of turbines and different durations. Using data from the recently commissioned Waubra wind farm in Victoria, a number of scenarios were simulated to quantify the benefits of using wind power forecasting to assist the maintenance scheduling process. It was found that the most benefit (albeit small) was achieved by scheduling tasks that required the shutdown of several turbines to occur at times when wind farm output is forecast to be below 10% of maximum capacity. By scheduling in this way, the annual energy production could be increased by 0.23% or 1.5 GWh for this particular wind farm, compared with the current practice of not using wind forecasts for scheduling. Improving the accuracy of wind forecasting would make little difference as a similar result was found when simulating perfect forecasting.

Keywords *wind power, wind forecasting, maintenance scheduling*

INTRODUCTION

Wind energy is a highly variable resource which presents challenges for grid integration; thus significant effort is going into developing systems to forecast the wind resource. Accurate wind forecasting provides a wide range of benefits to the wind industry, including increased network stability, reduced ancillary services, and more effective trading in electricity markets. Wind forecasting may also improve planning of maintenance work at wind farms (Giebel 2003). If wind speed can be predicted in advance, wind turbine maintenance can be scheduled during periods when low wind speeds are expected, thereby maximising the availability of wind turbines during periods when high energy production is possible. This will increase the overall annual energy production of the wind farm, thereby increasing the revenue stream.

In this paper we determine the optimal strategy for using wind power forecasts to improve maintenance scheduling at the Waubra wind farm in Victoria, owned and operated by Acciona Energy, and estimate the annual increase in energy production.

WIND POWER FORECASTING

What is Wind Power Forecasting?

The electrical power output of a wind farm depends on wind speed which is by its nature highly variable. Wind power forecasting attempts to predict the output of a wind turbine, a wind farm, or a group of wind farms.

The *forecast horizon* is the time period for which the forecast has been produced. This will typically depend on the intended application of the forecast. For example:

- A horizon of 5 minutes ahead may be used for dispatch planning by electricity network operators (Coppin & Katzkey 2003).
- A horizon of several hours ahead may be used for managing network flows and planning regional demand (Cutler 2006).
- A horizon of several days may be used for scheduling wind farm maintenance.
- A horizon of years ahead may be used for assessing the return on investment for a wind farm site, and for planning infrastructure development.

A forecast horizon of up to 14 days is generally classed as a *short-term forecast*.

A forecast *confidence interval* provides the end-user with an indication of the accuracy of the forecast. Typically a forecast is provided with an upper and lower bounds such that the probability of the actual value lying between these bounds is 95%. Confidence intervals are important as they provide the user of the forecast with more information about the range of possible values and the likelihood of a forecast being incorrect.

The size of the confidence interval of a forecast increases as the forecast horizon increases, i.e. forecasting further into the future has a greater level of uncertainty.

Why Forecast Wind Power?

Wind forecasting has a variety of applications for different participants in the electricity market. This section describes how participants may benefit from wind forecasting.

The *electricity network operator* is responsible for managing the transmission and delivery of electricity from generators to end customers. One of the primary functions of the network operator is to match demand and supply. Deviations between forecast and actual demand are corrected using regulation frequency control ancillary services, provided by quick response generators whose output can be controlled automatically by the Australian Energy Market Operator (AEMO) (NEMMCO 2001). For the electricity network operator, wind forecasting can be an important tool for managing the integration of wind energy into the overall mix of generation technologies. As the contribution of wind energy increases, the requirement for ancillary services may also increase. Using wind power forecasts can reduce the need for ancillary services, making wind energy less costly. Network operators must also ensure that the capacity of the network, including interconnectors between states, is not exceeded. Wind forecasting can also help operators to manage network flows.

A *renewable energy generator* (a participant in the electricity market that generates power from a renewable source) can also benefit from reliable wind power forecasts. In

Australia, wind farms greater than 30 MW commissioned from April 2009 are classified as semi-scheduled generators. These are required to submit a bid indicating how many MW of wind turbine capacity are available for generation. The Australian Wind Energy Forecasting System (see below) predicts their level of wind power generation (AEMC 2008). Since semi-scheduled bids are based on capacity (MW) rather than generation (MWh), the risk from the variability of the wind is not carried by the generator. This situation is distinct from other electricity markets and lessens the importance of forecasting for individual generators in Australia. On the other hand, companies that operate a portfolio of different renewable technologies may benefit more from forecasting. For example, companies with both wind farms and hydro power stations may use wind power forecasting to ensure that adequate hydro reserves are maintained to continue generation during periods of low wind (Cutler 2007).

For a *wind farm operator* wind forecasting provides benefits for managing individual wind farms. For example, when performing wind turbine maintenance, operators must meet minimum Occupational Health and Safety conditions. The Waubra Wind Farm employs increasing stringent access restrictions at wind speeds above 12 m/s: no external access to hub at 12 – 15 m/s; no internal access to hub at 15 – 20 m/s; no access to wind turbine at 20 – 25 m/s; and no access to wind farm above 25 m/s. (Acciona Energy 2009). By using wind forecasts, the operator can avoid scheduling maintenance work for periods where the wind conditions are outside safe working standards.

A key objective of the wind farm operator is to maximise energy production of the site. This must be balanced against the requirement to perform maintenance work in a timely manner. Using wind power forecasts, it is possible to adjust maintenance schedules to avoid shutting down turbines during times of high production.

WIND POWER FORECASTING IN THE AUSTRALIAN CONTEXT

The Australian Wind Energy Forecasting System

The amount of wind power in Australia is expected to increase greatly as a result of the expanded Renewable Energy Target. As of November 2009 around 6000 MW of new wind development was planned (AEMO 2009a). Consideration must be given to how such levels of wind power can be effectively integrated into the national electricity grid.

Following concerns raised by NEMMCO (2003) about the effect of wind power's variability on grid operation, particularly the increased need for ancillary services, the federal government announced in 2004 that it would provide $14 million to develop forecasting systems for wind power (DPMC 2004). NEMMCO (now AEMO) received funding to develop and deliver the Australian Wind Energy Forecasting System (AWEFS) – a centralised wind forecasting system that is integrated with the National Electricity Market (AEMO, 2009b).

NEMMCO selected ANEMOS, a European consortium with considerable experience with wind forecasting in Europe, as the implementer of AWEFS. The system went live in late 2008 and now produces power production forecasts for operational wind farms that participate in the National Electricity Market (AEMO 2009b).

The main objective of AWEFS is to provide forecasts that will improve the efficiency, stability and management of the National Electricity Market, to satisfy AEMO's obligations under the amended National Electricity Rules. However, AWEFS also provides benefits for wind farm operators. Participating wind farms can access

individual forecasts for a horizon of up to seven days. This should assist wind farm operators to maximise production by scheduling outages for periods of low wind.

To support the development of the AWEFS, the Bureau of Meteorology has been researching improvements to numerical weather prediction (NWP) models that would benefit wind forecasting, in particular the resolution and accuracy of Australian limited area NWP models (Kepert 2005). This should raise the quality of forecasts closer to those of Europe where country specific NWP models are already used.

Dr Peter Coppin from the CSIRO Wind Energy Research Unit has been researching how Australia's requirements for a wind forecasting system may differ from existing systems in other countries. In Australia, electricity end users and potential wind generation sites are spread over a large geographic area, with far lower population density than Europe; therefore the coverage area of the forecasting system will be larger than usual. Moreover, the Australian electricity grid is relatively weak which raises issues of network security. As a result, an Australian forecasting system will need to be more focussed on events that risk network security (Coppin 2005). On this theme, recent work has focussed on methods for predicting large changes in wind power (Cutler et al. 2009) (Davy et al. 2010).

Wind Energy and the Australian Electricity Market

The Australian Energy Market Operator (AEMO) is responsible for managing the trading of electricity between generators, retailers and end users. Trading is managed via a pool where the output of all generators is aggregated and scheduled to meet demand (NEMMCO 2008). Intermittent energy sources such as solar and wind present a challenge to this system as without some type of forecasting capability it is difficult to schedule the power produced on any given day. Therefore it is in the interests of network operators to be able to forecast electricity production for individual wind farms as well as aggregating forecasts for particular regions or across the whole network.

Although wind energy penetration in Australia is relatively low except in South Australia, significant growth is expected. The AEMC has amended the existing National Electricity Rules such that new intermittent generators greater than 30 MW are classed as semi-scheduled. Semi-scheduled generators must now meet a number of obligations in order to participate in the market including: providing plant availability for each generating unit; providing real time data feeds of atmospheric conditions including wind speed and direction; and submitting dispatch offers (i.e. bids), based on a per MW price. AWEFS is used to predict energy production taking into account the available information provided by the wind farms. (AEMC 2008).

FORECASTING WIND POWER FOR MAINTENANCE SCHEDULING

Project Overview

This project aims to use wind power forecasts to test whether improved maintenance scheduling algorithms will lead to increased energy production. By incorporating wind power forecasts into the maintenance planning cycle, energy production should be increased by ensuring that maintenance work requiring large numbers of turbines to be shutdown is not performed during times of high wind. Operating costs are reduced by ensuring that maintenance tasks are not scheduled for times when wind conditions would make such work unsafe or impact negatively on the production of the wind farm.

Computer simulations have been used to compare the algorithms and quantify the increase in total annual production. Data for this project comes from the Waubra Wind Farm, in mid Victoria. The wind farm has 128 turbines and maximum generation capacity of 192 MW. It began generating in 2009. NWP wind power forecasts have been provided by a Spanish company called Meteológica. The forecasts use 2 NWP models, the European Centre for Medium-Range Weather Forecasts (ECMWF) and the Global Forecast System (GFS). To improve the accuracy of the raw NWP forecasts, Meteológica applies a form of model output statistical downscaling using historical met mast data from the wind farm for initial configuration (Meteológica 2008).

Methodology

The various types of maintenance work performed at the wind farm have been identified and classified into two key categories: tasks that are amenable to re-scheduling using wind power forecasts, and those tasks that cannot easily be rescheduled.

The tasks that can be rescheduled are further classified according to the number of turbines that must be taken offline to complete the task. Since the wind turbines are grouped into distinct electrical circuits, certain tasks require the shutdown of multiple turbines. The more turbines shut down, the higher the losses to production.

The statistical accuracy of the wind power forecasts has been analysed to identify the optimal model and investigate methods to reduce error. Using real historical data, the error for two different NWP models provided by Meteológica has been calculated to select the best model. It was found that for forecast horizons between 0 – 172 hours the GFS model outperformed ECMWF. Systematic errors have been removed using bias correction.

A cost benefit analysis has been performed for all tasks to determine under which wind conditions it is economically beneficial to delay a task. This was calculated using the duration of the task, the number of turbines impacted, the electricity purchase price and the labour cost. This can be used as a decision point in the scheduling algorithm.

Using wind power forecasts a number of scheduling algorithms were developed. These algorithms have been tested using a computer simulation run with historical data and archived wind power forecasts. The simulation calculates the annual energy production using each scheduling algorithm. The scheduling algorithm with the highest annual energy production has been selected as the optimal mode.

Wind Farm Maintenance Work

Maintenance work on a wind farm can be corrective or preventive. Corrective maintenance occurs when the SCADA system detects a problem with a turbine that requires a corrective work job. Since the turbine does not generate until the fault is repaired, corrective work jobs should be completed as soon as possible. Hence wind power forecasts are not useful for scheduling corrective maintenance, except in ensuring that wind conditions are safe for workers.

Planned or preventive maintenance describes work that is performed regularly to ensure efficient operation and reduce the probability of failure. To comply with the wind turbine manufacturer's warranty, six monthly and twelve monthly maintenance must be performed within a specified timeframe. There is some flexibility as to the exact day on which maintenance is performed. If work is carried out during periods of low wind, lost

energy production may be minimised. Wind power forecasts can assist maintenance planners to ensure that high impact tasks are scheduled for days with low production.

Planned maintenance work includes tasks that impact on one turbine or multiple turbines. The Waubra Wind Farm consists of 5 substations. Each substation is fed by 3 to 5 circuits with 3 to 7 turbines on each circuit. Performing maintenance work on a circuit requires that all turbines in that circuit are stopped. Similarly if work needs to be performed on a substation, all turbines on all circuits feeding into that substation must be stopped. Therefore working on a circuit or a substation will reduce the production of the wind farm by a greater amount than maintenance of a single turbine. A summary of planned maintenance tasks and their impact is given below.

Description	Duration	Quantity	Turbines offline simultaneously
Turbine 6 monthly maintenance	3 days	128	1
Turbine 12 monthly maintenance	4 days	128	1
Circuit 6 monthly maintenance	1 day	21	3-7
Circuit 12 monthly maintenance	1 day	21	3-7

Table. 1: Summary of Planned Maintenance Tasks at Waubra Wind Farm

The greatest potential for minimising losses is by re-scheduling tasks that impact on a large number of wind turbines. This must be balanced against the requirement to progress the large number of maintenance tasks that must be performed in a year to avoid creating a backlog. For maintenance tasks that span several days, the work is performed such that the turbine can be returned to service at the end of each day. Therefore the turbine is only offline for 8 hours per day during a maintenance job.

Using Wind Power Forecasts to Improve Maintenance Scheduling

Requirements of a Forecasting System for Maintenance Scheduling

The forecasting requirements for maintenance scheduling are in part different to those required for energy trading, which has historically driven development of forecasting systems. Since maintenance planning occurs on a weekly cycle, forecast horizons of up to 168 hours are relevant. Importantly, timing and amplitude errors are less critical.

First, it is not important if the timing of a weather event is off by a few hours. To maximise production, forecasting is used to calculate the amount of energy that will be lost by shutting down one or more turbines for the duration of a task. When undergoing maintenance, a turbine is shutdown for 8 hours each day until the task is complete. Hence lost production is calculated by aggregating losses for each 8 hour period.

Second, amplitude errors may be of little consequence for maintenance planning. Since the forecasts are being used as a decision tool to choose between performing maintenance work on different days, the key requirement is that they can be used to distinguish between days of high wind vs. days of low wind.

Since forecasting requirements for maintenance planning are less stringent than for energy trading, and existing systems already produce forecasts at sufficient accuracy for maintenance planning, no additional development is required.

Labour Cost Versus Energy Revenue

In practice there is limited flexibility to reschedule maintenance work. The wind farm retains a permanent workforce, and maintenance scheduling must fit within the size of

the maintenance teams. The planned maintenance team at Waubra consists of 4 two man crews working 5 days per week. If a decision is made to not perform a maintenance task due to high wind, the technicians still need to be paid. Therefore the revenue from increased production must be balanced against the cost of labour.

Figure 1 shows the revenue from energy production compared to the hourly cost of a maintenance team. The energy revenue is shown as a function of power for different numbers of turbines. The dotted red line represents the hourly cost of a team of technicians. When the turbine revenue is greater than the technician cost it makes sense economically to delay a maintenance task, i.e. it is cheaper to pay the technicians to do nothing than to shut down the turbines.

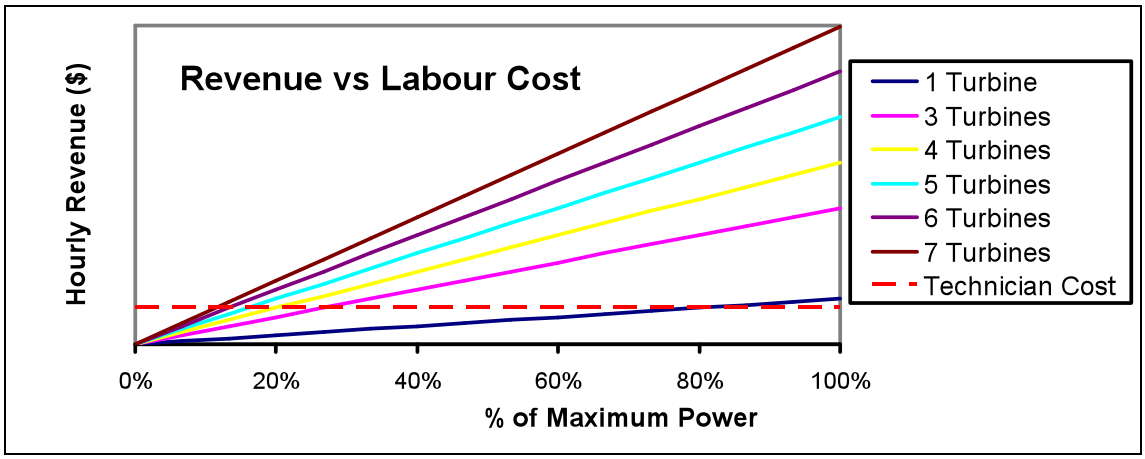

Figure 1: Energy revenue vs. cost of maintenance technicians

Figure 1 demonstrates that there is virtually no benefit in delaying maintenance on one turbine even when it is operating at maximum power. For maintenance tasks involving multiple turbines, the lost revenue from energy production usually outweighs the cost of paying the technicians. Therefore there is a benefit in rescheduling tasks that will impact on multiple turbines.

Hence a possible scheduling strategy would be to schedule maintenance tasks only for times where the labour cost is greater than the forecast production revenue. This would involve calculating the forecast lost energy production for each maintenance task based on the number of turbines involved and the duration of the task. The lost energy production for a specific task will vary according to when the task is performed so it should be scheduled for a time when the cost of labour is higher than the lost revenue from shutting down the turbines.

Using Climatic Trends for Maintenance Scheduling

A simple approach to improving maintenance scheduling could be to use climatic data to identify periods of low energy production. For example, at the Waubra Wind Farm the average daily energy production is slightly lower during the months from February to May. It may make sense to perform all maintenance work during these months. In practice this is problematic, since turbine maintenance must be completed within a prescribed window to comply with warranty conditions. It would also be impractical to squeeze maintenance for 128 turbines into 4 months. It would also be difficult to retain a team of skilled maintenance technicians if they are only required 4 months per year

We can also look at the average energy production for each hour of the day. At Waubra, the optimal timeframe for performing maintenance work is between 6 am and 2 pm.

Currently maintenance work is performed between 8am and 4 pm. So a potential improvement to the maintenance schedule would be to perform all maintenance work between the hours of 6 am and 2 pm. Provided that technicians are prepared to begin work at this time, there are no serious problems with this approach apart from during winter months when it is still dark at 6 am.

Simulation of Maintenance Scheduling Strategies

To test different scheduling strategies, a software simulation has been developed. The simulation tests each strategy by running it over a historical data set and calculating the total energy produced under each alternative scenario.

The simulation creates a list of maintenance tasks based on the job types in Table 1. The jobs are then assigned to maintenance crews and scheduled according to the rules of each scheduling strategy. Scheduling is performed at the beginning of each week using the most recent wind power forecast available at that time. Figure 2 shows a system flow for the software simulation model. A series of scheduling strategies were then run through the simulation.

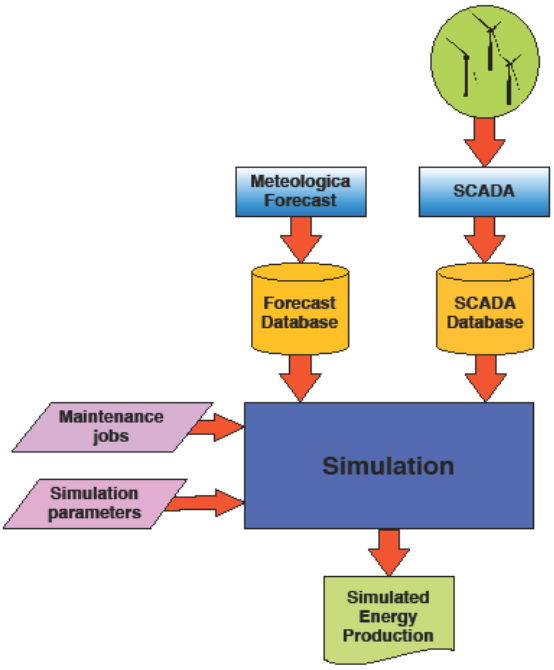

Figure 2 - System flow for simulation model

All strategies tested were relative to current practice, which we call *Naïve scheduling*. Under this strategy, wind power forecasts are not considered when scheduling maintenance work. Tasks are assigned to maintenance crews based only on their position in the job queue. The upper benchmark we call *'Perfect' forecasting'*. In this scenario the wind power forecasts are replaced with actual historical data. This is used to test the maximum possible improvement if the forecasts were 100% accurate.

1. *Scheduling based on labour cost:* Maintenance tasks are scheduled for times when the forecast energy revenue for the affected turbines is less than the cost of labour for the duration of the task. For each maintenance task, the number of turbines and the task duration are used to calculate lost energy production. The task is then scheduled for a window in the upcoming week that will minimise lost production. If there are no windows where forecast revenue is less than labour cost, the job is deferred to a later time. It has been assumed that the cost of labour does not vary within the different scenarios.
2. *Scheduling based on labour cost + 7 day working week:* This approach uses the same scheduling algorithm as the previous scenario with the modification that Saturdays and Sundays are available for planned maintenance work. This strategy is used to test whether the extra flexibility provided by a 7 day working week achieves any increase in production.
3. *Scheduling based on labour cost with perfect forecasting*: This approach uses the same scheduling algorithm, but perfect forecasts (historical data) are used.

4. *Pro-active scheduling of high impact work:* Under this scenario high impact jobs are pro-actively scheduled for times of low forecast production. High impact jobs are defined as those that take more than one turbine offline. A low production threshold is established such that high impact jobs are scheduled for times when the production forecast is below the threshold. For example, if the threshold is set to 10% of maximum production, then high impact jobs would be scheduled when the forecast production is less than 19.2 MW.
5. *Pro-active scheduling of high impact work with perfect forecasting*
6. *Scheduling based on climatic trends:* All maintenance work is shifted forward 2 hours so that work commences at 6am and finishes at 2pm. Wind power forecasts are not considered in this scenario.

Simulation Results

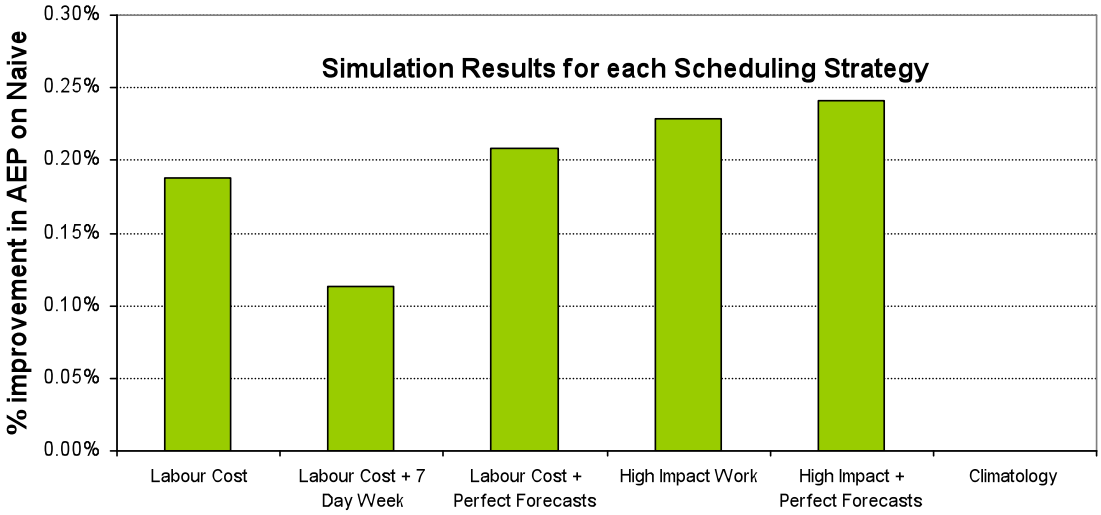

Figure 3: Simulation Results = Improvement in Annual Energy Production (AEP)

The results of the simulation are shown in Figure 3. The largest improvement is achieved by pro-actively scheduling high impact work. This achieved an increase in energy production of approximately 0.23%. Next comes scheduling based on labour cost, which achieved an increase in energy production of 0.19%. Surprisingly the added flexibility of allowing a 7 day week actually reduced the energy production under the simulation. This may be a result of the specific data set used for the simulation.

Using climatic trends to shift the working hours achieved virtually no benefit. This is probably because the existing working hours already include a large proportion of the times when average energy production is lowest. A more significant difference may be seen if comparing the hours of peak production with the hours of lowest production.

Using 'perfect' forecasts improves energy production for both of the scheduling algorithms that use wind power forecasts. In both cases the improvement due to the 'perfect' forecasts is approximately 0.01%. This suggests that the accuracy of the forecasts provided by Meteológica is sufficient for the purposes of maintenance scheduling and there is little benefit in using more accurate forecasting systems.

The increased production achieved with strategy 4 (pro-active scheduling of high impact work) is also dependant on the threshold set for scheduling high impact jobs. The simulation was run with several different threshold levels to see which achieved the

largest increase in energy production. Figure 4 shows that a threshold of 10% of total power achieved the largest increase; however all cases deomonstrated an improvement over the Labour Cost strategy.

In summary, it has been shown that the optimal strategy for maximising energy production is to pro-actively schedule jobs impacting more than one turbine for times where the forecast production is less than 10% of maximum production. This achieves an increase in annual energy production of 0.23% or 1.5 GWh. This increased efficiency can be achieved at no extra cost other than the cost of the forecasts, and will provide additional annual revenue of $142,500. The additional generation could reduce the amount of electricity that needs to be produced by coal generators thereby avoiding greenhouse gas emissions of 1830 tonnes CO_2-e (Department of Climate Change 2009).

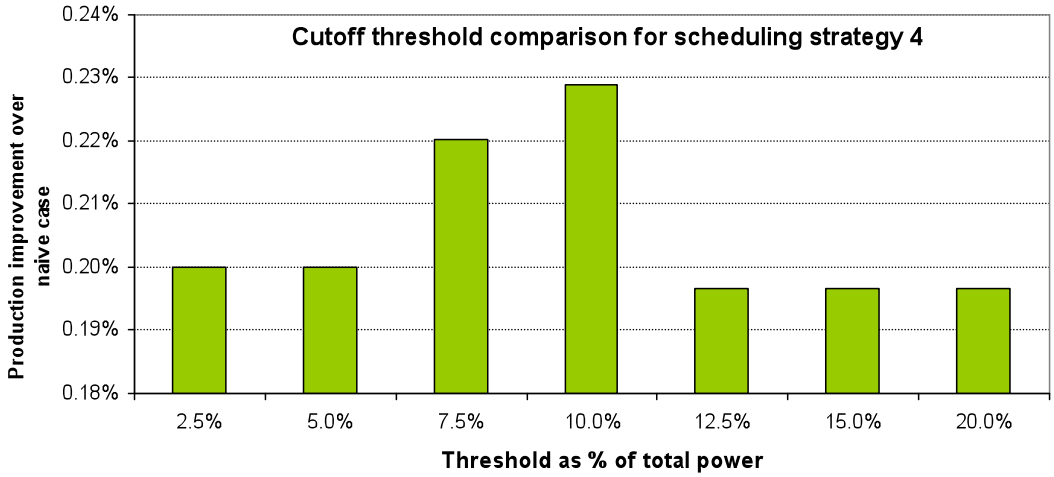

Figure 4 - Increased energy production for different threshold levels using strategy 4

CONCLUSION

This paper has demonstrated that wind power forecasting can be used to improve maintenance scheduling to increase the annual energy production of a wind farm. Forecasts based on a numerical weather prediction system proved the most useful. Highly accurate forecasts are not necessary for maintenance planning, as 'perfect' forecasting makes little improvement to annual energy production. Therefore existing forecasting systems can easily be adapted for maintenance planning.

Using wind power forecasts can increase the annual energy production of a wind farm by optimising maintenance work scheduling. At Waubra, the best scheduling algorithm—actively scheduling high impact work for times when electricity production was forecast to be below 10% of maximum capacity—increased production by 0.23% (1.5 GWh). It was found that there is little practical benefit in rescheduling tasks affecting only one turbine; however, for jobs that affect many turbines there can be large energy savings by performing the work at a time of low production. This applies to regular tasks such as circuit maintenance and also to one-off jobs such as substation maintenance that could impact on as many as 30 turbines.

REFERENCES

Acciona Energy (2009), *Wind Speed Chart*, Internal document

AEMO (2009a), *AEMO Committed NEM Non-Scheduled Generation*, http://www.aemo.com.au/data/gendata_comm.shtml

AEMO (2009b), *AWEFS Project Summary*, http://www.aemo.com.au/electricityops/awefs.html

AEMC (2008), *National Electricity Amendment (Central Dispatch and Integration of Wind and Other Intermittent Generation) Rule 2008 No. 2*.

Coppin, P & Katzfey, J (2003), *The Feasibility of Wind Power Production Forecasting in the Australian Context*, CSIRO Atmospheric Research, Aspendale, Victoria.

Coppin, P (2005), *Wind forecasting in Australia*, Workshop on wind energy forecasting and wind power system integration, CEEM, UNSW http://www.ceem.unsw.edu.au/windworkshop/

Cutler, N (2006), *Wind Energy Forecasting Issues Paper*, Centre for Energy and Environmental Markets, http://www.ceem.unsw.edu.au/windfornem/

Cutler, NJ, Kay, MJ, Jacka, K & Nielsen, TS (2007), 'Detecting, Categorizing and Forecasting Large Ramps in Wind Farm Power Output Using Meteorological Observations and WPPT', *Wind Energy*, Vol. 10, No. 5. pp. 453-470.

Cutler, NJ, Outhred, HR, MacGill, IF, Kay, MJ & Kepert, JD (2009). "Characterizing future large, rapid changes in aggregated wind power using Numerical Weather Prediction spatial fields".*Wind Energy,* Vol. 12, No. 6, pp. 542-555.

Davy, RJ, Woods, MJ, Russell, CJ and Coppin, PA (2010). "Statistical Downscaling of Wind Variability from Meteorological Fields". *Boundary Layer Meteorology*, Vol. 135, No. 1, pp. 161-175.

Department of Climate Change (2009), *National Greenhouse Accounts (NGA) Factors 2009*, Commonwealth of Australia.

Department of Prime Minister and Cabinet (2004), *Securing Australia's Energy Future*, Australian Government, Canberra

Giebel, G (2003), *The State-Of-The-Art in Short-Term Prediction of Wind Power*, Project ANEMOS, http://anemos.cma.fr

Kepert, J (2005), *NWP for Wind Energy: Local and Overseas*, Workshop on wind energy forecasting and wind power system integration, CEEM, UNSW, http://www.ceem.unsw.edu.au/windworkshop

Meteológica 2008, *Prediction System*, Metológica, viewed 7th July 2009, http://www.meteologica.es/meteologica/como_en.htm

NEMMCO 2001, *Guide to Ancillary Services in the National Electricity Market*, NEMMCO, http://www.aemo.com.au/electricityops/160-0056.pdf

NEMMCO (2003), *Intermittent Generation in the National Electricity Market*.

NEMMCO (2008) *An Introduction to Australia's National Electricity Market.*

BRIEF BIOGRAPHY OF PRESENTER

Iain Pople works as an Engineer for Acciona Energy in the Operations team, providing engineering support for all Australian Acciona wind farms. Iain began his time at Acciona working on the commissioning of the Waubra Wind Farm, at the time the

largest wind farm in the southern hemisphere. He is now focused on ensuring that all Acciona wind farms operate at their full potential. Iain has a Bachelor of Computer Engineering from the University of Melbourne and a Masters of Engineering (Sustainable Energy) from RMIT.

Forecasting scenarios of wind power generation for the next 48 hours to assist decision-making in the Australian National Electricity Market

Nicholas J. Cutler[1], Hugh R. Outhred[2], Iain F. MacGill[1]

[1]Centre for Energy and Environmental Markets
School of Electrical Engineering and Telecommunications
University of New South Wales
Sydney, NSW, 2052, Australia
n.cutler@unsw.edu.au

[2]School of Electrical Engineering and Telecommunications
University of New South Wales
Sydney, NSW, 2052, Australia

ABSTRACT

Wind power forecasts can assist decision-making in day-to-day power system operation, and thus facilitate wind power integration. This paper presents the work in progress for the current wind power forecasting project undertaken by the University of New South Wales in collaboration with the Australian Energy Market Operator (AEMO). The aim of the project is to develop a visual decision support tool to forecast large rapid changes in wind power to assist the management of power system security in the Australian National Electricity Market (NEM). The approach is to utilise Numerical Weather Prediction (NWP) data at multiple grid points in the vicinity of each wind farm of interest to produce automated multiple potential scenarios for wind farm generation. Data from the European Centre for Medium-Range Weather Forecasts (ECMWF) NWP global forecast model has been collected along with the observations from 18 wind farms in south-eastern Australia[1]. The methodologies and some resulting forecasts will be discussed and compared with more conventional wind power forecasting methods and presentation formats. The criterion for comparison is how the information could be interpreted by the forecast user and be used to assist decision-making.

Keywords: short-term wind power forecasting

INTRODUCTION AND BACKGROUND ON WIND POWER FORECASTING

Wind power forecasting can greatly assist decision-making by participants in an electricity industry with a high level of wind energy penetration. Wind farm operators can use short (5-minute) wind power forecasts for operational control and multi-day forecasts to prepare maintenance schedules. All generators and end-users participating in electricity markets can use wind power forecasts to improve their bidding strategies since in some electricity industries wind power may have an influence on market prices (Cutler *et al*. 2009a). Power system operators can benefit from information on critical events that threaten system security, such as a potential large rapid change in wind

[1] Source of wind power generation observations: http://www.aemo.com.au/data/csv.html

power generation. In each of the above cases an uncertain large and rapid change in wind power is likely to have significant albeit differing impacts on participant decision-making and its outcomes (from causing undesirable loadings on the wind turbines through to a rapid call for thermal unit start ups).

For all industry participants, the wind power forecasting techniques and presentation formats might best be tailored differently to meet the specific needs of the forecast user. For example, in some circumstances, the most useful forecast would be a single scenario, such as a "best-guess" that statistically has the smallest average forecast error (where the error is defined as the difference in amplitude between the forecast and observed values at each time-step). Commonly used chronology-independent average forecast error scores are the mean absolute error (MAE) and the root mean square error (RMSE) and great progress has been made on optimising wind power forecasts for these scores (Madsen *et al.* 2005, Ernst *et al.* 2008, Sanchez 2005). However, there are wind forecast applications for which chronology of wind power behaviour is important and optimising for error scores such as RMSE or MAE can compromise the chronological veracity of the forecast (Cutler *et al.* 2007, AWS Truewind 2008). An example of this is a tendency for the "best guess" forecast to hedge towards the climatological mean during periods of large, uncertain rapid changes to avoid increasing the average forecast error score. This paper discusses a forecasting approach that aims to provide useful chronological information for a single wind farm or a group of wind farms with a particular focus on large rapid changes in wind power. This is being developed in a UNSW research project, in conjunction with the Australian Electricity Market Operator (AEMO).

The paper is structured around three main sections followed by some concluding remarks. The first of the main sections provides some background for the wind power forecasting techniques being developed in the project and shows some examples of the results for the National Electricity Market. The second section provides more specific details for the project. The third section discusses various practical issues with wind power forecasting for managing power system security applications, including some specific issues for the Australian National Electricity Market and AEMO.

TECHNIQUES FOR FORECASTING LARGE RAPID CHANGES IN WIND POWER

As introduced above, this paper discusses a forecasting approach that aims to provide useful chronological information for a single wind farm or a group of wind farms. The most critical events of interest are when the chronological change in wind power is potentially highly significant, or in other words, when a large rapid change in wind power might occur. Large rapid changes in the power output of a single wind farm or a group of wind farms may not be well predicted using statistical techniques based on past on-site observations because there is unlikely to be any warning signal with a significant lead-time in on-site observations. Appropriately placed off-site observations can help predict large rapid changes for 1-2 hours ahead under specific conditions (Larson and Westrick 2007).

However, the most generally applicable tool to predict large rapid changes is a Numerical Weather Prediction (NWP) system. These mathematically based computer models of the atmosphere have been developed by weather forecast organisations around the world and are used routinely for a range of weather forecasting applications. They model the atmospheric region of interest with a three dimensional grid and undertake two main procedures to produce a forecast; first they estimate an initial state

of the atmosphere at each grid point and second, they solve equations representing the laws of atmospheric behaviour in response to exogenous drivers and disturbances to forecast how the initial state of the atmosphere might evolve in time. NWP systems are used to generate forecasts of atmospheric behaviour over forecast horizons of 48 hours or more. A relevant example is the European Centre for Medium Range Weather Forecasts (ECMWF) which has an NWP system that models the global atmosphere at a horizontal grid resolution of 16 km over a forecast horizon of several days (ECMWF 2010).

Recent research (Cutler *et al.* 2009b, Lange and Focken 2006) has highlighted some important traits of NWP systems for wind power forecasting. They have good skill in forecasting synoptic weather systems and how these influence near-surface wind features, but they may misplace these wind features relative to the earth's surface (Cutler *et al.* 2009b). This 'misplacement error' can be vertical or horizontal within the three-dimension model of the atmosphere, but for the Australian wind farms that we have studied misplacements of significance were found to be predominantly in the horizontal dimension. It is important to note that NWP models cannot resolve the fine scale near surface wind features below their grid resolution, such as turbulence and other topographical induced eddies. However these will generally cause only relatively small wind speed forecast errors and are unlikely to be the cause of large rapid changes in wind power except in the case of wind gusts that exceed the design shut-down wind speed of a group of wind turbines.

Single wind power forecast scenarios are usually derived from a single NWP forecast by compiling the wind forecasts from each NWP time-step over the forecast horizon at a single grid point (or interpolation of grid points) that represents the location of a wind farm of interest. Those wind forecasts are then transformed to wind power forecasts by using a previously estimated wind power curve for the wind farm. Because of uncertainty in forecasting rapid changes in wind power as highlighted above, forecast users might greatly benefit from multiple scenario forecasting techniques since it allows them to prepare for a set of potentially quite different yet plausible scenarios for wind farm power output. It is thus important that these multiple scenarios are each chronologically consistent with the underlying behaviour predicted by the NWP system.

Multiple wind power forecast scenarios are commonly produced using an ensemble of NWP forecasts that accounts for at least some uncertainty in the NWP modelling process. The NWP ensemble members may be based on slightly different initial conditions, or use different physical assumptions about atmospheric behaviour. Single forecast scenarios are extracted from each NWP ensemble method using the single grid point method described above to compile multiple forecast scenarios. However, NWP ensembles are more computationally expensive than single NWP forecasts at the same spatial resolution. Consequently, spatial resolution is usually compromised in NWP ensemble forecasting (eg 32 km instead of 16 km in the ECMWF case) and weather forecast organisations may set a higher price for them. The next section presents a different method to produce multiple scenarios utilising data from multiple grid points in a single NWP forecast.

The multiple grid point method

As described above, the conventional method for using forecast information from an NWP output data set is to extract the data at a single NWP grid point for each time step. Due to possible misplacement error, this method may miss useful information at nearby grid points in the NWP data set at a particular simulation time step. Additionally, the

single grid point forecast may miss further information due to temporal aliasing, since the NWP data set is only available at particular simulation time steps, such as hourly.

Utilising data at multiple NWP grid points at each simulation time step may provide more information on the possible future behaviour of wind farm power output. However the wind speed forecasts at each grid point are influenced by the way terrain local to that grid point is modelled in the NWP system. For example, wind speeds near the earth's surface over the ocean tend to be stronger than over land because the surface of the land is rougher than the ocean. Surface roughness effects are represented in the NWP model, so that if a given weather feature is over the ocean, higher near-surface wind speeds will be predicted than if the same weather feature was over the land. Hence, we have developed a 'terrain standardisation' method to establish relationships between predicted wind speeds at neighbouring grid points. This method uses a NWP data set that covers a long period of time (one year or more) to establish these relationships (Cutler *et al.* 2009b). The result is a horizontal grid of standardised wind speeds, where the wind farm of interest (or cluster of wind farms in close proximity) is located in the middle. A graphical example of the raw wind speeds and the standardised wind speeds is shown in **Figure 1** for a wind farm on the south coast of Australia, using a particular forecast from the ECMWF global model with a projection time of 15 hours ahead.

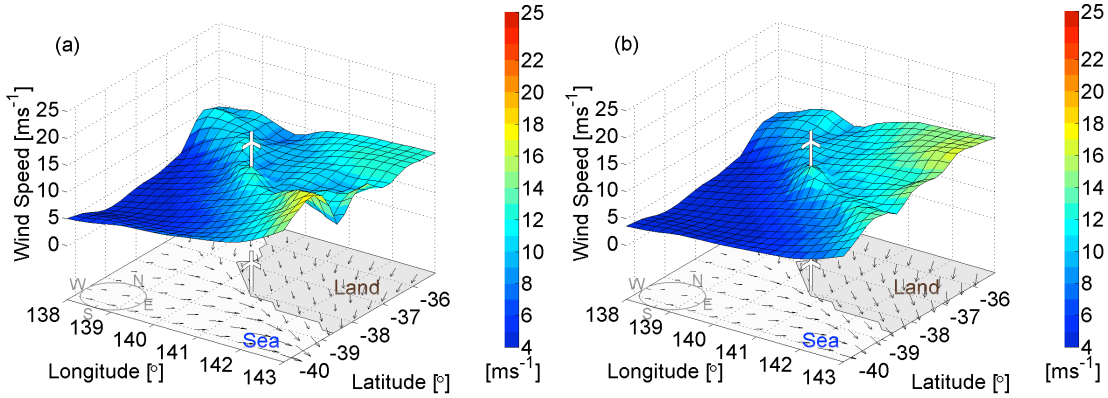

Figure 1: (a) raw and (b) standardised wind speed fields for an ECMWF forecast with projection time 15 hours ahead. Each plot (a) and (b) shows the wind speed fields in a 3D plot with the wind direction field shown on a 2D plot beneath it. The wind turbine symbol indicates the modelled location of the wind farm. Note how the standardised field has generally lower wind speeds over the ocean and higher over land compared with the raw field.

The standardised wind speed field can then be transformed to wind power (based on a wind power curve developed using past single grid point wind speed forecasts and wind power observations) to produce a 'site-equivalent wind power forecast field'. The wind power values are site-equivalent because of the terrain standardisation, meaning that all wind power values in the field are directly applicable to the targeted wind farm. Successive wind power forecast fields can be used to estimate the speed and direction of propagation of wind features (the algorithm for this will be published in a future paper). For the same example as in **Figure 1**, the wind power forecast field is shown in **Figure 2**, with several wind turbine symbols to indicate alternative scenario forecasts illustrating potential misplacement errors.

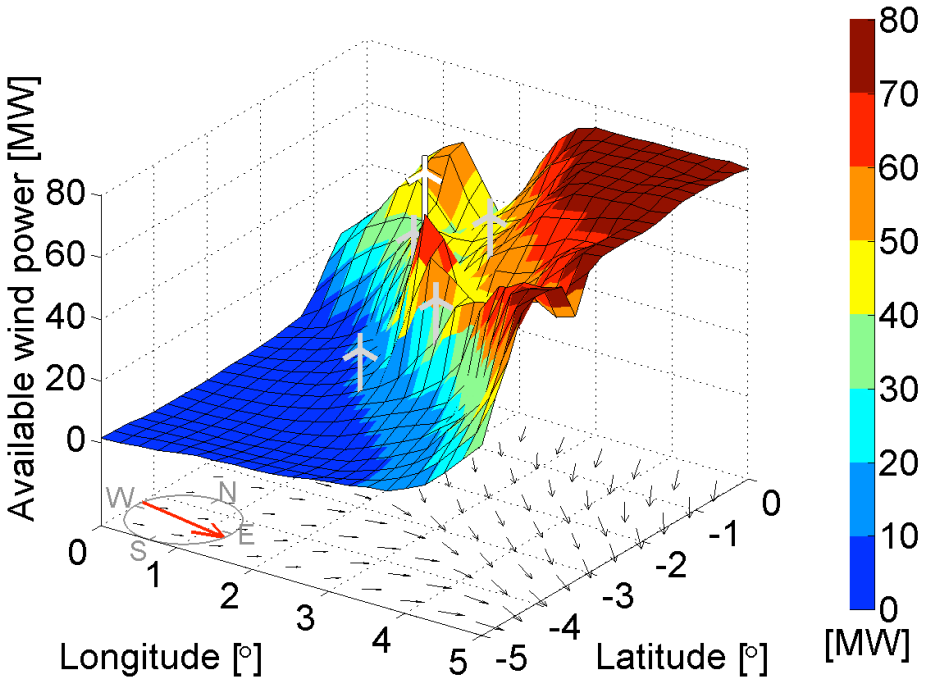

Figure 2: The wind power forecast field for the same example as in Figure 1. The modelled wind farm location is again shown with the white, outlined wind turbine symbol, and four other possible wind farm locations are shown that represent four illustrative misplacement errors. The estimated propagation direction for the wind features is indicated by red arrow on the compass, where the arrow length indicates the speed of propagation of the wind feature. The longitude and latitude values have been made generic to help clarify the misplacement concept where there are many possible positions of this wind power field relative to the surface of the earth

Displaying the site-equivalent wind power forecast field, such as in **Figure 2**, provides a visual tool to characterise uncertainty in the NWP system forecast. In this example, the white, uppermost wind turbine symbol, representing the actual location of a wind farm, is situated at a point of high wind power relative to the surrounding wind power field. The four grey wind turbine symbols on the wind power field represent possible misplacement errors of the wind feature forecast by the NWP with respect to the wind farm. They highlight that even a small misplacement error in any direction would result in a lower wind farm power at the particular time for which the forecast was issued. Thus we may infer that the predicted wind power value at the actual location of the wind farm has a low probability of being correct at the issued time.

Using the wind power field, a forecast user can also predict potential chronological changes in wind power by using the estimated speed and direction of propagation of the dominant wind power feature (shown by the red arrow in the compass). In **Figure 2**, the white wind turbine and each of the four grey misplaced turbines suggest five different scenarios for how the wind power may change. Furthermore, an animation of successive wind power fields for each time-step in the NWP data provides a visualisation of the propagation of wind power field features through a longer period of time. By contrast, a single grid point forecast may suffer from aliasing, or sampling error, such as if it falls on a sharp peak in the spatial wind power forecast (as in the example shown in **Figure 2**). This example highlights how a single grid point forecast can miss useful information because it provides only the predicted wind power value at the assumed wind farm location relative to the wind power field for each time step.

Figure 3 shows a single grid point forecast derived from twelve consecutive wind power fields at three-hour intervals (including the wind power field in Figure 2) along with some other potential scenarios that take into account possible misplacement errors. The corresponding half-hourly observations of wind power generation from the wind farm are also shown for comparison. At a projection time of 15 hours (corresponding with the wind power field in Figure 2), the single grid point prediction is above 70 MW and subsequently drops rapidly to around 10 MW in three hours. However the misplacement error scenarios indicate with a high level certainty that a rapid drop in wind power will occur, but that it may occur up to three hours earlier. The observations show that the wind power does indeed start to drop around three hours earlier than predicted by the single grid point forecast and then increases a little before dropping to less than 10 MW. In this example, the single grid point forecast was reasonably good for most of the 36-hour period, but had a large error at a projection time of about 15 hours. The wind power forecast fields provide additional insights about how the event might evolve, by highlighting the nature of the uncertainty around the projection time of 15 hours.

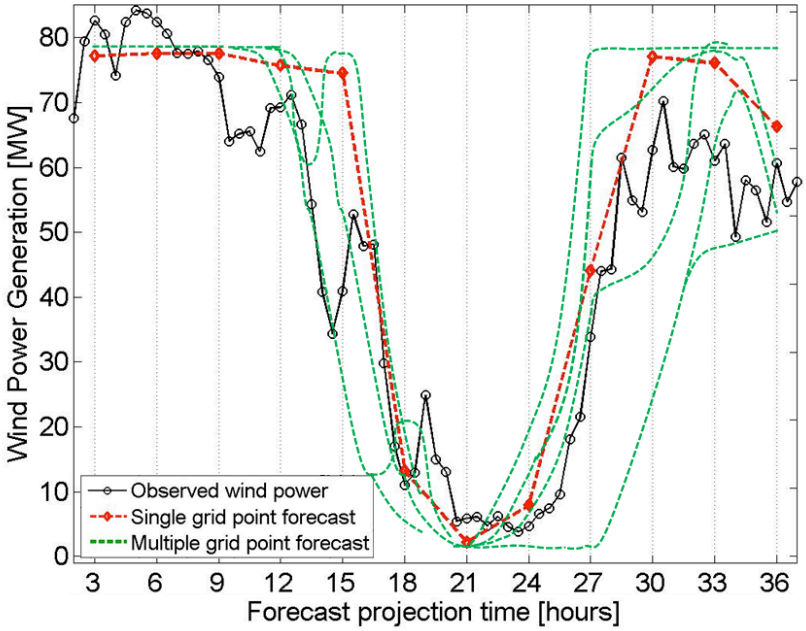

Figure 3: A time-series plot of the single grid point forecast and multiple scenarios from the ECMWF NWP system along with the actual half-hourly wind farm power observations

WIND POWER FORECASTING AT AEMO AND THIS SPECIFIC PROJECT

The Australian Energy Market Operator (AEMO) is funding and participating in this project, which is to develop a prototype tool for forecasting large rapid changes in wind power. If successful, this project might provide an enhancement to the Australian Wind Energy Forecasting System (AWEFS) project in which AEMO installed a commercial wind power forecasting system (AEMO 2010). The project was financed by the Commonwealth Department of Resources, Energy and Tourism (DRET) and is due to be completed in 2010. The successful supplier was the European consortium, ANEMOS[2]. These recent developments in wind power forecasting in Australia largely result from government planning for the rapid expansion of Australia's wind farm installations over the recent decade, particularly in the South Australian region of the

[2] Development of **A NE**xt Generation Wind Resource Forecasting Syste**M** for the Large-Scale Integration of **O**nshore and Off**S**hore Wind Farms. http://anemos.cma.fr/

Australian National Electricity Market. Australia currently has more than 1600 MW of wind power capacity installed, and more than half of this (868 MW) is installed in South Australia. Other recent studies on wind generation in South Australia include (Cutler *et al.* 2009, ESIPC 2009, Weston 2009).

In the current project, the prototype forecasting tool will undergo a user acceptance testing procedure in which AEMO personnel will assess its merit for possible further development into an operational tool as part of the AWEFS system in the power system control room. A set of critical large rapid change event categories have been identified on which to test the prototype tool. These are as follows:

Event category 1: Total wind generation in South Australia changes by more than a pre-specified amount in 30 minutes.

Event category 2: The summated wind generation from the south-east region of South Australia changes by more than a pre-specified amount in 30 minutes. The south-east region currently comprises of three wind farms: Canunda, Lake Bonney 1 and Lake Bonney 2 with a total installed capacity of 286 MW.

Event category 3: The total wind generation in Tasmania changes by more than a pre-specified amount in 30 minutes.

For each of these event categories, the prototype tool is to provide the following outputs:

- Raising alarms when there is the possibility of an event category occurring according to the most recently available NWP forecast,
- For each of the raised alarms, a presentation of the available forecast information is to be provided highlighting plausible multiple scenarios for wind power generation. This information will be provided in two forms (where both forms have been described in detail in the previous section):
    - An animation of successive wind power spatial fields,
    - A time-series plot showing the multiple scenarios, possibly with an indication of their associated probability.

The user acceptance test criteria will include an element of judgement assuming that the power system operator would prefer information that they can quickly assimilate to make a more informed decision. In addition to this, some evaluation scores have been defined as follows. These will be estimated for each event category.

- Number of alarms produced. This should be minimised so that the power system operators are not responding to too many alarms.
- Number of events that actually occur and were not alarmed, or 'missed' events. This should also be minimised.
- Number of events where the predicted timing of the event was within 60 minutes of the actual timing of the event. This should be maximised, since it is undesirable that a multiple scenario forecast would not contain at least one scenario where the event occurs within 60 minutes of the actual event.
- Average number of forecast scenarios provided for each alarmed event. This should be minimised to encourage that the uncertainty is reduced where possible, making the forecast information more useful.

PRACTICAL ISSUES FOR FORECASTING WIND POWER TO MANAGE POWER SYSTEM SECURITY

There are various unresolved issues regarding the implementation and operational use of wind power forecasts for the management of power system security. Some of the more important of these are as follows:

- **Input data quality.** As with any system, wind power forecasts are reliant on the quality of the input data to the forecasting system. This refers to the quality and reliability of the NWP system used as well as the historical observations at wind farms including wind power generation and wind turbine availability. High quality forecasts of wind turbine availability are also crucial to the accuracy of predictions of wind farm power output. Furthermore, NWP systems often only provide wind forecast data near turbine hub height with a temporal resolution of 3 hours whereas more frequent NWP data at hub height would be preferable, such as hourly. This is particularly important for operation forecasts in real time.
- **Decision-making procedure development.** Since wind power forecasts are a relatively new set of information for power system control rooms, additional decision-making procedures may be required to facilitate the most appropriate decisions being made, taking into account the state of the power system at the time.
- **Integrating wind power forecasts into the control room routine tasks.** Power system operators already manage a large number of tasks including assessing large quantities of time-varying information. Thus, they require wind power forecast presentation formats that allow them to quickly assess the situation and make informed decisions. Fortunately, NWP forecasts are provided for forecast horizons of 48 hours or more and a new NWP forecast is typically produced every 6 or 12 hours. This means that power system operators are likely to receive wind power predictions at least several hours and up to a day or two ahead. While time-series presentation of predicted behaviour may be more familiar, spatial field presentation can potentially take advantage of humans' superior pattern recognition skills and direct the eye to the more extreme scenarios of potential large rapid changes in wind power, which are the most important scenarios for managing power system security.

CONCLUSIONS AND FURTHER WORK

A wind power forecast system may be usefully designed to meet the intended user's specific needs beyond conventional forecasting methods and presentation techniques. Researchers in the field are still learning which wind power forecasting techniques and presentation methods might best meet the needs of forecast users. In this paper we have demonstrated a method that utilises data from multiple grid points in an NWP model to provide useful information on potential scenarios for wind power generation. The method shows promise for characterising large rapid changes in wind power and has been evaluated for some wind farm sites in Australia. The paper also describes a current application, in which we are developing a prototype tool for predicting large rapid changes in wind power for the Australian Energy Market Operator. Specific large rapid change event categories will be used to evaluate the prototype model. Progress to date is promising.

Potential future work includes investigating the development of a forecast tool for commercial decision-makers in the Australian NEM. Other research (Cutler *et al.* 2009a) suggests an emerging relationship between wind power and electricity prices in South Australia, including more common incidences of low or even negative prices at

times of high wind generation, and typically higher spot prices at times of low wind generation.

ACKNOWLEDGMENTS

This work is currently funded by the Australian Electricity Market Operator (AEMO) and follows from previous work in Nicholas Cutler's PhD project, which was financially supported by the Commonwealth Government (represented by the former Australian Greenhouse Office). The authors thank Jeffrey Kepert at the Australian Bureau of Meteorology for his contributions to this work.

REFERENCES

Australian Energy Market Operator (AEMO) website: http://www.aemo.com.au/electricityops/awefs.html. Accessed: 4 August 2010

AWS Truewind, *AWS Truewind's Final report for the Alberta forecasting pilot project*, in Wind Power Forecasting PILOT Project, AWS Truewind, Albany, NY, 2008. Available: http://www.aeso.ca/gridoperations/13825.html

Cutler NJ, MacGill IF. Outhred HR, *The integration of wind generation within the South Australian region of the Australian National Electricity Market.* Canberra : Environmental Economics Research Hub, 2009a. EERH Research Report No. 38.

Cutler NJ, Outhred HR, MacGill IF, Kay MJ, Kepert JD, "Predicting large changes in wind power using site-equivalent numerical weather prediction spatial fields", *Wind Energy*, 2009b; 12(6): 542-555.

Cutler NJ, Kay MJ, Jacka K, Nielsen TS, "Detecting, categorizing and forecasting large ramps in wind farm power output using meteorological observations and WPPT", *Wind Energy* 2007; 10(5): 453-470.

ECMWF web site. http://www.ecmwf.int/publications/cms/get/ecmwfnews/1264512002630

Energy Supply Industry Planning Council (ESIPC), "Annual Planning Report", Adelaide, 2009.

Ernst B, Oakleaf B, Ahlstrom M, Lange M, Möhrlen C, Lange B, Focken U, Rohrig K, "Predicting the Wind", *IEEE power & energy magazine*, 2008; 5(6): 78-89.

Lange M, Focken U. *Physical apporach to short-term wind prediction*. Oldenburg: Springer, 2006

Larson KA, Westrick K, "Short-term wind forecasting using off-site observations", *Wind Energy*, 2006*;* 9**:** 55-62.

Madsen H, Pinson P, Kariniotakis G, Nielsen HAa, Nielsen TS, "Standardizing the performance evaluation of short-term wind power prediction models", *Wind Engineering*, 2005; 29(6): 475-489.

Sanchez I, "Short-term prediction of wind energy production", *International Journal of Forecasting*, 2005; 22: 43-56.

Weston S, "Wind Energy – How Much is Enough?", Intelligent Energy Systems, *Insider Newsletter*, Issue 010, November 2009.

BRIEF BIOGRAPHY OF PRESENTER

Nicholas Cutler obtained his Bachelor degree in Electrical Engineering at the University of New South Wales in 2003, a Master of Science at the Technical University of Denmark in 2005 and was awarded his PhD in Electrical Engineering at the University of New South Wales in 2009. In 2003, he worked as a Projects Consultant for Pacific Solar. During his degree in Denmark he worked on a summer job in 2004 at Risø National Laboratory on Sound Detection and Ranging (SODAR) measurements. He is currently a post doctoral fellow at the University of New South Wales funded by the Australian Energy Market Operator to develop a prototype wind power forecasting model.

An Imaging Technique For Assessing the Optical Hazard Due to Solar Concentrators

Christopher J Fell[1,2] and Alex G Lehmann[1]

[1]CSIRO Energy Technology, 10 Murray Dwyer Cct, Mayfield West, NSW 2304
[2]School of Mathematical and Physical Sciences, University of Newcastle, Callaghan, NSW 2308
Ph: 02 4960 6032 Email: chris.fell@csiro.au

ABSTRACT

The bright glare associated with the receiver in concentrating solar power systems can be considered for the potential optical hazard presented to operators, people working nearby and members of the public passing by the site perimeter. This potential hazard is often treated superficially, using rules of thumb, for example, that the source is no larger or brighter than the sun in the sky, or that the natural aversion response should provide adequate protection. This treatment is insufficient with respect to operators of such systems, who have an operational requirement to look at or near the receiver for extended periods of time. Rigorous treatment of the hazard requires a detailed understanding of complex optical equipment and methodology, as well as the mathematical application of the equations for exposure limits. As a result, these treatments are usually performed by specialist consultants and are inconvenient to repeat every time system circumstances change.

We have radiometrically calibrated an inexpensive, consumer-grade digital camera, allowing the camera to be used for rapid analysis of emitted glare from any observer location. Our software analyzes images taken from the desired observer locations and calculates the exposure limits for each location according to international guidelines. Entering the required working time then allows a calculation of the shading requirements for personal protective equipment, such as eye glasses or window tinting.

Keywords: camera, concentrator, hazard, imaging, ocular, solar.

INTRODUCTION

Although facilities for concentrating solar power (CSP) have been in existence for decades, the wide variety of designs has hampered the development of uniform standards for protecting the health and safety of people in and around these facilities. One potential hazard associated with almost all such systems is the risk of ocular injury associated with accidental, casual or occupational viewing of the bright image of the sun that is projected onto the receiver. Assessing the degree of this hazard is challenging for a number of reasons:

- The link between the size, shape and brightness of the image and the resulting biological effects is non-trivial and not always intuitive. The eye is susceptible to several different types of damage, each of which requires a separate calculation that also depends on the degree of intent on behalf of the viewer.

- The degree of hazard varies significantly for different receiver design, collector optics, observer location, operating power and time of the day.
- Methods for measuring the relevant properties of the image are often complex, requiring specialist expertise and expensive equipment.

As a result of these challenges, this hazard is often treated in a very general sense. For non-occupational viewers a common treatment is to assume that the natural aversion response will be sufficient to protect the eye. Occupational viewers, such as operators, will often wear shaded eyewear, chosen based their own sense of comfort. These simple treatments fail to take advantage of the significant body of work that exists in the area of optical safety with respect to viewing of extended broadband sources of light. Literature in this area frequently references the early work of Sliney and Freasier (1973) whose findings have contributed to the formulation of international guidelines for exposure limits for broadband optical radiation by the International Commission on Non-Ionising Radiation Protection (ICNIRP 1997, 2004).

Since the degree of hazard depends most critically on the radiance and angular size of the bright object being observed, the analysis lends itself readily to assessment using imaging methods. Others have recognised this (Brumleve 1977, 1984) but in the past have not had access to modern digital photographic equipment and computers. A method that involves digital imaging, followed by software image analysis and calculation, would allow rapid assessment of the ocular hazard under the specific conditions at a given time, and from any observer location. This type of assessment would provide a much clearer picture of the degree of hazard, and allow a much more precise selection of control measures.

OCULAR HAZARD GUIDELINES

Viewing a bright light source beyond the exposure limit can result in one or more of five different types of ocular injury. Four of these injury types are applicable to the glare associated with CSP systems. In calculating the overall degree of hazard presented by a high-intensity light source, the four different pathological effects must be treated independently. This is necessary because they occur with different efficiencies, involve different parts of the wavelength spectrum, and are influenced differently by behavioural aspects of the viewer, such as involuntary eye movements and the degree of intent to view the hazard. The four types of ocular injury are briefly introduced here, along with the information required to determine the daily exposure limits as recommended by ICNIRP. Quantities necessary for interpretation of the guidelines include the radiance of the source, L, the angular extent of the source, α and the irradiance, E, produced by the source at the location of the observer.

Type 1: Photochemical injury to the cornea and lens (UV hazard)

This type of damage is caused by wavelengths in the range 180-400nm. The effects include photokeratitis, equivalent to sunburn of the cornea, and temporary or permanent clouding of the lens, known as cataracts. The effect is cumulative within any given day. Safe viewing requires that both of two exposure conditions be met:

$$\sum_{180}^{400} E_\lambda \cdot S(\lambda) \cdot \Delta\lambda \cdot t < 30\ \mathrm{Jm^{-2}} \quad \text{and} \quad \sum_{315}^{400} E_\lambda \cdot \Delta\lambda \cdot t < 10^4\ \mathrm{Jm^{-2}}$$

S(λ) is a spectral weighting function known as the action spectrum, or spectral effectiveness, for ultra-violet damage to biological organisms and can be found in (ICNIRP 2004).

Type 2: Photochemical injury to the retina (Blue-light hazard)

Light in the wavelength range 300-700nm passes through the cornea and lens, which together focus the light to produce an image of the viewed object onto the retina. Overexposure to these wavelengths creates an injury equivalent to sunburn in a localised area of the retina. Again being photochemical in nature, this effect is also considered cumulative within a given day. Recommended exposure limits are defined in two time regimes. For viewing times less than 10,000 seconds, the maximum viewing time is determined from:

$$\sum_{300}^{700} L_\lambda \cdot B(\lambda) \cdot \Delta\lambda \cdot t \le 1.0\ \mathrm{MJm^{-2}sr^{-1}} \qquad (\alpha \ge 11\ \mathrm{mrad})$$

$$\sum_{300}^{700} E_\lambda \cdot B(\lambda) \cdot \Delta\lambda \cdot t \le 100\ \mathrm{Jm^{-2}} \qquad (\alpha < 11\ \mathrm{mrad})$$

B(λ) is the action spectrum for blue-light photochemical damage to the retina and can be found in (ICNIRP 1997). For viewing times ≥ 10,000 seconds, the exposure limit becomes a maximum weighted radiance or irradiance:

$$\sum_{300}^{700} L_\lambda \cdot B(\lambda) \cdot \Delta\lambda \le 100\ \mathrm{Wm^{-2}sr^{-1}} \qquad (\alpha \ge 11\ \mathrm{mrad})$$

$$\sum_{300}^{700} E_\lambda \cdot B(\lambda) \cdot \Delta\lambda \le 10\ \mathrm{mWm^{-2}} \qquad (\alpha < 11\ \mathrm{mrad})$$

Type 3: Thermal injury to the retina (Retinal thermal hazard)

Light in the wavelength range 380-1400nm is also focussed onto the retina, but needs to be assessed with regard to the thermal damage it can cause. For bright hazards of angular size in the range 1.7 mrad < α < 100 mrad, and viewing times in the range 10μs < t < 10s, the exposure limit is a maximum radiance, determined according to:

$$\sum_{380}^{1400} L_\lambda \cdot R(\lambda) \cdot \Delta\lambda < 50{,}000/(\alpha \cdot t^{0.25})\ \ \mathrm{Wm^{-2}sr^{-1}}$$

R(λ) is the action spectrum for thermal damage to the retina and can be found in (ICNIRP 1997). For bright hazards with angular size or viewing time outside the ranges described above, the condition is applied assuming α and t are fixed at the corresponding limit of that range.

Type 4: Thermal injury to the cornea and lens (Near-infrared hazard)

If the bright source produces significant radiation in the wavelength range 780-3000nm, the irradiance should be considered for its potential to cause thermal injury to the front of the eye. The recommended maximum viewing time is determined according to:

$$\sum_{780}^{3000} E_\lambda \cdot \Delta\lambda < 100\ \mathrm{Wm^{-2}} \qquad (t > 1000\ \mathrm{s})$$

$$\sum_{780}^{3000} E_\lambda \cdot \Delta\lambda < 18{,}000 \cdot t^{-3/4}\ \mathrm{Wm^{-2}} \qquad (t \le 1000\ \mathrm{s})$$

MEASUREMENTS

Assessment of an arbitrary bright source against the exposure criteria above requires a measurement system to determine the source radiance, the source angular extent and the source irradiance at the location of the observer. Traditionally, radiance has been determined using radiometric equipment with a fixed field of view, with the measured value providing an average radiance over the field of view, which then serves as an effective angular extent. For accurate assessment of complex radiance profiles, such as often found with CSP systems, this measurement may need to be repeated using different aperture sizes. Repeat measurements are also required from different observer locations, since the source shape and angular extent vary with viewing angle and distance from the source respectively. This situation is compounded by the fact that the bright source can include specular reflections, making the radiance also dependent on viewing angle. The combination of expensive radiometric equipment, time-consuming measurements and the non-trivial mathematical interpretation above, mean that repeating the assessment frequently is often impractical.

Many CSP systems however, produce a bright spot hazard which varies regularly, due to either the number of heliostats in operation, changes to the receiver, or simply the changing position of the sun in the sky. Some of these systems are located in populated areas, leading to a need to assess the potential hazard from a number of different observer locations. We propose that a measurement system based on 2D digital imaging, coupled with software for extracting the key parameters and calculating the exposure limits, provides a much more effective tool for assessing the degree of hazard. We have developed a portable system based on a consumer-grade digital camera, with components costing less than US$1000. In the future such a system could be based on fixed digital video hardware, with on-board software for continuous, instantaneous monitoring of hazard conditions from key observer locations.

The obvious advantage of a digital imaging system for assessing an arbitrary glare hazard is the almost instantaneous capture of a complete, high-resolution radiance profile for the source. These data allow extraction of the average radiance and angular extent for any identified portion of even the most complex source profile. The same data also allows calculation of the irradiance at the observer location, with the particular advantage that the user can isolate the irradiance due only to a particular part of the image.

The accuracy of a digital imaging method for assessing glare however, depends critically on several calibration steps to characterise the performance of the particular detector, camera and lens being used. Of these, three steps are most important. The pixel domain must be calibrated across the full range of lens focal lengths, such that the x and y dimensions in the image correspond to the correct angular size at the source. The second calibration accounts for the non-linear response of the detector pixels to irradiance, and the third calibration is to determine the spectral response of the camera. Establishing the camera spectral response is critical if sources with arbitrary spectral composition are to be assessed. Precise knowledge of the camera response means that the source spectrum need only be known in a relative sense, and may include wavelengths outside the camera response range. The complete spectral irradiance of the source is inferred from the intensity of the image and the degree of overlap between source spectrum and camera response. This situation theoretically becomes untenable if

the overlap with the camera response is small or zero, however in CSP systems the spectrum of the bright hazard always contains a significant component in the visible range, and hence significantly overlaps the response of our camera. Establishing the relative spectrum of the source is achieved by one of several methods, depending on the accuracy required. In the simplest mode, our software allows the user to select from a number of standard solar spectra for the bright source, however for more accurate measurement we have incorporated the capability to enter either the relative spectral reflectances of mirrors and the receiver, or a direct measurement of the bright source spectrum.

In order to confirm that our calibrations were robust we conducted a number of tests. In one of these we used the camera to image a test source (20W compact fluorescent lamp in a diffuser housing) from progressively increasing observer distance. In Figure 1a we report the measured values for the size of the source. All measurements are in excellent agreement with the value for the source height measured using a ruler, which was 176mm. In Figure 1b we report the measured values for the irradiance at the observer locations. These are a clear fit to the inverse-square dependence with distance that is expected. At the time of writing we do not have an accurate alternative means of measuring the absolute irradiance for comparison purposes, however the numbers suggest an electrical to optical efficiency of 11%, which is believable, and in the next section it will be seen that our method provides an accurate absolute measurement of irradiance from the sun. In the same figure we have also plotted irradiance data for the case where a second bright light source was included in the image frame. Using our software we elected to measure the irradiance due only to the primary source, and the results are clearly equivalent to those where the image included only the primary source. This demonstrates the ability of the technique to isolate the irradiance at the observer location, attributable to a particular part of the image.

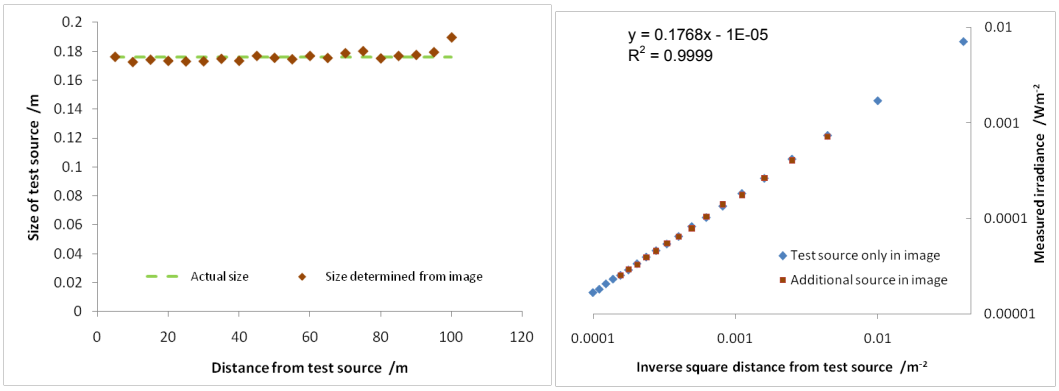

Fig. 1 (a) Values for the size of the test light source measured at different distances; (b) values for the irradiance due to the test source, measured at different distances.

SIMPLE IMAGES

As an example of the process applied to a simple source shape, we have conducted an assessment of the ocular hazard posed by viewing the sun directly. An image of the sun at AM1.64 was obtained on a clear day and is shown in Figure 2a, along with the corresponding calibrated radiance profile in Figure 2b. The measured peak radiance is

1.76×10^{7} $Wm^{-2}sr^{-1}$and the direct irradiance at the observer location is measured to be 848 Wm^{-2}. The latter is in good agreement with a concurrent measurement using an onsite pyrheliometer, which gives a direct solar irradiance of 836 Wm^{-2}. Our system determines the angular size of the solar disc to be 9.17 mrad, based on the radial point at which the radiance falls below the noise floor. The average radiance over this aperture is 1.28×10^{7} $Wm^{-2}sr^{-1}$. Both are in agreement with known typical values for the sun. The level of background noise for this measurement corresponds to a radiance of 1.4×10^{5} $Wm^{-2}sr^{-1}$, or 0.8% of the sun's maximum value. No circumsolar radiance is observed. This is consistent with published calculations that indicate circumsolar radiance on a clear day does not exceed 0.1% of the sun's maximum radiance (Thomalla 1983). An image of the sky adjacent to the position of the sun gave a value for sky radiance of 25 $Wm^{-2}sr^{-1}$, clearly well below the background level in our sun image.

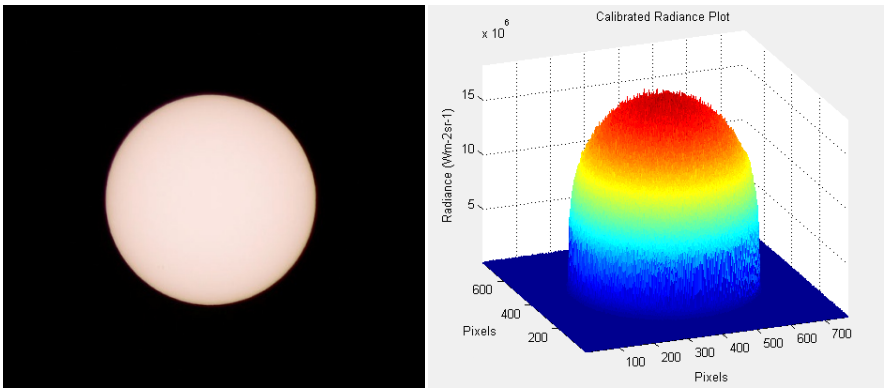

Fig. 2. (a) Uncalibrated photograph of the sun; (b) The corresponding calibrated radiance plot used to determine the degree of ocular hazard, daily exposure limits and suitable protective eyewear.

To determine the recommended exposure limits for viewing the sun, the measured functions L_λ and E_λ are first weighted against the specific action spectra for each injury type and then the resulting functions integrated to provide an effective radiance and irradiance for the particular ocular injury. These effective values are then compared against exposure guidelines which are different, depending on the angular size of the source and the intended viewing time. The dependence on intended viewing time takes into account the fact that ocular hazards may be more or less dangerous, depending on the intent of the viewer.

In Table 1a, b, c & d we present the results of our analysis against each of the four applicable injury types, for four different intended viewing times. In these tables we also present a preliminary determination of protective eyewear that would allow viewing for the intended period. The eyewear calculations take into account the spectral transmittance functions for the various shade ratings, interpolated from Australian Standards for optical protection equipment (AS/NZS 1992). We emphasise that the eyewear calculations are preliminary, and are presented here for the purpose of demonstrating an application of the method. Clearly, the eyewear to be used would be the highest of the shade numbers recommended against the four injury types.

Table 1a. Exposure limits for an observer with intent to view for 10 seconds. Preliminary calculations suggest AS/NZS Shade 4 would provide adequate protection.

Injury Type	ICNIRP Exposure Limit	Eyewear
1	Maximum exposure time 170 seconds	N/A
2	**Maximum exposure time 1.3 seconds**	**Shade 4**
3	Maximum exposure time 0.01 seconds	Shade 2
4	Maximum exposure time 190 seconds	N/A

Table 1b. Exposure limits for an observer with intent to view for 15 minutes. Preliminary calculations suggest AS/NZS Shade 7a would provide adequate protection.

Injury Type	ICNIRP Exposure Limit	Eyewear
1	Maximum exposure time 170 seconds	Shade 1.4
2	**Maximum exposure time 1.3 seconds**	**Shade 7a**
3	Maximum radiance 2.3×10^{6} $Wm^{-2}sr^{-1}$	Shade 2
4	Maximum exposure time 190 seconds	Shade 1.7

Table 1c. Exposure limits for an observer with intent to view for 1 hour. Preliminary calculations suggest AS/NZS Shade 9 would provide adequate protection.

Injury Type	ICNIRP Exposure Limit	Eyewear
1	Maximum exposure time 170 seconds	Shade 2.5
2	**Maximum exposure time 1.3 seconds**	**Shade 9**
3	Maximum radiance 2.3×10^{6} $Wm^{-2}sr^{-1}$	Shade 2
4	Maximum irradiance 240.8 Wm^{-2}	Shade 1.7

Table 1d. Exposure limits for an observer with intent to view for 8 hours. Preliminary calculations suggest AS/NZS Shade 12 would provide adequate protection.

Injury Type	ICNIRP Exposure Limit	Eyewear
1	Maximum exposure time 170 seconds	Shade 4
2	**Maximum irradiance 0.02 Wm^{-2}**	**Shade 12**
3	Maximum radiance 2.3×10^{6} $Wm^{-2}sr^{-1}$	Shade 2
4	Maximum irradiance 240.8 Wm^{-2}	Shade 1.7

COMPLEX IMAGES

In a real CSP system the radiance profile of the bright image is rarely as simple as in the previous example. This is particularly the case for research facilities, where experimental configurations are often in use and collector optics are not always optimised for every receiver. Point-focus systems using heliostats are particularly susceptible to a lack of precise overlap of images from the different mirrors. In order to demonstrate the use of our method on a more complex source, we installed an artificial receiver on our heliostat array system at Newcastle. The receiver was not actively cooled, meaning we could not run the system at high power, but the results are suitable for illustrating the method. Nineteen heliostats were used to produce an optical power of 34kW and a bright reflection approximately 0.8m in size. Digital images were taken from the viewpoint of the facility operator, a distance of approximately 45m from the receiver. An example image of the receiver in operation is shown in Figure 3a, with the corresponding calibrated radiance profile in Figure 3b.

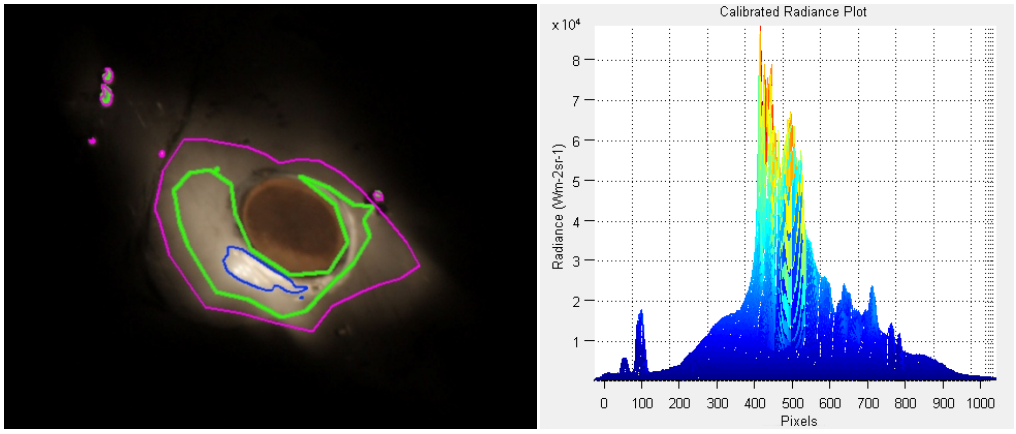

Fig. 3. (a) Uncalibrated photograph of the bright zone near the receiver entrance aperture. Blue, green and pink radiance contours (based on a calibrated image) are overlayed to indicate three different sized zones over which the angular size and average radiance of the hazard might be determined; (b) a 2D representation of the corresponding calibrated radiance profile.

The radiance profile of the image in Figure 3 is clearly non-uniform. In a conventional hazard assessment, this requires a decision on behalf of the assessor as to the choice of aperture for the radiance measurement. Existing methods use instrumentation with a fixed circular aperture, over which the measured radiance is averaged. An exhaustive investigation using such a method might include repeat measurements with different aperture sizes, including multiple measurements with small apertures, attempting to identify hotspots. This approach is time consuming, limited to circular apertures, produces large volumes of data for analysis, and is highly dependent on the skill of the consultant to identify combinations of aperture size and radiance that lead to the worst-case hazard.

Our software analyses the 2D radiance map of the bright area, identifying contours of constant radiance and calculating the ocular hazard and maximum exposure conditions at the various contour intervals. The worst-case scenario is identified and the

appropriate exposure limit reported, along with recommended eyewear. To demonstrate the importance of selecting the appropriate part of the image, three different radiance contours are identified in Figure 3a. The input parameters to the hazard calculation are presented in Table 2, along with the results and recommended shade for a full time operator, assuming a requirement to view the bright area for four hours over a working day. Clearly the radiance contour shown in green produces the worst-case hazard for these three options, recommending the darker Shade 4 eyewear, where the other two selections recommend Shade 2. A conventional hazard assessment may have missed this scenario if the consultant failed to identify the appropriate aperture size and bright zone.

Table 2. Characteristics of the bright light hazard in Figure 3, including the exposure limit criteria and recommended eyeglass shade number. Note the importance of selecting the appropriate sampling aperture (radiance contour) for averaging the radiance.

Colour of contour in Fig. 3	pink	green	blue
Radiance contour value /Wm^{-2}sr^{-1}	0.2×10^4	1.0×10^4	2.5×10^4
Effective angular size of zone /mrad	12.17	6.98	2.67
Average radiance in zone / Wm^{-2}sr^{-1}	7.13×10^3	1.37×10^4	3.9×10^4
Exposure limit	Max. radiance 1140.6 Wm^{-2}sr^{-1}	Max. irradiance 0.020 Wm^{-2}	Max. irradiance 0.020 Wm^{-2}
Recommended Shade	2	4	2

MAPPING THE REQUIREMENT FOR PROTECTIVE EYEWEAR

The ability to conduct comprehensive in-house assessment of potential bright-light hazards will be of value to CSIRO and any developers of CSP systems, particularly where such systems are constructed close to areas of human activity. Combining our assessment method with GPS and satellite mapping allows hazard maps to be prepared. One such map for an artificial set of operating conditions and a 4-hour occupational viewing requirement is shown in Figure 4.

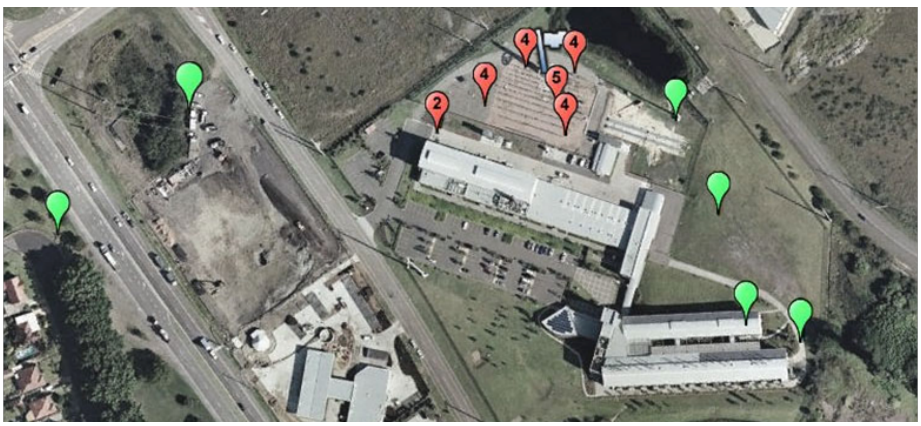

Fig. 4. A mock hazard analysis map for the CSIRO Energy Centre in Newcastle, showing markers at different locations where eye protection might be recommended for 4-hour per day occupational viewing of the solar reactor. Green markers indicate no need for protection; red markers indicate a recommended Australian Standard Shade Number. Original image source: Google Earth.

CONCLUSION

We have introduced a new technique for rapid assessment of potentially hazardous bright reflections in CSP systems. Testing has shown that the technique is applicable to both simple and complex source profiles, making it well suited to hazard analysis for a range of different systems. The method is both more rigorous and very much faster than existing methods. The capability of our tool to handle variations in spectral composition make it particularly attractive as collector and receiver materials with different spectral reflectivities are used. The flexibility of the technique to provide rapid, accurate hazard analysis at any time and from any viewer perspective makes it a highly useful tool in the development and management of solar concentrator systems. Where required, the method could be applied using fixed digital video hardware, with on-board software for continuous, instantaneous monitoring of hazard conditions from key observer locations.

ACKNOWLEDGEMENTS

This research was conducted at CSIRO's National Solar Energy Centre in Newcastle, Australia, with funding through the Energy Transformed National Research Flagship.

DISCLAIMER

The calculated AS/NZS standard shades in Table 1 are preliminary, and provided for the purpose of academic discussion only. They also apply only to the sun as it was at the time of our measurement. Whilst all care has been taken to ensure these values correctly reflect the ICNIRP guidelines, the authors do not provide any guarantee that these eyewear shades will protect viewers observing the sun for the durations specified. Neither the authors nor CSIRO will accept any liability for injuries resulting from the use of these figures in the selection of eyewear for safe viewing of the sun.

REFERENCES

AS/NZS 1338.1:1992

Brumleve, T.D., SAND76-8022, Sandia National Laboratories, Livermore, CA (1977)

Brumleve, T.D., SAND83-8035, Sandia National Laboratories, Livermore, CA (1984)

ICNIRP, *Health Physics* **73**(3):539-553 (1997)

ICNIRP, *Health Physics* **87**(2):171-186 (2004)

Sliney, D.H. and Freasier, B.C., *Applied Optics* **12**(1):1-24 (1973)

Thomalla, E, Kopke, P, Muller, H and Quenzel, H, *Solar Energy* **30**(6):575-587 (1983)

BRIEF BIOGRAPHY OF PRESENTER

Dr Fell is a Principal Research Scientist with CSIRO, based at the National Solar Energy Centre in Newcastle. His 15 year research career includes technology

development for both the semiconductor and telecommunications industries and an important contribution to a photovoltaic device now in commercial production.

A Novel System for Combined Power Generation and Water Desalination Using Renewable Energy

Fulaqi Bai, Abhijit Date, Aliakbar Akbarzadeh

Energy Conservation and Renewable Energy Group, School of Aerospace, Mechanical and Manufacturing Engineering, POBox: 71, Bundoora East Campus, RMIT University, Bundoora, Victoria 3083

Email: s3205876@student.rmit.edu.au, abhijit.date@rmit.edu.au , aliakbar.akbarzadeh@rmit.edu.au

ABSTRACT

The twin challenges of energy and fresh water shortage can be addressed simultaneously by a novel thermodynamic system for electrical power generation and water desalination, using a renewable energy source. This novel system is named the combined water desalination and power generation (CDP) unit and features a reaction turbine with two convergent-divergent nozzles. The system converts salt water, heated by solar energy, into a mixture of vapour and brine by using a trilateral flashing cycle. The flashing process occurs in a vacuum chamber, which is maintained at a low temperature by an internal water-cooled condensing coil. The reactive force from the flow exiting the nozzles generates torque on the rotor arms, which in turn drive an electrical generator for power production. A series of test results including power generation, fresh water production and system efficiency is presented. Moreover, results are shown from an improved CDP unit, which features a novel disk reaction turbine with curved nozzle designed to achieve much higher rotor speed. The performances of these two units are studied and compared. In addition, the performance of a salinity gradient solar pond, an evacuated tube solar water heater and geothermal sources are discussed as possible renewable energy sources for a system of this kind.

Keywords: *CDP, Reaction Turbine, Trilateral Flashing Cycle, nozzle efficiency, Renewable Energy*

1. INTRODUCTION

Within most areas of Australia the supply of natural fresh water is inadequate to meet increasing demand for agricultural, industrial and domestic uses. There are numerous projects underway to supplement fresh water supply, for example via desalination of seawater. The commercially favoured Reverse Osmosis technology for fresh water production from saline water requires large amounts of electrical energy. However, electricity is presently being generated from predominantly non-renewable and polluting fossil fuels and its generation is largely centralised. As with water, the demand for electricity is increasing driving an expansion in electricity generation capacity, which has environmental consequences relating to climate change and resource depletion. Therefore, in this context, Combined Desalination and Power generation

(CDP) using a renewable energy source becomes a technology of great interest with potentially high value and wide application [1].

In the CDP system developed, saline groundwater is heated by solar collectors to a temperature of 80°C, and enters a chamber under vacuum, with its pressure maintained at a low level by an internal water-cooled heat exchanger. This hot brine flashes as it flows through a two-phase reaction turbine, featuring two convergent-divergent nozzles. The turbine is coupled to an electrical generator for power production.

As a result of the flashing process, a mixture of low-temperature concentrated brine and water vapor is produced. The vapor is condensed on the heat exchanger cooling coils to form fresh water which is collected. While the liquid component of the mixture leaving the nozzles falls onto the bottom of the tank as more concentrated brine. The concentrated brine is collected, and reheated as a second stage of the same process, or used as the input to a salt production process. The flashing of hot water and the partial phase change causes a substantial increase in the specific volume of the two phase fluid in the nozzles, as a result of which a high-velocity jet is produced at the nozzle outlet. The reaction force from this jet drives the rotor and hence the generator to produce electrical power. The process described is illustrated in Fig. 1.

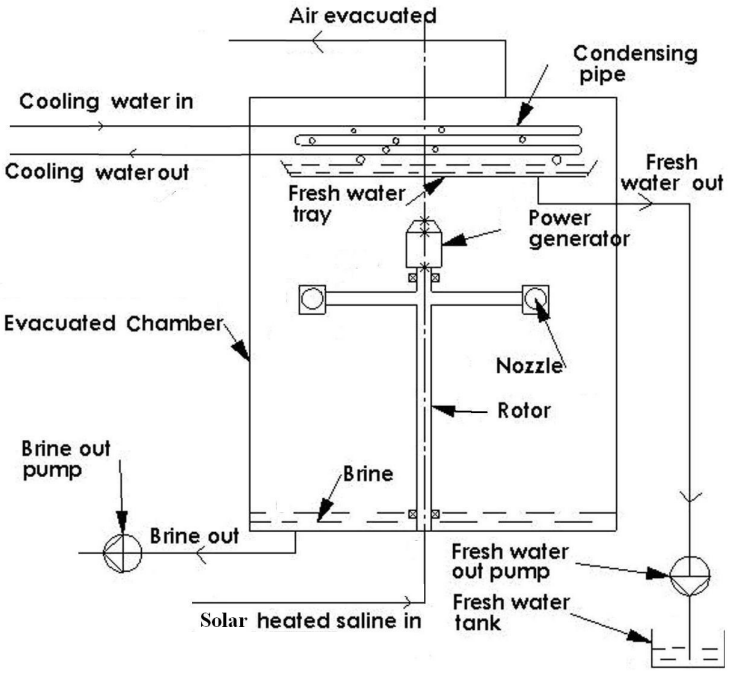

Fig. 1: Working Principle of a CDP unit

2. THE THERMODYNAMICS OF THE CDP UNIT

The CDP system is ideally a reversible single-stage water desalination system, whose thermodynamic process (T-S diagram) is shown in Fig. 2. Salt water, at atmospheric pressure and ambient temperature (point 1), goes through a solar heating system (process 1-2) and attains a higher temperature, T_2, but slightly lower pressure because of the pressure loss in the heater. The heated brine is introduced via the turbine into a vacuum chamber whose temperature, Tc (condenser temperature), is maintained lower

than T_2 through a water cooled heat exchanger. Introduction of the hot water into a cooler and lower pressure environment causes flashing, which results in a mixture of water vapor and brine. Whilst the enthalpy of the mixture is conserved its entropy is increased, as shown in process 2-3a. During this process the water temperature drops to Tc, which depends on temperature of the cooling water flowing through the condensing coil. The process 1-2-3a is a typical process of single stage water desalination. It basically uses the sensible heat available in hot salt water for the phase change needed for production of water vapor and from it fresh water. However, if power is extracted by the turbine, the working fluid enthalpy will fall. This power generation will be maximised when the expansion follows the path 2-3b that is isentropic process. The actual process is between 2-3a and 2-3b[2].

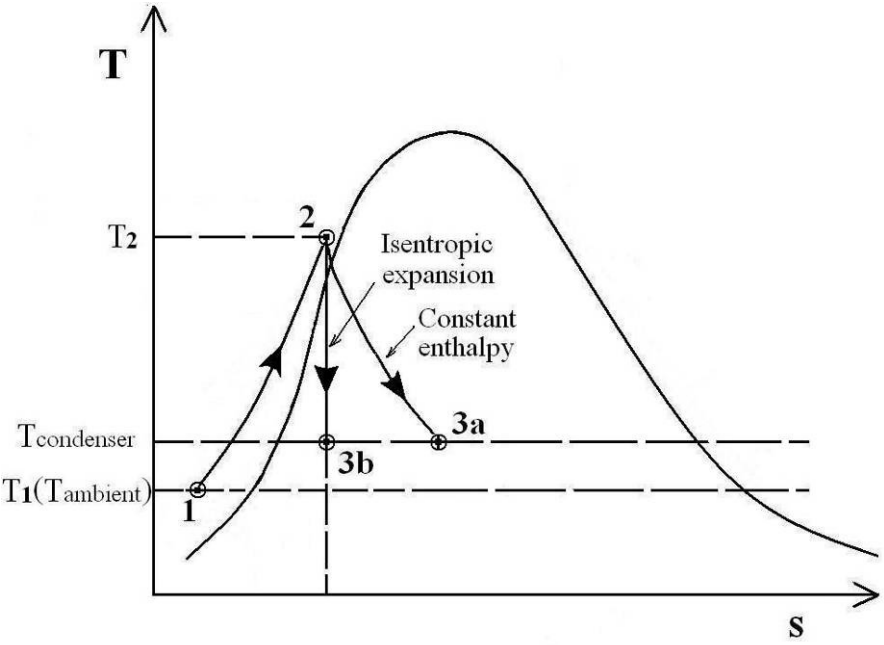

Fig. 2: The thermodynamic process of CDP unit

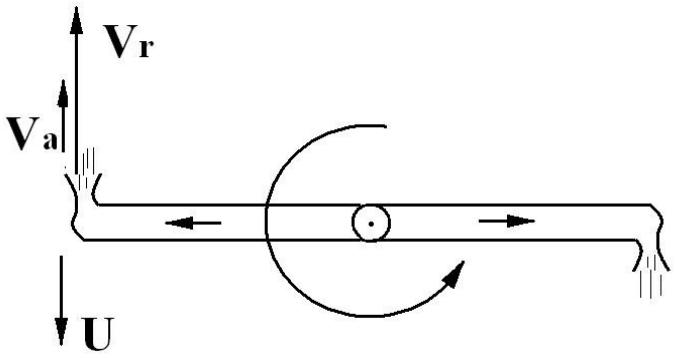

Fig. 3: Velocity diagram of the turbine rotor

As illustrated in Fig. 3, the high velocity jets at the nozzle exit exert a reaction force on the nozzle, which creates torque to rotate the turbine. In order to maximize the turbine efficiency, the absolute velocity of the mixture leaving the nozzles with respect to the

chamber, Va, should be as low as possible. This means that the tangential speed, U, of the nozzles should be as close as possible to the relative velocity of the mixture with respect to the nozzle outlets, Vr. At the same time, the output power increases as the relative velocity increases, consequently as rotor speed increases the opportunity increases for combining high turbine power output and high efficiency.

3. INSTALLATION OF THE NOVEL DISK TURBINE ROTOR

A new turbine has been made and installed in the CDP unit, which features a novel design of rotating reaction nozzles. The rotor of this novel turbine has superior mechanical design enabling it to run at substantially higher speeds.

Fig. 4: Novel disk reaction turbine rotor

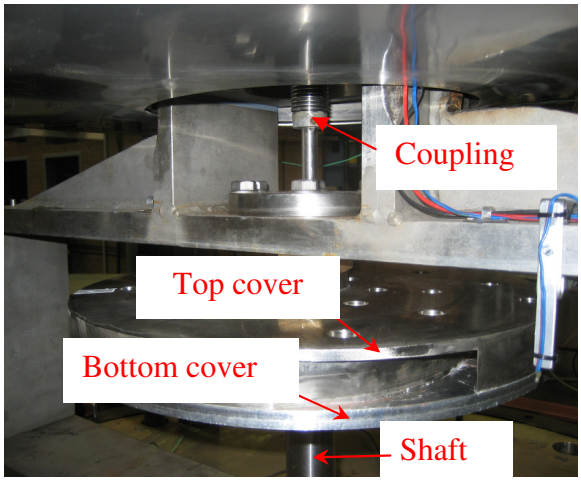

Fig. 5: Disk turbine in the CDP unit

There are two significant advantages over the previous reaction turbine arrangement, which is explained in details in the previous paper [3]. Firstly, the separation forces (acting laterally to stream wise directions in the nozzles) can be dramatically reduced, which is achieved by proprietary curving of the nozzles, as shown in Fig. 4. As a result of that, the slip loss will be greatly reduced. Secondly, the new design is expected to have a drastic reduction in abruptness of the flashing process. For the earlier turbine, passing pressurised water, with a large amount of centrifugal force, through very short convergent-divergent nozzles causes delay of flashing followed by explosive flashing. Such flashing is inefficient in terms of nozzle reaction forces. In contrast, the novel design effectively avoids the abrupt flashing for the following reasons. First of all, the new nozzles start much closer to the centre of the rotor. This minimises the centrifugal pumping effect due to rotation of the nozzles, which means that the pressure at the nozzle entry is almost the same as the saturation pressure of 85ºC water. In addition, the cross-section of the nozzles changes gradually along the nozzle flow path, which results in much more gradual de-pressurisation and flashing [4]. Fig. 5 shows the installation of the novel disk turbine to the CDP unit.

4. TEST RESULTS AND ANALYSIS

4.1 Simple reaction turbine

The CDP unit has been tested under various electrical loads, with resistance varying from 80 Ω to 250 Ω, in order to find out the optimal load condition which results in maximum power generation as shown in Fig. 6. It is found that the electrical power peaks at 440 W, when the load is at 100 Ω. This is probably due to the fact that the corresponding rotor speed, about 2350 RPM, is very close to the rated speed of the generator. In addition, based on the performance curves at each load, it is clear that the electrical power produced is directly proportional to the rotor speed [3].

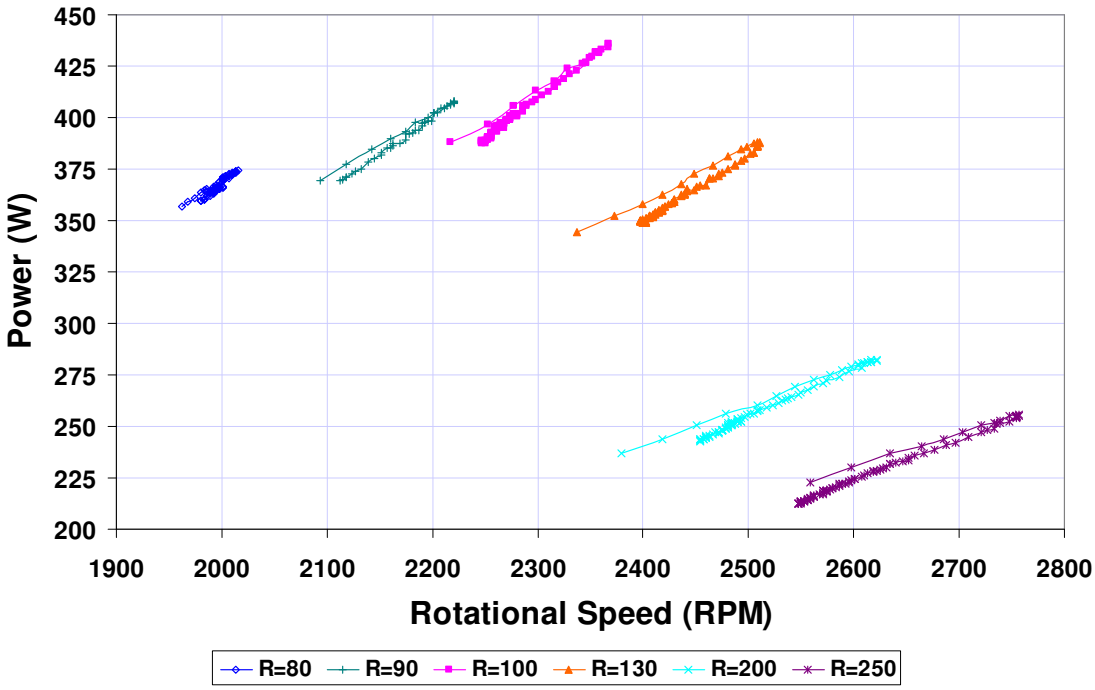

Fig. 6: Power generation vs rotor speed at various loads

In addition, nozzle (isentropic) efficiency, η_{isc}, is calculated for each data point, and plotted as a function of rotor speed, as shown in Fig. 7.

$$\eta_{isc} = \frac{\dot{W}_{act}}{\dot{W}_{isc}} = \frac{\dot{W}_{act}}{\dot{m}\,\Delta h_{isc}\eta_{mech}\eta_{gen}}$$

(Note: For mechanical efficiency, $\eta_{mech} \approx 0.8$ and for DC generator efficiency $\eta_{gen} \approx 0.85$)

Where, $\dot{W}_{isc}$ is defined as the theoretical electrical power the CDP unit would produce, if the hot water had gone through isentropic expansion process along the turbine nozzle.

That means, Δh_{isc} represents the enthalpy drop during an isentropic process, which is also the maximum possible enthalpy drop at the given temperature drop.

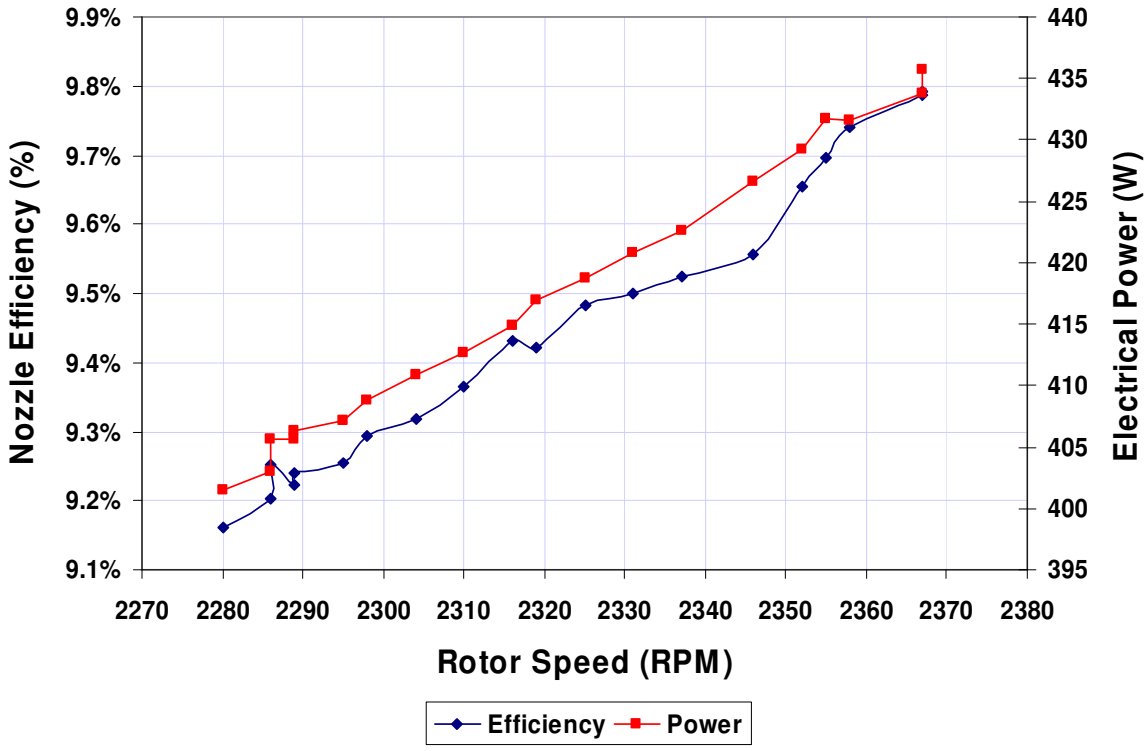

Fig. 7: Nozzle efficiency vs Rotor Speed

For testing conducted at the load resistance of 100 Ω, some data points have been selected when the unit is running at the steady state, and used to plot the efficiency curves. It shows in figure 7 that 9 % to 10 % can be achieved at the given operating condition. As with thermal efficiency, isentropic nozzle efficiency increases as the rotor speed, and shares a similar trend with the power generation graph.

4.2 Novel disk reaction turbine

Fig. 8 depicts a graph of rotor speed against time elapsed during one of the tests. It shows that disk rotor is initially left running freely in order to better accelerate up to a desired high speed. From then on, an electrical load of 250 Ω is connected to the unit so that electrical power starts to be produced. The graph clearly illustrates that the rotor maintains at a fairly steady speed, about 4000 RPM for a reasonable amount of time, about 200 seconds, before gradually slowing down.

It shows that compared with the previous turbine prototype, a relatively high rotational speed is achievable.

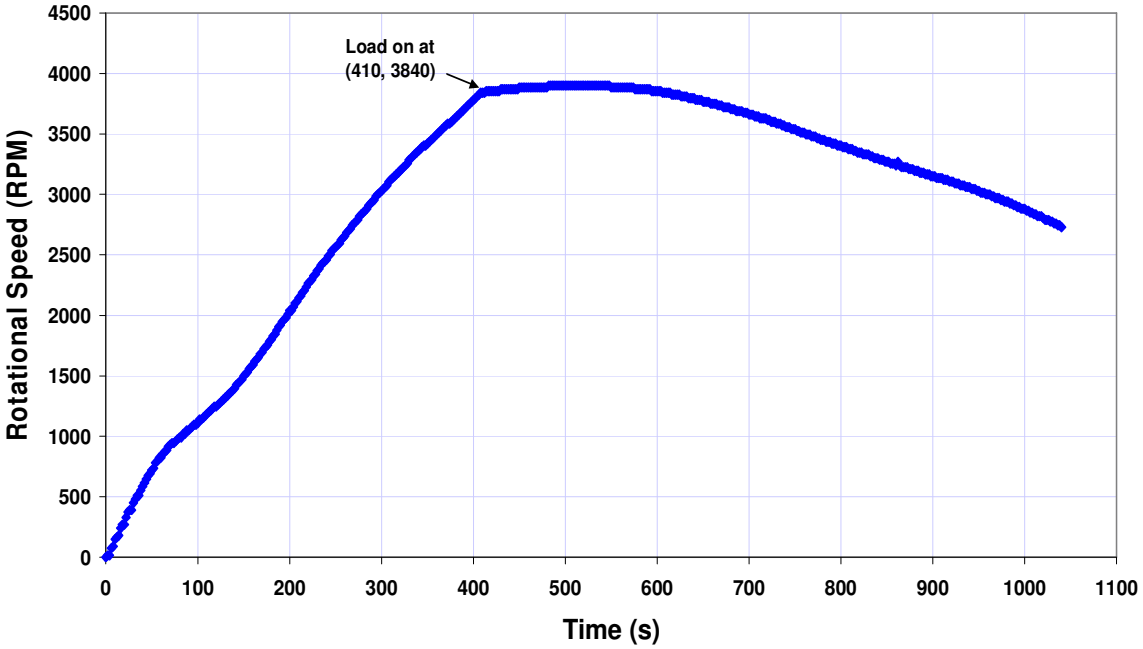

Fig. 8: Rotor Speed

Two digital flow meters have been installed to record the fresh water and brine water flow rate, and the sum of these two indicates the feed hot water flow rate. This is displayed in Fig. 9, which illustrates that the recovery rate of the system is about 12 – 15 %.

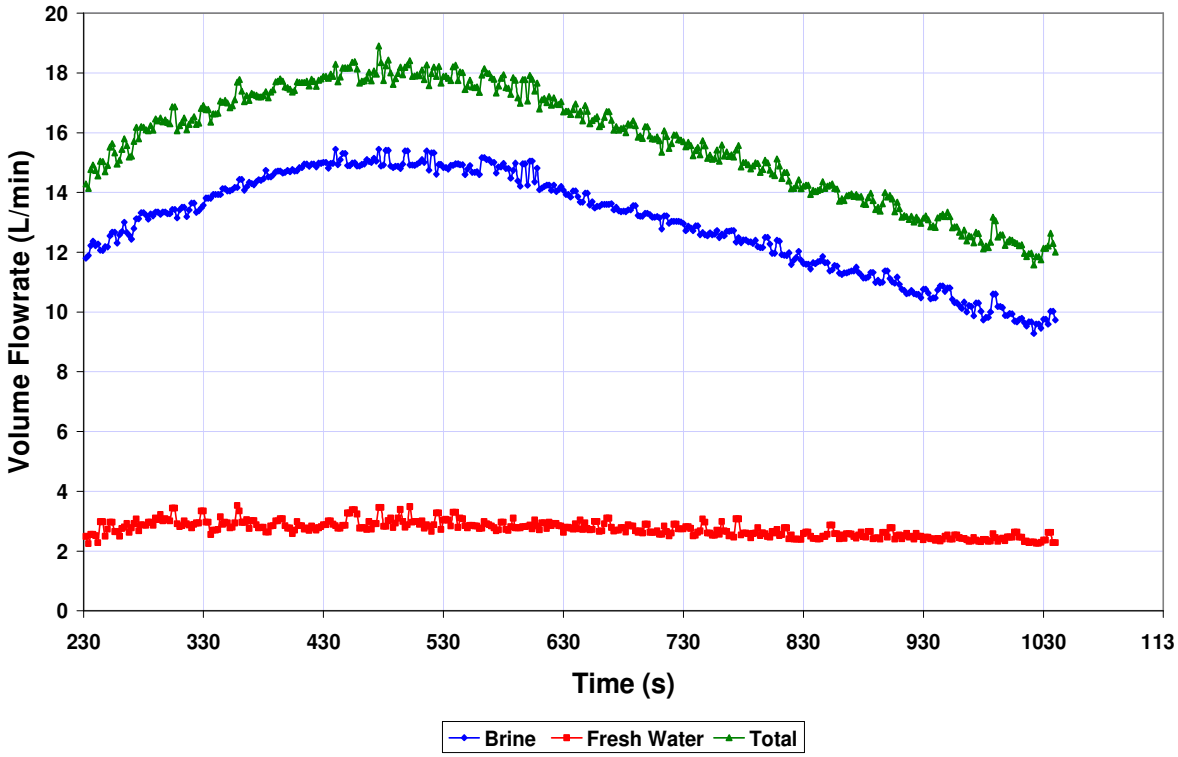

Fig. 9: Volume Flow rate

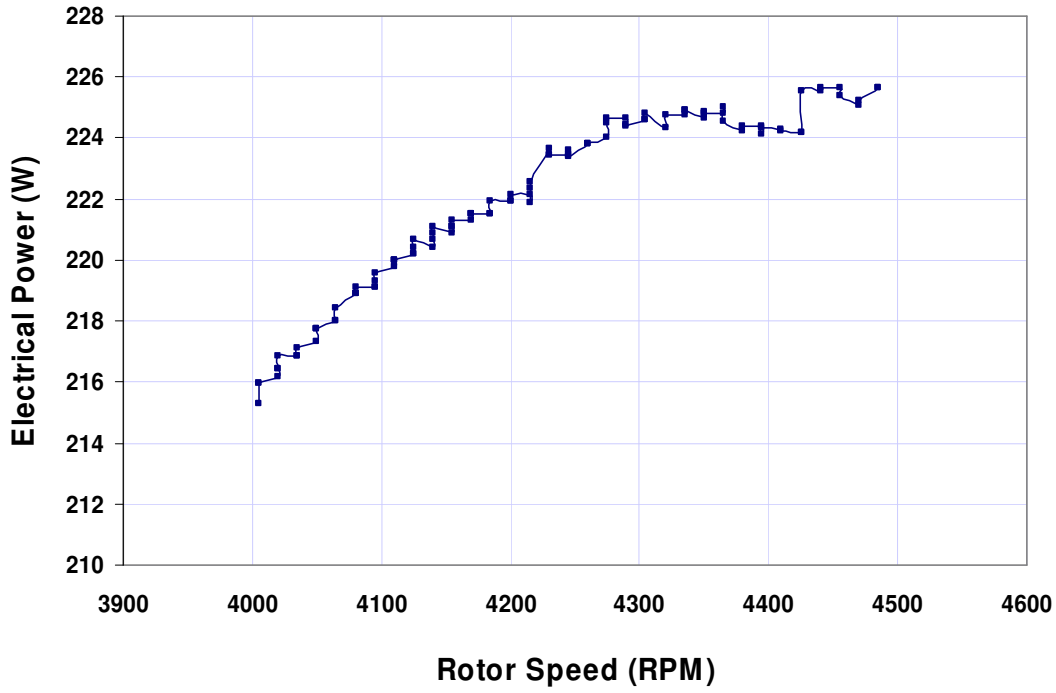

Fig. 10: Power generation v/s Rotor Speed

For power generation, an electrical load with resistance of 250 Ω was connected to the unit, which was running at 4500 RPM. As can be seen Fig. 10, after experiencing some abruptness at first, the rotor speed maintains at a steady level for a reasonable amount of time, during which time a peak power of 225 W has been produced, before it descends with a decreasing rotor speed. This indicates that the turbine rotor slows down, presumably due to the load connected to it. This raises the issue of proper electrical load selection which will be solved through more experimental testing in the near future.

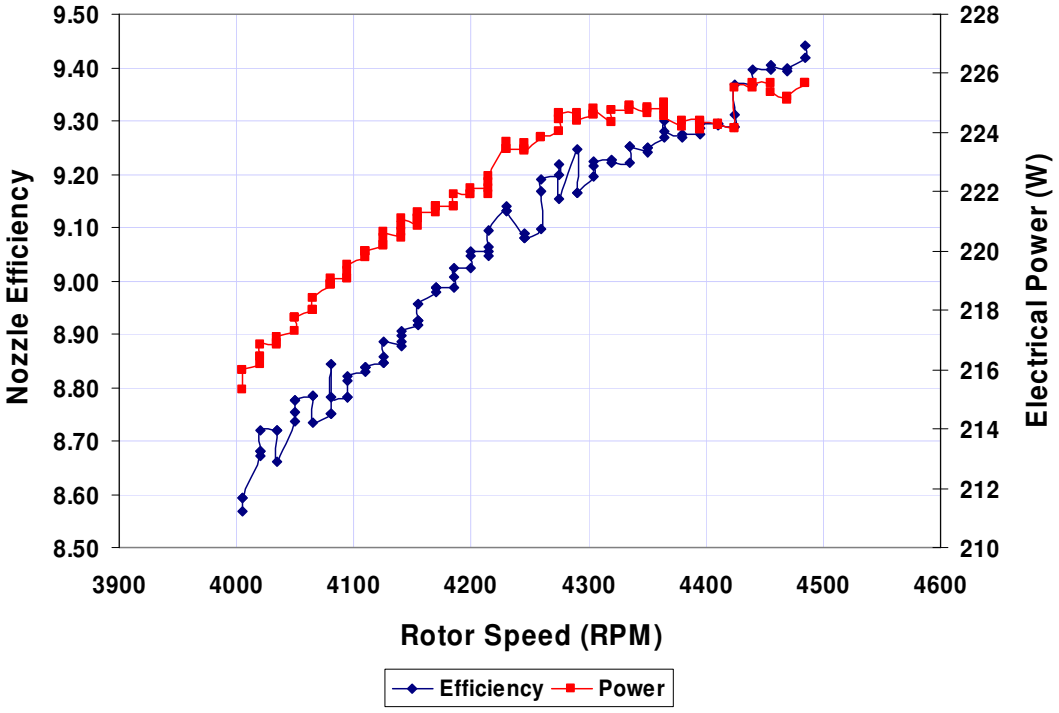

Fig. 11: Nozzle efficiency v/s Rotor Speed

Again, a curve of nozzle efficiency, in Fig. 11, has been produced to compare with the previous unit. It shows a similar trend as before, which explains how important a high rotor speed, and thus high power generation, is to the CDP unit performance, as the nozzle efficiency greatly depends on these two parameters.

5. FUTURE WORK

A new project, funded by the Australian Research Council (ARC), Greenearth Energy Ltd and RMIT University, known as a dual geothermal system for fresh water production and power generation', has been successfully launched. The primary aim of this project is to develop an efficient dual geothermal system to simultaneously produce electrical power and fresh water (See Fig. 12 for the basic concept). Naturally occurring hot saline water with temperatures between 90 °C and 150 °C, available from geothermal reservoirs at depths between 2,000 m and 4,000 m [5], will be utilised and introduced to the Combined Desalination and Power Generation (CDP) unit.

By taking 2000 L, or nominally 2000 kg, of hot saline water at a temperature of 150 °C, this dual geothermal system has the potential for producing 15 kWh of electricity as well as 400 L of fresh water, which are of the same order as the average energy and fresh water consumption of a standard household per day.

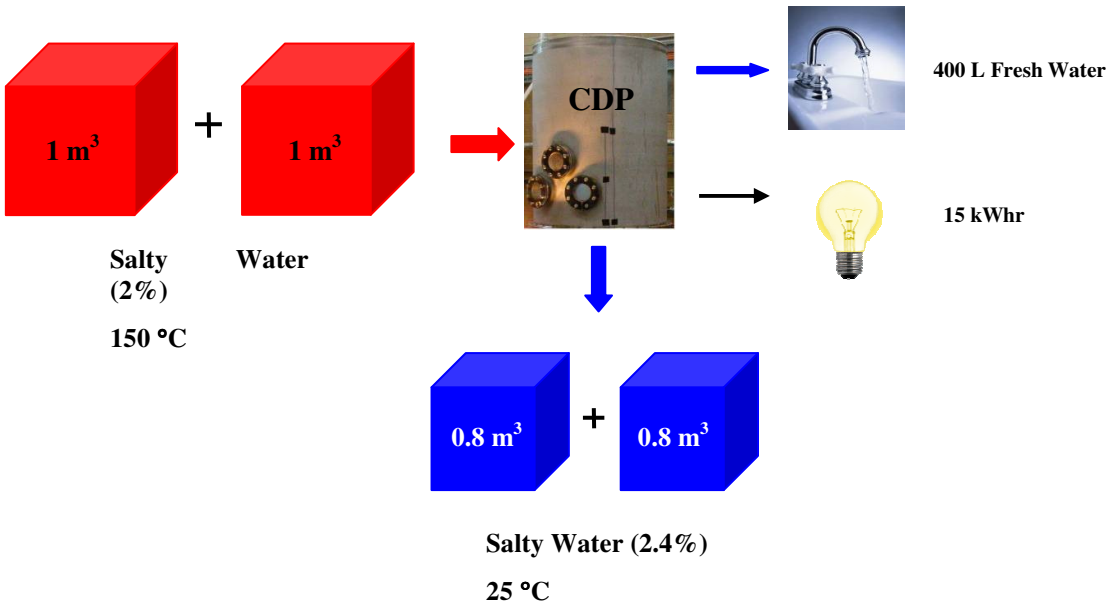

Fig. 12: Schematic explaining the novel dual system

6. CONCLUSION

The testing results and analysis have demonstrated that the prototype CDP unit is capable of producing electrical power in a range of 100 to 500 W, as well as fresh water at a rate of approximately 2 litres / min and recovery rate of about 15 %.

Although the CDP unit installed with a disk turbine rotor is able to operate at a much higher speed and therefore can produce a higher voltage, compared to the simple reaction turbine unit, in the preliminary tests, less power was generated. This is ascribed principally to the load restriction for the new unit, since an electrical load with too little resistance, such as 100 Ω, will be too much of a load to the heavy disk rotor which can drastically drags the its speed down. That also means that, maintaining the rotor at a high speed while producing electricity at a steady state has become an important task to be addressed for this new CDP unit.

In addition, it is promising to find that the nozzle efficiency of 8.5 % to 9.5 % remained similar despite less power generation, and only decreased by about 0.5 %, compared with the efficiency for previous unit. Also a lower feed hot water flow rate was achieved in the later prototype because of less centrifugal pumping effect, which also indicates potential for a better fresh water production rate.

Last but not least, a dual geothermal project for fresh water and power production is underway, which will utilize the hydrothermal resource as the input to the CDP unit.

7. REFERENCES

1. Zhao, Y., A. Akbarzadeh, and J. Andrews, *Simultaneous desalination and power generation using solar energy.* Renewable Energy, 2009. **34**(2): p. 401-408.
2. Smith, I.K., *DEVELOPMENT OF THE TRILATERAL FLASH CYCLE SYSTEM .1. FUNDAMENTAL CONSIDERATIONS - REPLY.* Proceedings of the Institution of Mechanical Engineers Part a-Journal of Power and Energy, 1994. **208**(A2): p. 154-154.
3. Bai, F., R. Sing, and A. Akbarzadeh, *A Novel System Of Combined Power Generation And Water Desalination Using Solar Energy*, in *Solar09, the 47th ANZSES Annual Conference*. 2009: Townsville.
4. Fabris, G., *Two-phase reaction turbine. Technical progress report for the period January-May 1999*, in *Other Information: PBD: 31 May 1999*. 1999. p. Medium: P; Size: vp.
5. DiPippo, R., *Geothermal Power Plants*. 2 ed. 2007, Oxford: Butterworth-Heinemann. 520.

BRIEF BIOGRAPHY OF PRESENTER

Fulaqi Bai is a postgraduate research student in the School of Aerospace Mechanical and Manufacturing Engineering. After completing the Bachelor Degree in Mechanical Engineering from the University of Melbourne in 2007, Mr Bai joined the Energy CARE Group in RMIT, and has been doing research study under the guidance of Professor Aliakbar Akbarzadeh. His research project involves power generation and water desalination using renewable energy sources, and two phase flow concepts.

Aliakbar Akbarzadeh is a professor in the mechanical engineering department and leader of the Energy Conservation and Renewable Energy Research (CARE) Group in the RMIT University (Melbourne, Australia) which he joined in 1986. Prof. Akbarzadeh is actively involved in various projects related to energy conservation technologies, renewable energy (wind and solar), heat pipes and production of power from low grade sources. He is the author/co-author of more than 75 scientific papers and two books concerned with his research and developments in the field of Energy Conservation and Renewable Energy.

Abhijit Date is a post doctorate research fellow in the School of Aerospace Mechanical and Manufacturing Engineering. His research involves work in the renewable energy field including hydro-electricity turbines, concentrated solar PV and solar thermal systems, solar desalination, low temperature heat engines, geothermal desalination and power generation and solar chimneys. His current focus is in the field of geothermal desalination and power generation technology, supported by an ARC linkage grant and includes the development of a dual geothermal system for desalination and power generation. This system will operate on thermodynamic trilateral cycle and will use a two-phase reaction turbine.

Understanding the Performance of Organic Photovoltaic Mini-modules

Christopher J. Fell[1,2], Timothy J. Nagle[1], Lynn J. Rozanski[1] and Krishna Feron[1,2]
[1]CSIRO Energy Technology, 10 Murray Dwyer Cct, Mayfield West, NSW 2304
[2]Centre for Organic Electronics, University of Newcastle, Callaghan, NSW 2308
Ph: 02 4960 6032 Email: chris.fell@csiro.au

ABSTRACT

Organic solar cells are considered an option for the long term future of photovoltaics, due to the potential for rapid, low cost manufacturing, low embodied energy and avoiding the depletion of scarce mineral resources. Successful implementation of this technology requires optimisation of both the multi-layered *axial* device structure and the monolithic *lateral* structure, including understanding the role of cell size and shape, interconnect regions, and series resistance of the contact layers. Although ultimately intended for a high-speed, roll-to-roll production process akin to printing, organic solar cells are often prepared by spin-coating on glass substrates, as this reduces the number of variables in the fabrication and encapsulation processes. Using information gathered from well-controlled experiments with small test cells, we take a systematic approach to understanding lateral device design, allowing us to accurately predict the performance of larger, multi-cell devices. This understanding has been used to prepare 10cm × 10cm mini-modules for demonstration and outdoor evaluation.

Keywords – modules, organic, photovoltaics, resistance, scale

INTRODUCTION

The discovery of organic semiconductors in the 1970s enabled the possibility of solution-processable photovoltaic materials, spawning research interest in printable solar cells that has continued to grow exponentially over the past decade. The subject has been reviewed extensively, for example, in the context of historical development (Spanggaard and Krebs, 2004), device structure (Steim *et al*., 2010), materials chemistry (Delgado *et al*., 2010), device physics (Pivrikas *et al*., 2007), and potential manufacturing costs (Kalowekamo and Baker, 2009). The most promising organic photovoltaic (OPV) design at present is based on the concept of a bulk heterojunction, involving a finely mixed blend that includes an electron donor and an electron acceptor material. With suitably chosen bandgaps and band edge energies for the donor and acceptor, photogenerated electron-hole pairs are efficiently isolated into the two material phases, with selective charge transport driven by concentration gradients and the difference in work function for the two electrodes.

Whilst significant research is underway worldwide to improve the efficiency and durability of laboratory-scale OPV devices (typically < 5mm × 5mm in size), the open literature contains little on the effects that limit performance when devices are fabricated at practical dimensions. Exceptions include Choi *et al.*, 2009, Servaites *et al.*, 2010 and Park *et al.*, 2010. The study presented here examines the role of two key factors that must be considered if the performance of larger devices is to be properly understood; electrode series resistance and device edge effects.

EXPERIMENTAL

Preparation of test devices

All devices for this study were fabricated using the common axial architecture comprising: glass/ITO/PEDOT:PSS/P3HT:PCBM/Al. The components of this structure are described in the following: Glass substrates with a pre-patterned layer of indium tin oxide (ITO), were sonicated at 85°C in a detergent solution, then again sequentially at room temperature in millipure water, acetone and isopropanol before being treated for 30 minutes in an air plasma. The anodic buffer layer was spin cast from a solution containing poly(3,4-ethylenedioxythiophene:poly(styrene sulfonate) (PEDOT:PSS) before being baked in a dry environment for 10 minutes at 140°C to form a 45nm thick film. All further sample preparation occurred under inert conditions in a glovebox. The donor material, regio-regular poly(3-hexylthiophene) (P3HT) and the acceptor material, [6,6]-phenyl-C_{61}-butyric acid methyl ester (PCBM) were mixed in a 1:1 weight ratio from two solutions, each at 10mg/ml in chlorobenzene. The solution was stirred for two hours, then filtered with a 0.2µm filter, before being spin-cast to form the active layer. The samples were then heated for 30 minutes at 120°C to anneal the bulk heterojunction. Finally, a cathode layer 100nm thick was deposited by evaporating aluminium through a shadow mask, producing the desired electrode pattern.

Series resistance

In order to examine the effect of electrode series resistance, R_s, a test cell configuration was designed such that four otherwise identical devices incorporated different path lengths through the ITO anode layer. The four cells were equally spaced, as shown in Figure 1. A Keithley 2400 Sourcemeter was used to obtain current-voltage curves for the four cells on each substrate in the dark. The series resistance for each cell was obtained by fitting the curves to the 1-parameter diode equation. The measurement was repeated for nine substrates, each with a different thicknesses for the active layer, ranging from 25nm to 310nm.

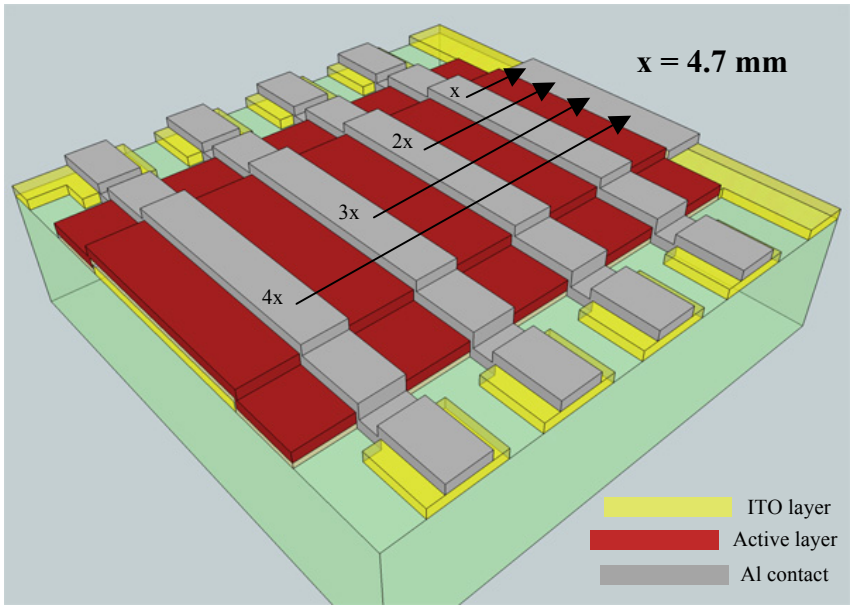

Fig. 1: OPV test cell configuration showing 2mm × 10mm cells at linearly increasing distance from an anode contact. The path length through the ITO (bottom) layer is the only difference between the cells.

The measured series resistance values for the nine devices are plotted in Figure 2, each clearly showing a linear relationship between R_s and the path length through the ITO layer. A linear least squares fit was used to extract the slopes and intercept values for the four cells on each substrate. Since the ITO layer was identical on each substrate, the nine slopes were averaged to determine a value of 8.67Ω for the incremental increase in R_s between cells. The average distance between the centres of adjacent cells was measured using a microscope to be 4.7mm, from which we extract an incremental R_s of 1.84Ωmm^{-1}. The width of the ITO track was 10mm, hence a value of 18.4Ω/□ was estimated for the sheet resistance of the ITO layer. The material was specified as nominally 15Ω/□, however a careful measurement of the sheet resistance using a four-point probe on a larger sample gave a value of 17.7Ω/□, in reasonable agreement with the value estimated from the current-voltage curves.

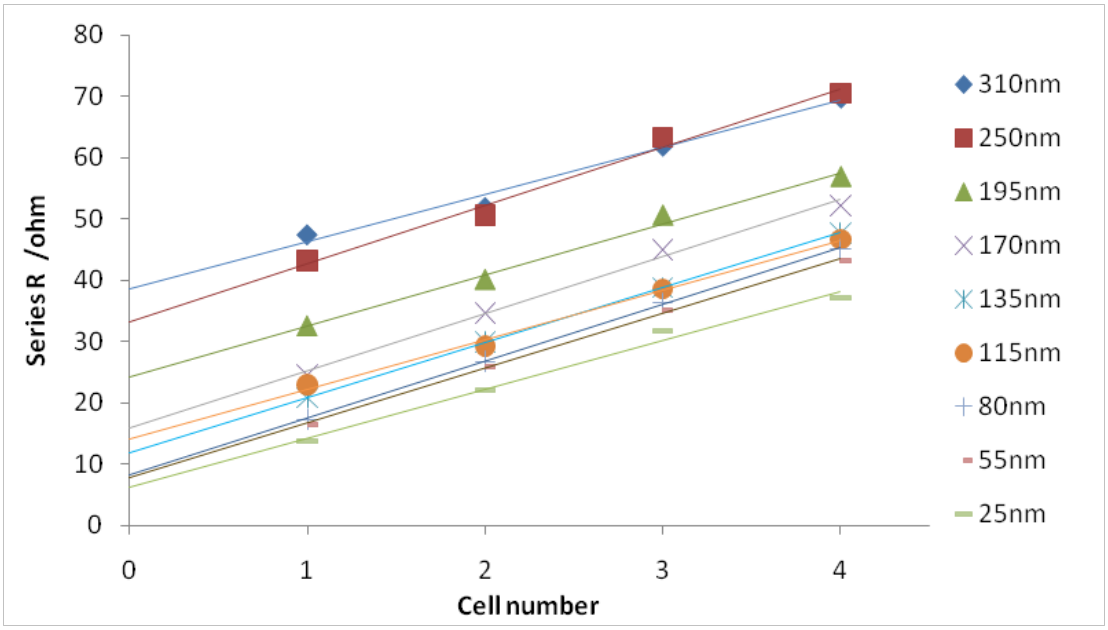

Fig. 2: Series resistance, R_s, obtained from dark current-voltage data for four test cells on each of nine substrates. The thickness of the OPV active layer is different for each substrate, as indicated in the legend.

The *y*-intercepts from the fits in Figure 2 indicate the contribution to the total R_s due to effects other than the ITO electrode. These contributions could include lateral transport through the metal cathode layer and/or axial transport through each of the layers in the device. When plotted against the thickness of the active layer for the nine samples, these values exhibit an approximately linear relationship, as can be seen in Figure 3. A linear least squares fit to the values in Figure 3 results in an intercept close to the origin (R_s = -0.3Ω) indicating that the only significant contribution to the remaining R_s is the series resistance of the active layer itself. The slope of this fit allows calculation of a specific series resistance for our bulk heterojunction active layer of 0.0244 Ωcm^{2}nm^{-1}, which is consistent with literature values for similar materials (Sievers *et al.*, 2006). These results indicate that for the common axial device structure glass/ITO/PEDOT:PSS/P3HT:PCBM/Al, the only components contributing significantly to the series resistance are the active layer (P3HT:PCBM) and the ITO layer. Hence, a relatively simple calculation is all that is needed to predict R_s for an arbitrary lateral device design.

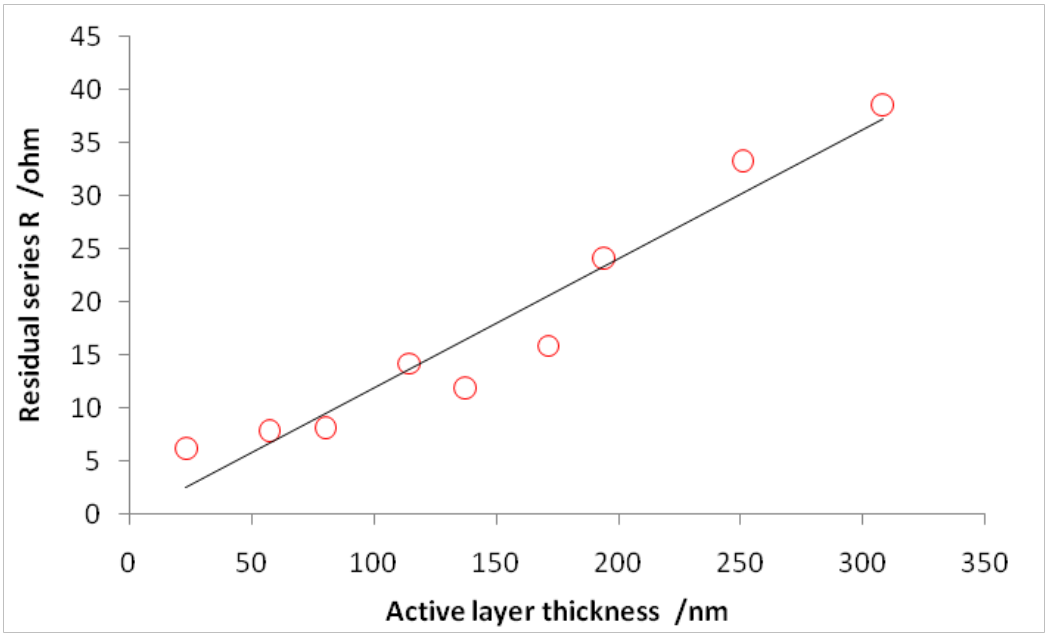

Fig. 3: Residual R_s, obtained from the y-intercept values of linear fits to the data in Figure 2. The proportional relationship with active layer thickness indicates no further significant contribution to R_s from other layers in the device.

Edge effects

Although in principle a photocurrent should be proportional to the area of a device, when extrapolating current density measurements between small and large devices it is useful to understand the enhancement of photocurrent that can result from effects occurring at the cell edge. These effects include light scattering into the cell from outside the active area, as well as collection of charges generated close to, but outside the active area. In order to study this effect, a second test cell configuration was designed as shown in Figure 4.

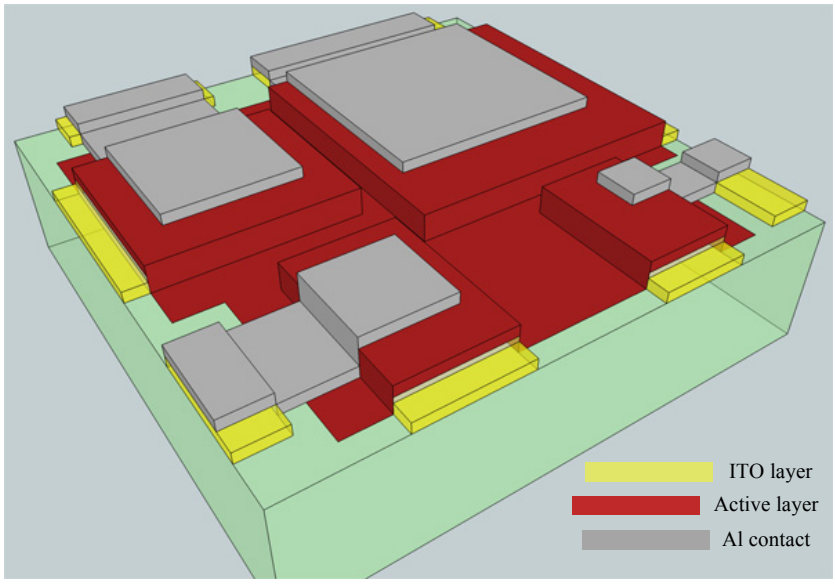

Fig. 4: OPV test cell configuration for studying the effect of cell edges on current density. Cell sizes (mm) are 2×2, 4×4, 6×6 and 10×10.

The test cell configuration shown in Figure 4 contains square cells at four different sizes; 2mm × 2mm, 4mm × 4mm, 6mm × 6mm, and 10mm × 10mm. Current-voltage curves for these cells were obtained at an irradiance of 1 sun, using a solar simulator rated at IEC60904 Class A. Cells were not masked during the measurement, meaning that the entire substrate was illuminated. Fits to the 1-parameter diode equation were used to extract values for the short-circuit current, I_{sc} for each cell. These values were divided by the cell area to calculate the short-circuit current density, J_{sc}. Values for J_{sc} are plotted against cell area in Figure 5.

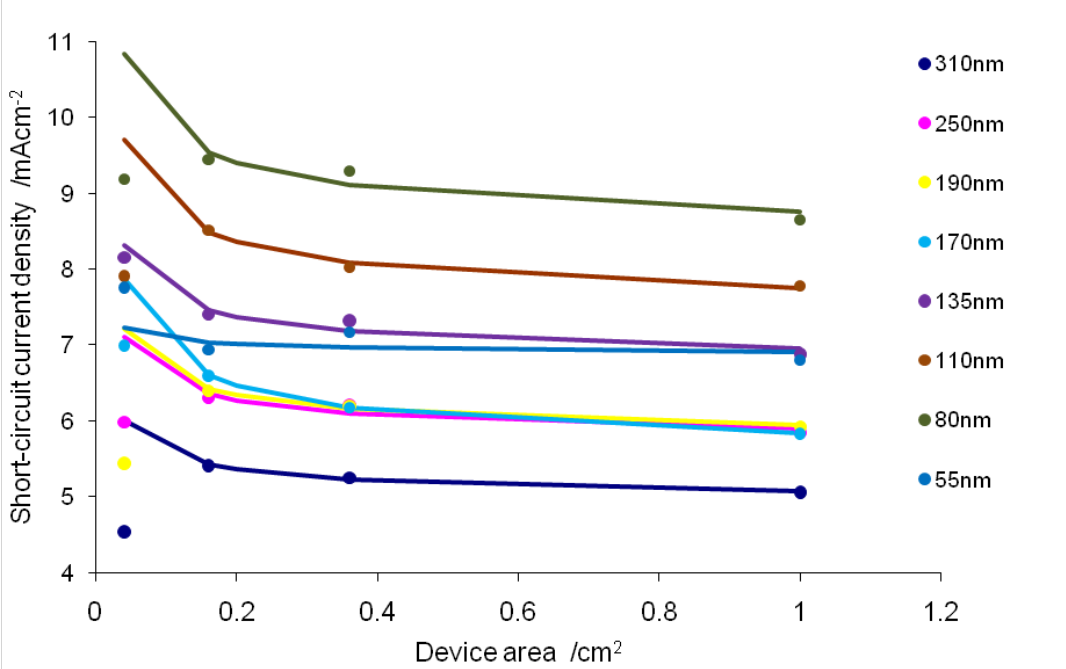

Fig. 5: Short-circuit current density, J_{sc}, for each of four test cells on nine substrates with different active layer thickness. The solid lines are least-squares fits to Equation 1.

The magnitude of the current enhancement at the cell edges can be quantified by assuming the J_{sc} values are influenced by an additional component that scales with the ratio of the cell perimeter length to the cell area. Since the test cells are all square, the perimeter-to-area ratio can be represented by the term $4\sqrt{A}/A$, where A is the cell area. We propose the following simple empirical form for the area-dependence of J_{sc}, where $J_{sc}^{edgefree}$ represents the short-circuit current density that would be observed in the absence of edge effects:

$$J_{sc} = k\frac{4\sqrt{A}}{A} + J_{sc}^{edgefree} \qquad \text{Equation 1}$$

The solid lines in Figure 5 are least-squares fits to the measured J_{sc} values in the form of Equation 1. The fits are poor for the very small devices (A = 0.04cm^2). A possible reason for this may be interactions between edge effects on opposite sides of the device. Fits for the larger three cells are reasonable however, permitting extraction of a single value for $J_{sc}^{edgefree}$ for each active layer thickness. This value is important as an input parameter for estimating the performance of larger OPV devices and modules.**

**A reader studying Figure 5 carefully may notice that $J_{sc}^{edgefree}$ does not scale intuitively with the thickness of the active layer. This is due to the role of optical interference effects, which significantly impacts the relationship between film thickness and absorption in the active layer.

The parameter, k, represents the contribution to edge-related cell current, per unit of perimeter length. Due to the difference in current density for the different film thicknesses, a different value of k was used to produce each of the nine fits in Figure 5, however when normalised to the value of $J_{sc}^{edgefree}$ the resulting values are all very similar, at around $k/J_{sc}^{edgefree} = 0.015\text{cm}^{-1}$. This is evidence that the data does indeed fit the form of Equation 1 and that the additional current density observed for small devices is due to edge effects.

PREDICTING PERFORMANCE OF MINI-MODULES

The lessons learned from the above two experiments have allowed the development of an empirical model for predicting the performance of an arbitrary lateral OPV device design, on the basis of results from small test cells. The details of the model will be discussed elsewhere (Fell *et al*. 2010). We have applied the model to predict the efficiency for OPV mini-modules containing a varying number of cells, monolithically interconnected in series at the longer edge. An example of one such mini-module is shown in Figure 6.

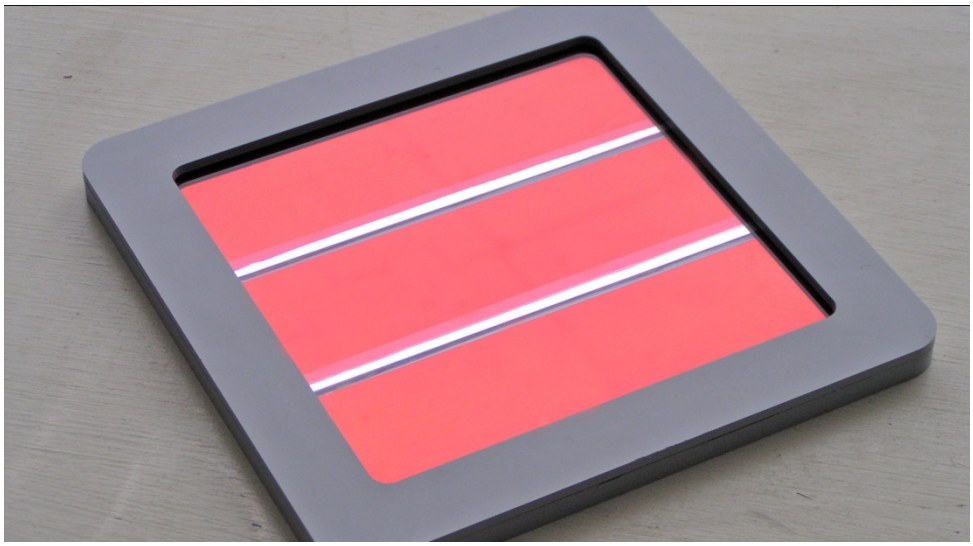

Fig. 6: Mini-module (10cm × 10cm) containing three organic photovoltaic cells, monolithically interconnected in series. The two external contacts are on the reverse side of the module.

Selected results of the model calculation are shown in Figure 7, which shows data sets for four possible design variations, based on the use of an ITO layer with sheet resistance of either 17.7Ω/□ or 5.0Ω/□, and a width for the (inactive) interconnect zone between cells of either 2mm or 6mm. The calculations assume the true area of the substrate (100cm^2) for the determination of efficiency, even though the aperture area of each mini-module is 70.5cm^2 and the active area exposed to sunlight is smaller still. The latter varies, depending on the width of the interconnect zones between the cells. From Figure 7 it can be seen that the module efficiency is optimised at a specific number of cells, and that the optimum number of cells varies, depending on the series resistance of the ITO contact layer and the amount of area lost to interconnects. The interconnect regions are described as “gaps” in the figure legend.

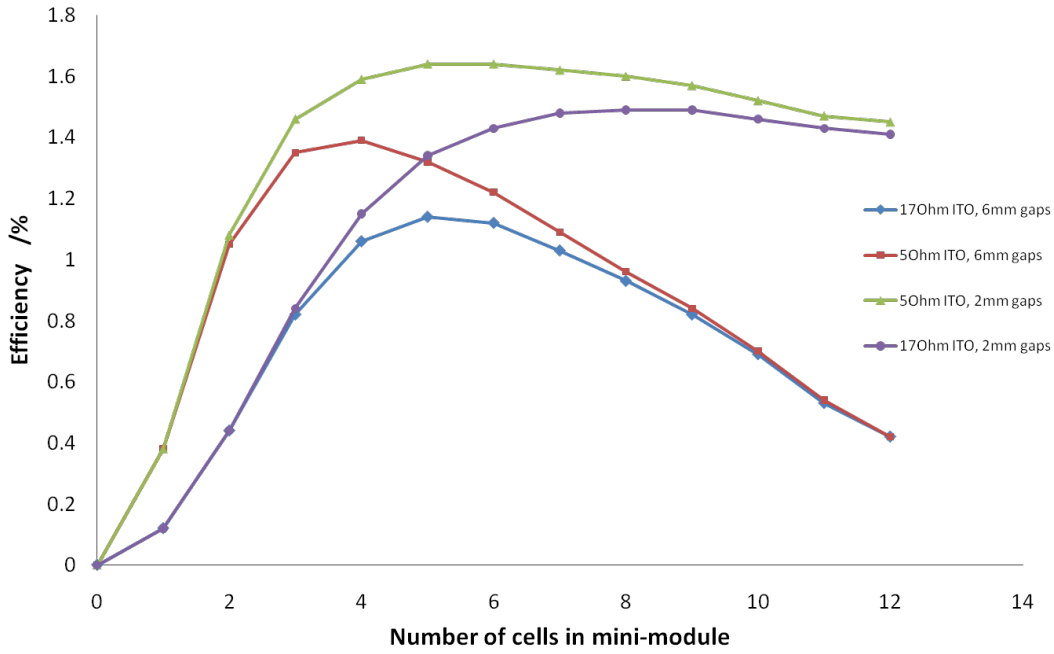

Fig. 7: Selected results of a model for predicting the efficiency of an OPV mini-module based on monolithically interconnected cells. The model uses input parameters taken from current-voltage measurements on small cells.

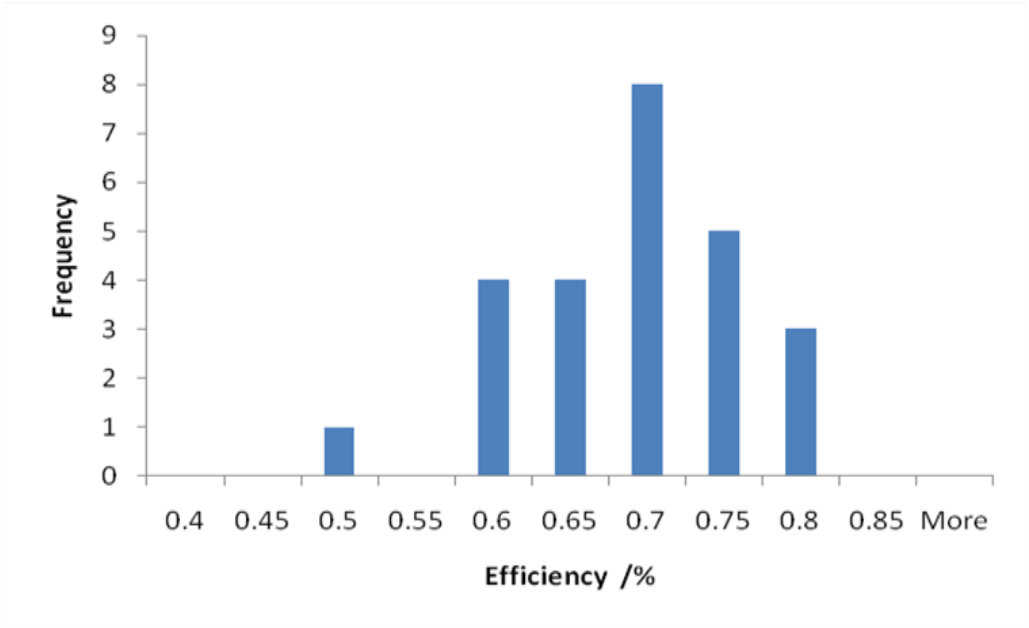

Fig. 8: Histogram showing measured efficiency for 20 OPV mini-modules. The maximum value of 0.8% is in agreement with the model results shown in Figure 6 for a three-cell module with a 17.7Ω/□ ITO layer.

In order to test the validity of the model, 20 mini-modules were prepared based on a three-cell lateral design, with 6mm wide interconnects and using substrates with an ITO sheet resistance of 17.7Ω/□. As can be seen in Figure 7, our model predicts an efficiency of approximately 0.8% for this design. The efficiency of each mini-module was measured and a histogram of the results is shown in Figure 8. The spread in the results indicates the variability of our fabrication process, which introduces a number of imperfections outside the scope of our simple model. Aside from these yield issues, the

histogram indicates good agreement with the model, with no results greater than 0.8% and most results within reasonable range of this value.

CONCLUSIONS

We have used a systematic study of the performance of small test cells to understand the role of series resistance and edge effects on the scalability of OPV devices. We confirm that the series resistance of the ITO anode layer is of critical importance as devices become larger. The sheet resistance of our ITO layer was determined from current-voltage curves on OPV devices, producing a value of 18.4Ω/□ that compares well with a direct four-point probe measurement. Our results also indicate that short-circuit current values taken from measurements on small devices cannot be assumed to increase proportionally with device area, unless the measurements are first corrected for the extra current occurring at the edges of the small device. These results have enabled us to develop a predictive model for optimising the lateral design for a 10cm × 10cm OPV mini-module.

ACKNOWLEDGEMENTS

This work was funded through CSIRO's National Research Flagships Program – Future Manufacturing.

REFERENCES

S. Choi, W.J. Potscavage, Jr., and Bernard Kippelen. Area-scaling of organic solar cells. *J. Appl. Phys*. 106, 054507 (2009)

J.L. Delgado, P-A. Bouit, S. Filippone, M.A. Herranza and N. Martın. Organic photovoltaics: a chemical approach, *Chem. Commun*., 46, 4853–4865 (2010)

C.J. Fell, T.J. Nagle, L.J. Rozanski and K. Feron. In preparation for *Solar Energy Materials and Solar Cells*.

J. Kalowekamo and E. Baker. Estimating the manufacturing cost of purely organic solar cells. *Solar Energy* 83, 1224–1231 (2009)

S-Y. Park, W-I. Jeong, D-G. Kim, J-K. Kim, D.C. Lim, J.H. Kim, J.J. Kim and J.W. Kang. Large-area organic solar cells with metal subelectrode on indium tin oxide anode. *Appl. Phys. Lett.* 96, 173301 (2010)

A. Pivrikas, N.S. Sariciftci, G. Juska and R. Osterbacka. A Review of Charge Transport and Recombination in Polymer/Fullerene Organic Solar Cells. *Prog. Photovolt: Res. Appl*. 15:677–696 (2007)

J.D. Servaites, S. Yeganeh, T.J. Marks and M.A. Ratner. Efficiency Enhancement in Organic Photovoltaic Cells: Consequences of Optimizing Series Resistance. *Adv. Funct. Mater.* 20, 97–104 (2010)

D.W. Sievers, V. Shrotriya, and Y. Yang. Modeling optical effects and thickness dependent current in polymer bulk-heterojunction solar cells. *J. Appl. Phys.* 100, 114509 (2006)

H. Spanggaard and F.C. Krebs. A brief history of the development of organic and polymeric photovoltaics. *Solar Energy Materials & Solar Cells* 83, 125–146 (2004)

R. Steim, F.R. Kogler and C.J. Brabec. Interface materials for organic solar cells. *J. Mater. Chem.*, 20, 2499–2512 (2010)

BRIEF BIOGRAPHY OF PRESENTER

Dr Fell is a Principal Research Scientist with CSIRO, based at the National Solar Energy Centre in Newcastle. His 15 year research career includes technology development for both the semiconductor and telecommunications industries and an important contribution to a photovoltaic device now in commercial production.

Assessing the potential impacts of electric vehicles on the electricity distribution network

Anna Cain[1], Iain MacGill[2], Anna Bruce[1]

[1]School of Photovoltaic & Renewable Energy Engineering
[2]Centre for Energy and Environmental Markets,
[2]School of Electrical Engineering and Telecommunications
University of New South Wales
Sydney NSW 2052 AUSTRALIA
anna.cain@student.unsw.edu.au

ABSTRACT

Despite the potential to deliver environmental, social and economic benefits compared with conventional, oil-fuelled vehicles, historically, electric vehicles (EVs) have not been commercially successful. However, improvements in battery technology and the development of electricity distribution network infrastructure seen over the last hundred years lend promise to widespread EV adoption. A transition to EV adoption will crucially hinge on successful integration into the existing electricity network. High-level studies have suggested that Australia could power all city and urban driving using existing off-peak electricity generation capacity. However, such studies give little indication of the ability of the current distribution network to charge EVs at particular locations, nor the impact on network operation. This paper investigates the impact of EV adoption on network loading and the potential to coordinate charging to best use existing network infrastructure. In particular, it reports modelling results from the deployment of EVs within a new distribution network simulation package. The results highlight the importance of charging coordination to minimise adverse operational impacts and network investment.

Keywords: demand management, electric vehicles, electricity distribution

INTRODUCTION

Australia depends on road transport for both commercial and private activities. In 2009, Australia's passenger vehicle fleet alone numbered over 12 million with an average annual growth rate of 2.5% (ABS, 2009). The national vehicle fleet is almost exclusively powered by carbon-dioxide emitting fossil fuels. The transport sector accounts for 14.6% of Australia's 541.2 Mt CO_2-e greenhouse gas (GHG) emissions (National Greenhouse Gas Inventory, 2009). Road transport makes up 12.7% of Australia's annual GHG emissions. Additionally, a range of gases and particulates including carbon monoxide (CO), non-methane volatile organic compounds (NMVOC), and oxides of nitrogen (NO_x) and particulates (PM10) are also emitted. These are harmful to the environment and human health, causing petrochemical smog and contributing to increased respiratory illness. In Sydney alone, the annual health cost of these pollutants is $AU2-3 billion and results in twice the deaths attributed to road accidents (Kearney, 2006). Electric vehicles (EVs) eliminate these emissions at the point of vehicle use. Despite Australia's highly GHG-intensive electricity generation (36.9 % of annual GHG emissions), overall GHG emissions and other environmental impacts are also reduced (Simpson, 2009). A number of studies, including Scott et al. (2007) and Went et al. (2008) have also noted a trend to lower

ownership costs compared with conventional internal combustion engine (ICE) vehicles. This trend is strengthened by the increasing and volatile price of oil.

EV technology has existed since the end of the nineteenth century (Wakefield, 1998). At that time however, the high cost of energy storage and absence of electricity distribution infrastructure prevented widespread EV adoption. This has been reinforced by ongoing investment in development of technological capacity and infrastructure for the competing ICE vehicle (Gagnon, 1999). However, this situation is changing with the emergence of lower cost lithium ion batteries. Australia, over the last hundred years, has also built an extensive electricity grid providing the previously missing distribution network. However, EV charging represents significant and mobile power and energy demand on residential and commercial distribution areas. Therefore, the successful adoption of EVs will depend on their capacity to integrate into the existing electricity network.

This paper first introduces stakeholders in planning and operation of Australia's electricity network, relevant earlier work and EV charging characteristics. It then presents an assessment of the impacts of adding EV charging to a single distributor and a distribution substation in Australia's electricity distribution network, the point where EV charging will occur. Implications of this additional load are discussed.

INTEGRATION OF EVS INTO AUSTRALIAN'S ELECTRICITY NETWORK

Electricity in Australia

Australians consume over 600 GWh of electricity per day (ESAA, 2009). This electricity is generated by private or state-owned entities that trade through the wholesale electricity market run by the Australian Energy Market Operator (AEMO). Electricity is transmitted to customers through a single, interconnected physical network. Planning for the network is conducted by Transmission (above 220 kV) and Distribution Network Service Providers (NSPs) in conjunction with AEMO. NSPs are monopoly businesses regulated by the Australian Energy Regulator (AER) to simulate competition (AER, 2009). Their role is to ensure that the network is able to reliably supply electricity. The nature of Australia's daily load cycle results in significant differences between peak and off-peak loading. Instantaneous supply-demand matching requires network infrastructure be rated for expected peak demand. Growth of this peak demand is a key driver for network investment. This leads to under-utilisation of network and generator assets, which could be exacerbated by EV charging, if added at times of peak demand. The flexibility of EV charging could also improve this utilisation.

Earlier Work

A number of studies from Europe and North America (Hadley, 2006, Kintner-Meyer et al., 2007, Perujo and Ciuffo, 2009, Scott et al., 2007) have supported off-peak charging of EVs as a way to provide the energy requirement for EV charging whilst limiting necessary generation and network expansion. An Australian study by Taylor et al. (2009) found that if 90% of Australia's peak annual capacity is available during off-peak, there is sufficient energy available over the network to support all city and urban passenger vehicle trips. This is an important result. However, it does not give any indication of the network's ability to supply the electricity to an EV at a particular

point in the network. This will depend on the configuration and loading of the distribution network where the EV is connected.

Electric Vehicle Charging Characteristics

An EV is a vehicle that uses electricity, generally stored in a battery to power its drive system. EV charging depends on its charger power and battery capacity. As EVs are not yet widely available in Australia, there is little understanding of how EV owners will undertake charging. However, charging can only take place when the EV is parked and has access to power. These requirements are clearly met when parked at the owner's home overnight. Medium sized EVs are expected to have 160 km range and driving efficiency in the order of 156 Wh/km (25 kWh battery) (Perujo and Ciuffo, 2009, Letendre and Watts, 2009). IEC 61851-1:2001, the international standard for EV conductive charging permits single and three phase charging up to 16 A (3.7 and 11 kW) (IEC, 2001).

ASSESSMENT OF EV LOADING ON DISTRIBUTION NETWORKS

Modelling Method

Based on the conditions discussed above, an EV with 25-kWh/160 km battery charging at 16 A, single phase between 6 pm–8 am (while the EV is plugged in) was considered. This load was connected to a low voltage (230 V) network area feeding residential load. An 808 A, 11 kV/ 400 V distribution substation feeding three 400 A distributors, each supplying 60 houses (20 per phase) was modelled. Fuse protection at both substation and distributor levels was assumed. Applying a 1.25 fusing factor, the minimum load for which a distributor fuse will operate is 500 A. For analysis, maximum load was assumed to be at 75 % of element rating. These assumptions are taken from EnergyAustralia's network standard NS110 Design and Construction of Underground Residential Distribution. To ensure secure operation of the network essentially minimising supply interruptions, thresholds are set by the NSP to trigger investment. For this study, distributor and substation thresholds of 95 % and 100 % respectively were assumed. These reflect current NSP thresholds at this voltage level.

The effect of introducing EV charging was assessed for two standard residential network load cycles, Low Penetration Water Heating and High Penetration Water Heating. Both load cycles incorporate the use of off-peak network capacity to power electric hot water at different areas (and thus different rates of use) within Sydney's distribution network. Off-peak electric water heating is being phased out over the next decade through a joint state and federal government greenhouse gas reduction initiative (DEWHA, 2010). Results then reflect current impacts for both load cycles and potential network investment considerations when planning network upgrades for High Penetration Water Heating network areas. Winter peaking conditions were assumed. Load cycles were kindly supplied by EnergyAustralia.

1 – Single distributor: EV charging as conventional load

This scenario investigates the situation where EV charging is connected as a conventional load. Charging begins and continues until battery is full. EV adoption rates of 5, 25 and 50 % were considered reflecting one, five and 10 EVs per phase per distributor. Four distance categories, 20 km, 40 km, 80 km and 160 km were tested.

Although compared to Sydney's average per capita Vehicle-Kilometres Travelled (VKT) of 18 km (NSW Transport Data Centre, 2010), these distances are quite long, they allow assessment of likely as well as possible worst case charging requirements. This also makes the assessment more relevant to different locations in the network as expected driving distance varies with location (Transport and Population Data Centre, 2005). The effect of existing Time-of-Use (TOU) price signals in managing EV charging is also assessed, based on EnergyAustralia's Residential Smart Power energy tariffs (EnergyAustralia, 2010). Charing start times of 6, 8 and 10 pm reflect Peak, Shoulder and Off-Peak charging as these are the times that EVs are plugged in and the TOU price begins in the evening. The experiment parameters are shown in **Tab. 1** below.

Tab. 1: Scenario 1 Test variables

Residential Load Cycle	Distance Travelled (km)	TOU Charging Regime	Adoption Rate (EV per phase, % per houses)
Low Penetration Water Heating	20	Peak – 6 pm start	1, 5
High Penetration Water Heating	40	Shoulder - 8 pm start	5, 25
	80	Off-Peak – 10 pm start	10, 50
	160		

To assess additional loading impacts, the maximum load on the distributor and number of hours above trigger threshold were recorded for each Charging Regime.

Load Cycle: Low Penetration Water Heating

Fig. 1 below shows the additonal load resulting from 50 % EV adoption at 160 km.

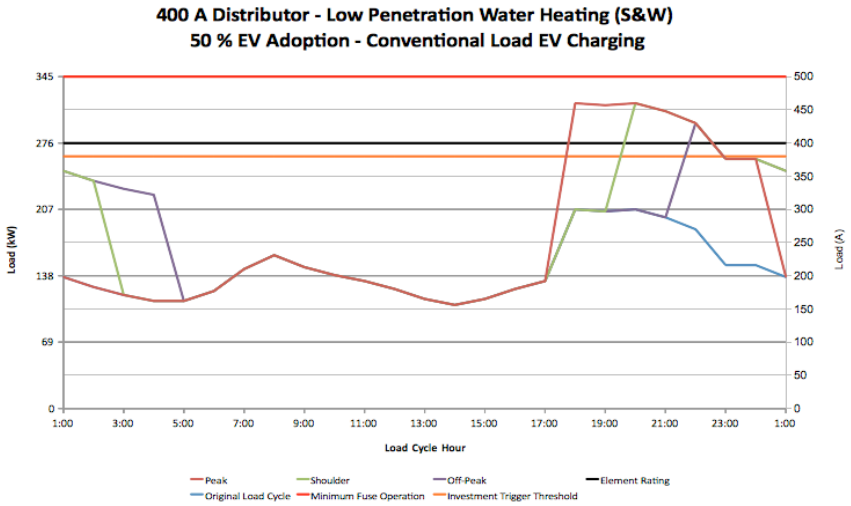

Fig. 1: Low Penetration Water Heating - Peak, Shoulder and Off-Peak Charging Regime – 50 % EV adoption 160 km scenario

For this scenario, Off-Peak charging has the lowest maximum load. This value exceeds the 95 % threshold trigger for network investment. The distributor rating (400 A) was also exceeded. This is not desirable, however, maximum load for this and indeed all charging scenarios would not result in fuse operation. Remaining results for the Low Penetration Water Heating load cycle are presented in **Tab. 2**. A comparison of maximum load values indicates that the magnitude of the new peak depends on the

number of EVs charging and the Charging Regime but not on the distance travelled. This is a consequence of the original load cycle shape, which peaks first at 6 pm. Interestingly, the orignal load shape peaks again at 8 pm, when the Shoulder Charging Regime and pricing begins. This explains the similarities in maximum load between Peak and Shoulder regimes and suggests that Shoulder pricing is an insufficient price signal for minimising EV charging loading.

Tab. 2: Load Cycle: Low Penetration Water Heating EV charging Results

Charging Regime		Peak		Shoulder		Off-Peak	
Distance (km)	EV Adoption (%)	Maximum load (%)	Time above 95 % (Hr)	Maximum load (%)	Time above 95 % (Hr)	Maximum load (%)	Time above 95 % (Hr)
20	5	79	0	79	0	75	0
	25	95	1	95	1	88	0
	50	115	1	115	1	108	1
40	5	79	0	79	0	75	0
	25	95	1	95	1	88	0
	50	115	2	115	2	108	1
80	5	79	0	79	0	75	0
	25	95	2	95	1	88	0
	50	115	4	115	4	108	4
160	5	79	0	79	0	75	0
	25	95	2	95	1	88	0
	50	115	5	115	3	108	1

In assessing the urgency of the trigger, the Distance cateory becomes important. As Distance increases, so does the length of Time above 95 %. Operating above this threshold reduces safety margins that protect the network from surges. Comparison of Charging Regimes shows improvement with delayed charging start time.

Load Cycle: High Penetration Water Heating

Results found are similar to the Low Penetration Water Heating load cycle considered above. This is evident in **Fig. 2**, showing the 50 % EV 160 km scenario.

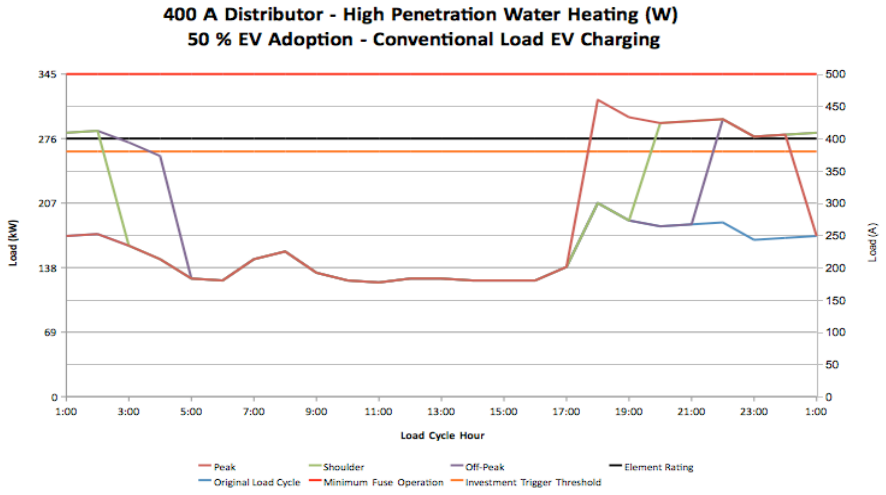

Fig. 2: High Penetration Water Heating - Peak, Shoulder and Off-Peak Charging Regime – 50 % EV adoption 160 km scenario

Although maximum load values in this case are generally slightly lower than the Low Penetration Water Heating case, the key difference between these load cycles is the length of operating time above the 95 % threshold. For the High Penetration Water Heating load cycle, these times are longer. Almost no improvement was found by delaying charging start time based on current TOU energy tariffs. This indicates for this load cycle, there is greater urgency for network investment planning to improve network safety margins if current TOU pricing is maintained. These trends also hold for shorter distances and are shown in **Tab. 3**.

Tab. 3: High Penetration Water Heating EV charging Results

Charging Regime		Peak		Shoulder		Off-Peak	
Distance (km)	EV Adoption (%)	Maximum load (%)	Time above 95 % (Hr)	Maximum load (%)	Time above 95 % (Hr)	Maximum load (%)	Time above 95 % (Hr)
20	5	79	0	75	0	75	0
	25	95	1	86	0	86	0
	50	115	1	106	1	106	1
40	5	79	0	75	0	75	0
	25	95	1	87	0	87	0
	50	115	2	107	2	107	2
80	5	79	0	75	0	75	0
	25	95	1	88	0	88	0
	50	115	4	108	4	108	4
160	5	79	0	75	0	75	0
	25	95	1	88	0	88	0
	50	115	7	108	7	108	6

From these results it appears that element loading could become a problem for distribution NSPs as EV adoption increases. This test, of course, represents an extreme case where all EVs charge simultaneously. If this were the case, network investment to allow for such loading would be significant. Results also show that there is scope to reduce loading problems by delaying charging start time, however, the existing Off-Peak price signal did not prevent load above the 95 % threshold. Essentially, the distributor could operationally cope with new EV load, but this load would need to be incorporated into network planning assumptions. A possible solution is to coordinated EV charging to minimise distributor loading. This may be necessary, particularly for higher EV adoption rates, to maintain safety margins for operation.

2 – Single distributor: Coordinated EV charging

This scenario investigates the extent to which EV loading on a 400 A distributor, initially loaded at 75 % capacity can be minimised by coordinating EV charging. For each time period, knowledge of instantaneous loading and charging distance for each EV were assumed. Charging Regime for each EV was determined based on this information under Peak, Shoulder and Off-Peak TOU price response.

Load Cycle: Low Penetration Water Heating

Compared to EV charging as a conventional load, coordinated charging significantly reduces distributor loading. The load curve resulting from adding 50 % EV adoption 160 km is shown in **Fig. 3** below. This was the charging scenario with the greatest impact identified above. Under a coordinated charging regime, EV charging is possible with a maximum load of 79 % (the same as the worst maximum load for conventional EV charging of a single vehicle), although higher loading is required when charging time is restricted to overnight Shoulder and Off-Peak TOU pricing. All other EV charging combinations could be completed with maximum load maintained at the initial 75 % maximum load.

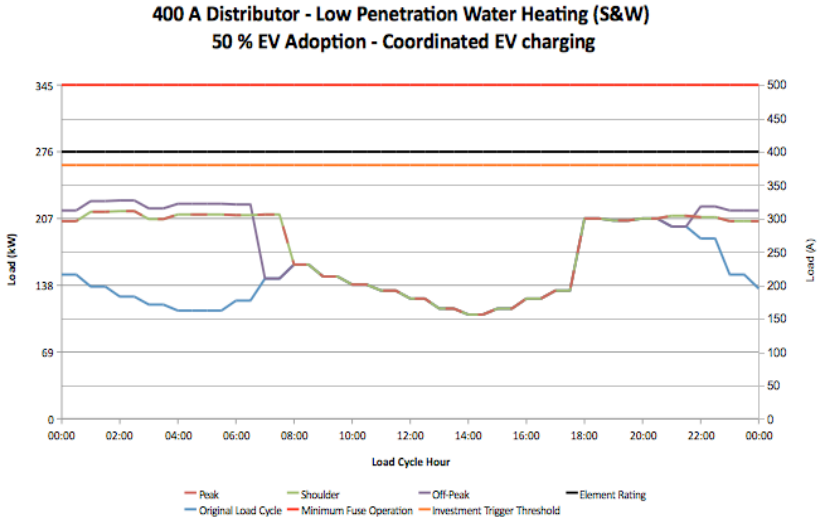

Fig. 3: Low Penetration Water Heating coordinated charging – 50 % EV adoption 160 km – maximum load can be maintained below 80 %.

Load Cycle: High Penetration Water Heating

Results were similar to those found for Low Penetration Water Heating. The load resulting from 50 % EV adoption 160 km is shown in Fig. 4 below. As for Low Penetration Water Heating, this was the loading with the largest distributor impact.

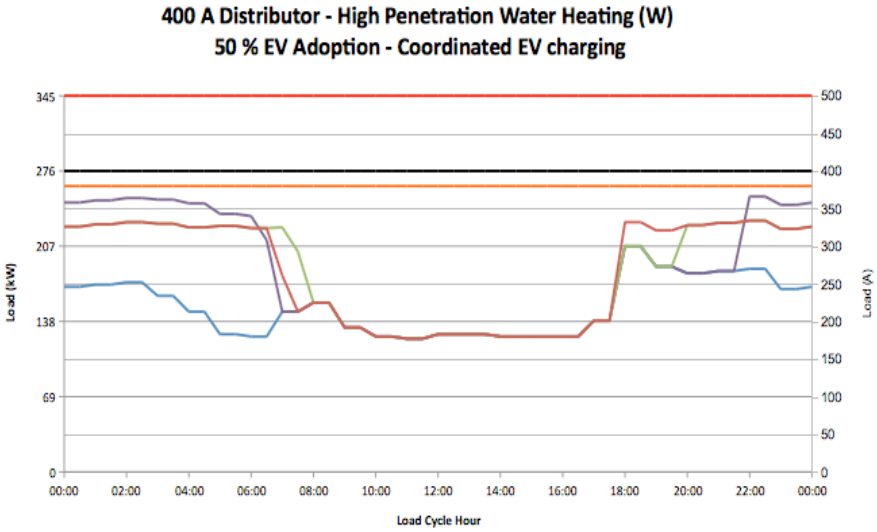

Fig. 4: High Penetration Water Heating coordinated charging – 50 % EV adoption 160 km – maximum load can be maintained below 83 %.

Under a coordinated charging regime, maximum load was restricted to below 83 %, less than the lowest maximum load for 25 % EV adoption charging. Again it is seen that higher loading is required for charging based on existing Shoulder and Off-Peak TOU pricing. With coordinated charging, all other charging combinations could be completed without exceeding 75 % loading. These results indicate that if coordinated charging is implemented, there is no longer a trigger for network investment. Further, the distributor utilisation is improved.

3 – Distribution Substation: Coordinated EV charging

To assess potential upstream network limitations for EV charging, coordinated charging algorithm was developed based on the 11-kV/400 V residential distribution substation feeding 60 houses per phase. Initial substation load (75 %) was divided equally between the three distributors. For each time period, EVs are charged based on rank (determined by charging distance required), TOU price signal response and network element loading. The resulting network load and EV characteristics were produced. This is shown in **Fig. 5** below.

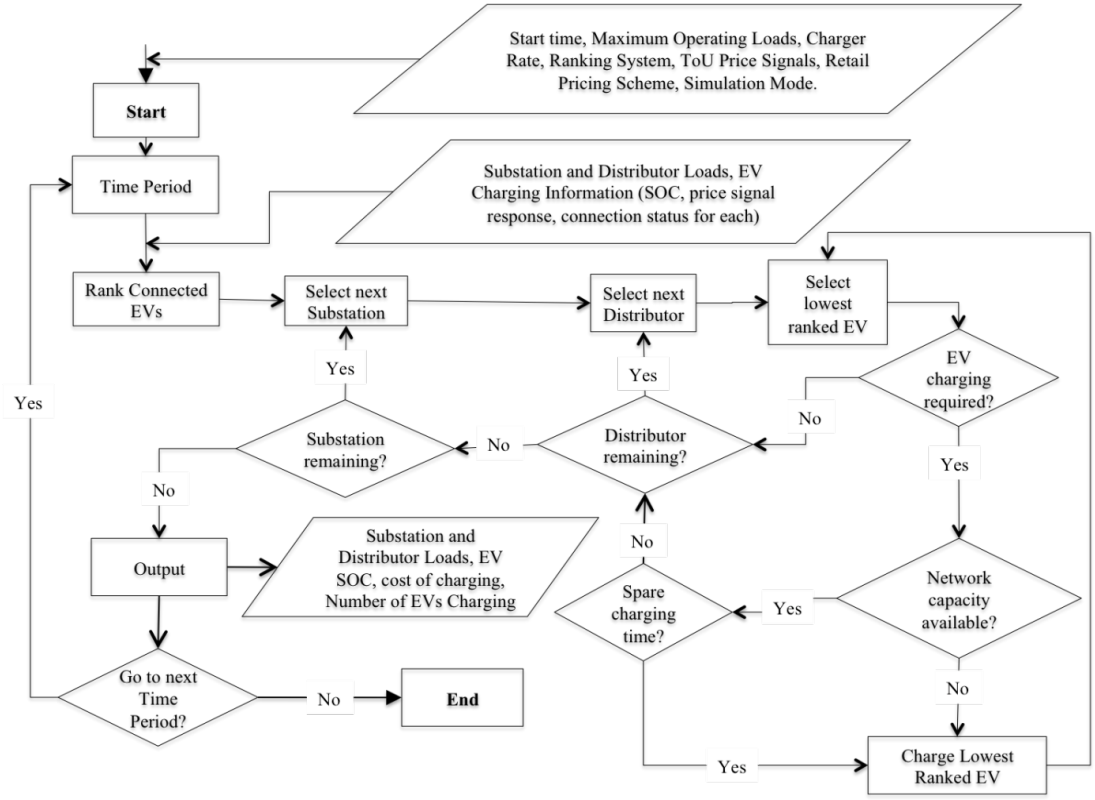

Fig. 5: Algorithm for determining network element loading and EV charging under coordinated EV charging

In this case, the network loading was limited by the substation capacity. For both Low and High Penetration Water Heating, maximum load was held at 75 % and the average resulting charging distance and corresponding state of charge (SOC) increase were obtained. Maximum load was then allowed to increase to allow 160 km (100 % SOC) charging per EV to be achieved. Results for 50 % EV adoption (10 EVs per distributor per phase) under Peak, Shoulder and Off-Peak Charging Regimes are presented in Tab. 4.

Tab. 4: Distribution Substation – Average EV SOC increase when coordinated charging is implemented to restrict network element loading greater than 75 %

Load Cycle	Charging Regime	Average SOC increase (%)	Equivalent Distance (km)	100% SOC increase possible	100% SOC increase maximum substation load (%)
Low Penetration Water Heating	Peak	61. 87	99	Y	89
	Shoulder	61. 87	99	Y	91
	Off-Peak	55.89	89	N	(100)
High Penetration Water Heating	Peak	46.14	74	Y	97
	Shoulder	45.67	73	Y	97
	Off-Peak	36.83	59	N	92.46% increase available at 100% loading

When maximum load is restricted to 75 % there is little or no difference in average SOC increase between Peak and Shoulder Charging Regimes for both load cycles. This shows that the price signal reflects the network loading. As charge start time is delayed with price signals, a trend to lower SOC increase holds for both load cycles. However, the lowest SOC increase would be sufficient to allow over 50 km of driving per EV. Given that daily VKT are generally lower than this value, the minimum SOC increase would satisfy most daily driving requirements without exceeding 75 % maximum load. However, this also shows that with higher EV adoption rates (or greater distance requirements), it may not possible to restrict charging to off-peak, as suggested in energy-based studies (discussed above). If this is the case, increased generation capacity and network augmentation may also be required.

The results in this section show that it is possible to coordinate EV charging to minimise network loading. However, for this coordinated charging regime to be implemented, the ability to remotely collect and analyse network loads and EV data will be required. The opportunity exists to incorporate these capabilities into future EV charging network infrastructure. A number of emerging businesses are taking this approach.

CONCLUSION

There are social, environmental and economic advantages in switching to EVs. However, charging EVs as conventional loads will increase maximum loading on distribution network elements. At significant deployment levels, this may accelerate network investment requirements. This impact may be reduced at low EV adoption rates if EV charging is delayed based on existing TOU Shoulder and Off-Peak pricing. If coordinating EV charging were implemented, this study suggests that it would be possible to minimise or eliminate these impacts without compromising expected daily driving distance at even the highest EV adoption rate examined.

ACKNOWLEGEMENTS

The authors gratefully acknowledge EnergyAustralia for providing the load cycle data for this study. Thanks also to Sali Torgoman of Better Place and Jay Parsons and David Hughes of EnergyAustralia for discussions that informed this work.

REFERENCES

ABS 2009. *Motor Vehicle Census,* Sydney, Australian Bureau of Statistics.

AER. 2009. *What we do in electricity* [Online]. Australian Energy Regulator. Available: http://www.aer.gov.au/content/index.phtml/itemId/659171 [Accessed 14 March 2010 2010].

DEWHA. 2010. *Renewable Energy Bonus Scheme - solar hot water rebate* [Online]. Canberra: Department of the Environment Water Heritage and the Arts. Available: http://www.environment.gov.au/energyefficiency/solarhotwater/index.html [Accessed 22 May 2010].

ENERGYAUSTRALIA 2010. EA Residential and business price list 2010. Sydney: Independent Pricing and Regulatory Tribunal (IPART) of NSW.

ESAA 2009. Annual Review 2008-2009. Melbourne: Energy Supply Association of Australia.

GAGNON, S. 1999. Strategic Challenges in Developing Electric Vehicles: A Literature Review. *International Journal of Vehicle Design,* 21, 21.

HADLEY, S. W. 2006. Impact of Plug-in Hybrid Vehicles on the Electric Grid. Oak Ridge: Oak Ridge National Laboratory

IEC 2001. Electric vehicle conductive charging system – Part 1: General requirements. Switzerland: International Electrotechnical Commission.

KEARNEY, R. 2006. Health Impacts of Fossil Fuels Ethanol-Blended Fuels are Mandatory. University of Sydney Department of Infectious Diseases and Immunology.

KINTNER-MEYER, M., SCHNEIDER, K. & PRATT, R. 2007. Impacts Assessment of Plug-in Hybrid Vehicles on Electric Utilities and Regional U.S. Power Grids Part 1: Technical Analysis. Pacific Northwest National Laboratory.

LETENDRE, S. & WATTS, R. A. 2009. Effects of Plug-In Hybrid Electric Vehicles on the Vermont Electric Transmission System. *Transportation Research Board 88th Annual Meeting 2009.* Washington, DC.

NATIONAL GREENHOUSE GAS INVENTORY 2009. Australia's National Greenhouse Accounts. Canberra: Department of Climate Change.

NSW TRANSPORT DATA CENTRE 2010. 2008/2009 Household Travel Survey. Sydney: NSW Ministry of Transport.

PERUJO, A. & CIUFFO, B. 2009. Potential Impact of Electric Vehicles on the Electric Supply System. Milan: JRC European Commission.

SCOTT, M. J., KINTNER-MEYER, M., ELLIOTT, D. B. & WARWICK, W. M. 2007. Impacts Assessment of Plug-in Hybrid Vehicles on Electric Utilities and Regional U.S. Power Grids Part 1: Economic Assessment. Pacific Northwest National Laboratory,.

SIMPSON, A. 2009. Environmental Attributes of Electric Vehicles in Australia. Curtin Universty sustainability Institute.

TAYLOR, M., PUDNEY, P., ZITO, R., HOLYOAK, N., ALBRECHT, A. & RAICU, R. 2009. Planning for Electric Vehicles in Australia-Can We Match Environmental Requirements, Technology and Travel Demand? : Planning and Transport Research Centre.

TRANSPORT AND POPULATION DATA CENTRE 2005. Car Travel in Sydney: Changes in the Last Decade. Sydney: Department of Infrastructure, Planning and Natural Resources.

WAKEFIELD, E. H. 1998. *History of the Electric Automobile Hybrid Electric Vehicles,* Warrendale, PA: Society of Automotive Engineers.

WENT, A., NEWMAN, P. & JAMES, W. 2008. Renewable Transport: How Renewable Energy and Electric Vehicles using Vehicle to Grid technology can make Carbon Free Urban Development. Perth: Curtin University of Technology.

BIOGRAPHY OF PRESENTER

Anna Cain is an engineering student at the University of New South Wales. Her undergraduate thesis investigates the impact of electric vehicle charging on electricity distribution networks.

Estimation of global and net solar radiation at the Earth surface using NWP model products or satellite observations

Zhian Sun[1]

[1]Author affiliation:
Centre for Australian Weather and Climate Research, Australian Bureau of Meteorology, Melbourne, Australia
700 Collins Street, Melbourne, Australia
z.sun@bom.gov.au

ABSTRACT

A parameterization for Estimation of the global, direct and net solar Radiation at the Earth's Surface (ERES) is developed based on series of radiative transfer calculations for various atmospheric conditions that occur in the atmosphere. The initial aim of this work is to improve the surface radiation budget modelling in a global NWP and climate model. The inputs required by the ERES for determining the solar radiation at the surface are total precipitable water in the atmosphere, CO_2 mixing ratio, total column ozone amount, cloud visible optical depth and cloud amount. All these variables are available in large-scale models as well as from satellite observations. Therefore, the scheme may be used either inside a NWP or climate model or run as an offline program to determine the solar energy at the surface using satellite observations. The evaluation of this scheme using the field experimental data has been done in this study. The evaluation using satellite data will be carried out in the future.

Test shows that the results determined by the ERES scheme and the sophisticated radiative transfer model are in excellent agreement. The scheme is also tested against observations from ARM field experiments for the clear sky conditions. The results show systematic biases indicating the need for including effects of atmospheric aerosols.

Keywords **solar** ***radiation, transmittance, albedo, cloud optical depth***

INTRODUCTION

Solar energy is an important renewable energy source. It is a clean, affordable energy source. Effective use of the solar energy will not only facilitate to meet increased demand on the energy consuming in the future but also reduce pollution and improve environment. Australia has the highest average solar radiation per square metre of any continent in the world (Australian Energy Resources Assessment, 2010). But the geographic distribution of the solar energy varies significantly from coast to inland. Therefore, it is important to accurately determine the distribution of solar energy to provide useful information for the solar energy industries. There are about 80 solar stations in Australia where the global solar radiation data at the surface are measured.

The geographic coverage of these stations is far less than the requirement for analysing the distribution of solar energy. It is possible to use Australian Bureau of Meteorology Numerical Weather forecasting Prediction (NWP) model to produce the solar energy distribution. However, due to the high computational cost of the radiative transfer calculations, the radiation time frequency used in the operational forecasting model is low (usually 1 or 3 hour interval), not good enough for sampling diurnal cycle of the solar radiation. It is therefore necessary to develop an appropriate model to estimate the solar energy at any time and any location.

In this study, we attempt to develop a fast yet accurate scheme ERES which can be used to determine the solar radiation at the surface at each model time step (about 10 ~ 30 minutes). The ERES is also designed for use as an offline program so that the solar radiation at any location may be determined using satellite observations. This application however requires further works to investigate if the accuracy and resolution of satellite data are met with requirements. The development of ERES is based on a sophisticated radiative transfer scheme as briefly introduced in next section.

BASE TOOL FOR DEVELOPMENT

The base tool we used for developing the ERES is a full radiation scheme known as Sun-Edwards-Slingo (SES), originally developed by Edwards and Slingo (1996) at the UK Met Office and modified by Sun and Rikus (1999) at the Australian Bureau of Meteorology. The code has been extensively validated against benchmarks determined using a line-by-line radiative transfer model and the error of the global solar radiation at the surface is less than 1 W m^{-2}. The modelled results are also examined against observations obtained from the Atmospheric Radiation Measurements (ARM) site at Oklahoma and model errors are within 4 W m^{-2}.

DEVELOPMENT OF ERES

The ERES scheme is developed based on a series of calculations using the SES radiation model for various atmospheric conditions. The 60 levels of mid-latitude summer (MLS) atmospheric profile are used for these calculations. In order to ensure that the scheme is applicable worldwide, the total column values of 3 major absorbing gases (H_2O, CO_2, O_3) have been varied to cover all possible values occurring in the global atmosphere. Precipitable water vapour amounts are varied from 0.2 to 20 cm; the ozone amounts are changed from 100 to 500 Dobson Unit (DU); and the carbon dioxide concentrations from 200 to 1000 ppmv. The impact of these changes is implemented into the radiation calculations by scaling the gaseous mixing ratio profile of the MLS atmosphere in such a way that the integrations of mixing ratios are equal to the altered values. The effects due to N_2O, CH_4, and O_2 are also included in the calculations, but since the radiative effects of these species are relatively less important compared with the major absorbing species, the changes in mixing ratios for these minor species are not included in the parameterization. The current values as reported in IPCC Third assessment (Houghton, *et al.,* 2001) are used in the full radiation calculations and the effects of these species are implicitly included in the parameterization. The solar zenith angle and surface albedo have a significant impact on the radiation at the surface and are required to include in the parameterization explicitly. Therefore, the solar zenith angle is varied from 0 to 90^o and surface albedo from 0 to 0.9, respectively. The Rayleigh scattering is treated explicitly and the method is described following the treatment of transmittance of the atmosphere due to molecular absorptions. The effects of clouds are considered in terms of cloud visible optical depth and cloud amount. The

cloud liquid/ice water content is varied to cover the range of values possibly occurring in the global atmosphere.

Table 1. Division of spectral bands of SES radiation model and major absorbing species in each band. The two bands used in the ERES (A, B) are also shown

Band	Spectral range (μm)	Species	ERES band
1	0.20~0.45	O_3	A: 0.2~0.7
2	0.45~0.50	O_3	
3	0.50~0.63	O_3, H_2O	
4	0.63~0.70	O_3, H_2O, O_2	
5	0.70~0.83	O_3, H_2O, O_2	
6	0.83~1.18	H_2O	B: 0.7~5.0
7	1.18~1.67	H_2O, CO_2, O_2	
8	1.67~2.50	H_2O, CO_2, CH_4, N_2O	
9	2.50~ 5.00	H_2O, CO_2, CH_4, N_2O	

Table 1 presents the SES radiation band structure and absorbing species in each spectral band. In the ERES scheme, two spectral bands are employed for the development, as indicated in the last column of Table 1.

Use of two distinct bands to parameterize, as opposed to a broadband, is expected to provide a more accurate representation of the Rayleigh scattering and gas absorption process, both of which have a strong spectral dependence.

In order to further simplify the problem, the molecular absorption and scattering are treated separately

Clear sky direct transmittance of solar radiation due to absorption

In band A, the direct solar radiation is strongly absorbed by ozone and weakly absorbed by water vapour. The direct transmittance of the atmosphere due to the absorption by ozone and water vapour can then be expressed by

$$T_1 = \frac{F_1}{\mu S_0} = f[\mu, U_{o3}, U_{h2o}] \tag{1}$$

where F_1 is the direct solar radiation at the surface; μ is the cosine of solar zenith angle; S_0 the solar constant; μS_0 then represents the incident direct solar radiation at the top of atmosphere; U_{o3} and U_{h2o} represent the total column ozone and water vapour

amount in cm. In order to determine this function, we first calculated T_1 for specified ranges of μ, water vapour and ozone amounts using the SES scheme as mentioned early. We then performed series numerical fittings to the SES model results for each of the dependent variables and obtained the following expressions:

$$\begin{aligned} T_1 &= a_1(\mu, U_{h2o}) \exp\{-b_1(\mu, U_{h2o}) U_{o3}\} \\ a_1(\mu, U_{h2o}) &= a_{11} \exp(a_{12} U_{h2o}) \\ b_1(\mu, U_{h2o}) &= b_{11} \exp(b_{12} U_{h2o}) \end{aligned} \tag{2}$$

$$\begin{aligned} a_{11} &= \sum_{i=0}^{3} a_{11i} \mu^i \\ a_{12} &= \sum_{i=0}^{5} a_{12i} \mu^i \\ b_{11} &= \sum_{i=0}^{3} b_{11i} \mu^i \\ b_{12} &= \sum_{i=0}^{7} b_{12i} \mu^i \end{aligned} \tag{3}$$

In the band B, the water vapour and carbon dioxide are dominant absorbing species and the transmittance due to these two species is parameterized as

$$\begin{aligned} T_2 &= a_2(\mu, U_{h2o}) + b_2(\mu, U_{h2o}) \log_{10}(U_{co2}) \\ a_2 &= a_{21} \exp\{a_{22} \log(U_{h2o}^m) \\ b_2 &= b_{21} + b_{22} \log_{10}(U_{h2o}^m) \\ U_{h2o}^m &= U_{h2o} + (U_{h2o})^{-0.000001} \\ a &= \sum_{i=0}^{8} a_i \mu^i \end{aligned} \tag{4}$$

where U_{co2} is co2 mixing ratio in ppmv; a in the last equation represents $a_{21,}$ $a_{22,}$ b_{21} *and* $b_{22,}$ respectively.

Transmittance and albedo due to Rayleigh scattering

Transmittance due to the Rayleigh scattering is determined by

$$T_r = \frac{F_r}{F_{TOA}} = a_r(\mu) \exp\{b_r(\mu), P\} \tag{5}$$

where F_r is the direct solar flux at the surface calculated by the SES scheme with both the gaseous absorption and surface albedo setting to zero to eliminate their effects, F_{TOA} is the solar incident flux in this band at the top of the atmosphere; and P is the surface pressure. F_r is calculated for μ between 0 ~ 1 and P between 1050 and 400 hPa. We use the surface pressure as a variable to represent the contribution to Rayleigh scattering due to different column amount of atmospheric molecules. The effect of the surface

pressure is implemented into the calculations by scaling the pressure profile of the MLS atmosphere by 14 specified surface pressures ranging between 400 and 1050 hPa. The results are first fitted in terms of right hand side equation for each μ and then fitted the derived coefficients a and b to μ using the following expressions:

$$a_s = \sum_{i=0}^{3} a_{si}\mu^i$$
$$b_s = \sum_{i=0}^{7} b_{si}\mu^i \tag{6}$$

Diffuse solar flux due to the Rayleigh scattering is considered by determining the Rayleigh albedo in both upward and downward directions as given below:

$$\alpha^{\uparrow} = \frac{F_0^{\uparrow}}{\mu S_0} \tag{7}$$

$$\alpha^{\downarrow} = \frac{F_A^{\downarrow} - F_0^{\downarrow}}{AF_A^{\downarrow}} \tag{8}$$

where $F_0^{\uparrow}$ is upward flux at the top of the atmosphere; A is the surface albedo; $F_A^{\downarrow}$ and $F_0^{\downarrow}$ are the solar flux determined with the surface albedos equal to A and 0. These albedos are then fitted with the following functions

$$\begin{pmatrix} \alpha^{\uparrow} \\ \alpha^{\downarrow} \end{pmatrix} = \gamma(\mu) P_0^{\kappa(\mu)} \tag{9}$$

$$\log_{10}(\gamma) = \sum_i \gamma_i \mu^i$$
$$\log_{10}(\kappa) = \sum_i \kappa_i \mu^i \tag{10}$$

The above fitting procedures are conducted for both band A and B to determine the coefficients of γ and κ as well as the limits of summation in the above equations.

Transmittance due to effects of clouds

The direct transmittance due to clouds is determined by

$$T_{cd} = \frac{F_{cd}}{F_{0d}} \tag{11}$$

where F_{cd} and F_{0d} represent the direct solar flux at the surface for the overcast and clear atmospheric conditions without including the effects of Rayleigh scattering. In addition to all clear sky conditions, the full radiation calculations are further expanded to include cloud liquid/ice content in a range between 0.0001 and 1.5 g m^{-3} to cover the possible values in cloudy atmosphere. The ice cloud is layer is inserted at 250 hpa and the water cloud layer at 800 hpa. The calculated results show that the direct transmittance determined by equation (11) follows the Bill's law and can be fitted by

$$T_{cd} = \exp(-c\tau / \mu) \tag{12}$$

where τ is the visible optical depth and c is a empirical constant determined for water and ice clouds in each band.

The total cloud transmittance T_{cT} is determined by F_{cT} / F_{0T} with F_{cT} and F_{0T} representing the total solar fluxes for cloudy and clear atmosphere. This quantity however is not a simple function of optical depth. The effect of the solar zenith angle must be treated separately. It also varies with gas absorber amount when gas absorption is strong.

In band A, the total transmittance for water cloud is fitted to the cloud optical depth in three optical depth ranges ($0 < \tau < 7$; $7 < \tau < 20$ and $\tau > 20$) in following equations

$$T_{cT} = a_{cT}^{i} \exp(b_{cT}^{i}\tau) \tag{13}$$

$$\begin{aligned} a_{cT}^{i} &= \sum_{k} a_k \mu^k \\ b_{cT}^{i} &= \sum_{k} b_k \mu^k \end{aligned} \tag{14}$$

where i=1, 2, 3 represents each range of τ. For ice cloud, the fittings are performed in two optical depth ranges and effect of ozone absorption must be taken into account. For $0 < \tau < 2$, we obtained following expressions:

$$\begin{aligned} T_{cT} &= \exp(a\tau) \\ a &= \sum_{i=0}^{3} a_i U_{o3}^{i} \\ a_i &= \sum_{j} a_{ij} \mu^j \end{aligned} \tag{15}$$

For $\tau \geq 2$, we have

$$\begin{aligned} T_{cT} &= a + b\log(\tau) \\ a &= \sum_{i=0}^{3} a_i U_{o3}^{i} \\ b &= \sum_{i=0}^{3} b_i U_{o3}^{i} \\ a_i &= \sum_{j} a_{ij} \mu^j \\ b_i &= \sum_{j} b_{ij} \mu^j \end{aligned} \tag{16}$$

In band B, the function forms are the same as in band A except replacing U_{o3} by U_{h2o}.

Direct and global solar radiation

After establishing the transmittance for clear and cloudy atmosphere, the global, direct and net solar radiation for band A and B at the surface can be determined by following equations:

$$F_b^{dir} = \mu S_0 T_a T_r T_{cdi} T_{cdd} \tag{17}$$

$$F_b^{TOT} = \mu S_0 T_a T_{cdi} T_{cdd} (1-\alpha^{\uparrow})/(1-A\alpha^{\downarrow}) \quad (18)$$

$$F_b^{net} = F_b^{TOT}(1-A) \quad (19)$$

where T_a is the transmittance due to gas absorption (T_1 or T_2); T_{cdi} and T_{cdd} are transmittance due to ice and water clouds (T_{cd}). The total fluxes are simply sum of the results in two bands.

VALIDATION OF THE SCHEME

We evaluate the ERES scheme by comparing results by this scheme with those determined by SES full radiation calculations. The calculations are performed for the solar zenith angles of 0 - 90^o; surface albedos of 0 – 0.90; column amount of water vapours of 0.2 - 20 cm; column amount of ozone 100 - 500 Dobson Unit and CO_2 mixing ratio of 200 - 1000 ppmv. In addition the range of these variables, the cloud liquid water/ice content are respectively varied from 0.0001 to 1.5 g m^{-3} for cloudy conditions.

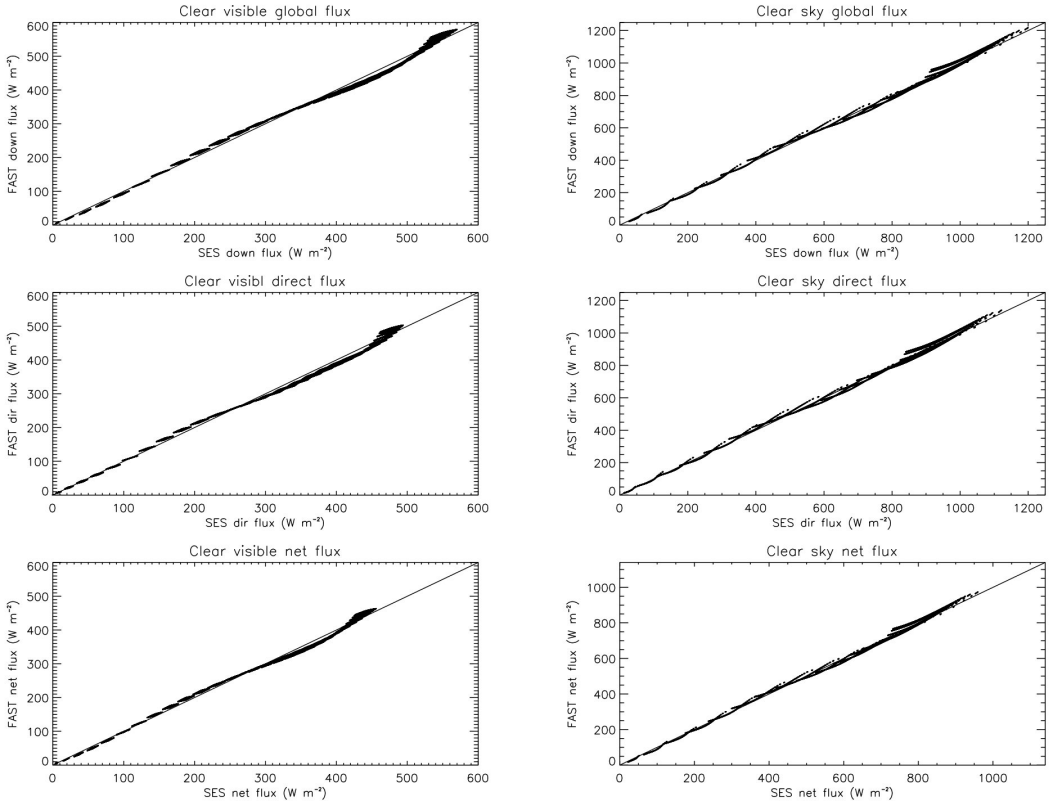

Figure 1. Comparison of solar flux (top: total, middle: direct; bottom: net) determined by the fast scheme with SES radiation scheme. Left column shows the results in band A (visible) and right column gives the results in full spectrum.

Figure 1 shows the results. It is seen that the agreement between the two schemes is excellent; the scatter points are closely distributed along the 45^o diagonal line. The mean

relative errors in total flux are 1.9% for all three components and rms errors are less than 0.06 W m^{-2}.

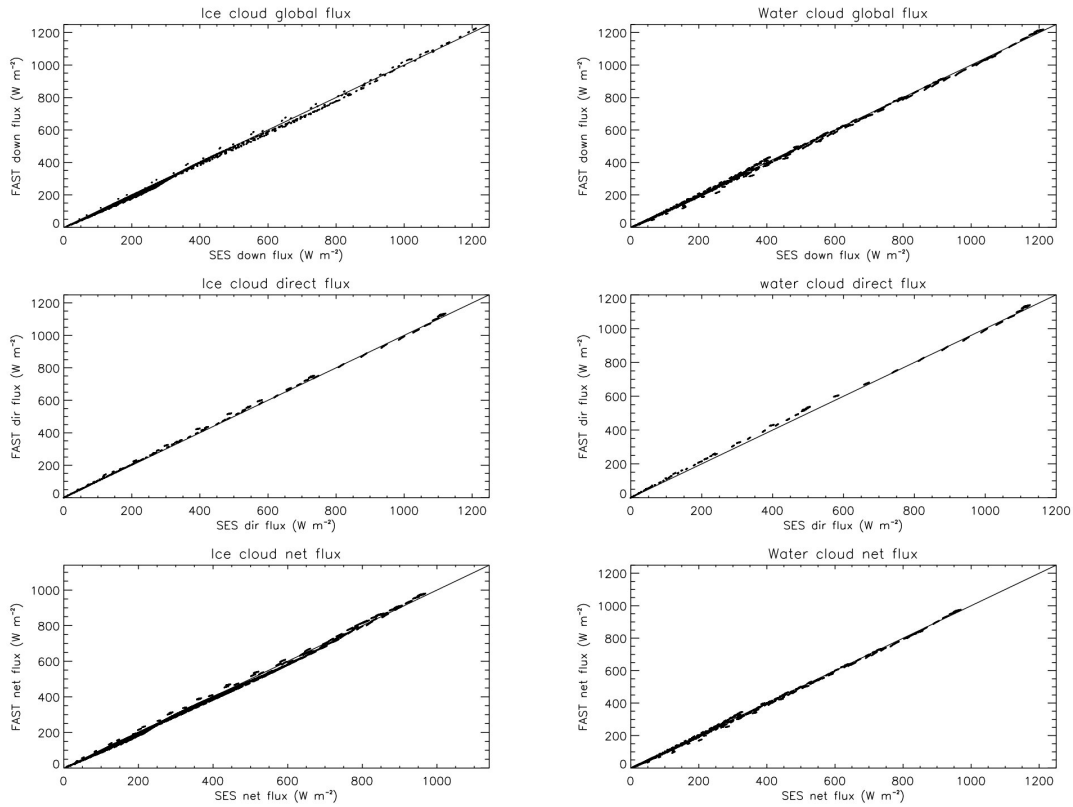

Figure 2. Same as figure 1 but including effect of ice cloud (left column) and water cloud (right).

Figure 2. presents the results for cloudy atmosphere. Again the results determined by the simple scheme for both ice and water clouds are in good agreement with those from the full radiation calculations. The mean relative error is 3.1 W m^{-2} for ice clouds and 3.4 W $^{-2}$ for water clouds. The rms errors are 0.015 and 0.009 W m^{-2}, respectively.

We further use the ARM data to test the scheme for the clear sky conditions. The test for cloudy atmosphere is still underway. One year of data in 2005 from three ARM sites were used in the comparisons. The data include the downward and upward solar flux at the surface, the Global Positioning System (GPS) column water vapour amount, and the fractional sky cover from the total sky imager. The radiation and fractional sky cover data are recorded in a frequency of a second and the GPS data are in 30 minutes. There are two types of cloud covers in the fractional sky cover dataset, the percentage of opaque clouds and the percentage of thin clouds. We accepted data as being cloudless when both the opaque and thin cloud percentages were less than 1% and sorted out the radiation and GPS water vapour data accordingly. Note that all ARM data used in the comparison are instantaneous observations. The real time daily total column ozone amounts are available from the Total Ozone Mapping Spectrometer (TOMS, http://toms.gsfc.nasa.gov/ozone/ozone_v8.html) for a global coverage with 1^{o} X 1.25^{o} latitude and longitude resolution. Data corresponding to the sorted clear sky days were used in the calculations. The ozone values at all four locations were determined by a linear interpolation from the TOMS data.

The results for the three ARM sites are shown in Figure 3. The agreements between the modelled and observed flux are also very good. The mean relative errors of global and

net solar irradiances are 6.15% and 6.19% at Lamont, 7.29% and 8.03% at Barrow and 4.06% and 4.11% at Nauru Island. The corresponding rms errors are 43.3 W m^{-2} and 35.6 W m^{-2} at Lamont, 41.7 W m^{-2} and 27.2 W m^{-2} at Barrow, and 39.7 W m^{-2} and 33.0 W m^{-2} at Nauru Island. It can be seen that the modelled results are systematically larger than observations. The positive biases are particularly apparent at Lamont and Barrow. The similar comparisons are also conducted using the observations obtained on the Tibetan Plateau (Gaize, 32.3 N, 84.06 E, 4420 m) and the results do not show systematically positive biases. Since the air over the Tibet is relatively clean and the effect of the atmospheric aerosols may not be significant there, the biases found in the ARM sites clearly reflect the effect of the atmospheric aerosols and indicate a necessity to include the aerosol radiative effect in the parameterization.

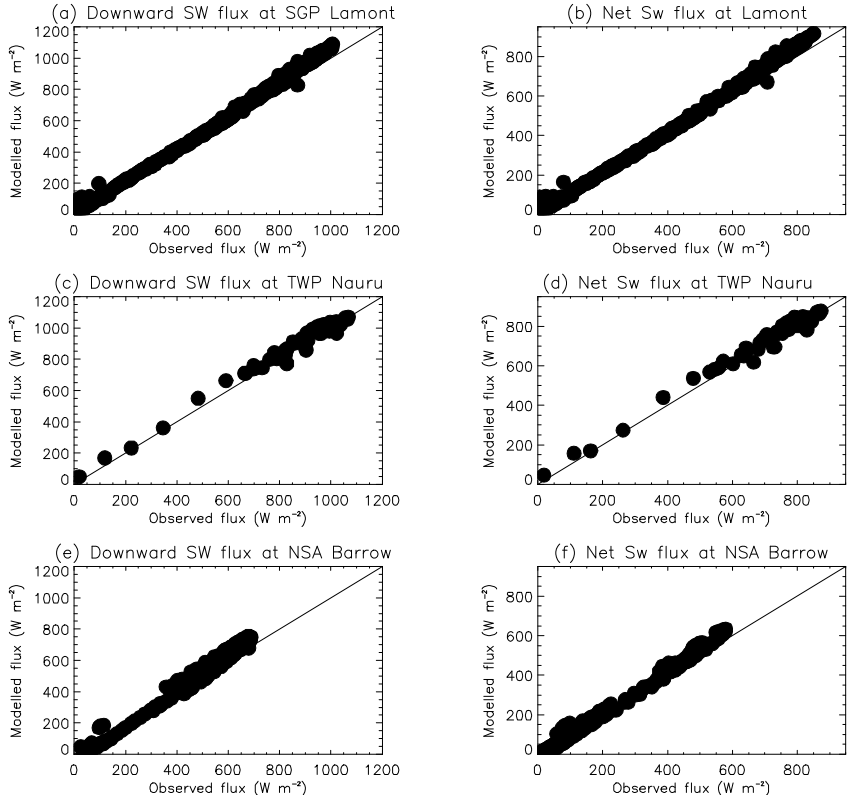

Figure 3. Comparison of global and net solar irradiances determined by the simple scheme with field observations at three ARM sites

CONCOLUSION

A fast scheme for calculating the global, direct and net solar radiation at the surface has been developed. It is based on detailed radiative transfer with input variables consisting in total precipitable water vapor amount, ozone and carbon dioxide amount, solar zenith angle and surface albedo, water and ice cloud optical depth. The effects of minor trace gases are implicitly included in the scheme. The atmospheric albedo due to the Rayleigh scattering is parameterized separately in terms of the solar zenith angle and surface pressure. The scheme reproduces the full radiation model calculations to a high level of accuracy. It is also tested against the observations obtained from the three ARM field research sites. The results show that the scheme systematically overestimates the solar radiation due to missing the effects of atmospheric aerosols in the calculations.

This study is continued on inclusion of effects of atmospheric aerosols. Once this part of work is finished the scheme will be implemented into the Australian Community Climate Earth System Simulator (ACCESS) to improve diurnal simulation of the surface process. The scheme can also be used to estimate the national or international geographic distribution of the solar energy.

REFERENCES

Australian Energy Resource Assessment, 2010. Geoscience Australia and ABARE, 2010, Australian Energy Resource Assessment, Canberra

Houghton, J. T., Ding, Y., Griggs, D. J., Noguer, M., van der Linden, P. J. and Xiaosu, D. 2001. IPCC Third Assessment Report: Climate Change 2001 (Eds.) Cambridge University Press, UK. pp 944

Edwards, J. M. and A. Slingo. Studies with a flexible new radiation code. I: Choosing a configuration for a large-scale model. *Quart. J. Roy. Meteor. Soc*., 1996, 122 (531) : 689-719.

Sun, Z. and L. Rikus, 1999: Improved application of exponential sum fitting transmissions to inhomogeneous atmosphere. *J. Geophys. Res.*, 104 (D6) : 6291-6304.

BRIEF BIOGRAPHY OF PRESENTER

Zhian Sun, PhD, Atmospheric physics team leader in Centre for Australian Weather and Climate Research, Australian Bureau of Meteorology working on atmospheric radiation modelling.

Solar Power Supply to Mitigate the Diurnal and Seasonal Electricity Demand in Victoria

Kwok-Keung Yum[1], George Grozev, Melissa James, and John Page

[1]CSIRO Ecosystem Sciences
37 Graham Road, Highett
Victoria 3190

ABSTRACT

This study aims at estimating the effect of solar power supply on the diurnal and seasonal electricity demand of the state of Victoria in Australia. There have been studies on the mitigating effect of solar power on the diurnal peak demand of electricity. Many of them are based on upscaling the net energy demand for a typical single house adopting grid-connected Photovoltaic (PV) technology. This work takes a different approach: it compares half-hourly solar power yield with Victoria's electricity demand over time; it focuses on centralised solar power generators (big PV or solar thermal generators) rather than distributed PV on house roofs; and it considers the impact of the solar power supply on the state-wide demand of electricity rather than on the individual home demand. The Australian Government has selected in May 2010 eight electricity generation and construction companies to participate in feasibility studies for centralised solar photovoltaic and solar thermal technologies to generate up to 150-250 MW electricity power. This adds timeliness and relevance to the study.

In the study we assume a future scenario that Victoria's solar power generators are able to supply up to 4500MW electrical maximum in day time, and that Victoria's base load demand (day and night) is supplied by conventional base load generators. We then match the Victorian daytime demand profile with the corresponding instant solar power supply profile. At anytime the outstanding demand will be supplied by other peak load and intermediate load generators; and the leftover solar energy will be stored away. The study provides a qualitative analysis of the impact of such arrangements on the peak demands and prices. The analysis demonstrates that matching the daytime demand profile with the corresponding instant solar power supply profile may help reducing peak demands and their prices. Further discussions argue that, when the cost of solar energy generation is not cheap enough to compete with fossil fuel generators, such arrangement can be achieved by delivering solar power as a non-scheduled energy source.

The study is based on a solar power generation model in CSIRO's NEMSIM electricity demand model (Grozev et al. 2005) and AEMO's electricity demand data of Victoria (AEMO 2010)

Keywords — Peak demand, solar power supply, bid stack, smart grid

Introduction

ABARE (2010) reports that Australia's solar power generation has a very low uptake base, but is expected to grow at an average annual rate of 17% from 2007 to 2030. Currently solar power generation in Australia is almost entirely sourced from distributed photovoltaic (PV) installations, but interest in centralised solar technology systems for large scale electricity generation (both solar thermal and PV) is increasing. In May 2010, the Australian Government (2010) selected eight electricity generation and construction companies to participate in feasibility studies for centralised solar

photovoltaic and solar thermal technologies to generate up to 150-250 MW electricity power each.

The strength of solar technology is that it generates electricity while producing very low levels of greenhouse-gas emission. It is a key technology for mitigating climate change (IEA 2010a). However, a full implementation of solar energy technology is not easy. It requires R&D efforts, planning and policy development to increase the market penetration of solar technology for electricity generation. And the market acceptance requires a holistic uptake of smart grid technologies, power storage and further improvements in high quality product components along the manufacturing supply chain (IEA 2010b).

This study aims at estimating the effect of solar power supply on the diurnal and seasonal electricity demand of the state of Victoria in Australia. There have been studies on the mitigating effect of solar power on the diurnal peak demand of electricity, e.g. Kamel (2009). However many of them are based on upscaling the net energy demand for a typical single house adopting grid-connected PV technology. This work takes a different approach: it compares half-hourly solar power yield with Victoria's electricity demand over time; it focuses on centralised solar power generators (big PV or solar thermal generators) rather than distributed PV on house roofs; and it considers the impact of the solar power supply on the state-wide demand of electricity rather than on the individual home demand.

The demand and supply profiles in Victoria

Demand for electricity in Victoria grows as investment and population rise. It is further pushed along in short term events such as heat spells and bush fires. The times for peak demand of electricity are hot days, and during daylight hours. During these times the electricity distributor has to buy electricity from every power generator available, including the much more expensive electricity from diesel generators. Fig. 1 shows the Victorian electricity demands and prices of the year 2009 (AEMO 2010). During the hot summer time in early 2009, high temperature caused simultaneously high electricity demand and network system failures in a short span of time. As a result the electricity prices shot up for hours in a shot span of a few days time.

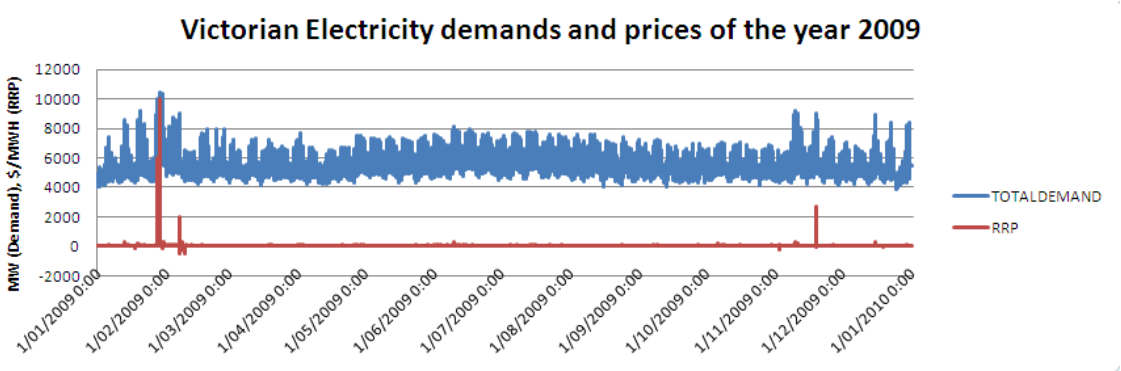

Fig. 1: Victorian electricity demands (MW) and Regional Reference Prices (RRP in $/MWh) of the year 2009.

Fig. 2 shows the daily demand of a summer and winter day in Victoria. A summer day has a peak demand at about the hour of 4:00pm; whereas in a winter day, there are morning and evening peaks which coincide with the usage pattern of households. The

same diagram illustrates the three different types of supply: base load power, intermediate load power and peak load power.

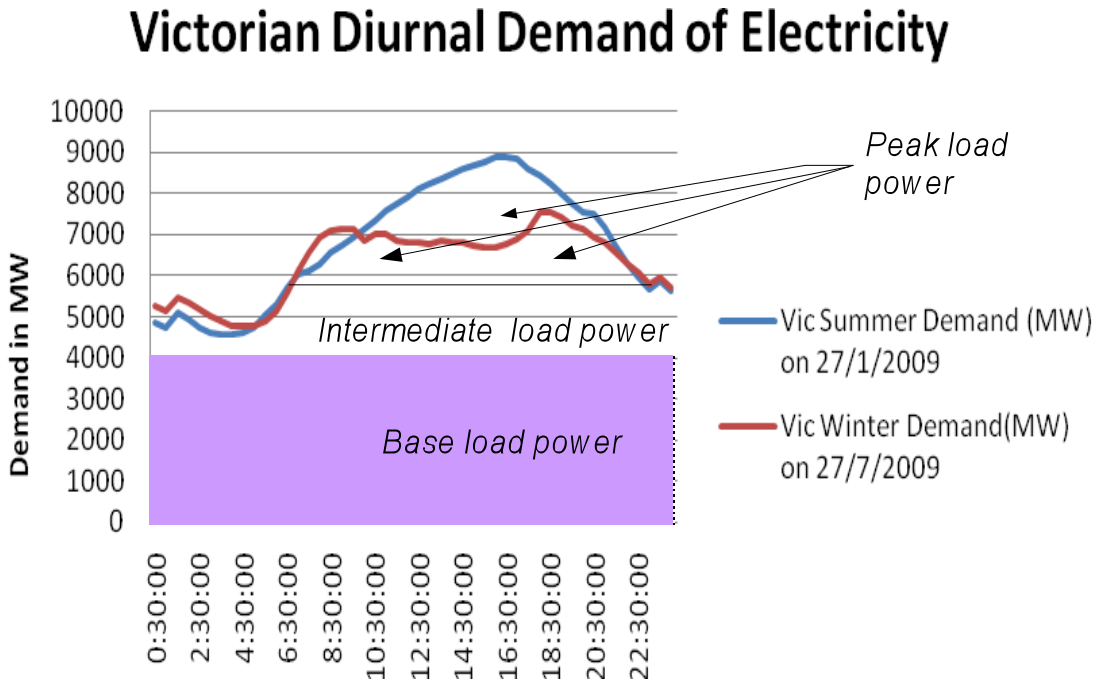

Fig. 2 Daily power demand and supply in typical summer and winter weekdays.

Base load power plants produce continuous, reliable and efficient power at low cost. They take a long time to start up and may not be efficient at less than full output. Base load plants run all times through the year except in the times for scheduled and non-scheduled maintenance. They are excellent candidates for long term agreements to provide stable power at attractive prices. Base load power plants include coal facilities. Geothermal and hydro plants can be used as base load using renewable energy sources.

Electricity demand fluctuates over the hours of a day, and there are weekly and seasonal variations. To meet the changing demand for power, peak load and intermediate load power plants come into play.

Peak load power plants specialise in providing power during peak system demand periods. They can be started up quickly and vary the output amount in minutes. Peak plants typically operate 10-15% of the time and are smaller in capacity than base load plants. They are expensive to run, given the amount of electricity they produce and the cost of fuel to power them. However they are less expensive to build because of their relatively small sizes. Peak plants are most often run on natural gas, but some are on light oil.

Intermediate load plants fill the gap between the base load and peak load plants. They run typically 30-60% of the time. Their costs of construction are considered to be higher than peak load plants but lower than base load plants.

Solar energy can be considered as an intermediate or sometimes peak load power source. It is intermittent in nature as its output fluctuates with weather patterns. It may not be suitable for use as a constant base load power. With suitable backup systems, solar power can be called in to dispatch intermediate or peak load power to reduce the demand for fossil fuels (Cordaro 2008).

High electricity demand events

Fig. 3 shows the daily peak demand for the few days 27-30 January 2009 when extreme heat occurred in Victoria just before the deadly Black Saturday Bushfire 7 February, 2009. NEM regions, in particular South Australia, Victoria and Tasmania, saw significant energy spot price fluctuations from trading interval 13:00hrs on 28 January 2009 to trading interval 18:00hrs on 30 January 2009. On 29 January, RRP spiked to the max allowable amount at the time of $10000.

The main contributor to the high energy prices in Victoria was high temperatures in excess of 40˚C in Melbourne between 28 and 31January 2009. This drove the demand to a record maximum of 10,494MW in Victoria on 29 January 2009 when temperatures peaked above 43˚C. The energy price in Victoria was manually set to $10000/MWh from 12:40hrs to 15:20hrs on 29 January 2009 when a Lack Of Resource (LOR) 3 condition was declared and instructions for load shedding were issued. This initial shedding of load in Victoria was large enough to relieve the shortage of supply. On 30 January 2009, an LOR 3 condition was again declared in Victoria. The energy prices in Victoria were capped at $300/MWh during the Administered Price Period on the day (AEMO 2009). Between dispatch interval 17:45hrs and 17:55hrs on 30 January 2009, the Victorian energy price collapsed to the administered price floor of -$300/MWh when 1200MW of load was shed from the western side of Melbourne.

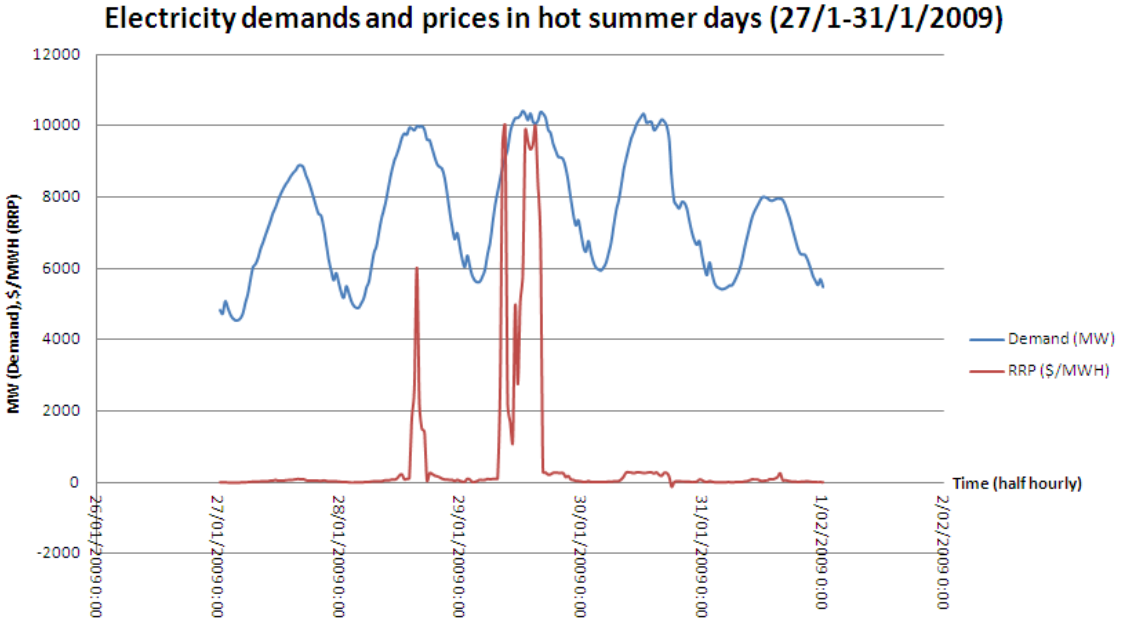

Fig. 3: Demand and peak demand prices in three hot summer days in Victoria in 2009.

Fig. 4 shows the 5-minute bid stack of the Victorian generators during the days 28-31 January 2009 (AEMO 2009). The chart displays the total capacity of electricity available during the peak demand period. The chart shows that there were times when Victoria's maximum capacity of electricity generation was reached.

In electricity grids, the demand for electricity is highly concentrated to the top 1 percent of hours (1 year = 8760 hours). According to Faruqui et al. (2007), in most part of the U.S., the top 1 % accounts for roughly 8-12% of the peak demand. In the Canadian province of Ontario, of 8,760 hours in all of 2006, peak electricity demand in the province only surpassed 25000 megawatts for 32 hours (0.37% of the total hours in a

year). We currently do not have the corresponding Australian figures, but believe that the demand for electricity is also highly concentrated to the top 1 percent of hours.

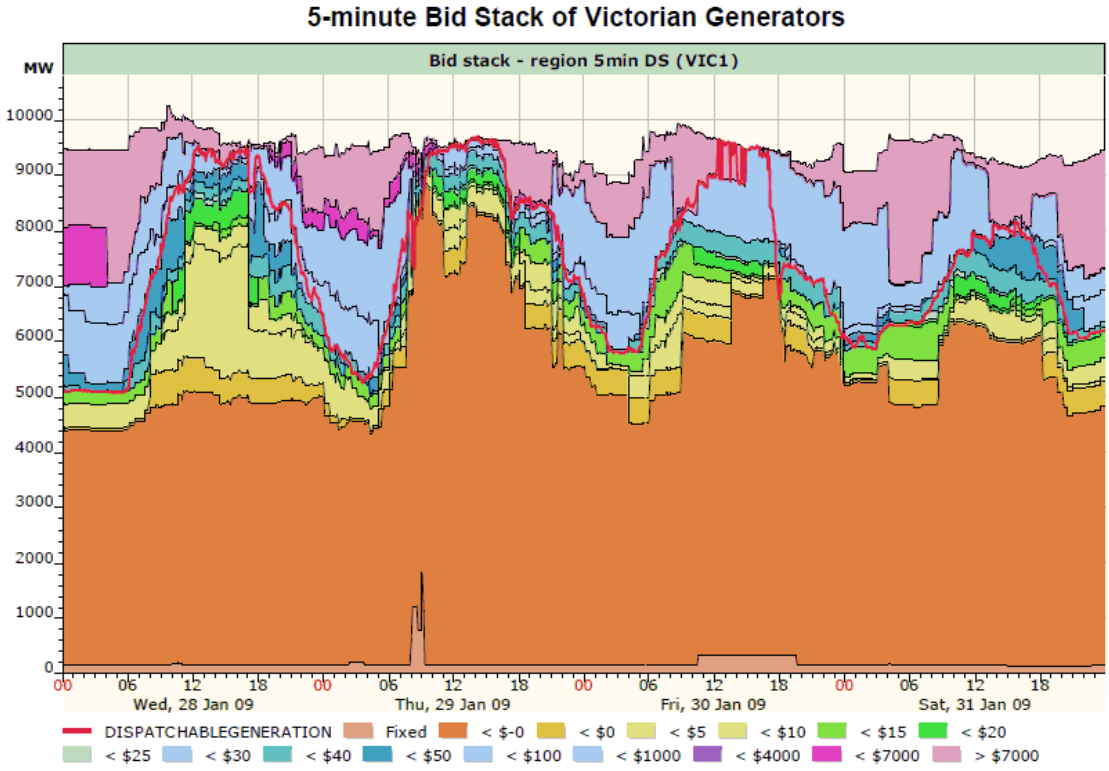

Fig. 4:5-minute bid stack and dispatch of Victorian generators on 28-31 January 2009 (AEMO 2009).

Matching demand profile with solar power generation profile

Currently the uptake of centralised solar technology is only at its embryonic stage. The major reason is the cost and the technology is not yet mature for industrial production. However, the cost of solar power relative to fossil fuel based technology will decrease over time because of (a) government incentive of developing renewable source of energy (carbon tax etc.), and (b) technological advancement of solar power. The Australian weather is generally hot, dry and sunny. In the longer term solar power will play a critical part of renewable energy supply.

Two rationales make the supply of solar power worthwhile. First, solar energy is a type of renewable energy source, the use of which helps reducing fossil fuel burning. Second, the bulk of human social and economic activities happen in daylight time, and as a result of this, the solar power supply profile roughly matches the electricity demand profile in daylight time.

In the research of this paper, we hypothesise that by matching demand profile with solar power generation profile, the outstanding peak demand will be reduced; lack of resource will be less likely to occur; and the electricity bidding prices are less likely to spike.

Let us assume a future scenario (Fig. 5) that the base load, up to 4500MW, is supplied by conventional power plants at both day and night times, and that the solar power plants are big enough to generate 4500 MW for the day light time only.

The theoretical estimation of solar power output in Fig. 5 is devoid of any atmospheric influence. This is a good approximation for a dry and sunny area like Mildura in

Victoria. As a rule of thumb, 1km^2 of PVs or heliostats can generate about 100MW electrical (MWe) of electricity power; so 4500 MWe of solar powers will take up about 45km^2 of PV or heliostats. As shown in the figure, solar power supplies about two third of the daylight demand. The oustanding demand (vertically shaded sections in Fig. 5) will be met with other peak load and/or intermediate load supplies.

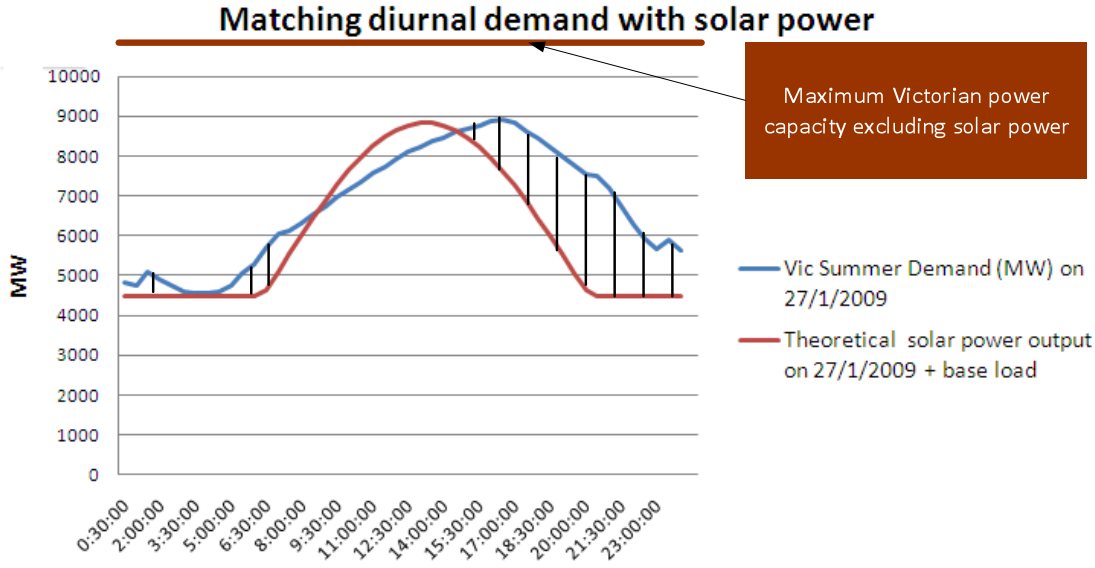

Fig. 5: Matching diurnal demand with solar power.

We also assume that the introduction of solar power in Victoria has not reduced Victoria's maximum power capacity excluding solar power. The assumption is reasonable as the operaion of the national electricity market is based on the assumption that all power generators are competing with each other in a market competition environment.

Without the supply of solar power, the summer time daily peak demand (i.e. the peak of the blue curve in Fig. 5 at 16:30, ~9000 MV) is very close to Victoria's maximum capacity ~11000 MV. This may create a competition for limited power supply. The competation can be further amplified if some generator systems and/or connectors fail due to high temperature.

With the supply of solar power, the outstanding demand (vertically shaded sections in Fig. 5) is much less than the maximum capacity of Victorian power system, excluding the solar power . As a result, the competition for limited power supply is expected to be less severe than the supply network without solar power. And it is less likely to have price spikes.

The above analysis is based on a theoretical solar power output. The argument will be strengthened by simulation results based on a solar power generator model and realistic solar irradiance data.

NEMSIM's solar power estimation model

This paper uses the solar power estimation model in CSIRO's NEMSIM simulation program (Grozev et al. 2005) to estimate solar power generation at half-hourly steps (Fig. 6). The aim of the model is to produce a time series of solar intensity (irradiance) received for each solar power generator site that has reasonable intra-day variability. The time series of solar energy received are then converted into electricity generated by

the power generator so that the effect of solar power on the market can be realistically investigated. The model can be used together with electricity demand, gas demand and hydro generation inflows to model various energy efficiency options. Currently we do not have any solar datasets derived from climate change models; instead we consider only historical solar time series that will give us a realistic inter-day variability.

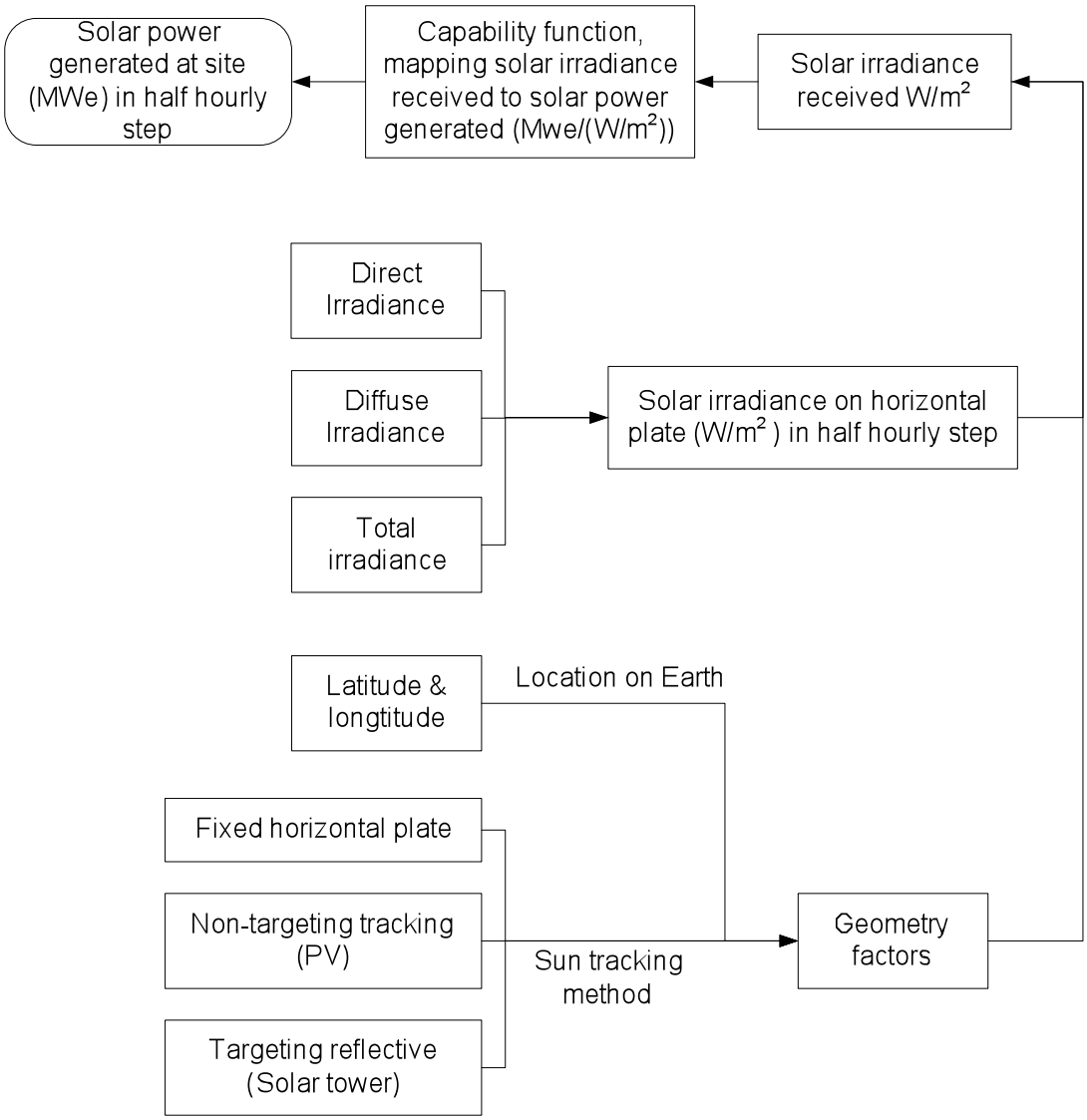

Fig.6: Parameterisation of NEMSIM's solar power generation model. Arrows show the direction of information flow.

Simulation results

Figures 7 and 8 demonstrate the simulation results of matching the half-hourly demand profile with solar power generated by some solar power generators in summer and winter days. The assumptions are:

(1) Demands data are taken from Victoria electricity demand in 2009 (AEMO 2009).
(2) Solar power generators are all situated in Mildura (latitude = 34.2°S, longitude = 142.1°E) and their generation technology is centralising PV with solar azimuth tracking capacity.
(3) The maximum solar output power of the year is about 4500MW, which requires about 45 km^2 of PVs.

(4) The base load power (~4500MW) is supplied by conventional base load power plants for low cost and stable supply of electricity.
(5) The time step for the simulation is half hourly, running on Australian standard time with *no* adjustment for daylight saving time.
(6) Mildura's total irradiance data is taken from Australian Climate Data Bank (Walsh *et al.* 1983).
(7) All solar power generated is immediately used to bid for dispatch.
(8) Being a renewable energy source, solar power generators are regarded as intermediate load dispatch, wedging between the dispatches from base load plants and peak load plants.
(9) Outstanding solar supply after dispatch is stored away (heating up water, etc.)
(10) Outstanding demand is covered by other peak load bids.

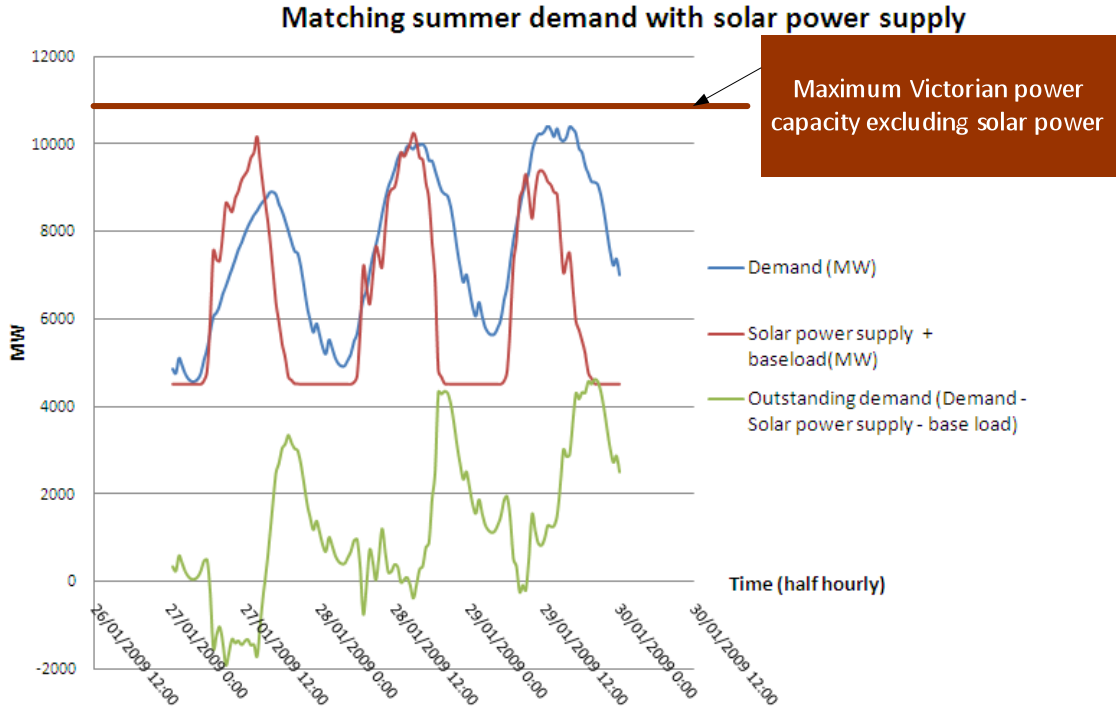

Fig, 7: Matching daily demand with solar power in summer.

Discussions

The assumption (8) above has a significant implication on the availability of solar power in AEMO central dispatch system. Solar power is only included in the system if either (a) the cost of solar power generation has been cheap enough to compete with other ordinary types of generator, or (b) it is included as non-scheduled energy source – no bidding is necessary. If we believe that it will take a long time for solar power generation to reduce its power generation cost, we may consider the option of including the solar power system as non-scheduled energy source, not controlled through AEMO's central dispatch process.

In Figures 7 and 8 the charts in pale green colour show the outstanding demands after the total demand is partially met by the base load supply and solar power supply. The portions of the graph below the horizontal axis indicate that there is an excess of (solar power) supply, which can be used for other things (power storage, etc.) The portions of the graph above the horizontal axis shows that there is a shortage of supply; and peak load generators can be called in to bid for the demand balance.

The maximum Victorian power capacity is about 11000MW at every time step. After deducting the base load of 4500MW, the remaining Victorian capacity is 6500MW, which is well above the peak of the outstanding demand (~4500 MW in Fig.7), even in the afternoon of the hottest day of the year 2009. In contrast, in the case of having no matching of demand profile with solar power generation profile (Fig. 4), the maximum Victorian power capacity has been reached on 29 January 2009. Consequently, in the central bidding process, generation supply (6500 MW) offers more choices than the peak outstanding demand (~4500 MW) can accept. As a result, the whole electricity generation system is less stressed and the possibility of bidding price spikes is greatly reduced.

Since winter consumes less power than summer, the introduction of solar energy power in winter time can offer even more choices than the peak outstanding demand can accept.

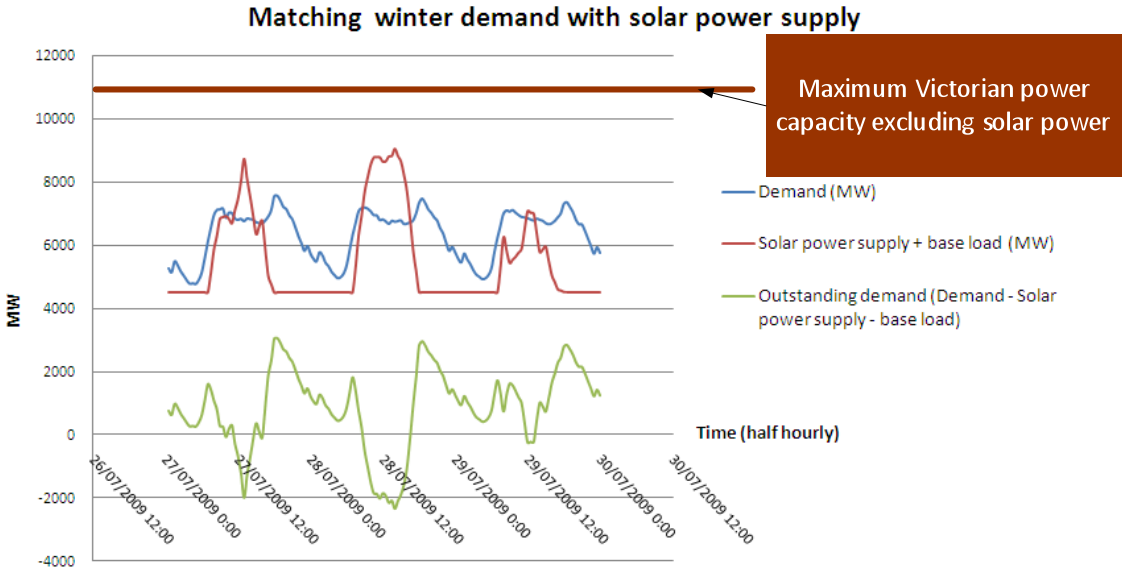

Fig, 8: Matching daily demand with solar power in winter.

Summary and future work

This study provides a system level description of how solar power can be used to mitigate the diurnal and seasonal electricity demand in Victoria. Through analysis and simulation, we demonstrates that by matching the day time demand profile with the solar power generation profile, the peak outstanding demand is greatly reduced to below Victoria's maximum power capacity level. Consequently, more power generators are reserved for meeting the outstanding demand; the network system is less likely to fail due to lack of reserve; and the bidding prices are less likely to spike.

The limitation of this work is that it offers only a qualitative description of mitigating the diurnal and seasonal electricity demand using solar power. In the future, when data and models are further collected and developed, a quantitative model may be needed for better prediction of bidding and prices when solar power is considered as an option for electricity supply.

REFERENCES

AEMO (2009) "Market Event Report: Record Demand in South Australia and Victoria 28 to 31 January 2009". 5 May 2009.

AEMO (2010) Australian Energy Market Operator Price and Demand Data Sets. http://www.aemo.com.au/data/price_demand.html

Australian Government (2010) Solar Flagship Program Round 1 Short List. http://www.government-grant.com.au/2010/05/solar-flagship-program-round-1-short-list/ (Last accessed in October 2010)

ABARE (2010) "Electricity generation major development projects – April 2010 listing". Australian Bureau of Agricultural and Resource Economics.

Cordaro, M. (2008) "Understanding base load power: What it is and why it matters". New York Affordable Reliable Electricity Alliance.

Faruqui, A., Hledik, R., Newell, S. and Pfeifenberger, H. (2007) "The Power of 5 Percent". The Electricity Journal, Volume 20, Issue 8, October 2007, Pages 68-77

Grozev G., Batten D., Anderson M., Lewis G., Mo J.P.T., Katzfey J. (2005) "NEMSIM: Agent-based Simulator for Australia's National Electricity Market". SimTecT 2005, Sydney, Australia, 9-12 May.

IEA (2010a) "Technology roadmap: Concentrating solar power". International Energy Agency.

IEA (2010b) "Technology roadmap: Solar photovoltaic energy". International Energy Agency.

Kamel, F. (2009) "Solar energy to mitigate electrical diurnal peak demand in Queensland". Solar09, the 47th ANZSES Annual Conference, 29 September- 2 October 2009, Townsville, Queensland, Australia.

Walsh, P.J., Munro, M.C., and Spenser, J.W. (1983) An Australian Climate Data Bank for use in the estimation of building energy use. CSIRO, Division of Building Research, ISBN 0 643 03500 1.

BRIEF BIOGRAPHY OF PRESENTER

Dr Kwok Yum is a research scientist in CSIRO Ecosystem Sciences. His expertise is in data interoperability, design and integration of systems and models. His application areas cover: energy efficiency workflows and standards, modelling solar power generation, uncertainty and risk integration for urban water management and for coastal cities, and building information modelling. He can be contacted by email at kwok-keung.yum@csiro.au.

Exposure of Pipe Insulation to High Temperatures from Domestic Pumped Storage (Split) Solar Water Heating Systems in Australia and New Zealand

Berrill[1,2], T.D, Jolly[2], P.G and Morrison[3], G.L
[1]QUT, School of Engineering Systems
tberrill@powerup.com.au
[2]Solaris Sustainable Homes
tberrill@powerup.com.au
pjolly@highlandspacific.com
[3]University NSW, Mechanical Engineering
g.morrison@unsw.edu.au

Acknowledgement: Dr Stephen Hodson,
Armacell Australia Pt Ltd,
PO Box 5202, Hallam Vic. 3803

ABSTRACT

Pipe insulation between the collector and storage tank on pumped storage (commonly called split), solar water heaters can be subject to high temperatures, with a maximum equal to the collector stagnation temperature. The frequency of occurrence of these temperatures is dependent on many factors including climate, hot water demand, system size and efficiency.

This paper outlines the findings of a computer modelling study to quantify the frequency of occurrence of pipe temperatures of 80°C or greater at the outlet of the collectors for these systems. This study will help insulation suppliers determine the suitability of their materials for this application.

The TRNSYS program was used to model the performance of a common size of domestic split solar system, using both flat plate and evacuated tube, selective surface collectors. Each system was modelled at a representative city in each of the 6 climate zones for Australia and New Zealand, according to AS/NZS4234 – Heat Water Systems – Calculation of energy consumption, and the ORER RECs calculation method. TRNSYS was used to predict the frequency of occurrence of the temperatures that the pipe insulation would be exposed to over an average year, for hot water consumption patterns specified in AS/NZS4234, and for worst case conditions in each of the climate zones.

The results show:

- For selectively surfaced, flat plate collectors in the hottest location (Alice Springs) with a medium size hot water demand according to AS/NZS2434, the annual frequency of occurrence of temperatures at and above 80°C was 33 hours. The frequency of temperatures at and above 140°C was insignificant.
- For evacuated tube collectors in the hottest location (Alice Springs), the annual frequency of temperatures at and above 80°C was 50 hours. Temperatures at and above 140°C were significant and were estimated to occur for more than 21 hours per year in this climate zone. Even in Melbourne, temperatures at and

above 80°C can occur for 12 hours per year and at and above 140°C for 5 hours per year.

- The worst case identified was for evacuated tube collectors in Alice Springs, with mostly afternoon loads in January. Under these conditions, the frequency of temperatures at and above 80°C was 10 hours for this month only. Temperatures at and above 140°C were predicted to occur for 5 hours in January.

Keywords Insulation damage, Pipe insulation, Solar hot water heating insulation, Stagnation temperatures.

INTRODUCTION

The aims of this study were to quantify by modeling, the frequency of occurrence over a year of pipe temperatures of 80°C and above, for split solar hot water systems. The pipes of interest were the supply and return pipes from the collector to the storage tank Both flat plate and evacuated tube systems were analyzed for the various climate zones in Australia and New Zealand for both typical and extreme load conditions.

The work was initiated to provide insulation manufacturers guidelines when specifying and rating their insulation material for this application.

The application of insulation on the supply and return pipes also resulted in considerable energy and greenhouse gas savings. This work is reported on in another paper presented during this conference.

LITERATURE REVIEW

A literature review was undertaken to determine the extent of previous research work by industry or government in this area.

Data from industry sources was not available due to commercial in confidence restrictions. However, personal communication with Dr Graham Morrison (Thermal Design Pty Ltd) and Mr Ken Guthrie (Sustainability Victoria) suggested that the main focus of industry or government testing to date has been on overall system performance such as the annual solar contribution and boost energy requirements. Details of the effects of piping insulation have not been investigated.

A search of the Solar Energy journal, Solar Energy Engineering Journal, Renewable Energy Journal and other energy journals shows that there were few research papers that reported on the effects of pipe insulation between collector and storage tank specifically for domestic split systems. While Hobbi *et al*. (2008) reported on system optimisation of most components, they overlooked the effect of supply and return pipes being uninsulated and simply assumed these pipes would be insulated at a specified level. El-Nashar (2006) did specifically examine **"**heat loss through the piping of a large solar collector field" but this was for large commercial systems and the results are not easily transferrable to small domestic systems. Lixing (2007) developed a model for heat losses from the storage tank to end-use points. These losses were estimated by the California Energy Commission to exceed 20 percent in many domestic systems.

Current methods to limit the solar collector heat delivered to the storage tank and hence control the maximum tank temperature include:

- Pressure/temperature relief valves at the tank that typically open around 95 to 99^0C, often dumping excessive amounts of hot water,
- Restrictor valves in thermosiphon pipes between the collector and tank that close off at set temperatures (thermosiphon systems only), or
- Switching off the circulating pump when the tank temperature exceeds a set temperature at the bottom of the tank (use for pumped storage (split) systems).

These strategies, while protecting the tank and hot water users, subject the collector and supply and return pipes between collector and storage tank to stagnation temperatures.

There are a range of research papers proposing methods to limit stagnation but none were found that specifically address the issue of the frequency of occurrence of temperatures that the insulation will be subjected to, at or below stagnation, during typical annual operation.

Methods to limit stagnation include:

a). Collector optical design - Grochola (2008) has patented a collector design using primarily the direct component of irradiation via reflectors that reflect less irradiation onto the absorber in summer. Slaman and Griessen (2009) incorporated a prismatic structure in a solar collector to control the amount of radiation reaching the solar absorber.

b). Ventilation of collector – Harrison *et al*. (2004) examined the use of temperature sensitive air valves that would open at a high temperature and vent air through the collector across the back of the absorber plate to cool the plate.

c). Shading of collector – A thermotropic resin coating on the collector transparent cover have been investigated by Resch *et al*. (2009). Retractable blinds over the collector have also been suggested and trialled.

d). Evacuated tube collector design - Pailthorpe *et al*. (1987) discuss a method of introducing a specific gas into evacuated tube collectors that is absorbed by the selective surface at lower temperatures but is released as temperatures increase. This gas decreases the vacuum within the tube and hence increases heat losses.

The results of the literature review showed that the modelling undertaken for this report was necessary to quantify the energy savings and cost savings of pipe insulation, and the frequency of exposure of the pipe insulation to high temperatures up to and including stagnation temperatures for typical domestic, split systems in Australia and New Zealand.

METHODOLOGY

The project involved the following tasks:

	Tasks
1	Literature research and consult with industry concerning typical operating temperatures and extreme conditions.
2	Define standard configurations from AS/NZS4234
3	Research and summarise supporting information from literature and industry consultation.
4	Define load types for average conditions.
5	Define load types for extreme conditions; stagnation during summer and summer holidays.
6	Build TRYNSYS models for each of the above.
7	Perform simulations using TRNSYS for Australian and NZ cities in each climate zone as per AS/NZS4234. Simulations would use various insulation thicknesses.
9	Determine temperature exposure for insulation for a typical year for each system, and worst case conditions.
10	Highlight potential problems if pipes are insulated / uninsulated.
11	Develop plumber friendly charts and graphs showing the merits of insulation.
12	Report on results of modelling.

The TRNSYS program was used to simulate the performance of typical size domestic, pumped storage (split), solar water heating systems. This program was used because it has been extensively tested and verified.

System Descriptions and Variables

Two domestic, split solar water heating systems were modelled. The first system used two 2 m^2 of selectively surfaced, flat plate collectors with electric boosting in the storage tank. The second system used a bank of 30, selectively surfaced, evacuated tube collectors with gas instantaneous boosting after the storage tank (known as solar pre-heat). Each system used a storage tank of 270 L. These were considered to be a common system size and collector types. Selectively surfaced collectors were used on both systems to make comparison consistent and to maximise performance (see Appendix 1 for collector and load details)

The pipe length modelled was 10 m. The R-value of standard 13 mm thick, closed-cell, polymer, pipe insulation was taken as 0.2 m^2K/W, as per the ORER RECs calculation method, instead of 0.3 m^2K/W. This allowed for increased convective losses for pipes exposed to ambient conditions for the full pipe length.

Reference standards for climate data, loads and calculation methods used were:

- AS/NZS4324 – Heat Water Systems – Calculation of energy consumption , and

- Office of the Renewable Energy Regulator's (ORER), renewable energy certificates (RECs) calculation method for systems of less than 700 litres storage capacity.

Climate data for the 6 climate zones in AS/NZS4234 were used across Australia and New Zealand. The locations for each climate zone are shown in tables 1 and 2 below. The orientation of the collectors is discussed later in the results section.

It was assumed that the plumbing of the return pipe from the collector to the storage tank would be according to AS/NZS4325 and AS3500 the pipe would be immediately routed downwards to restrict heat transfer along the pipe to the insulation during stagnation. Hence the insulation would be exposed to the high temperatures only when the collector circulating pump first switched back on after having been off for some time, and the collector had reached stagnation temperature or close to it.

The daily load patterns of hot water draw-off that were modelled are shown in Appendix 1. These consist of:

a) Load pattern for Australian according to AS/NZS 4324– Heated Water Systems – Calculation of energy consumption.
b) Load pattern for New Zealand according to AS/NZS 4324
c) AS/NZS4324 load pattern modified with no morning loads till 11 am.
d) AS/NZS4324 load pattern modified with no morning loads till 11 am and hourly small afternoon loads to maximise the possibility of stagnation of the collector.
e) No load (IE. no draw-off of hot water) at all for the month of January. So the only load is the heat lost from the tank and neighbouring pipes.

Several measures were taken to simulate worst case conditions.

Firstly, the collector was located facing north at an inclination angle of 25° in Australia and facing north and inclined at the latitude angle for New Zealand as specified in AS/NZS4234. This increases the irradiation on the collector. By comparison, under Office of the Renewable Energy Regulator (ORER) requirements for Australia, the orientation for the heat loss calculations was taken as 45 degrees west of north and the tilt angle is 20 degrees to simulate the range of non-ideal installations used in practice.

Secondly, selectively surfaced collectors were used in all locations where, in reality, a less efficient collector would be more suitable (and cheaper) in hotter climates or for smaller loads.

Thirdly, the reduction in morning loads and increase in afternoon loads was modelled as this produced the worst conditions. This is because the collector would more easily heat the tank to the maximum of 60^{o}C at the tank bottom. Hence, the pump would switch off by late morning and the collector could reach stagnation temperature or very high temperatures more frequently. Then, as hot water is drawn off during the afternoon and the tank temperature decreased, the circulating pump would switch on and off and send bursts of very hot water along the return pipe.

The no load condition for the month of January was also modelled to simulate the home owner going on holidays during the peak of summer. The only demand on the system would be the heat losses from the tank and neighbouring pipes, predominantly over night. The results show that this is not the worst condition as the pump operates from only a very short time in the morning, when the radiation is still low, before switching

off. Hence the pump sends very little hot water through the return pipe. This condition is satisfied provided that the collector outlet pipe is routed immediately down to restrict heat transfer along the pipe to the insulation while the collector is stagnating, as Australian Standard AS3500 requires. All locations were then modelled under each load pattern.

RESULTS

The TRNSYS program was used to model the frequency of occurrence of temperatures that the pipe insulation was likely to be exposed to near the collector outlet. The modelling time interval was reduced from the normal 6 minutes, used for Renewable Energy Certificate (REC) evaluation, to 1 minute to capture more accurately the frequency of occurrence of extreme temperatures over the year.

Tables 1 and 2 show the total hours equal to or greater than each temperature range, for Alice Springs, for flat plat and evacuated tube collectors respectively. This is the hottest climate and hence the worst case.

Alice Springs - Flat Plate							
			hours				
Temp. (C)	80	100	120	140	150	160	170
Jan	4.8	2.6	1.2	0.2	0.0	0.0	0.0
Feb	3.8	1.9	0.7	0.2	0.0	0.0	0.0
Mar	4.0	1.9	0.7	0.0	0.0	0.0	0.0
Apr	3.3	1.8	0.8	0.2	0.0	0.0	0.0
May	1.9	1.0	0.2	0.0	0.0	0.0	0.0
Jun	0.6	0.0	0.0	0.0	0.0	0.0	0.0
Jul	0.7	0.1	0.0	0.0	0.0	0.0	0.0
Aug	1.3	0.6	0.1	0.0	0.0	0.0	0.0
Sep	2.3	1.2	0.4	0.1	0.0	0.0	0.0
Oct	3.2	1.8	0.8	0.2	0.0	0.0	0.0
Nov	3.0	1.6	0.7	0.1	0.0	0.0	0.0
Dec	4.1	2.1	0.8	0.2	0.0	0.0	0.0
Annual	**32.9**	**16.5**	**6.4**	**1.0**	**0.0**	**0.0**	**0.0**
No load			**hours**				
Temp. (C)	80	100	120	140	150	160	170
Jan (hrs)	0.0	0.0	0.0	.0	0.0	0.0	0.0
No morning loads			**hours**				
Temp. (C)	80	100	120	140	150	160	170
Jan (hrs)	5.0	2.8	1.3	0.2	0.0	0.0	0.0
Afternoon loads only			**hours**				
Temp. (C)	80	100	120	140	150	160	170
Jan (hrs)	8.3	4.9	2.3	0.2	0.0	0.0	0.0

Table 1 – Temperature Frequency for Flat Plate Collector, Alice Springs

Notes:

1: Hours in each column are for the hours => the specified temperature (^{o}C)

2: Temperature intervals reduce from 20^{o}C to 10^{o}C above 140^{o}C.

Alice Springs - Evacuated Tube								
			hours					
Temp. (C)	80	100	120	140	160	180	200	220
Jan	7.0	5.3	3.8	3.0	2.2	1.5	0.7	0.1
Feb	5.6	4.2	3.1	2.4	1.6	1.1	0.4	0.1
Mar	6.1	4.4	3.3	2.5	1.7	1.3	0.6	0.0
Apr	4.7	3.6	2.9	2.1	1.6	1.3	0.7	0.2
May	3.2	2.3	1.9	1.4	1.0	0.5	0.0	0.0
Jun	1.1	0.9	0.6	0.4	0.2	0.0	0.0	0.0
Jul	1.4	1.1	0.8	0.6	0.4	0.1	0.0	0.0
Aug	2.7	1.8	1.6	1.0	0.9	0.5	0.1	0.0
Sep	3.5	2.5	2.2	1.6	1.3	0.7	0.4	0.0
Oct	4.6	3.5	2.7	2.1	1.6	1.1	0.5	0.1
Nov	4.3	3.2	2.5	1.9	1.4	0.9	0.3	0.0
Dec	5.6	4.2	3.1	2.4	1.7	1.1	0.6	0.1
Annual	**49.6**	**36.9**	**28.3**	**21.3**	**15.8**	**9.9**	**4.3**	**0.5**
No load								
Temp. (C)	80	100	120	140	160	180	200	220
Jan	0.1	0.1	0.1	0.0	0.0	0.0	0.0	0.0
No morning loads			**hours**					
Temp. (C)	80	100	120	140	160	180	200	220
Jan	7.1	5.7	4.0	3.4	2.5	2.0	1.0	0.0
Afternoon loads only			**hours**					
Temp. (C)	80	100	120	140	160	180	200	220
Jan	10.2	7.5	5.2	3.5	2.1	1.1	0.4	0.0

Table 2 – Temperature Frequency for Evacuated Tube Collector, Alice Springs

Notes:

1: Hours in each column are for the hours => the specified temperature (^{o}C)

2: Temperature intervals at 20^{o}C for all intervals.

Tables 1 and 2 show that:

- The "No Load" condition had negligible hours and was not the worst condition.
- The "Afternoon loads only" condition was the worst case for both collector types.

- For an average demand in the worst climate of Alice Spring, there were 50 hours annually at and above 80°C for evacuated tube collector system and 33 hours for selectively surfaced, flat plate systems. However, for selectively surfaced, flat plate collectors only 1 hour was in the temperature range of 140°C or greater. For evacuated tube collectors, there were 21 hours at this same temperature range.

The tables and graphs for other locations for other locations are not given in this paper due to space constraints. They can be obtained from the authors upon request.

Figures 1 and 2 show the temperature duration curves for each collector type in Alice Springs during January for average load demand and worst case month load demand conditions as outlined above.

The maximum temperature for evacuated tubes was set by the water supply pressure. Steam may be generated in an evacuated tube collector during stagnation however this is unlikely to become superheated. The maximum temperature would be 150°C for 5 bar supply pressure or 180°C for 10 bar pressure.

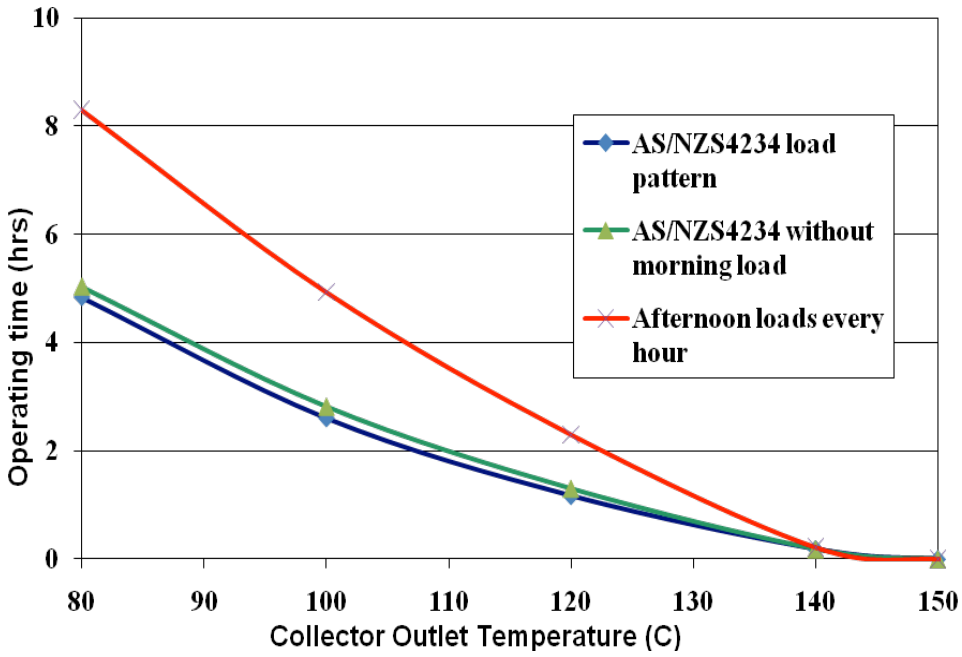

Figure 1 – Flat Plate Collector Temperature Duration Curve, Alice Springs January

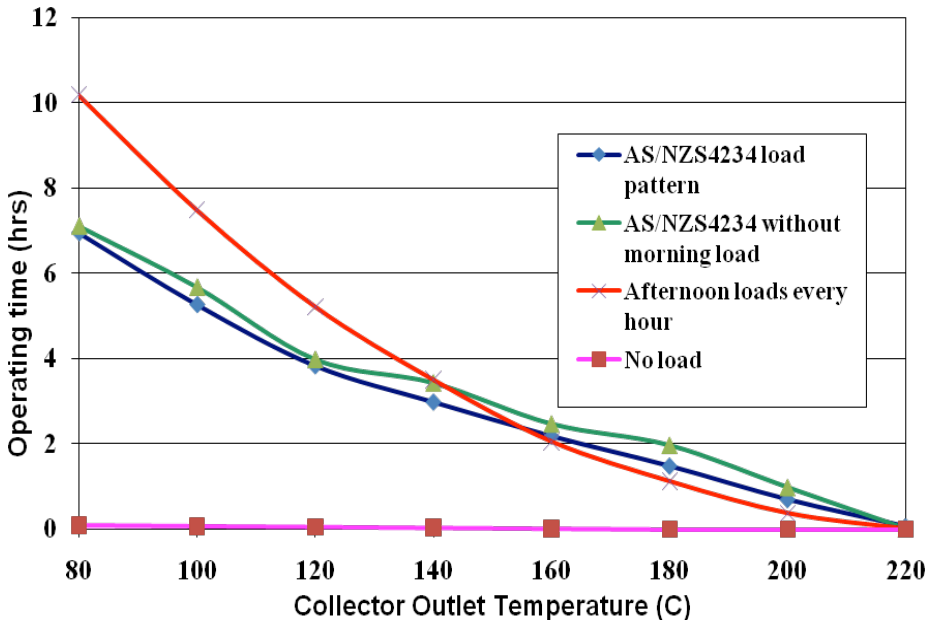

Figure 2 – Evacuated Tube Collector Temperature Duration Curve, Alice Springs January

CONCLUSIONS

For selectively surfaced, flat plate collectors in the hottest location (Alice Springs) with a medium size hot water demand according to AS/NZS2434, the annual frequency of occurrence of temperatures at and above 80°C was 33 hours. The frequency of temperatures at and above 140°C was insignificant.

For evacuated tube collectors in the hottest location, the frequency of temperatures at and above 80°C was 50 hours. Temperatures at and above 140°C were significant and were estimated to occur for more than 21 hours per year in this climate zone. Even in Melbourne, temperatures at and above 80°C occurred for 12 hours per year and at and above 140°C for 5 hours per year. Depending on the insulation's rated maximum temperature, extra care may have to be taken in the installation of pipe insulation for evacuated tube collector systems in most climates to avoid damaging or rapidly deteriorating the insulation.

The worst case simulated was evacuated tube collectors in Alice Springs, with mostly afternoon loads in January. Under these conditions, the frequency of temperatures at and above 80°C was 10 hours for this month only. Temperatures at and above 140°C were predicted to occur for 5 hours.

As a result of these frequencies, the following recommendations are made for solar water heating systems:

- That the pipe insulation is made from a material that can safely withstand the excessive temperatures that will occur throughout the year.
- That the collector outlet pipe must immediately be routed downwards to restrict heat transfer along the collector outlet pipe to the pipe insulation under stagnation or other high temperature conditions.

REFERENCES

El-Nashar, A. (2006). Heat loss through the piping of a large solar collector field. Energy, Volume 31, Issue 12, September 2006, Pages 2020-2035.

Grochola, G. (2008). Patent Application: Solar Collector - A low profile solar collector collects solar energy as heat, while limiting possible peak stagnant temperatures in the collector in summer months. www.wipo.int/pctdb/en/wo.jsp?WO=2008098283.

Gordon, J.M. et al (1980). Temperature-dependent collector properties from stagnation measurements. Solar Energy Volume 25, Issue 5, 1980, Pages 465-466.
Harrison, S.J. et al (2004). Integral Stagnation Temperature Control for Solar Collectors. Dept. of Mech. Engineering and Materials Engineering, Queen's University, Kingston, Ontario, Canada.

Heller, A. J. (2002). Heat-load modelling for large systems. Applied Energy Volume 72, Issue 1, May 2002, Pages 371-387.

Hobbi, A.(2009). Optimal design of a forced circulation solar water heating system for a residential unit in cold climate using TRNSYS. Solar Energy Volume 83, Issue 5, May 2009, Pages 700-714.
Lixing, G. (2007). A simplified hot water distribution system model. Florida Solar Energy Centre.

Marshall R. (1999). A generalized steady state collector model including pipe losses, heat exchangers, and pump powers. Solar Energy Volume 66, Issue 6, September 1999, Pages 469-477.

Matuska T. (2006). Façade solar collectors. Solar Energy Volume 80, Issue 11, November 2006, Pages 1443-1452.

Nagar, V.K. (1984). Emittance from stagnation temperature study. Solar Energy Volume 32, Issue 5, 1984, Pages 633-636.

Pailthorpe, B.A. (1987). Temperature limitation in evacuated solar collector tubes. Solar Energy Volume 39, Issue 1, 1987, Pages 73-75.

Resch, K. et al (2009). Phase separated thermotropic layers based on UV cured acrylate resins – Effect of material formulation on overheating protection properties and application in a solar collector. Solar Energy Volume 83, Issue 9, September 2009, Pages 1689-1697

Simpson, (1992). Measurements of heat losses from an insulated domestic hot water cylinder. Building Services Engineering Research and Technology 1992; 13; 43.

Slaman, M. (2009). Solar collector overheating protection. Solar Energy Volume 83, Issue 7, July 2009, Pages 982-987.

BRIEF BIOGRAPHY OF PRESENTER

The presenter, Peter Jolly, currently hold the position of General Manager of projects for Highlands Pacific. Prior to this worked 18 years in Asia as a technical manager and director for United Technologies and Emerson Corporation, both large multi-national American corporations. During the 1980's Peter worked at The University of Queensland's Solar Energy Centre as a senior research fellow. Peter received his PhD in solar crop drying from the University of the West Indies in 1981 and an honours degree from Melbourne University in 1975.

APPENDIX 1 - SYSTEM CONFIGURATION AND INPUT VARIABLES: PUMPED STORAGE (OR SPLIT) SYSTEMS

The diagram below shows the layout of the system analysed.

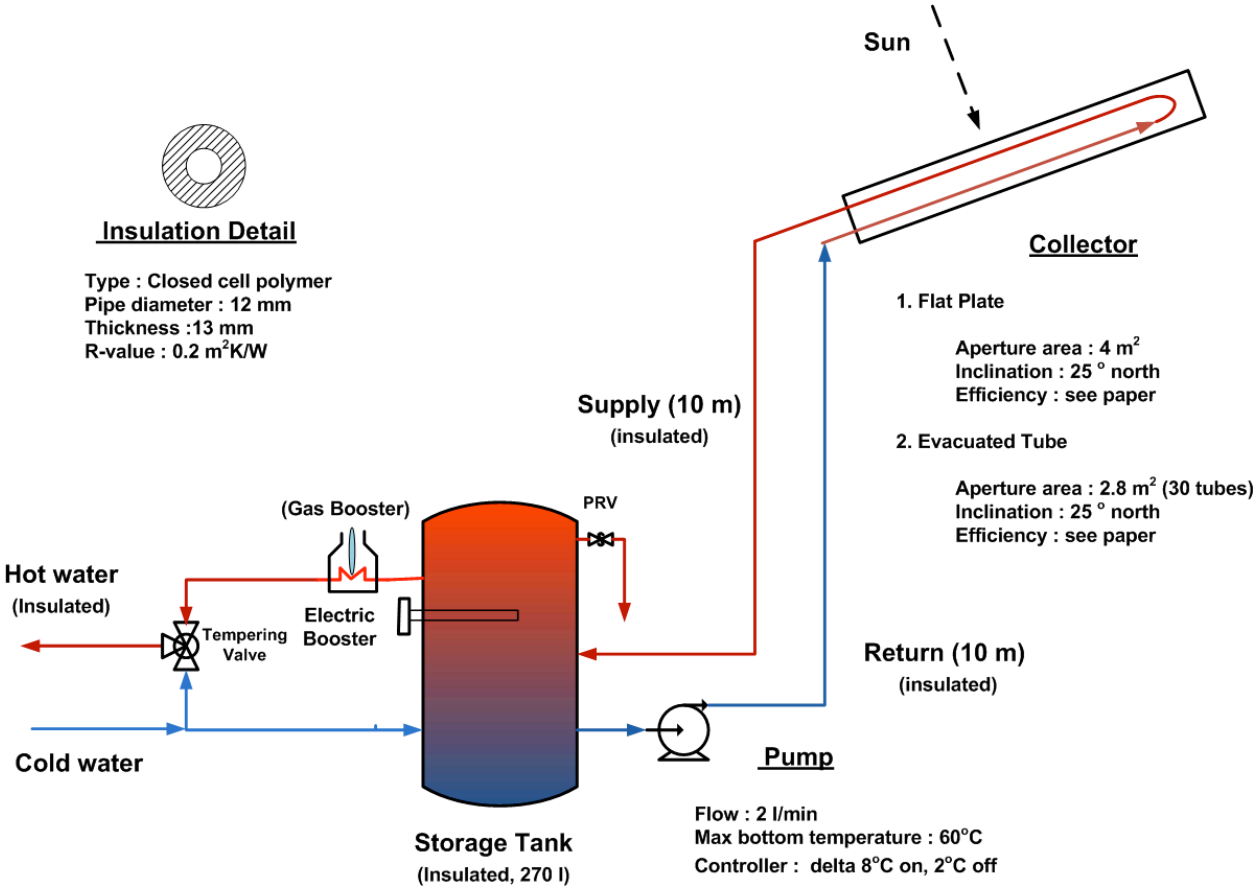

Figure Pumped Split Solar Hot Water System

Solar collector Details :

a). Flat Plate

Aperture area = 4 m^2

Efficiency = 0.8 – 5 dT/G -0.02 $(dT)^2/G$

Equivalent thermal mass = 6 kg water

Inclination = 25°

Orientation = north

b). Evacuated Tube

Aperture area = 2.8 m^2 (30 tubes)

Efficiency = 0.687 – 1.505 dT/G -0.011 $(dT)^2/G$

Incidence angle modifiers are modelled (see figure below)

Equivalent thermal mass = 3 kg water

Inclination = 25°

Orientation = north

Storage tank

Volume = 270 L

Heat loss = 2.4 kWh/d

Auxiliary boost volume = 135 L

Boost tariff = continuous

Pump Operation

Flow rate = 2 L/min

Differential temperature controller 8 K on, 2 K off

Maximum bottom temperature in tank = 60°C

Collector loop piping

Piping length = 10 m each way

Piping diameter = 12 mm

Insulation thickness = 13 mm

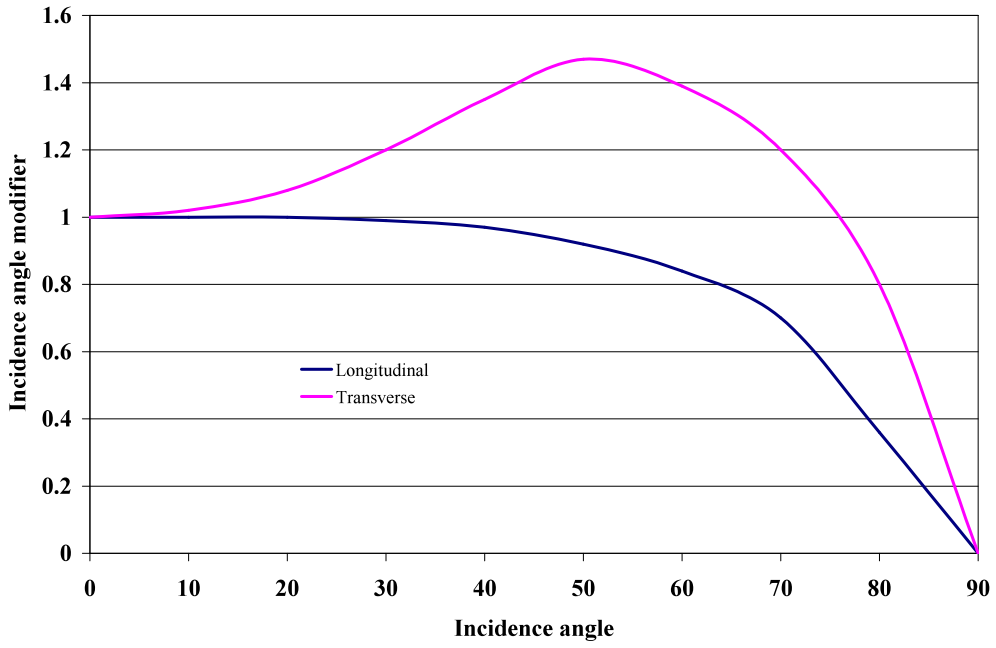

Figure Incident Angle Modifier for evaculated tube collectors

Locations modelled

Alice Springs

Rockhampton

Sydney

Melbourne

Auckland

Dunedin

Load Profiles

AS/NZS4234 (Australia)		AS/NZS4234 (New Zealand)		January Loads			
Time	Load	Time	Load	No morning load		Afternoon loads	
7	0.150	6	0.050	Time	Load	Time	Load
8	0.150	8	0.160	11	0.100	11	0.100
11	0.100	10	0.150	13	0.100	12	0.100
13	0.100	12	0.110	15	0.125	13	0.100
15	0.125	14	0.080	16	0.125	14	0.100
16	0.125	16	0.070	17	0.125	15	0.125
17	0.125	18	0.110	18	0.125	16	0.125
18	0.125	20	0.130			17	0.125
		22	0.110			18	0.125

Energy and Cost Savings from Pipe Insulation on Domestic, Pumped Storage (Split), Solar Water Heating Systems in Australia and New Zealand.

Berrill[1,2], T.D, Jolly[2], P.G and Morrison[3], G.L
[1]QUT, School of Engineering Systems
tberrill@powerup.com.au
[2]Solaris Sustainable Homes
tberrill@powerup.com.au
pjolly@highlandspacific.com
[3]University NSW, Mechanical Engineering
g.morrison@unsw.edu.au

Acknowledgement: Dr Stephen Hodson,
Armacell Australia Pt Ltd,
PO Box 5202, Hallam Vic. 3803

ABSTRACT

Appropriate pipe insulation on domestic, pumped storage (split), solar water heating systems forms an integral part of energy conservation measures of well engineered systems. However, its importance over the life of the system is often overlooked.

This study outlines the findings of computer modelling to quantify the energy and cost savings by using pipe insulation between the collector and storage tank. System sizes of 270Litre storage tank, together with either selectively surfaced, flat plate collectors (4m^2 area), or 30 evacuated tube collectors, were used. Insulation thicknesses of 13mm and 15mm, pipe runs both ways of 10, 15 and 20 metres and both electric and gas boosting of systems were all considered.

The TRNSYS program was used to model the system performance at a representative city in each of the 6 climate zones for Australia and New Zealand, according to AS/NZS4234 – Heat Water Systems – Calculation of energy consumption and the ORER RECs calculation method. The results show:

- Energy savings from pipe insulation are very significant, even in mild climates such as Rockhampton. Across all climates zones, savings ranged from 0.16 to 3.5GJ per system per year, or about 2 to 23 percent of the annual load.

- There is very little advantage in increasing the insulation thickness from 13 to 15mm.

- For electricity at 19c/kWh and gas at 2 c/MJ, cost savings of between $27 and $100 per year are achieved across the climate zones. Both energy and cost

savings would increase in colder climates with increased system size, solar contribution and water temperatures.

- The pipe insulation substantially improves the solar contribution (or fraction) and Renewable Energy Certificates (RECs), as well as giving small savings in circulating pump running costs in milder climates. Solar contribution increased by up to 23 percent points and RECs by over 7 in some cases.

- The study highlights the need to install and maintain the integrity of appropriate pipe insulation on solar water heaters over their life time in Australia and New Zealand.

Keywords — Pipe insulation, energy savings, domestic solar water heaters

INTRODUCTION

The paper reports on the results of a study to model energy savings for boosting and cost savings through the use of closed cell polymer, insulation on typical domestic, pumped storage, solar water heating systems (commonly called split systems) in Australia and New Zealand (see figure1 below). The study examined insulation thicknesses of 13mm and 15mm, pipe runs both ways of 10, 15 and 20 metres and both electric and gas boosting of systems.

LITERATURE REVIEW

A literature review was undertaken to determine the extent of previous research work by industry or government in this area. Data from industry sources was not available due to commercial in confidence restrictions. However, personal communication with Dr Graham Morrison (Thermal Design Pty Ltd) and Mr Ken Guthrie (Sustainability Victoria) suggested that the main focus of industry or government testing to date has been on overall system performance such as the annual solar contribution and boost energy requirements. Details of the effects of piping insulation have not been investigated.

A search of the Solar Energy journal, Solar Energy Engineering journal, Renewable Energy journal and other energy journals shows that there were few research papers that reported on the effects of pipe insulation between collector and storage tank specifically for domestic split systems. While Hobbi et al (2008) reported on system optimisation of most components, they overlooked the effect of supply and return pipes being uninsulated and simply assumed these pipes would be insulated at a specified level. El-Nashar (2006) did specifically examine **"**heat loss through the piping of a large solar collector field" but this was for large commercial systems and the results are not easily transferrable to small domestic systems. Lixing (2007) developed a model for heat losses from the storage tank to end-use points. These losses were estimated by the California Energy Commission to exceed 20 percent in many domestic systems.

The results of the literature review showed that the modelling undertaken for this study was necessary to quantify the energy savings and cost savings of pipe insulation for typical domestic, split systems in Australia and New Zealand.

METHODOLOGY

The project involved the following tasks:

	Tasks
1	Literature research and consult with industry re typical operating temperatures and extreme conditions.
2	Define standard configurations from AS/NZS4234 including electric boosted, gas boosted, continuous boost, off-peak boost. Consider various pipe lengths.
3	Research and summarise supporting information from literature and industry consultation.
4	Define load types for average conditions.
5	Build TRYNSYS models for each of the above.
6	Perform simulations using TRNSYS for Australian and NZ cities in each climate zone as per AS/NZS4234. Simulations would use various insulation thicknesses.
7	Quantity potential energy and economic savings using insulation.
8	Report on results of modelling.

The TRNSYS program was used to simulate the performance of typical size domestic, pumped storage (split), solar water heating systems as shown in figure 1 below. This program was used because it has been extensively tested and verified. (Source: Wikipedia).

SYSTEM DESCRIPTIONS AND VARIABLES

Two domestic, split solar water heating systems were modelled. The first system used two $2m^2$ of selectively surfaced, flat plate collectors. The second system used a bank of 30, selectively surfaced, evacuated tube collectors. Both systems were modelled with electric boosting in the storage tank and with gas instantaneous boosting after the storage tank (known as solar pre-heat). Each system used a storage tank of 270Litres. These were considered to be common system sizes and collector types. Selectively surfaced collectors were used on both systems to make comparison consistent and to maximise performance.

Reference standards for climate data, loads, system orientation and tilt, and calculation methods used were:

- AS/NZS4324 – Heat Water Systems – Calculation of energy consumption , and
- Office of the Renewable Energy Regulator's (ORER), renewable energy certificates (RECs) calculation method for systems of less than 700 litres storage capacity.

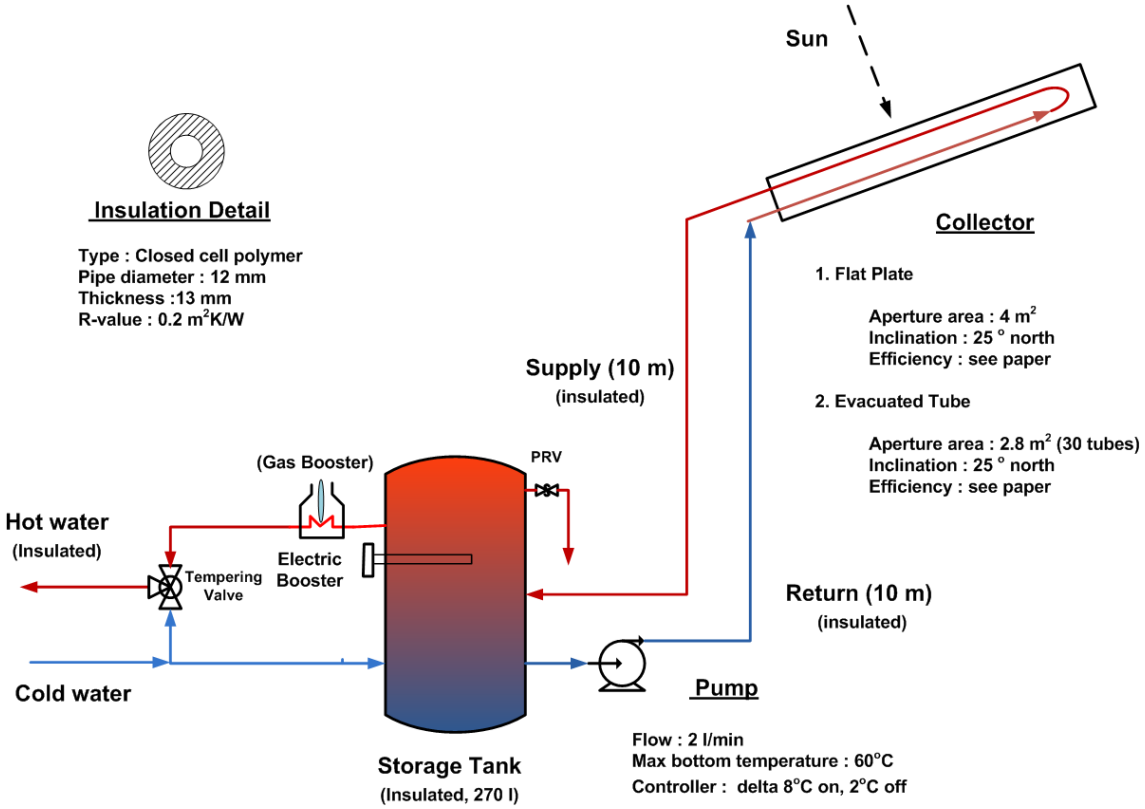

Figure 1 – Typical Split System Configuration with either Electric or Gas boosting.

Climate data for the 6 climate zones in AS/NZS4234 were used across Australia and New Zealand. The locations for each climate zone are shown in tables 1 and 2 below.

The orientation and tilt of the collectors were as per AS/NZS4234 - collector orientation (azimuth) 45 degrees west of North, tilt 20 degrees (climate zones 1 to 4); azimuth 0 degrees, tilt 40 degrees (climate zone 5), and azimuth 0 degrees, tilt 45 degrees (climate zone 6).

Pipe lengths between collector and storage tank of 10, 15 and 20metres were modelled to allow for both single and two storey homes where pipe runs are longer. The R-value of standard 13mm thick, closed-cell, polymer, pipe insulation was taken as 0.2m^2.K/W, as per the ORER RECs calculation method, instead of 0.3m^2.K/W. This allowed for increased convective losses for pipes exposed to ambient conditions for the full pipe length.

Annual loads varied from between about 10 and 14GJ for electrically boosted systems to between about 15 to 21GJ for the gas boosted systems. This increase in loads for gas boosted systems is required under the ORER's RECs calculation method. This is problematic as it:

- Penalises the performance of the gas boosted systems in all climate zones, the worst case being Dunedin, with 20 metre pipe run, where the solar contribution was only about 16 percent. Even with low solar contributions, the absolute value of energy savings was still significant in colder climates.

- Ignores the trend of decreasing household occupancy across Australia, which is currently about 2.5 persons per household and falling. This low occupancy together with water saving appliances is likely to result in lower hot water demand.
- Results in lower energy and cost savings in the colder climates than if larger systems are used for the same hot water demand.

This highlights the need to increase system size in colder climates accordingly for increasing hot water demand. In practice this would be done by using a larger tank and collector area. This was not done in this study so the potential energy and cost savings are conservatively estimated.

Full details of the system specifications and input variables are shown in Appendix 1.

RESULTS

Results for energy and cost savings are shown in tables 1 and 2 below. These tables are for the 15 metre pipe lengths, electric and gas boosting with electricity priced at the general domestic tariff in Victoria of 19c/kWh (See www.victoriaelectricity.com.au/electricity-rates.php), and gas at 2c/MJ, for locations in each climate zones as specified in AS/NZS4234. Cost savings from pipe insulation will depend on the electricity tariffs and local gas prices used in each climate zone.

Flat Plate

Location & Climate Zone	Insulation Thickness	Annual Load	Annual Pipe Losses	Annual Tank Loss	Annual Boost Energy	Boost Energy Savings	Annual Boost Energy Costs	Annual Savings for Electricity at c/kWh
	mm	GJ/yr	GJ/yr	GJ/yr	GJ/yr	GJ/yr	$/yr	**19.00** $/yr
Alice Springs	0	9.897	3.824	1.917	0.889		$46.91	
2	13	9.897	1.229	2.029	0.535	0.354	$28.23	$18.68
	15	9.897	1.163	2.031	0.530	0.359	$27.98	$18.93
Rockhampton	0	9.896	4.066	1.731	1.610		$84.97	
1	13	9.896	1.270	1.858	0.968	0.642	$51.09	$33.88
	15	9.896	1.201	1.861	0.952	0.658	$50.24	$34.73
Sydney	0	12.540	3.530	1.731	3.930		$207.42	
3	13	12.540	1.109	1.838	3.027	0.903	$159.76	$47.66
	15	12.540	1.047	1.840	3.007	0.923	$158.70	$48.71
Melbourne	0	13.860	2.870	1.735	6.693		$353.24	
4	13	13.860	0.887	1.807	5.785	0.908	$305.32	$47.92
	15	13.860	0.837	1.809	5.766	0.927	$304.32	$48.93
Auckland	0	10.990	3.266	1.776	4.749		$250.64	
5	13	10.990	1.041	1.881	3.758	0.991	$198.34	$52.30
	15	10.990	0.983	1.884	3.736	1.013	$197.18	$53.46
Dunedin	0	10.990	2.090	1.831	6.676		$352.34	
6	13	10.990	0.643	1.905	5.809	0.867	$306.59	$45.76
	15	10.990	0.608	1.907	5.783	0.893	$305.21	$47.13

Table 1 – Electrical Boost Energy and Cost Savings, Flat Plate Collector and 15 metre Pipe Length

Evacuated Tube

Location & Climate Zone	Insulation Thickness	Annual Load	Annual Pipe Losses	Annual Tank Loss	Annual Boost Energy	Boost Energy Savings	Boost Energy Annual Costs	Annual Savings for Electricity at c/kWh
								19.00
	mm	GJ/yr	GJ/yr	GJ/yr	GJ/yr	GJ/yr	$/yr	$/yr
Alice Springs	0	9.897	4.412	1.923	0.986		$52.03	
2	13	9.898	1.479	2.105	0.472	0.514	$24.92	$27.11
	15	9.898	1.403	2.109	0.464	0.522	$24.50	$27.53
Rockhampton	0	9.897	4.449	1.740	1.646		$86.87	
1	13	9.898	1.425	1.945	0.766	0.880	$40.42	$46.46
	15	9.898	1.349	1.950	0.748	0.898	$39.50	$47.37
Sydney	0	12.540	3.814	1.718	4.255		$224.57	
3	13	12.540	1.260	1.857	2.938	1.317	$155.06	$69.51
	15	12.540	1.190	1.861	2.907	1.348	$153.43	$71.14
Melbourne	0	13.860	3.238	1.738	6.940		$366.28	
4	13	13.860	1.067	1.838	5.718	1.222	$301.78	$64.49
	15	13.860	1.007	1.842	5.693	1.247	$300.46	$65.81
Auckland	0	10.990	3.780	1.771	4.927		$260.04	
5	13	10.990	1.260	1.936	3.543	1.384	$186.99	$73.04
	15	10.990	1.194	1.940	3.510	1.417	$185.25	$74.79
Dunedin	0	10.990	3.037	1.851	6.740		$355.72	
6	13	10.990	1.052	1.979	5.457	1.283	$288.01	$67.71
	15	10.990	0.995	1.983	5.430	1.310	$286.58	$69.14

Table 2 – Electrical Boost Energy and Cost Savings, Evacuated Tube Collector and 15 metre Pipe Length

Figure 2 shows annual boost energy graphically for 3 locations north to south across Australia, namely Rockhampton, Sydney and Melbourne.

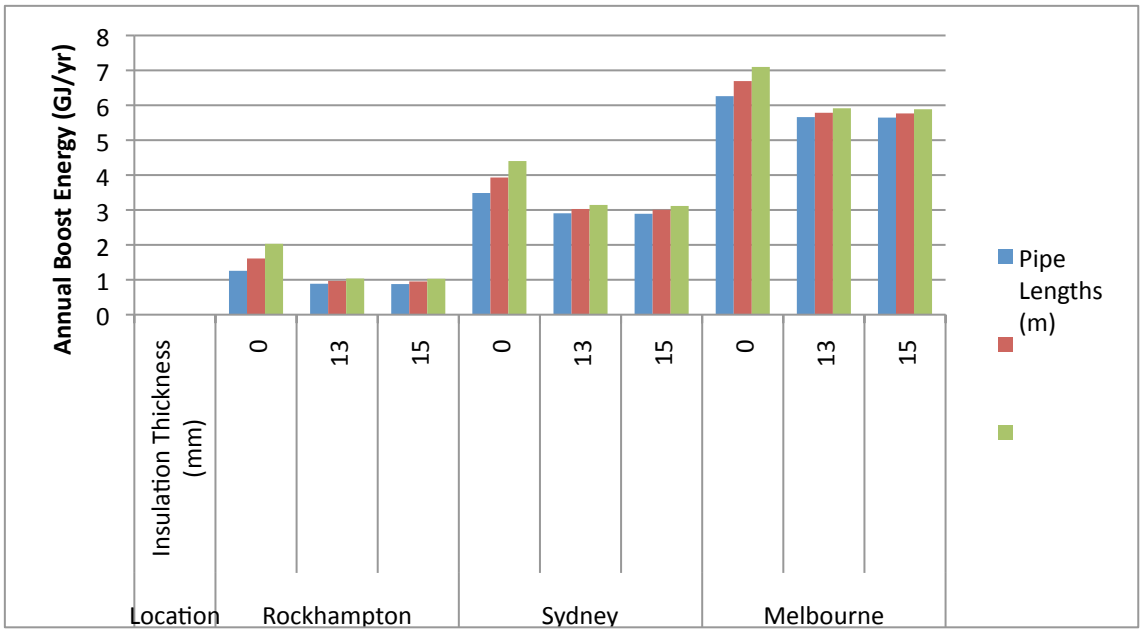

Figure 2 – Annual Boost Energy for varying Insulation Thickness (0, 13 & 15mm) and Pipe Lengths (10, 15 and 20m) for 3 Sites

Explanations of aspects of tables 1 and 2 are as follows:

- Losses from the tanks depend on the water temperature and ambient conditions. Both pipe insulation and improved collector performance from evacuated tubes collectors increase the pipe temperatures and tank water temperatures in the top of the tank, increasing losses from both the pipes and tank. This can be seen for Melbourne by comparing the pipe losses, tank losses and boost energy for flat plate and evacuated tube collectors.

- As the pipe losses decrease, the tank losses increase a little due to higher water temperatures. However, the boost energy savings do not reflect the full savings from the decrease in pipe losses. This is because the table does not show the full heat balance including losses from the collector. These increase as the collector inlet water temperature increases, due to higher tank temperatures, for the same ambient conditions.

- The solar contribution and the number of Renewable Energy Certificates (RECs), not shown in the tables, improved with pipe insulation for all climate zones. This was to be expected as energy was being saved and the solar systems were performing better overall.

- For electrically boosted systems, the evacuated tube collector systems performed marginally better due to higher collector efficiencies at higher water temperatures associated with in-tank boosting. For gas instantaneous boosting after the tank, the flat plate collectors performed marginally better due to higher collector efficiencies at lower water temperatures.

- Even with high loads and low solar contributions, the absolute energy savings were significant as collectors are more efficient at lower average tank water temperatures.

- Annual tank losses were lower in gas boosted systems due to lower tank temperatures, but overall boost energy requirements are higher due to losses in the gas booster.

- Energy used by the circulation pump and controller was listed separately as electrical energy. This was in the range of about 0.23 to 0.73GJ per year. Pipe insulation reduced pump run time a little in all but the coldest climates.

- In very cold climates, pump energy increased due to the pump running for longer times to prevent freezing in the collectors and pipes.

CONCLUSIONS

The following conclusions can be drawn from the results above.

- Energy savings from pipe insulation are very significant, even in mild climates such as Rockhampton. Across all climates zones, savings ranged from 0.16 to 3.5GJ per system per year, or about 2 to 23 percent of the annual load.
- For colder climates such as Melbourne (Climate Zone 4) with the worst case of 20 metre pipe runs, energy savings of between 1.2 and 2.4GJ per year per system were achieved. This is equivalent to between about 9 and 12 percent of the annual average load. This would increase with increasing system size and solar contribution as pipe water temperatures would be higher on average. For milder climates such as Rockhampton (Climate Zone 1), energy savings were also very significant, and range between 1.0 and 3.5GJ per year (about 10 to 23 percent of the load). The higher upper boundary in this milder climate was due to the high solar contribution and higher temperatures achieved by the solar collectors relative to ambient air temperatures in this climate zone. This resulted in higher pipe losses.
- There was very little advantage in increasing the insulation thickness from 13 to 15mm.
- For electricity at 19c/kWh and gas at 2 c/MJ, cost savings of between $27 and $100 per year were achieved across the climate zones. This would increase with increased system size and solar contribution in colder climates as heat losses would increase with higher solar contributions and water temperatures.
- The pipe insulation also improved the solar contribution (or fraction) and Renewable Energy Certificates (RECs), as well as giving small savings in circulating pump running costs in milder climates. Solar contribution increased by up to 23 percent points and RECs by over 7 in some cases.
- The study highlights the need to install and maintain the integrity of appropriate pipe insulation on solar water heaters over their life time in Australia and New Zealand.

REFERENCES

El-Nashar, A. (2006). Heat loss through the piping of a large solar collector field. Energy, Volume 31, Issue 12, Pages 2020-2035.

Heller, A. J. (2002). Heat-load modelling for large systems. Applied Energy Volume 72, Issue 1, Pages 371-387.

Hobbi, A.(2009). Optimal design of a forced circulation solar water heating system for a residential unit in cold climate using TRNSYS. Solar Energy Volume 83, Issue 5, Pages 700-714.

Lixing, G. (2007). A simplified hot water distribution system model. Florida Solar Energy Centre.

Marshall R. (1999). A generalised steady state collector model including pipe losses, heat exchangers, and pump powers. Solar Energy Volume 66, Issue 6, Pages 469-477.

Parker, G.J. (1981). The performance of a solar water heating system in a dwelling in Christchurch, New Zealand. Solar Energy, Volume 26, Issue 3, Pages 189-197.

Simpson, (1992). Measurements of heat losses from an insulated domestic hot water cylinder. Building Services Engineering Research and Technology. Volume 13, Page 43.

BRIEF BIOGRAPHY OF PRESENTER

Trevor Berrill has worked in the renewable energy industry for more than 30 years, as a researcher, system designer/installer, educator and in policy work. He is trained in mechanical engineering and has a masters degree (honours) in environmental education. He currently works as a private consultant in sustainable energy systems and undertakes research and teaching, part-time, at the Queensland University of Technology.

APPENDIX 1 - SYSTEM CONFIGURATION AND INPUT VARIABLES: PUMPED STORAGE (OR SPLIT) SYSTEMS

Storage tank

Volume = 270 L

Heat loss = 2.4 kWh/d

Auxiliary boost volume = 135 L

Electric Boost tariff = continuous

Pump

Flow rate = 2 L/min

Differential temperature controller 8 K ON, 2 K OFF

Maximum bottom temperature in tank = 60°C

Gas booster

Thermal efficiency = 80%

Heating capacity (gas input) = 180 MJ/h

Start-up loss = 0.5 MJ

Standby electric power = 7 W

Fan power = 40W

Set temperature = 60°C

Collector loop piping

Piping length = 10, 15 & 20m each way

Piping diameter = 12 mm

Insulation thickness = 0, 13 and 15 mm

Flat Plate Solar Collector

Aperture area = 4 m^2

Efficiency = 0.8 – 5 dT/G -0.02 $(dT)^2/G$

Equivalent thermal mass = 6 kg water

Evacuated Tube Solar Collector

Aperture area = 2.8 m^2 (30 tubes)

Efficiency = 0.687 – 1.505 dT/G -0.011 $(dT)^2/G$

Incidence angle modifiers

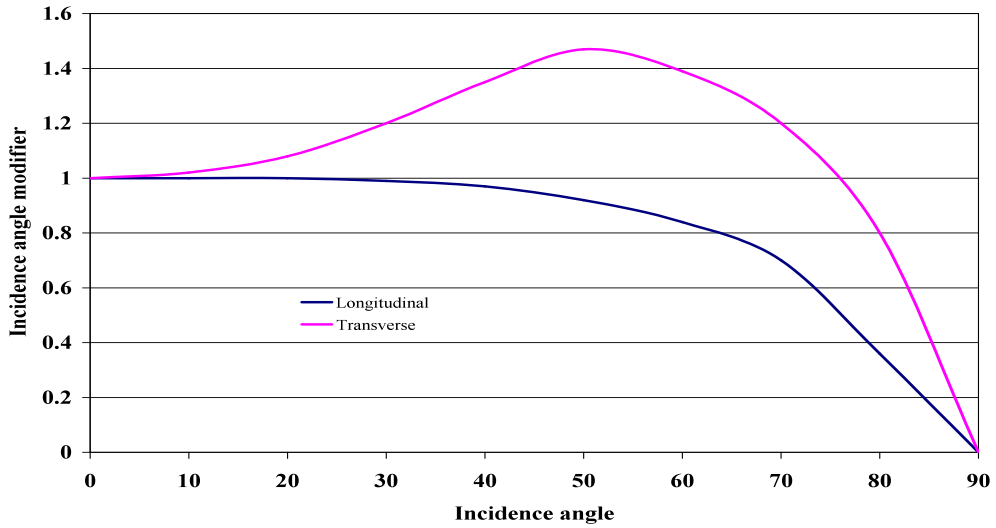

Equivalent thermal mass = 3 kg water

The maximum temperature for evacuated tubes is set by the water supply pressure. Steam may be generated in an evacuated tube collector during stagnation however this it is unlikely to become superheated. The maximum temperature would be 150°C for 5 bar supply pressure or 180°C for 10 bar pressure.

LOCATIONS

Alice Springs, Rockhampton, Sydney and Melbourne

Auckland and Dunedin

LOAD PATTERNS

AS/NZS4234 (Australia)

Time	7	8	11	13	15	16	17	18
Load	0.15	0.15	0.1	.1	0.125	0.125	0.125	0.125

AS/NZS4234 (New Zealand)

Time	6	8	10	12	14	16	18	20	22	23
Load	0.05	0.16	0.15	0.11	0.08	0.07	0.11	0.13	0.11	0.03

A Review of Heat-reflective Paints

John Pockett[1] and Martin Belusko[1]
[1]Sustainable Energy Centre
University of South Australia
Mawson Lakes SA5095
John.Pockett@UniSA.edu.au

ABSTRACT

In recent years, there have been a number of heat-reflective paints come on the Australian market. These provide the same visible colour range as standard products but perform quite differently in the infra-red region of the spectrum, reflecting more of the invisible part of the solar spectrum. Are they effective in meeting their advertised claims and if/when is there a benefit for their use? This paper reviews the advertising material and data to assess their value in a field where there is little sound scientific literature on some products and the technology of others is hidden for IP reasons.

Sunlight at ground-level incorporates incident radiation in the ultraviolet, visible and infra-red regions with wavelengths spanning 300 to 2500 nm. Any part of the solar spectrum where a surface absorbs incoming sunlight will cause an increase in surface temperature above ambient temperatures. If heat cannot be re-radiated to the sky, it will conduct through roof spaces towards the ceiling and radiate downwards through insulation batts. This produces a heat load on buildings, resulting in loss of comfort or an increase in electricity bills and greenhouse gas emissions for air-conditioning.

The main approaches used individually or in combination are to;

- select pigments to match visible colours using pigments that also naturally reflect more infra-red radiation,
- utilise hollow silica/ceramic microsphere additives that reflect the longer wavelength solar radiation and
- improve the ability to radiate any heat build-up out to the sky.

Attempts to simplify a complex situation for public consumption means advertising, comments and claims are often made that are technically incorrect. Measurements from some paint suppliers show not only the benefits of the paints but also claims of 'insulation' that are unsubstantiated and simply incorrect. Heat conduction through the paint layer actually plays an insignificant role compared to the total solar reflectivity and emissivity with lighter colours providing the best surface temperature reduction. It is also shown that the use of a heat reflective paint instead of a standard paint for a particular (visible) colour reduces the surface temperature. The benefits of heat-reflective paints are generally smaller for lighter colours and very small for pure white. Heat-reflective paints can attract a premium so there is a point where the added costs do not warrant use in moderate climate zones.

It can be concluded that the most cost effective solution for coating roofs of houses against the heat from sunlight is to paint the roof with a high build gloss Vivid White paint. In many cases, this is not practical because of the glare. The next best option is to start with as light as possible a colour and then to use one or another type of heat-reflective paint with high reflectance in the infra-red to minimise the surface temperature increase.

Keywords **heat-reflective, infra-red, paint, sunlight, surface, temperature**

BODY OF PAPER

Introduction

Heat-reflective paints have been available for fifteen years and are used to reflect the heat component of incident sunlight. They are a radiative barrier minimising surface heating rather than providing an insulating layer that reduces conductive heat flow. These paints can lead to a reduction of exterior surface temperatures, and heat load, on buildings, external electrical and electronic equipment, pipes transporting oil or water; insulated pipes used to transport refrigerated wine from one vat to another, insulated outdoor storage vats and hulls of ships. They are beginning to be used in industrial and architectural applications to give significant cost savings through reduced energy use for temperature control. They could contribute to reduced regional peak electricity generation capacity required for coping with air-conditioning on very hot summer days. They can also reduce greenhouse gas emissions caused by air-conditioning and urban heat islands.

This paper explains how many heat-reflective paints function and reviews some of the advertising material and claims in an area hardly covered in the relevant scientific literature.

Heat-reflective paints reduce the absorption of infra-red radiation at surfaces exposed to sunlight without changing the visible colour. Figure 1 plotted from an MS Excel spreadsheet (Renewable Resource Data Center, viewed 21/10/2010 shows the solar spectrum from 300 nm to 2.5 μm and highlights the portion visible to the human eye representing nearly half of the incident energy, with infra-red being most of the remainder.

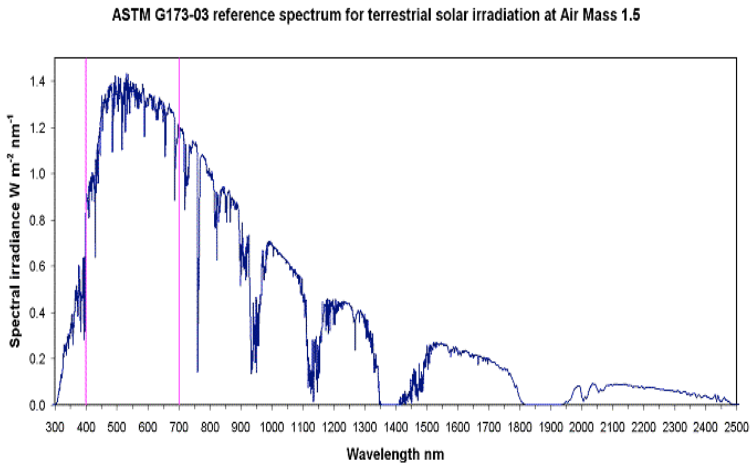

Figure 1 Solar Radiation Spectrum at Sea level showing ultra violet (<400 nm), visible (400 – 700 nm) and infra-red (> 700 nm) components including absorption bands for water, O_2 and CO_2 in the atmosphere. (Data plotted from Renewable Resource Data Center, viewed 21/10/2010.)

Radiation not reflected at various wavelengths across the spectrum is absorbed at the surface, leading to increased surface temperature. That increased surface temperature leads to a heat load on the building resulting in increased temperatures inside or increased energy useage to retain comfortable interior temperatures. It results in a greater stress on thermal insulation systems and also to increased radiaion passing directly through any insulation to the interior. If the reflectance at different wavelengths is weighted according to ASTM G173-03 (2008), the solar spectrum at ground level, a

single value of Total Solar Reflectance (TSR) can be derived. Reflected sunlight can be increased by increasing infra-red reflectance, and hence the TSR, without changing the perceived colour. Dark colours will still absorb strongly in the visible region contributing to higher surface temperatures than lighter colours with the same level of infra-red reflectance.

Surface temperatures are a function of the emissivity, a material property that determines the long wavelength infra-red radiation emitted from a surface. An emissivity of unity maximises this radiation, reducing excess surface temperatures. Many materials have an emissivity in the range 0.8 to 0.9 but bright metal roofs become very hot despite high reflectivity because the emissivity is low.

In 1908, Mie published a paper on light scattering from particles approximately the same size as their wavelength (Mie, 1908) which is quite different to the highly wavelength-dependant Rayleigh scattering from molecules in the atmosphere that lead to the sky's characteristic blue colour. Mie scattering depends upon the difference in refractive index (RI) of the scattering particle from the medium that light is traversing, the diameter of the scatterer and, to a certain extent, the wavelength of the light. From each Mie scattering there will be a range of angles where light is scattered and some will be scattered in a backwards direction.

An example of particles having higher RI than the medium is given with clouds. White light can be seen scattered out of the cloud from multiple water droplets or ice particles. It allows us to see the total volume of the cloud where there are Mie scatterers. Milk is another example with an oil-based emulsion in a water-based bulk. Light coloured paints with high reflectance in the visible spectrum have TiO_2 particles with high refractive index that also scatter infra-red light reasonably well.

In a standard paint formulation with 1 μm TiO_2 particles there will be approximately 11 percent backscattering efficiency at 450 nm (blue light) reducing to 1.6 percent at 2 μm infra-red wavelengths. Doubling the TiO_2 particle size boosts the infra-red backscattering at 2 μm wavelength to 4.4 percent (Prahl, viewed 17/6/2010).

It is also possible to select coloured pigments that have absorption in the visible spectrum giving their visible colour but with high RI in the infra-red and little absorption, allowing them to reflect much of the infra-red. It is also possible, as seen in Figures 2 & 3, to even create black paints and near black paints with judicious use of combined 'infra-red' pigments that absorb across the visible. This is done whilst reflecting moderately well in the infra-red instead of absorbing right across the spectrum like traditional paints based on carbon black pigment. An example of an Australian company with this approach is the Dulux/AcraTex range of InfraCOOL paints (Dulux, viewed 21/10/2010).

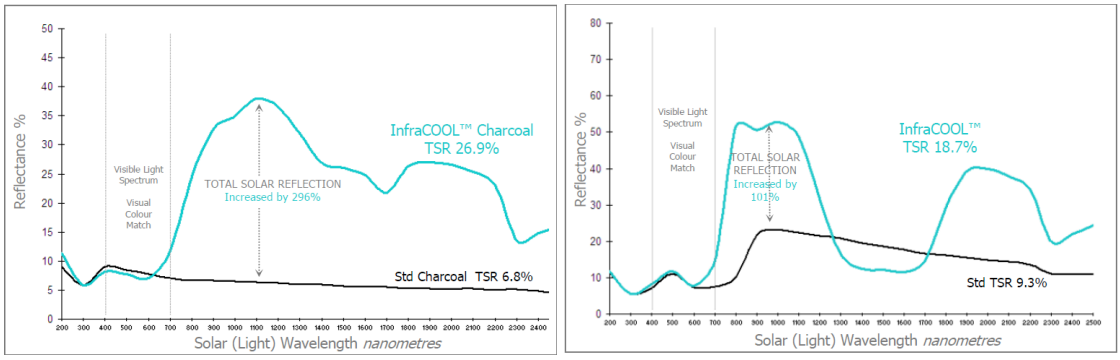

Figures 2 & 3 Standard Dulux and InfraCOOL Charcoal and Mid Brunswick Green paints demonstrating how pigment selection can lead to enhanced infra-red reflection. (test reports at Dulux, viewed 22/10/2010.)

An alternative situation, not often considered for Mie scattering, occurs when the RI of the 'particle' is less than that of the medium. Figure 4 provides an example of this, where microscopic air bubbles are entrained in water. We can see through the water to the milky volume, where the small underwater bubbles are reflecting ambient light towards the viewer. Similarly, studies have been made of light scattering from small bubbles in water-based bioreactors (Berberoglu *et al*, 2007). These examples with water are similar to the effect achieved in the infra-red for paints that include hollow microspheres with the paint medium as the bulk material.

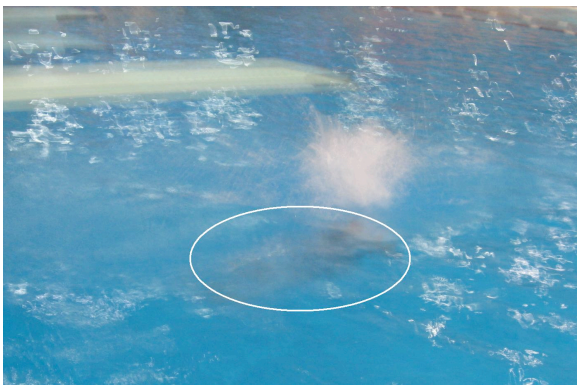

Figure 4 Highlighted milkiness obscuring the diver beneath her entry point in the water, is caused by Mie scattering of fine air bubbles reflecting ambient light. The medium has a refractive index of 1.3 and the bubbles a refractive index close to 1.0.

One approach for creating a heat-reflective paint is to add hollow microspheres that do not scatter light in the visible spectrum but scatter effectively in the infra-red region (Dombrovsky, 2005), (Dombrovsky, *et al*, 2005), (Dombrovsky, *et al*, 2007). In the US, there are several companies producing hollow microspheres including INSULADD, Hy-Tech and 3M. The first two of these are spinoff companies from NASA projects but have no relationship to the technologies and mechanisms for space shuttle tiles. In Australia, the microsphere additives appear to be dominated by INSULADD and Thermilate which both come from the same source. An example of a company using the INSULADD/Thermilate approach in Adelaide is Acryloc's additive products (Acryloc, viewed 20/10/2010) plus their roof formulations (Acryloc, viewed 19/10/2010). Acryloc imply in their documentation that they combine the 'infra-red pigment' approach with the microspheres for their tinted colour formulations.

Another approach is to formulate the paint combining one or both of the above two methods while making sure that emissivity is high in the 8 to 13 μm wavelength region. There is a transmission window in the atmosphere that is relatively independent of the

moisture level such that heat can effectively be removed from the surface, and even the whole building, by radiative transfer processes. The broad peak for black body radiation at surface temperatures between –10 °C and +100 °C lies in this region and extends from wavelengths of 3 μm to 40 μm. An example of an Australian company that uses this approach is SkyCool. (SkyCool, viewed 24/05/2010), (Wojtysiak, 2002). SkyCool is a highly reflective white paint combined with a claimed high emissivity of 0.94. This is claimed to have reduced air-conditioning costs in a southern Queensland supermarket by 40% p.a. (Davidson, 2004) but in cooler climates would increase winter heating. The Wojtysiac patent above only refers to selective emissivity in the 8 to 13 μm region achieved, at least in part, with hollow microspheres but does not describe the mechanisms for enhancing emissivity. It is known that at least one other heat-reflective paint manufacturer chemically formulates the paint medium to enhance emissivity.

ASTEC, who produce the Energy Star range of paints (ASTEC, viewed 19/10/2010), will not divulge the technical approach they take for IP reasons but claim (ASTEC, 2010) that it is a radically different approach in optimising IR reflectance to the above methods.

Heat-reflective paints rely on maximising reflection of the whole solar spectrum at the surface. This requires minimising any absorption and therefore any contaminants trapped at the surface that absorb the solar radiation. A gloss surface will more likely have contaminants washed off by rain or blown away than for a matte or low-sheen paint that can trap absorbing particles in surface crevices over time and lower solar reflectance. Products such as ASTEC's Dirtguard and the Dulux InfraCOOL range, have been chemically formulated to ensure low dirt pickup over an extended period. Generally a thicker layer is required to produce a layer opaque to infra-red radiation because of less efficient scattering at the longer wavelengths. A 'membrane' having a thickness of 150 μm or more would typically be required for a heat-reflective paint.

Advertising

It is difficult to advertise to non-technical people about infra-red, heat radiation as distinct from heat conduction and, in particular, about effects that are dependent upon emissivity. As a result, the advertising explanations are often not technically correct as to how these paints function.

Much of the advertising for paints with hollow microspheres incorrectly state or imply that the paints function as an insulating layer (Hy-Tech, viewed 20/10/2010) with the hollow microspheres acting as 'thermos bottle'-like cells (Hy-Tech, viewed 21/10/2010) with empty interstitial volumes. A similar idea is found in cartoons for INSULADD (INSULADD, viewed 20/10/2010). Paint layers containing more than 40 percent total volume of pigments and microspheres would have insufficient cohesion to be a viable layer against abrasion and would not provide corrosion protection. The thermal conductivity through a thin membrane made of microspheres, pigment particles and paint medium will be almost identical to that of a similar thickness of a layer without the microspheres. Even high quality thermal insulation batts which are almost entirely made of void require 50 to 150 mm thickness to achieve good thermal insulation. The heat reflecting paint layers have only a small proportion of voids and are usually well under 1 mm in thickness. It is not possible for a properly formulated heat reflective paint containing hollow microspheres and forming a cohesive, integral layer of less than 1 mm thick to act as an effective thermal insulator. Despite advertising material to the contrary, thermal conduction plays an insignificant role compared with the importance of Total Solar Reflectance and emissivity in minimising temperature build-up.

The Australian-based Heat Reflective Paints website (Heat Reflective Paints, viewed 21/10/2010) provides some information about brands such as ASTEC, DuroBond, NuTech, ShieldCoat and SolaCoat. The website expresses disappointment in the way some of the paints and additives are marketed with such technical inaccuracies.

Comparisons with conventional paints

Reflectance spectra given in advertising with any resulting TSRs and temperature increases calculated to the ASTM E903/C-1549 standards should be able to be trusted. Specific temperature differentials where the paint company has done correctly instrumented tests under outdoor conditions may well provide useful comparisons but tests done under infra-red lamps will grossly exaggerate the benefits of heat reflective paints. Generalised advertising claims by manufacturers that their paint will lower room temperatures by a given number of degrees should be ignored because of the complexities involved.

INSULADD provide comparisons as seen in Figure 5 (INSULADD, viewed 21/10/2010). They show lower surface temperatures of INSULADD white paint compared with other paints and materials for Central Texas in August (Summer) with an ambient of 33 °C in clear sunlight. These tests clearly demonstrate the benefits of the white, heat-reflective paint over the other alternatives for the particular testing regime chosen.

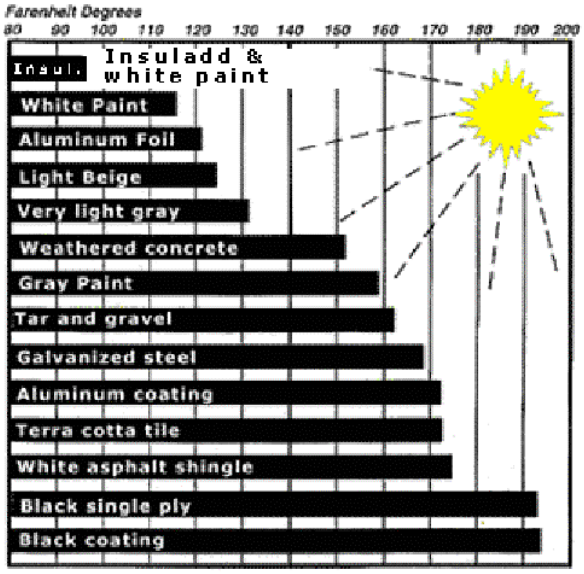

Figure 5 Temperatures (°F) of coatings and other materials in August sunlight conditions in Central Texas in at an ambient of 90 °F (33 °C) and a clear sky (from INSULADD, viewed 21/10/2010).

In Figure 6, is shown the reflectance comparison by ASTEC of a conventional black paint with their Energy Star Black (ASTEC, viewed 19/10/2010). Whilst there are large infra-red reflectance gains at wavelengths over 1000 nm, it should be remembered from Figure 1 that there is a major part of the incident infra-red from sunlight between 700 nm and 1000 nm. A truly effective heat-reflective black paint would rise sharply in reflectance to high values at wavelengths very close to 700 nm with greater TSR effect.

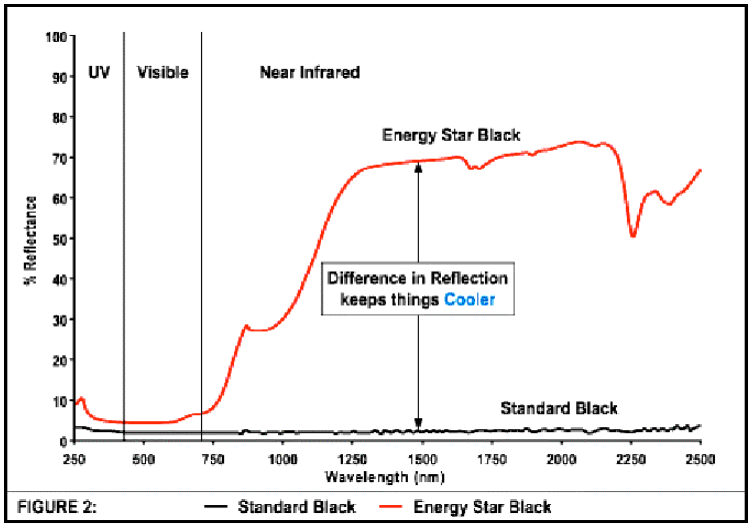

Figure 6 ASTEC comparison of their heat reflective Energy Star Black with a standard black paint demonstrating substantially increased infra-red reflectance at wavelengths above 1000 nm (ASTEC, viewed 19/10/2010).

A comparison of reflectance for conventional and heat-reflective Off White paint from ASTEC data (ASTEC, viewed 19/10/2010) is portrayed in Figure 7. This shows less advantage in infra-red reflectance for Energy Star paint over standard paint when compared with Figure 6 for a black colour. Between 90 and 95 percent of pigment in a standard off-white colour will be TiO_2 and that already scatters strongly in the infra-red, leaving less room for improvement in infra-red reflectance when using Energy Star paint.

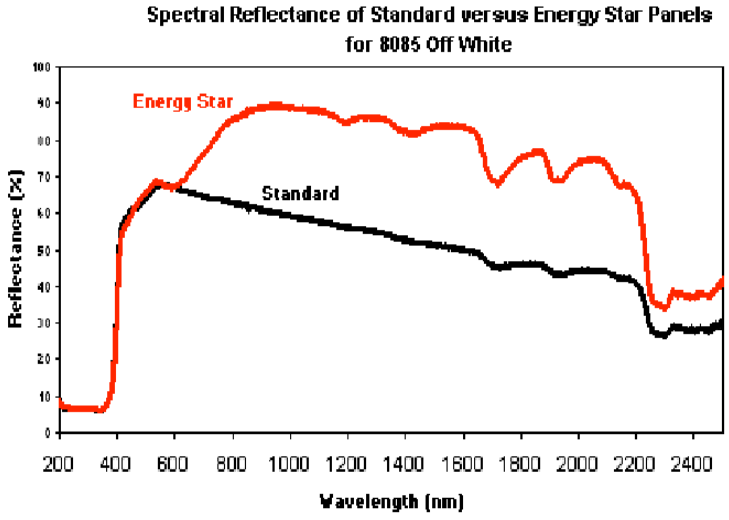

Figure 7 ASTEC comparison of their heat reflective Energy Star Off White with a standard off white paint demonstrating substantially increased infra-red reflectance at wavelengths over 800 nm.

Information on TSRs to ASTM C-1549 was plotted from ASTEC's data (ASTEC, viewed 20/10/2010) and is shown in Figure 8. It demonstrates that TSRs can be improved by up to 31 percent for dark colours reducing to 4 percent for pure white.

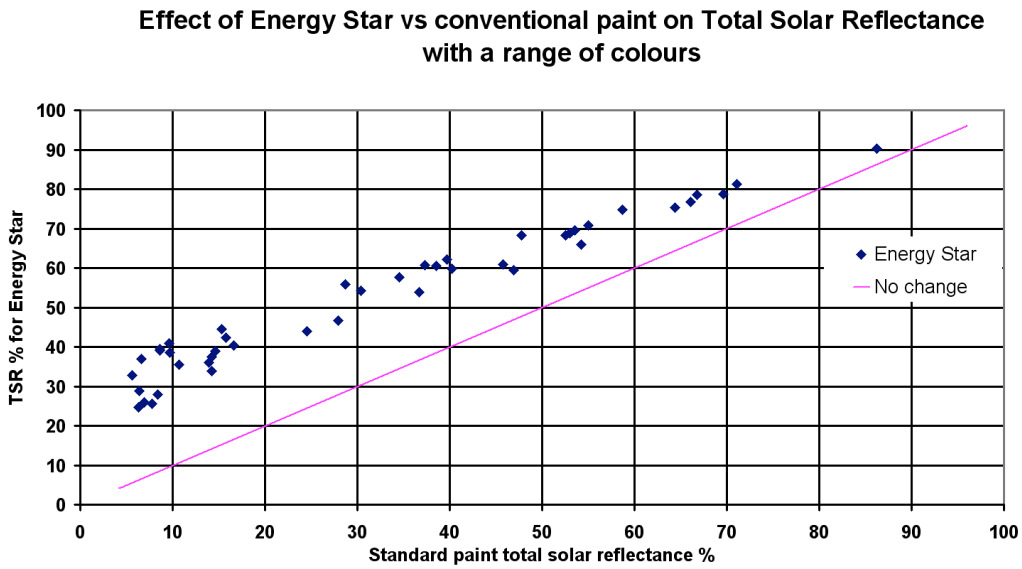

Figure 8 Comparisons between heat reflective and conventional paints compiled from ASTEC data (ASTEC, viewed 19/10/2010) and graphed with MS Excel. These show increased TSR for Energy Star versions of the same colours.

Some of the colours in the ASTEC website material also had information about surface temperatures in sunlight where surface temperatures are calculated to ASTM E903/C1549 for low wind conditions. Low wind conditions are chosen because these are the worst conditions for heat buildup and often very hot days have low wind conditions. Dulux/AcraTex had similar information available to ASTM C-1549 based on their TSRs for standard Dulux and their InfraCOOL paints so these can be directly compared with the ASTEC data. Plots were made in MS Excel for the conventional and heat-reflective versions of colours from the data available from both companies. These are presented in Figure 9 and provide an interesting insight into the importance of TSR to the surface temperatures in sunlight according to the ASTM calculations. The plotted data based on ASTM calculations for low wind conditions directly show that the higher the TSR, the lower the surface temperature is. They also show clearly that there is very little difference between conventional and heat-reflective paints in terms of surface temperature once TSR is taken into account. The major factor affecting surface temperature is the TSR, with emissivity being of lesser importance.

Unfortunately there was no data available from Acryloc or SkyCool on TSR data and resulting temperature rises calculated to the relevant ASTM standards. These products incorporated hollow microspheres.

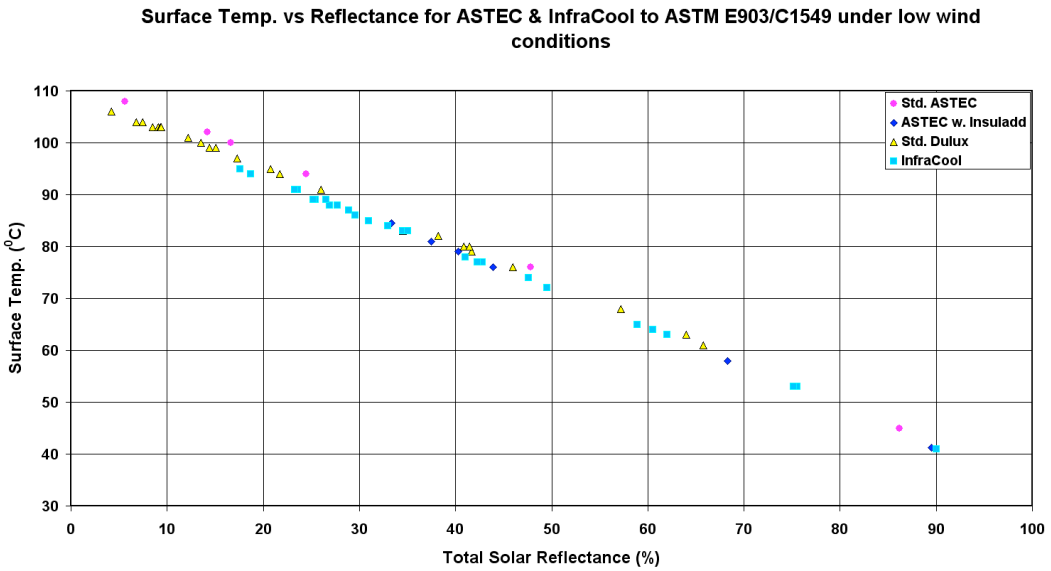

Figure 9 Demonstrating the direct influence of TSR with various colours on the surface temperature and the relatively small effect of whether the paint was a heat reflective or a conventional one and based on ASTM C-1549 low wind calculations. This graph was plotted from ASTEC and Dulux data.

Amongst the Dulux standard and InfraCOOL paints (without microspheres) there is a slight difference with standard paints a degree or so higher in temperature, most likely due to the lower emissivity of standard paints at 0.85 as compared with 0.9 for the InfraCOOL which has been formulated to better emit absorbed heat. The ASTEC heat-reflective paints with emissivity of 0.88 fall between both Dulux paint types in temperature rises. ASTEC heat-reflective white performs nearly to the same as the InfraCOOL white.

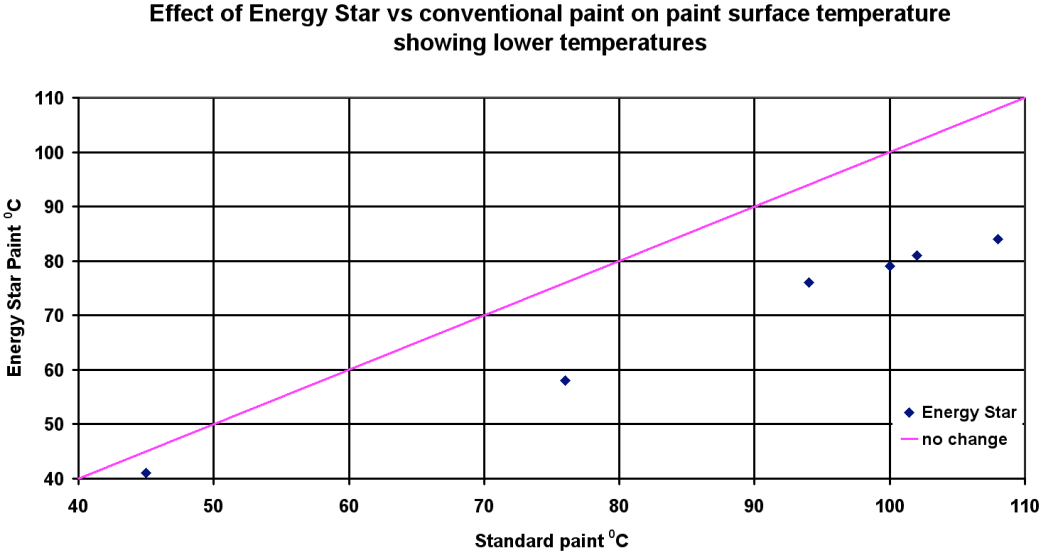

Figure 10 Reductions in surface temperature for a range of colours as plotted from ASTEC data based on the ASTM calculations.

The effect of reducing surface temperature for heat reflective paints is shown in Figure 10, which compares ASTEC temperature data for a range of coloured paints in standard and Energy Star paints as calculated by ASTM methods. The effect is smaller (4 °C) for

pure white paint than for darker coloured paints (24 °C). This raises the question as to the benefits gained for the added expense in opting for heat-reflective white paint.

In Table 1 (scanned from Acryloc brochure, 2008), Acryloc provide surface temperature reductions in a Roofcote brochure comparing their heat-reflective Roofcote (with Thermilate) to their standard equivalents of the same nominal colour when placed under infra-red lamps. These lamps do *not* reproduce the solar spectrum and exaggerate the temperature differences compared with summer sunlight or lamps correctly simulating the solar spectrum (and having an intensity of 1 kW/m^2.at the test sample). Temperature differences in sunlight would be much less since half the energy in sunlight is in the visible part of the spectrum and the two versions of the same 'colour' will be absorbing the same amount of energy in the visible region. ASTEC (ASTEC, viewed 21/10/2010) presents an Amdel report, 05MAAD10444 Part 1, that gives surface temperatures from 41 to 90 °C under low wind conditions and an ambient of 27 °C calculated for ASTM E1980-01. If this is compared with Acryloc's extreme temperatures of 81 to 136 °C for their heat-reflective paints under infra-red lamps, then the overall trends are similar to ASTEC data but the magnitude is exaggerated. Darker colours, in both cases, will benefit much more than lighter ones from the use of the infra-red reflecting paints but they come from an unfavourable starting point. They are also similar in that pure white heat reflective paint will only provide a slight benefit to using a conventional white paint.

Table 1 Acryloc comparison of surface temperatures with the heat reflective Roofcote products based on Thermilate compared with Acryloc's standard products under infra-red lamps. The effects under sunlight would not be as good.

Colour	Cooler than CRC Equiv by
Arctic White	3°
Blue Ridge	16°
Brunswick Green	-
Bushland	
Charcoal	22°
Classic Cream	13°
Cottage Green	40°
Deep Ocean	15°
Dune	
Headland	15°
Ironstone	39°
Jasper	37°
Manor Red	19°
Night Sky	36°
Pale Eucalypt	
Paperbark	25°
Plantation	28°
Sandbank	29
Shale Grey	26°
Sienna Clay	14°
Stone	29°
Surfmist	
Wheat	31°
Wilderness	27°
Windspray	29°
Woodland Grey	17°

Cost Implications

Using a heat-reflective paint does come at a cost premium to a conventional paint. For example, in Adelaide in 2008, the quote for high pressure water cleaning of 50 m^2 of a weathered, galvanised iron roof followed by priming and two coats of Vivid White gloss acrylic paint was $1000 whilst the same process with topcoats of Acryloc heat-reflective paint using Thermilate was $1400 using the same contractor. There was a

similar differential with ASTEC heat-reflective paint. The additional cost to a $3000 professional job in painting a 180 m^2 house roof with Dulux InfraCOOL rather than standard paint would be $500 to $1000.

The cost differential for critical industrial applications, where there are aesthetic or local government colour restraints or for extreme climates such as Darwin, or elsewhere in far northern Australia, may well make it worth while to opt for the more expensive heat-reflective paint option.

Conclusions and recommendations

Advertising of heat-reflective paints often refers to insulation properties; however, restricting heat flow through paint films is not a significant part of the benefits of heat reflective paints. The predominant factor reducing solar heat load on buildings etc. is the Total Solar Reflectance of the exterior surface and not thermal conductivity, but emissivity does play a small role. There is a lack of technical accuracy in much advertising material.

The most cost effective solution for non-critical applications is using two coats, for infra-red opacity, of a conventional gloss white acrylic paint over an appropriate primer to reflect heat and reduce the heat load from sunlight. Gloss paint is recommended to minimise dust and dirt collection. It is preferable to spray the gloss paint wet to attain the smoothest surface possible that will not quickly capture dirt and dust.

If the application is critical, such as coatings over insulation around piping carrying refrigerated fluids, or in extremely hot climates, then optimal solar heat reflection can be attained with a heat-reflective version of a pure white paint.

If architectural or aesthetic reasons eliminate the use of a pure white paint because of the glare, then as light as possible coloured paint should be used. The paint should be heat-reflective to ensure that as much infra-red as possible is reflected at the surface and reduce the heat load on buildings and pipework.

References

Acryloc, viewed 19/10/2010, *Acryloc Roofcote Supa Cool incorporating Thermilate,* <http://www.acryloc.com.au/cgi-bin/products.cgi?category=%22Roof%20Membranes%22>.

Acryloc, viewed 20/10/2010 *Thermilate Additive Pack,* <http://www.acryloc.com.au/cgi-bin/image_popup.cgi?image_name=/products/images/16100.jpg>.

ASTEC, 2010, personal telephone discussion with the Managing Director, Mr. Mark Waters .

ASTEC, viewed 19/10/2010, *How do They Work ?,* <www.astecpaints.com.au/energystar/how_do_they_work.htm>.

ASTEC, viewed 21/10/2010, *Slar Reflectance Index Test Reports – Energy Star EC-100 Dirtguard*, .< http://www.astecpaints.com.au/energystar/downloads/sri/ec100_dirtguard.pdf >.

ASTEC, viewed 20/10/2010, *TSR Test Reports to ASTM C-1549,,* <via www.astecpaints.com.au/energystar/about_energystar.htm >.

ASTM G173-03, (2008), *Reference Solar Spectral Irradiance: Air Mass 1.5,* American Society for Testing and Materials.

Berberoglu H, Yin J, Pilon L. (2007) *Light transfer in bubble sparged photobioreactors for H_2 production and CO_2 mitigation* Peer Reviewed, Permalink <http://escholarship.org/uc/item/4g62323h>.

Davidson S. (2004) *SkyCool – extraordinary paint on a hot tin roof,* ECOS (CSIRO publication), Issue **119**, Apr-Jun 2004, p. 12

Dombrovsky L. (2005), *Modeling of Thermal Radiation of Polymer Coating Containing Hollow Microspheres* High Temperature. Vol. **43**, No. 2, pp. 247–258. Translated from Teplofizika Vysokikh Temperatur, Vol. **43**, No. 2, 2005, pp. 256–266.

Dombrovsky L., Randrianalisoa J. Baillis D. Pilon L. (2005) *Use of Mie theory to analyze experimental data to identify infrared properties of fused quartz containing bubbles.* <http://www.escholarship.org/uc/item/96w8k08s> Peer Reviewed Permalink.

Dombrovsky L. Randrianalisoa J. & Baillis D. (2007) *Infrared radiative properties of polymer coatings containing hollow microspheres* International Journal of Heat and Mass Transfer **50** 1516–1527

Dulux, viewed 21/10/2010 *Dulux AcraTex 962 Cool Roof,* <http://www.dulux.com.au/specifier/our-brands/dulux-acratex/products/roof-restoration/high-build-membrane/product-detail?product=7365>.

Dulux, viewed 22/10/2010, test reports at *InfraCOOL Heat Reflective Coating Technology*, < http://www.dulux.com.au/specifier/our-brands/dulux-acratex/infracool/infracool-information>.

Heat Reflective Paints, viewed 21/10/2010, *Compare Brands*, <http://www.heatreflectivepaints.net.au/Compare-Brands>.

Hy-Tech, viewed 20/10/2010 *How Ceramic Paint Saves Energy*, <http://www.ceramicadditive.com/conduction_heat.html>.

Hy-Tech, viewed 21/10/2010, *Insulating Ceramic Microspheres What they are and how they make paint Insulate,* <http://www.ceramicadditive.com/work.html>.

INSULADD, viewed 21/10/2010, *How It Works,* <http://www.insuladd.com/howitworks.html>.

INSULADD, viewed 20/10/2010, cartoon in *History,* <http://www.insuladd.com/insulating-paint-history.html>.

Mie G., (1908) *Beiträger zur Optiek trüber Medien, speziell kolloidaler Metallösungen* Annalen der Physik Vierte Volge 25, 3, 377-445 in German and translated to English by Crossland, Barbara in 1976 to *Contributions to The Optics of Turbid Media, Particularly of Colloidal Metal Solutions* for the Royal Aircraft Establishment Library

Prahl, viewed 17/6/2010, *Mie Scattering Calculator* with 1 μm TiO_2 particles of RI =2.68 in medium of RI=1.5 calculated at <http:// omlc.ogi.edu/calc/mie_calc.html>.

Renewable Resource Data Center, viewed 21/10/2010 *Reference Solar Spectral Irradiance: Air Mass 1.5 – downloaded MS Excel spreadsheet,* <http://rredc.nrel.gov/solar/spectra/am1.5/>.

SkyCool, viewed 24/5/2010 , *SkyCool - In the business of Cooling Buildings,* <http://www.skycool.com.au/>.

Wojtysiak C. S., (2002) *Radiative cooling surface coatings.* Australian Patent Application no. 20023002117.

BRIEF BIOGRAPHY OF PRESENTER

John Pockett has had a broad career mainly in industrial R&D, process/product improvements and data analysis across a range of industries, leading-edge technologies and working across engineering and scientific disciplines. He has worked in areas such as paint, medical equipment, electronics, ophthalmic, laser, printing, photovoltaics, electrophotography and biofuels. He has had practical experience in independent research. Innovations have led, amongst other things, to patented IP and IP utilised as Trade Secrets. He has been employed in organisations such as Dulux, Optische

Industrie, Philips, Adelaide University, SOLA Optical, Research Labs of Australia, Uni. of SA, Flinders Uni, and carried out consultancy work in John Pockett & Associates. His original BSc in Physics and Maths was supplemented in recent years by a PhD in Materials Science (Polymer Chemistry) on a part-time/full-time basis whilst continuing with his consultancy work.

In the last three years, he has also played a part-time role in University of South Australia's Sustainable Energy Centre as an Adjunct Senior Research Fellow working on projects with other researchers and students. These projects include retrofitting vehicles to make them hybrids, phase change materials, roof insulation, radiative cooling and heat-reflective paints.

He is a Fellow of the Australian Institute of Physics, a Chartered Chemist member of the Royal Australian Chemistry Institute, a member of the SA Committee for the Australian Solar Energy Society, a member of the Organising Committee for the recent Chemeca2010 conference and is currently Chair of the Joint Chemical Engineering Committee in SA.

Valuation of Renewable Energy Storage Capacity

Trevor Jack[1], Robyn Bateup[2], Vernie Everett[3]
Author affiliation:
[1]Jack Actuarial Consulting Pty Ltd
[2]Bateup Actuarial + Consulting Services Pty Ltd
[3]Centre for Sustainable Energy Systems
Australian National University, Canberra, Australia

Corresponding author: vernie.everett@anu.edu.au

1 Background

A large proportion of the public does not accept the likely viability of utility scale solar power because "…I want electricity when the sun doesn't shine…".

The need for storage is evident and there are many potential, and some realised, solutions. This paper investigates the gross value of storage capacity. The value is assessed from different viewpoints. These different viewpoints are essentially a commercial investor's view and a public policy view where in the latter case the focus is on carbon pollution reduction.

Two storage technologies are considered. Firstly, thermal storage integrated with a Concentrated Solar Thermal (CST) generator. Secondly, a generic storage/dispatch system which is characterised only by storage capacity, cycle efficiency and dispatch capacity. In this second case, the discussion is framed around pumped hydro – but other current technologies, other technologies in development or possibly as yet unconceived technologies that can be characterised, at a high level, in these terms would also be covered by the approaches considered in this paper.

The cost of developing/constructing the modelled storage capacity is not considered.

The calculations in the paper focus on determination of annual generator income and carbon abatement which can be attributed to storage capacity. The generator income is based on current pricing and hence, by definition, on the current grid structure. The uncertainties around future wholesale pricing trajectories, and all other aspects of the wholesale electricity market, are so great as to make capitalisation of annual values by simple annuity factors somewhat meaningless. Nevertheless, given the range of viewpoints that are considered, approximate capitalisation/annuity factors which may be appropriate to these different viewpoints are considered in section 4. All values presented in this paper are not capitalised.

2 CST with thermal storage

2.1 Methodology

The approach adopted was to build a very simple model of a utility scale CST generator, with storage capacity, and optimally dispatch energy to the NEM. The only parameters of the design are the solar multiple (SM) and reservoir capacity. The SM is the electrical equivalent energy capture capacity, relative to the generator capacity. Taking all figures relative to a 1MW generator, a solar multiple of 2 would indicate that the solar field could deliver 2MW(e). The size of the (thermal) reservoir is expressed in the number of hours that it could supply the generator. So a 4 hour reservoir at a 1MW plant has a capacity of 4MWHr(e).

For each combination of reservoir capacity and solar multiple examined, the assessment is done over the 35,000 half hour dispatch periods during 2008 and 2009. For each design combination, the value of storage is calculated as the difference between the incomes received for a generator with storage, using a dispatch algorithm that optimally allocates energy from the collector field to dispatch or storage, and that for a generator without storage.

Consider a simplified example where there are just two periods, rather than the 35,000 actually modelled. The two periods are at 2pm and 8pm on a day with reasonable insolation. The units for energy collected, dispatched, stored and dumped are MWhr(e). The RRP is $/MWhr from 10 July 2009 (chosen somewhat randomly) and the value is the product of the RRP and energy dispatched.

TABLE 2.1

Calculation of value of storage

	Energy collected	Dispatched	Stored	Dumped	Price (RRP)	Value
Generator without storage						
2pm	1.6	1	0	0.6	$24.0	$24.0
8pm	0	0	0	0	$36.1	$0.0
Income to generator without storage:						$24.0
Generator with storage						
2pm	1.6	0.6	1	0	$24.0	$14.4
8pm	0	1	-1	0	$36.1	$36.1
Income to generator with storage:						$50.5
Value of storage capacity:						$26.5

The overall model uses the same insolation and energy conversion models as are used in Jack et al. The results presented here are for a notional CST generator at Roma in SW Qld and RRPs are for Queensland.

2.2 Commercial view

This section considers the average value of the specified storage capacity over a period of a year from the perspective of a commercial investor. That is, we consider the value arising from selling into the wholesale electricity market at market prices. There are some surprising results. Recall that the model uses data for two years, namely 2008 and 2009.

2.2.1 Value based on NEM RRP

Many of the results from this analysis will be presented in a table of the following form where the value, in this case over a year using NEM RRP, is shown for each combination of Reservoir and SM modelled. The hypothetical CST generator has a 1MW generating capacity.

TABLE 2.2

Annual value of storage ($000)

Reservoir (hrs)\SM	1	1.5	2	2.5	3
2	24	26	28	28	29
4	28	38	46	47	48
8	28	40	65	73	76
12	28	40	68	86	92
16	28	40	68	89	98

An alternative view would be the value over a year per MWhr of storage capacity:

TABLE 2.3

Annual value of storage per MWhr ($000)

Reservoir (hrs)\SM	1	1.5	2	2.5	3
2	12.1	13.0	13.9	14.0	14.4
4	6.9	9.6	11.4	11.8	12.0
8	3.4	5.0	8.1	9.1	9.4
12	2.3	3.3	5.6	7.2	7.7
16	1.7	2.5	4.2	5.6	6.1

2.2.2 Low SM case

The annual value of storage for a solar multiple of 1 varies very little across reservoir sizes. This is not surprising. The energy available for deferral is clearly limited when the SM is 1. The high pricing periods typically only extend for a few hours. So whether one has 4 hours capacity or 8, the value from deferring relates only to a few hours.

With perfect long term forecasting, one might expect the higher reservoirs to show slightly better value in total (though not when expressed per MWhr of storage capacity) as deferral might be such as to cover a few evening peaks during a period when insolation was low. During a period of several days of low insolation, the small reservoir cases would not be replenished from one night to the next whereas the higher reservoir cases could defer sufficient from a period of good insolation to cover several evening peaks.

The current model does not allow for such perfect long term forecasting - so the higher reservoir cases would be exhausted over just one evening peak and the following night. A more sophisticated model allowing for better forecasting would, for this low SM case, be expected to show a marginally increasing storage value as a function of storage capacity.

2.2.3 Increasing value with higher SM

Clearly as SM increases, the annual value of storage increases. A high SM without a large reservoir is useless as much energy is dumped. A higher storage capacity allows deferral of dispatch until overnight. In these cases, the extra value simply comes from dispatching more hours in the day and not from targeting high price periods (though this is a direct consequence).

2.2.4 Decreasing returns to scale

The annual value per MWhr of storage capacity clearly decreases as a function of increasing storage capacity. The reason for this is essentially the same as described in Section 2.2.2. That is, the low storage capacity cases capture most, in many cases all, of the value of storage because the high price periods are short enough that only a small amount of storage is necessary in order to capture the full peak.

2.2.5 Monthly view

A monthly view of the value development is instructive. The SM=2 case is shown.

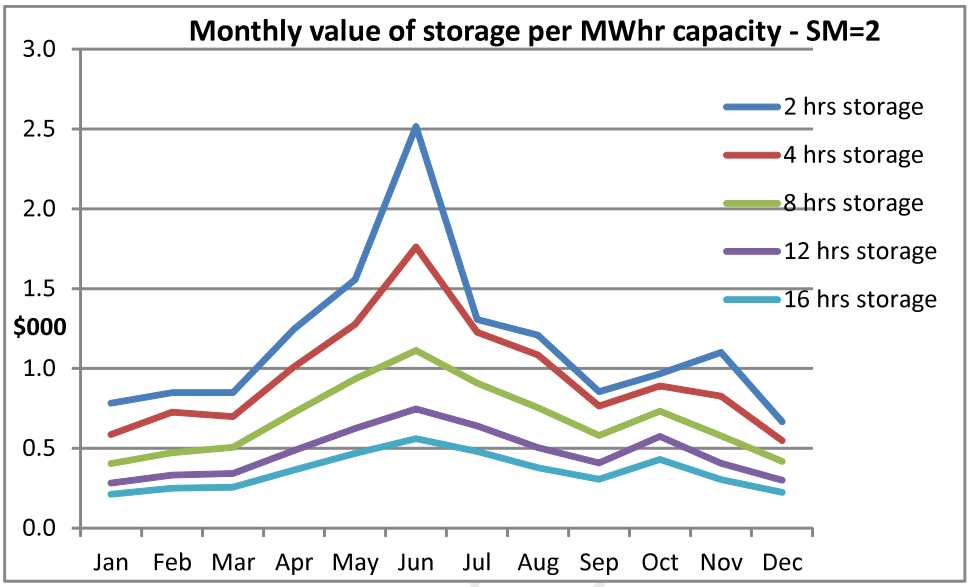

The winter peak, at least for the low SM cases, is not at all surprising. The value arising from deferral in summer is limited, particularly with a SM of 2. During the summer air conditioning peak periods, this SM would typically provide sufficient capacity to run the generator at maximum capacity without needing to augment from the reservoir. So, the value that is gained from storage arises only from deferral into the second peak of the day, which is much lower.

A reservoir would of course be valuable in the summer if the SM were only 1.

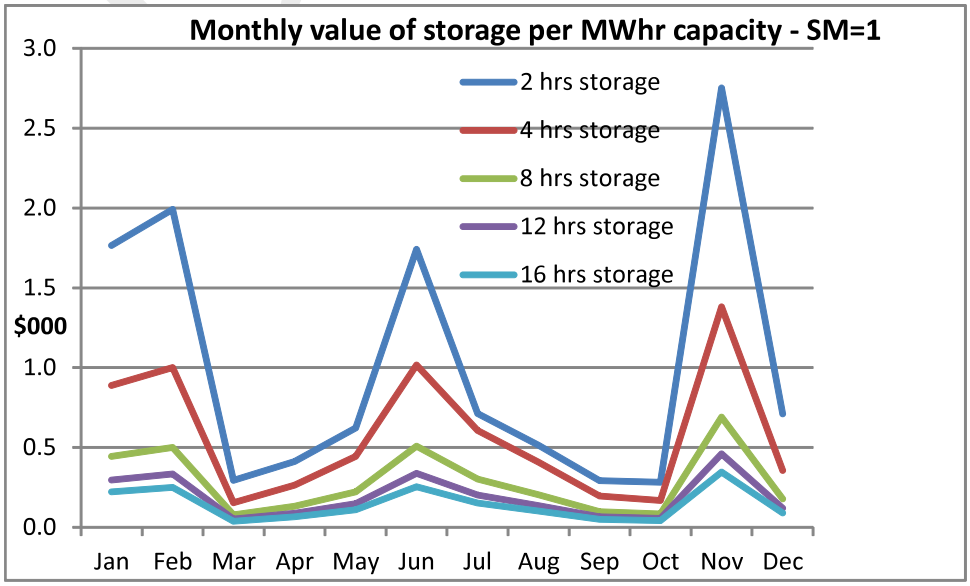

In this case, because of the extreme height of some summer peaks, there is considerable value in the reservoir enabling the generator to run at peak capacity rather than even slightly less than peak, due to insolation not being sufficient.

2.3 Value based on constant price (eg carbon offset value) – the community view

The previous section considered the value of storage when it enhances generator value by essentially deferring dispatch to high price periods. This is the appropriate approach for a commercial generator to take. However, other stakeholders with different viewpoints, for example government as the representative of the community as a whole, could value storage differently. For example, the effect of carbon pollution is not dependent on when it is produced – so the value of displacing carbon pollution by use of solar power is not dependent on the timing.

The value of displacing carbon pollution can be easily calculated. It is simply the additional energy dispatched by a renewable generator with storage capacity, compared to one without storage capacity, multiplied by the value of carbon displaced. Using, as an example, $40 per tonne for carbon and a carbon intensity of 0.75 tonne/MWhr, gives a value of $30 per MWhr.

TABLE 2.4

Annual value of storage per MWhr ($000)

Reservoir (hrs)\SM	1	1.5	2	2.5	3
2	0.5	3.9	4.9	5.1	5.4
4	0.3	3.2	4.9	5.4	5.7
8	0.1	1.9	6.6	8.1	8.6
12	0.1	1.2	4.5	6.5	7.1
16	0.1	0.9	3.4	5.1	5.7

Not surprisingly given the flat "price" over time, values are much smaller than those for the commercial view.

2.4 Long term storage

Long term (seasonal) thermal storage is not considered for CST as it is unlikely ever to be a realistic option.

3 Pumped hydro

3.1 Background

A critical aspect of a high solar penetration grid would be seasonal supply/demand mismatch. With a high solar penetration there would need to be deferral of excess generation in the summer to the winter periods when the solar resource is deficient. Pumped hydro is the obvious choice for this – though there may well be others.

A pumped hydro facility can be specified quite simply, for the purposes of this analysis, by its storage and generation capacity and cycle efficiency. For this model a cycle efficiency of 80% is assumed. The methodology used here relies only on these three parameters: generation capacity, storage capacity, and cycle efficiency. Storage capacity is, unless otherwise indicated, specified relative to a notional 1MW generation capacity.

3.2 Short term storage

First consider the short term case – essentially diurnal storage and generation.

3.2.1 Methodology

The methodology adopted for valuing storage of the character of pumped hydro requires choosing dispatch and charging periods. Each day is considered independently. The length of the dispatch period, assumed to be one contiguous period, is determined by the storage capacity and its timing is determined by pricing. Offset against the value of dispatch is the cost of charging the reservoir. For the cases discussed below (4 and 2 hours storage capacity), 5 and 2.5 hours of contiguous pumping is assumed – these lengths reflect the 80% cycle efficiency assumption. Charging periods are taken as 1am until 6am for the 4 hour reservoir case and 3am until 5:30am for the 2 hour reservoir case.

3.2.2 Results

For a generator with 4 hours storage capacity the pricing (Qld RRP) over 2008 and 2009 indicates a value for storage of $27,800 per MWhr p.a. For a 2MWhr capacity, the value is $41,100 per MWhr p.a.

As for the CST case, these figures are heavily seasonal:

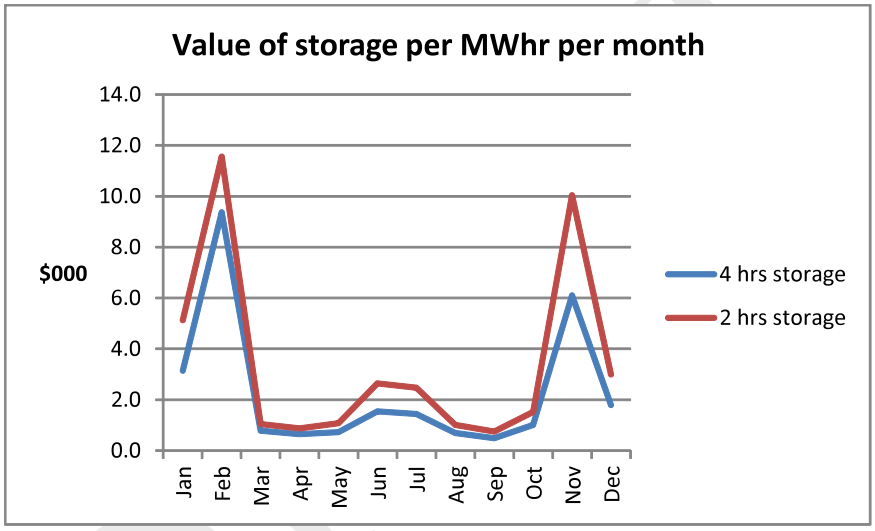

3.2.3 Constrained pricing

Much of the value assessed from the above methodology arises from a small number of dispatch periods with very high prices. For example, consider altering the above by limiting the RRP to $2,000 per MWhr (roughly 100 times a typical daily low price of $20 per MWhr). For the 4 hour capacity case this gives a value of $17,900 per MWhr p.a. (cf $27,800 above) and $26,100 per MWhr p.a. (cf $41,100 above)for the 2 hour capacity case.

3.2.4 Flat pricing – the community view

In the current environment, the marginal production that would be used to charge a pumped hydro facility would be from fossil fuelled sources – black coal in Queensland. This is likely to be the case for a long time. Accordingly, on the methodology employed in this paper, pumped hydro storage has a negative benefit to the community (ie negative contribution to carbon emissions) as 25% more carbon would be emitted, because of the assumed 80% cycle efficiency, using fossil fuelled charging.

In fact it would be more negative than this because pumped hydro production would likely displace gas fired peaking generators which have a lower carbon intensity than the coal that would be used to charge the pumped hydro.

3.3 Long term storage

In the current commercial context there is essentially no value in long term storage because of the absence of a price on carbon and, therefore, the existence of cheap electricity from fossil fuels.

If solar power were ever to provide a significant contribution to Australia's electricity demands there would clearly be seasonal supply variability – ie higher in summer and lower in winter. It is unlikely that demand would change from the current seasonal pattern so much that it would match this supply variability[1]. Accordingly, inherent in any high solar penetration energy solution is either wasted summer capacity or the need for a seasonal (ie high capacity and long term) storage solution[2].

If a storage solution were introduced in order to provide the required seasonal balancing, it would have to dispatch over quite long periods – that is, it could not just pick out the peak pricing periods. However, almost by definition, the high flexibility (essentially high ramp rates and no resource constraints[3]) of pumped hydro would mean that it would be more valuable, on a commercial assessment, than alternatives without such flexibility. In particular, in a grid with a high renewable penetration, pricing in high renewable resource periods (eg good winter insolation days or windy days if there were a high wind penetration) would be relatively low and pumped hydro would not be used. In low renewable resource periods, there would, by definition, be lower supply and hence a higher price. This higher price would be accessed by the pumped hydro.

Quantifying the value of such long term/high capacity storage would involve so many assumptions as to be almost meaningless at this stage; however, it is clear that such a facility would access much higher wholesale electricity prices than average.

4 Capitalising the annual value

There will clearly be major changes in the electricity supply over the coming years and decades – ie over the life of any new storage asset. Such changes will include higher (possibly much higher) renewable penetration, at least some smart grid improvements including some demand management, some changes in overall demand patterns and many others. This paper does not try to project what these changes will be.

All the changes to the overall supply/demand mix will have some impact on wholesale pricing. Accordingly capitalising the one year values using simple annuity factors would give only the simplest view of possible present values. This section is introduced to suggest the range of approaches that may be taken, rather than for the purpose of calculating actual values. Annuity factors have been calculated using a 30 year design life with no allowance for deterioration in storage efficiency.

[1] Though much higher air conditioning penetration, not something the authors advocate, would tend to improve the seasonal supply/demand correlation.

[2] A balancing supply technology, one that is "naturally" high in winter and low in summer, could be a solution – but no such technology, existing or potential, is known to the authors.

[3] Assuming that it was sufficiently charged in the summer and/or had access to winter recharging from some true base load capability in the system.

Three possible approaches to capitalisation are considered:

(a) Commercial: A commercial investor would seek to get a return at least as great as the weighted average cost of capital. A representative value of 12%p.a. has been used for this example. We have allowed for wholesale price inflation at 2.5%p.a. the midpoint of the Reserve Bank of Australia's target range for CPI inflation.

(b) Risk Free rate: Loan guarantees are policy instruments that are used in some jurisdictions to encourage investment in infrastructure which may be considered to be in the public interest but which may not be commercially viable. The government can provide loan guarantees (without specifically charging for the guarantee) at risk free rates. A representative long term value for a Commonwealth government cost of funds is 6%p.a. This has been used.

(c) Stern. Sir Nicholas Stern's investigation of climate change and subsequent report to the then British Chancellor of the Exchequer used a discount rate of 1.4%p.a. to discount future value/costs for the purposes of comparing values across time. This rate was made up of a 0.1%p.a. extinction probability and the balance allowed for the projected real rate of economic growth. Use of the real rate of economic growth as a discount rate gives effect to an assumption that the marginal utility of consumption is inversely proportional to income. There is some contention regarding this assumption – however, this paper does not enter that debate. (Note that inflation is not specifically allowed for in this case as the assumption of 1.3%p.a. rate of growth is net of inflation.)

TABLE 4.1

Representative annuity rates for different approaches to capitalisation

	Commercial	Risk free rate	Stern
Discount rate	12%	6%	1.4%
Price inflation	2.5%	2.5%	0
Annuity factor	11.0	19.2	24.7

5 Conclusions

5.1 Low renewable penetration

The calculations in this paper have used recent data. They are therefore based on the current supply infrastructure which has black coal (base load) and gas (peaking) as the marginal suppliers. These therefore determine pricing for, and carbon intensity displaced by, renewable power.

5.1.1 CST

The commercial value of marginal thermal storage associated with CST power is highest for low storage capacities. Increasing thermal storage capacities above a few hours allows dispatch over longer time periods – but most of the value from accessing peak price periods is achieved with relatively low thermal storage capacities.

Thermal storage associated with CST may allow some energy to be dispatched that would otherwise be dumped. Indeed this would be expected to occur in a high SM high storage capacity CST design. In such case the thermal storage contributes to a reduction in carbon emissions because the additional dispatched energy would displace marginal supply from a fossil fuel source.

On the other hand, if thermal storage is used simply to defer dispatch, and thereby dispatch in peak pricing periods rather than lower priced periods, it could contribute to higher carbon emissions. This is because the marginal supply displaced in peak periods is from relatively low carbon intensity OCGT whereas the marginal supply displaced in lower priced periods is from higher carbon intensity black coal.

5.1.2 Pumped hydro (or other)

The paper has estimated a value for pumped hydro storage. The storage characteristics used in this derivation are only the capacity and cycle efficiency. So the results apply to any storage solution that can be characterised in this way. For example, a large EV fleet in a smart grid with smart charging might be valued similarly[4]. Of course EV storage would necessarily be short term (of order diurnal) rather than longer term (seasonal).

As for the CST thermal storage case, and for the same reasons, the marginal value of an extra MWhr of storage capacity is highest for relatively low storage capacities.

The commercial value of an independent storage solution is shown to be greater than for the integrated thermal storage of a CST plant. This is essentially because the independent storage, with good cycle efficiency, can always fully access peak pricing periods, because of access to cheap off peak power. The CST storage does not necessarily allow this as it is only available if there is sufficient insolation.

The carbon offset value of independent storage is negative as the availability of storage essentially replaces peak generator production at a relatively low carbon intensity (gas) with base load production of a higher amount of electricity (due to the cycle efficiency being less than 1) at a higher carbon intensity.

5.1.3 Costs

This paper has not considered the costs of different storage options. The values of different options have only been assessed on a gross basis. Incorporating at least approximate costs into the analysis would provide more useful insight.

5.2 High renewable penetration

A high renewable penetration, which included a high solar contribution, would require seasonal storage in addition to diurnal storage. Thermal storage associated with CST is unlikely to be able to fill this need.

[4] Value has only been assessed for the utility scale generation. Distributed storage solutions (eg EV fleet) would provide both the storage value and, in many cases, considerably greater value from the removal of the need for network augmentation – but network augmentation avoidance has not been considered in this paper.

If wind or other variable resources were significant contributors to a high renewable penetration, they would contribute additional variability to the supply side. Diversification of resources and, for each resource, geographic diversification would attenuate overall supply variability. However, there would still be a substantial need for both short and long term storage to smooth out overall variability. Thermal storage associated with CST is clearly not suitable for storage of energy captured other than thermally and locally.

5.3 Public policy implications

If Australia is to have a substantial utility scale solar thermal contribution to supply, then clearly some thermal storage is necessary and likely to be cost effective. However other storage options may provide much better commercial value, even in the low penetration case, and will be necessary for any seasonal smoothing in the high solar penetration case. Moreover, non thermal storage technologies, such as pumped hydro, would be appropriate for PV, wind and other variable renewable sources and thereby provide buffering to the whole system rather than just the CST component.

Public policy aimed at reducing carbon emissions should be framed based on an understanding of the commercial value that may arise from different storage technologies. In general, we believe that the market should be allowed to choose the technology. However, uncertainty over the future makeup of the overall market means that making commercial assessments is currently very difficult. This, combined with the long lead times for investments, suggests that the market may be a poor mechanism for developing optimal storage solutions that will be appropriate for a high renewable penetration supply. This indicates the need for direct public investment in research and indeed development and construction of storage solutions.

T Jack, V Everett, “A Supply-Demand Model for a Zero-Carbon Australia”, AuSES Solar 2010

Progress in Australian Solar Resource Assessment

Ian Muirhead[1], Ian Grant[1], Lawrence Rikus[1], Paul Gregory[1] and Greg Scott[2]

[1]Bureau of Meteorology
GPO Box 1289, Melbourne VIC 3001, Australia
[2]Geoscience Australia
GPO Box 378, Canberra ACT 2601, Australia
i.muirhead@bom.gov.au

ABSTRACT

This paper describes recent work by the Bureau of Meteorology (the Bureau) and Geoscience Australia (GA) in response to a rapidly expanding industry demand for enhanced solar resource assessment tools and data sets for Australia.

GA and the Bureau are collaborating to provide a coordinated source of pre-competitive solar resource prospectivity data to support decision making in the expanding solar industry and research community. Mapping layers include digital elevation, proximity to energy infrastructure, land tenure, water sources and solar radiation datasets. Following the release of an initial database in 2010, the database will be progressively further refined in consultation with stakeholders, including industry and jurisdictions.

The Bureau's ground network currently comprises nine stations providing one-minute statistics on global, diffuse and direct normal solar exposure, together with downward longwave irradiance and direct spectral transmission. The 95% uncertainty for any quantity measured is well within 3% or 15 W m^{-2} (whichever is the greater) after the post-measurement verification is completed. Progress is continuing in the reprocessing of historical data and provision of access to one-minute solar data.

The Bureau has been providing satellite-based, Australia-wide daily global solar exposure for approximately 20 years. A comparison between satellite and ground data indicates typical errors in the satellite-derived data of around 0.8 MJ m^{-2} in winter and 1.5 MJ m^{-2} in summer. More recently, datasets of approximately ten years of hourly global horizontal irradiance and direct normal irradiance covering Australia have been developed, presented both as time series and climatological summaries.

The Australian Community Climate and Earth System Simulator (ACCESS) is a coupled climate and earth system simulator based on the Unified Model from the UK MetOffice. It became the operational Numerical Weather Prediction (NWP) system for the Bureau of Meteorology in mid-2010. Validation studies for surface solar radiation have commenced but are currently limited by the duration of operation. Overall, the forecasts appear to show comparable accuracy to the satellite-based solar exposure upscaled to the model resolution for the short periods of validation data available.

Keywords – Forecast, mapping, resource, satellite, solar

INTRODUCTION

The Commonwealth Department of Resources, Energy and Tourism has tasked Geoscience Australia (GA) to develop an authoritative solar mapping capability under the Solar Flagships Program. Within this context, GA and the Bureau of Meteorology (the Bureau) aim to provide spatial information for solar resource mapping relating to high solar prospectivity regions, and expansion of the solar observation network. The intention of the capability is to assist the solar industry and research community to make better decisions through the provision of pre-competitive solar resource prospectivity data and analysis. This paper describes the plans for the development of the new capability, and the sources of solar radiation information that will contribute to it.

TRANSFORMING SOLAR DATA INTO A PRE-COMPETITIVE RESOURCE FOR INDUSTRY

GA has a long and proven history as a provider of pre-competitive spatial data and information for the benefit of the mining and petroleum industries. Building upon this expertise, GA is now expanding this capability to the renewable energy sector with a specific focus on solar prospectivity in response to the Clean Energy Initiative (CEI) Solar Flagships Program managed by the Commonwealth Department of Resources Energy and Tourism (RET).

RET has tasked GA to develop an authoritative solar mapping capability, in collaboration with the Bureau, which will provide spatial information for solar resource mapping related to high solar prospectivity regions. In addition, a study will be conducted on the existing solar observation network to recommend optimal expansion of the network in time for increasing the collection of data over the 2011/12 and 2012/13 summer seasons.

The primary aim of the capability is to assist the solar industry and research community to make more informed decisions through the provision of pre-competitive solar resource prospectivity data and analysis. It is intended that the data will continue to evolve and be refined over time in consultation with stakeholders and through feedback from industry. This pre-competitive solar mapping capability will be an enduring asset for the solar research community and the solar power industry as the potential for this sector of the renewable energy market continues to expand in the future.

Background

Solar energy, from a government policy and energy security perspective, is being seen as the next big renewable energy source, following on from wind. Electricity generation from solar energy is projected to increase from 0.1 TWh in 2007–08 to just under 4 TWh in 2029–30 (Figure 1) (AERA 2010). However, the outlook for electricity generation from solar energy depends critically on the commercialisation of large-scale solar energy technologies that will reduce investment costs and risks.

The role of renewable energy is projected to increase significantly in coming years, reflecting government policies and proposed greenhouse emissions reduction targets. The CEI was created to assist the Government's Carbon Pollution Reduction Scheme and enhanced Renewable Energy Target, by supporting the research, development and

demonstration of low-emission energy technologies, including solar energy. A key component of the CEI is the $1.5 billion Solar Flagships Program.

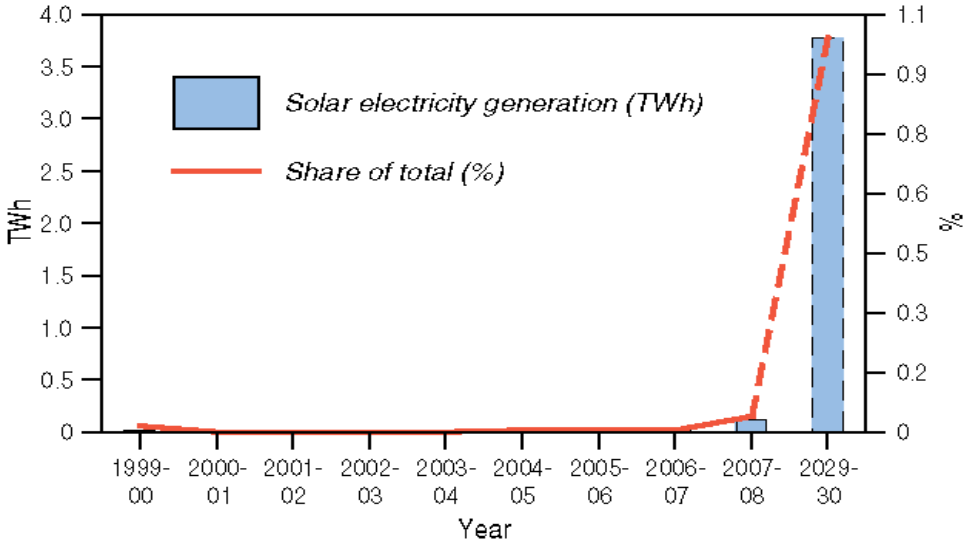

Fig. 1: Projected electricity generation from solar energy in Australia.
(Source: ABARE 2009)

The main objective of the Solar Flagships Program is to provide the foundation for large-scale, grid connected, solar power to develop into a significant energy source within a competitive electricity market. The expectation is that this will be achieved by supporting the construction and demonstration of large-scale, grid connected solar thermal and photovoltaic power stations and associated energy technologies. Additionally, further benefits of the program include: developing the solar industry in Australia, encouraging regional development, providing research infrastructure, developing intellectual property in solar power generation, and developing and sharing technical and economic knowledge.

Essential to the objectives of the Solar Flagships Program is government, research and industry access to publicly available and relevant information to assist in identifying optimal sites for the development of solar thermal and photovoltaic power generation. In recognition of this requirement RET has tasked GA to develop a nationally consistent pre-competitive solar mapping resource.

Developing a pre-competitive solar mapping resource

The potential for using solar energy at a given location depends largely on the solar radiation, climate, proximity to electricity load centres, existing infrastructure, frequency of natural hazards and the availability of suitable sites (AERA 2010). Depending upon the technology and location, large scale solar power plants may require up to approximately 2 hectares of land per MW of power. Therefore to underpin the prospectivity of potential solar power generation sites, geographic analysis and portrayal of a range of key indicators is an important requirement for investing in solar.

GA's National Geographic Information Group (NGIG) is responsible for maintaining the national topographic database which, in various forms over many years, has been the essential ingredient to delivering numerous government policies and programs. The topographic database provides an authoritative and nationally consistent base which has been built upon and extended through the acquisition and integration of energy infrastructure and solar radiation datasets to create the first baseline release of the *Australian Solar Energy Information System* (ASEIS).

The first version of ASEIS has initially been released as a self contained GIS product containing broad 'themes' of data distributed on DVD under a Creative Commons by attribution license. The themes have been split into solar irradiance, energy infrastructure and topography (Table 1), and represent a compilation of existing accessible data relevant to the requirements of the industry for determining potentially high solar prospectivity.

Tab. 1: ASEIS v1, dataset descriptions

Theme	**Dataset description**
Solar Irradiance	Global Horizontal Irradiance
	Direct Normal Irradiance
	Bureau Monitoring stations
Energy Infrastructure	Transmission lines
	Power station Locations
	Electricity Distribution Zones
	Fossil Fuel Resources such as gas pipelines, gas producing basins, black and brown coal basins.
Topography	Digital Elevation Model – 3 second DEM
	DEM derivatives - Slope, Aspect, Hillshade
	Water Resources - Lakes, Reservoirs, Rivers
	Roads and transportation infrastructure
	Administrative boundaries
	Land tenure

The objective of the first version of ASEIS is to provide a valuable foundation from which GA will gather feedback through consultations with industry and identified stakeholders to inform future releases. Further refinement of the datasets and the integration of new data such as natural hazards, pollution, and soil classifications may also be included. Future technical development of ASEIS will migrate the database and application from a DVD product to streamlined and more accessible web delivered services.

To further complement and strengthen the solar data available through this program a study is being conducted to examine the options available for the optimal expansion of the existing solar observation network. This study is being carried out by the Bureau, and in collaboration with GA, recommendations within the scope of this project will be

implemented to augment and extend the solar observation network prior to the 2011/12 and 2012/13 summer seasons. The data collected over this timeframe will be integrated into more comprehensive solar radiation datasets and included in future releases of the ASEIS, contributing to an enriched publicly available resource.

The initial delivery, ongoing enhancement and maintenance of the ASEIS and augmented solar observation network will provide a solid, nationally consistent framework and valuable pre-competitive solar information resource to support a rapidly growing segment of the renewable energy sector.

OBSERVATIONAL DATA FROM THE BUREAU OF METEOROLOGY

Satellite-based datasets

The Bureau of Meteorology has distributed solar data products derived from satellite data since the early 1990s. The Bureau's satellite solar radiation system processes hourly visible-band images from geostationary meteorological satellites to estimates of hourly instantaneous solar global horizontal irradiance (GHI) at ground level, using a two-spectral-band physical model (Weymouth & Le Marshall 2001). The hourly irradiance gridded datasets cover Australia with a resolution of 0.05° (approximately 5 km) in latitude and longitude, but with further work may be refined to 0.02° in future.

The Bureau has derived several datasets from the hourly irradiance estimates. The Bureau has been providing satellite-based daily global solar exposure for approximately 20 years (Figure 3 (left)). A comparison between satellite and ground data indicates typical errors in the satellite-derived daily exposures of around 0.8 MJ m^{-2} in winter and 1.5 MJ m^{-2} in summer. In 2009, monthly climatologies of hourly global horizontal exposure and hourly direct normal exposure were produced (Figure 3 (right)). Hourly time series spatial data sets of global horizontal irradiance (GHI) and direct normal irradiance (DNI) were produced in 2010 (Figure 4). All of these datasets are on a 0.05° grid. The direct normal quantities are derived from global horizontal quantities using conversion relations for Australian conditions which are based on the work of Boland (Boland *et al*. 2008, Ridley *et al*. 2010).

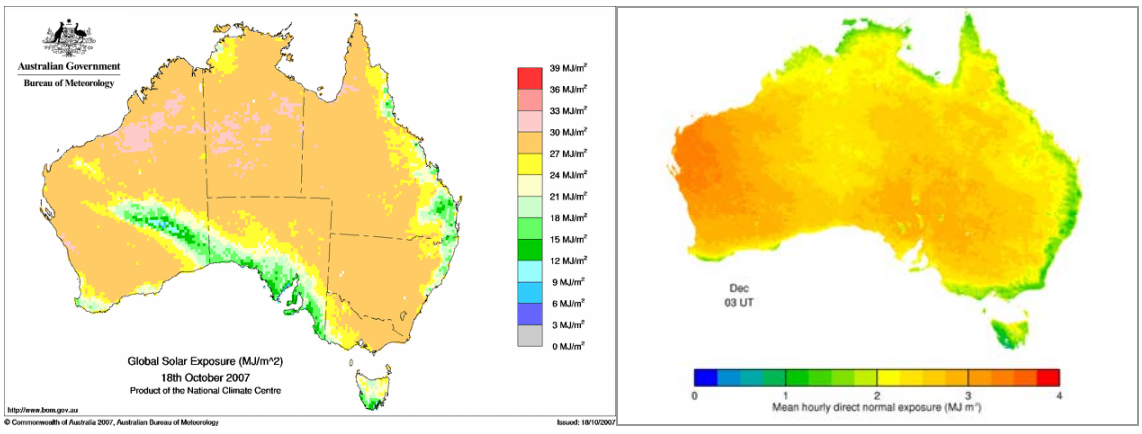

Fig. 3: *Left*: Daily global solar exposure map from the Bureau of Meteorology website *Right*: Monthly mean of 1-hour direct normal exposure for 02-03 UT in December

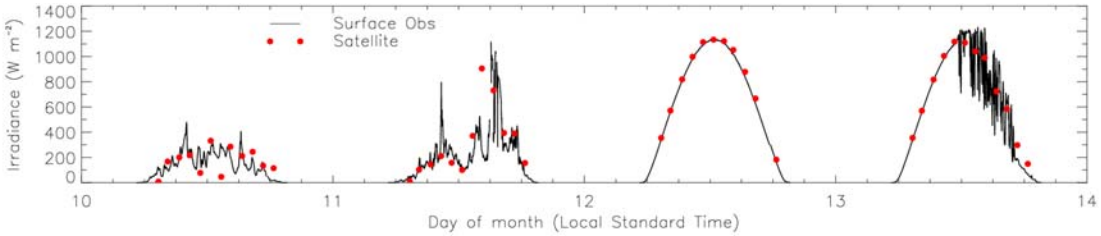

Fig. 4: A comparison between satellite-derived and ground-measured GHI at Alice Springs (Dec 1999) shows good agreement, especially under clear sky conditions

Historical climate data

The Bureau of Meteorology's ground network currently comprises nine Australian stations (including Cocos Island). These stations provide one-minute statistics on global, diffuse and direct normal solar exposure, together with downward longwave irradiance and direct spectral transmission (currently 412, 500, 610, and 778 nm, but it is planned to add 368, 812 and 868 nm by the end of 2010). The 95% uncertainty for any quantity measured is well within 3% or 15Wm^{-2} (whichever is the greater) after the post measurement verification is completed.

The one minute data are used by the Bureau for research purposes, and to assist in removing any bias associated with the Bureau's satellite-derived solar exposure data. They are also the basis of the half hourly solar exposure data products available from the Bureau. Given the growing demand for high temporal resolution information, in early 2010 the Bureau began work to establish a system to facilitate access to these data though the Bureau's regular climate data request service. The first stage of this work is expected to be finished by the end of 2010. When the project is complete, one minute irradiance data for around 26 locations (Figure 5) will be available by contacting the Bureau (i.e. these data will not yet be available online). Periods of available data vary between locations, but the longest record will be from 1993 to present day.

Climate Data Online

Over the past four years the Bureau has been establishing the infrastructure and tools to provide access to the historical climate data held within the Australian Data Archive for Meteorology (ADAM). This system, known as Climate Data Online, has delivered more than two million HTML pages, graphs and data files in the two years since the first data product – monthly rainfall – became operational.

The initial phase of Climate Data Online was to provide climate statistics on a monthly and daily basis for around 1200 Australian locations, daily and monthly rainfall information for around 19,000 locations, and maximum and minimum temperature data on daily and monthly timeframes for approximately 1700 Australian locations. This work was completed in July 2010. In 2010 work began on providing access to daily solar exposure information derived from the Bureau's solar-satellite model. The spatial data are mapped to existing station locations to utilize the current station-based data interface. Current intentions are to provide these data via a spatially enabled data management system in future. Once the work is completed daily global solar exposure dating back to 1990 will be available for all 19,000 Bureau station locations.

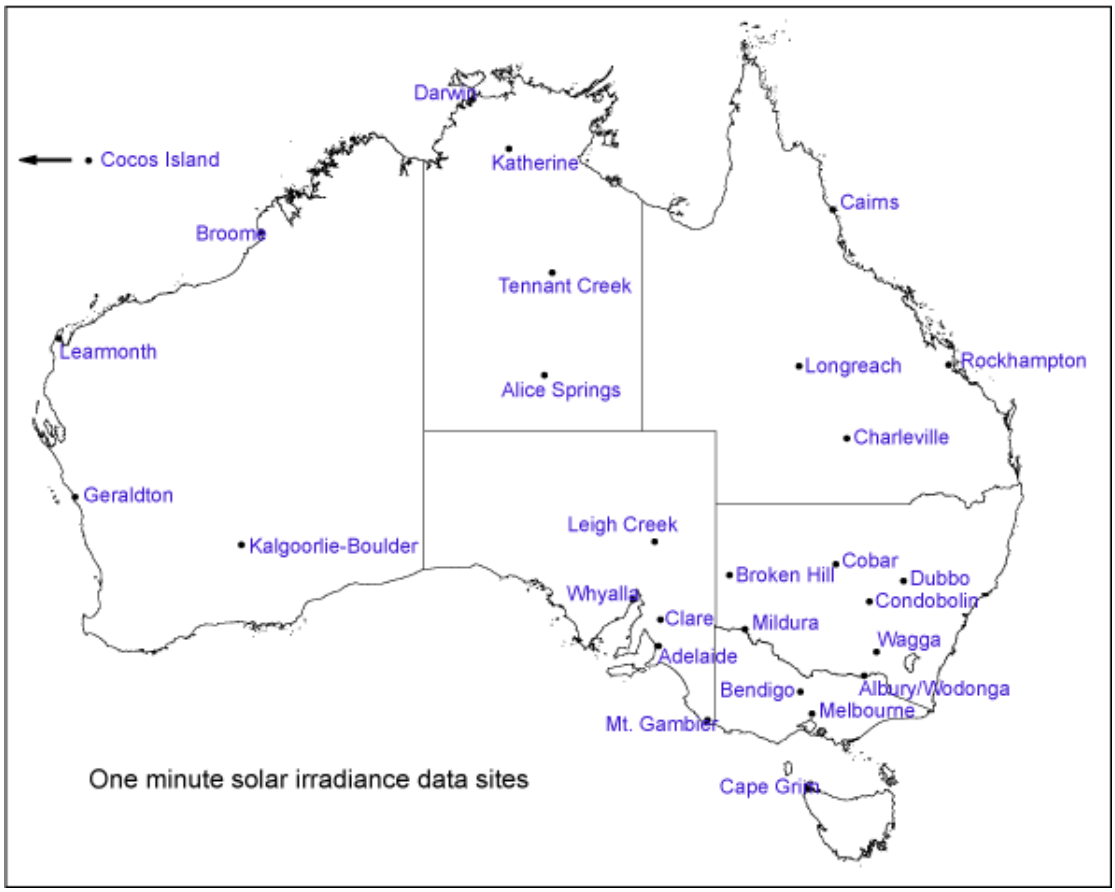

Fig. 5: Location of sites with one minute solar irradiance information

Climate Data Online will implement the first of several planned data information portals to support the rapidly increasing interest in solar energy systems, which will cater for the small domestic photovoltaic system through to large grid-connected solar plants. Access to this information will increase the capacity of users to make informed decisions about what data are available for particular applications, and their suitability for purpose.

SOLAR RADIATION FORECASTS

The Bureau has an operational suite of regional numerical weather prediction (NWP) models which are used to forecast the weather over the Australian continent up to 3 days in advance. These suites are based on a sophisticated data assimilation scheme which ingests millions of data values from ground and satellite observations, and other sources each day to produce an accurate description of the state of the atmosphere at analysis times. The analyses are the initial conditions for the forecasts. Since NWP models are based on physical equations describing the evolution of energy, momentum and cloud fields in the atmosphere they include forecasts of the solar radiation incident on the ground for each hour of the forecast as well as the standard weather elements. The largest scale system is the global domain with a nominal resolution of 75 km and forecast length of 10 days. This provides boundary conditions for the regional model (nominal horizontal resolution of 40 km for 3 day forecasts) and the mesoscale model

(10 km for 2 day forecasts) which both extend over the Australian continent. The analysis and forecast data from these models have been archived for a number of years at a temporal frequency of one hour. In addition there are a number of higher resolution (5 km and 2 day forecasts) models run over restricted domains centred around the major Australian cities.

The skill of the old operational system

Up until July 2010 the operational NWP system at the Bureau was based on a 3-D Optimal Interpolation Assimilation scheme (Seaman *et al*. 1995). For the hourly radiative transfer calculations the model diagnosed cloud amount based on the grid point relative humidity and static stability. The cloud condensate content used to calculate the optical depth of the clouds was estimated from a function of the cloud level temperature (Lemus *et al*. 1997) which is known to severely underestimate the ice content for high convective anvil cloud. The radiative transfer scheme for solar wavelengths was based on the Lacis & Hansen (1974) scheme and assumed that all radiation is diffuse below the first level at which cloud is encountered and hence only calculates global irradiance at the surface. Despite these limitations the model solar insolation forecasts show some degree of skill.

Plots of the monthly mean solar exposure averaged over the Australian continent over the 2 day forecasts from the old mesoscale (12 km) system (MALAPS) are shown in Figure 6 along with the corresponding satellite estimates (Grant *et al*. 2008). Note that the performance of the models does not vary greatly over the 2 or 3 day period and that on the whole good agreement is obtained with the satellite data.

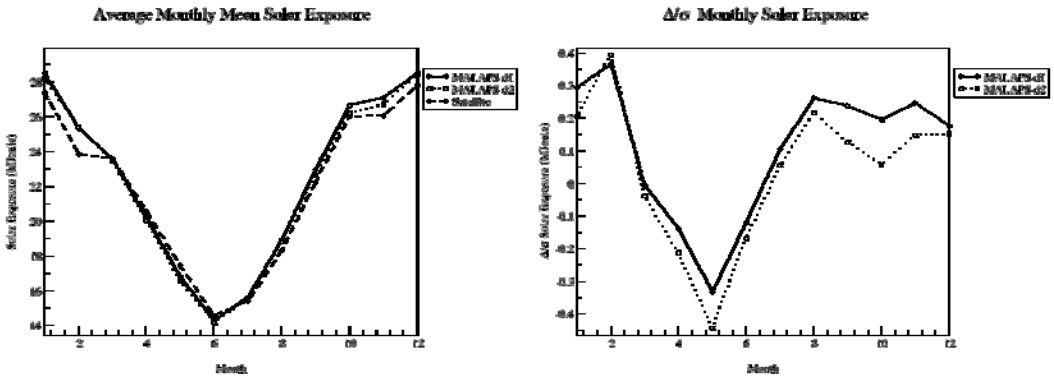

Fig. 6: Averaged monthly solar exposure over continental Australia for the old mesoscale (12 km) model (MALAPS) (left) with differences between MALAPS and satellite data (right). Suffixes ‘d1’ and ‘d2’ refer to 1st and 2nd day forecasts respectively.

A limited comparison with surface measurements from the Bureau's eight surface radiation measurement sites (not shown) also shows skill. For the comparison of monthly means, the model is generally better than the satellite for mid-latitude stations such as Melbourne, Cape Grim and Adelaide, and (perhaps surprisingly given the

known problems with the prediction of local convection) Darwin. The satellite does better overall at Alice Springs, Rockhampton, Broome and Wagga Wagga. For the essentially clear skies over Alice Springs the model is slightly more accurate than the satellite, although for most other months the satellite is better. At most sites and times, the overall patterns are generally in agreement with the observational data but there are extended periods where the model over-estimates the solar insolation (e.g. early May at Adelaide). Investigations into sample days of disagreement indicate the main source of these errors is the model's transparent high cloud.

The skill of the ACCESS system

The Australian Community Climate and Earth System Simulator (ACCESS) is a coupled climate and earth system simulator being developed as a joint initiative of the Bureau and CSIRO in cooperation with the university community in Australia. NWP suites based on this system became operational in July 2010. The main improvement over the old systems is the implementation of a highly sophisticated data assimilation scheme (Rawlins *et al*. 2007) which forces greater consistency between the meteorological fields and allows for much more data to be ingested resulting in better analysed meteorology including cloud fields. The heart of the NWP system is the unified model from the United Kingdom Meteorological Office. The main advantages of this model in the context of surface solar radiation is that it uses a prognostic cloud scheme which maintains a 'memory' of the cloud amount and condensate fields between model time-steps and evaluates the changes due to cloud formation and dissipation continuously. This results in greater skill in defining the cloud fields and because it 'tracks' cloud condensate it produces much more realistic optical depths for high and middle level cloud than the old model which relied on a temperature dependent diagnostic scheme. Validation studies for surface solar radiation have commenced but are currently limited by the lack of surface measurements for the periods for which the new Australian region NWP suites have been run. The new model also has the capability to forecast direct and diffuse solar radiation at the surface but this is yet to be validated against measurements. The systems are expected to move to higher horizontal resolution in the near future.

Preliminary comparisons of the regional (12 km) models MALAPS and, its equivalent in the new NWP system, ACCESS-A are shown in Figure 7 for a selection of the Bureau's surface radiation sites for October 2008. Overall, there is an improvement in the forecasts although there are some instances where ACCESS-A is not as good as MALAPS. Note that the model results are grid scale quantities and a true comparison at finer scales such as those represented by the measurement sites should really take this discrepancy in scale into account using some type of downscaling technique.

Summary of solar forecasting

Modern NWP systems provide the best possible estimate of the state of the atmosphere at analysis times. Using these as initial conditions for the physical based numerical forecast models produces an accurate evolution of large-scale cloud fields which can provide estimates of solar exposure at the surface which are comparable with the estimates from satellite data. The main advantage of the NWP based solar insolation product is that it is a forecast which shows skill out to at least 3 days.

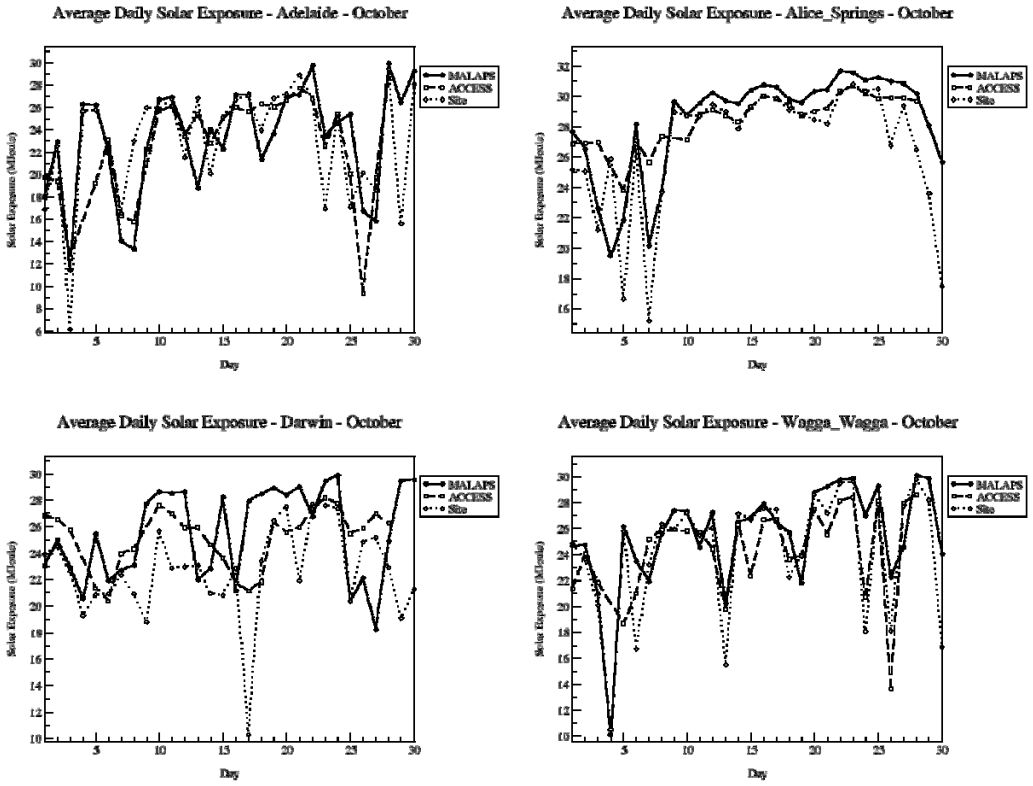

Fig. 7: Plots of daily solar exposure for October at selected sites within Australia for the 1st-day forecasts of the mesoscale (12 km) models ACCESS-A and MALAPS

The forecasts from the Bureau's old operational regional models have been compared with the satellite estimates of daily insolation and generally agree well, particularly for time and space means. The verification against the Bureau's limited number of surface solar radiation sites again shows comparable skill for daily exposure although some of the known limitations in the old model are apparent. A preliminary investigation into the current generation of the Bureau's NWP systems shows it to be better in most respects than the old systems.

This work was supported by the Australian Government as a funded project with the Department of Resources, Environment and Tourism.

CONCLUSION

The Australian Government has tasked GA with the development of an authoritative, pre-competitive solar resource mapping capability to support the solar industry and research community. GA and the Bureau will collaborate to provide spatial information relevant to high solar prospectivity regions, building on the Bureau's expertise and current activities in its surface-based solar observation network, satellite-based solar mapping, and data distribution. The Bureau's operational numerical weather prediction modelling also offers a solar forecasting capability.

REFERENCES

ABARE (2009). Australian Energy Statistics, Canberra, August.

Australian Energy Resource Assessment (AERA) (2010). Chapter 10 – Solar Energy, <https://www.ga.gov.au/products/servlet/controller?event=GEOCAT_DETAILS&catno=70142>

Bureau of Meteorology (2009). Average Daily Solar Exposure, < http://www.bom.gov.au/jsp/ncc/climate_averages/solar-exposure/index.jsp >

Boland, J., Ridley, B., and Brown, B., (2008). "Models of diffuse solar radiation", Ren. Energy, 33, 575-584.

Bourke, W., Hart, T., Steinle, P., Seaman, R., Embery, G., Naughton, M., and Rikus, L. (1995). "Evolution of the Bureau of Meteorology's Global Assimilation and Prediction system. Part 2: Resolution enhancements and case studies", Australian Met. Mag., 44, 19-40.

Grant, I., Jones, D., Wang, W., Fawcett, R., and Barratt, D., (2008). "'Meteorological and Remotely Sensed Datasets for Hydrological Modelling: A Contribution to the Australian Water Availability Project", CAHMDA-III International Workshop on Hydrologic Prediction: Modelling, Observation and Data Assimilation, 2008 Melbourne, Victoria, Australia.

Lacis, A.A., and Hansen, J.E., (1974). "A parameterization for the absorption of solar radiation in the earth's atmosphere", J. Atmos. Sci., 31, 118-133.

Lemus, L., Rikus, L., and Platt, C.M.R., (1997). "Global cloud liquid water path simulations", J. Climate, 10, 52-64.

Seaman, R., Bourke, W., Steinle, P., Hart, T., Embery, G., Naughton, M., and Rikus, L., (1995). "Evolution of the Bureau of Meteorology's Global Assimilation and Prediction system. Part 1: Analysis and initialisation", Australian Met. Mag., 44, 1-18.

Rawlins, F., Ballard, S.P., Bovis, K.J., Clayton, A.M., Li, D., Inverarity, G.W., Lorenc, A.C., and Payne, T.J., (2007). "The Met Office global four-dimensional variational data assimilation scheme", Q. J. R. Meteorol. Soc., 133, 347-362.

Ridley B., Boland J., and Lauret P., (2010). "Modelling of diffuse solar fraction with multiple predictors", Ren. Energy, 35, 478-483.

Weymouth, G.T. and Le Marshall, J.F., (2001). "Estimate of daily surface solar exposure using GMS-5 stretched-VISSR observations. The system and basic results", Aust. Meteor. Mag., 50, 263-278.

BRIEF BIOGRAPHY OF PRESENTER

Ian Muirhead first became involved in renewable energy while undertaking a Master of Environmental Studies at Melbourne University, where his thesis studied the potential for large-scale wind power generation in Victoria. After 13 years working in remote area power systems design at Telstra Research Laboratories, Ian joined the Bureau of Meteorology in 1998. He is currently managing product development for the Bureau's Climate Data Online project, but is actively involved in helping develop the Bureau's renewable energy activities within the Bureau.

Australian solar patents: Are they up to scratch?

Justin Blows and George Mokdsi
Griffith Hack Patent and Trade Mark Attorneys
100 Miller Street, North Sydney NSW 2060
justin.blows@griffithhack.com.au

ABSTRACT

The quality of solar patents from various countries including Australia has been investigated. It appears that the quality of solar patents by Australian entities has declined in recent years. Policy makers need to urgently focus their attention on the Australian Solar Industry to secure its future.

Keywords* *Australian solar patent quality, patents.

INTRODUCTION

It is universally accepted that a high quality patent is more desirable than a low quality patent. A high quality patent may provide immense leverage in commercial negotiations, protect the underlying technological concept broadly and robustly, and have a higher monetary value associated with its sale or licence. Typically, high quality patents are for inventions having higher foundational and lesser incremental characteristics, which correlate with the sophistication of the protected technology. High quality patents may also have a higher value to academia and research. Put simply, the quality of the patents an entity has is an important measure of its commercial readiness.

We have investigated the quality of patents related to solar technologies ("solar patents"). The quality of solar patents by Australians generally is compared to that of solar patents by others elsewhere. We have also determined the highest quality Australian patents and the associated inventors.

Regrettably, we report that Australian patents generally are of modest quality. We do note, however, that this is primarily a phenomenon of the last few years and we are confident that this situation could be rapidly turned around by appropriate efforts by government and industry.

WHAT IS PATENT QUALITY AND HOW WE MEASURE IT

Patent quality means different things to different people and can be difficult to quantify. Many methods of measuring patent quality have been proposed, each method corresponding to a respective definition of quality. Each method places a different weight on each of the aspects that collectively constitute patent quality. However, most methods use for their base information relating to the number of times a patent has been cited during prosecution of a latter filed patent. A patent that discloses a technology with strong foundational characteristics is likely to be cited during the prosecution of a latter filed patent that discloses incremental advances on the same technology. Often, the foundational patent will force down the scope of protection afforded by latter filed patents. Thus, patents with high citation counts generally provide broad and robust protection. Patents that are cited often are also likely to involve a technology that is highly relevant to the needs of industry, and may well protect a 'keystone' technology that others need access too.

The metric for patent quality used here is the number of times a patent has been cited. Separate to this study, Griffith Hack has developed a more comprehensive and sophisticated algorithm for determining patent quality using citation data, which involves an analysis of the network formed by patent citations. A network analysis may provide a better result. The metric used here, however, provides, with relative ease, a sufficiently accurate determination of patent quality trends.

We have restricted our analysis to US patents filed by Australian applicants and applicants from other countries including the US. We have done so because the patent citation data held by the United States Patent and Trade Mark Office is superior, thus facilitating our approach. The trends observed are thus a highly accurate representation of the situation in the US generally. We also believe that the results can be extrapolated globally because the US solar market is a fair enough representation of the global market.

Griffith Hack patent searchers searched the US patent database through the Thomson Innovation platform provided by Thomson Reuters. The search included both granted patents and published applications filed from the year 2000 and was based on a keyword and IPC mark search query targeting solar photovoltaic and solar thermal technologies. Altogether around 35,000 individual patents were found.

RESULTS

Figure 1 shows the average number of times a patent from each of several countries is cited, between the years 2000-2010. The countries represented in Figure 1 are the 10 best performing countries and China. Patents from the US are on average cited the most, at 2.9 times per application. By this metric, US solar patents have on average the highest quality. Broadly speaking, the "tier 1" countries with more then 2 citations per patent on average are the US, Great Britain (GB), Japan (JP) and Germany (DE). The "tier 2" countries with more than 1 citation per patent on average are France (FR), Australia (AU), Italy (IT), Korea (KR), and Taiwan (TW). Over the period considered, Australia was ranked 6th for patent quality.

China is included because of its emerging status and enormous potential as a manufacturer. The number of US solar patents filed by Chinese entities rose from 1 in 2000 to 118 in 2008, a rate of growth far in excess of that of any other country. However, the patent quality is still low, at around 0.36, and the overall number of US patents filed is a very small proportion of all the patents filed (US and Japan combined filed 1,800 patents in 2008). Thus, Chinese patentees are unlikely to greatly shape solar innovation in the near feature.

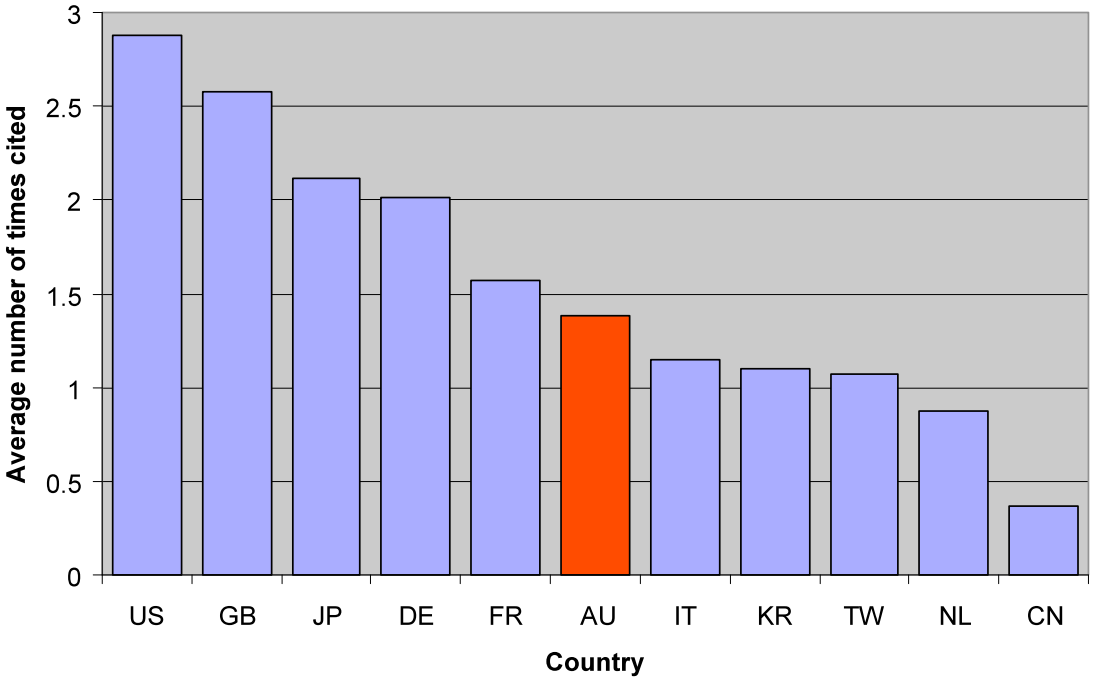

Figure 1. Average number of times a patent from each of several countries is cited.

Figure 2 shows normalised average citation index data for US patents by entities from Japan, the US, Korea, China and Australia, between 2000 and 2008. This graph indicates how patent quality has changed over time. Younger patents are less likely to be cited than older patents. To control for this age bias, we have divided, for each year, each country's average number of citations per patent by the average number of citations for every patent. The data from 2009/2010 is not yet fully available and so these years have not been considered. The general

trend for Japan is for increasing patent quality, for the US decreasing patent quality and unchanging for Korean patent quality.

Australia appears to have declining patent quality. The normalised citation index for Australian patents may increase as the patents age, however. The uncertainty of the results with respect to Australia (and China) may be significant because the number of US patents by Australian and Chinese entities is quite small.

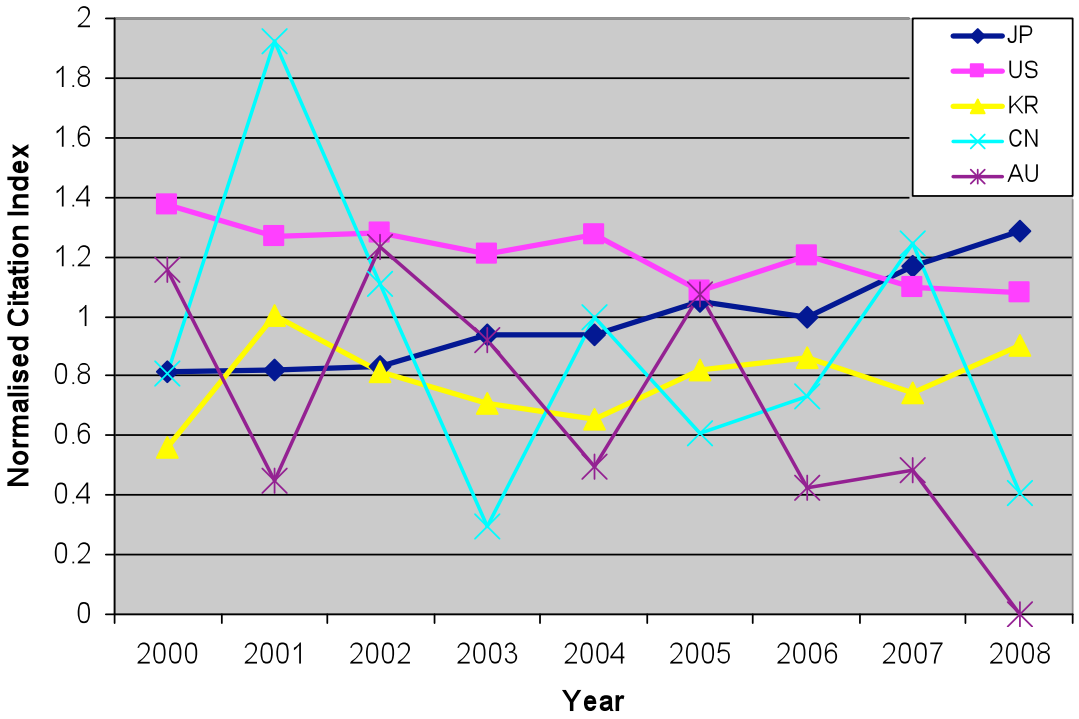

Figure 2. Normalised average citation index for US patents by entities from Japan, US, Korea, China and Australia.

Figure 3 shows the number of patents that cite patents by the 11 most cited Australian inventors. The inventors have been grouped according to the most cited patents. The leading inventors are Martin Green and Stuart Wenham (University of NSW), closely followed by George Phani, Jason Hopkins, David Vittorio and Igor Skryabin (Sustainable Technologies International).

Figure 4 shows the number of patents citing the 10 most cited US patents by an Australian entity. The highest quality patent was US6429037, having been cited 17 times. This makes US6429037 the 712th most cited US solar patent. For comparison, the most cited US solar patent, US6297539B1, has been cited 181 times.

CONCLUSION

Using patent citation data we have made a measure of the quality of solar patents by Australian entities. Overall, Australian solar patents have been of an intermediate level over the last ten years. Disturbingly, Australian patent quality appears to have declined in the last few years. One possible reason for this may be a recent tendency for Australian solar companies to greatly undervalue the importance of patents – which would undermine their competitiveness. Another reason may be that there is a significant problem with solar research and innovation in Australia. Australian policy makers should urgently focus their attention on this problem with a view to ensuring the future of Australian solar innovation. Fortunately, the decline in Australian patent quality is only recent and may be still turned around.

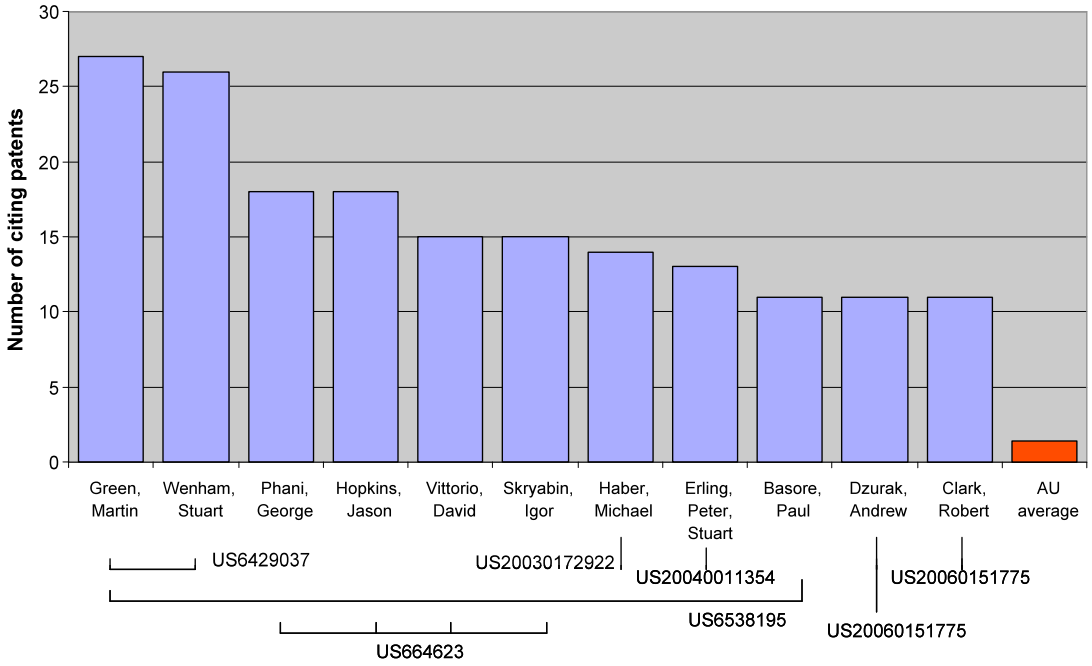

Figure 3. The number of patents that cite the 11 most cited Australian inventors.

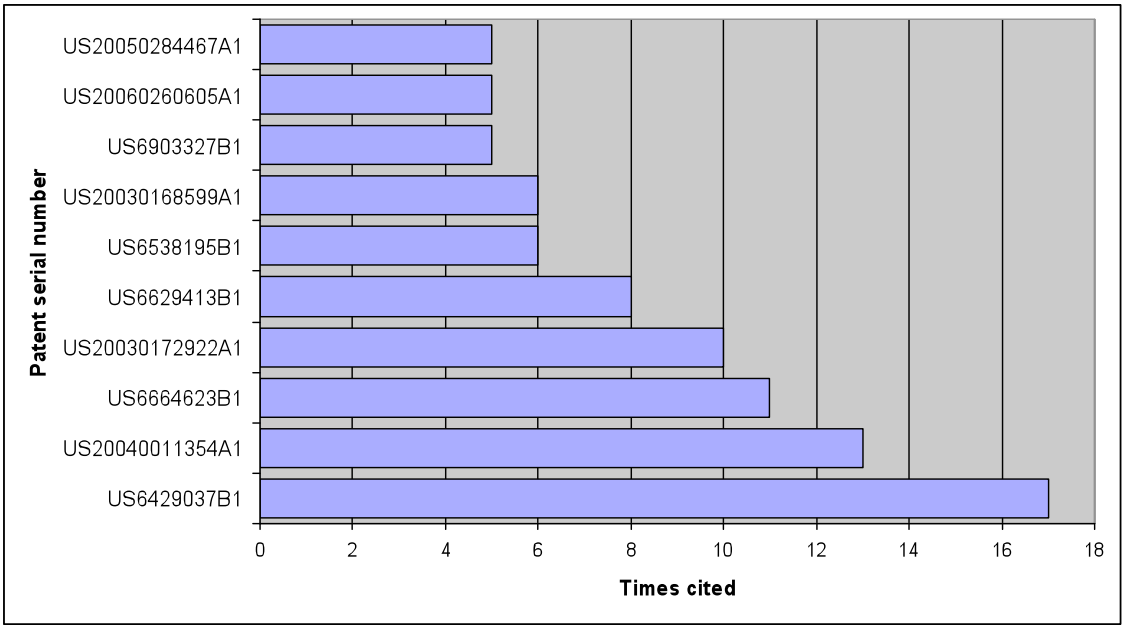

Figure 4 shows the number of patents citing the 10 most cited US patents by an Australian entity.

BIOGRAPHY OF PRESENTER

Justin Blows completed his PhD in applied laser physics at Macquarie University in 1997. He was a project leader at the Optical Fibre Technology Centre, The University of Sydney, and was subsequently a Chief Investigator at the ARC Centre of Excellence CUDOS, The University of Sydney, leading a group researching ultrafast optical devices for telecommunications. Justin commenced practice as a patent attorney in 2005 and takes a keen interest in protecting clean and sustainable technologies, particularly solar technologies. He has authored reports on Australian patents relating to clean coal, solar and hybrid vehicle technology, and is the principle contributor to the blog *www.cleanip.com.au*.

Photovoltaic Panels + Air Conditioners + Multi-Objective Evolutionary Algorithms = A win-win situation

Cristian Perfumo[1,2], John K. Ward[1] and Julio Braslavsky[2]

[1]CSIRO Energy Technology
Newcastle, Australia
{cristian.perfumo, john.k.ward}@csiro.au

[2]CDSC, University of Newcastle
Newcastle, Australia
julio.braslavsky@newcastle.edu.au

ABSTRACT

Electricity peak demand represents a serious threat to the power infrastructure and can lead to blackouts when the lines cannot cope with the required load. As the use of commercial and residential air conditioning (AC) increases, these peaks can only become higher. Connecting a set of these devices to photovoltaic panels (PV) can help mitigate this problem under the proper management. This paper models a group of air-conditioned rooms, whose ACs are partly powered by photovoltaic panels. A multi-objective evolutionary algorithm (MOEA) is used to quantify trade-offs amongst peak demand, energy cost and thermal comfort. We model and study a scenario with 8 air conditioners connected to different configurations of photovoltaic panels and compare our findings against the case of having all ACs working independently, irrespective of the renewable generation.

Keywords – Air conditioning, Evolutionary algorithms, Photovoltaic, Solar power, Renewable energy.

INTRODUCTION

As energy demand increases with the popularity of power-hungry appliances like air conditioners (ACs), so does the awareness for reducing CO_2 emissions to stop global warming. The most popular way out of this catch-22 is incorporating renewable sources of energy such as solar and wind. Although these energy sources are clean and virtually infinite, their main handicap is the lack of steadiness of the power output they supply. Batteries are a way of counteracting this situation but they are expensive and contaminate the environment. Demand-side load management appears, then, as an appealing alternative for energy storage and standardisation work (such as the Australian standard AS4755) has already started trying to define the interfaces used to control air-conditioning systems. Load management makes it also possible to harness renewables by, for instance, powering cycle-based devices such as ACs, pool pumps and water heater only when enough energy is available for them.

In our previous work (Perfumo, Ward, & Braslavsky, 2010) we modelled and studied a scenario with 8 ACs and compared our findings against the case of having all ACs working independently, irrespective of global goals. This paper incorporates renewable generation in the form of photovoltaic panels partly powering our AC load. One example of such a scenario in real life would be a motel in which every room has its own, independent, AC but the owner cares about the aggregate energy consumption. The question this paper attempts to answer is what could be achieved by combining load management in the form of coordinating those ACs with the generation output from a set of solar panels.

A multi-objective evolutionary algorithm (MOEA) (Goldberg, 1989) is used to quantify trade-offs amongst peak demand, energy cost and thermal comfort and how those trade-

offs change when the air conditioners are coordinated in order to work in awareness of the renewable generation.

DESCRIPTION OF THE AC MODEL & PV DATASET

In this paper we consider the interaction of eight independent AC systems that operate under a basic on/off thermostat control, which is a situation representative of many of the existing installed residential AC systems.

For each of the rooms modelled, the temperature of the air inside the room is given by the difference equation

$$T_{int}(k+1) = T_{int}(k) + P\frac{UA}{C}\left(T_{out}(k) - T_{int}(k)\right) + Q_{int}(k)\frac{P}{C} - Q_{ac}(k)\frac{P}{C}$$

where

- $T_{int}(k)$ is the temperature inside the room at time interval k ($C°$),
- $T_{out}(k)$ is the outside temperature at time interval k ($C°$),
- P is the duration of an interval of time (*seconds*),
- U is the heat transfer coefficient of the walls, floor and ceiling of the room ($W/m^2C°$),
- A is the total area of the of the walls, floor and ceiling of the room (m^2),
- C is the heat capacity of the room ($J/C°$),
- $Q_{int}(k)$ is the heat transmission from internal load at time interval k (W),
- $Q_{ac}(k)$ is the heat transmission from the AC at time interval k (W).

For the sake of simplicity, in this study we assume that all of the rooms are identical, i.e. they have the same thermal load and mass and their ACs have the same cooling power. Figure 1 illustrates a typical sequence of on-off periods of the AC system corresponding to one room (lowest square waveform) to maintain the temperature of the room (middle saw-tooth waveform) within comfort limits in the face of the evolution of the external ambient temperature (top curve) on a typical hot summer day between 8 a.m. and 6 p.m. We can see how the room temperature decreases every time the AC is switched on, and increases when it is switched off, while the external ambient temperature is higher than the maximum set-point level of comfort. We also see that the AC on-periods are wider when the external temperature is higher in the day.

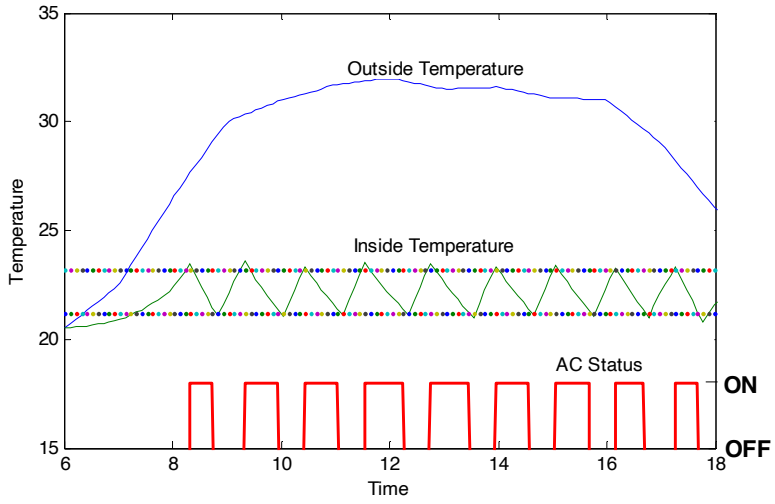

Figure 1: External and internal temperature and AC activity for one room

Figure 2 represents a possible scenario with eight AC systems operating in a completely decentralised and uncoordinated way. The figure shows on-off periods and temperature evolution plots, as in Figure 1, for each of the eight rooms. The plot in the lowest right hand side corner represents the evolution of aggregate energy consumption (red), energy generation (green) and their difference, which is the energy taken from the electricity grid (blue).

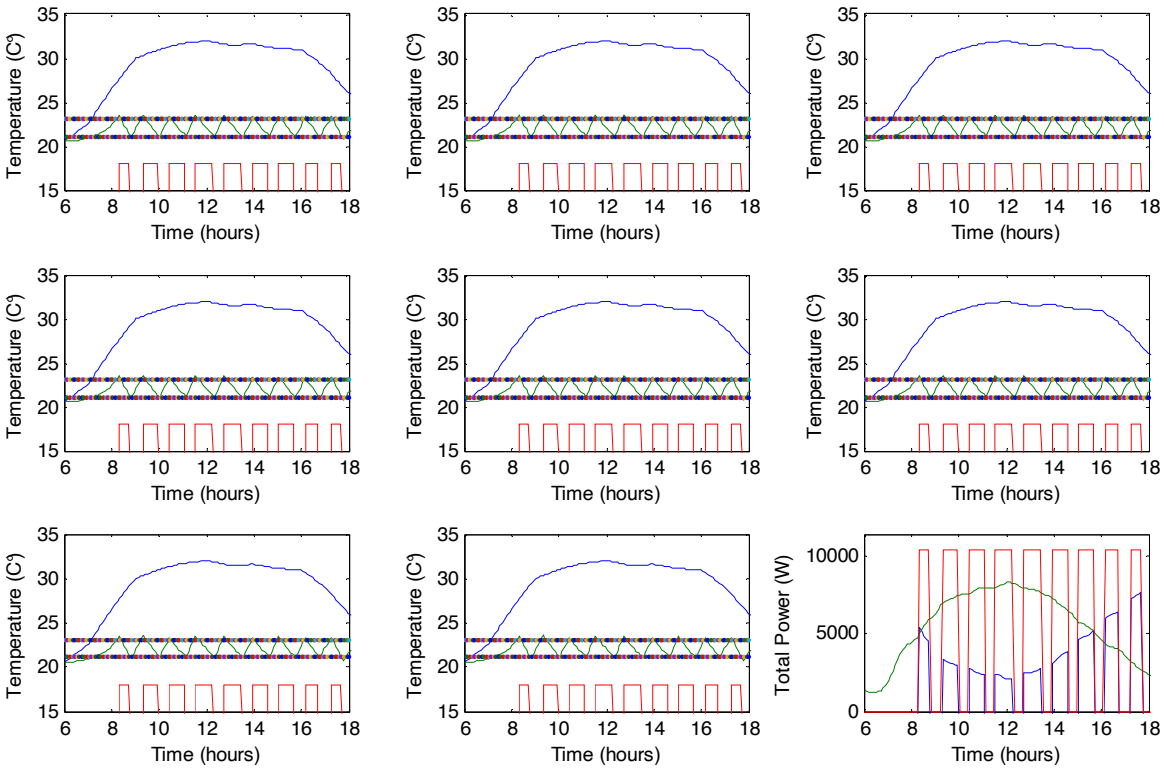

Figure 2: One possible scenario, where all the ACs work in phase. *In all but the bottom-right plot, blue is external temperature, green is internal temperature and red is the AC state (high=on and low = off). In bottom-right plot, green is predicted PV generation, red is power consumption and blue is power imported from the electricity grid.*

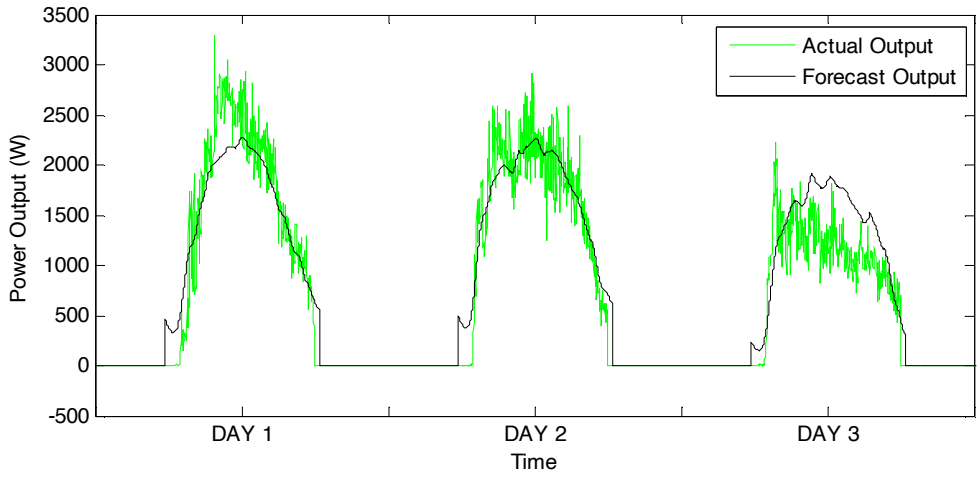

Figure 3: Real and forecast PV power output for three days in Newcastle, Australia.

The energy generation data used in this work is real data collected from photovoltaic panels installed at the several sites that form CSIRO's Virtual Power Station, based at the CSIRO Energy Centre, Newcastle Australia (Ward, Platt, & Li, 2008). Based on actual generation data, a support vector machine predicts the PV output based on weather forecasts from the Australian Bureau of Meteorology and historic output data (West, 2005). Figure 3 shows actual and forecast data for three days in March 2010. Our optimisation algorithm uses the predicted data of day 1 as the generation dataset.

For the scenario in Figure 2 we chose to set the peak predicted generation of the photovoltaic panels to 80% of the maximum aggregate consumption of the ACs. Throughout this paper we will say that there is a *p% of renewable generation* in our system when the peak of the predicted generation represents a *p%* of the maximum load (all the ACs turned on). In the results section of this paper we present a sensitivity analysis varying the amount of renewables from 0% to 150% with 10% steps.

In Figure 2 we see a potential worst-case scenario, in which the eight AC systems tend to be synchronised (in this case they are exactly in phase because of identical initial and functioning conditions of the rooms over time), yielding very undesirable large amplitude oscillations in the aggregate energy consumption. Section "Our MOEA and the results" presents an alternative solution for this situation that we later use to compare against the results of our optimisation algorithm.

THE OPTIMISATION PROBLEM

We are interested in finding sequences of on-off periods for each room that minimise the following three competing objectives:

- *Discomfort*: the occupants of the rooms should be as comfortable as possible.
- *Energy cost*: the electricity bill should be as cheap as possible.
- *Demand during on-peak hours*: the highest instantaneous energy consumption during the period of the day with highest electricity rates should be as low as possible.

We use the widely-accepted Percentage of People Dissatisfied (PPD) as a discomfort metric. PPD is defined by the American Society of Heating, Refrigerating and Air-Conditioning Engineers (ASHRAE) (Parsons, 2005) and it estimates the percentage of people that would vote that they are uncomfortably cold or hot if they were surveyed. PPD is calculated as a function of temperature, clothing, activity level of the occupants and air velocity (Parsons, 2005). Because the PPD is an instantaneous measurement, the arithmetic mean of the PPD in all the rooms at all time intervals is used as the objective to minimise.

The energy cost in dollars is calculated based on the residential rates offered by Energy Australia in New South Wales, Australia. Under this scheme, there are three different tariff time bands: *off peak*, *shoulder* and *peak*, each of them with a different price. Table 1 summarises these costs.

Table 1: Residential electricity rates in Australia as of 1 July 2009

Rate	Hours	Price (*cents/kWh*)
Off Peak	10 p.m. to 7 a.m. every day	7.4
Shoulder	7 a.m. to 2 p.m. and 8 p.m. to 10 p.m. weekdays - 7 a.m. to 10 p.m. on Sat, Sun and public holidays	12.8
Peak	2 p.m. to 8 p.m. on working weekdays	32.4

For the residential tariffs shown in Table 1, the maximum demand (in *W*) during the peak hours does not directly affect the end-user bill. However, energy retailers do care about peak demand (which is the reason for higher prices during peak hours), since generation and network capacity must be sized to cope with the highest load, no matter how infrequent it may be. Moreover, some industrial and commercial tariffs explicitly include peak demand charges.

The mathematical formulation of the objectives to minimise: discomfort, energy cost, and demand during peak hours is given by

$$\mathrm{Df} = \frac{1}{R}\sum_{r=1}^{R}\left(\frac{1}{|I|}\sum_{\forall i \in I}\mathrm{PPD}_{ri}\right),$$

$$M = \sum_{r=1}^{R}\left(\sum_{\forall i \in I_{\mathrm{off}}}(W_{ri} - G_i) * M_{\mathrm{off}} + \sum_{\forall j \in I_{\mathrm{sho}}}\left(W_{rj} - G_j\right) * M_{\mathrm{sho}} + \sum_{\forall k \in I_{\mathrm{peak}}}(W_{rk} - G_k) * M_{\mathrm{peak}}\right),$$

$$D = \max_i\left(W_{\mathrm{AGG}_i} - G_i\right), \text{ where } i \in I_{\mathrm{peak}}$$

where

- *Df*, *M* and *D* are discomfort, energy cost and maximum demand respectively (*%*, *$* and *W*),
- PPD_{ri} is the Percentage of People Dissatisfied for the room *r* at the time interval *i* (*%*)
- I_{off}, I_{sho} and I_{peak} are the intervals of time falling into the off-peak, shoulder and peak hours respectively, $I = I_{\mathrm{off}} \cup I_{\mathrm{sho}} \cup I_{\mathrm{peak}}$; $|I|$ is the cardinality of *I*,
- M_{off}, M_{sho} and M_{peak} are the costs of one interval of time at the off-peak, shoulder and peak hours respectively (these prices are taken from Table 1 (*$*))
- *R* is the total number of rooms, or ACs,
- W_{ri} is the power used (assumed at a constant rate) by the AC for room *r* during the time interval *i* (*W*),
- W_{AGG_i} is the power used (assumed at a constant rate) by all the ACs (aggregate) at the time interval *i* (*W*).
- G_i is the power generated (assumed at a constant rate) by the solar panels during the time interval *i* (*W*).

It can be seen in the above equation defining *M* that if the generation is more than the consumption, the energy cost will be negative. In other words, when there is more energy being generated than the amount needed to run the ACs, that energy is sold to the grid and made available for others to use it. In this case, our model assumes a feed-in-tariff where the energy is bought from and sold to the grid at the same price. We chose this scheme for simplicity, although there are several other agreements between generators owners and energy retailers. In some cases the energy might even be exported to the grid at a higher price than it is bought from the grid, because green sources are highly appreciated.

Since more than one conflicting objective is taken into account, there is no single optimal solution to be found but a set of trade-off solutions, each of them giving

different degrees of importance to comfort, cost and demand. Multi objective techniques aim to work on many objectives simultaneously without forcing the user to make the *a priori* decision of selecting weights and aggregating the objectives into one weighted sum. Also, the search space grows exponentially as the number of rooms or time intervals increases, making the problem well suited for population-based techniques such as evolutionary algorithms (EAs). The way we applied MOEAs to the problem described in this work is explained next.

RESULTS USING THE MULTI-OBJECTIVE EVOLUTIONARY ALGORITHM

Multi-objective optimisation techniques aim to find a group of solutions that are as close as possible to the optimal set of non-dominated solutions known as *the Pareto front*. A solution *X* is said to *dominate* another solution *Y* if, at the same time: *(a) X* is not worse than *Y* in terms of any objective and *(b) X* is better than *Y* in terms of at least one objective (Deb K. , 2005).

In this paper we use the NSGA-II algorithm (Deb, Pratap, Agarwal, & Meyarivan, 2000), whose main features are the usage of elitism, an explicit diversity preserving mechanism, with emphasis on non-dominated solutions.

The representation of solutions as well as the genetic operators (i.e. crossover and mutation) were designed as follows:

- *Representation*: For simplicity, each solution is coded as a binary matrix. Rows represent air conditioners and columns, intervals of time. So, if *S* is a solution, then *S(i,j)=1 iff* the *i*-th air conditioner is *on* during the *j*-th period of time. In this paper we use six-minute intervals of time.
- *Crossover*: Two solutions (parents) are used to generate two new solutions (offspring) by randomly picking a row cross point and a column cross point. These cross points generate four sub-matrices for each parent. The top-left and bottom-right sub-matrices of one parent are combined with the top-right and bottom-left parts of the other, forming the first offspring. The unused sub-matrices create the second offspring. Either (but not both) cross points can be zero, leading to two sub-matrices per parent instead of four.
- *Mutation 1*: One random bit in the solution is flipped. This is the traditional mutation operator and its objective is to explore new solutions.
- *Mutation 2*: For one randomly-picked AC, a random number of consecutive bits within the peak hours is shifted left or right a random number of time intervals between 1 and 3, making sure to never exceed the boundaries of the peak-hours period. The idea behind this mutation is that by shifting the control bits, less spiky solutions (in terms of the electricity consumption chart) are encouraged. Preliminary results showed that the introduction of this operator improves the quality of the solution with respect to the peak demand objective.

Table 2: Evolutionary algorithm parameters

Population	50	**Crossover probability**	0.8
Initial pop.	Random	**Mutation 1 probability**	0.1
Generations	9000	**Mutation 2 probability**	0.1
Hard constrain		*mean(PPD) < 6*	

After evaluating preliminary results, the parameters chosen to run the EA are the ones summarised in Table 2.

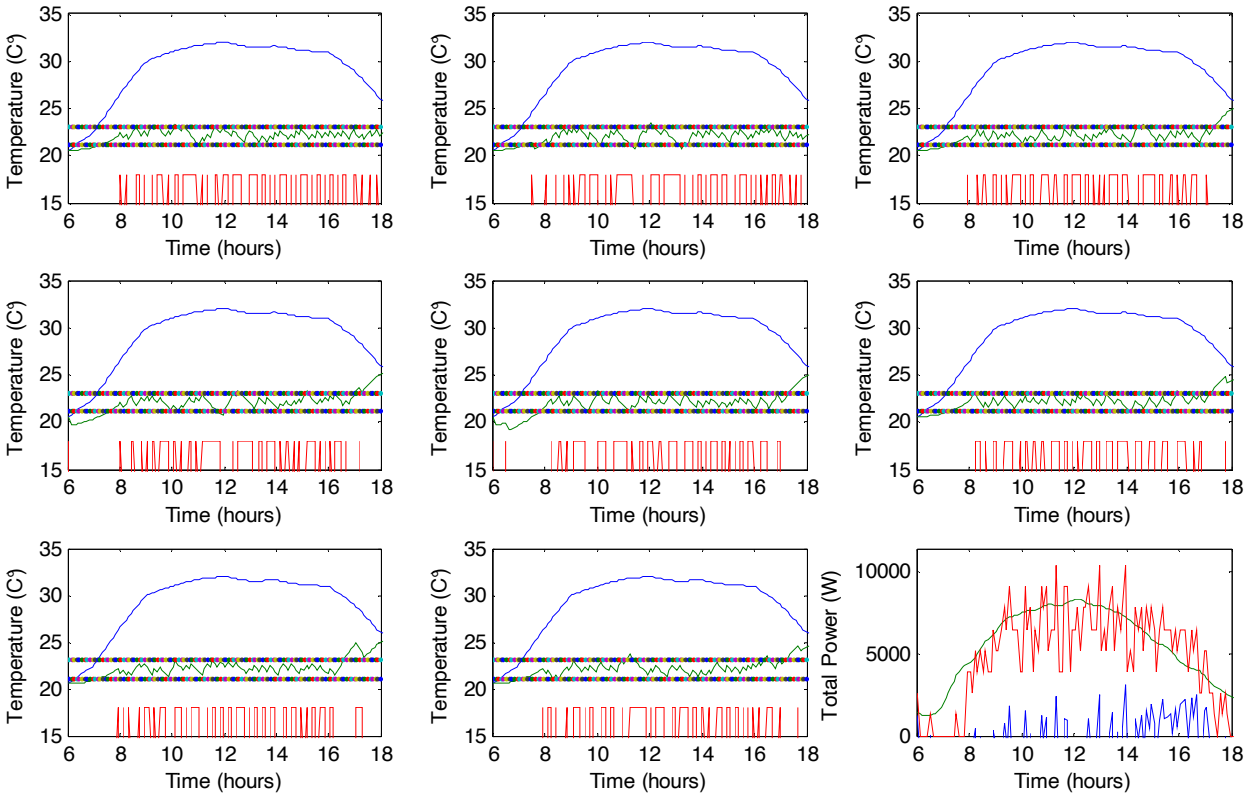

Figure 4: The selected tradeoff solution for 80% renewables. *In all but the bottom-right plot, blue is external temperature, green is internal temperature and red is the AC state (high=on and low = off). In bottom-right plot, green is predicted PV generation, red is power consumption and blue is power imported from the electricity grid.*

This optimisation algorithm returns a set of non-dominated tradeoffs solutions known as the Pareto front. Ideally, the selection of one tradeoff solution amongst all of the ones in the Pareto front should be made by an expert in the area. However, we selected the solution using an automatic algorithm that is described later in this paper. The selected solution after running the MOEA for 80% renewables is depicted in Figure 4. Compared to the solution of Figure 2, the selected tradeoff solution exhibits:

- Negative energy cost (profit), as opposed to positive cost (expense),
- 1.8% less PPD (more comfortable),
- 59.2% less demand on peak hours,
- 5.2% less energy consumed.

The first three items indicate that the selected trade-off dominates the one shown in Figure 2. Note that the fourth item above is not an objective that the MOEA takes into account for the optimisation. However, it is still worth looking at it since it confirms that the improvements achieved are not at the expense of using more energy.
It is fair to compare our results against Figure 2 in terms of comfort and energy cost, since it is a realistic situation. However, it is an unfair comparison in terms of the aggregate demand during peak hours, because in the base case, the ACs are (improbably) “in phase” (switching on and off simultaneously).

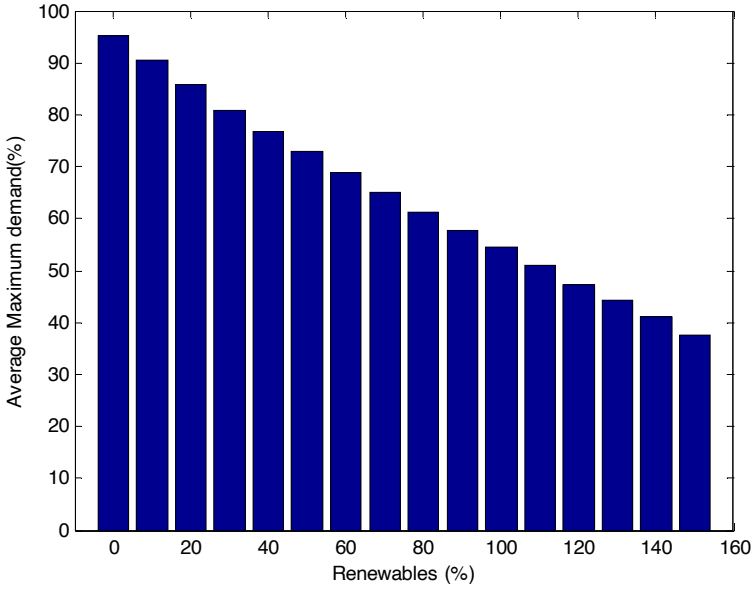

Figure 5: Average maximum demand (normalised to the maximum possible demand, using in-phase switching, with no renewables) for different percentages of renewables.

It would be interesting to quantify by how much the average maximum demand (AMD) is outperformed with our algorithm. In this work we estimate the AMD for our 8-room example by randomly generating solutions that use the same amount of energy as the one in Figure 2. Figure 5, shows the AMD for different amounts of renewables from 0% to 150%.

We define, therefore the business-as-usual (BAU) solution as the solution that exhibits the same energy use, price and comfort as the one in Figure 2 with a maximum demand from the grid during peak hours equals to the AMD in Figure 5 for the corresponding amount of renewables. Note that this underestimates actual BAU peak demand and capacity charges, since these are typically calculated over a month or year –so rather than considering an average peak over one realisation, charges reflect the maximum over 30 to 365 realisations.

Table 3: Running cost, discomfort, peak demand (from grid) and total energy for MOEA and BAU solutions for different amounts of renewables

% Renewables		**0**	**10**	**20**	**30**	**40**	**50**	**60**	**70**	**80**	**90**	**100**
Energy cost ($)	BAU	**20.68**	**18.28**	**15.87**	**13.46**	**11.06**	**8.65**	**6.24**	**3.84**	**1.43**	**-0.97**	**-3.38**
	MOEA	**17.42**	**15.04**	**12.44**	**10.02**	**7.26**	**5.80**	**2.85**	**0.45**	**-1.49**	**-4.96**	**-6.84**
Dis-comfort (PPD)	BAU	**5.59**	**5.59**	**5.59**	**5.59**	**5.59**	**5.59**	**5.59**	**5.59**	**5.59**	**5.59**	**5.59**
	MOEA	**5.46**	**5.44**	**5.53**	**5.56**	**5.59**	**5.37**	**5.62**	**5.49**	**5.55**	**5.66**	**5.56**
Peak (kW)	BAU	**9.89**	**9.41**	**8.91**	**8.41**	**8.00**	**7.58**	**7.16**	**6.76**	**6.39**	**6.00**	**5.66**
	MOEA	**6.50**	**6.06**	**5.58**	**5.59**	**4.76**	**4.26**	**3.15**	**3.37**	**2.47**	**1.76**	**1.39**
Total Energy (kWh)	BAU	**624**	**624**	**624**	**624**	**624**	**624**	**624**	**624**	**624**	**624**	**624**
	MOEA	**686**	**591**	**580**	**584**	**578**	**591**	**582**	**586**	**591**	**573**	**577**

Table 3 shows comparisons in terms of running price, PPD, demand on peak hours, and total energy consumed between the business-as-usual and optimised solutions. We ran

one optimisation algorithm for each different percentage of renewable generation, varying from 0% to 100%[1] with 10% intervals. For each of the categories the comparison is made on, the table presents the values for the BAU solution and the MOEA one. For example, for 80% renewables, the energy cost is $1.43 for the BAU solution and $-1.49 (profit) for the tradeoff solution found running the MOEA.

The tradeoff solutions in Table 3 were chosen using a quantifiable criterion. Populating Table 3 with human-selected tradeoff solutions would not guarantee consistency in the selection criteria, making it impossible to compare columns in the table. For each Pareto front obtained from our optimisations (one for every different percentage of renewable generation) we included in the table the solution with the maximum hypervolume.

The hypervolume of one solution for an *n*-objective problem is the *n*-dimension volume enclosed by that solution and one arbitrarily-chosen reference point *r* so that everything within the hypervolume is dominated by the solution (Bradstreet, While, & Barone, 2008). For each Pareto front we construct *r* with the worst objective values in the whole set of solutions.

Table 3 reveals that in terms of energy cost, the relative improvement of the optimised solution over the BAU increases with the amount of renewables. The reason for this trend is the fact that the MOEA-optimised solution tries to consume the on-site generated energy when the energy price is cheap and sell it to the grid when it is expensive.

The most significant improvements from using the MOEA approach occur in the peak system demand. Peak demand is reduced by around 35% for renewable penetrations smaller than 30%, increasing almost linearly with peak demand reductions of 75% achieved with 100% renewable penetration. The MOEA achieves these improvements by accommodating most of the consumption during the periods of time when generation is available, therefore reducing as much as possible the energy that needs to be imported from the grid to satisfy the demand. Consequently, more generation gives the MOEA more room to place the consumption during the right period of time, producing in turn higher improvements.

The improvements on the peak demand are not at the expense of reduced comfort for the building occupants, as it can be seen from the row in Table 3 showing PPD. The changes are not significant, but if there is a trend, it is that of improving the thermal comfort, since in seven out of ten cases the optimised solution is more comfortable than the BAU one.

On average, the optimised solution consumes 6.4% less energy than the BAU solution, since the temperatures in the rooms at the end of the studied period are higher for the MOEA solution as can be seen from Figure 2 and Figure 4.

It is worth noticing that our MOEA only takes into account the number of times the compressors switch on and off indirectly, by making sure it uses a coarse-enough time quantisation (6 minutes in our case). However, a constraint can be added to the algorithm to explicitly ensure an upper bound on the toggling frequency.

[1] Note that there is no reason to stop at 100% (in fact Figure 5 shows results up to 150%). However, very high proportion of renewables is not representative of the scenarios foreseeable in the near future.

CONCLUSIONS AND FUTURE WORK

When a group of ACs are coordinated to work in awareness of the renewable generation they are connected to, substantial savings in energy cost and maximum peak can be achieved. Managing this peak demand simultaneously benefits consumers, electricity retailers and utilities.

In particular, our proposed MOEA is able to find several solutions that are strictly better than the scenario where the ACs are considered independently, which is representative of the incumbent operation of residential air conditioning. At the same time, optimised solutions help even out the demand during the day, reducing the stress on the network. Moreover, the present research can be applied with no or minor changes to other devices with energy storage such as space and water heaters, fridges and pool pumps.

The optimisation presented in this work assumes that the amount of energy generated by the solar panels as well as the thermal loads of all rooms are known in advance. In practice it is not trivial to obtain this information, since people are not necessarily in their places all the time and also the weather forecast can be inaccurate. Our group is also conducting research on PV prediction (West, 2005; Ward, Platt, & Li, 2008) to improve this forecast. However, the forecast will never be perfect and our algorithm provides a best-effort solution with the data available, leaving it to the implementers of the control system to deal with disturbances.

Summarising, we have clearly demonstrated that by coordinating solar generation and AC loads, there is substantial benefit to both the end user and the electricity network operator. This benefit is currently not being exploited.

REFERENCES

Bradstreet, L., While, R. L., & Barone, L. (2008). A Fast Incremental Hypervolume Algorithm. *IEEE Trans. Evolutionary Computation* , 714-723.

de Ia Rue du Can, S., & Price, L. (2008). Sectoral trends in global energy use and greenhouse gas emissions. *Energy Policy* , 1386-1403.

Deb, K. (2005). Multi-Objective optimization. In *Search Methodologies: Introductory Tutorials in Optimization and Decision Support Techniques* (p. Chapter 10). Springer.

Deb, K., Pratap, A., Agarwal, S., & Meyarivan, T. (2000). A Fast Elitist Multi-Objective Genetic Algorithm: NSGA-II. *IEEE Transactions on Evolutionary Computation* , 182-197.

Goldberg, D. E. (1989). *Genetic Algorithms in Search, Optimization and Machine Learning*. Boston, MA, USA}.

Parsons, R. (2005). *ASHRAE Handbook: Fundamentals*. American Society of Heating, Refrigerating and.

Perfumo, C., Ward, J. K., & Braslavsky, J. (2010). Reducing Energy Use and Operational Cost of Air Conditioning Systems with Multi-objective Evolutionary Algorithms. *IEEE Congress on Evolutionary Computation*. Barcelona, Spain.

Ürge-Vorsatz, D., & Novikova, A. (2008). Potentials and Costs of Carbon Dioxide Mitigation in the World's Buildings. *Energy Policy* , 642-661.

Ward, J. K., Platt, G., & Li, J. (2008). The Virtual Power Station – Reliably Meeting Electricity System Demands With Photovoltaics. *ISES-AP - 3rd International Solar Energy Society Conference – Asia Pacific Region (ISES-AP-08)*. Sydney, Australia.

West, S. (2005). *Photovoltaic Power Forecasting with Support Vector Machines*. Newcastle, NSW, Australia: Final year project, CSIRO Energy Technology and University of Newcastle.

ASI funded Solar Thermal Storage and Steam Programs at the CSIRO and ANU

R. McNaughton[1], R. Benito[1], G Burgess[2], G.J. Duffy[1], J.H. Edwards[1], J.S. Kim[1], K Lovegrove[2], J Pye[2], and W. Stein[1]

[1]CSIRO Energy Technology
10 Murray Dwyer Circuit Mayfield West NSW 2304 Australia
Robbie.Mcnaughton@csiro.au
[2]Department of Engineering, Australian National University, Canberra, ACT 0200, Australia

ABSTRACT

The use of concentrated solar thermal energy for the production of electricity has been achieved commercially with the generation of steam in trough or tower concentrating systems. More recently, solar power stations such as the AndaSol 1 have also included 1,010 MW·h of heat storage, enough to run the turbine for about 7.5 hours at full-load. The thermal storage in the AnderSol 1 solar power station is a molten salt mixture of 60% sodium nitrate and 40% potassium nitrate that is stored in large insulated tanks at temperatures up to 380 º C.

These first generation commercial systems have some limitations in their operation when compared to state of the art fossil fuelled generators; the most significant of these is the temperature and pressure of the resultant steam that is generated and the types of steam turbines that can be utilised. Other major limitations are the ability of the solar system to produce a consistent steam quality required for operation of a steam turbine, and the upper temperature limit that molten salt can be safely stored before it begins to decompose.

The CSIRO and Australian National University (ANU) have recently begun two Australian Solar Institute (ASI) funded projects, one looking at development of high temperature thermal storage systems, and a second investigating techniques for the generation of high pressure and temperature steam. These projects will be undertaken over the next three years.

The high temperature thermal storage project will examine a wide range of techniques, fluids, materials and process designs that will enable the storage of solar thermal heat at temperatures beyond the limitations of the salts used in current solar power generation facilities.

The advanced steam generation project will address the challenges of producing steam at the conditions required to couple solar thermal with state of the art power generation turbines, and through the use of storage technologies enable production of reliable, consistent and high quality steam.

This paper outlines the research directions and the areas of focus of the two projects.

Keywords — solar, concentrating solar, CSP, steam, storage

Introduction

The Australian Solar Institute has recently approved support for two projects to enable the development of critical solar thermal technologies that can make substantial advancements in the ability of solar thermal systems to produce clean reliable electricity.

The projects involve the storage of the heat produced by concentrating solar energy and the conversion of the heat to electricity via the production of steam.

The projects have many areas of interaction.

The thermal storage project

Cost-effective thermal storage systems are required for solar thermal energy to make a significant contribution to Australia's electricity generating sector and to supply the energy requirements of its energy-intensive industries. Such storage systems are required to accommodate periods of cloud cover, overnight operation and, in the case of electricity generation, meet peak power needs that occur outside the hours of maximum insolation rates. In doing so, thermal storage removes many of the intermittent characteristics of solar electricity generation, improves its dispatchability, thereby increasing its level of contribution to total electricity supply.

About half the cost of a solar central tower power generation system is associated with the heliostat field that focuses sunlight on the high temperature receiver located on the tower. The remainder of the cost is associated with absorbing the heat and converting it into electricity. The heliostat system is almost independent of the power conversion technology and thus improvements in power conversion efficiency through the use of higher temperature steam cycles can have a major impact on total power plant costs per unit of electricity generated.

Most electricity generation technologies are based on the Carnot thermodynamic cycle (eg. Brayton gas turbine and Rankine steam cycles) and their theoretical thermal efficiencies increase with increasing the inlet or peak temperature at which the cycle operates. As demonstrated in large solar applications overseas (e.g. Solar One, Solar Two and SEGS and most recently Andasol 1), solar thermal energy storage technologies can provide a continuous supply of high grade, high temperature energy for electricity generation, although the reliability of such systems has been problematic. New solar plants for electricity generation are now also being developed or under construction overseas (e.g. Solar Tres) to implement improvements to earlier designs, but with conventional molten nitrate salts these are restricted to maximum storage temperatures of 565^{o}C, which limits the maximum temperature of the steam produced to 538^{o}C, typical of coal-fired subcritical plants. However, new steam-based power generation technology has advanced to the use of supercritical (566^{o}C) and ultra-supercritical (605^{o}C) steam cycles, as these higher steam temperatures result in higher thermodynamic efficiency. If solar thermal power generation plants are to take advantage of such developments, maintain their compatibility with existing fossil fuel-fired plants and to generate power when the sun is not available there is a need for solar thermal storage systems that can operate well above 565^{o}C.

To date the highest temperature thermal storage systems have used nitrate salts. However, with conventional molten nitrate salts the maximum storage temperature is around 565^{o}C, which limits the maximum temperature of the steam produced to 538^{o}C and thus restricts the options for power generation to the use of lower efficiency

subcritical steam cycles. There is a need to look at means of increasing the storage temperature for the solar energy collected to around 750°C to make possible the use of thermodynamic cycles that operate at higher temperatures and achieve higher efficiencies, hence increasing the power output per unit of capital invested.

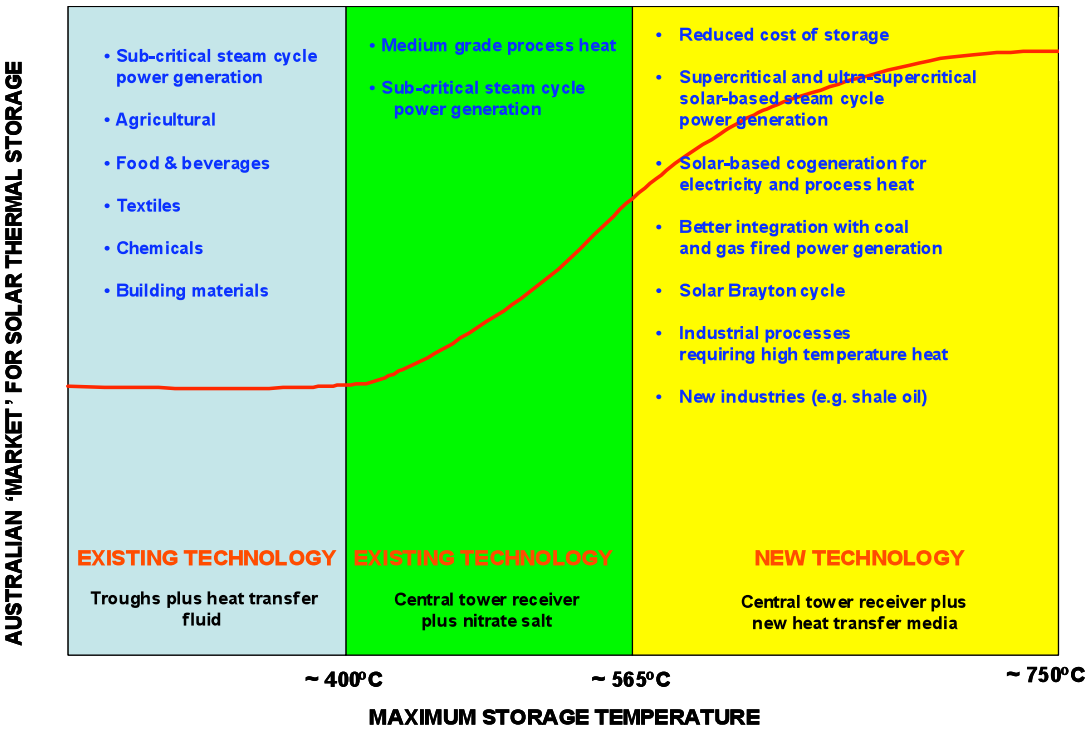

Figure 1 – Benefits of existing and new solar thermal energy storage technologies

This storage project will therefore identify, develop and demonstrate solar thermal energy storage technologies that can operate at as high a temperature as can be reliably achieved (up to 750°C) in order to encourage the widespread use of solar thermal energy by Australian industry and make possible some of the benefits shown in Figure 1.

An important aspect of this project will be to show proof-of-concept of the integration of a solar thermal storage system with a solar energy concentrator/receiver facility to store high grade heat that can be subsequently used on demand by electricity generators and industrial processes relevant to the Australian situation. While new molten salts such as fluorides and fluoroborates will be investigated, other processes utilising gases or solids as the heat transfer media will also be considered. Integration of the heat transfer medium with storage media, such as graphite blocks or other suitable solids or phase change materials, will also be investigated. Results from this phase of the project will then lead to a decision on the type of solar thermal storage loop to be constructed for integration with CSIRO's central tower facility at Newcastle.

Outcomes from this project will be quantification of the potential for integrating solar thermal storage with Australian electricity generation and industrial processes, development of a system that can store solar thermal energy at temperatures up to 750°C, proof-of-concept performance assessment of the optimized storage system under real solar conditions and development of the paths to commercialization for most prospective applications of this technology in Australia. This project will obviously

have a strong link to the steam generation project and will play a crucial role in ensuring the early uptake of solar thermal technologies by Australian industry.

The steam generation project

Rankine cycle power generation is the basis of the production for the majority of the world's electricity normally with thermal energy supply from either coal , oil or nuclear sources. There is a natural fit with CST technology and consequently by far the bulk of commercial CST activity and plant construction uses steam Rankine cycles. This link is a major enabling factor that should allow the level of installed capacity in CST power generation to grow extremely fast. Many of the systems currently being installed use Rankine cycle systems that are less efficient than might otherwise be the case due to the use of steam of limited pressure and temperature. This is a limitation of the linear reflector, whether trough or Fresnel, and the use of oil as the heat transfer medium, mandated by the difficulties of a two-phase fluid over long receiver lengths. Given the high capital cost associated with the collector field, a power conversion efficiency improvement afforded by higher temperature steam means less cost associated with the oil system, less required mirror area and subsequent reduction in levelised energy cost of the output.

The advanced steam project has identified four areas to address:

- To maximise the efficiency of solar receiver systems that produce superheated steam for Rankine cycle power generation
- To produce optimal combinations of heat source and steam temperature such that linear concentrators or geothermal heat sources can be complemented by high concentration collectors.
- To match steam from CST systems to the highest efficiency turbines available.
- To explore the possibility of integrating other energy conversion cycles to produce a higher efficiency combined cycle system, without compromising the reliability of the Rankine cycle approach.

The project will test Steam receivers designed to match the highest efficiency commercial turbines, including supercritical steam turbines (ie more advanced Rankine cycles such as those in the coal-fired power stations most recently deployed in Queensland). It will also test the concept of developing superheating receivers and associated systems suitable for increasing the temperature and efficiency of low temperature thermal technologies such as linear Fresnel or geothermal to above 500°C. Going beyond this the technical and economic feasibility of adding Thermoelectric generating elements to receiver tubes for additional electricity production will be investigated.

The optical, material and heat transfer principles associated with the development of high temperature solar steam generation will translate to most other CST technologies and as such this project can also form a backbone for future CST work.

Strategies for the thermal energy storage project

The objectives for this project are :

1. To assess the Australian market potential for solar thermal energy storage systems that can supply heat at appropriate temperatures (up to 750^{o}C) for both power generation and industrial process applications on a dispatchable basis.

2. To identify suitable heat transfer and storage media for operation at temperatures required in applications identified in Objective 1.
3. To design a solar thermal energy storage system to meet the requirements determined in Objectives 1 and 2.
4. To design receiver systems for tower and dish concentrators suitable for transferring solar energy to the heat transfer medium at temperatures up to 750^{o}C.
5. To construct and operate a proof-of-concept solar thermal energy storage loop, integrated with one of CSIRO's Newcastle solar concentrating field/tower facilities.
6. In conjunction with the steam generation project to evaluate methods for heat recovery from the solar thermal energy storage system.

The strategies to achieve these objectives involve the following activities:

1. A study evaluating the requirements for process heat in Australian industries.
   This will involve identification of the geographic distribution of energy-intensive Australian industries, both current and future (e.g. oil shale processing) and for each significant industrial site, quantification of the demand for process heat, it will include assessment of on-site daily, seasonal and annual insolation rates and other issues (e.g. land availability) to determine the potential for co-locating solar thermal generation adjacent to the industrial site. Economic and systems modelling studies will be carried out to quantify the benefits that solar thermal storage can have on increasing the market penetration of solar thermal energy in Australia. This would include quantifying the curve shown in Figure 1.
2. Identification of the most appropriate heat transfer and storage media suitable for the applications
   From our review of the literature to date on thermal storage it is clear that each of the basic types of thermal storage (sensible heat, latent heat and thermochemical) has its own advantages and limitations. However, what is not yet clear is which one has the best potential for extending the upper storage temperature limit from its current level of 565^{o}C to something approaching 750^{o}C.
   Preparation and characterisation of the preferred heat transfer and storage media in the laboratory will be performed to determine operating envelopes as will the assessment of the impact of such media on the selection of the materials of construction of heat transfer loops and containment vessels. Various system configurations will be simulated using a range of heat transfer and storage media to establish the optimum system that can proceed to detailed design. The design study will be guided by previous CSIRO experience in reactor and heat exchanger design using computational fluid dynamics (CFD) and finite element analysis (FEA).
3. Design of solar receiver systems for tower and dish concentrators unit for the effective collection and transfer of solar energy to the heat transfer medium
   The designs will be guided by previous CSIRO experience in reactor and heat exchanger design using CFD and FEA. Control strategies will need to be developed to link control of receiver temperature with the heliostat operating system.
4. Construction and operation of the solar thermal energy storage system fully integrated with the solar thermal concentrating facility at Newcastle
   This will see the construction of a facility with a storage capacity of around 750 kWh. This stored heat will then be used within the steam project to generate high temperature and pressure steam that can drive a steam turbine.

Strategies for advanced steam generation project

The broad objective of this project is to develop high temperature (>540°C) steam generating solar receivers that maximise the efficiency and cost performance of solar towers or distributed dish systems in the near to medium term.

Each case below incorporates the development and assessment of the receiver in the context of overall plant thermo-economic performance. It is not the intention to develop receivers in isolation.

The specific objectives are:

1. Steam receivers with outputs to match highest efficiency commercial turbines
2. Superheating steam receivers
3. Thermo-economic of solar steam systems
4. Feasibility studies of hybrid steam/thermoelectric receivers

Objective 1

Conventional Rankine cycles have used subcritical steam conditions and this remains the receiver which would be most readily developed under this project. However these steam conditions are still 540°C and 16MPa at the turbine inlet (so higher at the receiver) and no commercial solar plants are operating at this condition in the world. State of the art large scale Rankine cycle power generation utilises supercritical steam for the highest possible conversion efficiencies. This means steam at over 22.5MPa, with temperatures up to 600^{o}C or higher. Under these conditions water does not "boil" in the traditional sense, rather the distinction between liquid and gas is progressive. These temperatures and pressures have been explored in solar receivers in the course of previous work. High strength nickel alloys are required and new approaches to construction geometry must be developed.

Specific strategies to address the first objective will be:

- Establish methods for design and performance modelling of steam receivers and confirm their validity against experimental data
- Develop and test high efficiency receivers for once through to superheat operation at pressures in excess of 10MPa for large dish or tower concentrators. This may include subcritical and supercritical.
    - Review of steam turbines on the market in terms of their allowable inlet condition parameters and subsequent impact on receiver design, including transient temperatures, start-up and shut-down and combination solar/coal –fired operation. This will provide the boundary conditions for receiver design.
    - Assessment of boiler materials - allowable creep/fatigue life, radiant flux, heat transfer, and temperature excursion. This invokes the real-world limitation of available materials, and will investigate more novel possibilities.
    - Consideration of above in relation to recirculation and once-through-type boilers and selection of preferred design/s. Both types of receivers are technically feasible for subcritical, and only once through for supercritical. Both offer various advantages in relation to operational control and cost. These will be assessed in relation to dish and tower systems.

- Use proven models to explore performance of possible geometric arrangements
- Use proven transient models to examine the tradeoffs associated with increased receiver thermal mass

Objective 2

The value of high concentration systems such as dishes and towers lies in their ability to convert energy at higher temperatures than linear concentrators. Consequently in the context of steam based conversion, the feedwater heating and boiling stages underutilise their potential. Other sources such as Geothermal HDR heat or linear concentrators can effectively provide the lower temperatures in bulk. The motivation for consideration of superheat only receivers is the high exergy value gained from introducing only a small level of energy, but at high temperature. The information gained from the once through receivers will be the starting point for these investigations.

Specific strategies anticipated are:

- Determine the most appropriate operating parameters for a receiver designed to superheat saturated steam produced by other sources.
  - Conduct a review in three areas that will provide the design parameters for a superheat steam receiver:
    1. linear reflectors
    2. geothermal technologies
    3. complete system models
  - Construct and test receiver including a front-end system capable of emulating the condition that would be provided by the linear reflector or geothermal heat source in practice.
- Develop and test a receiver system for large dish concentrators suitable for superheating at the required pressures and to > 500°C the saturated steam produced by other lower temperature thermal systems for both dish an tower concentrators
  - Use proven models to explore performance of possible geometric arrangements and transient models to examine the tradeoffs associated with increased receiver thermal mass
  - Model the thermodynamics of integration of the two systems in terms of controlling variable pressure drop, flows and temperatures at the inlet to the superheater.
  - Optimise design including geometry and aperture and complete structural analysis and technical drawings
  - Fabricate, including full instrumentation. Consider use of superheated steam outlet with heat exchanger to simulate the variable low temperature inlet.
  - Test, analyse data, verify and calibrate models.

Objective 3

Each of the receivers above will exhibit different characteristics in relation to operation of large-scale systems. Past steam generation projects in Australia have exhibited issues

with aggregation of steam from multiple point sources. This stream will develop a combined thermodynamic and economic model of complete systems for towers and dishes. This will allow optimisation of tower size vs steam transport path to be conducted.

- Complete analysis of the superheat receiver and thermo-economic modelling in conjunction with industry developers of the low temperature technology.
- Modelling and annual thermo-economic assessment of a supercritical receiver in a complete system and analysis of any refinements that might be recommended.

Objective 4

The intention of this stream is to conduct high level modelling of the potential for thermoelectric devices incorporated into steam receivers. This will provide the framework for another project where devices will be developed, fabricated and tested on sun at small scale.

- Assess the technical and economic feasibility of improving system performance of steam receivers by incorporating thermo-electric elements.
- Provide feedback to researchers working on device development and fabrication in other projects.

Concluding remarks

Over the next 3 years these two projects will develop and demonstrate technologies that will enable solar thermal to be a realistic option for the production on solar thermal based electricity in both the peaking and baseload markets for Australia.

The high temperature thermal storage project will examine a wide range of techniques, fluids, materials and process designs that will enable the storage of solar thermal heat at temperatures beyond the limitations of the salts used in current solar power generation facilities.

The advanced steam generation project will address the challenges of producing steam at the conditions required to couple solar thermal with state of the art power generation turbines, and through the use of storage technologies enable production of reliable, consistent and high quality steam.

Together these projects address the critical issues to allow deployment of solar thermal power in Australia.

This project has been supported by the Australian Government through the Australian Solar Institute (ASI), part of the Clean Energy Initiative. The Australian Government, through the ASI, is supporting Australian research and development in solar photovoltaic and solar thermal technologies to help solar power become cost competitive with other energy sources."

Development of a Low Cost Solar Electric Generator with Thermal Energy Storage

Kame Khouzam
School of Engineering Systems
Queensland University of Technology
2 George St., Brisbane, Qld 4000
Email: k.khouzam@qut.edu.au

Jason Meiklejohn
Global Production Manager
International Clean Energy Pty Ltd
Springwood, Brisbane, Qld 4127
Email: jason.m@icenrg.com

ABSTRACT

The paper presents an experimental study to demonstrate the technical viability of a low cost modular system for generating electricity using a modified Organic Rankine Cycle. The pilot plant comprises of a number of evacuated tube solar collectors filled with a heat transfer medium, a dual heat-exchange system using organic fluid, a heat-storage tank, and a specially designed engine driving an electrical generator. The solar system is designed to raise the working fluid temperature to 150^{o}C using low cost components and local manufacturing techniques. The design intent is to deliver peak power of 5 kW_e providing a predictable and stable output. Depending on the particular needs, the stored energy can be converted to electricity and dispatched to the grid for accommodation of peak load requirement, provide base load capability, power provision in remote areas or other heating applications. Market research substantiates significant demand for this solar system, particularly in many island nations, mining sites and third world countries.

Keywords −evacuated tube collector, organic Rankine cycle, solar thermal energy

INTRODUCTION

Global warming and climate change rightfully continue to be major political issues and as such legislations are being implemented to limit carbon emissions from a number of sectors. Power generation in particular receives significant attention. In addition, many households want to participate in the solution by lowering their own emissions. As such, governments around the world have had the foresight to offer attractive incentives such as renewable energy certificates and feed in tariffs (FIT) for solar power generation.

From the utilities perspectives, these small solar electric generators enables power to be generated where it is needed, mitigates transmission losses, lengthens the life of existing power infrastructure and reduces ongoing capital expenditure. By government providing FIT's, it also enables a significant number of people to remain employed.

However, notwithstanding Australia has embraced FIT legislation, it remains behind by continuing to limit eligible solar power generation to photovoltaic. A significant number of countries around the world have adopted a broader approach to their FIT legislation by including all solar power technologies. By allowing broader application of the FIT in Australia, it would facilitate more technology development, more competition, more job creation and more power generation.

THERMAL ENERGY STORAGE SYSTEM (TESS)

Despite growth in photovoltaic (PV) devices and the introduction of several incentive programs; the uptake of small-scale generation such as PV has been slow especially in industrial and commercial sectors. PV modules are costly and their efficiencies are affected by temperature and incidence angle; thus their output in kWh/kWp is considered low. Such systems operate normally during sun hours with either grid or battery backup. Electro-chemical energy storage is expensive and is complicated by regular maintenance, hazards and replacement costs. Because of high upfront cost, base load capability has been a challenge with PV generation.

Solar thermal electric conversion could be a solution to current technical and economic limitations of small-scale solar power generation by allowing efficient and low cost heat storage and conversion to electricity. Depending on the particular need, the stored energy can be discharged to the grid to accommodate for peak load requirements, provide base load capability or power provision in remote sites. This power generation can be used in residential and commercial applications, and as many of these systems come on line, base load generation will mitigate the need for coal fired generation. Excess thermal energy can be utilised for other purposes such as space heating (or cooling) or just water heating.

TESS Advantage

A large percentage of the overall energy use in a society is required as heat. It is a far better investment to let the sun provide a major share of the energy for low and medium heat applications, in order to recover the benefits of the displaced fossil fuel resources. Thus, less proportion of conventional energy is required. The solar-displaced fuel is returned to power other important elements of the economy. The money that would have been spent for fossil fuels becomes money spent instead, for example, on jobs to produce, install and maintain solar electric generators, and those jobs also enhance the strength of local economy.

Solar heating is hardly a new technology, but even with the continued growth being experienced, it still falls short of its potential. The potential for TESS is huge when approximately 50% of the sun's radiant energy is emitted in the red and infrared regions of the electromagnetic spectrum, a large portion of which cannot be utilised by PV devices (which require minimum photon energy to produce an electron-hole pair). Contrary, solar thermal collectors can utilise almost the entire spectrum and thus are more efficient than PV modules.

The Solution the TESS Presents

TESS efficiently captures solar energy, converts it to electricity using a generator (via a thermodynamic cycle) and stores excess energy in thermal form. The system continues to produce power in conditions that PV would not, thus has the capacity to provide base power capability. This will lower the cost of electricity (compared to PV), improve performance and allow discharge to the grid at required times (such as peak times).

The TESS relies on the use of highly efficient solar evacuated tube collectors to utilise solar heat at temperatures up to 160^{o}C. A heat transfer medium is used to run a modified Organic Rankine Cycle. The pilot plant comprises of a dual heat-exchange system using organic fluid, a heat-store system, and a specially designed scroll compressor driving an

electrical generator. The system is designed for a maximum power output of 5 kW with thermal energy storage to maintain supply for a design period, potentially 24 hours. Notwithstanding the current system is being developed for small-scale industrial use, it can potentially be scaled up.

TESS Innovation

TESS is designed to utilise low cost components and materials such as thermal energy storage, evacuated tubes and a modified scroll engine (adapted from refrigeration). Aside from the evacuated tubes all parts are readily available and simple to manufacture and integrate using local expertise.

The proposed power plant is designed for stand-alone or grid-connected electricity. The peak efficiency is estimated at eight percent. Due to the nature of this system, TESS may lead to a stronger acceptance of solar electric generators, help reduce the stress on the current electricity infrastructure, which is in line with and facilitate many objectives of governments and utilities. Solar generation can make a significant contribution to meeting Australia's targets for the reduction of CO_2 emissions, a social obligation not governed by simple cost considerations.

TECHNICAL DESCRIPTION OF THE TESS

The pilot plant comprises of several modules of evacuated tube (ET) solar collector systems filled with a heat transfer medium, a dual heat-exchange system using organic fluid, a heat-store system, and a specially designed compressor driving an electrical generator. The solar power system is designed to raise the working fluid temperature typically up to 160^{o}C (minimum 120^{o}C) using low cost components and manufacturing techniques. The total efficiency of TESS was modelled using the solar collector (49%), heat storage (98%), thermodynamic cycle (14%) and the generator (91%). Although this is somewhat inferior to PV, the cost per kWh is estimated at roughly two-thirds of PV electricity. A simple block diagram of the system is shown in Fig. 1.

Solar energy (appr. 2000 MJ) is converted to heat by high performance evacuated tubes and transferred to a heat transfer fluid (water) via a heat exchanger in the manifold. This transfer fluid is pumped by a variable speed pump to large scale thermal storage tanks. The fluid is then pumped through a heat exchanger where the energy is transferred to an organic gas under pressure. The gas enters the heat exchanger as a liquid and flashes into its gaseous state as a result of the exchange of heat. This rapid expansion of the gas drives a scroll expander connected to a dc generator to produce electricity, which is then converted to ac using an inverter for grid connection.

Depending on user's requirement, the solar collector and heat tanks are modularised to allow energy for autonomous operation with provision for either:

- Electric power generation of up to 5 kW peak with thermal storage of energy (for up to 24 hours);
- The fluid exiting the heat exchanger can then be applied to an absorption chiller which supplies chilled water to fan units for air conditioning or cool drinking water;
- The stored fluid could also be pumped through the heat exchange coil in a solar hot water tank to maintain hot water at 75^{o}C for supply to a tempering valve in the house plumbing.

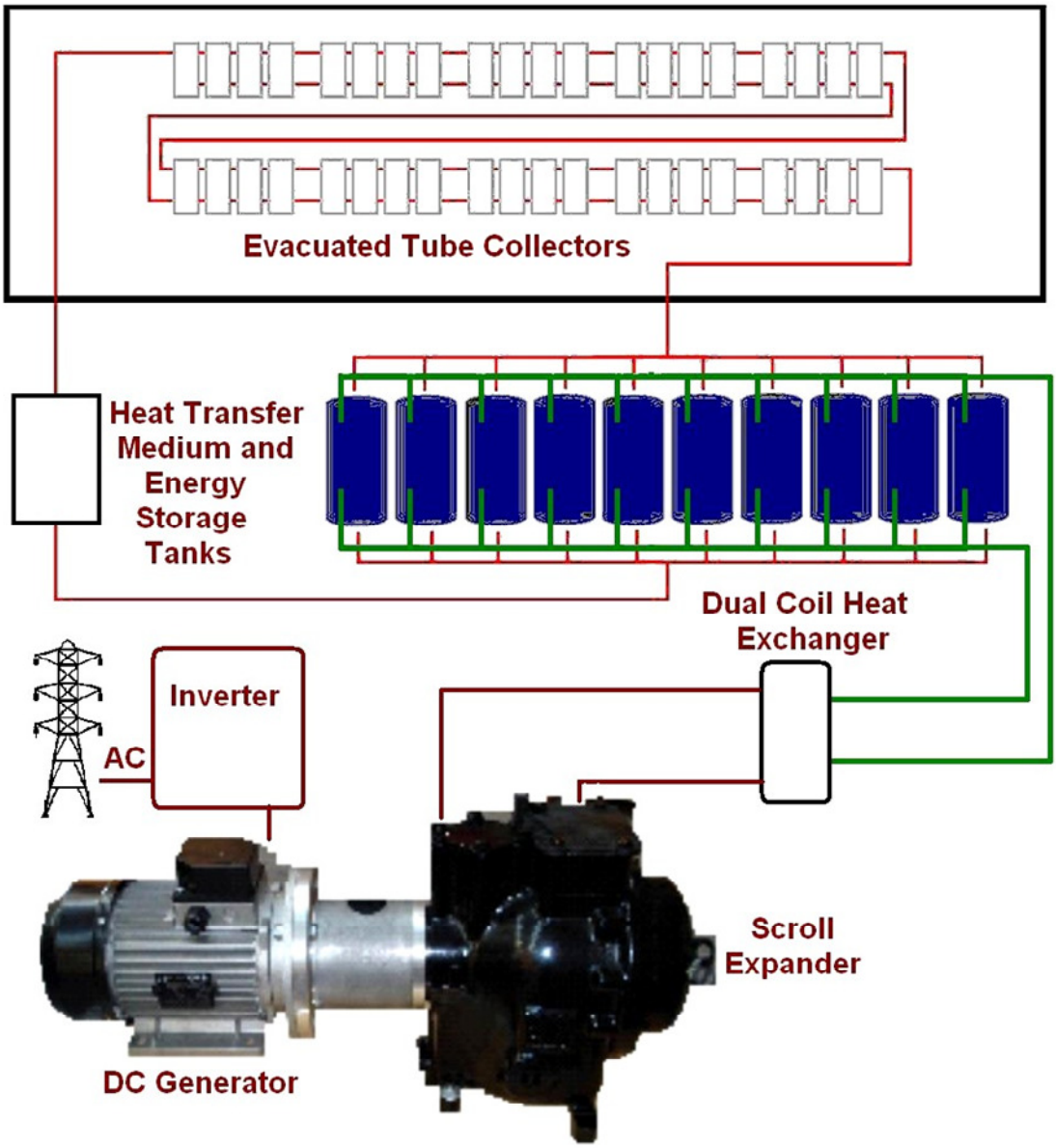

Fig. 1: Schematic of the solar thermal energy system (TESS) for electricity generation

TEST RESULTS AND ANALYSIS

The TESS was designed applying engineering logic and based on the knowledge at the time, the best estimate of what the anticipated component and flow rate requirements were. Once the original prototype was constructed, testing of each aspect of the system (including type of expansion motor, refrigerant type, etc) was undertaken to quantify the inter-relationship between each of the components and empirically verifying the performance of the system (as a whole and individual components). The adopted testing regime facilitated system optimization.

The last testing utilised a scroll compressor operating in reverse as the expansion motor and using R-245FA refrigerant. Our objective was to achieve 18 Bar inlet pressure, but, due to climatic conditions at the time, we were only able to achieve approx. 16 Bar inlet pressure. Table 1 gives a summary of a test result.

Tab. 1: Summary of TESS testing results (sample)

Parameter – Description	Amount
Max (typical) inlet pressure induced	15.6 Bar
Max (typical) outlet pressure induced	7.5 Bar
Max (typical) pressure differential across expander	8.5 Bar
Water inlet temp at max (typical) gas temp	132^{o}C
Water outlet temp at max (typical) gas temp	113^{o}C
Max (typical) gas temp to inlet of expander	126^{o}C
Corresponding gas temp at outlet of expander with max (typical) inlet temp to expander	100^{o}C
Corresponding gas temp from condenser with max (typical) inlet temp to expander	67^{o}C
Power produced at 15 Bar inlet pressure	550 W
Power produced at 16.1 Bar inlet pressure	900 W
Ambient temperature (at time of test)	22^{o}C

Despite unfortunately not achieving the desired 18 Bar inlet pressure, the conclusions were:

- The latest scroll tested is much quieter and starts significantly easier than any previous expansion motors trialled in low temperature applications;
- Need to consider alternative methods of gearing the shaft of the scroll to the PMG;
- Back-pressure must be reduced to enable a higher output. Notwithstanding we have tried to largely utilise components that can be readily accessed, we will need to consider significantly modifying the existing equipment or searching for innovative alternatives;
- Comparing the recent scroll tests (S2) to another test some time ago (S1); they both had similar behavioural characteristics under the conditions tested. A correlation of performance between S1 and S2 was drawn. S1 historically was tested up to 22 Bar inlet pressure (10 Bar outlet pressure) and at that time produced 1.3 kW (ambient temperature appr. 15^{o}C). Given S2 has an expansion ratio of up to 5:1, compared to S1 of 3.5:1, S2 potentially could produce substantially more power than S1 should we reduce the back pressure and/or increase the inlet pressure to approx. 20 – 22 Bar. By virtue of the larger potential expansion ratio, S2 should be thermally more efficient in the process of conversion of thermal to electrical energy relative to S1.

Although it is possible to have a higher expansion ratio with S2 scroll, at this point it is believed that the current design is commercially the most viable solution. When further testing is completed the possibility of increasing the expansion ratio will be considered.

Optimisation of the prototype continues with the primary focus at this stage for power generation. As such, other options for the utilisation of stored energy will be considered at a later time. Of the factors that have been optimised as a result of the testing regime, empirical values have shown that the system is operating as expected. Most key parameters have been investigated, with the completion of the remaining key areas to be evaluated over the next few months. The largest challenge we are currently facing is to achieve adequate pressure differential across the expansion motor. Major work in this area is currently underway including replacing the collector tubes with more efficient ones, incorporating a new heat exchanger and a condenser.

MARKET ASSESSMENT

It is known (Electricity Supply Association of Australia 2009) that an estimated increase of 30,000 MW of new generation plant will be required in Australia by 2030. In addition, Australia's physical energy infrastructure is expected to require renewal and expansion costing around $30 billion over the next ten years. Solar distributed plants can be part of this expansion. Market research conducted by the second author (as part of International Clean Energy) identified demand for TESS in certain countries. This is particularly true with the fact that nearly 25% of the world's population still have no access to electricity.

Several associations including the International Solar Energy Society (ISES) indicate a surge in production of wind and solar electricity worldwide in coming decades. Today, most countries have ambitious goals as it is no longer a question of whether to connect renewable energy, but rather how much will be connected to electric transmission and distribution grids. Consequently, a strong worldwide market exists for the production of renewable power equipment focussing on low cost equipment capable of providing base load generation or discharge of power during peak load at reasonable cost. This would also make carbon reduction more viable in many parts of the world.

An issue of concern to the utility is the variable characteristics of wind and solar power, which call for practices to plan and operate systems expansion. TESS has the ability to provide a more predictable and dependable output. Given TESS base load capacity, and low cost, every roof or available land is an opportunity to generate power. It is clear that solar intermittence can be alleviated by adopting decentralised stations approach and using a mixture of generation options rather than the conventional centralised approach.

Another reason for the existence of favourable market for the TESS is its low energy cost, locally manufactured and reduced carbon footprint from the manufacture and disposal of used product. This is also supported by regulations to reduce emissions of fossil fuels (including carbon tax). The economic benefit of solar thermal electricity in particular justifies research and incentive programs by governments; and expected to yield enormous competitive advantages.

The ultimate goal of TESS is to enable:

- the system owner to be remunerated for the additional energy produced. This would in turn provide incentive to home/business owners and therefore assist in mitigation of the financial challenges they may be experiencing;
- mitigation of brown/black-outs and therefore improved level of reliability to the community;
- the supply of electricity whenever needed such as at peak times (not necessarily during daylight hours);
- reduced demand on escalation of power delivery infrastructure;
- reduced water demands in this industry, given the reduced necessity of generation by coal fired power stations;
- the provision of central heating, air conditioning or hot water, should the owner choose to;
- the possibility to efficiently operate in remote applications;
- reduced greenhouse emissions; and
- job creation opportunities.

Initial survey into other technologies were conducted and showed that the TESS would offer competitive market advantage not only for its capacity to deliver base load power but also for the fact that the system (except for few parts) can be produced in Australia using existing know-how. In time imported parts can be manufactured in Australia, thus providing for our local economy and creating a much needed export income.

COMPETITIVE TECHNOLOGIES

Photovoltaic Arrays

Photovoltaic (PV) arrays are well known and are in use in remote and grid connected applications. After nearly 60 years, they have reached maturity in development and cost. In spite the extensive deal of research and development in PV cells their cost is still high resulting in a total installed cost of about $9 per watt (before subsidy). Since more than 75% of the world's production of PV is based on high grade c-Si, the cost is dependent on the availability of silicon; competing for demand with the electronic chips industry. Commercial PV modules have efficiencies of 14% to 18% at STC (1000 W/m^2, AM1.5, 25^{o}C). Although PV modules are reliable, the daily average (energy) efficiency is low at less than 12%, due to many factors; the most significant of which is temperature effect followed by spectral distribution mismatch, incidence angle loss and dust accumulation. The use of multi-junction cells in concentrators is emerging to improve the efficiency and may lower the cost of PV generation on a large scale; but not to the level required to competing with coal or gas fired power generation.

Although government subsidies exist for residential PV the market uptake is growing rather slow. Considering feed-in-tariff schemes of 44 cents/kWh such as in Queensland, the economic value of PV for home use can only be achieved with PV of more than 1.5 kW exporting at least 75% with a load of less than 10 kWh per day. This scenario can hardly be attained when the average domestic electricity consumption is 21 kWh (tariff 11); equating to more than 3 times the output of a 1.5 kW system (Khouzam and McClymont 2009).

Storage of electricity is normally in the form of electrochemical battery that poses risks, costs, reliability and maintenance issues. Therefore, grid connected PV systems usually do not incorporate battery storage, which diminishes the value of PV generation at least from the utilities perspective. A PV system's contribution is a reduction in fuel burning only during generation. The conventional infrastructure remains to supply the bulk of electricity as base load.

It is worth noting that the making of silicon and non-silicon based devices is not without risks. Many substances and chemicals used in the PV industry are toxic and pose health and safety hazards. The use of silane gas is the most significant hazard in the fabrication of c-Si because it is extremely explosive and presents a potential danger to workers and communities (Fthenakis and Moskowitz, 1990). Accidental releases of silane have been known to spontaneously explode, and the semiconductor industry reports several silane incidents every year (Fthenakis, 2008). PV can leave a toxic legacy if they end up in landfills, where the materials they contain can leach into ground water; or incinerators where burning can release toxic materials into the atmosphere (Silicon Valley Toxics Coalition, 2009).

Concentrating Collectors

Flat plate collectors (FPC) are widely used in hot water systems, but cannot be used in electricity generation due to their low efficiency and low temperature operation. When high temperatures are required a concentrating collector is used. These collectors reflect and concentrate sunlight from a wide area thus simultaneously increasing working fluid temperature and reducing losses. One such equipment, a solar furnace, was installed in Odeillo, France and has several acres of mirrors focused on a single target. The energy concentrated at the target is 3,000 times that received by a single mirror, and the unit produces temperatures of up to 2,000^{o}C.

Another structure, the 'power tower' plant near Barstow, California, generates 10 MW of electricity. Central receiver tower technology, typified by the Barstow Solar One and Solar Two plants, is a second concentrator option. Solar Two has demonstrated 24 hour operation using molten salt as the heat transfer and storage medium. The world's first commercial scale installations (PS10 and PS20) were commissioned in the past year in Spain. These are generally large systems and range of few hundred kWs to few MWs (Frier 2009). Here, the furnace acts as a boiler and generates steam for a steam turbine-electric power plant. In these concentrating collectors such as the tower, each mirror is rotated by a heliostat that directs the sun's rays from the mirror to the target.

Dish systems are a third type in which a parabolic dish focuses light onto a thermal receiver, which may be a Stirling engine or a steam generator. Steam may be generated at the receiver to run an engine or transported to a centralised turbine. Australian National University has worked on the development of large, potentially grid-connected steam generating dishes since 1994 (Lovegrove and Dennis 2006). According to Lovegrove (2009) paraboloidal dish concentrators offer the highest thermal and optical efficiencies of all the concentrator options. This must be set against a higher cost of construction per unit area, compared to linear systems.

Less costly collectors can produce temperatures lower than those of concentrating tower heliostats. For example, parabolic reflectors that concentrate sunlight on black pipes can produce fluid temperatures of 240^{o} to 320^{o}C. Parabolic trough plants have already been developed at the utility-scale, particularly in the US and Spain. Trough technology is integrated into larger combined-cycle plants to help improve the solar economics, as demonstrated at the Solar Electric Generating Systems (SEGS) in California. A number of these plants, with capacity of 354 MWe (Kramer), were built in the 1980's and continue to operate successfully and economically. In Spain, Europe's first parabolic-trough plant came on-line in 2008 with a capacity 50 MW (Andasol 1). More recently, in Morocco and Algeria similar solar installations are being constructed. One of the advantages of solar thermal power, in addition to the cost benefit, is the potential for power storage (Brosseau *et al* 2004).

A more recent option being deployed is Linear Fresnel Reflector technology, in which long reflector rows are aimed at an inverted linear absorber on a linear tower. Mills and Lièvre (Solar Heat and Power 2004) were involved in developing a highly ground area efficient form of this technology called the Compact Linear Fresnel Reflector which has moved to US. The potential cost advantage gained by low temperature operation derives from a combination of a low cost array technology, large low cost low temperature turbines, and an inexpensive storage concept, that suits the particular temperature range. This proposed concept is likely to be the most cost-effective and low risk solar thermal

electricity development path, as it uses simple solar collector technology already being installed, and a proven turbine from the nuclear industry. Levelised costs of around 4 cents per kWh seem achievable with this type of plants (Mills 2007).

Wind power generators are limited to certain locations and may not be practical in urban areas. They are more relevant in remote and hybrid power supply applications and thus will not be considered in this discussion.

EVACUATED TUBE COLLECTORS

Evacuated tube collectors (ETC) have been tested by researchers worldwide including Morrison *et al* (2004). These perform better in comparison to flat plate collectors (FPC) in particular for high temperature operations. They can provide hot water at temperature above 95^{o}C or low-pressure steam at 140^{o}C at efficiency reaching 55%. Tremendous cost reduction in this technology has been achieved in the last few years by way of improved processes and mass production (Walker *et al* 2004).

Previously ETC provided no competition to FPC in Australia because of manufacturing issues and market penetration. This is changing as demand for high temperature and high efficiency applications are needed in the industrial and commercial sectors. The evacuated tube collectors have reached a high level of maturity and low cost production resulting in their widespread use in many parts of the world. ETC now comprise over 65% of 7 million m^2/year solar collector market in China. Indications are that rising energy prices will make ETC economically attractive. Industrial managers constantly search for ways to lower costs of production and ensure maximum efficiency. The potential to produce low cost steam using ETC and thermal storage is possible in particular for applications such as in food and beverage processing.

As indicated the world market for solar collectors is expanding dramatically, resulting in large-scale developments of new technologies and improved quality products. The proposed TESS technology does not require highly sophisticated production facilities such as those used in making silicon devices; when all PV modules in Australia today are imported. TESS has the potential to deliver base power generation at nearly the same efficiency as PV systems but with less cost and using local industries.

CONCLUSION

Concerns over climate change and advances in technology present opportunities as well as pressures to diversify electricity from renewable resources. A low cost modular solar electric generator with thermal storage (TESS) is currently being developed and tested aimed at small scale generation of few kWs. The system uses evacuated tube collectors to heat an organic fluid which in turn operate a modified Rankine cycle engine. Further optimisation of key parameters is still in progress. A market assessment was conducted and favoured this type of generation for grid and non-grid applications. The proposed TESS offers the following advantages:

- Provision of predictable and dependable output;
- Low energy cost, locally manufactured and reduced carbon footprint from the manufacture and disposal of used product;
- Reduction in fossil fuel consumption and associated emissions;

- When completed, it will contribute to the renewable energy industry in Australia as the electricity is generated from solar panels;
- A large amount of electricity can be generated when the grid is highly stressed especially during peak summer times (1 to 4 pm in Queensland);
- The reductions in peak electricity demand will defer and may eliminate the need for construction of new coal-fired power stations; and
- This will save funds towards other critical areas of the economy and help meet emission targets.

Given strong regulations to reduce emissions of fossil fuels (including carbon tax); it is to the benefit of our economy to promote and accelerate solar energy use. The economic benefit of solar thermal electricity in particular justifies research and incentive programs by governments and as such would yield enormous competitive advantages.

REFERENCES

- Doug A. Brosseau, Paul F. Hlava, Michael J. Kelly (2004), *Testing Thermocline Filler Materials and Molten Salt Heat Transfer Fluids for Thermal Energy Storage Systems Used in Parabolic Trough Solar Power Plants,* SAND2004-3207, Sandia National Laboratories, Albuquerque, New Mexico, July 2004.
- Scott Frier (2009), *Solar power for a sustainable world*, Proc. ANZSES Conference, Townsville, Queensland, September 2009.
- Vasilis Fthenakis and Paul Moskowitz, "*An Assessment of Silane Explosion Hazards*," *Solid State Technology* 33(1):81–85, 1990.
- Vasilis Fthenakis, "National PV Environmental Research Center: Summary Review of Silane Ignition Studies," http://www.bnl.gov/pv/abs/abs_149.asp (accessed May 20, 2008).
- K. Khouzam and W. McClymont (2009), *Economic Study of Residential Grid-Connected PV Systems*, Proc. ANZSES Conference, Townsville, September 2009.
- K. Lovegrove and M. Dennis (2006), *Solar thermal energy systems in Australia*, International Journal of Environmental Studies, 63 (6): 791–802.
- K. Lovegrove (2009), *Concentrating solar thermal gathers momentum*, Proceedings ANZSES 2009, Townsville.
- G. L. Morrison, I. Budihardjo and M. Behnia, *Water-in-glass evacuated tube solar water heaters*, Solar Energy, 76, 135-140, 2004.
- D. Mills and P. Le Lièvre (Solar Heat and Power), *Competitive Solar Electricity,* Proceedings of ANZSES Conference, 2004.
- D. Mills (Ausra Inc), *Solar thermal power as the plausible basis of grid supply*, Proceedings of International Solar Energy Society, China, September 2007.
- Silicon Valley Toxics Coalition, *Toward a just and sustainable solar energy industry*, January 14, 2009.
- A. Walker, F. Mahjouri, and R. Stiteler (2004), *Evacuated-tube heat pipe solar collectors applied to the recirculation loop in a Federal Building,* Proc. ASES Conference, Portland, Oregon, July 2004.

Value Creation and the 'Less than Zero' Cost of Renewable Energy Deployment

David Edwards

Renewable Energy Coordinator – Islanded Systems Development

Horizon Power
18, Brodie Hall Drive, Technology Park
Bentley, 6102, Western Australia
www.horizonpower.com.au

david.edwards@horizonpower.com.au
http://au.linkedin.com/in/davidnedwards

ABSTRACT

The most successful organisations understand that the purpose of any business is to create value for customers, employees and investors, and that the interests of these three groups are inextricably linked. Therefore sustainable value cannot be created for one group unless it is created for all three. The first focus should be on creating value for the customer, but this cannot be achieved unless the right employees are selected, developed and rewarded, and unless investors receive consistently attractive returns.

If we can effectively employ a triple bottom line approach to our energy service delivery, sensitively positioning customer engagement; quality of supply; energy efficiency; renewable energy generation and demand side management; if we can empower our customers to make informed choices about their energy use whilst at the same time investing in appropriate technology solutions and research and development into future solutions, we will be able to create real and lasting value for our customers, their communities, the environment, our shareholders, our stakeholders and the industry at large.

This presentation examines a utility scale approach to sustainable service delivery in remote and isolated communities in Western Australia and promotes a methodology which can be employed anywhere in the world. The appropriate use of carefully selected technologies and culturally sensitive deployment models will create transcendent and lasting value reaching far beyond the customer as the first recipient, the monetary value of which, if correctly addressed can be folded back into the initial project justification and business case process.

BRIEF BIOGRAPHY OF PRESENTER

David Edwards is the Renewable Energy Coordinator in Islanded Systems Development at Horizon Power based in Perth, Western Australia. David has experience in utility scale Biogas based generation; the hybridisation of solar concentration and external combustion engine technology; Wind farm development and has contributed to government publications on Biomass Utilisation and Renewable Energy Development.

David is currently working on the development of the Modular, Automated, Renewable and Scaleable (MARS) model for remote generation, the implementation of high penetration solar generation and energy storage management on isolated (or islanded) grid systems and limited RFI power generation for use in Radioastronomy projects.

Energy Efficiency in Remote Indigenous Communities

Fleur Crowe

Sustainable Development Coordinator
Horizon Power Corporation
18 Brodie Hall Drive
fleur.crowe@horizonpower.com.au

ABSTRACT

Implementing energy efficiency and conservation in indigenous Australian communities has helped improve the resident's quality of life, health and wellbeing. Consumers are often unaware of the true cost of running their household appliances and are often surprised by the its cost. Through community engagement and education about energy efficiency, the residents gain a true understanding of their energy use. Horizon Power has developed an Energy Efficiency Engagement Program to assist the community in achieving these goals.

Horizon Power's education program focuses on household energy use. Our energy audit enables residents to understand their energy use in heating, cooling, cooking, lighting and appliances. A profile is then developed which identifies opportunities for energy savings. This assists residents to make informed decisions on how to best use their appliances and purchase energy efficient appliances. Recommendations are made from this program to provide refits to existing housing with assistance from the Office of Energy.

Horizon Power achieves energy efficiency and conservation without compromising standards of living while creating sustainable and long lasting positive impact.

Renewable Energy Penetration Limits for Isolated Remote Area Power Systems

Dr. Worawit Tayati and Gordon Pack

Technical Services
Horizon Power
18 Brodie Hall Drive, Bentley WA 6102
Worawit.tayati@horizonpower.com.au

ABSTRACT

Currently Horizon Power are operating 38 isolated power systems ranging from hundreds kW to tens of MW in generating capacity. These fossil fuel based generation systems are expensive to run and have large carbon footprint. Renewable energy (RE) generation in small isolated and remote power systems is desirable considering its contribution to economic, environment and social benefits. However, the quality of power supply may be deteriorated as a result of high penetration of RE generation installed in customer premises. These systems usually connect to low voltage network and can have adverse effects on increasing power station spinning reserve requirements and causing feeder voltage rises, voltage unbalanced and neutral voltage rises.

This paper investigates step load and voltage rise limits when integrating distributed renewable energy generation systems into Horizon Power's LV network. Mitigation options were addressed and future vision will be presented focusing on emerging technologies such as Advanced Metering Infrastructure (AMI) and Smart Grid.

The step load limit is a result of a sudden and significant loss of overall RE distributed generation such as clouding on PV installations. This can affect the power station stability leading to power supply outage and hence system reliability. Sophisticated integration technology with energy storage is usually required to mitigate this problem but only economically viable for centralised RE generation systems. Alternative mitigation options suitable for distributed RE generation that had been field trialled by Horizon Power are under frequency load shedding schemes at customers equipment e.g. air conditioner, freezer compressor, pump, hot water system etc.

The voltage rise limit is dependent on local conditions and can occur any where in the network. The paper focuses on voltage rise occurring at customer main switchboard which may cause nuisance inverter disconnect. Voltage rise problems can be mitigated by effective LV network design practices and careful consideration in inverter design and installation.

Keywords: Renewable Energy Penetration Limit, Voltage Rise, Step Load Capability, Remote Area Power System

INTRODUCTION

Horizon Power is a vertically integrated, state owned electricity utility responsible for procurement, transport and supplying electricity to regional and remote towns in Western Australia. Horizon Power's service area covers over 2 millions square kilometres with approximately 40,000 customers. This illustrates unique characteristics of dispersed power demand requiring small, distributed and isolated power generation systems close to the demand. Currently there are 38 isolated power systems ranging from hundreds kW to tens of MW in generating capacity.

Horizon Power have been continuously promoting and supporting renewable generation and efficient use of electricity under renewable energy buy back scheme (REBS) and a current feed in tariff. Unfortunately, small generation systems have a limited capacity to accept intermittent renewable generation such as solar PV and wind. This is due to a step load capability of fossil fuel internal combustion engine driven generators which is limited to approximately 30% - 50% of the unit power rating. High penetration of renewable generation in small and remote power systems is major concern of Horizon Power to ensure that the quality of power supply is maintained within acceptable limits.

Furthermore, high RE penetration in low voltage network can have adverse effects on feeder voltage especially voltage rise as reported by Liu and Bebic (2008). Utilities worldwide are aware of this voltage rise issue. Particularly in Australia, inverters manufactured in Europe were reported to disconnect from the grid due to excessive voltage rise.

This paper reports investigations into technical limits of isolated power systems in accommodating high penetration of renewable energy generation. Power system modellings were undertaken to evaluate the technical impacts of high penetration of decentralised renewable generation on LV network. The limits considered include generation, network feeder and transformer capacities and operational performance parameters such as voltage and frequency regulation.

Voltage rise in customer premises were given special attention in this paper. Possible solutions to mitigate limit violation and to allow high level of integration of renewable energy generation to isolated power supply systems are recommended.

REMOTE TOWN PENETRATION LIMITS

Remote community power generation is usually based on multiple diesel or gas engine driven electric generators as shown in Fig 1. Horizon Power's power station operation design philosophy is such that N-1 criterion is maintained i.e. an unplanned loss of a single unit will not cause loss of supply or system performance limit violation.

For example, Fig. 2 shows frequency deviations of a 360kW diesel generator after sudden load increases of 200kW and 300kW from no load and a 200kW step load increase from initial loading of 100kW are applied at t=0 s. This represents a condition of loss of a generating unit. The generator frequency deviations are proportional to the step load magnitude. It is noted that for the same step load of 200kW, the initial generator loading of 100kW resulted in a greater frequency drop than when the generator initially carried no load. It can be seen that at a step load of 200kW the system frequency quickly recovered to within 5% (2.5Hz) in 3 seconds which is deemed acceptable.

Horizon Power had undertaken comprehensive studies attempting to identify the town RE penetration limiting criteria. The study recommended the minimum of the following three criteria as the limit.

1. *Approximately 50% of the smallest generator capacity installed at the power plant*
2. *Approximately 30% of instantaneous network load at the time of peak renewable generation*
3. *Approximately 15% of the annual peak demand*

Studies had been undertaken to determine the limit for each town. The result was published as a guideline for Horizon Power's internal assessment of generation connection applications.

When Horizon Power considers integrating renewable generation in power station design, the allowable penetration level for our customers will be reduced.

move this text to after figs 1&2

(a)

Preferably move figs 1a) & b) to a single page, on page 3.

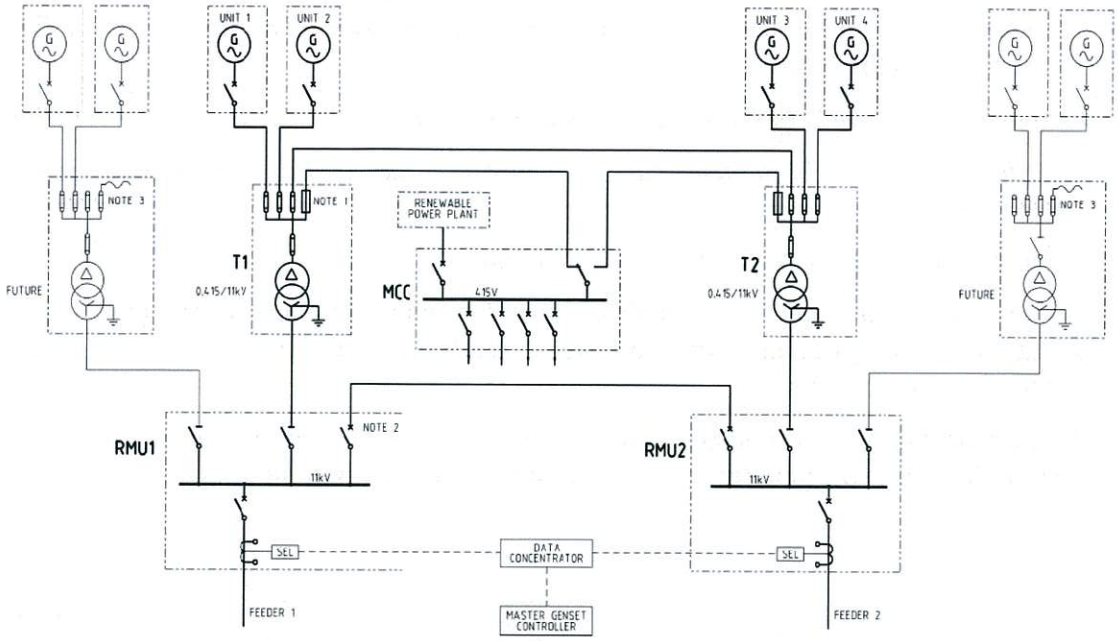

(b)

Fig. 1 (a) Aerial View and (b) Power Supply Diagram of a Typical Remote Community

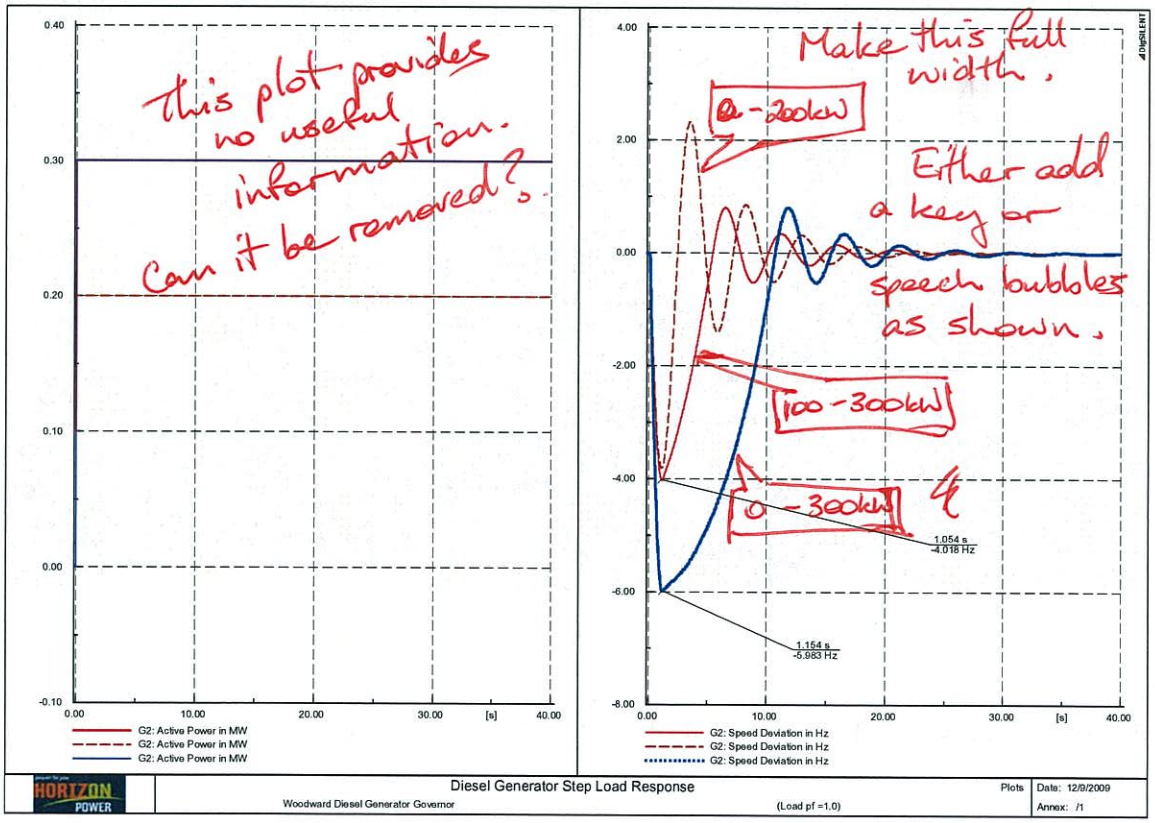

Fig. 2 System frequency excursion following step load changes

Discussion

Horizon Power has been investigating options to mitigate the generating unit step load capability limit. The principle is to maintain balance of system load and generation at all time. This includes distributed under frequency load shedding at customer deferrable loads such as air conditioner, freezer compressor, pump, hot water system etc. Field trials had been undertaken using commercial devices for demand response enabling devices such as Enermet's SWITCHit low frequency load shedding. This device will switch off electrical appliances when the system frequency drops below a set point. And hence reducing the magnitude of step load seen by generating units following any load increase and/or any loss of generation. Advanced Metering Infrastructure (AMI), when implemented, can provide two-way communications which will enhance effectiveness of the distributed UFLS scheme.

LOW VOLTAGE (LV) NETWORK PENETRATION LIMITS

Horizon Power had investigated voltage rise as a result of high penetration of PV on LV networks and the study outcome was reported by Tayati and Pack (2009). Horizon Power in collaboration with Western Power has recently put in place a simplified technical assessment policy described in Section 15 Embedded Generation of Western Australian Distribution Connection Manual (2010). This provides simplified processes for the assessment of applications to connect renewable energy systems to a network in regional towns serviced by Horizon Power. The technical assessment process adopted by Horizon Power, which assumed an approved inverter is used, is summarised below.

System Categories

Systems will be categorised according to the inverter rating. Where the intended installed renewable capacity is lower than the inverter capacity the application will be assessed according to the inverter rating. This provides a one pass assessment of the greatest system impact allowing for the possible future expansion of the renewable energy source.

Category One System:-

One single phase inverter with a power (Pmax) rating less than or equal to 1.75kW

Category Two System:-

One or more single phase inverters with a total combined Pmax rating greater than 1.75kW and less than or equal to 3.3kW

Category Three System:-

One or more single phase inverters with a total combined Pmax rating greater than 3.3kW and less than 10kW per phase

Category Four System:-

Systems with Pmax greater than 10kW per phase

Requirement for Technical Review

Category 1 and 2 systems may not require technical review unless the conditions below apply. Technical review shall be required for any of the following conditions:-

- Systems with an inverter rating greater than 3.3kW – category 3 and 4
- Distribution transformer is less than 63kVA
- There are less than 10 customers on the network
- The inverter is not on the approved list

- Multiple inverters are being used
- A second application is made for an existing installation
- Any of the stated limits are exceeded for the total number of installations on a system
- Any of the stated limits are exceeded for the installation

Assessment

Renewable energy applications will be assessed to ensure:-

- Embedded generation can not operate in an islanded situation
- System generation step load capability is not exceeded. Ref section 9.3
- Voltage rise at customer point of supply meets requirements
- Network thermal limits are not exceeded
- Neutral current due to imbalance between phases is limited
- Potential rise on earth circuits is limited

Assessment criteria

Customer Service Connection Rating Limit

Individual systems will be limited to 33% of the service connection rating.

Tab. 1 Customer connection limits

Typical Service Lead Rating	Inverter Rating
Rural 32 Amp connection	2.5kW
Town 63 Amp single phase	5kW
Town 32 Amp three phase	2.5kW per phase/7.5kW total

Feeder/Transformer Limits

To ensure voltage regulation within the required limits is maintained, WA Distribution Connection Manual 2010 required that the total embedded generation on any feeder will not exceed 30% of the transformer rating.

Embedded generation feeding into a network causes the voltage at the customer rise above the network voltage which if it is not controlled can cause customer voltage to exceed upper limits and risk damage to their installation. However, a more typical outcome is that the inverter will disconnect if these situations persist over 10 minutes period.

Tab. 2 Customer voltage rise analysis results

Scenario	Voltage at PoS (pu)	Voltage at Inverter (pu)
No load	1.042	1.042
3kW load – No PV	1.042	1.035
5kW load – No PV	1.042	1.030
7.5kW load – No PV	1.042	1.024
3kW PV – No load	1.042	1.049
5kW PV– No load	1.042	1.054
7.5kW PV– No load	1.042	1.060
7.5kW PV– No load*	**1.042**	**1.051**

Note * Two connecting cables are connected in parallel to halve cable impedance.

Analysis of the Results

Table 2 indicates that a PV system with inverter rating capacity of 3kW, 5kW and 7.5kW capacity result in a voltage rise at the inverter terminal of 0.7%, 1.2% and 1.8% respectively. At voltage of 1.054p.u or 253V, a conventional inverter design practice such as SMA (2002) would disconnect the inverter from the grid to avoid excessive network voltage rise.

The analysis result confirms that with 2.5kW PV installation on a 32A customer circuit would not cause voltage rise beyond the acceptable limit. And the inverter disconnect will not occur provided that the point of supply voltage is less than 250V (1.042 pu).

Mitigation Options

It is recommended that the LV network design taking into account voltage rise in addition to a compliance with the wiring rules. Table 2 shows that employing two 4 mm^2 cables in parallel for 7.5kW PV installations the voltage rise is maintained within the limit.

Inverter with reactive power or voltage control capability is generally envisaged as an alternative option to mitigate voltage rise problem. However, at low voltage level where network impedance is predominantly resistance (R/X ratio greater than 50) this option is ineffective and is not recommended. Though voltage rise can be controlled by reducing inverter power output, the benefit of renewable energy generation is lost.

Discussion

The voltage rise issue which resulted in inverter disconnection is Australian specific issue arising from incompatibility between utility practice and Australian Standards. A majority of Australian utilities adopt 240/415V as LV standard voltage and +/-6% voltage variation during normal operating condition. On the other hand, the Australian Standards has attempted to be in line with IEC standard and has recommended 230/400V as the standard voltage. IEC compliance inverters were factory set as a default to disconnect at 10% voltage rise (i.e. 253V). The setting has caused nuisance trips in Australian installations. It may be viable that the setting is modified to meet the Australian conditions.

HORIZON POWER LV NETWORK DESIGN STANDARD

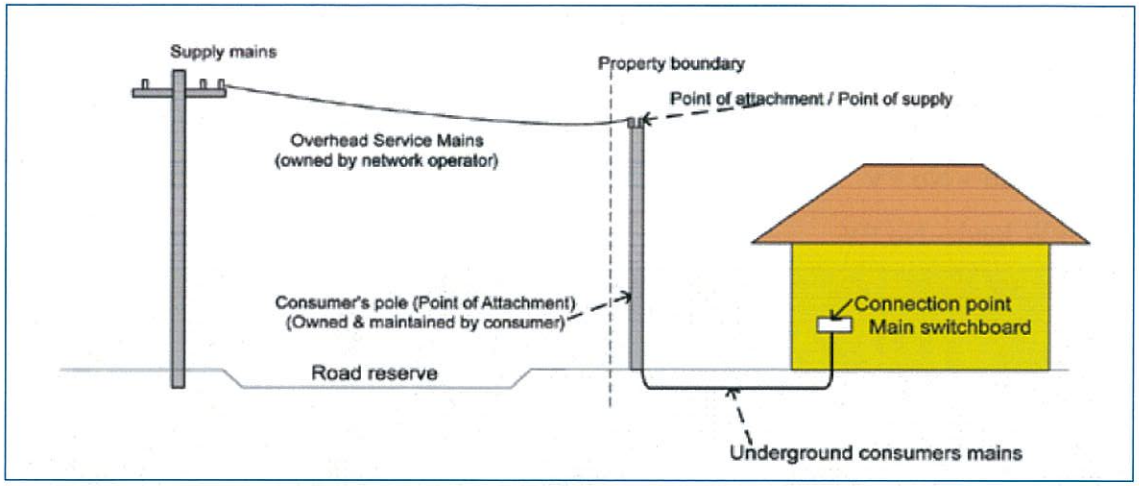

Fig. 3 Typical LV net work design

Horizon Power design standard for residential LV network are summarised below.

- Overhead service mains (6 mm^2 conductors) are selected for 32A circuit capacity and allows for voltage range +/-6% at point of supply.
- Consumer mains are sized for 32A circuit capacity and allows for negligible small voltage drop between point of supply and main switchboard. Horizon Power adopted 16 mm^2 conductors as standard consumer mains, taking into consideration being surrounded by thermal insulation and hence de-rating.

CONSUMER VOLTAGE RISE ANALYSIS

Customer voltage rise analysis was carried out to assess voltage variation at customer switchboard and at point of utilisation due to a single PV installation within the customer premise. The analysis studied cases included various demand and PV generation output conditions.

PV systems are connected via inverters to the LV network at the customer main switchboard via a connecting cable running from inverter output terminal. Customer voltage rise is analysed based on Horizon Power's design standard and the following assumptions.

- Customer circuit rating is 32A, single phase.
- Voltage at point of supply and customer switchboard is maintained at 250V (i.e. + 4.2% of 240Vnominal).
- Inverter cable employed is 25meters of 4 mm^2 conductors with impedance of 5.61 +j0.102 ohm/km (R/X ratio = 55).

How can you know this is true ?

The analysis results are given in table below.

CONCLUSIONS

This paper presents technical limits relating to high penetration level of small renewable energy generation systems to Horizon Power's LV network. The limits identified are related to the power station step load capability and network voltage rise. The step load limit is due to overall system penetration while the voltage rise limit can occur any where in the network e.g. at customer main switchboard. Voltage rise problem can be mitigated by effective LV network design practices.

REFERENCES

A.F. Povlsen, "Impacts of Power Penetration from photovoltaic power system in distribution network," Report IEA-PVPS Task 5, February 2002

E. Liu and J. Bebic, "Distribution System Voltage Performance Analysis for High-Penetration Photovoltaics", National Renewable Energy Laboratory (NREL) Report, NREL/SR-581-42298, February 2008

SMA Solar Technology AG, Technical Information, "Grid Connection – Influence of the grid conditions in terms of connected power of PV inverters". http://download.sma.de/smaprosa/dateien/7418/Netzanschluss-UEN083010.pdf

W. Tayati and G. Pack (2009) "Determination of PV Penetration Limit in LV Network" ANZSES Annual Conference, Townville, QLD 2009

Western Power and Horizon Power, "Western Australian Distribution Connections Manual", 2010

BRIEF BIOGRAPHY OF PRESENTER

Worawit Tayati is a power systems engineer with Technical Services, Horizon Power based in Perth, Western Australia. He has extensive experiences in power system analysis including planning, power systems studies e.g. motor starting, interconnection of new load and generation. He has also worked in the field of hybrid diesel and renewable energy generation for remote area power supply (RAPS) for more than ten years. Worawit has worked with an international organisation promoting renewable energy for remote islands and villages in developing countries in South and South East Asia.

Fabrication of Refractory Thermionic Emitter Materials for Direct Solar Energy Conversion – Work in Progress

Heber O. Sugo [1] and Erich Kisi [2]

[1]Senior Research Fellow
School of Engineering
Faculty of Engineering and Built Environment
The University of Newcastle
Callaghan, NSW 2308
Heber.Sugo@newcastle.edu.au

[2]Professor
School of Engineering
Faculty of Engineering and Built Environment
The University of Newcastle
Callaghan, NSW 2308
Erich.Kisi@newcastle.edu.au

ABSTRACT

The conversion of thermal energy directly into electricity is ideally suited for concentrated solar thermal applications. The direct conversion of thermal energy to electricity is possible via thermoelectric, thermionic or combinations of these phenomena. The development of high temperature thermionic devices is being undertaken at the University of Newcastle, School of Engineering with funding from the Australian Solar Institute. The research phase is currently focused on producing and characterizing emissive cathode materials which are stable at elevated temperatures. This report provides a brief description of the project and outlines the work in progress.

Keywords* *direct energy conversion, thermionic, work function measurement

INTRODUCTION

The conversion of thermal energy directly into electricity by solid-state devices has been used for several decades for power sources in space vehicles. The potential exists to apply these principles to harvest solar energy. The direct conversion of heat to electricity is possible by utilizing materials which exhibit thermoelectric or thermionic phenomena. Thermionic devices are of special interest due to the potential for higher operating efficiency and working temperatures of 1000-1500ºC which are easily achieved via concentrated solar arrays (Krieder 1979).

Theoretical analyses of thermionic emission are presented by Krieder (1979) and Angrist (1982). In simple terms, the thermionic process can be described as electrons "boiling off" from the hot surface (emitter), traversing across the emitter/collector gap and condensing on the cooler electrode (collector). The flow of electrons can be used via an external circuit to provide electrical energy as shown in Figure 1.

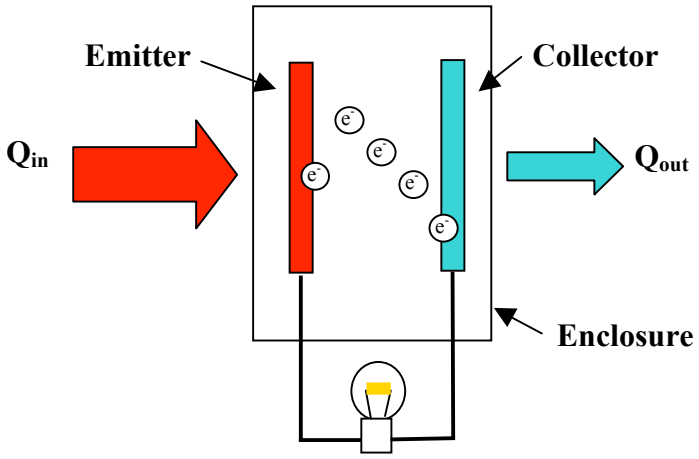

Figure 1. Vacuum Type Thermionic Converter

Due to the possible build up of free electrons (space-charge) which hinders further emission, the electrode spacing plays an important role in determining the output current of the device. Various separation techniques are used and these include evacuated space with and without the introduction of caesium ions or solid (semiconductor) materials. Under optimum space charge and collector conditions, the saturation current from the emitter is described by the Richardson-Dushman equation (see Angrist 1982):

$$J = A_1 T^2 \exp[-\phi/(kT)]$$

where: T is the electrode Temperature (Kelvin)
A_1 is the emission constant (120A/cm^2.K^2)
k is Boltzmann constant
and ϕ is the work function of the emitting material

The ability of the electrodes to emit and collect electrons is therefore also important and requires the determination of the electronic work function for candidate materials. Typical emitter materials included metallic tungsten and tungsten-ceramic composites however recent advances involve the use of diamond and carbon nanotubes (Koeck *et a*l 2009 and Raffaelle *et a*l 2005).

Thermionic devices can also be used in tandem with thermoelectric materials to increase the overall energy recovery. However, the focus of this research project is to construct a working prototype thermionic device capable of operating at elevated temperatures and high heat fluxes for use in concentrated solar thermal systems.

This proof-of-concept is being undertaken at the University of Newcastle, School of Engineering with funding assistance from the Australian Solar Institute. The research phase is currently focused on producing and characterizing emissive cathode materials which are stable at elevated temperatures. This report outlines the work in progress.

RESEARCH PROGRAM AND WORK IN PROGRESS

The project duration is three years and the research activities can be summarized into three phases:

Phase 1: Fabrication and process optimization for the production of thermionic emissive substrates with low work function and high current density characteristics. Evaluation of substrate physical and electronic properties.

Phase 2: Establish collector compatibility with emitter material. Optimization of the device fabrication with consideration given to vacuum/space separation requirements.

Phase 3: Performance testing: long-term current-voltage characteristics, poisoning of emitter/collector electrodes, diffusion of atmospheric gases and microstructural changes. Monitor physical modes of failure, thermal shock and dimensional stability.

The high temperature usage of thermionic devices necessitates the use of refractory materials. This in turn, places special demands on the synthesis and shaping of the emissive materials. Efforts are being directed at both conventional high temperature processes (1600-2000ºC) and novel low-temperature paths.

Scanning electron microscopy and x-ray diffraction of synthesized emitter materials is underway. Various substrates will be manufactured over the next few months and characterised prior to measurement of work function and current density outputs.

SUMMARY

This presentation provides a brief overview of work-in-progress at the University of Newcastle to fabricate thermionic devices suitable for concentrated solar thermal applications. This is part of a three year project funded by the Australian Solar Institute. This research is necessary to demonstrate that thermionic devices; capable of working at elevated temperatures are a viable method of converting solar energy to electricity. This proof-of-concept development work is essential to bring the technology to a level which is attractive to industry for wide-scale deployment of the technology.

ACKNOWLEDGEMENTS

The authors would like to thank the Australian Solar Institute for providing financial support to carry out this work.

REFERENCES

Angrist, S., W., "Chapter 6. Thermionic Generators in 'Direct Energy Conversion'." Allyn and Bacon, Boston, 1982, 4th Edition.

Koeck, F. A.M., Nemanich. R.J., Lazea. A. and Haenen, K. "Thermionic electron emission from low work-function phosphorous doped diamond films." Diamond and Related & Materials, 18, pp.789-791, 2009.

Krieder, J., "Chapter V, Solar Thermionics in 'Medium and High Temperature Solar Processes' ". Academic Press Ltd., London, 1979.

Raffaelle, R.P., Landi, B.J. Harris, J.D., Bailey, S.G. and Hepp, A.F. "Carbon nanotubes for power applications." Materials Science and Engineering B116, 2205, pp 233-243.

BRIEF BIOGRAPHY OF PRESENTER

Dr Heber Sugo has a background in materials science. He has worked in industry and academia for 25 years and has a wide range of interests ranging from passive solar design of buildings, materials for energy harvesting and the use of cementitious materials to reduce embodied energy.

Low cost, building integrated CPV using standard solar panels[1]

Dr. Alonso Marquez[2]

[2]Ideasol Australia Pty Ltd

alonsom@tpg.com.au Ph: 0416168563

Abstract

The objective of our project has been to create a commercially viable, low maintenance solution for solar electricity generation using Concentrated Photovoltaic (CPV) technology.

During the development of a low cost, commercially viable CPV product we've faced the following challenges:

(1) Limitations on the availability of specialized CPV cells in contrast to the relatively low efficiency and larger size of commercial panels.

(2) Technical complexity associated with Sun tracking systems versus intrinsic limitations of non tracking concentrators.

The high cost of specialized solar cells for CPV and a continuos fall in the price of solar panels has driven our decision to use commercial solar cells/panels in our project. However, commercial solar panels are two orders of magnitude larger in size than specialized solar cells for CPV (around 1 cm). Our challenge was that none of the current concentrator designs would be compact enough to fit a commercial solar panel within a building integrated CPV.

We focused our initial development effort in non tracking concentration due to its lower manufacturing and maintenance costs. Using innovative non imaging concentration techniques we have been able to come reasonably close to the limits of static concentration in a very compact design that minimizes reflection losses by using Total Internal Reflection (TIR).

We have developed a first prototype using low cost materials (acrylic) and widely available manufacturing processes. This initial version uses standard 1.75 Watt solar cells, is translucent to Sun light (the solar cell is placed in a vertical position) and is compact enough to be fit in the roof of a house. This design could theoretically achieve a concentration over x5 (assuming no reflection losses and an optical grade cutting of the acrylic pieces). Our current tests show an increment of x3.5 in energy generation of the solar cell and we expect additional improvements through the use of more sophisticated manufacturing techniques.

We are currently designing a second generation prototype using bifacial solar panels. This second prototype will concentrate x4 the light on each side of the panel, achieving a reduction of around x7 on the surface of solar panels required in contrast to current commercial PV systems of similar capacity.

In both cases the potential savings are quite significant. The innovative concentration technique created will allow for a great variety of forms and shapes to generate electricity and hot water (e.g. facades, building roof tops, etc). More advanced manufacturing strategies are currently been explored.

[1]We are proudly assisted by Business and Industry Development, ACT Government.

World's First Solar/Diesel Hybrid Generation Power Marble Bar and Nullagine– A Post Implementation Review

David Edwards

Renewable Energy Coordinator – Islanded Systems Development

Horizon Power
18, Brodie Hall Drive, Technology Park
Bentley, 6102, Western Australia
www.horizonpower.com.au

david.edwards@horizonpower.com.au
http://au.linkedin.com/in/davidnedwards

ABSTRACT

Horizon Power has built the world's first two high penetration solar/diesel hybrid power stations in Marble Bar and Nullagine in the Pilbara region of Western Australia, two of the hottest towns in the country. These two power stations use a unique combination of flywheel - kinetic energy storage; single axis tracking photovoltaic solar arrays; diesel generation and an integrated control system to achieve a penetration of up to 87% of renewable energy into the town distribution networks during the hours of sunlight. The annual penetration of around 30% sets a new standard for utility scale deployment of solar energy into regional towns.

This presentation is a post implementation review of the stations design; the deployment methodology; technical performance to date and a vision for future projects.

BRIEF BIOGRAPHY OF PRESENTER

David Edwards is the Renewable Energy Coordinator in Islanded Systems Development at Horizon Power based in Perth, Western Australia. David has experience in utility scale Biogas based generation; the hybridisation of solar concentration and external combustion engine technology; Wind farm development and has contributed to government publications on Biomass Utilisation and Renewable Energy Development.

David is currently working on the development of the Modular, Automated, Renewable and Scaleable (MARS) model for remote generation, the implementation of high penetration solar generation and energy storage management on isolated (or islanded) grid systems and limited RFI power generation for use in Radioastronomy projects.

A Supply-Demand Model for a Zero-Carbon Australia

Trevor Jack[1], Robyn Bateup[2], Vernie Everett[3]

[1]Jack Actuarial Consulting (JAC) Pty Ltd
[2]Bateup Actuarial + Consulting Services Pty Ltd
[3]Centre for Sustainable Energy Systems
The Australian National University, Canberra, Australia
vernie.everett@anu.edu.au

ABSTRACT

The primary intent of the paper is to expose a mechanism for more rationally debating the question "Can intermittent renewable power replace base-load coal?" A national demand scenario is compared with renewable supply model sourced from Beyond Zero Emissions' proposed Zero Carbon Australia 2020 (ZCA) Stationary Energy Plan [1]. Both supply and demand models, at half hourly periods over 2008 and 2009 use real NEM demand, NEM wind supply and satellite derived insolation data to identify the extent to which the proposed renewable energy mix would meet demand. The ZCA plan aims for 40% wind and 60% concentrating solar thermal (CST).

The paper covers development of the detailed demand model, conversion of NEM wind supply data to that based on 50 GW capacity and conversion of satellite derived daily global horizontal insolation to half hourly direct normal insolation, and then, through a power tower, to electrical supply.

The analysis reveals that:

- the proposed supply mix meets 98% of demand without use of biomass;
- the biomass boiler capacity of approximately 10 GW is adequate to meet otherwise unmet demand; and
- approximately 23% of harvestable solar energy is lost due to poor seasonal solar/demand correlation.

Keywords: base-load renewables, renewable supply-demand model, Zero Carbon Australia

INTRODUCTION

Climate Change imperatives present strong drivers to reduce carbon emissions. Beyond Zero Emissions (*BZE*) has recently drafted a plan [Wright, Hearps, 2010] to de-carbonize Australia by 2020 – the Zero Carbon Australia (*ZCA*) plan. In order to test the capacity of the proposed renewable generating capability to meet demand, a fine time-scale supply-demand correlation model has been developed. The model uses actual data for insolation, wind, and NEM demand for 2008 and 2009 and uses estimated changes in demand to reflect, at a high level, various aspects of the full BZE plan. This paper reports on the results of that model.

Although demand and supply have been modeled, the model does not include any allowance for transmission constraints or losses. The generating mix is that proposed by BZE. There has been no attempt by the authors to estimate the costs associated with this generating mix, or to assess the optimality of the proposed mix. Also not questioned as part of this study, was the overall demand level which, amongst other

considerations, was assumed by BZE to incorporate substantial energy efficiency improvements, energy source switching, and reduction in private vehicle use.

DEMAND MODEL

The demand model is the sum of:

(a) Existing National Electricity Market (NEM) demand, which in 2008 and 2009 averaged 206 TWh, scaled down to 175 TWh to reflect energy efficiency gains without changing the half hourly pattern; and

new demands for

(b) Heating, ventilation and cooling (HVAC) totalling 66 TWh p.a., with demand higher at times of low insolation in Victoria in winter, and at times of high insolation in Queensland in summer; and

(c) Industrial use and transport (IT) totalling 83 TWh p.a.

The total demand is 325 TWh p.a. as projected by [Wright et. al., 2010]. Details of the model components can be obtained from the authors.

SUPPLY MODEL

Transmission constraints and line loss considerations have not been explicitly incorporated in this model, although there is implicit allowance since the total energy supply is built up from current generator output which covers these losses.

Concentrating Solar Thermal (*CST*) generation

It was inappropriate to use Typical Meteorological Year (*TMY*) data, since the task involved investigation of the correlation of renewable sources of power with actual demand, albeit as modified by scaling and addition of HVAC and IT. Accordingly, actual renewable resource data were used rather than TMY data. Data for calendar years 2008 and 2009 have been used. The ZCA plan proposes 42.5 GW of CST spread evenly across 12 sites.

Daily Global Horizontal Insolation (*GHI*) estimates, derived from satellite imagery by the Bureau of Meteorology, are available at a fine grid across Australia. Data for the 12 ZCA CST sites were used, with daily GHI transformed to estimated half hourly Direct Normal Insolation (*DNI*) by site. The ZCA stationary energy report [Wright, Hearps, 2010] details a 217 MW solar power tower that is the basis for most of the projected solar thermal power generation. The design of this system is covered by Sargent et al. (2003), with the Solar 220 standard plant having a solar multiple of 2.6, and a storage capacity, using molten salt technology, of 17 hours. A solar multiple of 2.6 indicates that, at maximum insolation, the collector field would deliver energy to the receiver at 2.6 times the rate required to run the generator at rated capacity. 17 hours storage indicates that a fully charged reservoir could run the generator at rated capacity for 17 hours with no insolation.

The electrical equivalent power captured each half hour at each CST site from estimated DNI derived from Erbs et al (1982) is calculated by:

(Estimated DNI/reference DNI) x solar multiple x site capacity x relative field efficiency factor

= (Estimated DNI /1.15 kWm^{-2}) x 2.6 x 42.6 GW/12 x relative field efficiency factor

= Estimated DNI x 8.03 GW x relative field efficiency factor.

The reference DNI, 1.15 kWm^{-2}, derived from Sargent et al specifications, is the DNI required for the plant to capture thermal energy at maximum capacity. The relative field efficiency factor, higher in summer and for lower latitudes, allows for the variation in cosine losses by latitude and season. It averages 99% and varies from 105% (summer) to 97% (winter) for Prairie (latitude = 21º S) and from 100% to 87% for Mildura (latitude = 34º S). Each of the 12 sites is considered to have the same generating capacity, solar field, and storage capacity.

The Solar 220 performance, including a 72% capacity factor, is based on DNI, quoted by Sargent, of 8.054 $kWhm^{-2}$. The average daily DNI over the full 2 years and across all CST sites was 8.314 $kWhm^{-2}$. The annual capacity factor with no load constraints, using the above DNI to electrical equivalent net energy conversion for all 12 ZCA sites, was 75% for 2008 and 80% for 2009. These are higher than the Sargent & Lundy capacity factor because of higher Australian insolation and higher average field efficiency due to the lower average latitudes.

Wind

The ZCA plan proposes 49.5 GW of wind capacity across 24 sites. Energy production data from 9 NEM wind generators were extracted from NEM publicly available data sets, providing power output at 5 minute intervals, averaged to half hour periods. The sites available are fewer in number and less geographically diverse than proposed by the ZCA model. Nevertheless, these were the best data sets in real time that were available.

Recorded power production during each half hour for each site was converted to a capacity factor using the published capacity of each power station. The overall ZCA wind capacity of 49.5 GW was distributed evenly across the 9 sites for which wind data were used, set at 5.5 GW at each site. The derived capacity factor, by site and period, was multiplied by this 5.5 GW capacity to obtain energy production by site by period.

Biomass

In order to allow for periods of low insolation, the ZCA stationary energy plan provides for subsidiary biomass boilers at the CST plants; allowing the plants to be characterised as hybrid CST/biomass plants. Total biomass boiler capacity has not been separately attributed to different sites, and optimal distribution has not been considered in this model. It has been assumed that the biomass boilers would operate only to charge the reservoir. They have been incorporated in this model by simply providing for the specified capacity to be converted, at full capacity, from biomass to thermal energy stored in the reservoir. While this does not reflect actual operating conditions, errors introduced by this assumption are inconsequential to the overall model. Different biomass boiler capacities were tested.

Secondary biomass boilers, at a pre-determined proportion of the CST plants, are considered as strictly subsidiary with the thermal energy converted and stored in the reservoir available for dispatch when the overall stored thermal energy drops below a specified minimum reserve capacity; but only up to the level of generator capacity. A range of these minima, referred to as reservoir trigger levels, have been tested in the model.

Hydro

The hydro model is very simple, with 5 GW total capacity assumed. Reservoir capacity is not considered, and energy is assumed to be available for dispatch, but only up to the level of generator capacity.

Dispatch

A very simple dispatch model is used with the order of dispatch being wind, then CST, then hydro.

Biomass capacity is not directly dispatched to the grid. Rather, biomass boilers are triggered as required to heat the CST reservoir, with the energy in the reservoir dispatched through normal CST generation. For the purposes of this model, the transmission capacity is assumed to be infinite and lossless. There is no provision for storage of wind-generated power, so all wind power is dispatched at the time of capture.

CST is assumed to be dispatched as necessary to meet demand. This is constrained by thermal lag, turbine capacity, and thermal storage capacity. The calculation process for each half hour period is to;

(a) add captured energy to the thermal reservoir, on a site-by-site basis, if the site reservoir has unused capacity; and

(b) dispatch energy to meet demand in such a manner that each site retains a similar reserve energy level in the reservoir.

The reservoir balancing process can be affected by local conditions on a time-scale of days, for example, with one site suffering a significant cloud event and therefore not being recharged over a few days, while reservoirs at other sites not suffering cloud shading, would become more highly charged. Accordingly, energy from these latter sites would subsequently be dispatched in preference to the sites with lower reservoirs.

Smart grid, load shedding, and EV charging

No allowance has been made for a smart grid. It is likely that a smart grid would allow load shifting and load management procedures sufficient to remove the effects, or adequately manage the periods, of short term unmet demand on the time-scale of hours. A smart grid would not be able to contribute to ameliorating the seasonal mismatch of supply and demand.

The demand model does not provide for the additional load shifting, or demand management, that would be possible with a substantial private EV fleet; nor for EV fleet to supply the grid.

RESULTS

All of the results in this section, whether shown as annual, monthly, daily, or hourly, arise from summing data from half-hourly projections using the model described above.

Seasonal supply/demand mismatch

There is a substantial aggregate oversupply during the warmer months – available energy from wind and CST in December is 41 TWh against demand of 26.8 TWh. The corresponding figures for June are 29.8 TWh of wind and CST supply and demand of 28.0 TWh. Figure 1 shows averages over 2008 and 2009 for June and December. Although supply exceeds demand in June in aggregate, this masks a small unmet demand of 0.2 TWh as shown in Figure 1, which arises when the supply and demand are poorly correlated.

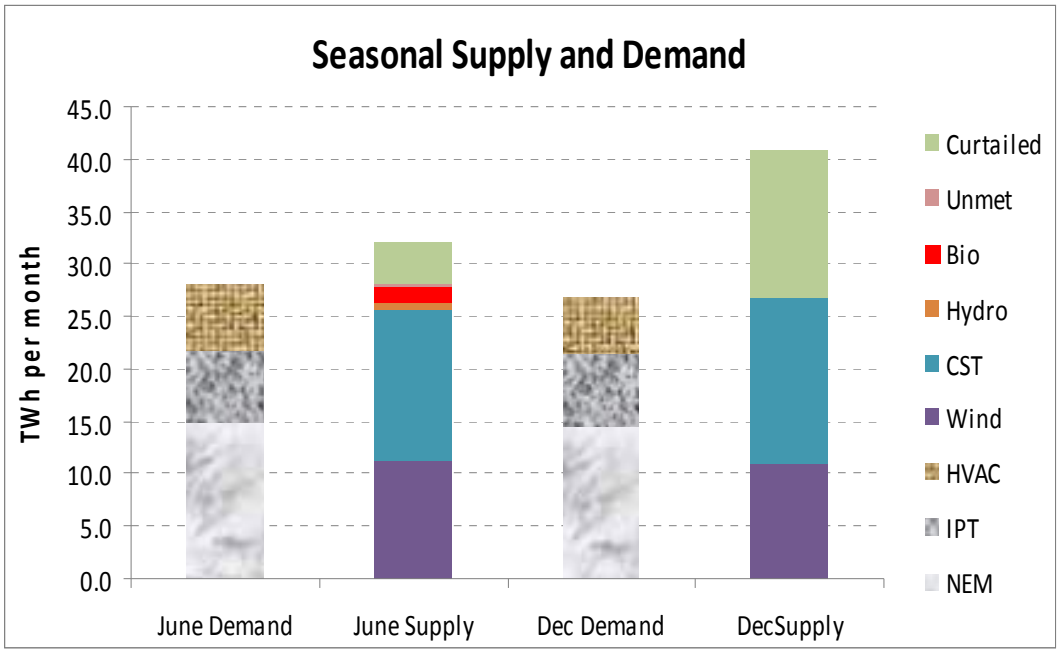

Fig. 1: Average modelled supply and demand for various energy sources for 2008 and 2009.

Major Supply Components

Figure 2, covering the full years 2008 and 2009, shows a summary of monthly energy supply contributions by various technologies to the total supply, and demonstrates that supply is dominated by wind and CST. Small values for unmet, hydro, and biomass appear in the annual summarised Table 1 below.

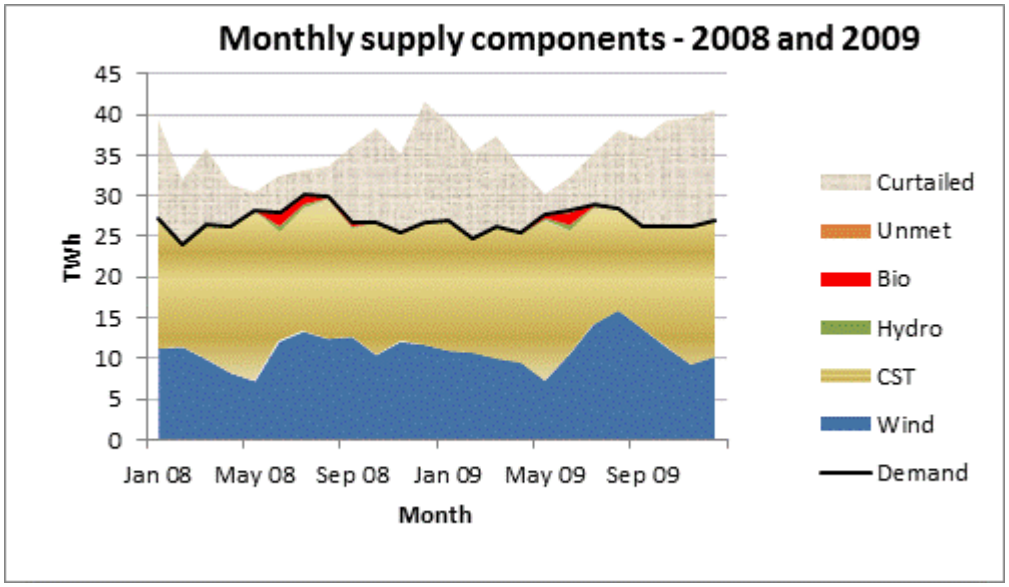

Fig. 2: Modelled monthly supply components for 2008 and 2009.

Tab. 1: Annualised summaries of modelled supply components and related capacity factors for 2008 and 2009.

Supply components				
TWh per annum			**Capacity Factors**	
	2008	**2009**	**2008**	**2009**
Wind	132	134	30%	31%
CST	188	185	50%	50%
Hydro	1	1	3%	3%
Bio	3	3	4%	3%
Total	326	323		
Demand	325	322		
Unmet	0.1	0.1		
Curtailment	92	113		
Solar supply + curtailment	281	298	75%	80%

Unmet Demand

Although modelled unmet demand is low in aggregate, amounting to less than 0.1 TWh in each of 2008 and 2009, it is important to consider the distribution of this unmet demand. With 10 GW biomass boiler capacity and boiler triggering at 5 hours reservoir capacity, there were 13 days over the 2 years where there was some period, in some cases as little as half an hour, of unmet demand. The modelled total deficiency of supply, and the maximum hourly deficit for each day on which there was any deficiency for the two cases of 5-hour and 8-hour reserve capacity triggering, are shown in **Error! Reference source not found.**.

Tab. 2: Unmet demand for modelled supply components and related capacity factors for 2008 and 2009.

Unmet demand				
	5Hr trigger, 10GW cap		8Hr trigger, 10GW cap	
	Total (GWh)	Maximum (GW)	Total (GWh)	Maximum (GW)
3/06/2008	3.6	3.6	0	0
9/06/2008	13.9	9.0	0	0
10/06/2008	24.6	5.9	0	0
28/07/2008	21.2	18.0	0	0
29/07/2008	8.1	8.1	0	0
20/05/2009	4.9	4.9	0	0
2/06/2009	0.4	0.4	0	0
3/06/2009	3.7	3.7	0	0
4/06/2009	14.1	13.3	0	0
24/06/2009	0.1	0.1	0.1	0.1
26/06/2009	51.5	20.7	0	0
27/06/2009	118.6	22.1	106.4	21.6
17/07/2009	39.3	16.6	0	0

In the case of 8-hour triggering, there were only 2 days on which there was any unmet demand. On the first of these, 24 June 2009, unmet demand was 114 MW during a one hour period from 6pm to 7pm. During this period, the wind contribution was only 0.9 GW, which is less than 2% of capacity, and demand was unusually high at 48.6 GW. The unmet demand arose even though the CST reservoirs were not empty. The model projected that the CST turbines ran at full capacity – that is, 42.6 GW. However, the sum of the CST full turbine capacity, the full hydro capacity of 5 GW and the poor wind

contribution of only 0.9 GW was deficient by 0.1 GW. Increasing biomass boiler capacity or triggering biomass firing earlier would clearly not deal with this deficit.

The second day with unmet demand in the 10 GW, 8-hour trigger case was 27 June 2009. Here the overall deficit was 106 GWh with a maximum of 21.6 GW. This result is not materially better than the deficit on the same day that is projected for the 10 GW, 5-hour reservoir trigger. The overall deficit of 106 GWh represents about 2.5 hours of storage.

With a 15 GW boiler capacity the small deficit on 24 June is not eliminated, as this is a total generating capacity and wind issue, rather than a storage issue, as described above. If, however, a 15 GW boiler capacity is combined with an 8 hour trigger, the deficit on 27 June is eliminated. That the 15 GW boiler capacity can eliminate a deficit, relative to the case of a 10 GW boiler capacity, which includes a maximum of 21.6 GW may appear counter-intuitive. However, the greater boiler capacity would be firing for several hours before the advent of the largest deficit – these several hours of firing would have contributed to the reservoir which can then be dispatched through the CST generators.

No optimisation of biomass boiler capacity versus trigger level reserve capacity, for any given CST and wind mix, has been performed. However, some results, using various biomass trigger points and boiler capacity combinations to determine the unmet demand, the quantity of biomass energy electrical equivalent consumed, and any "wasted" biomass capacity, will assist in structuring the optimisation procedure.

Tab. 3: Unmet demand for modelled biomass usage for a range of trigger reserve capacity rates for 2008 and 2009.

Unmet demand, biomass usage, and biomass curtailment									
TWh	Bio Boiler (GW):	5	10	15	20	5	10	15	20
	Trigger (hrs)	2008				2009			
Unmet	2	2	1	0	0	2	1	0	0
	3	2	1	0	0	1	1	0	0
	5	1	0	0	0	1	0	0	0
	8	1	0	0	0	1	0	0	0
Bio	2	2	3	3	4	1	2	3	3
	3	2	3	4	4	1	3	3	3
	5	3	4	5	5	2	4	4	4
	8	4	6	7	7	3	5	6	6
Wasted	2	0	0	0	0	0	0	0	0
	3	0	0	0	1	0	1	1	1
	5	1	1	1	1	1	1	1	2
	8	2	3	3	4	2	3	3	4

The biomass firing model makes no allowance for forecasting capacity. That is, the trigger is used regardless of forecast future renewable resources. For example, in the 10 GW 5-hour trigger case, if the thermal reservoir dropped below 213 GWh(e) at 9am on a day forecast to have strong winds, clear skies and good insolation, the biomass boilers would still be fired at that point. If, however, forecasting were taken into account, it is improbable that the biomass boilers would be fired.

Correspondingly, if a period of several days of poor wind and high cloud were forecast, even though the thermal reservoirs were quite full the biomass boilers might be fired in order to store more energy to get through the forecast lean renewable energy period. Consequently, the biomass indicated as being "wasted" by the model in Table 3 above

sets an upper bound on biomass curtailment given that any allowance for forecasting would improve firing efficiency, almost regardless of the sophistication of the prediction.

Capacity Factors

The following chart shows monthly capacity factors. The insolation series shows the expected CST capacity factors without curtailment. That is, the expected capacity factor given that all available power could have been dispatched. The annual capacity factors for 2008 and 2009 were, respectively, 30% and 31% for wind, 50% each year for CST and 75% and 80% for insolation.

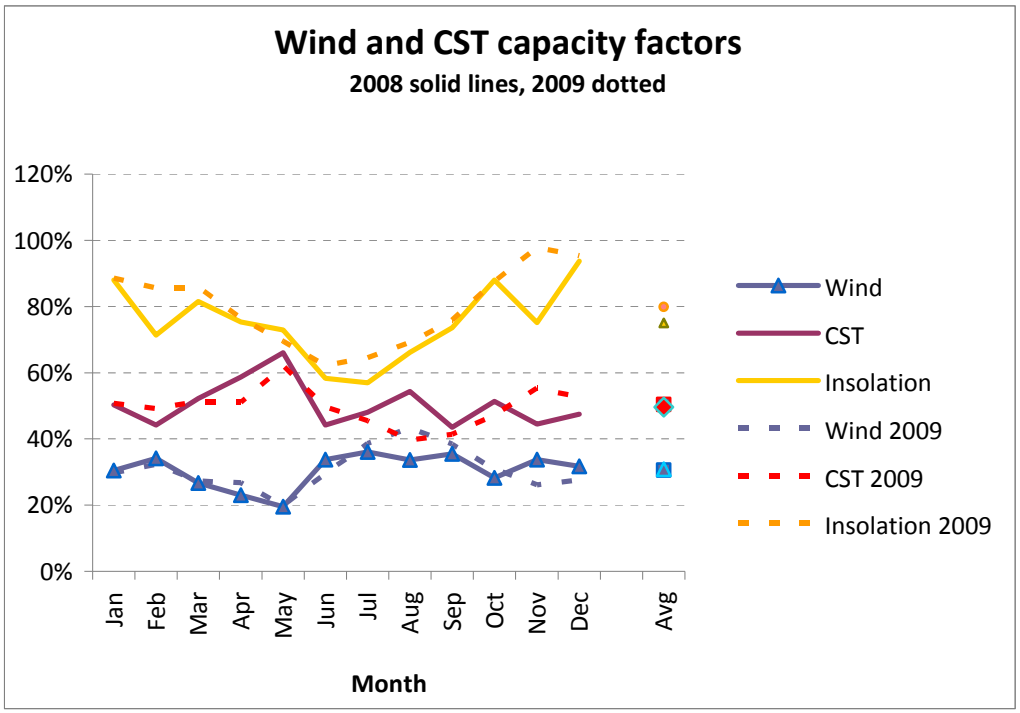

Fig. 3: Wind and CST capacity factors for 2008 and 2009

INTERPRETATION OF RESULTS – OPTIMISATION CONSIDERATIONS

The supply mix that has been modelled was specified by BZE. The BZE specification was essentially derived from aggregate and average considerations of demand and CST and wind capacity factors. The fine time-scale modelling reported here has been performed primarily to verify that the high-level design determined from these aggregate/average factors is sufficient to continuously meet demand. Subject to the model deficiencies discussed below, our model confirms supply adequacy except for the short periods of unmet demand discussed above.

As previously mentioned, there has been no attempt in this model to optimise the supply mix. Notwithstanding this limitation, the modelled results suggest various changes to the overall supply mix structure which may be closer to the optimal arrangement. Therefore, the considerations presented in this section should be considered speculative, since they represent conceptual structures for further research, rather than well-developed, detailed proposals.

Seasonal supply – pumped hydro

Unless demand is changed substantially to switch from winter to summer, substantial CST curtailment would arise in the summer with the proposed supply mix. Replacing

some CST capacity with pumped hydro might introduce the ability to shift, for example, 30 TWh of energy captured by CST in the summer to pumped hydro storage primarily for dispatch in the winter.

Even with relatively small storage capacities, but significant generating capacity, pumped hydro could provide the supply mix with significantly greater robustness. Because pumped hydro has very short response times compared with thermal systems, it is ideal for meeting peak generating demand. On a daily time scale, pumped hydro storage capacity infrastructure requirements are quite small. Higher storage capacities would provide seasonal redistribution capacity and also allow for greater short term robustness. Pumped hydro could also replace CST biomass backup. A further advantage of pumped storage in comparison with CST biomass backup is the significantly higher complete cycle efficiency.

CST versus biomass backup

Excess usage of biomass occurs when the firing algorithm, essentially the pre-determined reservoir level that triggers firing, causes biomass boilers to be fired but the subsequent combination of wind, insolation and demand are such that, had the biomass not been fired, there would have been no unmet demand. This excess firing of biomass is determined from the current model by subtracting the reduction in the unmet demand, that is, the demand that is met as a result of firing the biomass boilers, from the quantity of biomass energy consumed in terms of its electrical equivalent. This modelled excess is found to be relatively small.

The fact that excess biomass usage is minor suggests that the combination of biomass, solar multiple, and reservoir storage may be far from optimal, particularly in terms of the allocation of capital cost. In order to quantify this, it is instructive to examine the modelled distribution of reservoir storage over time. The results, shown in Table 4, detail the specific proportion of modelled half-hour periods in which the reservoir has a particular reserve storage capacity. These data represent the reservoir level before any allowance for biomass charging. The reservoir is clearly well-charged for the majority of the time. This suggests the need to investigate a lower storage capacity, and in particular, alternative methods, or blend of methods, for meeting short-term demand.

Tab. 4: Reservoir status as a function of reserve capacity.

Reservoir distribution	
Reservoir capacity 'R' (hrs)	Relative Frequency
R<3	5%
3 <= R <5	2%
5 <= R <8	4%
8 <= R <10	6%
10<= R <13	19%
13 <= R <17	64%

MODEL DEFICIENCY ANALYSIS

The model constructed for this analysis is a high level structure, and either ignores or only deals approximately with many second-order factors. This section provides details, with limited exposition, of the more important factors that would need to be included in a more comprehensive model for a zero carbon supply-demand system.

(a) Transmission constraints: not included in the present model.
(b) Thermal losses from reservoir: not included in the present model.

(c) Accuracy of DNI – further research is required into the accuracy of the data available, including the transformation from GHI to DNI at a local level.

(d) The wind sites used don't match the ZCA. Supply reliability is likely to be better with the ZCA-planned wind farm distribution than with the modelled results reported here as the ZCA sites would provide far greater diversity.

(e) Some of the wind data appears to be deficient: there are some very low wind periods. This may be due to data errors rather than real-world events, but this has not been verified. Data errors of this type would result in understating the reliability of modelled supply.

(f) The shape of the demand model, particularly diurnally and weekly, requires more investigation. But this work would be more useful if integrated with modelling the sort of demand management strategies that could be put in place in the same timeframe as the proposed fundamental stationary energy supply.

CONCLUSION

The Beyond Zero Emissions plan to de-carbonise Australia by 2020 is an ambitious and visionary proposal. With no reference to, or analysis of, the practicality or costs associated with any of the proposed technologies, the plan has been analysed with a high-level supply-demand model. The capacity of the proposed renewable generating capability to meet demand, on a fine time-scale supply-demand basis, has been examined. The results show that the proposal is basically quite sound and that significantly improved outcomes are readily attainable with comparatively simple fine-tuning.

Further work is required to refine the model and incorporate second-order parameters in order to deliver finer time-scale detail and provide a robust basis for optimisation of the generation and storage mix. This will also allow other renewable resources to be included in the generation mix. Installation, operation and maintenance, and lifetime system costs will be included to subsequent models to allow informed selection of the best mix of energy capture, storage, and transformation.

REFERENCES

D. G. Erbs, S. A. Klein and J. A. Duffie "Estimation of the Diffuse Radiation Fraction for Hourly, Daily and Monthly-Average Global Radiation", Solar Energy Lab, University of Wisconsin, Madison. Published in Solar Energy, Vol 28, No 4. 1982

Matthew Wright,Executive Director, Beyond Zero Emissions: Patrick Hearps, University of Melbourne "Australian Sustainable Energy: Zero Carbon Australia Stationary Energy Plan", http://media.beyondzeroemissions.org/ZCA2020_Stationary_Energy_Report_v1.pdf

Sargent & Lundy LLC, Chicago, Illinois, 2003: "Assessment of Parabolic Trough and Power Tower Solar Technology Cost and Performance Forecasts", National Renewable Energy Laboratories, http://www.nrel.gov/csp/pdfs/35060.pdf, Accessed: 2010-01-11

BRIEF BIOGRAPHY OF PRESENTER

Trevor and Robyn are independent consulting actuaries who wish to contribute to more rational public debate on climate change.

Dynamic Stability Analysis of Photovoltaic Systems using Lyapunov Functions

M. A. Mahmud, M. J. Hossain, and H. R. Pota

The University of New South Wales at Australian Defence Force Academy (UNSW@ADFA), Northcott Drive, Canberra, ACT 2600, Australia.
Email: Md.Mahmud@student.adfa.edu.au, (m.hossain and h.pota)@adfa.edu.au

ABSTRACT

This paper proposes a novel approach based on Lyapunov function method to analyse the stability of photovoltaic (PV) systems. The Lyapunov function is formulated using the method of quadratic forms, i.e., Krasovskii's method. The stability of the photovoltaic systems under different operating conditions is analysed based on the formulated Lyapunov function. A comparison of stability analysis using eigenvalues and Lyapunov function is also presented in this paper.

Keywords Lyapunov function, photovoltaic systems, stability.

INTRODUCTION

Demand for electricity grows with great rapidity as a nation modernizes and its economy develops. The growth rate for electricity demand has outstripped that for other forms of energy. Renewable energy which comes from natural resources such as sunlight, wind, rain, tides, and geothermal heat, is the best choice as alternative sources of energy.

In 2006, about 18.4% of global final energy consumption came from renewable energy sources, with 13% coming from traditional biomass, which is mainly used for heating, and 3% from hydroelectricity. New renewable energy sources (small hydro, modern biomass, wind, solar, geothermal, and bio fuels) accounted for another 2.4% and are growing very rapidly, REN21 *et al.* 2008. Wind power is growing at the rate of 30% annually, with a worldwide installed capacity of 157,900 megawatts (MW) in 2009, Lars Kroldrup *et al.* 2010 and REN21 *et al.* 2009 and is widely used in Europe, Asia, and the US. At the end of 2009, cumulative global photovoltaic (PV) installations surpassed 21,000 MW, REN21 *et al.* 2009 and PV power stations are popular in Germany and Spain.

Renewable energy projects and productions are suitable for large-scale as well as small off-grid applications, sometimes in rural and remote areas, where energy is often crucial in human development. Kenya is the world leader in the number of solar power systems installed per capita (but not the number of watts added). More than 30,000 very small solar panels, each producing 12 to 100 watts, are sold in Kenya annually. More Kenyans adopt solar power every year than make connections to the country's electric grid.

Photovoltaic systems as alternative sources of energy have been attracting a growing amount of environmental, political, and commercial interest. As the PV installations are increasing day by day, the stability of PV systems becomes a major concern. The dynamic stability and transient response of PV systems connected to a large utility grid is analysed in Li Wang, and Ying-Hao Lin *et al*. 2000, C. Rodriguez and G. A. J. Amaratunga *et al.* 2004 and Li Wang and Tzu-Ching Lin *et al.* 2004. In these papers, the stability of PV systems based on the eigenvalue analysis and also the dynamics of the converters and inverters are considered.

The dynamic behaviour of PV systems changes a lot with the change in atmospheric condition. If the light emitted by sun is changed, then the equilibrium points of the PV systems also change. Therefore, it is essential to do the dynamic analysis of the PV systems.

The aim of this paper is to analyse the dynamic stability of PV systems by using a novel approach based on the formulation of Lyapunov function. In this paper, the Lyapunov function is formulated using the methods of quadratic forms, i.e. Krasovskii's method. The dynamic stability of the PV systems is also analysed based on the eigenvalues. Finally, a comparison is shown between the stability analysis using eigenvalues and Lyapunov function method.

The rest of the paper is organized as follows. The mathematical model of PV system is shown first. After that, an overview of Lyapunov function is given. Dynamic stability analysis using eigenvalues and Lyapunov function method are presented then. Finally, the paper is concluded with brief remarks and future trends.

MATHEMATICAL MODEL OF PV SYSTEM

Photovoltaic systems are characterized by the constant power injection into the grid. For the sake of simplicity, we consider the dynamics of the PV systems with constant power load and neglect all the internal resistive components. The simplified circuit is shown in Fig. 1.

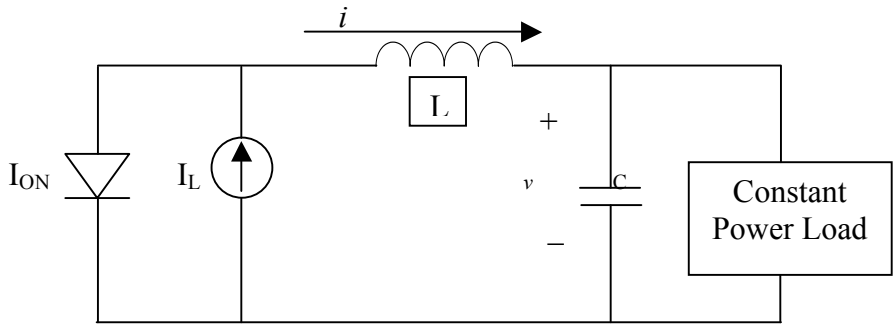

Fig. 1: PV Systems

Here, we have considered the constant power load instead of constant impedance or constant current loads because in practical cases most of the PV cells are connected to the grid and in planning stages, it is assumed that they are supplying constant power. Therefore, the assumption of constant power load is practical.

By applying Kirchhoff's current law at both nodes of Fig. 1 we get

$$I_L - I_s\left\{\exp\left[\alpha\left(v + L\frac{di}{dt}\right)\right] - 1\right\} - i = 0 \tag{1}$$

$$i - \frac{p}{v} - C\frac{dv}{dt} = 0 \tag{2}$$

In equation (1), the exponential terms comes due to the diode current. Finally, the dynamics of the systems are given by,

$$\frac{di}{dt} = \frac{1}{L}\left[\frac{1}{\alpha}\ln\left(\frac{I_L - i}{I_s} + 1\right) - v\right] \tag{3}$$

$$\frac{dv}{dt} = \frac{1}{C}\left[i - \frac{p}{v}\right] \tag{4}$$

Here, $\alpha = {}^{q}\!/_{nsKT}$, $q = 1.6022\times10^{-19}$ is the charge of electron, $k = 1.3807\times10^{-23}$ J/K is the Boltzmann's constant, $ns = 72$, is the number of cells connected in series in the PV system, $T = 298$ K is the temperature, $I_L = 4.7$ A for irradiance at 1000 W/m^2 is the light generated current, $p = 130$ W is the constant power drawn by load, $I_s = 9e-11$ A is the saturation current of the diode, $L = 1\mu H$ is the series inductance of the PV system, $C = 10mF$ is shunt capacitance of the PV system, i and v are the output current and output voltage of PV system respectively.

Equations (3)-(4) represent a nonlinear, time-varying system which define the dynamics of photovoltaic system and can be written in the following form:

$$\dot{x} = f(x,t) \tag{5}$$

where $x \in R = \begin{bmatrix} i & v \end{bmatrix}^T$ is the vector of states, $t \in R_+$ are the time values greater than zero, and $f \in R_+ \times R^n \to R^n$ is a vector function. Therefore, the equilibrium point of (5) must satisfy

$$f(x,t) = 0 \tag{6}$$

The i-v characteristic curve and power loading of PV system is shown in Fig. 2.

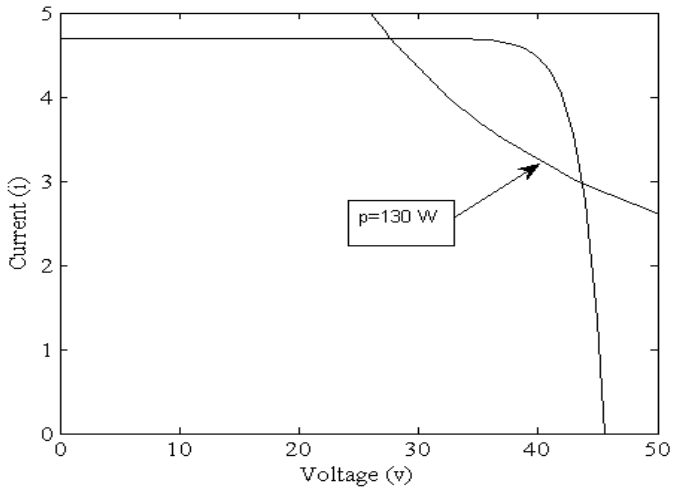

Fig. 2: i-v characteristic curve and power loading of PV system.

The i-v characteristic curve may shift with changing atmospheric condition, thus there is the probability of two solutions which can be obtained by solving the following two nonlinear equations:

$$\left[\frac{1}{\alpha}\ln\left(\frac{I_L - i}{I_s} + 1\right) - v\right] = 0 \tag{7}$$

$$\left[i - \frac{p}{v}\right] = 0 \tag{8}$$

Equations (7)-(8) are solved numerically through Newton-Raphson method which gives two solutions:

$$(\tilde{v},\ \tilde{i}) = \left[(2.9691,\ 4.6997),\ (43.7837,\ 27.6612)\right]$$

Now, our aim is to analyse the stability at this two points which is discussed in the subsequent section.

LYAPUNOV FUNCTION

Lyapunov functions are functions which are applicable to the stability analysis of the equilibrium states for dynamical systems. The Lyapunov stability theory includes two methods, Lyapunov's first method and Lyapunov's direct method. Lyapunov's first method is a technique which simply uses the idea of system linearization (lowest order approximation) around a given point. Lyapunov's direct method is the most important tool for design and analysis of nonlinear system. The definition of Lyapunov function in Slotine and Li *et al.* 1991 for the stability of nonlinear system is given as follows:

If a function $V(x,t)$ ***is positive definite and if its time derivative along any state trajectory of the system*** $\dot{x} = f(x,t)$ ***is negative definite, i.e.*** $\dot{V}(x,t) \leq 0$***, then*** $V(x,t)$ ***is said to be a Lyapunov function.***

In this paper, the Lyapunov function is formulated by using Krasovskii's method, Slotine and Li *et al.* 1991. An overview of this method is given below:

Any nonlinear system with equilibrium point can be described by equations (5)-(6). Let, $A(x,t)$ *is the Jacobian matrix of the system, i.e.,*

$$A(x,t) = \frac{\partial f}{\partial x} \tag{9}$$

If the matrix $F = A + A^T$ *is negative definite in a neighbourhood* Ω*, then the equilibrium point at the origin is asymptotically stable. A Lyapunov function for the system is*

$$V(x,t) = f^T(x,t) f(x,t) \tag{10}$$

Proof: The derivative of equation (10) is

$$\dot{V} = \dot{f}^T f + f^T \dot{f}$$

We can write

$$\dot{f} = Af$$

Thus,

$$\dot{V} = f^T A^T f + f^T A f = f^T (A^T + A) f$$

$$\Rightarrow \dot{V} = f^T F f$$

The negative definiteness of F implies the negative definiteness of $\dot{V}$.

DYNAMIC STABILITY ANALYSIS USING EIGEN VALUES

The system as described by equation (5) can be written as the following linearised form:

$$\Delta \dot{x} = A \Delta x \tag{12}$$

where the Jacobian matrix A can be written as

$$A = \begin{bmatrix} -\frac{1}{\alpha L}\left(\frac{I_S}{(I_L - i) + I_s}\right) & -\frac{1}{L} \\ \frac{1}{C} & \frac{p}{cv^2} \end{bmatrix} \tag{13}$$

The eigenvalues of A can determined from

$$\lambda_{1,2} = \frac{(a_{11} + a_{22}) \pm \sqrt{(a_{11} - a_{22})^2 + 4a_{12}a_{21}}}{2} \tag{14}$$

Practically in PV systems, the inductance is only due to the intrinsic parameters of the cable and is in the order of μH, whereas the capacitance is used for the filtering

purposes and is in the order of mF. Thus, the ratio L/C is in the order of 0.001 and the roots of the characteristic polynomial of (13), i.e., are real.

As a result, the stability of PV systems is assessed through the following way:

If we assume the radical in (14) is positive, the system will be stable iff,

$$(a_{11} + a_{22}) \pm \sqrt{(a_{11} - a_{22})^2 + 4a_{12}a_{21}} < 0$$

As the radical is considered as positive, the system will also be stable if

$$(a_{11} + a_{22}) < 0$$

$$\therefore \ |(a_{11} + a_{22})| > \left|\sqrt{(a_{11} - a_{22})^2 + 4a_{12}a_{21}}\right|$$

$$\Rightarrow (a_{11} + a_{22})^2 > \left(\sqrt{(a_{11} - a_{22})^2 + 4a_{12}a_{21}}\right)$$

$$\Rightarrow a_{11}a_{22} > a_{12}a_{21} \tag{15}$$

By substituting the values from (13) into (15) and following some manipulation, the condition for stability of PV system can be written as

$$v^2 > \frac{p}{\alpha[I_L - i + I_s]} \qquad \text{for } v > 0,\ i < I_L \tag{16}$$

The stability assessed through the condition (16) is tabulated in Table-I.

Table-I

Stability Assessment using the Concept of Eigenvalues

Current (i)	Voltage (v)	Status
2.9691	43.7837	Stable
4.69697	27.6612	Unstable

DYNAMIC STABILITY ANALYSIS USING LYAPUNOV FUNCTION

The Jacobian matrix of the system is given by equation (13). Therefore,

$$A^T = \begin{bmatrix} -\frac{1}{\alpha L}\left(\frac{I_S}{(I_L - i) + I_s}\right) & \frac{1}{C} \\ -\frac{1}{L} & \frac{p}{cv^2} \end{bmatrix} \tag{17}$$

The matrix F can be written as

$$F = A + A^T = \begin{bmatrix} -\frac{2}{\alpha L}\left(\frac{I_S}{(I_L - i) + I_s}\right) & -\left(\frac{1}{L} - \frac{1}{C}\right) \\ -\left(\frac{1}{L} - \frac{1}{C}\right) & \frac{2p}{cv^2} \end{bmatrix} \tag{18}$$

The matrix F is negative definite for $v > 0$, $i < I_L$. Therefore, the Lyapunov function for PV system can be written as

$$V = \tilde{f}^T \tilde{f}$$

$$\Rightarrow V = \begin{bmatrix} \tilde{f}_1 & \tilde{f}_2 \end{bmatrix} \begin{bmatrix} \tilde{f}_1 \\ \tilde{f}_2 \end{bmatrix}$$

$$\therefore V = \tilde{f}_1^2 + \tilde{f}_2^2 \tag{19}$$

where, $\tilde{f}_1 = \frac{1}{L}\left[\frac{1}{\alpha}\ln\left(\frac{I_L - \tilde{i}}{I_s} + 1\right) - \tilde{v}\right]$ and $\tilde{f}_2 = \frac{1}{C}\left[\tilde{i} - \frac{p}{\tilde{v}}\right]$ and the superscripts '~' denotes the value at equilibrium points.

The derivative of V from equation (19) can be written as

$$\dot{V} = 2\left(f_1 \dot{f}_2 + f_2 \dot{f}_2\right)$$

The values of $\dot{V}$ and the status of PV system at the equilibrium points are given in Table-II.

Table-II

Stability Assessment using Lyapunov function

Current (i)	Voltage (v)	$\dot{V}$	Status
2.9691	43.7837	-1.755×10^{7}	Stable
4.69697	27.6612	3.6×10^{10}	Unstable

CONCLUSION

This paper presents the stability analysis of PV systems through eigenvalue approach and Lyapunov function method. The eigenvalues, i.e. the roots of the characteristic equation do not provide any information about stability of PV system. That is why we need formulate a condition which gives information about the stability of PV systems. But using Lyapunov function the stability of the PV systems is analysed directly as the system is represented by nonlinear equations. Moreover, before implementing a PV cell into a practical system, the stability of the system can easily be analysed using the proposed Lyapunov function. In this paper, though one constant power load is considered, the stability of any practical system with different loads can also be analysed. Future works will deal with the extension of the proposed method to handle PV systems with different loads as well as converter and inverter dynamics.

REFERENCES

REN21 (2008), "*Global Status Report 2007*". Available at: http://www.ren21.net/pdf/RE2007_Global_Status_Report.pdf

REN21 (2009), "*Global Status Report 2009*". Available at: http://www.ren21.net/pdf/RE_GSR_2009_update.pdf

Lars Kroldrup (2010), *"Gains in Global Wind Capacity Reported,"* Green Inc.

Li Wang, and Ying-Hao Lin (2000), "Dynamic stability analysis of photovoltaic array connected to a large utility grid," *IEEE Power Engineering Society Winter Meeting,* 23 Jan 2000 - 27 Jan 2000, pp. 476 - 480.

Li Wang and Tzu-Ching Lin (2004), "Dynamic stability and transient responses of multiple grid-connected PV systems*," IEEE Transaction on Energy Conversion,* 19(4), pp. 748-755.

C. Rodriguez and G. A. J. Amaratunga (2004), "Dynamic stability of grid-connected photovoltaic systems," *IEEE Power Engineering Society General Meeting.*

J. J. E. Slotine and W. Li (1991), *"Applied Nonlinear Control,"* New Jersey: Prentice-Hall.

BRIEF BIOGRAPHY OF AUTHORS

Md. Apel Mahmud was born in Rajshahi, Bangladesh in 1987. He has received the B.Sc. in Electrical & Electronic Engineering with honours from Rajshahi University of Engineering and Technology (RUET), Bangladesh, in 2008. He is currently a PhD candidate at the University of New South Wales, Australian Defence Force Academy.

His research interests are dynamic stability power systems, solar integration and stabilization, voltage stability, distributed generation, nonlinear control, electrical machine, and HVDC transmission system.

Hossain (S'10) was born in Bangladesh, on October 30, the B.Sc. and M.Sc. Eng. Rajshahi University of Technology (RUET), and 2005, respectively, all in electronic engineering. He is toward the Ph.D. degree at the South Wales, Australian Academy.

His research interests are wind generator integration and voltage stability, micro grids, electrical machine, FACTS devices, and energy storage systems

M. Jahangir Rajshahi, 1976. He received degrees from Engineering and Bangladesh, in 2001 electrical and currently working University of New Defence Force

power systems, stabilization, robust control,

Hemanshu R. Pota received the B.E. degree from SVRCET, Surat, India, in 1979, the M.E. degree from the IISc, Bangalore, India, in 1981, and the Ph.D. degree from the University of Newcastle, NSW, Australia, in 1985, all in electrical engineering.

He is currently an Associate Professor at the University of New South Wales, Australian Defence Force Academy, Canberra, Australia. He has held visiting appointments at the University of Delaware; Iowa State University; Kansas State University; Old Dominion University; the University of California, San Diego; and the Centre for AI and Robotics, Bangalore. He has a continuing interest in the area of power system dynamics and control, flexible structures, and UAVs.

Methods to Increase Renewable Content at Islanded Power Stations

Dr James Darbyshire

Horizon Power
18 Brodie Hall Drive
Bentley, Western Australia
james.darbyshire@horizonpower.com.au

ABSTRACT

Significant technical issues exist when increasing the renewable generation content on islanded networks. Many of the concepts which underpin the "normal" operating methodology used in reliable power stations and networks is challenged when increasing the renewable quotient. Up to 30% renewable penetration may be achieved with no or little external control requirement, however beyond this consumer reliability can be affected. Horizon Power has pioneered using flywheel technology in its Marble Bar and Nullagine Solar Power Stations to allow up to 87% renewable energy content during the day. We have created new modelling techniques and are developing novel power electronic interfaces and control systems which we believe will allow us to turn off the fossil fuel based energy sources when sufficient renewable energy is available. This presentation outlines a vision to increase the renewable content at our remote power stations to 100% and the building blocks we hope will allow this to be realised.

Keywords - Renewable Energy, Isolated Networks, Short Term Energy Storage, Long Term Energy Storage

BRIEF BIOGRAPHY OF PRESENTER

James Darbyshire has managed and designed renewable energy projects and a renewable energy consultancy since 2006. He has experience in both solar and wind projects for on and off-grid applications. He is an electrical and electronic engineer and completed his PhD in 2010 in power electronics design and renewable system integration for small isolated power systems. His project experience includes all aspects from carrying out initial feasibility studies, completing electrical system and control design, project financing and rebate procurement, component sourcing, and liaison between suppliers, engineers, and trade staff. Currently, James works for Horizon Power as part of the Sustainable Energy Solutions team and has recently completed work on the Marble Bar hybrid PV power station as commissioning engineer.

Investigating Demand Side Management in Regional Western Australia

Timothy Wong

Power Systems Engineer
Horizon Power Corporation
18 Brodie Hall Drive
tim.wong@horizonpower.com.au

ABSTRACT

Horizon Power is currently undertaking a number of Demand Side Management projects in regional Western Australia which aim to achieve energy savings of at least 10%. Demand Side Management refers to reducing the quantity of energy consumed and changing patterns of energy use. It comprises Demand Response, Energy Efficiency and Energy Conservation. It is often overlooked by engineers, policymakers and consumers because the technology and potential savings are poorly understood.

Demand Response aims to manage consumer energy use in response to supply conditions such as pricing mechanisms and reducing usage during peak grid load times. Energy Efficiency involves using less energy to achieve the same task. Energy Conservation is an overall reduction in energy use, achieved through behavioural change.

Demand Side Management is regaining its relevance as concerns grow over the sustainable use of non-renewable energy resources and the aging power infrastructure in many countries. The solutions used to achieve demand side management are comprised of both technical and non-technical solutions. There are a number of engineering standards and technologies which enable Demand Side Management. This paper looks at the different options for Demand Side Management and its future potential.

BIOGRAPHY

Timothy Wong currently works in the Islanded Systems Development division at Horizon Power. He graduated from the University of Western Australia with a Bachelor of Electrical & Electronics Engineering and Computer Science. Timothy is actively involved as a volunteer with the IEEE at a local and international level.

Impacts of Distributed Wind Generation on Distribution Networks

N. K. Roy, H. R. Pota, M. A. Mahmud, and M. J. Hossain

The University of New South Wales at Australian Defence Force Academy (UNSW@ADFA), Northcott Drive, Canberra, ACT 2600, Australia.
Email: N.Roy@student.adfa.edu.au, h.pota@adfa.edu.au, Md.Mahmud@student.adfa.edu.au, m.hossain@adfa.edu.au

ABSTRACT

This paper analyses the impacts of distributed wind generation on distribution networks of power systems. The analysis is done over a test distribution system representative of the Kumamoto area in Japan. The detailed mathematical modelling of the system is also presented. The power losses at various nodes of the system as well as in the whole system with and without the integration of wind generator are presented. This paper also provides simulation results showing the effects of higher and lower penetration of distributed wind generation on voltage dynamics in a faulted system.

Keywords *Distributed generation (DG), distribution system, eigenvalues, wind turbine.*

INTRODUCTION

The integration of renewable power offers a promising solution, and is consequently the subject of increasing research efforts around the world. During the next ten years, renewable energy will emerge as a major enabler of the smart grid for the integration of small and medium sized renewable energy into the Australian electricity grid. Multiple mini-grids, connected into the distribution level network, will form new systems exhibiting potentially new collective (emergent) behaviour. Distributed supply based on renewable energy sources is one main element in all scenarios for the worldwide energy supply in the future. Solar energy, wind energy, bio fuel, and hydro power will be the basic components of a long-term sustainable energy supply. The integration of distributed generators into supply networks has already become a relevant issue in many countries. The costs of energy production of renewable sources will become more and more competitive as compared to the increasing cost for fossil fuels in the coming years. Important developments have occurred in the last few years in the fields of electrical system technology for distributed generation; see Walmir Freitas *et al.* (2006), Stratis Tapanlis and Michael Wollny (2009).

Some analytic and utility case studies on the impacts of wind power on existing power systems are described by B. Parsons *et al.* (2003). A definite conclusion was not given in this paper. A capacity credit of wind power is calculated by Yi Zhang *et al.* (2010). An overview of dynamic models for transient stability analysis of transmission and distribution systems with DG is given by Jens C. Boemer *et al.* (2009). The authors state that the inclusion of squirrel cage induction generator (SCIG) does not have a large influence on transient stability. But it significantly affects the voltage stability of the system; see Genevieve Coath and Majid Al-Dabbagh (2005), Ching-Yin Lee *et al.*

(2009). Problems related to voltage instability in power systems are one of the major concerns in power system planning and operation; see Per-Anders LÖf *et al.* (1993).

Recent work tends to focus on assessing how distributed generation can be integrated into existing grids without compromising grid reliability or protection schemes or causing other problems, consistent with the minimum standards for all connected devices. However, the effect of a potentially rising penetration of DG upon the distribution systems has attracted much less attention. Very little work has examined its impact on distribution network. The aim of this proposed work is to discuss the potential impact of the DG on distribution systems, i.e., how the integration of wind generation affects the behaviour of the distribution system with line flows and losses. Moreover, the effects of voltage rise under fault condition with different penetration of DG are also analysed.

The organisation of the paper is as follows. Firstly, the mathematical model of a distribution system with distributed generation (wind generation) is presented. Then the simulation results of the test system with and without distributed generation are presented and the power losses in the system are also described. The variations of terminal voltage of wind generator for different levels of DG penetration are also provided through simulation in this section. Finally, the paper is concluded with the extension of the proposed analysis with different types of distributed energy resources and loads.

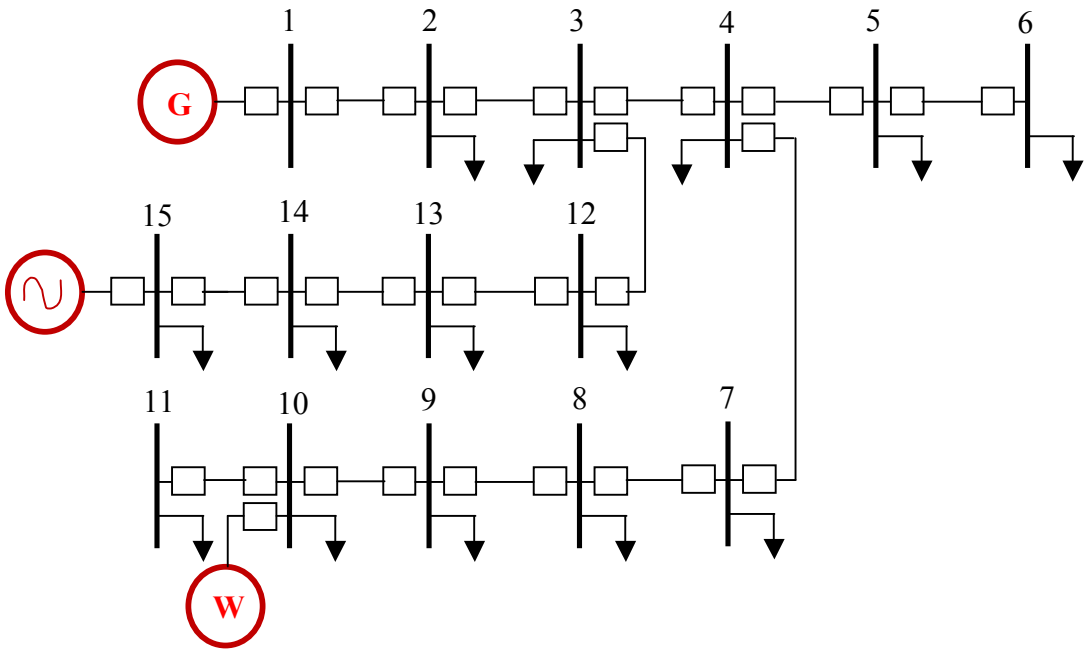

Fig. 1: Single line diagram of Modified Kumamoto 15-bus distribution system; see Fracisco M. González-Longatt (2007)

MATHEMATICAL MODEL

The basic features of a distribution system can be represented through the widely used Kumamoto 15 bus distribution test system as shown in Fig. 1 which is a benchmark system. For the analysis in this paper, we modified the 15 bus distribution system by

connecting a wind generator at bus 10. Moreover, we connected a small synchronous generator at bus 1 and considered bus 15 as slack bus. The line and load data of the test system are given in Appendix.

The most important components of a constant speed wind are rotor, drive train, and the generator. The rotor of the wind turbine, with radius R_i, converts the energy from the wind to the rotor shaft, rotating at the speed ω_m. The power from the wind depends on the wind speed, V_w, the air density, ρ, and the swept area A_{wt}. From the available power in the swept area, the power on the rotor is given based on the power coefficient $c_p(\lambda, \theta)$, which depends on the pitch angle of the blade, θ, and the ratio between the speed of the blade tip and the wind speed ratio, $\lambda_r = \frac{\omega_m R}{V_w}$. The aerodynamic torque applied to the rotor for the turbine by the effective wind passing through the rotor is given as; see Ackermann *et al.* (2005), M. J. Hossain *et al.* (2010):

$$T_{ae} = \frac{\rho}{2\omega_m} A_{wt} c_p(\lambda_r, \theta) V_w^3 \tag{1}$$

where c_p is approximated by the following relation; see Abdin and Xu *et al*. (2000):

$$c_p = (0.44 - 0.0167\theta)\sin\left[\frac{\pi(\lambda - 3)}{15 - 0.3\theta}\right] - 0.00184(\lambda - 3)\theta \tag{2}$$

A two-mass drive train model of a wind turbine generator system (WTGS) is used in this paper as the drive train modelling can satisfactorily reproduce the dynamic characteristics of WTGS. The drive train is attached to the wind turbine converts the aerodynamic torque T_{ae} on the rotor into the torque on the low speed-shaft, which is scaled down through the gearbox to the torque on the high-speed shaft. The first mass term stands for the blades, hub and low-speed shaft, while the second mass term stands for the high speed shaft having the inertia constants H_m and H_g. The shafts are interconnected by the gear ratio, N_g, combined with torsion stiffness, K_s, and torsion damping, D_m and D_g resulting in torsion angle λ. The normal grid frequency is f. The dynamics of the shaft can be represented as follows; see Ackermann *et al.* (2005), M. J. Hossain *et al.* (2010):

$$\dot{\omega}_m = \frac{1}{2H_m}\left[T_{ae} - K_s\lambda - D_m\omega_m\right] \tag{3}$$

$$\dot{\omega}_g = \frac{1}{2H_g}\left[K_s\lambda - T_{ae} - D_g\omega_g\right] \tag{4}$$

$$\dot{\lambda} = 2\pi f\left(\omega_m - \frac{1}{N_g}\omega_g\right) \tag{5}$$

The induction generator gets the power from the gear box through the stiff shaft. The relationship between the mechanical torque and torsional angle is given by:

$$T_m = K_s\lambda \tag{6}$$

The mechanical torque depends on torsion stiffness (*Ks*), torsion angle (λ), rotor speed (ω_g) etc. In this work, time domain simulation is carried out with full non-linear model of the wind turbine generation system considering variable mechanical torque.

A transient model of a SCIG can be described by the following algebraic-differential equations; see Mahmud, Hossain, and Pota (2010):

$$\dot{E}'_{qr} = -\frac{1}{T'_o}\left[E'_{qr} + (X - X')i_{ds} + s\omega_s T'_o E'_{dr}\right] \quad (7)$$

$$\dot{E}'_{dr} = -\frac{1}{T'_o}\left[E'_{dr} - (X - X')i_{qs} - s\omega_s T'_o E'_{qr}\right] \quad (8)$$

$$\dot{s} = \frac{1}{2H_g}\left(T_m - T_e\right) \quad (9)$$

$$\left(v_{ds} + j\,v_{qs}\right) = \left(R_s + jX'\right)\left(i_{ds} + j\,i_{qs}\right) + j\left(E'_{qr} - jE'_{dr}\right) \quad (10)$$

Here, $X' = X_s + \frac{X_m X_r}{X_m + X_r}$ is the transient reactance, R_s is the stator resistance which is assumed to be zero, X_r is the rotor reactance, X_m is the magnetizing reactance, $X = X_s + X_m$ is the rotor open circuit reactance, T'_o is transient open circuit time constant, T_m is the mechanical torque, s is the slip, $T_e = E'_{dr} i_{ds} + E'_{qr} i_{qs}$ is the electrical torque, E'_{dr} and E'_{qr} are the direct and quadrature axis transient voltages respectively, i_{ds} and i_{qs} are the direct and quadrature axis currents respectively, and ω_s is the synchronous speed.

SIMULATION RESULTS

The Kumamoto 15-bus distribution network shown in Figure 1 is used to exhibit the effectiveness of the proposed analysis. Firstly, it is modified by connecting a small synchronous generator at bus 1 and considering bus 15 connected to the main grid (infinite bus). The eigenvalues of modified Kumamoto test system without and with wind generation are shown in Fig. 2. Here the base power is 10 MVA and the base voltage is 6.6 kV, total load on the system is 6.3 MW, 0.0446 Mvar. The wind farm is next installed at bus 10 to provide 20 percent of the total power. The nodal voltages without and with installing DGs are given in Figure 3. The integration of wind generator increases the voltage at the adjacent nodes. The eigenvalues of the system without and with wind generator are given in Table-1. The participation matrix combines the right and left eigenvectors according to I. J. Pe'rez-Arriaga *et al.* (1992), Denis Lee Hau Aik and Goran Andersson (1998) as follows:

$$P_{ki} = \xi_{ki}.\eta_{ik} \quad (11)$$

Where,

P_{ki}: participation factor of the bus *k* in the *i-th* mode

$\xi_{ki}.\eta_{ik}$: *k-th* element of the right-column and left-row eigenvector, respectively, associated with the *i-th* mode eigenvalue λ_i.

The participation factors computed from the eigenvectors associated with the critical mode provide information on the critical system location of instability. The mode which

dominates the behaviour of the system is called critical mode. In this case, the marginally stable mode is critical mode.

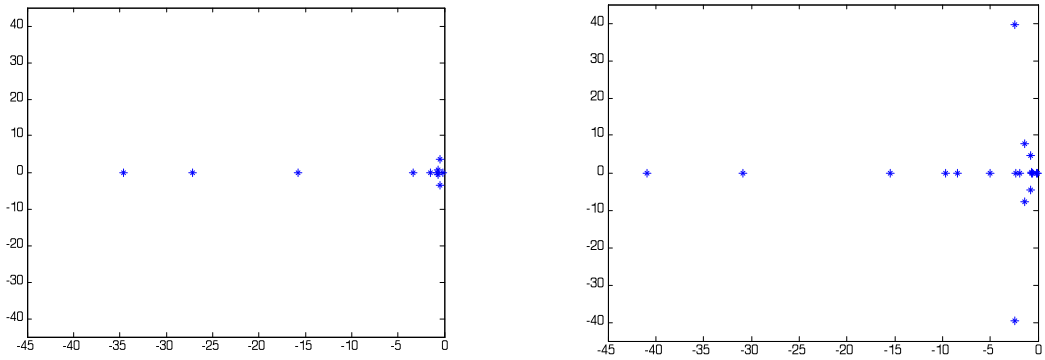

(a) (b)

Fig. 2: Eigenvalues of modified Kumamoto 15 bus distribution test system (a) without wind generation and (b) with wind generation

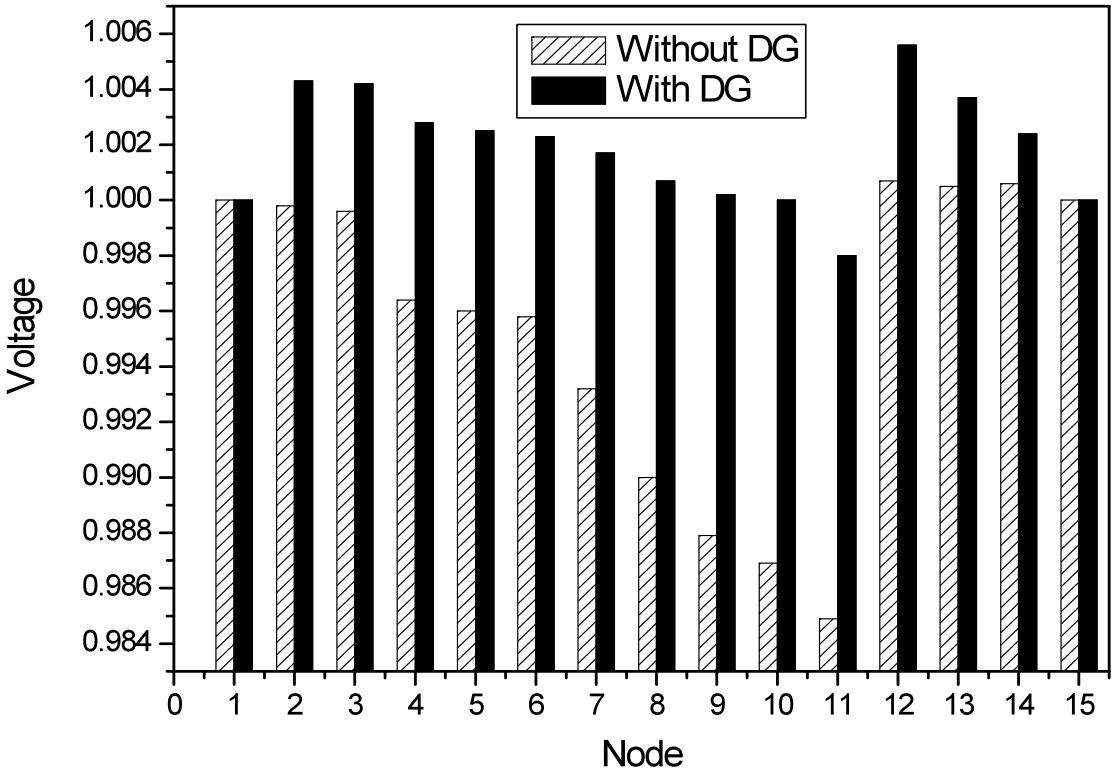

Fig. 3: Nodal voltages without and with distributed wind generation

From the eigenvalues, it can be seen that Modes 18 and 19 make the system marginally stable compared to without wind generation. The participation factors of dominating modes are given in Table-2 from which it is clear that direct and quadrature axis transient voltages are responsible for this situation. Here, the marginally stable mode is

monotonic. From the participation factor, it is clear that it is related to reactive power mismatch. The power losses at various nodes are given in Table-3. It is shown that total power loss with DG is less than without DG. This is due to wind generator consuming reactive power.

To analyse the voltage profile, the test system is tested with different penetration levels of wind generation under fault condition with outage of the line connecting buses 3 and 12 for 2 sec. A fault is applied at t = 1 second and removed at t = 3 second. The terminal voltage of wind generator for 20%, 50%, and 80% wind generation penetration under pre-fault, faulted, and post-fault condition are shown in Figure 4. This shows that higher penetration of distributed wind generation causes significant voltage rise and oscillations in distribution system. However, in this analysis, the system returns to its pre-fault condition in case of high penetration also. In other cases, it may become unstable with high penetration in case of shortage of reactive power. It also depends on the operating conditions, system configuration etc. The parameters of wind generator are specified by M. J. Hossain *et al.* (2009).

Tab. 1: Eigenvalues of Kumamoto 15 bus distribution system without and with wind generator

Mode	Without wind generation		With wind generation	
	Real	Imaginary	Real	Imaginary
1	-0.47818	3.5149	-2.4659	39.639
2	-0.47818	-3.5149	-2.4659	-39.639
3	-0.68737	0.65034	-1.3866	7.7508
4	-0.68737	-0.65034	-1.3866	-7.7508
5	-34.634	0	-0.80380	4.7237
6	-27.142	0	-0.80380	-4.7237
7	-15.725	0	-0.70685	0.12431
8	-3.3653	0	-0.70685	-0.12431
9	-1.5443	0	-40.954	0
10	-0.74740	0	-30.928	0
11	-0.15910	0	-15.460	0
12			-9.6406	0
13			-8.4765	0
14			-5.0684	0
15			-2.3399	0
16			-1.9592	0
17			-0.51747	0
18			-0.16229	0
19			-0.11304E-04	0

Tab. 2: Participation factors

Modes	Participation factors	
18	$\Delta Eq'$= 1.0	$\Delta E_d'$=0.38805
19	$\Delta Eq'$=0.0001	

Tab. 3: Power losses at various nodes

Sending Node	Ending Node	Power loss without DG (MW)	Power loss with DG (MW)
1	2	1.26×10^{-4}	0.023
2	3	1.21×10^{-3}	3.03×10^{-4}
3	4	2.16×10^{-2}	1.49×10^{-3}
4	5	2.76×10^{-4}	2.82×10^{-5}
5	6	2.82×10^{-5}	5×10^{-5}
4	7	8.73×10^{-3}	8×10^{-4}
7	8	1.26×10^{-5}	4×10^{-4}
8	9	2.52×10^{-4}	5.71×10^{-5}
9	10	3.39×10^{-2}	0
10	11	1.28×10^{-4}	4.44×10^{-3}
3	12	1.13×10^{-2}	0
12	13	6.3×10^{-3}	3.17×10^{-4}
13	14	0	7.35×10^{-3}
14	15	1×10^{-3}	4.6×10^{-4}
Total		0.0851	0.0387

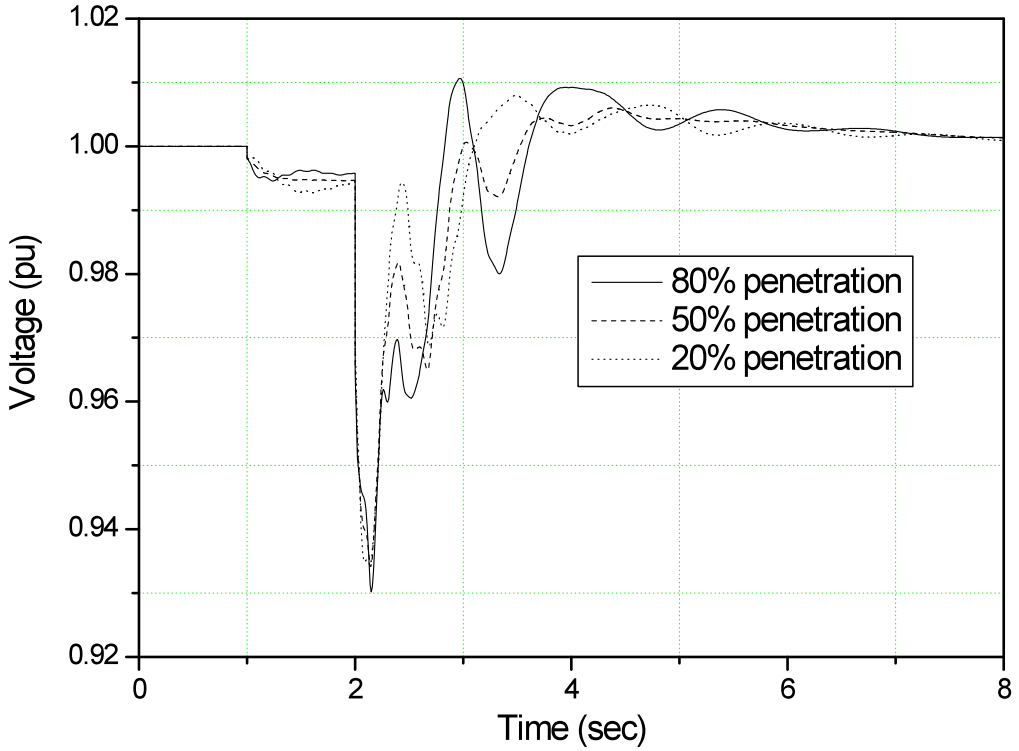

Fig. 4: Voltage profile of bus 10 with different penetration level

CONCLUSION

We have investigated the impacts of wind farm dynamics on a distribution network. The analysis shows that the integration of wind generation significantly affects the voltage

stability of the system. The penetration of wind generation has impact on the frequency of the modes. The analysis also shows that the voltage rise has a significant impact on the amount of DG capacity that can be connected to the distribution network. The total power losses of the system with DG are less than without DG. The aim of the future work is the dynamic analysis of distribution network with various types of distributed energy sources and loads.

REFERENCES

B. Parsons *et al.* (2003), *"Grids impacts of wind power: summary of recent studies in the United States,"* NREL/CP-500-34318, National Renewable Energy Laboratory.

Ching-Yin Lee *et al.* (2009), *"The Impact of SCIG Wind Farm Connecting into a Distribution System,"* Asia-Pacific Power and Energy Engineering Conference (APPEEC 2009), China.

Denis Lee Hau Aik and Goran Andersson (1998), "*Use of participation factors in modal voltage stability analysis of multi-infeed HVDC systems,*" IEEE Transactions on Power Delivery, vol. 13, no. 1, pp. 203-211.

E. S. Abdin and W. Xu (2000), *"Control design and dynamic performance analysis of wind turbine-induction generator unit,"* IEEE Trans. on Energy Conversion, vol. 15, no. 1, pp. 91-96.

Fracisco M. González-Longatt (2007), "*Impact of distributed generation over power losses on distribution system,*" 9th International Conference on Electrical Power Quality and Utilisation, Barcelona.

Genevieve Coath and Majid Al-Dabbagh (2005), *"Effect of Steady-State Wind Turbine Generator Models on Power Flow Convergence and Voltage Stability Limit,"* Australasian Universities Power Engineering Conference (AUPEC 2005), Tasmania, Australia.

I. J. Pe'rez-Arriaga *et al.* (1992), "*Selective modal analysis with applications to electric power systems, Part I: Heuristic Introduction,*" IEEE Transactions on Power Apparatus and Systems, vol. PAS-101, no. 9, pp. 3117–3125.

Jens C. Boemer *et al.* (2009), "*Dynamic models for transient stability analysis of transmission and distribution systems with distributed generation: an overview,*" IEEE Bucharest Power Tech Conference, Bucharest, Romania.

M. A. Mahmud, M. J. Hossain, and H. R. Pota (2010), *"Investigation of critical parameters for power system stability with dynamic loads,"* IEEE PES General Meeting, Minneapolis, Minnesota, USA.

M. J. Hossain, H. R. Pota, V. Ugrinovskii, and R. A. Ramos (2009), *"A novel STATCOM control to augment LVRT capability of fixed speed wind generators,"* in 48th IEEE Conference on Decision and Control, Shanghai, P. R. China, pp. 7843-7848.

M. J. Hossain, H. R. Pota, V. Ugrinovskii, and R. A. Ramos (2010), *"Simultaneous STATCOM and pitch angle control for improved LVRT capability of fixed-speed wind turbines,"* IEEE Trans. on Sustainable Energy, vol. 1, no. 3, pp. 142-151.

Per-Anders LÖf, David J Hill, Stefan Arnborg, and GÖran Andersson (1993), *"On the analysis of long-term voltage stability,"* International Journal of Electrical Power & Energy Systems, vol. 15, no. 4, pp. 229-237.

Stratis Tapanlis and Michael Wollny (2009), *"Advanced active and reactive power control for mini grids,"* World Climate & Energy Event, pp.111- 117, Rio de Janeiro, Brazil.

S. Li, Tomsovic, and T. Hiyama (2000), "*Load following functions using distributed energy resources*" Proceedings of the IEEE PES Summer Meeting, Seattle.
T. Ackermann, *"Wind Power in Power Systems,"* John Wiley & Sons Ltd, England, 2005.
Walmir Freitas *et al.* (2006), "*Comparative analysis between synchronous and induction machines for distributed generation applications,*" IEEE Transactions on Power Systems, vol. 21, no. 1, pp. 301–311.
Yi Zhang, Sadrul Ula and Yibin Zhang (2010), "*Wind power availability and increased capacity credit for multiple wind farms,*" IEEE PES General Meeting, Minneapolis, Minnesota, USA.

Appendix:

Tab. 4: Line and load data of Kumamoto distribution system; see S. Li *et al.* (2000)

Sending Node	Ending Node	R (p.u)	X (p.u)	B (p.u)	P_{load} (p.u)	Q_{load} (p.u)
1	2	0.00315	0.075207	0.00000	0.02080	0.0021
2	3	0.00033	0.001849	0.00150	0.04950	0.0051
3	4	0.00667	0.030808	0.03525	0.09580	0.0098
4	5	0.00579	0.014949	0.00250	0.04420	0.0045
5	6	0.01414	0.036547	0.00000	0.01130	0.0012
4	7	0.00800	0.036961	0.03120	0.06380	0.0066
7	8	0.00900	0.041575	0.00000	0.03230	0.0033
8	9	0.00700	0.032346	0.00150	0.02130	0.0022
9	10	0.00367	0.01694	0.00350	0.02800	0.0029
10	11	0.00900	0.041575	0.00200	0.21700	0.0022
3	12	0.02750	0.127043	0.00000	0.01320	0.0014
12	13	0.03150	0.081405	0.00000	0.00290	0.0003
13	14	0.03965	0.102984	0.00000	0.01610	0.0016
14	15	0.01061	0.004153	0.00000	0.01390	0.0014

Bus voltage=6.6 kV, Base MVA= 10 MVA

BRIEF BIOGRAPHY OF AUTHORS

Naruttam Kumar Roy was born in Mymensingh, Bangladesh in 1985. He received his B.Sc. degree in Electrical & Electronic Engineering from Khulna University of Engineering and Technology (KUET), Bangladesh, in 2007. He is currently a PhD student in the University of New South Wales at Australian Defence Force Academy, Canberra, Australia.

His research interests include distributed generation, renewable energy, smart grids, electrical machines, artificial intelligence, power electronics, and control applications.

Hemanshu R. Pota received the B.E. degree from SVRCET, Surat, India, in 1979, the M.E. degree from the IISc, Bangalore, India, in 1981, and the Ph.D. degree from the University of Newcastle, NSW, Australia, in 1985, all in electrical engineering.

He is currently an Associate Professor at the University of New South Wales, Australian Defence Force Academy, Canberra, Australia. He has held visiting appointments at the University of Delaware; Iowa State University; Kansas State University; Old Dominion University; the University of California, San Diego; and the Centre for AI and Robotics, Bangalore. He has a continuing interest in the area of power system dynamics and control, flexible structures, and UAVs.

Md. Apel Mahmud was born in Rajshahi, Bangladesh in 1987. He has received the B.Sc. in Electrical & Electronic Engineering with honours from Rajshahi University of Engineering and Technology (RUET), Bangladesh, in 2008. He is currently a PhD candidate at the University of New South Wales, Australian Defence Force Academy.

His research interests are dynamic stability power systems, solar integration and stabilization, voltage stability, distributed generation, nonlinear control, electrical machine, and HVDC transmission system.

M. Jahangir Hossain was born in Rajshahi, Bangladesh, on October 30, 1976. He received the B.Sc. and M.Sc. Eng. degrees from Rajshahi University of Engineering and Technology (RUET), Bangladesh, in 2001 and 2005, respectively, all in electrical and electronic engineering. He is currently working toward the Ph.D. degree at the University of New South Wales, Australian Defence Force Academy.

His research interests are power systems, wind generator integration and stabilization, voltage stability, micro grids, robust control, electrical machine, FACTS devices, and energy storage systems.

Analysis of the Impact of Wind Turbines and FACTS Device Penetration on the Dynamic Performance of Power Systems

M. J. Hossain[1], H. R. Pota[1] and R. A. Ramos[2]

[1]The University of New South Wales at Australian Defence Force Academy (UNSW@ADFA), Northcott Drive, Canberra, ACT 2600, Australia.
Email: (m.hossain and h.pota)@adfa.edu.au
[2]The Engineering School of Sao Carlos, Brazil.
Email: ramos@sel.eese.usp.br

ABSTRACT

The complexity of power systems has been increased in recent years due to increased utilization of the existing transmission lines using FACTS (flexible AC transmission system) devices and for changing the generation mechanism with more intermittent sources and lower inertial units. This changing nature of power systems has considerable effect on its dynamic behaviour resulting from power swings, dynamic interaction between different power system devices and less synchronized coupling. This paper will analyse the changing nature of systems and its dynamic behaviour to identify critical issues that limits the large scale integration of wind generators and FACTS devices. The studies in this paper are conducted on a 16 Machine, five area New England and New York power system. In this paper, the study of dynamic behaviour includes modal analysis, PV analysis, eigenvalue tracking, and dynamic simulations to investigate the dynamic behaviour of a complex power system under both small and large disturbances..

Keywords – Wind Turbines, FACTS Devices, stability, Dynamic Performance.

INTRODUCTION

Power systems are complex systems that evolve in response to economic growth and continuously increasing power demands. With growing population and the industrialisation of the developing world, more energy is required to satisfy basic needs and to attain improved standards of human welfare (Anderson et. al. 2002). The structure of the modern power system is becoming highly complex in order to make energy available economically with reduced carbon emissions and the use of renewable energy.

In recent years, power demand has increased substantially while the expansion of power transmission lines has been severely limited due to inadequate resources and environmental restrictions. As a consequence, some transmission lines are heavily loaded and system stability becomes a power transfer-limiting factor. FACTS controllers have been used to solve various power system steady-state control problems, therefore, enhancing power system stability in addition to their main function of power-flow control (Qiao et. al. 2006).

Dynamic reactive devices, such as thyristor-controlled series capacitors (TCSCs), mechanically switched capacitors (MSCs), static VAr (volt-ampere-reactive) compensators (SVCs) and static synchronous compensators (STATCOMs) do not require extensive amounts of land nor are they especially visible when compared with major new EHV (extra-high voltage) transmission lines. These characteristics make them much more acceptable to government agencies and the public and, thus, to

transmission system operators who are responsible for providing reliable electricity delivery services.

In many cases, these dynamic reactive devices are much less expensive to build than the equivalent number of new transmission lines that may otherwise be necessary. Employed in moderation, such devices are useful additions to the set of tools that system planners and operators should use to relieve voltage or VAr problems and provide flexibility. However, if used to excess, such devices will likely increase the risk of uncontrolled system collapse and significantly increase the complexity of system design and operation. This complexity may introduce new failure modes into the system and reduce its overall reliability in unexpected ways.

Following the issuance of the renewable energy regulations in recent years to give impetus to the development of renewable energy by governments in Denmark, Germany, USA, China, Ireland, Australia and India, a large number of wind farms are currently interconnected into transmission networks at the 220kV voltage level with higher installed capacities than those of connected wind generators. Being connected to a higher voltage level, their impact is becoming more widespread. The European Wind Energy Association (EWEA) projects that there will be 230 GW and 300 GW of total installed wind power capacity in Europe in 2020 and 2030, respectively. This will result in wind power generation of the same order of magnitude as the contributions from conventional technologies developed over the past century. An overview of the historical development of wind energy technology and the current world-wide status of grid-connected, as well as stand-alone, wind power generation is given (Ackermann et. al 2002). The present and progressive scale of integration has brought to a head serious concern about the impact of such a scale of wind penetration on the future safety, stability, reliability and security of the electricity systems.

Voltage instability is also highly influenced due to the integration of induction generators into grids. There are several technical constraints, including steady-state or dynamic stability, which may limit wind power integration into a power system. A majority of large wind farms, including proposed large wind projects, are geographically far away from load centres and connected into relatively weak transmission networks (Rathi et al. 2005). The presence of wind farms in such weak transmission networks raises serious concerns about system security and stability. Concerns regarding power system utilities are shifting focus from power quality issues to stability problems caused by wind power integration. In the grid impact studies of wind power integration, the voltage stability issue is a key problem because a large proportion of existing wind farms are based on fixed-speed wind turbines (FSWTs) equipped with simple squirrel-cage induction generators (SCIGs) (Palsson et al 2002).

SCIGs consume reactive power and behave similarly to IMs during a system contingency and deteriorate the local grid voltage stability (Hossain et. al 2009). Presently, variable-speed wind turbines (VSWTs) equipped with doubly-fed induction generators (DFIGs) are becoming more widely used due to their advanced reactive power and voltage control capability. DFIGs make use of power electronic converters and are, thus, able to regulate their own reactive power in order to operate at a given power factor or to control grid voltage. However, because of the limited capacity of the PWM (pulse-width modulation) converter, the voltage control capability of a DFIG cannot match that of a synchronous generator. When the voltage control requirement is beyond the capability of a DFIG, the voltage stability of a grid is also affected.

Recently, a lot of work has been done on analysing the effects of the large-scale integration of wind generators on dynamic stability. The effect of wind power on oscillations and damping has been investigated by gradually replacing the power generated by synchronous generators in a system by power from either constant or variable-speed wind generators (Slootweg et al. 2003, Hagstrom et. al. 2005). Only the impact on electromechanical modes are investigated (Slootweg et al. 2003) despite the voltage modes also being influenced by the penetration of wind generators. The limits for voltage stability at different wind power integration levels and grid alternatives are illustrated (Palsson et. al. 2002) for situations both with and without extra stabilising controls in the system and for different characteristics of wind turbine generators. Detailed dynamic load modelling and fault analysis are not treated (Palsson et. al. 2002). However, load characteristics are closely related to voltage instability.

Although much work has been done, the following issues have not yet been addressed in detail: (i) the effects of importing a higher level of power from remote generation with high a penetration of FACTS devices; (ii) the effects of a high penetration of DFIGs on voltage stability during transients when they behave as SCIGs; (iii) the effects of integrating FACTS devices into power systems with different structures; (iv) the critical interactions between FACTS devices; and (v) the effects of the integration of FSWTs and FACTS devices with substantial amounts of dynamic load. Large wind generation facilities are evolving to look more and more like conventional generating plants in terms of their abilities to interact with a transmission network, other generating units and FACTS devices in a way that does not compromise performance or system reliability. But many challenges and new breakthroughs are needed before their use becomes a reality.

The high penetration of wind power is foreseen in many countries and regions globally. FACTS devices will mainly be used to integrate the large-scale wind energy into power systems. The dynamics of power systems will likely to be dominated by the dynamics of wind turbines and FACTS devices in the near future. Therefore, the impacts of wind power and FACTS devices on power system stability and reliability need to be thoroughly analysed before they are integrated into existing power system networks. This paper will analyse the changing nature of systems and their dynamic behaviours to identify future issues that need to be either resolved or to have limits defined to a degree that can be tolerated. The following cases are considered in this paper: (i) the possible effects of higher FACTS density on the dynamic performance of a distributed power system; (ii) the critical interactions amongst FACTS devices; (iii) whether there is a level of wind generation capacity and FACTS devices above which a system's dynamic behaviour is unstable and has poor controllability.

TEST SYSTEM AND POWER SYSTEM MODEL

A 16 machine, 69 bus system is considered in this paper (Pal et. al. 2005). The single line diagram of the system is shown in Fig.1. This is reduced order equivalent of the interconnected New England test system (NETS) and New York power system (NYPS). There are five geographical regions, out of which NETS and NYPS are represented by a group of generators whereas, import from each of the three other neighbouring areas 3, 4 and 5 are approximated by generator equivalent models. The generators, loads and imports from other neighbouring areas are representative of operating conditions in the early 1970s. The total load on the system is P_L=17620.65 MW, Q_L=1971.76 MVAr and generation P_G=18408.00 MW. The line loss in the system is 152.2 MW. Generators G_1

to G_9 are the equivalent representation of the NETS generator whilst machines G_{10} to G_{13} represent the generation of the NYPS. Generators G_{14} to G_{16} are the dynamics equivalents of the three neighbouring areas connected to the NYPS. There are three major transmission corridors between NETS and NYPS connecting buses 60-61, 53-54 and 27-53. All these corridors have double-circuit tie-lines. In steady state, the tie-line power exchange between NETS and NYPS is 700 MW in total. The NYPS is required to import 1500 MW from area 5. The system and generator data are given (Pal et. al. 2005).

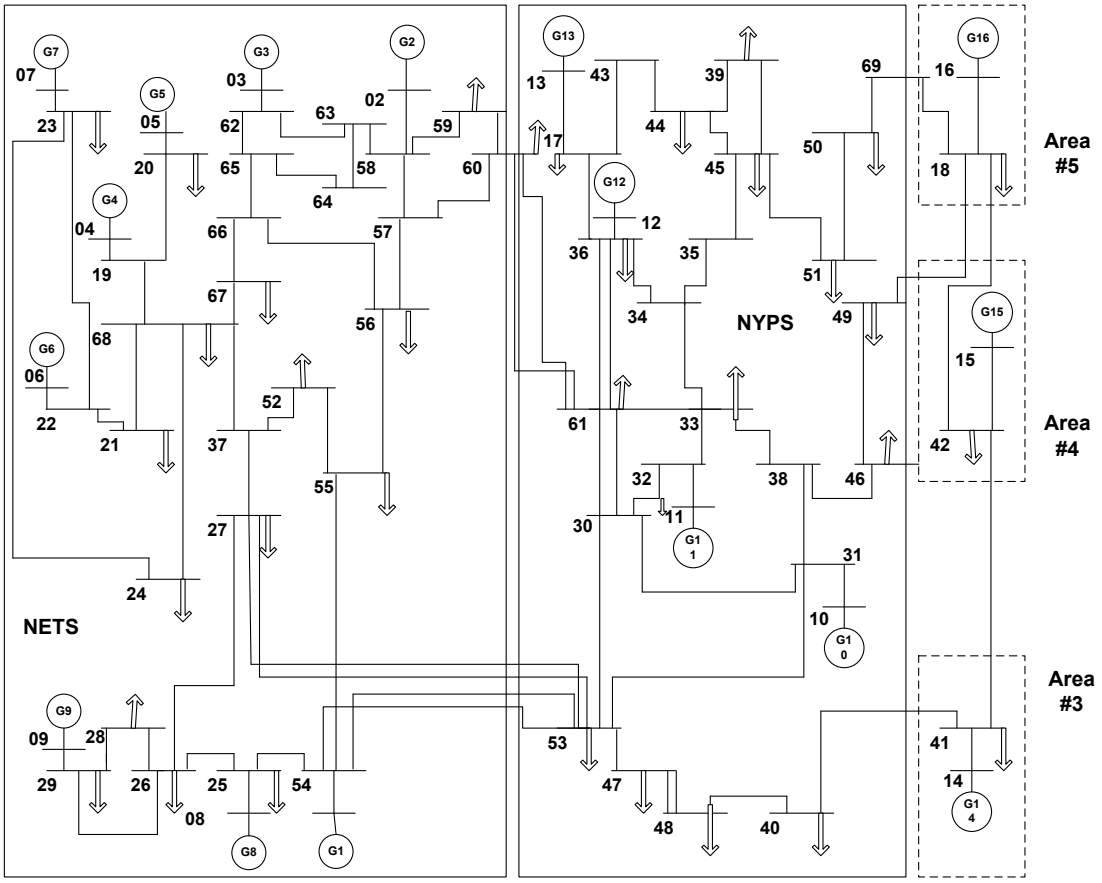

Fig1. 16 Machine 69 bus test system

All the generators of the test system (G_1 to G_{16}) have been represented by a sub-transient model (Pal et. al. 2005). The mechanical input power to the generators is assumed to be constant during the disturbance. The generators G_1 to G_8 are equipped with slow excitation system (IEEE-DC1A) whilst G_9 is equipped with a fast acting static excitation system (IEEE-ST1A) (Pal et. al. 2005). The fast acting static excitation system at generator G_9 is equipped with a power system stabilizer to provide supplementary damping control for the local modes. The rest of the generators are under manual excitation control (Pal et. al. 2005). The load is modelled as (i) 20% large induction motor load, (ii) 25% small induction motor load, and (iii) 45% static load. The active components of static loads are represented by constant current models and the reactive components by constant impedance models.

The modelling of induction generators for power flow and dynamic analysis has been discussed (Hossain et. al. 2009). A general model for representation of doubly-fed wind turbines in power system dynamics simulations has been presented (Slootweg et. al

2003). The SVC is a shunt connected static VAr generator or absorber whose output is adjusted to exchange capacitive or inductive current so as to maintain or control specific variables of the electrical power system (Pal et. al. 2005). A TCSC is a capacitive reactance compensator which consists of a series capacitor bank shunted by a thyristor controlled reactor in order to provide a smooth variation in series capacitive reactance (Pal et. al. 2005). The main task of the TCSC is to control the power flow and to increase the stability limit. The basic reason for installing a STATCOM in a power system is to provide a controllable AC voltage source. This is done by a voltage source inverter connected to a DC capacitor. Basic STATCOM circuit consists of a voltage source converter (VSC) and a DC capacitor (Hossain et. al. 2009).

.

CASE STUDIES

A number of cases are considered to get a deeper insight into these complex issues.

Load area fed by high import

A large amount of compensation is needed within the load area of this test system. This is due to the high demand for reactive power by the loads, the need for a lot of reactive power by the feeding lines and the lack of generation units within the load area which could deliver reactive power as a by-product. A large amount of reactive compensation results in a P-V curve that is flat to a certain point and then falls very steeply whereas in a moderately compensated system this P-V curve has a slow gradient and it curves towards the critical point. The effect is that the voltages are on a good level for a long time and nobody can see a problem. However, in reality the security margin of voltage instability is very small and a small event can pull the system down.

The P-V curve for bus 49 in area NYPS which is highly compensated (750 MVAr) and the load (P=1350 MW and Q=29 MVAr) is supplied from the NETS, as shown in Fig. 2. The system is operated with an 864 MW load at bus 49 and the voltage remains constant for this loaded condition. A three-phase fault is applied at the middle of one of the lines 60-61 and the resulting voltage at bus 49 is shown in Fig. 3 in which it is clear that, although the system is highly compensated and operated at a constant voltage, instability occurs due to the small security margin.

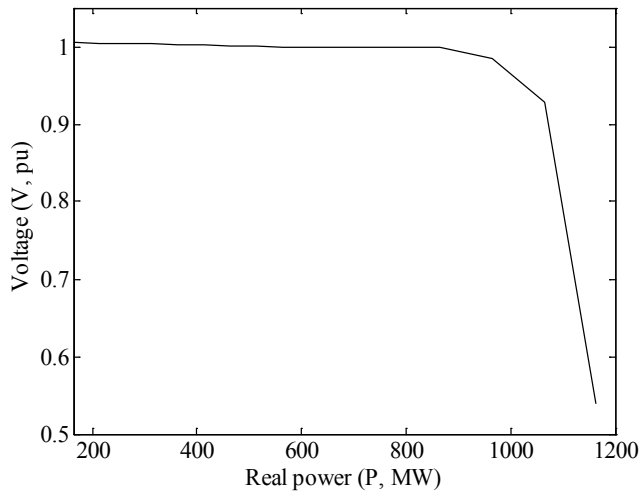

Fig. 2. P-V relationship at bus 49

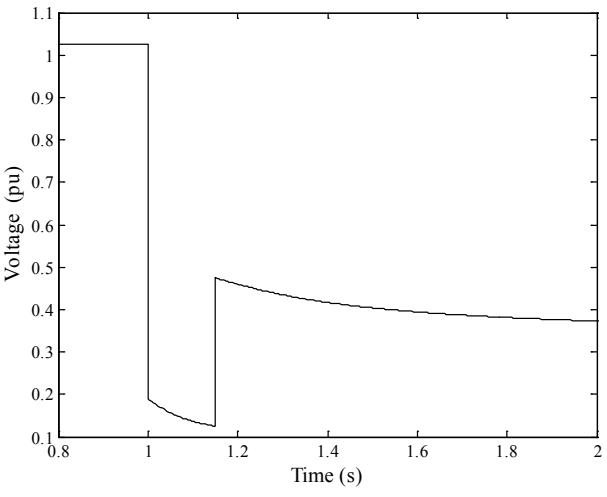

Fig. 3. Voltage at bus 49 for three-phase fault

Lots of DFIG type wind farms and a few synchronous generators

Statically, DFIGs often do not deliver as much reactive power as do synchronous generators and, dynamically, they cannot produce the same short-circuit current. The post-fault voltage support provided by feeding the reactive power is normally worse for a DFIG than for a synchronous machine. Although, recent work shows that an improvement in the area of voltage support may be possible. Due to the inferior behaviour of DFIGs compared to the synchronous generators, a system dominated by them behaves worse than one with synchronous generation. Normally, the effect is that more reactive compensation is needed in such a system. During deep voltage sags, a synchronous generator feeds in more reactive current than does a DFIG-based wind farm and, thus, provides a stronger support to the grid voltage. Also, DFIGs consume reactive power when they behave as SCIGs during transients and can reduce the voltage stability limit.

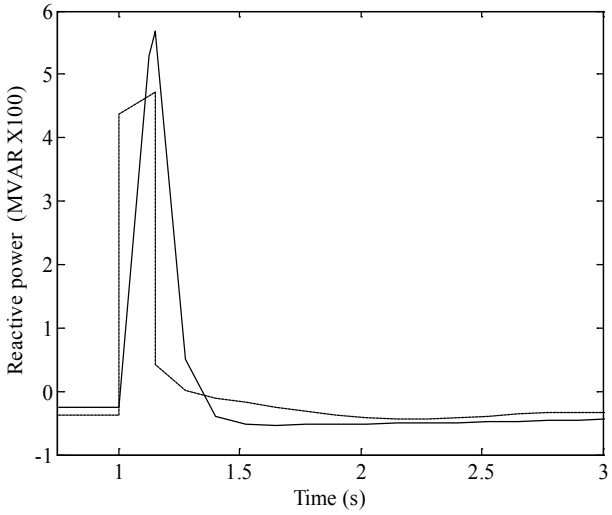

Fig. 4. Reactive power for three-phase fault

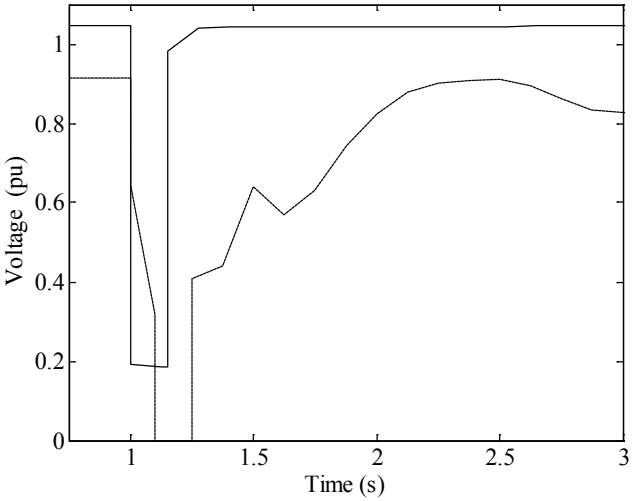

Fig. 5. Voltage for three-phase fault

Fig. 4 shows the reactive power supplies from a synchronous generator (G_{10}) and a DFIG of the same capacity during a three phase fault at the middle of one of the lines 60--61. Voltage transients for a power system with only synchronous generators (SGs) and one with a combination of 60% DFIGs and 40% synchronous generators of total generation for the same fault are shown in Fig. 5. The synchronous generators supply more reactive power and, thus, provide better performances in contrast to DFIG when recovering post-fault voltage. In some countries the grid-codes are so rigid that the DFIGs must be combined with static synchronous compensators (STATCOMs) in order to achieve similar behaviour to that of synchronous generators. In these cases, wind generation can be considered to be equivalent to conventional power generation.

Interactions amongst different FACTS devices

Interactions amongst the FACTS devices in a multi-machine system can adversely influence the damping properties of individual FACTS devices. In some critical cases, it may even amplify power swings or increase voltage deviations. Due to local, uncoordinated control strategies used in many power systems, destabilising interactions amongst FACTS controls are possible. This problem may occur especially after the clearance of a critical fault, if shunt and series connected devices, e.g., SVC or STATCOM and TCSC, are applied in the same area. Interactions amongst FACTS controls can adversely influence the rotor damping of generators and for weakly

interconnected system conditions it can even cause dynamic instability and restrict the operating power range of the generators. The following two case studies are conducted: (i) a STATCOM at bus 31; and (ii) a STATCOM at bus 31, an MSC at bus 53 and a TCSC at the middle of the line 30-31. Fig. 6 shows the rotor angle for both the cases with three-phase fault at the middle of one of the lines 60--61. It is clear that the addition of TCSC and MSC nearest to STATCOM increases the rotor angle oscillations. To improve overall system dynamic performance, interactions amongst FACTS controls must be minimised or prevented.

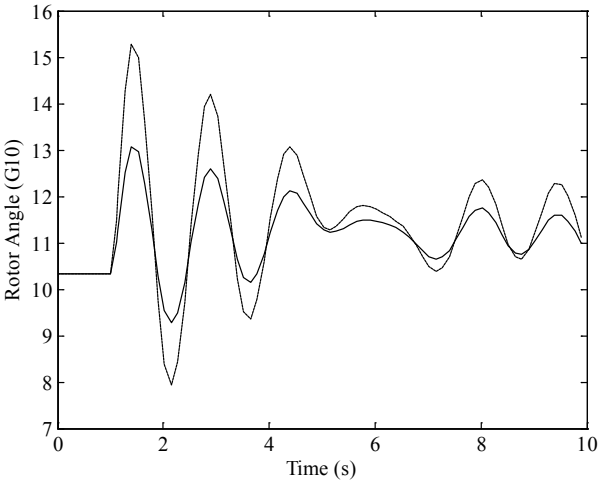

Fig. 6. Rotor angle for three-phase fault

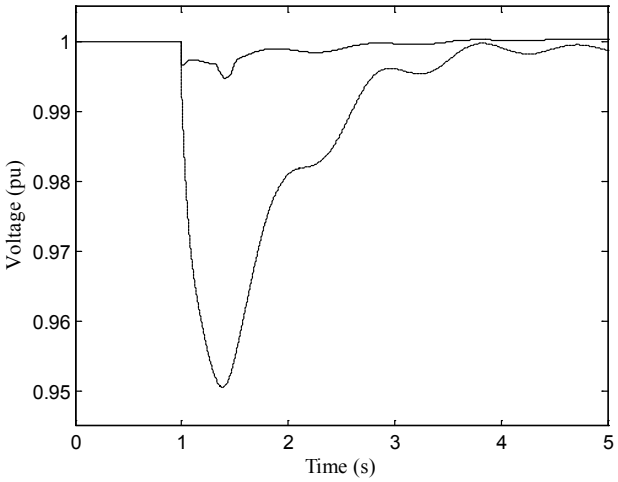

Fig. 7. Voltage for three-phase fault

Comparison of different compensation devices

A possible way of assessing the 'quality' of a compensation device concerning voltage stability may be that the reactive power output of several devices are not compared at the rated voltage of the devices but at the minimum voltage that is accepted in the grid. It could be the voltage at which power plants trip due to under-voltage (or other under-voltage criteria). An SVC has constant impedance and its reactive power output decreases in proportion to the square of the voltage. It is an active fast reacting device. If it is not yet at its limit before the fault, it can improve the voltage recovery after fault by activating the reserve. A STATCOM is a constant current source and its reactive power output decreases linearly with the voltage. It is also an active fast reacting device with limited energy storage. Because it can inject a constant current, it can better improve the voltage recovery after fault. Fig. 7 shows the bus voltage with a STATCOM and a SVC for a three phase fault in the middle of line 60--61. It is clear that during low voltage the STATCOM provides better response and the lower voltage with the STATCOM is much higher that that of the SVC.

Effects of integration of large-scale fixed-speed wind turbines (FSWTs)

A grid-connected wind turbine generation system consists of both mechanical and electrical systems which are connected to the distribution system to form part of the existing utility network. The analyses described in this section show that, for an interconnected power system, stability is likely to be affected by various factors contributed to by the constituent distribution system and the wind turbine's mechanical and electrical properties. Modal analysis [P. Khundur 1994] is conducted on the test system by replacing the synchronous generator by fixed speed wind turbines. Fig. 8 shows the monotonic mode under different FSWT integration levels. Fig.9 shows the

damping and frequency of the mechanical modes as a function of the shaft stiffness. From the participation factors [P. Khundur 1994], we find that the instability is caused mainly by shaft stiffness and the operating slip.

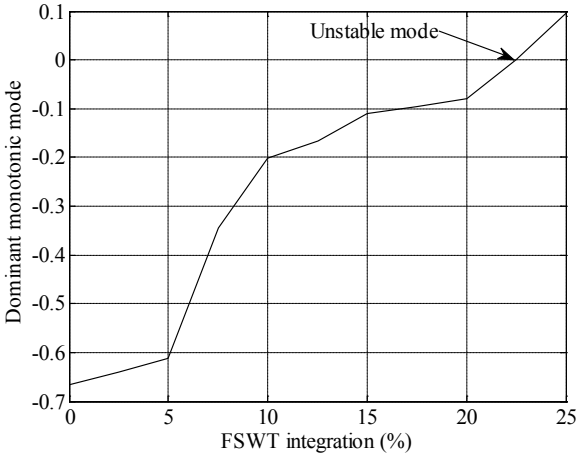

Fig. 8. Monotonic mode as a function of FSWT integration.

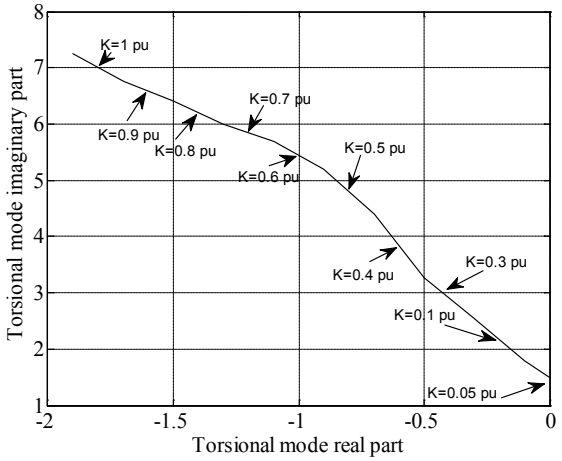

Fig. 9. PCC voltage for three-phase fault

Integration of FSWTs by using STATCOM

In the case of renewable energy, FACTS devices are especially advantageous when integrated with wind generators. As wind farms become a larger part of total power generation and as their penetration levels increase, issues related to integration, such as transient stability and voltage control are becoming increasingly important. For wind generation applications, FACTS can be implemented for voltage control in the form of shunt-connected SVCs or STATCOMs configurations.

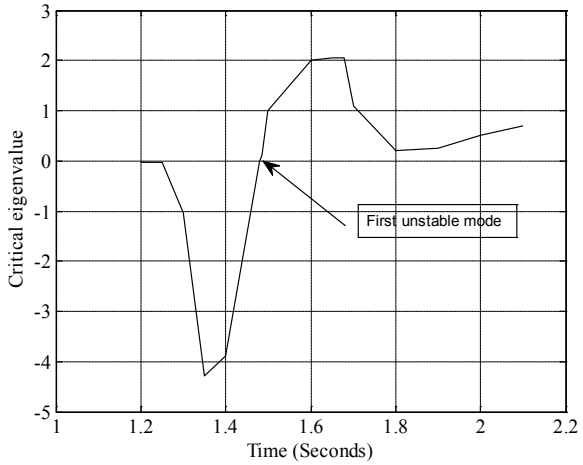

Fig. 10. Evolution of critical modes.

FSWT (MW)	*4500*	*6300*	*7325*	*8120*
STATC-OM (MVA)	*100*	*200*	*300*	*400*
Capacit-or (MVAr)	*500*	*100*	*1500*	*2000*

Table 1. FSWT integration and compensations

FSWTs and STATCOMs are integrated into the system repeatedly to find a certain level at which the system becomes unstable. The upper limits for certain amounts of compensation (STATCOM and shunt capacitor) are shown in Table 1. It is found that a 100 MVA STATCOM with a 500 MVAr capacitor is required to integrate a 24.5% level of FSWTs in different areas of the test system. For identifying the nature of instability

during transients at the upper limit, the method of eigenvalue tracking is used. In this method, the system is repeatedly linearised at selected time instants during the simulation and the system eigenvalues are computed at each snapshot. With a fixed compensation level (500 MVAr capacitor), the system becomes unstable after the integration of a certain level of FSWTs (4500 MW) which is decided depending on the acceptable voltage level and dynamic stability. Online linearisation and eigenvalue tracking show that, after fault clearing, the monotonic mode shown in Fig. 10 is correlated to generator slip and the mechanical state is the first to become unstable. The conclusions, drawn from Fig. 10 are an indication of potential instability.

CONCLUSION

In this paper, the impact of high compensation and large scale wind power integration on power system dynamic performance has been investigated. Modal analysis, participation factors, eigenvalue tracking and dynamic simulations have been used to analyse the nature of system behaviour under large scale wind turbine and FACTS device integrations. Due to local, uncoordinated control strategies used in many power systems, destabilizing interactions among FACTS controls are possible. High compensation reduces the security limit under certain operating conditions. Series compensation, such as TCSC does not have adverse effects on power flow. New transmission lines may be needed where the wind generation is situated far from the existing network. The modes related to operating slip and shaft stiffness are most critical and they may limit the large scale integration of wind generation.

REFERENCES

P. M. Anderson and A. A. Fouad (2002), *"Power System Control and Stability,"* Wiley, John & Sons, USA.

W. Qiao, R. G. Harley, G. K. Venayagamoorthy (2006), "Effects of FACTS Devices on a Power System Which Includes a Large Wind Farm," *IEEE PES Power Systems Conference and Exposition,* October 29-November 1, Atlanta, GA, pp. 2070-2076.

T. Ackermann and L. Soder (2002), "An overview of wind energy-status 2002," Renewable *and Sustainable Energy Reviews*, 6(1), pp. 67-128.

M. R. Rathi and N. Mohan (2005), "A novel robust low voltage and fault ride through for wind turbine application operating in weak grids," *31st Annual Conference of IEEE Industrial Electronics Society,* November 6--10, pp. 2481-2486.

M. P. Palsson, T. Toftevaag and K. Uhlen et. al. (2002), "Large-scale wind power integration and voltage stability limits in regional networks," *IEEE Power Engineering Society Summer Meeting,* July 25, Chicago, USA, pp. 762-769.

M. J. Hossain, H. R. Pota and V. Ugrinovskii et. al. (2009), "Robust STATCOM control for the enhancement of fault ride-through capability of fixed-speed wind generators," *IEEE Multi-Conference on Systems and Control,* July 8-10, Saint Petersburg, Russia, pp. 1505-1510.

J. G. Slootweg and W. L. Kling (2003), "The impact of large scale wind power generation on power system oscillations," *Electric Power Systems Research*, 67(1), pp. 9-20.

J. Hagstrom, I. Norheim and K. Uhlen (2005), "Large-scale Wind Power Integration in Norway and Impact on Damping in the Nordic Grid," *Wind Energy*, 8(3), pp. 375-384.

M. P. Palsson and T. Toftevaag and K. Uhlen et. al. (2002), "Large-scale wind power integration and voltage stability limits in regional networks," *IEEE Power Engineering Society Summer Meeting,* July 25, Chicago, USA, pp. 762-769.

P. Khundur (1994), *"Power System and Stability and Control,"* McGraw-Hill, USA.

BRIEF BIOGRAPHY OF AUTHORS

M. Jahangir Hossain (S'10) was born in Rajshahi, Bangladesh, on October 30, 1976. He received the B.Sc. and M.Sc. Eng. degrees from Rajshahi University of Engineering and Technology (RUET), Bangladesh, in 2001 and 2005, respectively, all in electrical and electronic engineering. He is currently working toward the Ph.D. degree at the University of New South Wales, Australian Defence Force Academy.

His research interests are power systems, wind generator integration and stabilization, voltage stability, micro grids, robust control, electrical machine, FACTS devices, and energy storage systems

Hemanshu R. Pota received the B.E. degree from SVRCET, Surat, India, in 1979, the M.E. degree from the IISc, Bangalore, India, in 1981, and the Ph.D. degree from the University of Newcastle, NSW, Australia, in 1985, all in electrical engineering. He is currently an Associate Professor at the University of New South Wales, Australian Defence Force Academy, Canberra, Australia. He has held visiting appointments at the University of Delaware; Iowa State University; Kansas State University; Old Dominion University; the University of California, San Diego; and the Centre for AI and Robotics, Bangalore. He has a continuing interest in the area of power system dynamics and control, flexible structures, and UAVs.

Rodrigo A. Ramos (S'97-M'03-SM'08) received the B.Sc.degree in 1997, the M.Sc. degree in 1999, and the Ph.D. degree in 2002 from Escola de Engenharia de Sao Carlos - University of Sao Paulo (EESC/USP), Sao Carlos, Brazil.

He is currently an Assistant Professor at EESC/USP. His research interests are in the fields of power system dynamic performance, stability and robust control

Pumped hydro for large scale storage of solar generated electricity in Australia

Andrew Blakers, James Pittock, Mishka Talent and Francis Markham
Australian National University
Canberra 0200
Andrew.Blakers@anu.edu.au

ABSTRACT

Pumped hydro storage is efficient, flexible, economical and commercially available on a vast scale. Indeed, it is the only large scale storage technology currently available to the electricity industry, with some 130 GW of capacity installed world wide including 2.5 GW in Australia. Competing storage techniques, such as compressed air, high temperature thermal storage in conjunction with CST, and advanced batteries, are considerably more costly or less developed. The paper describes a project aimed at quantifying the capacity of pumped hydro to provide adequate back up to allow solar and wind generation to provide most of Australia's electricity. Initial results suggest that there are vastly more suitable pumped hydro storage sites than required for this task.

Keywords *Energy Storage, Pumped Hydro, Solar Energy*

INTRODUCTION

It is sometimes claimed that solar energy (and wind energy) can't provide baseload power and is therefore limited to small penetrations of the national electricity grid by day/night and weather-related intermittency [ABC 7:30 Report, 2007]. However, the potential of pumped hydro to accommodate the intermittency and storage of solar energy often overlooked.

Traditional hydro electric schemes typically involve large dams on a river, sufficient to provide seasonal storage (usually winter to summer). Water is released to meet electricity demand. Since hydro can respond to electricity demand variations quickly, hydro plant typically follows load fluctuations, and is rarely used to provide constant baseload. The value (and price) of electricity produced on demand, such as from hydroelectricity, is higher than baseload electricity from coal or nuclear power stations.

Pumped hydro storage involves pumping water from a lower reservoir to an upper reservoir located at an altitude that is 100 - 1,000 metres higher during times when capacity exceeds demand, and releasing that water through a pump/turbine on demand. Many pumped hydro systems are associated with large conventional hydroelectric systems. An example is the Tumut 3 pumped hydro storage system in the Snowy Mountains, which has a capacity of 1.5 GW and a head of 151m.

Tumut 3 1500 MW pumped hydro storage system in the Snowy Mountains

A new breed of pumped hydro storage is being deployed around the world. These systems have relatively small reservoirs, with storage of only hours or days of turbine capacity. Reservoirs can be "off-river" (since only evaporation needs to be replaced), and sea water can be used. For example, reservoirs can be excavations located atop hills next to the sea, or pairs of oversized "farm dams" located close to each other at different elevations. The cost of these systems is much more heavily weighted to power production (pump/turbines, pipes & tunnels, interconnection to the grid) rather than energy storage (dams & lakes). Their role is to smooth short term fluctuations in demand and supply.

Pumped hydro storage is efficient, flexible, economical and commercially available on a vast scale. Indeed, it is the only large scale storage technology currently available to the electricity industry. Competing storage techniques, such as compressed air, high temperature thermal storage in conjunction with concentrating solar thermal (CST), and advanced batteries, are considerably more costly or less developed.

An internet search reveals that there are more than 200 large pumped hydro systems currently deployed around the world with a combined capacity of about 130 GW, including 2.5 GW in Australia. This capacity is far larger than the combined size of all other energy storage technologies available to the electricity industry. The median elevation difference between upper and lower reservoirs is 250m, and ranges from 12m to 1260m. The power capacity ranges from less than 1 MW up to 2700MW, with a median of 420MW.

Storage of Australia's entire electrical output for 24 hours using pumped hydro would require combined upper and lower lakes of about 100 km^2 (about 5 m^2 per Australian citizen), which suggests that it should be possible to find enough sites for very large scale storage of solar electricity. This calculation assumes that the lakes are 15m deep, there is an elevation difference between the upper and lower lakes of 400m, and that the round trip efficiency is 80%. Round trip efficiency refers to the proportion of energy

recovered compared with the energy expended in pumping the water to the upper reservoir. Pumped hydro storage could be in the form of a few large systems, or could comprise many small systems scattered over the populated regions of Australia.

LARGE SCALE SOLAR

Increasingly large scale deployment of CST power and PV technology is expected to continue to result in continued learning-curve and technology-driven cost reductions. Very rapid and sustained growth of the solar and wind energy industries has occurred over the past decade. Indeed, should growth rates that were experienced from 2000 to 2010 continue, all of the world's electricity could be supplied by solar energy by 2028. However, large scale deployment could be inhibited by problems, or perceived problems, relating to the intermittency of solar (and wind) energy.

Solar indeed has an issue of intermittency. One type of intermittency is completely predictable (day/night and summer/winter). Day/night intermittency can be ameliorated by moving loads from night to day instead of the reverse, which happens at present.

Another type of intermittency relates to weather events. This type can be ameliorated by wide geographical distribution of PV and CST systems, by taking advantage of the availability of sophisticated solar monitoring satellites, by weather modelling, and by establishing a networked array of many low cost sun-sensors throughout the populated regions of Australia. The latter would allow early detection of local cloud missed by satellites and weather modelling.

A third type of intermittency is common to all generation technologies, and relates to generator and grid reliability. In this case, the output of large numbers of moderately sized and widely distributed CST and PV generators are more predictable than the output of a small numbers of large conventional generators.

In summary, solar intermittency exists but can be highly predictable on every time scale from seconds to years – more so than the load itself. There will usually be adequate warning of cloud cover to allow alternative measures to be taken, including firing up fossil fuel generators, shedding non-firm load and drawing from storage. Pumped hydro storage is ideal in this respect because it has no standing losses and can respond quickly.

The availability of solar electricity is generally well matched to demand from commercial activities for electricity. However, the air conditioning load lags the solar availability by several hours. In addition, demand for electricity in domestic dwellings is high during the early evening. Short term storage of solar electricity (3-6 hours) confers a substantially higher value to solar electricity. Longer term storage (24 hours) allows energy shifting from one day to another, to cope with poor weather.

GIS STUDY OF PUMPED HYDRO OPTIONS

Recent advances in Geographic Information System (GIS) tools, GIS data and computing power make it possible to comprehensively analyse the eastern and south-western Australian land mass for feasible pumped hydro storage sites. Substantial preliminary work has been undertaken to systematically identify and assess sites capable for use in pumped storage across the landscape. Our pilot work uses 9 arcsecond and 3 arcsecond digital elevation models to identify locations with relatively flat land suitable for construction of upper and lower pumped hydro storages that are

separated by the minimum required elevation (head) and gradient. The shape of the ponds is determined by flat terrain, and by parameters set to minimize required earthworks. Consequently opportunities for impoundments in steep valleys are overlooked using this method.

This pilot model performs better than published best practice assessment systems from overseas. However preliminary work has been limited by the need to refine the software to better locate more reservoir sites on undulating sites (eg. in gullies of the required volume), and by the need to upgrade the software to run finer resolution (<100 m) digital elevation model data on parallel computer architectures (i.e. a super computer) to assess broader areas.

Substantial "ground truthing" using tools such as Google Earth and site visits will be required. Overlays to eliminate sites that conflict with environmental, urban and economic uses will be applied. Proximity to a source of water will need to be identified for each site, together with analysis of rainfall and evaporation data, water value and water stress within particular catchments. Sites with proximity to the high voltage transmission network will be advantageous. The interaction of variably distributed energy sources (solar and wind) with variable loads is an important area of study.

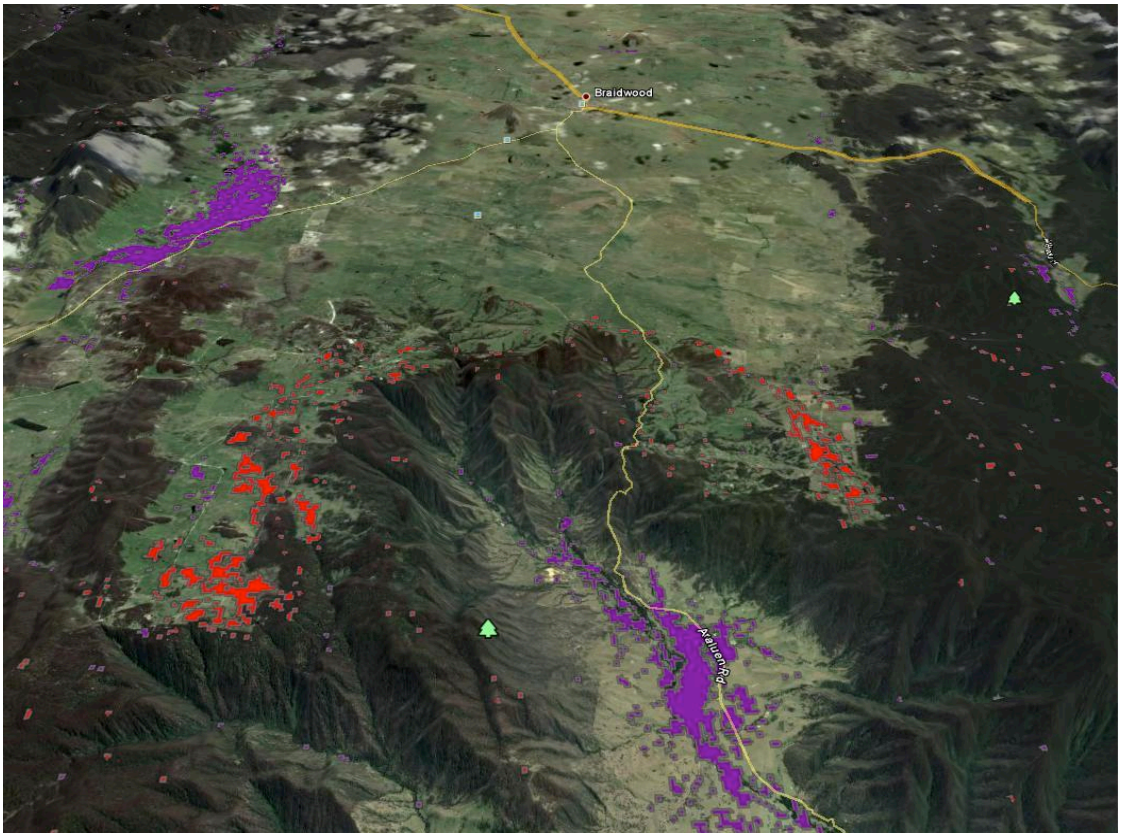

Figure 2: Potential pumped hydro sites in the Araluen Valley near Canberra. Note that only geographical constraints have yet been applied.

Our pilot work in the greater Canberra region and central Tasmania has already identified many suitable sites. Figure 2 illustrates potential sites in the Araluen Valley

near Canberra. There is an elevation difference of about 400m between the potential upper reservoir sites (red) and lower reservoir sites (purple).

Central Tasmania alone appears to have far more than enough sites to back up the entire Australian electricity grid for 24 hours. Figure 3 shows our model run for central Tasmania and includes potential pumped storage sites with greater than 20GWh storage capacity. The elevation difference between upper and lower reservoirs is about 800 m. The paired ponds are shown in red, linked by pink pipelines. Deeper red indicates ponds used more than once by linked ponds. About 20 of these sites (i.e. 20 of the "pink pipelines") would be sufficient to provide 24 hour storage for Australia's entire electricity production. It should be noted that environmental, urban, cultural, economic and other constraints have yet to be applied.

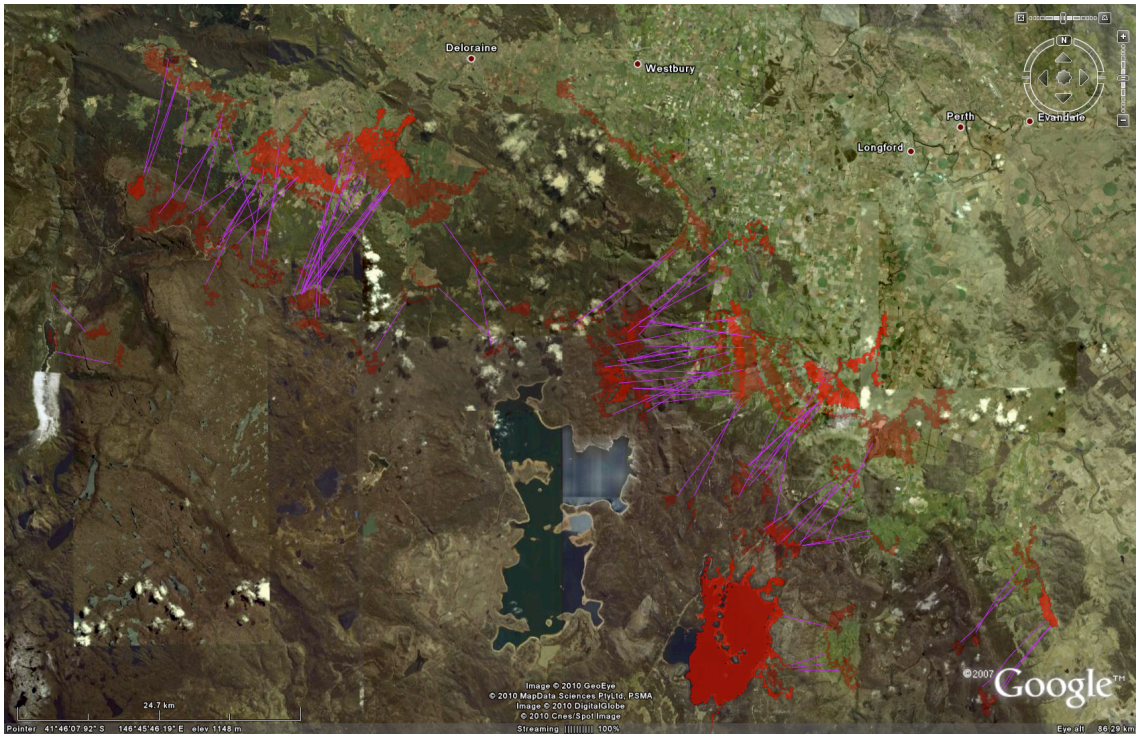

Fig. 3: Potential pumped hydro sites in central Tasmania. Note that only geographical constraints are accounted for - no environmental, urban, cultural, economic or other constraints have yet been applied.

ECONOMIC MATTERS

A study of the economic efficacy of pumped hydro is needed in parallel with GIS analysis of potential sites. Since pumped hydro storage is daily rather than the seasonal storage available from most current hydroelectric systems such as in the Snowy Mountains and in Tasmania, far smaller and less costly lakes are required. Most of the cost is in the power components: pipes & tunnels, pump-turbines and grid interconnection. Is most of the value of storage captured by extending the solar peak into the early evening (4 hours storage), or is 24 hour storage preferred? Should the storage be a smaller number of GW-rated systems, or are a large number of smaller

systems better? Can distributed pumped hydro alleviate the need to upgrade transmission infrastructure? What additional value does mass pumped hydro storage have in terms of managing short and long term load and supply fluctuations and peaks, independent of its role in backing up high penetrations of wind and solar? And finally, what is the additional cost of pumped hydro?

Thorough analysis of the physical and economic potential of pumped hydro will support the solar (and wind) energy industry as it grows to become a major source of electricity.

REFERENCES

Malcolm Turnbull and John Howard quoted in ABC's 7:30 Report, 1st October 2007, http://www.abc.net.au/7.30/content/2007/s2047734.htm

BRIEF BIOGRAPHY OF ANDREW BLAKERS

Professor Andrew Blakers is the Director of the ARC Centre for Solar Energy Systems and the Centre for Sustainable Energy Systems at the Australian National University. He was a Humboldt Fellow and has held Australian Research Council QEII and Senior Research Fellowships. He is a Fellow of the Academy of Technological Sciences & Engineering, the Institute of Energy and the Institute of Physics. He has published approximately 200 papers and 12 patents. His research interests are in the areas of photovoltaic and solar energy systems; particularly advanced thin film silicon solar cell technology and solar concentrator solar cells, components and systems. He also has interest in sustainable energy policy.

Brine Clarity Maintenance in Salinity-Gradient Solar Ponds

Neus Gasulla, Yusli Yaakob, Jimmy Leblanc and Aliakbar Akbarzadeh

Energy Conservation and Renewable Energy Group
School of Aerospace, Mechanical and Manufacturing Engineering
RMIT University
P.O Box 71, Bundoora, Victoria, 3083, Australia

Email: neus.gasulla@rmit.edu.au, yusli.yaakob@rmit.edu.au, jimmy.leblanc@rmit.edu.au and aliakbar.akbarzadeh@rmit.edu.au

ABSTRACT

Brine transparency is an important part of the maintenance of a salinity-gradient solar pond as it affects the amount of solar radiation reaching the storage zone and hence has an influence on the thermal performance. There is a wide range of factors that can hinder the transmission of light in a solar pond. Algal and microbial growths are the most common problems encountered in working solar ponds and control of their densities is essential to maintain transparency. Two different chemical treatment methods for algae growth prevention are described in this paper: chlorine and a novel chemical product - copper ethylamine complex. The latter method has never been implemented previously in a working pond. This paper discusses the theory of the algae control methods used and presents the experimental results of the chemical treatments. The results showed that Cupricide is more effective than chlorine and is therefore the recommended chemical for algae control in solar ponds; it improves the water transparency especially in the Upper Convective Zone and Lower Convective Zone with all measurement values less than 1 NTU. Chlorine was found to be more corrosive than Cupricide due to the acidic effect it has on the pH. The preliminary cost analysis showed that granular chlorine is the cheapest chemical. A more detailed financial analysis is nevertheless required to refine these costs.

Keywords – Algae, Chlorine, Clarity, Cupricide, Salinity-Gradient Solar Pond, Turbidity.

INTRODUCTION

A salinity-gradient solar pond (SGSP) is a combined solar energy collector and heat storage system reliant upon an aqueous solution of salt at varying densities to suppress natural convection and store thermal energy (Hull *et al.*, 1988). Solar ponds generally consist of three regions, the upper convective zone (UCZ), the non-convective zone (NCZ) and the lower convective zone (LCZ), as shown in Figure 1. The UCZ is the topmost layer of the solar pond. It is a relatively thin layer which consists almost wholly of fresh water. The NCZ is the layer below the UCZ and has an increasing salt concentration relative to the UCZ. The LCZ is the layer which contains saturated salt; energy is absorbed and stored in this region.

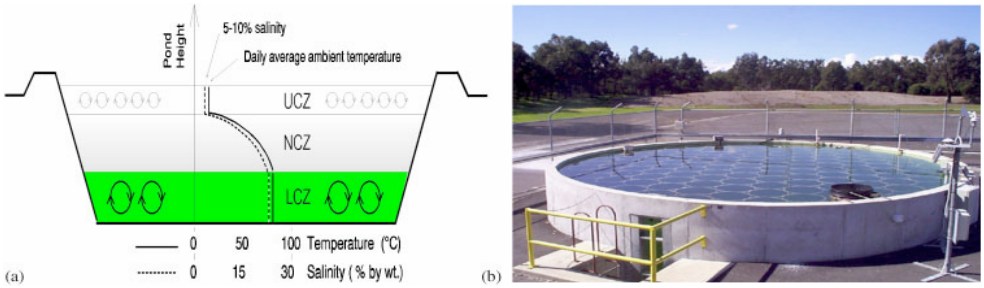

(a) Schematic (b) 50 m^2 solar pond at RMIT

Fig. 1: Salinity-gradient solar pond

Solar ponds have the potential to supply low-temperature heat at competitive costs. It is technically possible to generate electricity from the heat stored in a solar pond, as demonstrated, in Israel near the Dead Sea (5 MW), at Alice Springs in Australia (15 kW) and at the University of Texas in El Paso, USA (70 kW) (Hull *et al.*, 1988). Moreover, thermal desalination processes such as multi-stage flash and multi-effect evaporation may use solar ponds to heat the incoming saltwater (Leblanc and Andrews, 2007; Leblanc *et al.*, 2010a). Integration of solar ponds into salinity mitigation or interception schemes is another attractive potential application (Akbarzadeh *et al.*, 2005; Akbarzadeh *et al*., 2008).

In 1998, a 53 square metre experimental solar pond was constructed in the Renewable Energy Park of the School of Aerospace, Mechanical and Manufacturing Engineering, RMIT University located in Melbourne, Australia. Attempts have been made to maintain the clarity in this experimental solar pond using brine shrimps (‘Artemia salina’ and ‘Artemia fransiscana’ species), which swim in the pond feeding on algal populations and detritus - the main sources of turbidity. In spite of initial success, the population of brine shrimps decreased gradually to extinction. A possible explanation of this loss was lack of dissolved oxygen in the water (Alagao *et al.*, 1994). Another practical way of maintaining the clarity is to reduce the pH of the brine to 4 or less by adding hydrochloric acid (Hull, 1990). At the RMIT pond, chemical treatment was administered from January 2007 to February 2009 by injecting HCL acid at different heights using PVC pipes to maintain the pH below 4. However, HCL acid injection caused corrosion of metal brackets (Leblanc *et al.*, 2010b).

In the present article, two different chemical treatment methods for algae growth prevention are described: chlorine and a novel chemical product, which has never been implemented previously in a working pond, known as copper ethylamine complex. The theory of the algae control methods used is discussed and the experimental results of the chemical treatment are presented.

CLARITY MONITORING

Monitoring the clarity is an important part of the maintenance process in pond operations. Turbidity is the primary parameter measured at the RMIT solar pond to monitor the brine transparency. An increase of turbidity values indicates an increase in the concentration of suspended matter in the pond. Turbidity measurement provides the means for monitoring and controlling the clarity of brine by indicating the necessity for brine treatment when turbidity levels are higher than desirable. At the El Paso solar pond, the upper limit allowed was an NTU reading of 3, determined from experience

(Xu *et al.*, 1993). At Bundoora solar pond, the turbidity was measured using the Hanna instruments HI 93703 turbidity meter.

RELATIVE LIGHT TRANSMISSION INDEX

The thermal performance of a solar pond depends on the nature of light absorption in the body of the water and hence is largely affected by the clarity. In the RMIT solar pond, a photovoltaic solar cell has been used as an alternative method to quantify light absorption by measuring the relative light transmission index values. The index values are obtained by dividing the maximum power obtained when using distillate water with the maximum power obtained from the different brine samples, as represented by the following equation.

$$I_{RLT} = \frac{Power_{\ pond\ water}}{Power_{\ distillated\ water}} \quad (1)$$

In order to develop the I-V characteristics curve, the open circuit voltage (V_{oc}) was measured first. The electric current is zero at this point. Then the electrical resistance was decreased in a stepwise process which resulted in an increase in the electric current and a simultaneous decrease in the voltage. Finally, the short-circuit current (I_{sc}) was measured which corresponds a voltage of zero. The corresponding power values for each measurement value were also calculated.

Figure 2 shows the equipment set-up. The voltmeter was connected in parallel with the variable resistance and an ammeter was connected in series. The solar cell was placed in a PVC pipe and exposed to a constant light source of 100 Watts. The difference in turbidity would affect the radiation reaching the solar cell and hence produce different performance curves. The performance curves were developed for five different positions: UCZ, NCZ (at 37 cm, 63 cm and 88 cm from the UCZ) and LCZ.

(a) Equipment set-up (b) Schematic

Fig. 2: Solar cell experiment set-up

POND TREATMENT USING CUPRICIDE

Cupricide Operation Principle

In 1956, Maloney and Palmer found that copper ions in solutions at concentrations of 0.1 – 0.5 ppm (mg/L) were capable of killing all algal cells, depending on the species tested (Agmin, 2009). It was later found that there is a range of chemical reactions between copper ions and fresh water algae. These early algaecides were based on

copper sulphate, which has several disadvantages. Later on, a new stable copper-based algaecide, named Cupricide, was developed. It combines the copper ions with organic complexing agents known as ethanolamines (Agmin, 2009). The effectiveness and benefits of Cupricide over copper sulphate are overwhelming. Cupricide has been proven in controlled laboratory test with blue-green algae to be an effective algicide at 0.2 mg/L copper compared to copper sulphate at 1.0 mg/L (Agmin, 2007).

Cupricide contains copper chelate which stabilizes copper solutions, preventing precipitations of copper hydroxy salts in alkaline, hard water. Whereas, copper sulphate is readily precipitated in these waters and thus reduces the algicidal effectiveness. Moreover, because of the chelate structure in Cupricide, it is rapidly and specifically absorbed by algal cells, which are inactivated within 12-24 hours. These properties provide significant advantages over solid or crystalline products such as copper sulphate, which are difficult to handle, dispense and dissolve in water. For the reasons mentioned above, Cupricide was chosen as a potential candidate for further algae control experimental tests at the Bundoora experimental solar pond.

Application

The quantity of Cupricide required in the form of available copper is related to the volume of water to be treated. The concentration of copper in parts per million (ppm) is determined after consideration of the types of algae present and their susceptibility or resistance to copper. The total water volume of the Bundoora experimental solar pond was found to be 108 m^3. Based on this volume, the amount of Cupricide needed was found to be approximately one litre. Cupricide has been applied at different levels in the pond (within the UCZ and NCZ). It was applied each week with different doses to improve the effectiveness of the chemical treatment as detailed in Table 1.

Tab. 1: Total Cupricide volume applied at different levels of solar pond water

	Cupricide Volume Applied (ml)			
Date / Level	**3.12.09**	**11.12.09**	**18.12.09**	**29.12.09**
UCZ	150	50	50	50
NCZ (37cm)	400	600	1000	1000
NCZ (63cm)	350	300	400	500
NCZ (88cm)	100	50	50	50
TOTAL	**1000**	**1000**	**1500**	**1600**

Cupricide was mixed with the pond water in a proportion of 1:10. The pond water was extracted from different levels using the variable depth sample taker. After mixing the chemical with the brine, the mixture was reintroduced at the same level in order to avoid disturbance of the gradient. For this propose, PVC pipes of varying length were used to inject the mixture. Horizontal diffusion of the Cupricide mixture was noticeable during injection.

Experimental results

Figure 3 shows the turbidity profile before applying Cupricide and five weeks after application. It can be seen that there is an improvement in the brine transparency during the chemical treatment. Prior to the chemical treatment, the highest recorded NTU measurement was at the top of the NCZ with values around 7 NTU. There was an improvement in the solar pond water transparency five weeks after application, especially in the UCZ and LCZ with all values less than 1 NTU. The brine NTU values in the NCZ were still high but there have been some improvements.

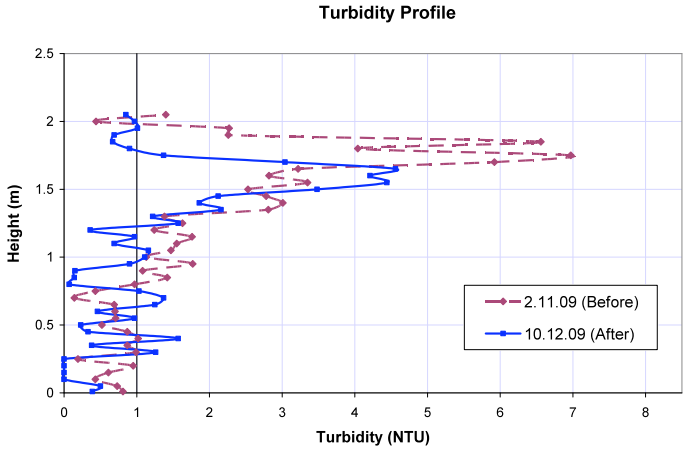

Fig. 3: Turbidity profiles during Cupricide treatment

The solar cell I-V characteristics curves and power values from the solar cell experimental tests are directly related to the brine transparency. The solar cell I-V and power performance graphs obtained for the brine sample from the NCZ (37 cm from UCZ) during the Cupricide treatment are illustrated in Figure 4. It can be seen from the figure that the maximum current (short-circuit current) and maximum power has increased during the treatment (from 13.15mW to 16.40 mW). This increase in power (~ 20 %) shows that the brine transparency has improved with the application of Cupricide.

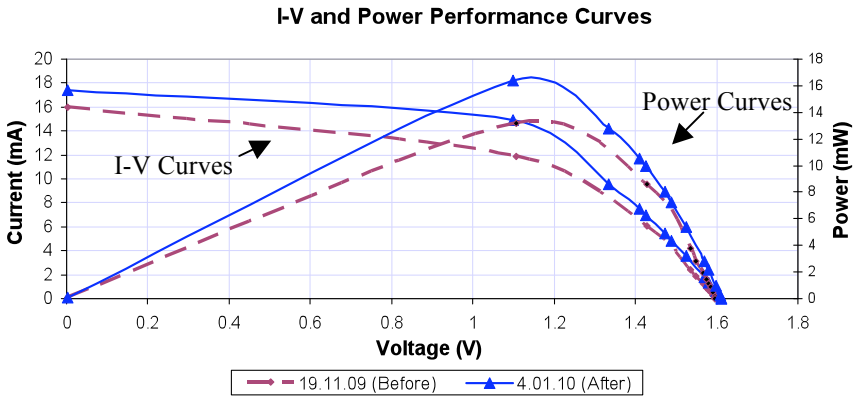

Fig. 4: I-V and power performance curves before and after Cupricide treatment (for sample from NCZ - 37 cm from UCZ)

The relative light transmission index was calculated using equation (1). The index values prior to the treatment and after application, for brine samples at different locations in the pond, are shown in Table 2. The level of brine samples in the PVC pipe was fixed at a height of 0.154 m from the solar cell. It can be appreciate that the difference between the indexes and the reference index (distilled water) has reduced after treatment indicating better brine transparency.

Tab. 2 : Relative Light Transmission Index obtained for Cupricide Treatment

	Before Cupricide treatment (19.11.09)		**After Cupricide Treatment (14.01.10)**	
	Maximum Power	**Index**	**Maximum Power**	**Index**
Distilled water	19.87	1	18.37	1
Pond Water From UCZ	17.06	0.86	17.99	0.98
Pond Water From NCZ (37cm)	13.59	0.68	16.07	0.87
Pond Water From NCZ (63cm)	13.77	0.69	16.77	0.91
Pond Water From NCZ (88cm)	18.07	0.91	17.25	0.94
Pond Water From	18.37	0.92	18.10	0.98

In order to establish the cause of turbidity in the solar pond, an Olympus optical microscope has been used. Before starting the chemical treatment, some optical observations have being carried out. It has been found that Blue-green algae is the type of algae that inhabit RMIT's solar pond. Filamentous and unicells have been observed and different components of the algae structure have been identified as shown in Figure 5. The decomposition of cytoplasm unicells and filamentous was observed during and after the Cupricide treatment (Figure 5).

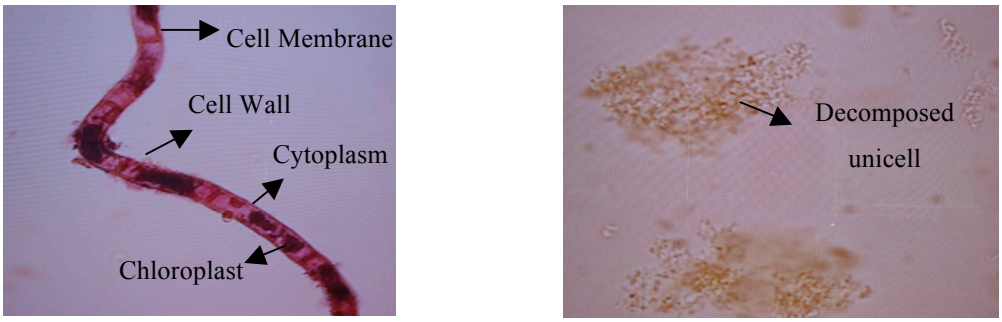

(a) Filamentous algae structure (b) Unicell decomposition

Fig. 5: Filamentous algae and unicell (400x magnification)

POND TREATMENT USING CHLORINE

Chlorine Operation Principle

Two types of granular chlorine have been tested. Initially, chlorine without stabilizer has been applied in order to produce a shock treatment. Later on, chlorine with stabilizer has been introduced, which helps the chlorine last longer and therefore reduces consumption.

Application

The quantities of the premium granular pool chlorine low residue formula (with active constituent: 700g/kg chlorine present as calcium hypochlorite) and the amount of the stabilised dichlor pool chlorine (with active Constituent: 560 g/kg chlorine present as sodium dichloroisocyanurate) applied are shown in Table 3.

Tab. 3: Quantities of chlorine applied

	Granular Chlorine quantity applied	**Quantity of Stabilized Chlorine Applied (g)**		
Date / Level	**27.01.10**	**5.02.10**	**15.02.10**	**23.02.10**
UCZ	300	100	100	50
NCZ (37 cm)	400	400	400	500
NCZ (63 cm)	150	150	150	150
NCZ (88 cm)	150	150	150	50
NCZ (140 cm)	400	200	200	250
Total	**1400**	**1000**	**100**	**1000**

Experimental Results

The turbidity profiles obtained before and after the chlorine treatment show that there was a slight improvement in the brine transparency (Figure 6). However, it can be seen that the chlorine treatment was not as effective as the Cupricide treatment; only a few locations had NTU values less than 1. This can be attributed to non-uniformity in the chemical distribution. In addition, despite the large quantity of chlorine applied at the most affected level (NCZ 37 cm), no significant improvement was noticed. This could be due to dead algae settling at this particular level. Further tests are needed to address this issue. It is noteworthy that high turbidity values were obtained near the NCZ-LCZ interface due to the crystallization of sodium chloride after adding granular chlorine to this level.

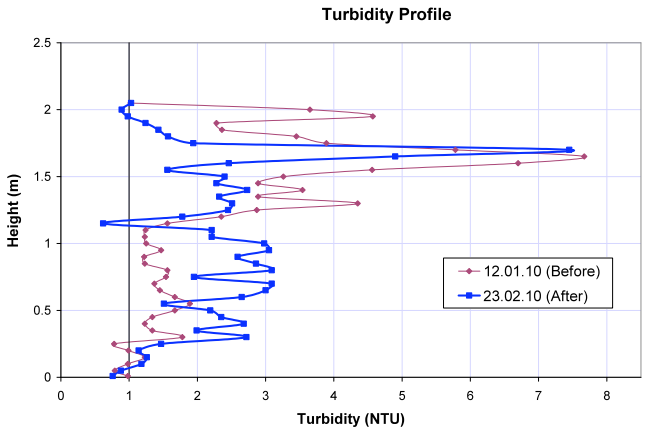

Fig. 6: Turbidity profiles during chlorine treatment

Figure 7 shows the solar cell I-V and power performance graphs obtained for the brine sample from the NCZ (37 cm from UCZ) during the chlorine treatment. The figure shows that the maximum power has increased by ~ 14% after the treatment (from 11.21 mW to 13.05 mW).

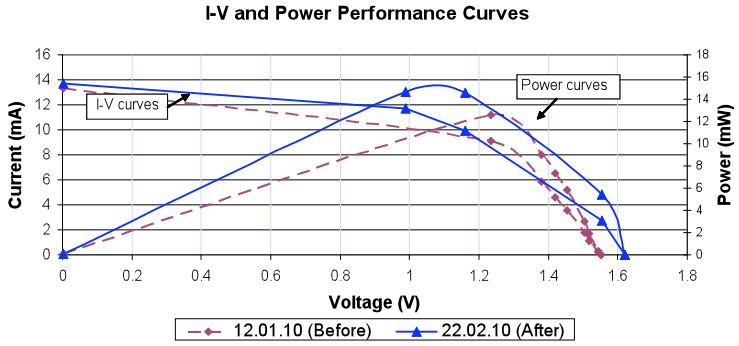

Fig. 7: I-V and power performance curves before and after chlorine treatment

The relative light transmission index was calculated using equation (1). The index values prior to the treatment and after application, for brine samples at different locations in the pond, are shown in Figure 8 and Figure 9, respectively. For more accurate results, the height of the brine samples in the PVC tube containing the photovoltaic solar cell was varied (0.061, 0.081, 0.154 and 0.197 m) to obtain four index values for each sample. The figures clearly show that the difference between the indexes and the reference index (using distilled water) has reduced after treatment, confirming that the brine transparency has improved.

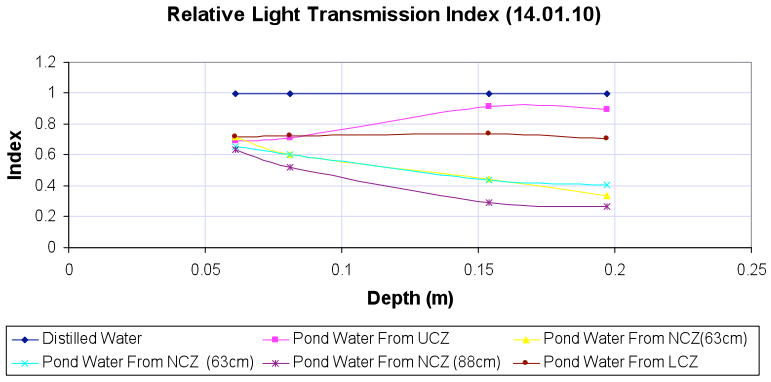

Fig. 8: Relative light transmission index before chlorine treatment

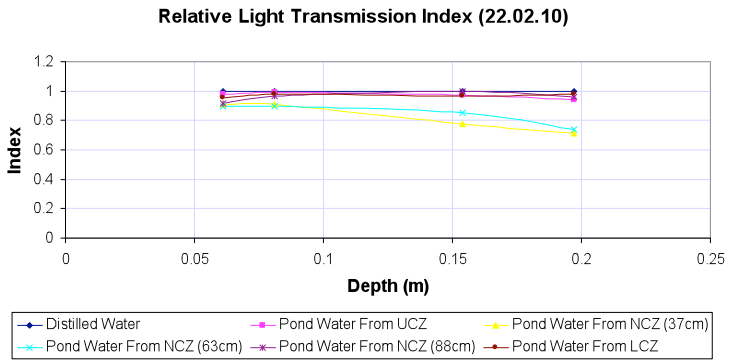

Fig. 9: Relative light transmission index after chlorine treatment

COMPARATIVE ANALYSIS

Turbidity profiles

It is clear from the comparative turbidity profiles (Figure 10) that Cupricide treatment was more effective that granular chlorine treatment.

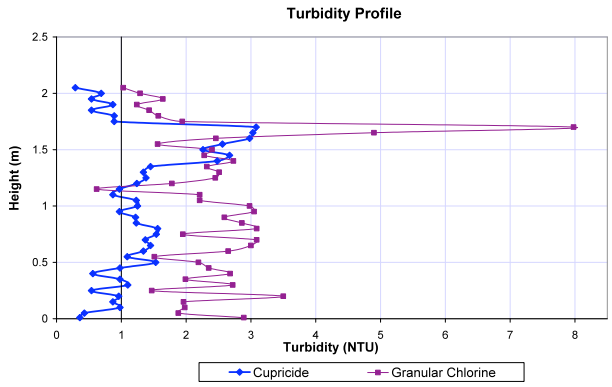

Fig. 10: Turbidity profiles at the end of Cupricide and chlorine treatments

Cupricide treatment improved the water transparency especially in the UCZ and LCZ with all values less than 1 NTU. With chlorine, despite the large quantity of chlorine applied at the most affected level (NCZ 37 cm), no significant improvement was noticed. As mentioned earlier, this could be due to dead algae settling at this particular level. This is still an open question and further tests are needed to address this issue.

Power performance curves

In order to have a meaningful comparison, the same conditions were observed during the solar cell experimental tests. Figure 4 showed that the maximum power obtained increase ~ 20% after Cupricide. Similarly, Figure 7 showed that the chlorine treatment resulted in an increase of ~ 14% in the maximum power. It is clear from the results that the Cupricide treatment had an advantage over chlorine.

Economical aspects

A preliminary simple cost analysis for all chemicals investigated is shown in Table 4. It is obvious that granular chlorine is the cheapest chemical but was found to be less effective than the more expensive Cupricide chemical. A more detailed financial analysis is nevertheless required to refine these costs.

Tab. 4 : Unit and total price of chemical compounds applied

	Unit price	Quantity applied	Total price
Granular pool chlorine low residue formula	AUD $ 15 / kg	1.1 kg	AUD $ 16.5
Stabilised dichlor pool chlorine	AUD $ 21 / kg	1.1 kg	AUD $ 23.5
Cupricide	AUD $ 22 / L	1.275 L	AUD $ 28.05

Adverse Effect on Equipment

One of the main disadvantages of having a low pH during chemical treatment is the rapid deterioration of metal fittings in the pond. The heat exchanger supports are made of galvanised iron and corrosion was observed, especially during the chlorine treatment.

Samples of galvanized iron were placed in Cupricide and chlorine solutions for 24 hours in order to observe the chemical reaction and compare the rate of corrosion. Figure 11 shows that both chemicals are corrosive in nature. However, chlorine was found to be much more corrosive due to the acidic effect it has on the pH. The corrosion weight loss for the samples dipped in Cupricide and chlorine solutions were estimated to be 0.94 mdd and 4 mdd, respectively.

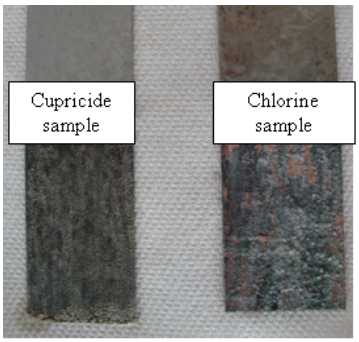

Fig. 11: Corrosion observed during chemical treatments

CONCLUSIONS

In this paper, the different chemical treatments as an algae control method for the clarity maintenance of salinity-gradient solar ponds have been presented. Blue-green algae has been found to be the type of algae that inhabit at RMIT solar pond. Both filamentous and unicell algae have been found to affect the brine clarity. Two different chemical treatment methods for algae growth prevention have been investigated during a trial period at Bundoora solar pond: granular chlorine and cooper ethylamine complex. The results showed that both chemicals improve the brine transparency. Cupricide is more effective than chlorine; it improves the water transparency especially in the UCZ and LCZ with all values less than 1 NTU. On the other hand, with the chlorine treatment, despite the large quantity of chlorine applied at the most affected level, no significant improvement has been noticed. The solar cell experimental tests showed that Cupricide treatment increased the maximum power by ~ 20%, compared to 14% in the case of chlorine treatment. The difficulty in treating a particular region in the NCZ (37 cm from UCZ) is still unknown and remains an open question. The preliminary cost analysis showed that granular chlorine is the cheapest chemical. A more detailed financial analysis is nevertheless required to refine these costs. Chlorine was found to be more

corrosive than Cupricide due to the acidic effect it has on the pH. The approximate corrosion weight loss for the samples dipped in Cupricide and chlorine solutions were found to be 0.94 mdd and 4 mdd, respectively. From this preliminary study, Cupricide is the recommended chemical because of its effectiveness, consumption and environmental benefits. However, further work is needed to study the effectiveness in more detail. The use of flocculants, which can withstand acidic conditions, to eliminate suspended particles need to be investigated.

REFERENCES

Agmin 2007, *Comparative effectiveness of Cupricide against Copper Sulphate,* Agmin Newsletter nº 224, Agmin Chelates Pty Ltd, available online at <http://www.cupricide.com/newsletters.html>.

Agmin 2009, *Background of Cupricide – Cupricide – The Affordable Algicide*, Agmin Chelates Pty Ltd, viewed March 2010, <http://cupricide.com/aboutcupricide.html>.

Akbarzadeh, A., Andrews, J., Golding, P., 2005. 'Integration of solar ponds in salinity mitigation schemes and production of low grade heat for industrial process, desalination and power' in Proceedings of 2005 Solar World Congress - Bringing Water to the World, 8–12 August 2005, Orlando, FL, USA.

Akbarzadeh, A., Andrews, J. and Golding, P., 2008, 'Solar Ponds', in *Solar Energy Conversion and Photoenergy Systems*, [Eds. Julian Blanco Galvez, Sixto Malato Rodriguez], in *Encyclopedia of Life Support Systems (EOLSS),* Developed under the Auspices of the UNESCO, Eolss Publishers, Oxford, UK.

Alagao, F., Akbarzadeh, A. and Johnson, P., 1994, 'The Design, Construction and Initial Operation of a Closed Cycle Salt Gradient Solar Pond', *Solar Energy*, vol. 53, pp. 343-351.

Green, M. A., 1988, 'Solar Cell-Operating Principles, Technology and System Applications', Prentice-Hall Inc.N.J.

Hull, J. R., 1990, 'Maintenance of brine transparency in salinity gradient solar ponds', *Journal of Solar Energy Engineering*, vol. 112, pp. 65-69.

Hull, J. R., Nielsen, C. E. and Golding, P., 1988, 'Salinity Gradient Solar Ponds', CRC Press, Florida.

Leblanc, J. and Andrews, J., 2007, 'Low-Temperature Multi-Effect Evaporation Desalination Systems Coupled With Salinity-Gradient Solar Ponds', International Solar Energy Society (ISES) 2007 Conference - Solar Energy and Human Settlement, Beijing, China, September 18-21, 2007.

Leblanc, J., Andrews, J., and Akbarzadeh, A., 2010a, 'Low-temperature solar-thermal multi-effect evaporation desalination systems', *International Journal of Energy Research*, vol. 34, no. 5, pp 393-403.

Leblanc, J., Akbarzadeh, A., Andrews, J., Golding, P. and Lu, H. 2010b, 'Heat Extraction Methods from Salinity-Gradient Solar Pond and Introduction of a Novel System of Heat Extraction for Improved Efficiency', *Solar Energy*, in Press, doi:10.1016/j.solener.2010.06.005.

Xu, H., Sandoval, J., Lu, H., and Ybarra, A., 1993, 'Operating Experience with the El Paso Solar Pond,' Proceedings of the 3rd International Conference on Progress in Solar Ponds, El Paso, TX.

BRIEF BIOGRAPHY OF PRESENTER

Miss Neus Gasulla obtained her Master degree in Chemical Engineering from the Technical University of Catalonia, Spain in 2010. As a formal requirement of her Master's degree she completed a six months internship project with the Energy Conservation and Renewable Energy (Energy CARE) group of the School of Aerospace, Mechanical and Manufacturing Engineering at RMIT University, Melbourne. During her master's degree, she also worked as a researcher for Cetaqua - a water management technology research centre in Spain. She has now just started another internship at RMIT University, which would be a pathway for further PhD studies. Her research interests include water treatment, heat transfer and fluid flow.

Smart Energy Zones:

Showcasing local sustainable energy projects in Victoria (including Solar Cities)

Susan Lindsay

Sustainability Victoria
50 Lonsdale Street, Melbourne 3000
Susan.Lindsay@sustainability.vic.gov.au

ABSTRACT

Seven creative and innovative energy projects across Victoria are demonstrating a dynamic shift in thinking when it comes to managing energy supply and demand whilst bringing the notion of energy closer to the local community.

The Smart Energy Zones program expands on the Federal Government's Solar Cities initiative and includes the Moreland and Central Victoria Solar City projects, as well as projects with local councils, community groups and other government bodies.

Their approaches involve energy efficiency, shared energy across site boundaries, decentralised energy generation, such as solar technologies, tri-generation, wind and biogas and explore market based mechanisms to address local energy needs in a sustainable way across a precinct.

The Smart Energy Zones projects aim for replication of these examples that are leading the way in environmental, social and economic outcomes. Results to date include:

- Completion of two solar PV parks with tracking and battery storage technology in Bendigo and Ballarat which are supplying solar energy for 300 homes (Central Victoria Solar City).
- Construction of buildings which feature best practice eco-principles and sustainable design measures at the Centre for Education and Research in Environmental Strategies (CERES). In particular the restaurant incorporates natural ventilation, ceiling fans, hydronic heating, double-glazing and energy efficient induction stoves.
- Installation of solar PV panels, natural gas fired cogeneration system and energy efficient retrofits, including lighting at the Ashburton Pool and Recreation centre and neighbouring buildings (City of Boroondara).

This paper will explore the lessons learnt from projects which have been completed or are nearing completion and will explore the achievements and barriers faced in the current regulatory environment in order to transition to local decentralised energy systems.

Keywords: community, energy demand, energy supply, precinct, solar city

INTRODUCTION

Green Communities – Smart Energy Zones

Building on the momentum established by the Federal Government's Solar Cities program, the Victorian Government announced the Green Communities - Smart Energy Zones initiative as part of the Our Environment, Our Future: Sustainability Action Statement in 2006.

Through this initiative the Victorian government committed to investing "$4 million over four years to show how leading Victorian communities can dramatically cut greenhouse emissions" (Department of Sustainability and Environment 2006).

At this time, it was acknowledged that opportunities for Victorian communities to meet their own power needs had been largely untapped and this initiative aimed to showcase this possibility in preparing Victoria for a low carbon future. Support was targeted to go towards:

- Existing solar city projects in Victoria, integrating energy efficiency measures, smart meters, retail tariff incentives, solar panels and demand management.
- Additional projects, exploring opportunities for localised sustainable energy generation such as solar power and small scale wind within major activity centres.

Sustainability Victoria's role

Sustainability Victoria (SV), an agency of the Victorian Government, was given the responsibility for delivering the Smart Energy Zones (SEZ) program. The framework for this social change strategy included key environmental, economic and social sustainability objectives around:

- The efficient integration of precinct energy supply and demand infrastructure.
- Strong community demonstration and engagement programs.
- Innovative projects.
- Potential for replication.
- Financially viable solutions.
- Understanding and solutions to regulatory barriers.
- Significant reductions in greenhouse emissions.

SV is working in partnership with the SEZ project developers, providing funding and in-kind support (technical advice, information and facilitation).

The delivery of each project has been undertaken by the project partner, who provides SV regular reports on project status, challenges faced and key outcomes. Project partners have also formed relationships with electricity distribution and retail businesses, local governments, technology providers and consumer participants.

Progress to date

In June 2008 and June 2009, partnerships were established with the two Victorian Solar Cities projects at Central Victoria and Moreland, respectively.

In July 2009, additional projects with local government, State government and community group were confirmed.

The program is currently in its implementation phase and has been working with seven projects.

Tab. 1: Smart Energy Zones program timeline

	2006/07	2007/08	2008/09	2009/10	2010/11	2011/12
Program planning						
Partnerships established						
Project implementation						
Monitoring and evaluation						

SMART ENERGY ZONES

SEZ is designed to demonstrate that communities can cost-effectively reduce their greenhouse emissions through increased community engagement, renewable energy, low emission technologies, sustainable building design and energy efficiency.

Alternative Energy Models

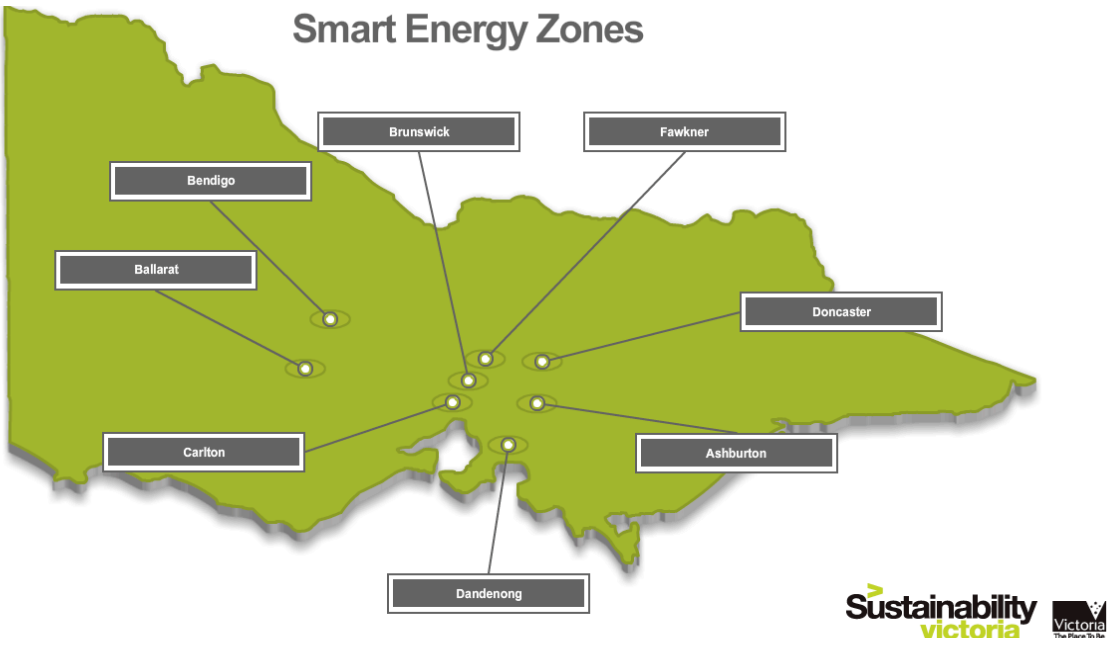

Fig. 1: Locations of Smart Energy Zones projects

Seven SEZ projects across Victoria are demonstrating alternative models of energy efficiency, distributed generation and energy use. Each of these projects is unique which is crucial as solutions are specific to the surrounding environment.

The alternative energy models within the projects explore the most efficient way to supply local energy needs on a precinct scale. The objective is to lower the greenhouse emissions due to energy. This is achieved by:

- Ensuring all new and existing buildings incorporate passive design principles, for example taking into account solar orientation, insulation and designing for climate conditions on site.

- Incorporating measures to lower energy consumption, demand and managing peak/off-peak use of energy, for example utilising smart meter displays and facilitating consumer awareness, attitudes and behaviour.
- Lastly, once the energy requirement is deemed to be as low as possible, the rest is supplemented by low emission and renewable energy generation.

Communities within a SEZ aim to empower the local residents to create and manage their own energy needs. This has huge social change implications as there is a move from energy simply being an outlet on the wall towards it being a precious commodity that can be sourced from a variety of resources and methods – each having their own environmental, social, economic and technical implications and benefits. Table 2 outlines the technologies being explored for the SEZ projects.

Tab. 2: SEZ project outlines, updates and sustainable technologies

Central Victoria Solar City: Solar PV Parks, Bendigo and Ballarat		
Outline: SEZ has supported the installation of two 300kW community solar photovoltaic (PV) parks at Ballarat and Bendigo with emphasis on the use and testing of tracking systems and battery storage technologies.	**Update:** The parks commenced construction in July 2009 and were completed and formally launched four months later. Twelve month data monitoring and verification reports for both parks are currently in progress.	**Technologies:** • Solar photovoltaic parks • Energy efficiency • Smart metering & time-of-use tariffs
Moreland Solar City: Moreland Energy Services, Fawkner		
Outline: SEZ is supporting the development of an energy services model in the Fawkner area, which will deliver local sustainable energy generation through technologies such as cogeneration and solar photovoltaic.	**Update:** The feasibility study and business plan for the site have been completed, with construction of supporting infrastructure and delivery of the embedded generation systems due to start early next year.	**Technologies:** • Solar photovoltaic panels • Solar hot water • Cogeneration • Energy efficiency • Smart metering
Partnering for Zero Emissions, CERES - Brunswick		

Outline:	Update:	Technologies:
CERES environmental park in Brunswick is working with a local shopping centre to take their organic waste to feed a biogas digester, which will power the CERES site alongside new solar and wind generation. The CERES van will be converted to an electric vehicle and a solar PV charging station constructed.	Construction of three energy efficient buildings (Education centre, Eco-House and Van Raay Centre) has been completed. Detailed design is currently in progress for the biogas digester pilot, electric vehicle conversion, solar charging station, aquaponics smart energy management system, solar thermal electricity generation, solar cooking, solar pavilion and solar refrigeration.	• Solar thermal generator • Solar pavilion • Solar charging station for electric vehicles • Solar photovoltaic panels • Solar cooking equipment • Biogas digester plant • Wind turbines • Electric vehicle conversion • Aquaponics system • Passive building design
Zero-Carbon Social Housing, Department of Human Services - Carlton		
Outline:	**Update:**	**Technologies:**
The Department of Human Services (DHS) is aiming to supply new public and social housing buildings at the Carlton redevelopment with gas fired cogeneration. The gas utilised by the plant will be off-set through electricity provided on-site by both wind turbines and solar PV panels to achieve a 'Zero Carbon' development. The decentralised energy will compliment energy efficiency measures already incorporated in the redevelopment design.	The first stage of construction of the new housing precinct began in early 2010 (to be completed September 2011). The second stage of construction will begin early 2011 (to be completed September 2012). The third and final stage is expected to be completed in March 2014.	• Solar photovoltaic panels • Solar hot water • Cogeneration • Wind turbines • Energy efficiency • Metering and monitoring
Doncaster Hill Smart Energy Zone, Manningham City Council - Doncaster		
Outline:	**Update:**	**Technologies:**
Manningham City Council is developing a green civic precinct and will use gas-fired trigeneration to supply a new community centre (including a sustainability education hub) and the existing council offices. The project will incorporate a micro-	The project was officially launched in September 2010 when construction commenced and is due for completion in June 2012.	• Solar photovoltaic panels • Trigeneration • High efficiency lighting • Natural/hybrid ventilation

grid, real time monitoring and energy efficiency measures including natural ventilation and high efficiency lighting.		• Activated thermal mass • Integrated BMS • Smart meters
Ashburton Community Precinct Project, Boroondara City Council – Ashburton		
Outline: Boroondara City Council is installing a gas-fired cogeneration plant to supply heat and electricity to the Ashburton pool and recreation centre and electricity to a nearby child care facility. Neighbouring buildings will receive solar PV panels, energy efficient lighting retrofits, variable speed drive system upgrades and other efficiency measures.	**Update:** Installation of technologies has been completed with commissioning and operation due in March 2011.	**Technologies:** • Solar photovoltaic panels • Cogeneration • Mini distribution network • Efficient lighting retrofit • Energy monitoring equipment
Revitalising Central Dandenong – Central Trigeneration Facility, VicUrban – Dandenong		
Outline: VicUrban is revitalising the central business area of Dandenong as part of a major urban revitalisation, Revitalising Central Dandenong (RCD). Among the suite of sustainability initiatives for the RCD Project, VicUrban is planning to incorporate a central trigeneration facility to supply electricity, heating and cooling for the precinct.	**Update:** The project is in the process of securing an operator/financier for the project and finalising detailed design.	**Technologies:** • Trigeneration • Reticulation Infrastructure/ pipeworks • Sustainable building design and construction

LESSONS LEARNED

Innovative projects of this nature that are testing the regulatory waters in an uncertain environment have inevitably come across barriers which have caused a change in the original course for most projects. The process itself has proved to be just as important to understand and learn from as the outcome. The following is a list of the most important lessons learnt to date. In terms of replication this is important to comprehend and build on. The most significant issues - both positive and those needing improvement, to developing local energy solutions can be classified into the areas below.

Dealing with complex and uncertain electricity grid connection processes

The process of negotiating electricity network connection agreements between distributed generators and distribution network service providers (DNSPs) has been

complex, time-consuming and costly. There is currently a lack of information regarding the connection processes in Victoria, standard connection agreements, network connection requirements, payments for network benefits, optimal sizing, negotiation and approvals processes, which has caused time delays.

The cost of connection is also variable and can be a large percentage of the overall cost of the system, particularly for small (under 1MW) distributed generation systems.

Projects have had to factor in extended timelines to account for approval from DNSPs to connect to the main grid and to distribute electricity across land title boundaries.

There should be a streamlined processes for small-scale projects (less than 1MW) which identifies standardised costs and timelines. This should include a negotiation framework which includes setting timelines for the negotiation processes and network connection cost allocation guidelines.

Project planning and design - difficulty in accessing relevant skill sets

Finding appropriately skilled personnel with the specialised technical abilities has been particularly challenging. The delivery of these projects has highlighted a lack of knowledge and market readiness, as consultants follow traditional models. It has been a challenge sourcing the appropriate skills and experience needed to deliver some of the local energy options proposed in the SEZ projects, resulting in either having to go back out to tender for some aspects of work or obtaining multiple reviews of work by various consultants.

Lack of precedents is also a significant barrier. Innovation carries with it inherent and perceived risks which make securing support at a management level more difficult. This also makes the process of finding relevant information about practical implementation issues much harder. Government financial incentives can assist not only in offsetting the financial impact of such risks, but also in demonstrating support for such innovations.

Presenting new ways of looking at governance and business models

Establishing the business case for innovative technologies has posed a challenge, as these business models must be redesigned to more accurately reflect costs/benefits compared to Business as Usual (BaU). Long term sustainability values and goals have to be factored in. Each project partner was provided with a business case template to reflect these requirements as highlighted in Table 3, but challenges have still arisen in the implementation phase of the projects.

Project developers have had challenges in reframing the way conventional ownership models are viewed when implementing new technology/models. Risk identification has included identifying who is best placed to manage/own the risks and the most appropriate contractual agreements (with long term arrangements, performance measures, guaranteed minimum levels of consumption and penalties).

Facilitating a sustainable energy community of practice

Sustainability Victoria has acted as facilitator for these local sustainable energy projects, providing advice and technical assistance and resources through the establishment and maintenance of a “community of practice”. This has allowed project partners to share and workshop through common barriers they are facing and has proved invaluable in sharing and continual learning as they move towards their individual visions and program goals.

Learning from the program and communication with stakeholders

The SEZ program successes and challenges are continually being communicated to stakeholders to enable change and allow for continuous improvement of the program itself. Lessons learned from the program are fed back into the program, which is fluid in its implementation and has a clear sight on its goals and whether these are being achieved (see Table 3).

Tab. 3: Smart Energy Zones goals and indicators for success

Goal	**Has the goal been achieved?**	**Indicators for success (over life of program)**
Innovation across the projects in the program	Projects are innovative in their use of technology rather than the type of technology. Most projects include solar, wind and/or cogeneration. Given the timing of these projects, the solutions presented are chosen for their innovation and commercial viability.	12,150kW of investment in renewable energy generation and energy efficient enabling technologies
Strong demonstration value and community focused projects	All locations for the program are either in major or principal activity centres and they showcase the local generation opportunities. For example, solar panels and wind turbines have an immediate visual effect. One project aims to create a glass case around a trigeneration system. All will have signage, open days and enhanced communication programs. Additionally, SV promotes the programs through an extensive communication plan, which involves a web based animation tool showcasing the location, technologies and business cases of each.	10,000 individuals participating 10 businesses / organisations participating 50 local governments, state governments, project developers participating
Potential for replication	This measure is difficult to quantify at present as the program is in project delivery stage. The potential for replication however can be determined across the project types, the influence of the organisation and the number of similar organisations and sites across Victoria.	Number of similar sites across Victoria
Financially viable solutions	Projects have completed high level financial analysis through business cases. At this stage only one project has been completed – with funding that enabled innovative solar tracking and battery storage technology Financial models also need to capture the avoided transmission and distribution charges resulting from embedded generation. A lot of initial financial planning factored in	7 successful communities with technology commissioned and operational 7 projects successfully implemented as set out in business case

	a price on carbon and the cost effectiveness of reducing emissions. The ownership of the plant and equipment needs to include not just financial risks but operation and maintenance.	Leverage of Government investment
Understanding and solutions to regulatory barriers	Mainly in relation to electricity distribution across boundaries, grid connection, feed in to grid	Qualitative measures of understanding as outlined by projects
Significant reductions in greenhouse emissions	To be measured both as a result of the project and due to replication across Victoria. The significance will be greater when projects are replicated and have overcome barriers to mass implementation at the conclusion of the program. Reduction in peak demand and infrastructure investment will become more apparent towards the conclusion of the program.	Tonnes of greenhouse gas savings over life of projects: 850,000 Reduction in peak electricity demand Reduction in electricity infrastructure investment

CONCLUSION

The SEZ program has been largely successful to date. Successes of the program include a high investment in energy efficient technologies and local sustainable energy generation. All projects have potential for high demonstration value and there is enough variety in the types of projects/sites to enable replication.
The implementation phase has overcome and side stepped many obstacles encountered. Stakeholder feedback into the process has been positive. There has been support and flexibility in allowing the program to achieve its objectives.
There have been areas of improvement identified such as a need to extend the programs' timelines beyond the four year commitment. The program also requires a replication strategy to achieve dramatic cuts in emissions. There are continual challenges in addressing both technical and regulatory issues.

SEZ is showcasing energy efficiency, renewable energy technologies and low emission sustainable energy generation. Due to timing, resources and market preparedness, SEZ pushes the boundaries of conventional energy systems and shows what is possible, utilising current available technologies in the current regulatory environment.

REFERENCES

Department of Sustainability and Environment 2006, Our environment our future - sustainability action statement, Victorian Department of Sustainability and Environment, Melbourne.

Dunstan, C., & Daly, J. 2009, Smart Energy Zones: Policy and Regulation Discussion Paper, Institute for Sustainable Futures, University of Technology, Sydney for Sustainability Victoria, August.

Jennings, R. 2010, Smart Energy Zones: Lessons Learned, Sustainability Victoria, September.

BRIEF BIOGRAPHY OF PRESENTER

Susan Lindsay is currently managing the Smart Energy Zones program at Sustainability Victoria (SV). She is also completing a fellowship with the Centre for Sustainability Leadership developing management and leadership skills.
She is two-thirds of the way through completing a Master of Engineering (Sustainable Energy) with acquired skills in triple bottom line analysis, energy auditing, Life Cycle Assessment (LCA), financial modelling, energy policy, sustainability strategies and local/international business management. She is contributing to the development of the Green Building Council's Green Star Communities Tool as a member of the Technical Working Committee. At SV, she is an active member of staff with roles as a Green Leader and Equal Opportunity Contact Officer.

Urban Wind Generation in Victoria

Sonja Ott[1], John Edgoose
[1]Sustainability Victoria
L28/50 Lonsdale Street
sonja.ott@sustainability.vic.gov.au

ABSTRACT

Victoria has one of the worlds best wind resources and the wind energy market is growing rapidly. Victoria has currently 428MW of installed capacity and 2,047MW are approved. However, the market of small scale wind turbines (<100kW) is also growing internationally and in Australia. There is currently less than 400kW of installed small wind turbines in Australia [1]. The application of this technology ranges from off-grid applications such as powering remote houses and water pumping to on-grid applications such as build integrated systems on rooftops of dwellings and commercial buildings or installed in the backyard or arranged as small wind farms in communities.

There has been increasing interest in small wind turbines from those living in cities. It is commonly known that the best wind resource is found in open rural areas however wind can be very unpredictable and degraded in city and suburban locations.

Sustainability Victoria worked with the Australian Technology Association to monitor and analyse the wind speeds and turbulence at a range of locations in Melbourne. The project involved wind speed and direction monitoring on or near houses and buildings at ten sites. Turbulence data was collected with an ultrasonic anemometer. The wind resource was represented by wind roses and turbulence charts.

Subsequently to the study Sustainability Victoria also produced a Victorian Consumer Guide to Small Wind Turbine Generation which provides information to enable an informed decision to be made about whether a site is suitable for a small wind turbine and information on turbine selection.

This paper presents a summary of the wind monitoring study in suburban Melbourne and key points in the Victorian Consumer Guide to Small Wind Generation.

Keywords *Small wind turbines, small wind generation, urban wind generation*

BACKGROUND

Victoria – good wind resource & installation wind farms

Victoria has one of the best wind resources in the world. Currently, eight wind farms with 428MW of wind generation capacity are installed at sites located in open areas and on top of hills in regional Victoria and 2,047MW of wind capacity is approved

What are small wind turbines?

Small scale wind turbines have a capacity of less than 100kW and are mostly between 1-10kW. There are two types of small-scale wind turbines distinguished by their axis of rotation: horizontal axis and vertical axis.

Horizontal axis turbines are the most recognizable common turbine design as they dominate the market of large scale wind turbines. Their design is most efficient in clear wind streams but do not handle turbulence very well as the turbine is constantly twisting around its vertical axis increasing wear and tear. However, although vertical axis turbines have lower efficiencies they are less sensitive to changing wind directions and hence turbulence because they do not have to yaw and face into the wind [2].

A small wind turbine system consists of several components as shown in Figure 1 for a grid-connected system. The wind turbine generates direct current (DC) electricity which is converted to alternating current (AC) electricity in the inverter. The generated electricity is either used by household or office appliances or exported into the electricity grid. The meter records how much electricity is exported to the grid. The wind turbine controller ensures the turbine operates within safe limits [3].

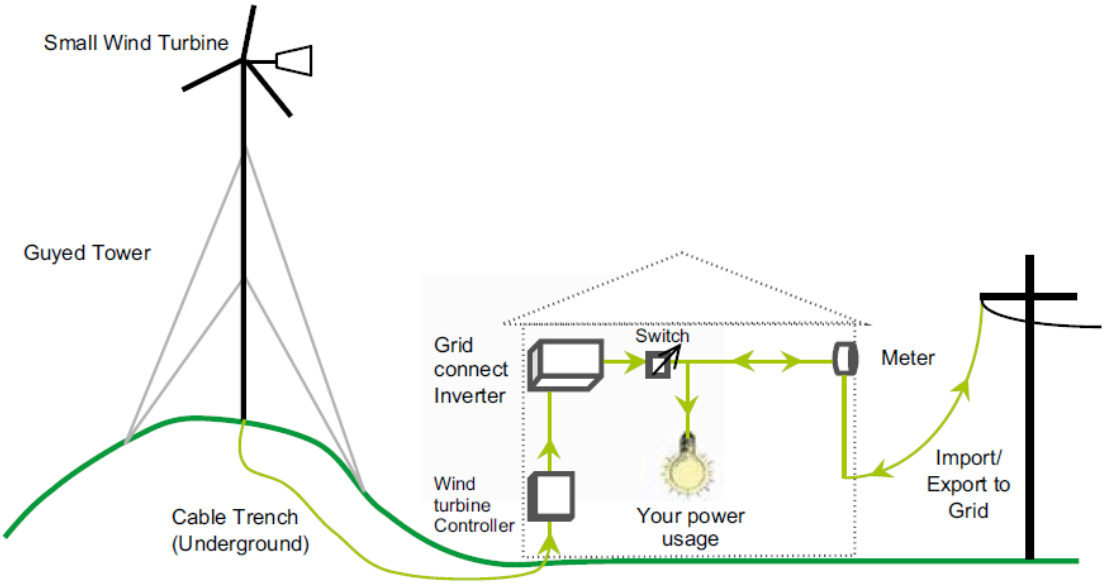

Figure 1 System components of a grid-connected small wind turbine [3]

The application of this technology ranges from off-grid applications such as powering remote houses and water pumping to on-grid applications such as build integrated systems on rooftops of dwellings and commercial buildings or installed in the backyard or arranged as small wind farms in communities.

Why did we do the study?

There has been increasing interest in small wind turbines from those living in cities. It is commonly known that the best wind resource is found in open rural areas however wind can be very unpredictable and degraded in city and suburban locations.

The study *The viability of domestic wind turbines for urban Melbourne* developed by the Alternative Technology Association (ATA) for Sustainability Victoria showed that most urban wind turbine projects overseas demonstrate poor economic performance and long pay back periods due to a lack of accurate wind monitoring in the project assessment stage.

The results of this first study led Sustainability Victoria to work with the Australian Technology Association to monitor and analyse the wind speeds and turbulences at various locations in Melbourne in order to identify the suitability of small wind turbines in Melbourne's suburban environment.

Turbulence intensity is the traditional characteristic used to measure the scale of turbulence in a flow. Turbulence is a non-dimensionalised factor obtained by dividing the standard deviation of wind speed by the mean wind speed. It is a relative measure how much a flow is varying.

METHODOLOGY

How did we select the sites?

In 2009, Sustainability Victoria worked with ATA to monitor and analyse the wind speeds and turbulence at ten sites located within 25km of Melbourne's CBD (Figure 2). The sites were selected based on a questionnaire which was sent to all ATA members. The guiding principle of the site selection process was to identify the most suitable locations for small wind generation such as clear aspects in all directions with minimised geographic and architectural obstructions such as relatively high roof peaks and buildings situated on hills. Other practical features such as the presence of accessible power outlets were also considered. The site on a high rise CBD building was chosen in line with a partnership project between Sustainability Victoria and the occupant of that specific building.

The distribution of site types can be broken down as follows:

- Three sites with anemometers installed on pitched roofs and 10 meter masts in open backyard areas
- Two sites with anemometers installed on flat roofs and 10 meter masts in open backyard areas
- Two sites with anemometers installed on flat roofs
- Two sites with anemometers installed on 10 meter masts
- One site with anemometer installed on a communication tower at height of 9 meter above the roof of a high rise building in the CBD

All participants took part on a voluntary basis in what was a non-commercial agreement.

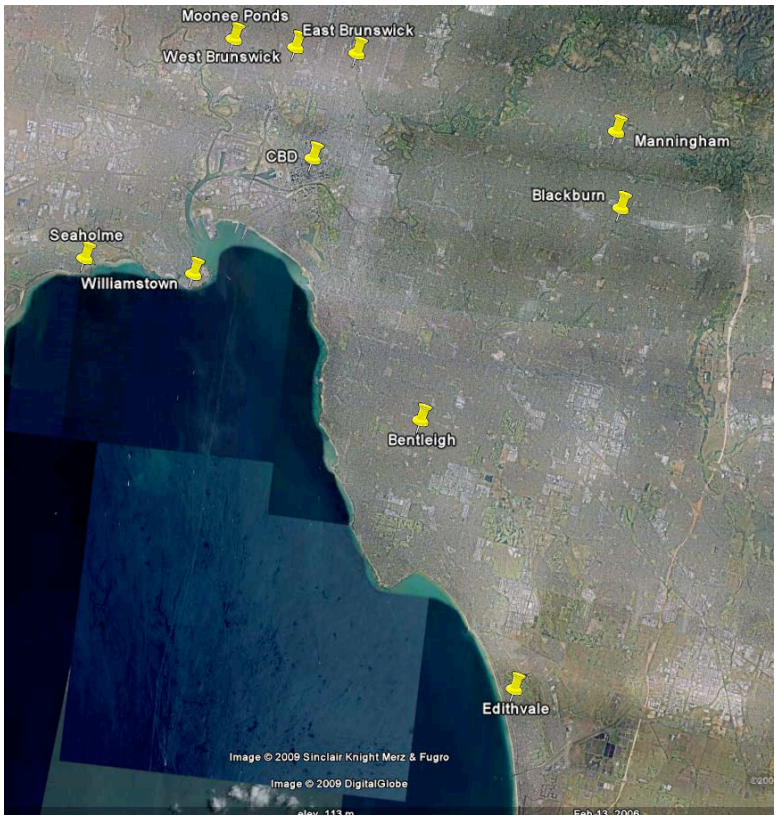

Figure 2 Satellite image of site locations

How did we do the measurement?

The project involved wind speed and direction monitoring at ten different locations including 15 different measurement sites (rooftops, backyards, sports oval). The aim of multiple anemometer siting was to examine if there are any apparent differences in the energy availability and turbulence at the particular site. The anemometers were positioned at heights to be likely for installation of a small wind turbine without the usage of additional mounting infrastructure ranging from one and a half meter to three meters above the roof surface. Anemometers installed on a mast were positioned 10 meters above the ground which is consistent with international meteorological measurement standards. Two Gill ultrasonic anemometers were moved from site to site and collected wind turbulence data over a period of two weeks at each site. One Gill ultrasonic anemometer was installed over a period of three month at the CBD location. Fourteen NRG cup anemometers collected wind speed and wind direction data over a period of three month at each location.

The short period of time over which the ultrasonic anemometers were installed at each site limits the strength of any conclusions that may be drawn from this data. Hence, the study focused on apparent trends in the data instead of more general marks.

Table 1 shows information on data sampling and logging.

Measured data	**Sampling frequency**	**Averaging and logging intervals**
Horizontal wind speed (m/s)	5 to 10Hz	1 minute & 10 minute
Vertical Wind Speed (m/s)	5 to 10 Hz	1 minute & 10 minute
Horizontal wind direction	5 to 10 Hz	1 minute & 10 minute
Temperature (^{o}C)	5 sec intervals	1 minute & 10 minute

Table 1 Data sampling and logging information

OUTCOMES

What were the outcomes?

Table 2 shows the summary data for each site over a period between 66 and 146 days produced from the data collection of the cup anemometers. Most of the sites assessed had a measured average horizontal wind speed between 3 and 3.79 meters per second (m/s). There were no apparent differences in wind power availability between anemometer installations on pitched roof, flat roof or in backyards. The influence on the anemometer position appears to be rather small when compared to features like the positioning height above the ground and the roughness of the surrounding terrain.

The collected data suggests that only the sites in Williamstown and CBD are likely suitable for small wind turbine installations. The characteristic of the site in Williamstown is the openness of the terrain around the measurement site (sports oval at the seashore) which is quite uncommon in domestic urban areas. The CBD building is around 185 meters high and relative without any built up obstructions at roof level which results in exposure to much higher wind speeds than what is experienced near ground level. The data suggests that small wind turbine installations at all other sites are likely perform with low capacity factors and with long energy and financial payback periods.

Replace 2009 average wind speed with 2010 data in the table!!!

Site	2009 Revision										2010 Revision		Suitability for Turbine Installation
	Install type	Terrain type	Average speed [ms^{-1}]	BOM moderated average wind speed [ms^{-1}]	Weibull scale constant *k*	Weibull shape constant *c*	Quality of Weibull Fit	Percentage of with speed above 3 ms^{-1}	Forecast Output from Ampair 600 230 [kWh]	Number of days of data	Average speed [ms^{-1}]	Number of days of data (equivalent)	
West Brunswick A	Mast	Urban	3.48	3.36	2.08	3.93	Good	57%	419	147	3.48	145	Marginal
West Brunswick B	Pitched Roof	Urban	3.40	3.17	1.95	3.83	Good	54%	416	101	3.44	87	Marginal
East Brunswick A	Mast	Urban	2.18	2.08	1.63	2.43	Fair	24%	112	171	2.20	130	Very Poor
East Brunswick B	Pitched Roof	Urban	3.12	3.03	1.89	3.51	Good	48%	323	171	3.31	130	Poor
Edithvale A	Mast	Coastal	3.76	3.62	2.04	4.24	Good	58%	550	119	3.71	146	Marginal
Edithvale B	Pitched Roof	Coastal	3.61	3.40	1.87	4.06	Good	57%	528	130	3.57	125	Marginal
Seaholme A	Mast	Coastal	3.79	3.59	1.75	4.26	Good	58%	654	124	3.92	89	Marginal
Seaholme B	Flat Roof	Coastal	3.66	3.51	1.81	4.11	Good	57%	569	122	3.85	92	Marginal
Moonee Ponds A	Mast	Urban	3.05	2.90	1.66	3.41	Good	45%	367	102	3.03	98	Poor
Moonee Ponds B	Flat Roof	Urban	2.70	2.61	1.47	2.96	Good	36%	281	102	3.21	29	Poor
Manningham	Flat Roof	Urban	3.16	3.09	1.98	3.56	Fair	49%	318	133	3.16	132	Poor
Blackburn	Flat Roof	Urban	1.61	1.55	1.54	1.79	Poor	11%	38	109	1.44	72	Very Poor
Williamstown	Light Tower	Open Coastal	5.82	5.46	2.12	6.59	Good	83%	1677	131	5.83	130	Excellent
Bentleigh	Mast	Urban	3.15	3.03	1.78	3.55	Fair	48%	366	125	3.15	124	Poor
CBD*	Comm Tower	Central Urban	3.94	NA	1.59	4.39	Good	NA	NA	75	3.94	66	NA

* CBD site data summary based on 1 minute average 3D velocity

Table 2 Summary of cup anemometer data

Turbulence

Figure 3 shows the average turbulence intensity calculated over 0.5 m/s bins of average 3D velocity for all sites. The data was produced from the ultrasonic anemometers over a period of two weeks at each site. The graph shows that turbulence intensity (y-axis) is highest for wind speeds (x-axis) below 3.5 m/s. The Williamstown site has the lowest turbulence intensity for wind speeds above 3 m/s due to the open characteristics of the site. The turbulence intensity of the CBD building is in the lower range of all sites.

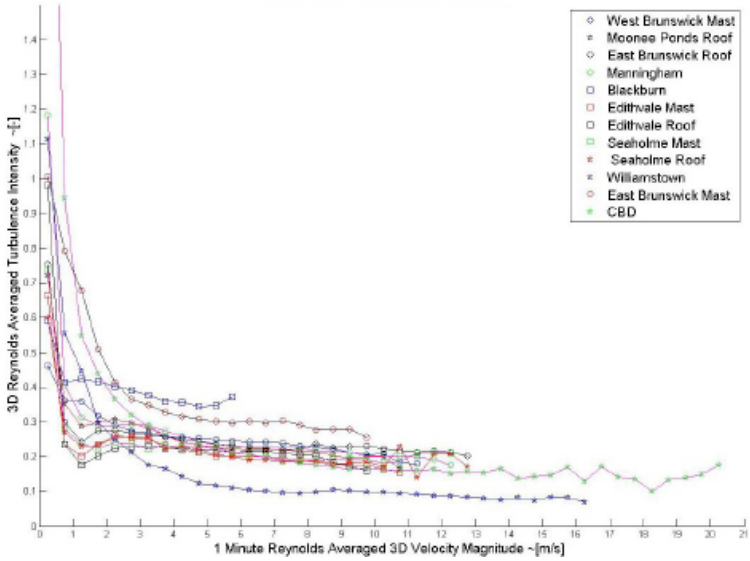

Figure 3 Binned average turbulence intensity versus 3D wind velocity for all sites

Estimating turbine performance

The output of a wind turbine can be estimated using a turbines power curve and measured wind speed data. The power curve gives the instantaneous power output at various wind speeds. In this study the power curve of the model Ampair 600-230 (Figure 4) which is a vertical axis small wind turbine was chosen to estimate the turbine performance and suitability of the site. The selection of this wind turbine was purely arbitrary. The graph shows that the energy output (vertical axis) increases with wind speed (horizontal axis). The selected wind turbine has a nominal rating of 698 Watts and has a cut in wind speed of 3 m/s.

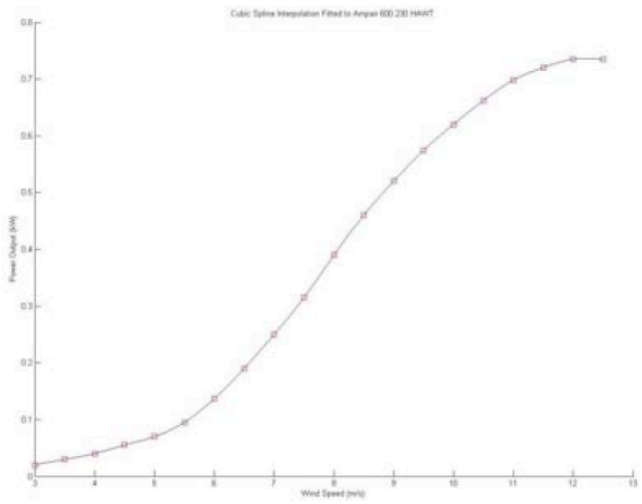

Figure 4 Ampair 600-230 power curve

Table 3 shows the wind characteristics and modelled output of the small wind turbine for all sites except the CBD using Weibull probability curves. The modelled output does not include parasitic energy usage and losses of the system. The output is also depending on the accuracy of the manufacturer's power curve and effects of turbulence. The results suggest that only Williamstown has an excellent wind resource with a forecasted annual output of 1,677 kilowatt hours (kWh).

Replace 2009 average wind speed with 2010 data in the table!!!

Site	2009 Analysis				2010 Revision	Suitability for Turbine Installation
	Average speed [ms^{-1}]	BOM moderated average wind speed [ms^{-1}]	Percentage of time at speed above 3 ms^{-1}	Forecast Output from Ampair 600 230 [kWh]	Average speed [ms^{-1}]	
West Brunswick A	3.48	3.36	57%	419	3.48	Marginal
West Brunswick B	3.40	3.17	54%	416	3.44	Marginal
East Brunswick A	2.18	2.08	24%	112	2.20	Very Poor
East Brunswick B	3.12	3.03	48%	323	3.31	Poor
Edithvale A	3.76	3.62	58%	550	3.71	Marginal
Edithvale B	3.61	3.40	57%	528	3.57	Marginal
Seaholme A	3.79	3.45	58%	654	3.92	Marginal
Seaholme B	3.66	3.37	57%	569	3.85	Marginal
Moonee Ponds A	3.05	2.90	45%	357	3.03	Poor
Moonee Ponds B	2.70	2.61	36%	281	3.21	Poor
Manningham	3.16	3.09	49%	318	3.16	Poor
Blackburn	1.61	1.55	11%	38	1.44	Very Poor
Williamstown	5.83	5.25	83%	1677	5.83	Excellent
Bentleigh	3.15	3.03	48%	366	3.15	Poor

Table 3 Wind energy characteristics and modelled small wind turbine output for all sites (except CBD)

SUMMARY

Sustainability Victoria worked with the Australian Technology Association to monitor and analyse the wind speeds and turbulence at a range of locations in Melbourne. The project involved wind speed and direction monitoring on or near houses and buildings at ten sites. Turbulence data was collected with an ultrasonic anemometer.

The collected data suggests that only the sites in Williamstown and CBD are likely suitable for small wind turbine installations. The characteristic of the site in Williamstown is the openness of the terrain around the measurement site (sports oval at the seashore) which is quite uncommon in domestic urban areas. The CBD building is around 185 meters high and relative without any built up obstructions at roof level which results in exposure to much higher wind speeds than what is experienced near ground level. The data suggests that small wind turbine installations at all other sites are likely perform with low capacity factors and with long energy and financial payback periods.

REFERENCES

[1] Office of Renewable Energy Regulator. (2010). Own calculations based on *Search Register of Renewable Energy Certificates*. (Online: https://www.rec-registry.gov.au/getSearchPublicRecHoldings.shtml, accessed 28.09.2010)

[2] Sustainability Victoria. (2007). *The viability of domestic wind turbines for urban Melbourne*. Report developed by the Alternative Technology Association (ATA). (Online: http://www.sustainability.vic.gov.au/www/html/2770-wind-in-urban-areas.asp?intSiteID=4, accessed 04.10.2010)

[3] Sustainability Victoria. (2010). *Victorian consumer guide to small wind turbine generation*. Guide developed by Enhar. (Online: http://www.sustainability.vic.gov.au/www/html/2770-wind-in-urban-areas.asp?intSiteID=4, accessed 04.10.2010)

BRIEF BIOGRAPHY OF PRESENTER

Sonja Ott is an Industrial Engineer in Energy and Environmental Management and works as a project manager in the Renewable Energy team at Sustainability Victoria. She worked on various small renewable energy generation projects including small wind turbines, photovoltaic, domestic and commercial solar hot water systems and solar cooling.

Design and Simulation of a Linear Flat Mirror Concentrator

Hui Zhang[1,2,a], Li Zhu[3,b], Yiping Wang[1,3,c], Yong Sun[1,d]

[1]School of Chemical Engineering and Technology
Tianjin University, Tianjin, 300072, China
[2]Center for Sustainable Energy Systems
Australian National University, ACT, 0200, Australia
[3]School of Architecture
Tianjin University, Tianjin, 300072, China
[a]Zhanghui201000000@163.com, [b]zly_tj@163.com, [c]wyp56@tju.edu.cn,
[d]sunyong-1984@163.com

ABSTRACT

A linear flat mirror concentrator was designed and developed for low cost and low control power consumption. The optical performance was calculated as well as simulated. The real concentrator was set up and the light intensity at the focus area was measured. The agreement between the theoretical values and the experimental data is significantly good. The concentration ratio is around 20 and the focus has a uniform illumination. The presented concentrator is aimed at low cost linear concentrating photovoltaic systems for economic green power.

Keywords □ Concentrating photovoltaic, linear flat mirror concentrator, optical simulation, solar flux intensity uniformity

INTRODUCTION

In modern society, with the development of economy but the shortage of energy, the development and utilization of renewable energies has become a common task of the whole world (Jefferson 2006, Omer 2008). Since it is ubiquitous, inexhaustible and pollution-free, solar energy has won people's favor, in which photovoltaic (PV) wins more attention (Hoffmann 2006, Lewis *et al.* 2007). However, because of its high cost, PV could hardly compete with traditional forms of power generation (Lewis *et al.* 2007). Concentrating photovoltaic (CPV) system uses cheaper concentrators to make partial substitution of expensive solar cells, not only making the sunlight collected together, to overcome the defect of low solar flux density, but also greatly reducing the costs of the whole system (Blakers 1999, Swanson 2000, Tian *et al*. 2005).

There are many kinds of concentrators currently, according to different standards, there are different classifications. The Linear Flat Mirror Concentrator (LFMC) presents in this paper is a variation of the linear Fresnel concentrator. It has been several decades since the idea of the linear Fresnel concentrator emerged. A lot of work has been done over this period, including calculation and experiments. But due to constrain of low accuracy tracker and lack of optimization, the concentrating results were not satisfactory.

So in this time, most linear Fresnel concentrators were applied in the solar thermal field (Nelson et al. 1975, Mills & Morrison, 2000, Ryu, et al, 2006). In accordance with optical principle, the LFMC can be categorized into the reflective concentrator (Yuan & Wang 2009). Compared with the refractive linear Fresnel concentrators, the LFMC uses common flat mirrors other than Fresnel lens which need to be specially processed. This LFMC uses 24 pieces of flat mirror to get near 20 times concentration ratio, which greatly increases the sun's power density. By using low cost flat mirrors to replace the expensive solar cells the investment cost of concentrating photovoltaic power generation can be greatly reduced. Compared with other concentrators, its biggest feature is that it can provide an even focal beam with dense solar flux, which will improve the performance of the concentration solar module, and then increase the solar energy conversion efficiency.

DESIGN OF THE LFMC

In order to provide a uniform linear focal beam as an outdoor test platform for the research of Liquid Immersion CPV at TJU, and also in order to verify the consistency between the simulation result and the actual result of its concentration, we built up this mini-scale LFMC. Fig. 1 shows the mini-scale LFMC designed and developed at Tianjin University. There are 24 pieces of 1000mm long and 50mm wide flat mirrors assembled in it and its geometry concentration ratio is 24.

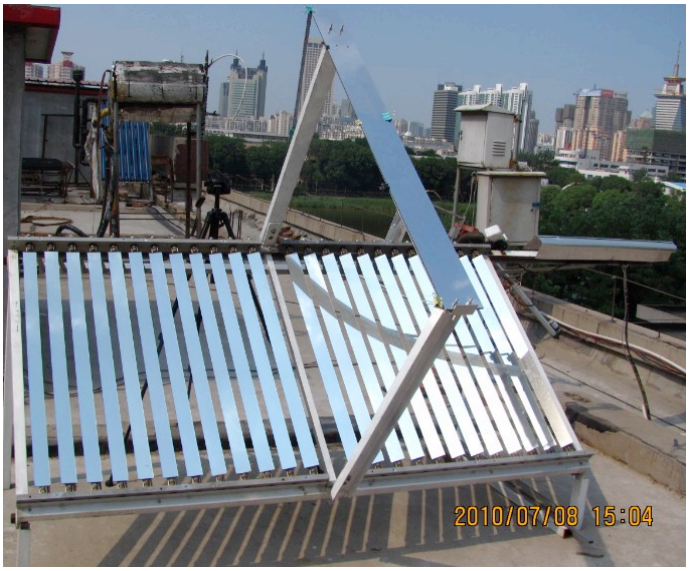

Fig. 1: Picture of the mini-scale LFMC

Many parameters need to be considered for the design of the LFMC, such as the installation height of the receiver, the width of the mirror, the space between mirrors and so on. All these parameters directly affect the concentration. If the parameters chosen improperly, it will lead to the block between each mirror, not only a waste of material, but also greatly reducing the effect of concentration. Table 1 shows the design parameters of the mini-scale concentrator.

Tab.1: Design parameters of the mini-scale LFMC

Design parameters	Value

Geometry concentration ratio	24
Dimensions of the concentrator (mm)	1000(L)×2000(W)
Installation height of the receiver (mm)	1000
Size of flat mirror (mm)	50×1000
Space between mirrors (mm)	80

Fig. 2 gives the views of the structure of the mini-scale LFMC. In order to get the maximum exposure to the sun all year around, the slope angle of the concentrator installation plane was designed to be 39°, which is the geographic latitude in Tianjin.

Due to the limitation of each mirror's rotation angle during the day, in order to reduce the tracking error, we use the linking devices to enlarge the limited rotation, which greatly improved the stability of the whole system. The tracking mode is one-axis close-loop tracking and the mirrors can track the azimuth by using links. The link transmission system we designed is quite simple but functional. By using high precision photoelectric sensor, the mirrors can track the sun in high accuracy of 0.2°.

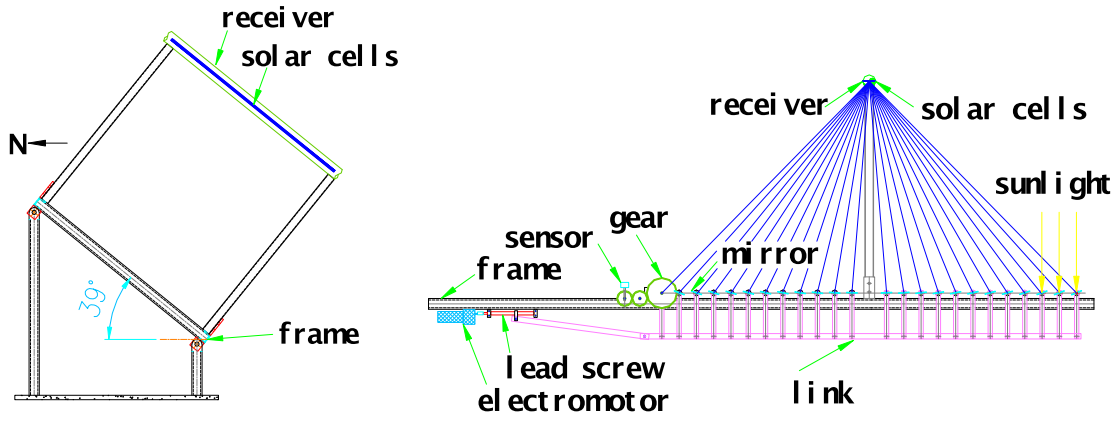

(a) Side view (b) Rear view

Fig. 2: The structure sketches of the designed concentrator

It is noted that the mini-scale LFMC was initially adjusted at solar noon. The installation angles of each mirror at solar noon are shown in Table 2. The real concentration ratio was obtained by comparing the I_{sc} of a concentrator solar cell at the middle of the focus and at one sun and the value is calculated as 16.8. After the right initial adjustment, all the mirrors can achieve accurate tracking of the sun by rotating a same angle. The sun tracker changes the position signals of the sun into electrical signals. The signals are transmitted to the motor which supplies power to the mirrors by the links driving each mirror to rotate along with the position change of the sun, gathering the sunlight to the receiver position.

Tab.2: Angle related values of each mirror slice at solar noon

Number of mirror	Installation angle	Cosine value	Number of mirror	Installation angle	Cosine value
1	43.8	0.72	13	4.6	0.997
2	41.3	0.75	14	9.1	0.987
3	38.7	0.78	15	13.5	0.97
4	35.8	0.81	16	17.7	0.95

5	32.6	0.84	17	21.8	0.93
6	29.2	0.87	18	25.6	0.90
7	25.6	0.90	19	29.2	0.87
8	21.8	0.93	20	32.6	0.84
9	17.7	0.95	21	35.8	0.81
10	13.5	0.97	22	38.7	0.78
11	9.1	0.987	23	41.3	0.75
12	4.6	0.997	24	43.8	0.72

The installation angle of the mirrors is equal to the incidence angle of the sun at noon time. Table 2 presents the Cosine values of each mirror showing the effect of incident angle. The corresponding theoretical number of concentration ratio is 21.0, which is higher than the real value. This is mainly because of the assumption of 100% reflectivity of the mirrors, the neglect of dust degradation and light mismatch.

OPTICAL CALCULATION BY AUTOCAD

In order to obtain the ideal focus beam, at the beginning of the design of the LFMC, we have made some appropriate optimization of its parameters, and ultimately determined the optimal parameters as shown in Table 1. In order to determine the maximum width of the ideal focus beam it can provide, we drew the rotation of the mirrors and the irradiation of the sunlight in the software AutoCAD at every sharp time from 9:00am to 15:00pm. In these drawings we can clearly and visually see the optical journey of the sunlight, and we can get every mirror's precise width of the focus beam and its position. Fig. 3 shows every mirror's width of the focus beam at every sharp time from 9:00am to 15:00pm. It is assumed that the solar noon time is 12:00pm, and the sunlight is symmetrical before and after that time.

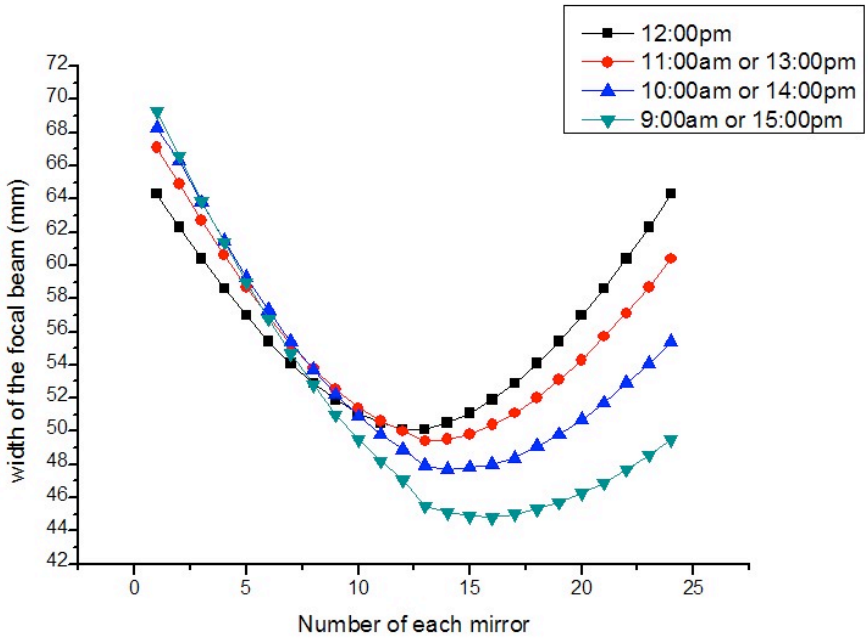

Fig. 3: The width of the focus beam from each mirror at sharp times

By summing up the width of the focus beam from every mirror at every sharp time from 9:00am to 15:00pm, the width of the intersection and of the union of the linear focus at

every sharp time are listed in Table 3. The minimum width of the intersection is 44.8mm, which means that a 24X even geometry concentration ratio can be obtained in this width. The maximum width is 69.3mm, a secondary concentrator can be used for the most collection of the incoming sunlight.

Tab.3: The width of the intersection and union focus at various sharp times

Time	Intersection focus width (mm)	Union focus width (mm)
12:00pm	50	64.3
11:00am(13:00pm)	49.4	67.1
10:00am(14:00pm)	47.7	68.3
09:00am(15:00pm)	44.8	69.3

OPTICAL SIMULATION BY TRACEPRO

The simulation model

The simulation in the present paper was done by an optical simulation tool, Tracepro4.16_demo. Special thanks to the Lambda Research Corporation, thanks for providing a free version for us to do the simulation research. Tracepro uses Monte Carlo ray-tracing to compute optical flux as it propagates through a model. It also allows data exchange with popular lens design programs and mechanical CAD and analysis programs. The simulation settings usually require the optical properties of the materials and the light source.

We established the geometry models in the 3-dimensional drawing software Solidworks and then imported the geometrical model to the optical tool. Fig. 4 shows the model at solar noon established in Solidworks.

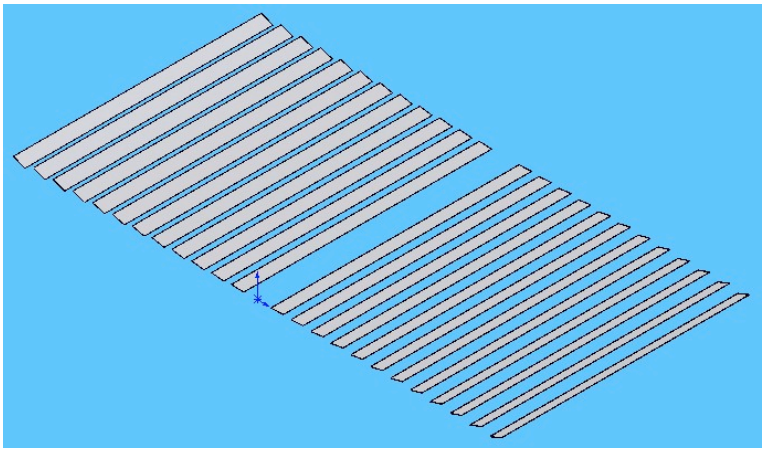

Fig. 4: The model at solar noon established in Solidworks.

The same with the real concentrator, the model consists of 24 pieces of 1000mm long, 50mm wide mirrors with the installation angles as shown in Fig. 2. By counting the rotation angle of 7.5^{o} per hour of the mirrors based on the sun's 15^{o} rotation per hour, the mirrors at other sharp times like 9:00am (15:00pm), 10:00am (14:00pm), and 11:00am (13:00pm) were respectively set with an inclination angle of 22.5^{o}, 15^{o} and 7.5^{o}.

The surfaces facing the incident lights of the mirrors were set as the reflective surface

with the absorptivity of 0.05 and the specular reflectivity of 0.95. In order to make sure that the concentrator (2000mmW×1000mmL) is completely covered under the light irradiation, we established a surface light source (2200mmW×1000mmL) in the vertical direction 2000mm from the concentrator, and defined the light source as illumination form. The irradiance was assumed as 1000W/m^2 radiating the light ray number of 22,000,000 which was uniformly distributed on the light source surface. A 50mmW×1000mmL plane was set as the light output surface to evaluate the flux which was vertically placed 1000mm above the concentrator.

Results and analysis

Fig. 5 is the light distribution chart at 9:00am (15:00pm), 10:00am (14:00pm), 11:00am (13:00pm) and 12:00pm. For the clearness of showing the light reflection and blockage, only the light paths of those reflected to the light output surface are shown. It is confirmed that there is no mutual blockage of the 50mm wide mirrors, and the incoming sunlight on the mirrors can be best used.

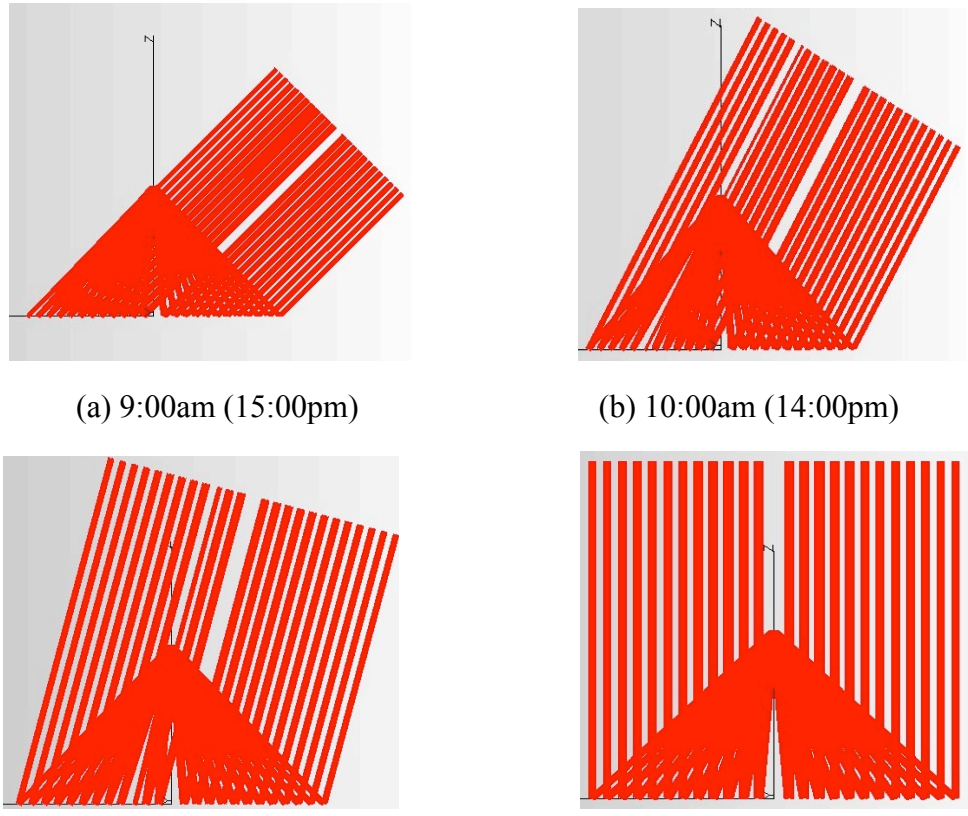

(a) 9:00am (15:00pm) (b) 10:00am (14:00pm)

(c) 11:00am (13:00pm) (d) 12:00pm

Fig. 5: Light distribution charts at various sharp times

Fig. 6 shows the irradiance analysis chart at solar noon, where we can see the simulated even flux distribution at the focus plane at noon time. The 50mmW×1000mmL receiver area was evenly covered with the irradiance of about 20kW/m^2.

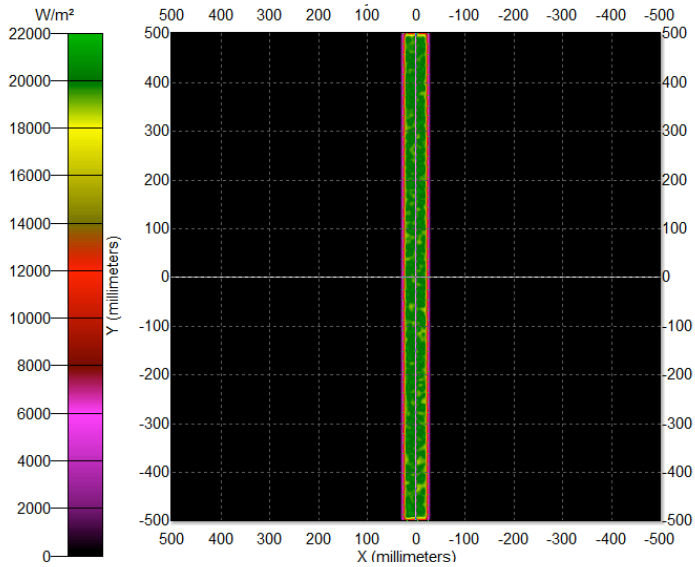

Fig. 6: Irradiance analysis chart at solar noon

Similarly, we can get the irradiance analysis charts at other sharp times, the simulation results are shown in Table 4.

Tab.4: Simulation results of the flux and its distribution at different sharp time

Time	Average irradiance (kW/m^2)	Number of the incident light on the receiver	Equivalent concentration ratio
12:00pm(solar noon)	19.9	1,051,648	19.9
11:00am(13:00pm)	19.5	1,030,420	19.5
10:00am(14:00pm)	19.1	1,011,741	19.1
09:00am(15:00pm)	18.9	1,000,076	18.9

It is shown that the concentration ratio in the period from 9:00am to 15:00pm is 18.9~19.9, which is very close to the one we get in the ideal condition showed in Table 2, but still higher than the real concentration ratio due to the same ideal assumptions. The ratio peaks 12:00pm since the incident angle of sunlight is lower at the noon time, which causes lower cosine loss of the light intensity. We defined the light source as one light per square millimeter and is in even distribution, since the size of the concentrator is 2000mmW×1000mmL, the total number of the incident light on the concentrator is 2,000,000. The number of the incident light rays indicates the light collecting range of the concentrator.

CONCLUSION

The calculation and simulation work was done on a linear flat mirror concentrator. The calculated width of the linear focus is 44.8mm in minimum and 69.3mm in maximum. A uniform 24 suns flux can be obtained for the minimum case and a secondary concentrator is suggested for the most collection of the incoming sunlight for the maximum case. The simulation results show that there is no mutual blockage of the 50mm wide mirrors, and the incoming sunlight on the mirrors can be best used. At solar noon the 50mmW×1000mmL receiver area is evenly covered with the irradiance of

about 20kW/m^2. The concentration ratio from 9:00am to 15:00pm is 18.9~19.9, and the ratio peaks 12:00pm since the incident angle of sunlight is lower at the noon time, which causes lower cosine loss of the light intensity. A real concentrator based on the optimal sizes and structure was established, and the comparisons between real data, calculation and simulation results are quite good.

The design parameters still need to be optimized, and since the simulation results do have a very good consistency with the real data, in the future we will accomplish the optimization work with the help of the optical simulation tool.

REFERENCES

[1] A.W. Blakers, "PHOTOVOLTAICS AT ANU", World Renewable Energy Network Conf, Perth, 1999

[2] Abdeen Mustafa Omer, "Energy, environment and sustainable development", Renewable and Sustainable Energy Reviews, Vol. 12(9): 2265-2300, 2008

[3] Aiyi Yuan, Liangxing Wang, "Research and prospect of concentrating photovoltaics generation technology", Shanghai power, Vol. 1:13-18, 2009(In Chinese)

[4] David R. Mills, Graham L. Morrison, "Compact linear Fresnel reflector solar thermal powerplants", Solar Energy, Vol.68, No.3:263-283, 2000

[5] D.T. Nelson, et al, "Linear Fresnel lens concentrators", Solar Energy, Vol.17:285-289, 1975

[6] Kwangsun Ryu, et al, "Concept and design of modular Fresnel lenses for concentration solar PV system", Solar Energy, Vol.80:1580-1587, 2006

[7] Michael Jefferson, "Sustainable energy development: performance and prospects", Renewable Energy, Vol. 31(5): 571-582, 2006

[8] Nathan S. Lewis, et al, "Toward Cost-Effective Solar Energy Use", Science, Vol. 315, 798-801, 2007

[9] R.M. Swanson, "The Promise of Concentrators", Progress In Photovoltaics, Vol. 8: 93-111, 2000

[10] Wei Tian, Yingping Wang, Lijun Han, "Development of concentrating photovoltaic system", Acta Energiae Solaris Sinica, Vol. 26(4):597-603, 2005 (In Chinese)

[11] Winfried Hoffmann, "PV solar electricity industry: Market growth and perspective", Solar Energy Materials and Solar Cells, Vol. 90(18-19): 3285-3311, 2006

BRIEF BIOGRAPHY OF PRESENTER

My name is Hui Zhang, I am a master student in Tianjin University (China) majored in Chemical Processing Machinery. My research topic is Concentrator Photovoltaic Systems. Now I am a visiting student in Center for Sustainable Energy System (CSES) at ANU for 5 months, doing some tests related to the direct liquid immersion cooling CPV (till 20/Jan/2011).

Factors Affecting Long-Wave Atmospheric Radiation: Experimental and Theoretical Investigations

Maghrabi, A.H.

National Centre For Mathematics and Physics, King Abdulaziz City For Science and Technology,
P.O. Box 6086 Riyadh 11442, Saudi Arabia
amaghrabi@kacst.edu.sa

ABSTRACT

Infrared (IR) atmospheric radiation (wavelength 4.0–100 μm) is a key term in the surface energy budget and is vitally important for climatological and meteorological studies and in applications such as agricultural meteorology and designing solar heat collectors and building heating/cooling systems. Previous studies have concentrated on the measurements and evaluation of the total and spectral IR radiative flux. Most of these studies were limited to clear sky conditions and a few attempted to include the effects of cloud cover. It has been well established previously that the atmospheric radiation in normal conditions is considerably affected by both atmospheric water contents and screen temperatures. Several models using both parameters were previously proposed. However other parameters are expected to have some effect on the atmospheric emissions. The main objective of this study is to use the atmospheric modelling program MODTRAN to investigate the impact of various parameters on the atmospheric radiation. These parameters are zenith angles variations, amount of cloud, the influence of screen level temperature, the precipitable water vapour (PWV), aerosol type, and altitude of the site. The results showed that these parameters affect the total and the spectral atmospheric radiation differently. Experimental justifications on the impact of these parameters on the atmospheric radiation will be presented.

Keywords – atmospheric radiation, sky temperature, PWV, MODTRAN

INTRODUCTION

The knowledge and study of infrared (IR) atmospheric radiation at the Earth's surface is of fundamental importance for many applications and has long been studied both empirically and theoretically. Infrared radiation from the sky depends strongly on the water vapour, carbon dioxide, and ozone content of the atmosphere, and trace gases such as nitrous oxides and carbon monoxide (Ramsey et al., 1982). Previous studies have concentrated on the measurements and evaluation of the total and spectral IR radiative flux (Kjaersgaard et al., 2007; Lhomme et al., 2007). Most of these studies were limited to clear sky conditions and a few attempted to include the effects of cloud cover (e.g. Duarte et al., 2006). It has been well established previously that the atmospheric radiation, in normal conditions, is considerably affected by both atmospheric water contents and screen temperatures. These two parameters have a great impact on the IR clear sky atmospheric emission and both were used to model the IR

clear sky radiance (e.g. Prata, 1996; Garcıa, 2004; Ruckstuhl et al., 2007). However other parameters are expected to have some effect on atmospheric emissions. Their effects vary in importance according to the wavelength, atmospheric conditions, and other factors such as the geography of the site.

The main objective of this paper is to use the atmospheric modelling program MODTRAN to investigate the impact of several parameters on the IR spectral and total radiance. These parameters are clouds, zenith angle, screen level temperature, the precipitable water vapour (PWV), aerosol type, and altitude of the site. Comparisons between theoretical results and experimental data will be presented

DATA USED AND METHODOLOGY

IR sky temperatures were obtained using a single-pixel, broadband IR detector designed in a collaborative work between King Abdulaziz City for Science and Technology (KACST) and the University of Adelaide, Australia. The construction of this instrument, its calibration, and all related technical issues have been described in detail in a number of previous articles (Clay et al., 1998; Maghrabi, 2007; Maghrabi and Clay, 2008; Maghrabi et al., 2009). The basic detector is a Heimann TPS 534 thermopile. In this study, its angular field of view was set to 3° using a Fresnel lens. The spectral range extends from 6.6 μm to above 50 μm if only the transmission of the lens is taken into account.

Theoretical simulations were conducted using MODTRAN software Version 3, Revision 1. MODTRAN is a "Moderate Resolution Transmission" program calculating atmospheric radiance/transmittance at a moderate resolution. MODTRAN was developed by the US Air Force Research Laboratory (AFRL) program beginning in the early 1970s and has been used in various applications and studies (Wang et al., 2002; Rothman et al., 1992; Berk et al., 1989; Rothman et al., 2003).

The methodology of the simulations and the approach of calculations are detailed in Maghrabi (2007) and will be briefly discussed below.

The simulation steps consist of (1) choosing the desired atmospheric profile, (2) assigning the input parameters, (3) running MODTRAN, and (4) processing the outputs. Sky temperatures were calculated by integrating the simulated spectral radiance between the desired wavelength ranges and over the sky dome. By assuming the atmosphere to be a uniform blackbody having a uniform temperature, Tsky, and using the Stefan Boltzman law, the integrated radiance is then converted into temperature, which is conventional for the purposes of investigations conducted in this study.

RESULTS AND DISCUSSIONS

IR spectrum at the zenith and at different zenith angles

Figure (1.a) shows the typical clear sky spectral distribution of energy emitted by the atmosphere at the zenith and at different zenith angles superimposed by a black body curve as simulated by MODTRAN in the region of 5–50 μm for a mid-latitude atmosphere. The main feature of the clear IR atmospheric emission obtained at the zenith is that the atmosphere emits as a blackbody below 7.6 μm, between 14 μm and 16 μm, and beyond 22 μm. Water vapour, H_2O, is the main emitter at these wavelengths. A wide band of emission from 13 μm and 17 μm is due to carbon dioxide,

CO_2. Emission of ozone, O_3, peaks at 9.6 µm. Relatively little energy is emitted by the atmosphere in the "atmospheric window" extending from 8 µm to 14 µm.

The most observable spectral change observed at different zenith angles is the increase in the sky emission in the atmospheric window as the zenith angle increases. This increase is due to the amount of the atmosphere increasing as one moves toward the horizon, where the system reaches that of a black body. Also, it is clear that the effect of the ozone emission increases as the elevation angle increases. Figure (1.b) shows a plot of the *simulated* and the *measured* sky temperatures as a function of the logarithm of the secant of the zenith angle from the zenith to 87° on a typical clear sky day in Adelaide. It can be seen that both temperatures increase monotonically as one moves toward larger air masses and this variation is almost linear with the logarithm of the air mass. In addition a perfect agreement between the simulated and measured temperatures is evident.

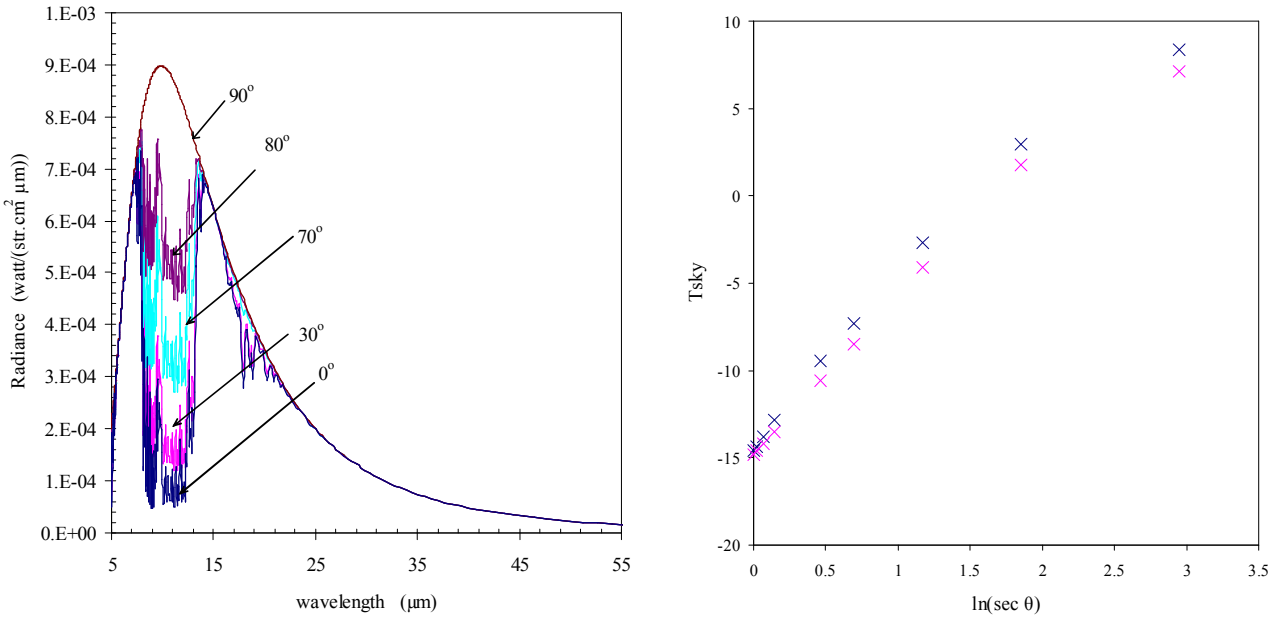

Fig. 1: (a) Shows IR clear sky radiance of typical MLS profile with Tair = 21 °C, RH = 75.9% and the PWV = 1 cm for zenith angles of 0° (zenith), 30°, 70°, 80°, and 90° (horizon). (b) Shows the integrated sky temperatures (Tsky) by MODTRAN (blue) and measured (pink) as a function of the logarithm of air mass.

Cloudy sky spectrum

Cloud has a strong effect on the IR atmospheric radiation. This decreases in importance with altitude because higher clouds are usually colder than low clouds (Kondratyev, 1965; Riordan et al., 2005). The effect of clouds upon the atmospheric radiation may be seen in Figure (2). It shows the effect of clouds of different altitudes on the spectral distribution of the IR atmospheric radiation. Due to their higher altitude, the spectrum of the cirrus clouds is similar to that of clear skies. The integrated Tsky between 6.6 µm and 50 µm was –10.5 °C for cirrus and –12 °C for the clear sky. On the other hand, the basic effect of the low level clouds (stratus in this case) is to close off the atmospheric window to the atmospheric radiation and emit as a blackbody with a temperature close to that of the screen level. The Tsky for the stratus spectrum was 15 °C. Experimental

data for one year of sky Tsky in Adelaide have shown Tsky values between 10 and 20 ^{o}C with a mean value of 16 ^{o}C for stratus, which is comparable with the simulated value.

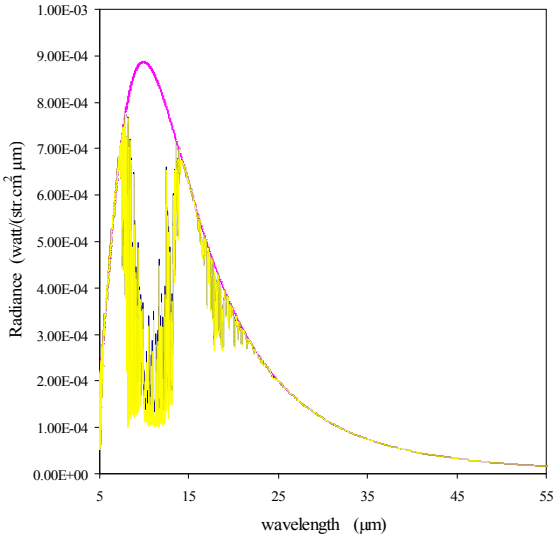

Fig. 2: Shows a typical IR spectrum of the cloudy sky at the zenith for MLS standard atmosphere for stratus (pink) and cirrus (blue) compared with the clear sky spectrum (yellow).

The effect of screen temperature

In this section we investigate the impact of the screen temperatures on the clear sky atmospheric emission, while the effect of the PWV will be discussed in the following section. MODTRAN has six standard atmospheres that cover a wide range of screen level temperatures from warm conditions of 27 ^{o}C at the tropics to very extreme cold conditions of –15 ^{o}C found in the sub-Antarctic winter. MODTRAN was run at the zenith for the entire range of standard atmospheres. Figure (3.a) shows a plot of Tsky as a function of screen level temperatures (T) for a value of 1 cm of PWV, whereas the hourly variations of one year of experimental data for the Tsky as a function of T are shown in Figure (3.b). The equations of the linear regression analysis between the two temperatures are presented in the figures. It is clear that the sky temperatures increase progressively with increasing screen level temperatures. Although there is a scatter on the experimental data which may be due to the effect of different atmospheric conditions throughout the year, the increasing trend of Tsky with T is observable. A comparison of the regression results (slopes and intercepts) between the simulated and the measured temperatures shows that the regression coefficients of the experimental formula are close to those obtained theoretically.

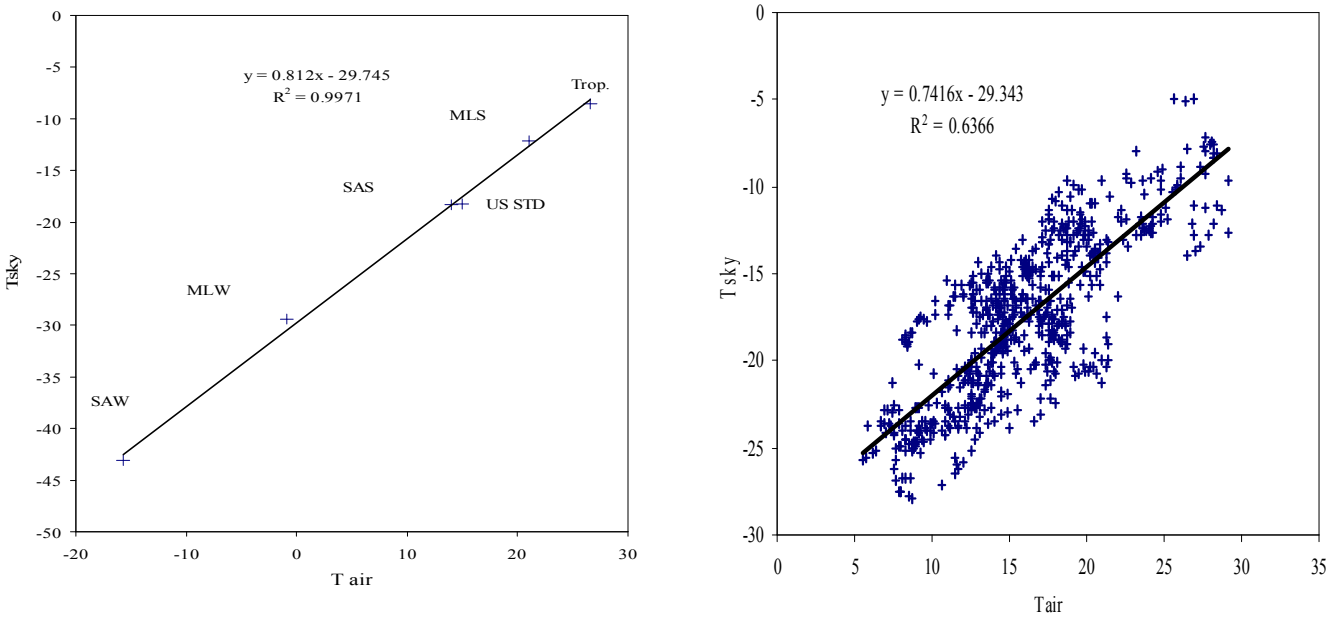

Fig. 3: (a) The simulated Tsky at the zenith for different screen level temperatures for six standard atmospheres as marked for 1 cm of PWV. (b) Shows the relationship between hourly clear Tsky and T. Both temperatures are in ^{o}C.

The effect of amount of water content

Figure (4) shows the spectral distribution of IR flux obtained by MODTRAN for mid-latitude summer at the zenith for various amounts of PWV. An increase in the area under the curves can be observed as the amount of water is increased. At very low values of water (0.00005 cm), the emission due to water vapour is negligible and the atmospheric emission is only due to carbon dioxide and ozone and some other minor gases, for example methane. As the amount of PWV is increased, the emission from the water vapour first approaches the blackbody emission in the spectral region on each side of the relatively low emissive atmospheric window. A further increase in the PWV is accompanied by an increase in emission from the spectral atmospheric window towards the blackbody values. At a value of 20 cm of PWV the atmosphere is nearly emitting as a black body, and when the PWV gets to its maximum value, the atmosphere becomes a total black body emitter at the screen level temperature.

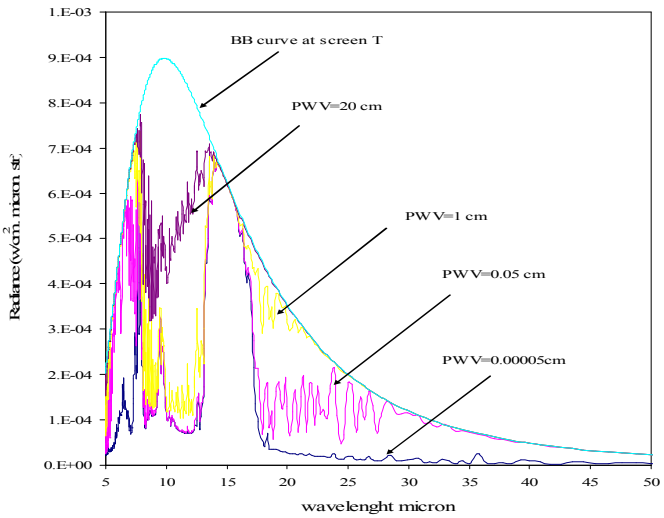

Fig. 4: The spectral distributions for IR clear sky radiance at the zenith for different amounts of PWV. The simulations were conducted for a mid-latitude summer (MLS) at the specified amounts of water.

Figure (5.a) shows a plot of the PWV values against the integrated Tsky from MODTRAN. Figure (5.b) shows the hourly variations of one year of experimental data for the Tsky as a function of PWV. The PWV data were obtained from a GPS receiver deployed at the Buckland Park (BP) field site about 30 km from Adelaide; see Maghrabi (2007) and Maghrabi et al. (2009) for more details. The equations of the regression results are also shown in both figures. Although there is some scatter on the experimental data, it is clear from both figures that the sky temperatures increase monotonically with increases in the amount of PWV. The numerical values of both the slope and the intercept of the regression equations are different from each other. One explanation for these dissimilarities between the measured and simulated sky temperatures is that the range of the PWV values covered experimentally was between 0.2 and 2 cm. This is narrower than that covered by the simulations (0.2–4 cm). Instrumental error either in the IR detector or in the GPS receiver may cause part of this deviation. We also expect that the variations in the measured screen temperature have an impact in causing the scatter in the equation as shown in Figure (5.b), while the fixed screen temperature at MLS gives a perfect fit as shown in Figure (5.a)

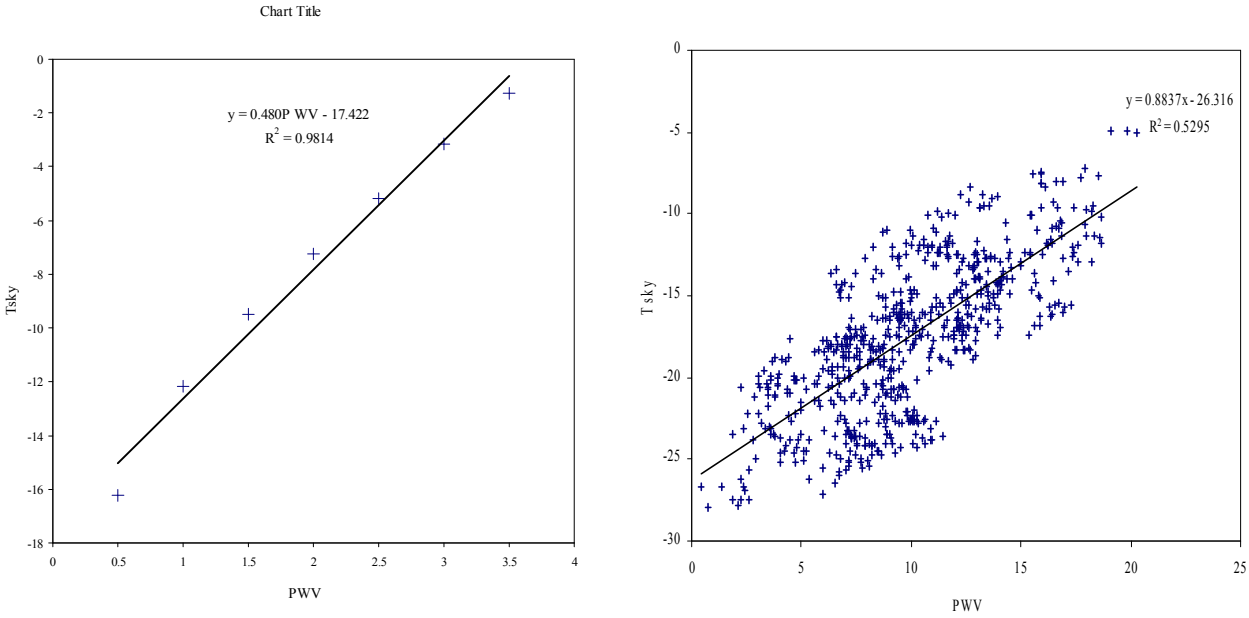

Fig. 5: (a) The simulated sky temperatures in oC for the MLS atmosphere as a function of the PWV in centimetres. (b) Shows the relationship between hourly Tsky and PWV in mm.

Figure (6) and Table (1) summarize the effects of both T and PWV on the sky temperatures. It shows the relationship between Tsky as predicted by MODTRAN for the different atmospheres (different screen temperatures) and for different values of the PWV. Generally speaking, in the normal conditions such those found in the MLS, US, STD, and tropical atmospheres (which have a similar range of temperatures to that experienced in Adelaide), the amount of atmospheric water content and screen level temperature can be used together and assumed to be the most effective parameters in

modelling the IR radiation with a high accuracy. For example from the table and the figure, a difference of 5 °C can be observed in MLS if the amount of PWV increases by 1 cm. This value is similar to the value found experimentally for the same increase in the amount of PWV. However, in very extreme conditions such as those found in the SAW and MLW, even when increasing or decreasing the PWV (RH up to 100%), the amount of water will have no practical impact on the sky temperatures. This is mainly due to the fact that in such extreme conditions of very low screen temperature the atmosphere is very dry and it is impossible to achieve a higher PWV.

Tab. 1: Integrated sky temperature results at the zenith (in °C) of MODTRAN simulations for six standard atmospheres for different amounts of PWV for 6.6–50 µm simulations. The T column is the screen level temperature for the standard atmosphere.

Atmosphere	T °C	PWV 0.5 cm	PWV 1 cm	PWV 2 cm	PWV 3 cm
Tropical (Trop)	26.6	–12.6	–8.5	–3.6	0.4
Mid-latitude summer (MLS)	21.0	–16.2	–12.2	–7.3	–3.2
Mid-latitude winter (MLW)	–0.9	–33.7	–29.4	–28.0	–28.0
Sub-Antarctic summer(SAS)	14.0	–22.5	–18.4	–13.4	–9.6
Sub-Antarctic winter(SAW)	–15.8	–44.2	–43.1	–43.1	–43.1
US STD	15.0	–22.5	–18.2	–13.2	–9.5

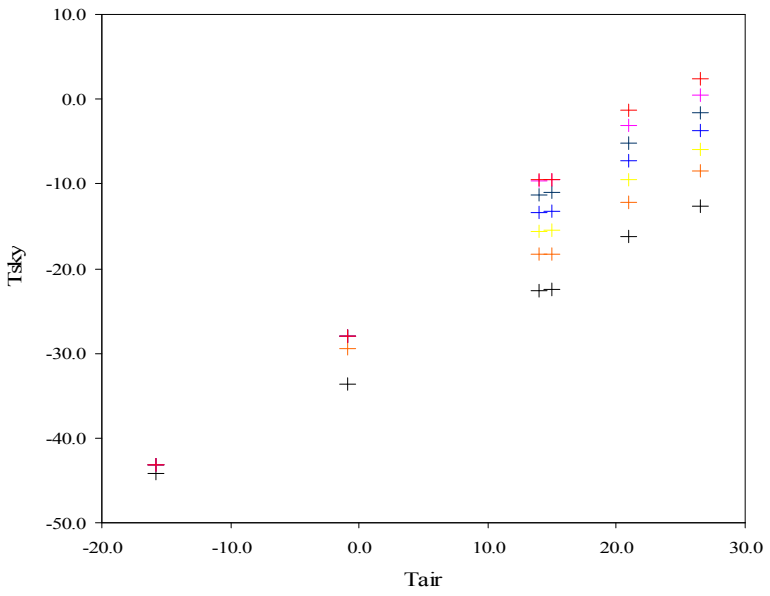

Fig.6: The simulated Tsky (in °C) for different screen level temperatures (in °C) for six standard atmospheres (from top right diagonally to bottom left: tropical, MLS, US standard atmosphere, SAS, MLW, and SAW atmospheres). Each atmosphere has 0.5 cm (black), 1 cm (orange), 1.5 cm (yellow), 2 cm (light blue), 2.5 cm (dark blue), 3 cm (pink), and 3.5 cm (red) of PWV.

The effect of other parameters

The effect of atmospheric aerosol

The effect of aerosol on atmospheric emission was examined using MODTRAN's standard MLS atmosphere and aerosol type, "urban". The spectra and the sky temperatures were obtained by assigning different values of visibility range from clear to totally turbid conditions. Visibility is related to the presence of aerosols in the atmosphere and has an effect on the visible range of wavelengths. Their influence may be extended to the IR part of the spectrum if the size of the aerosol particles becomes comparable with the IR wavelengths. Starting with a high visibility, increasing amounts of aerosol were added, corresponding to visibilities of 25 km, 20 km, 8 km, 2.5 km, 500 m, 100 m, 50 m, and 1 m. Figure (7.a) shows the spectral distribution of atmospheric radiation for the selected visibilities. For high visibilities (clear non-turbid atmosphere) greater than 8 km, no major changes in the spectral distribution were found. The atmospheric radiation distribution at all wavelengths resembles that of the clear sky. However, for a visibility of 2 km and below, the effect of the emission of atmospheric water and other atmospheric gases outside the atmospheric window remains the same and the effect of the aerosol on the atmospheric window is evident. A dramatic increase in the atmospheric radiation in the window occurs for visibilities of 50 m and 10 m. With 1 m visibility the atmospheric window is totally closed and the atmospheric emission resembles that of a blackbody. In this case the presence of larger sizes of aerosols may work as a lid causing more emission in this part of the spectrum. Figure (7.b) shows the integrated sky temperature for the values of visibilities used here. The sky temperature increases by 3.5 ^{o}C for visibility ranges from 25 to 1.5 km. At these visibilities, in normal atmospheric conditions, the effects of other meteorological parameters such as water vapour contents and air temperature are dominant. However, for visibilities below 1 km the sky temperature increases exponentially with decreases in the visibility. For example at a visibility of 0.5 km the sky temperature was –4.2 ^{o}C, while at a visibility of 0.3 km the sky temperature was –0.8 ^{o}C, an increase of about 3.5 ^{o}C. For a visibility of 1 m the integrated sky temperature was 16.5 ^{o}C. This simulated temperature is identical to the observed temperature of 16 ^{o}C recorded by our IR detector placed in Riydah, Saudi Arabia, during the severe storm that occurred on 9 March 2009. It is clear that the visibility factor, which is related to the presence of aerosols in the atmosphere, has an enhanced effect on the IR part of the spectrum because the size of the aerosol particles becomes comparable with the IR wavelengths.

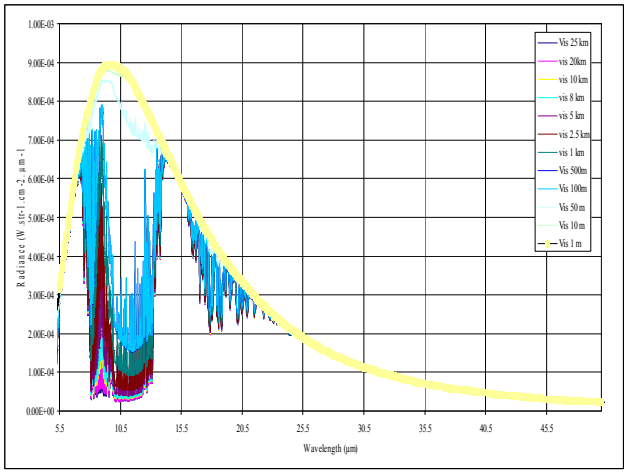

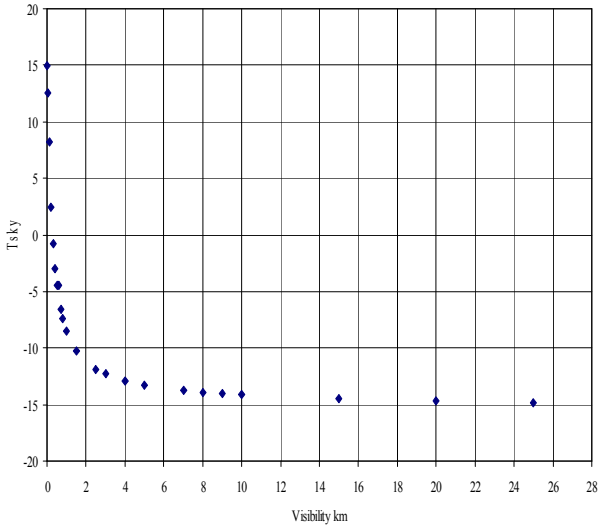

Fig. 7.: The clear sky atmospheric spectra for MLS atmosphere with varying visibility of aerosols as indicated. The model has 1 cm of PWV.

The effect of site altitude

In investigating the effect of the site elevation upon the IR atmospheric emission for clear sky, MODTRAN was run for an MLS standard atmosphere at six arbitrary altitudes: 0, 0.5, 1, 2, 3, and 4 km. Figure (8) shows the IR clear sky spectra obtained at these altitudes. For lower altitudes (0, 0.5, and 1 km) the main features of the atmospheric IR spectra do not change very much. The absorption bands of CO_2, O_3, H_2O, and other minor gases dominate. As the altitude increases, the amount of total water vapour above the considered base altitude decreases. However, the CO_2 amount remains sufficient to close the window between 14 and 16 μm. Inside the atmospheric window, ozone emission is visible at any altitude. Outside the atmospheric window the atmospheric radiance is that of a blackbody at an air temperature corresponding to the considered base altitude (not shown in the figure). Figure (11) shows the sky temperature plotted against the site's altitude for the two wavelengths. It is clear that for both wavelength ranges the sky temperature does decrease as the altitude increases. This is explained by the decrease in the amount of atmospheric water content as the altitude increases.

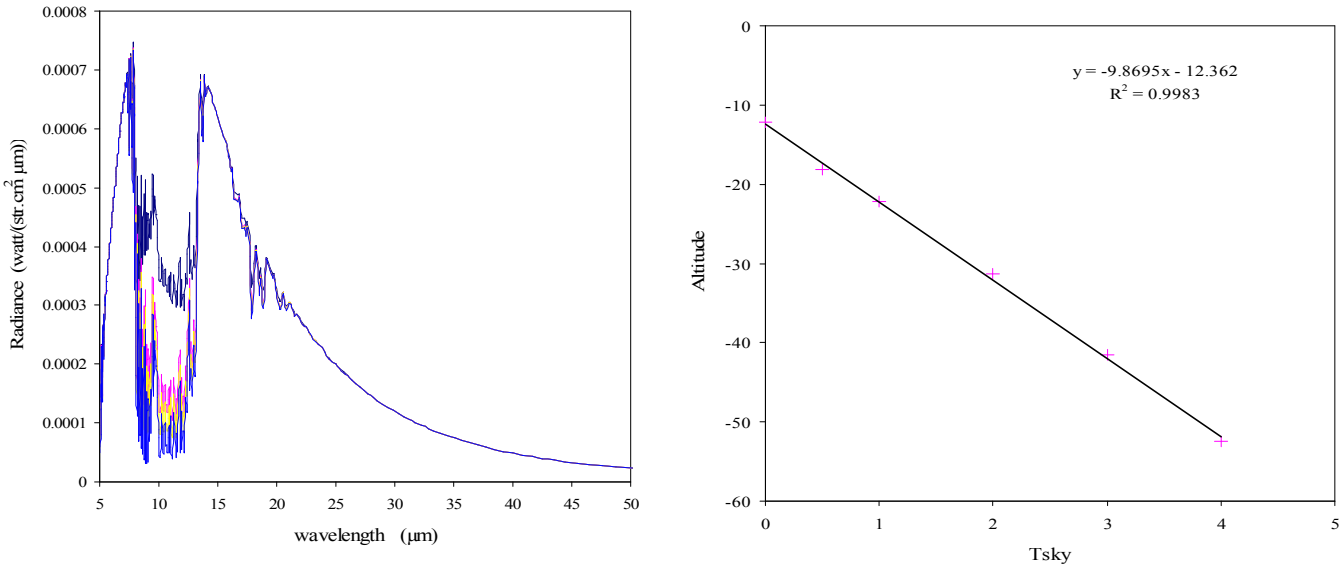

Fig. 8: (a). Atmospheric spectral radiance for different altitudes (dark blue: 0 km; pink: 0.5 km; yellow: 1 km; turquoise: 2 km; grey: 3 km; and brown: 4 km) obtained for MODTRAN standard MLS summer atmosphere with an amount of 1 cm of PWV.

(b)A plot between sky temperature (in ^oC) and the altitude (in km) .

CONCLUSION

Using MODTRAN it was confirmed that the screen level temperatures and the water vapour content, represented here as the PWV, have the greatest impact in determining the broadband IR clear sky temperatures. However, as pointed out by some researchers, other parameters may impact on studies of IR sky temperatures,. Here, we studied the

effect of two factors, aerosol type and altitude effect. We have shown that these two factors have different effects on the sky temperatures. Experimental justifications on the impact of these parameters on the atmospheric radiation were presented and a great agreements were found.

ACKNOWLEDGMENTS

This work was supported by King Abdulaziz City for Science and Technology (KACST). The meteorological data were provided by the Presidency of Meteorology and Environment (PME).

REFERENCES

Berk, A., *et al*., 1989, Rpt. No.GL-TR-89-0122, Air Force Geophys. Lab., MA.

Clay, R.W., N.R. Wild, D.J. Bird, B.R. Dawson, M. Johnston, R. Patrick, and A. Sewell (1998), A cloud monitoring system for remote sites. *Pub. Astron. Soc. Aust*., *15*, 332–335.

Duarte, H.F., N.L. Dias, and S.R. Maggiotto (2006), Assessing daytime downward longwave radiation estimates for clear and cloudy skies in southern Brazil, *Agric. For. Meteorol.*, *139*, 171–181.

Garcıa M. P, (2004), Simplified modelling of the nocturnal clear sky atmospheric radiation for environmental applications Ecological Modelling 180, 395–406

Kjaersgaard, J.H, F.L. Plauborg, and S. Hansen (2007), Comparison of models for calculating daytime long-wave irradiance using long term data set, *Agric. For. Meteorol.*, *143*, 49–63.

Kondratyev, K.Y., 1969, "Radiation in the Atmosphere "Academic Press, NY.

Lhomme, J.P., J.J. Vacher, and A. Rocheteau (2007), Estimating downward long-wave radiation on the Andean Altiplano, *Agric. For. Meteorol.*, *145*, 139–148.

Maghrabi, A.H, Clay, R.W,Riordan, D.,(2009), DETECTING CLOUD WITH A SIMPLE INFRA-RED SENSOR, Accepted for publication , *Transactions of the Royal Society of S. Aust.*

Maghrabi, A.H. (2007), Ground based measurements of IR atmospheric radiation from Clear and Cloudy Skies, Ph.D. thesis, University of Adelaide, Adelaide, Australia.

Maghrabi, A.H. and Clay, R.W., (2008) Results from a Simple Infrared Cloud detector, Accepted as a peer reviewed paper in the International Solar Energy Society- Asia Pacific Conf. 25-28 Nov 2008.(WC0160)

Maghrabi, A.H. Clay, R.W,Dawson, B and Wild N.(2009) Design and Development of a Simple Infrared Monitor for Cloud Detection, Energy and Conservation managements , (50); 2732-2737.

Prata, A.J. (1996), A new long-wave formula for estimating downward clear-sky radiation at the surface, *Q. J. R. Meteorol. Soc*., *122*, 1127–1151.

Ramsey, J.W., H.D. Chiang, and R.J. Goldstein (1982), A study of the incoming long wave atmospheric radiation from a clear sky, *J. Appl. Meteorol*., *21*, 566–578.

Riordan, D., R. Clay, A. Maghrabi, B. Dawson, and N. Wild (2005), Cloud base temperature measurements using a simple longwave infrared cloud detection system, *J. Geophys. Res.*, *110*, D03207, doi:10.1029/2004JD005390.

Rothman, L.S.*, et al*. 2003, J. Quant. Spectrosc. Radiat. Transfer, 82, 5

Rothman, L.S., *et al*., 1992 J. Quant. Spectrosc. Radiat. Transfer, 48, (5/6) 469.

Ruckstuhl, C., R. Philipona, J. Morland, and A. Ohmura (2007), Observed relationship between surface specific humidity, integrated water vapor, and longwave downward radiation at different altitudes, *J. Geophys. Res.*, *112*, D03302, doi:10.1029/2006JD007850.

BRIEF BIOGRAPHY OF PRESENTER

Dr . Abdullrahman H. Maghrabi

Assistance Professor of Research

Deputy Director for Scientific Affairs

National Center For Mathematics and Physics, King Abdulaziz City For Science and Technology

Fields of Interest

Solar energy applications, atmospheric studies – particularly long wave radiation, low energy cosmic rays, and observational astrophysics.

2007: PhD, the University of Adelaide (Infrared Atmospheric Monitoring)

2000: MSc, the University of Adelaide (High Energy Astrophysics)

1996: BSc, King AbdulAziz University, Jeddah, Saudi Arabia (Physics – Astronomy)

Dye solar cells – pushing efficiency boundaries for industrial size cells

Ravi Harikisun, Nancy Jiang, Yanek Hebting, Richard Cordiner and Hans Desilvestro[1]
[1]Dyesol Australia Pty Ltd
3 Dominion Place, Queanbeyan NSW 2620, Australia
hansd@dyesol.com

ABSTRACT

Dye solar cell efficiencies as high as 12.2% (Grätzel 2009) have been reported for laboratory cells based on small active area and highly volatile solvents. However, efficiencies for industrial sized dye solar cells with cell widths of around 1cm and using high-boiling solvents are generally lower. In order to be commercially competitive with other thin-film technologies, dye solar cell full panel efficiencies need to attain between 8 to 10%. Furthermore, high device stability is required in the long term and production costs need to be relatively low.

This paper explores realistically achievable cell and DSC panel performance based on today's materials and provides strategies on how to optimally select and fine tune the dye, the semiconductors and the hole conductor system. Even for industrially viable cell designs, efficiencies of close to 16% are anticipated with the standard I_3^-/I^- redox system. If energy losses for dye regeneration can be reduced by 0.3 eV, close to 19% active area efficiency is estimated to become realistically achievable with industrial devices, which translates in full panel efficiencies of >16%.

Keywords *dye solar cells, materials for optimum performance, ruthenium dyes*

INTRODUCTION

O'Regan and Grätzel reported in their seminal 1991 paper on a first successful realisation of a non-aqueous electrolyte, nano material-based dye solar cell (DSC) a AM 1.5 efficiency of 7.1%, with 7.9% at 0.1 sun light intensity (O'Regan & Grätzel 1991). Efficiencies of small laboratory cells were then relatively quickly increased to 10%, followed, as shown in Fig. 1, by a 10^+ year period of little progress in terms of cell efficiency. Only very recently 12.2% has been presented (Grätzel 2009). In order for DSC to be competitive with more established solid-state thin film technologies such as CIGS (copper indium gallium diselenide) or CdTe (cadmium telluride), it is important to further increase cell and thus ultimately panel efficiency. This paper will explore some of the practical boundaries imposed by today's and future materials and designs for DSC.

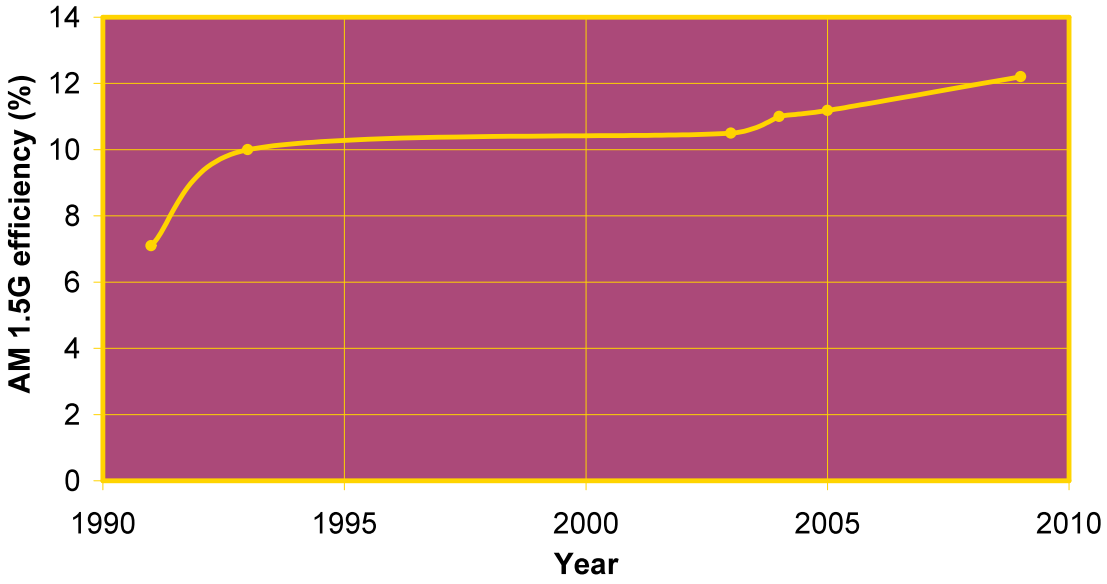

Fig. 1: Historic record efficiencies of laboratory DSCs

Laboratory cells are often based on an active area of <0.2 cm^2, on low viscosity, i.e. high volatility [1)], and possibly toxic solvents and tend to employ the highest performing components irrespective of materials and processing costs. In contrast, industrially feasible devices have to provide high performance at the panel level. Thus module design and optimisation of the ratio active area to seal widths as well as current collection paths become very important. For building integrated (BIPV) applications, product life times of at least 20-25 years are required and cost-wise DSC will be judged against low cost thin film technologies such as CdTe available at less then 1$/$W_p$. It has to be cautioned however that the $/$W_p$ metric insufficiently characterises cost of PV in most practical applications. On sides of buildings and/or under hazy or cloudy conditions DSC can outperform silicon PV in terms of annual output (kWh/m^2) and even in terms of levelised cost of energy, LCOE (Desilvestro 2010). The different development criteria for laboratory and industrially feasible DSC, normally leads to a 2-3% performance gap, based on active area, between the two types of devices. For well-designed DSC panels the active area will be close to 80%. Thus a laboratory cell yielding 12%, will realistically only provide around 7% at the panel level. Therefore pushing efficiency of small cells beyond the "12% hurdle" is very important for very large scale commercialisation of DSC, where mainly LCOE will count. The following discussion will theoretically explore what cell efficiencies can realistically be expected for DSC.

WHERE ARE THE LIMITS?

Recently Hamann et al stated, based on an analysis of the energy level diagram (see Fig. 2 below), open circuit voltage V_{oc} and limiting photocurrents, i.e. theoretical short circuit currents j_{sc}: "Efficiencies exceeding 16% are reasonably achievable, and there

[1)] Acetonitrile often used in high-performance laboratory cells has a boiling point of 82°C, a temperature which can easily be attained by a DSC panel fully exposed to sunlight.

are many combinations of dyes and redox shuttles to get there" (Hamann et al 2008). In the present work, we will use a similar analysis, but in addition, include realistically estimated fill factors for 2 types of cell designs. Our analysis will provide guidelines for optimised combinations of dye, redox couple and semiconductor energy levels.

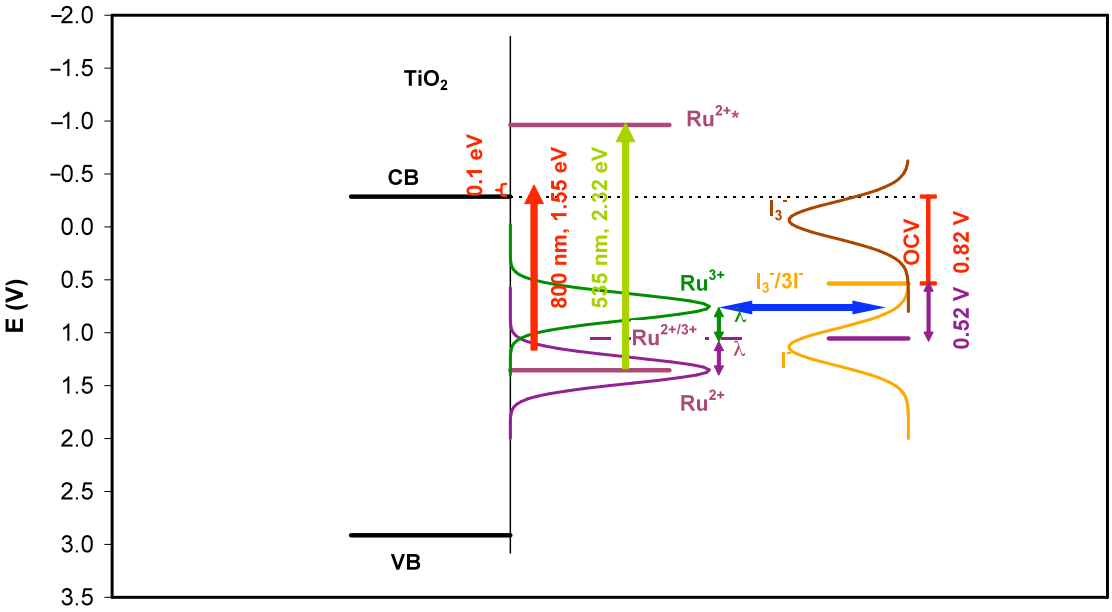

Fig. 2: DSC energy level diagram vs NHE. Ru^{3+}/Ru^{2+} reorganisation energy of ~0.35 eV is presented to scale, while the I_3^- and I^- electronic states are depicted schematically only.

Limits imposed by energy losses and V_{oc}

Because the I_3^-/I^- couple is electrokinetically rather slow and characterised by a cascade of electron transfer processes with intermediates $I^\bullet$ (Ru^{3+} stabilised) and $I_2^{-\bullet}$, a relatively high driving force of 0.5-0.6 eV is required for dye regeneration (Hagfeldt et al 2010). In addition, it is further estimated that at least 0.1 eV "driving force" between the dye LUMO (lowest unoccupied molecular orbital) and the TiO_2 conduction band is required. Thus the total driving force $E_{dr.force}$ required for charge exchange within the dye-TiO_2-redox system is **at least 0.6 eV**. The reorganisation energy λ of the N3 dye in its ground state has been estimated to 0.35 eV, which is characteristic for a fast redox couple (Boschloo et al 2002). Since the I_3^-/I^- couple is much more sluggish the electronic overlap between Ru^{3+} and I^- states is relatively poor (see blue arrow in Fig. 2), indicating that dye regeneration by I^- needs to be accounted for by a rather high I^- concentration.

For energy balance reasons the light energy has to fulfil the following relation:

$$E_{light} \geq E_{dr.force} + qV_{oc} \qquad [1]$$

q represents the elementary charge. For a driving force of 0.6 eV and V_{oc} = 0.8 V, only light with $\lambda_{min} \leq 886$ nm can be converted to electrical energy.

j_{sc} limits

Limits for short circuit photocurrents are mainly governed by the Incident-Photon-to-electron Conversion Efficiency, IPCE, and the spectrum of the adsorbed dye on TiO_2. j_{sc}

values can easily be calculated through integration over the IPCE spectrum. Fig. 3a shows that j_{sc} can in principle, i.e. if no limits were imposed by driving force requirements, reach values of almost 40 mA/cm^2 for the IPCE peaking at 85% and for a dye with an absorption tail approaching 1300 nm.

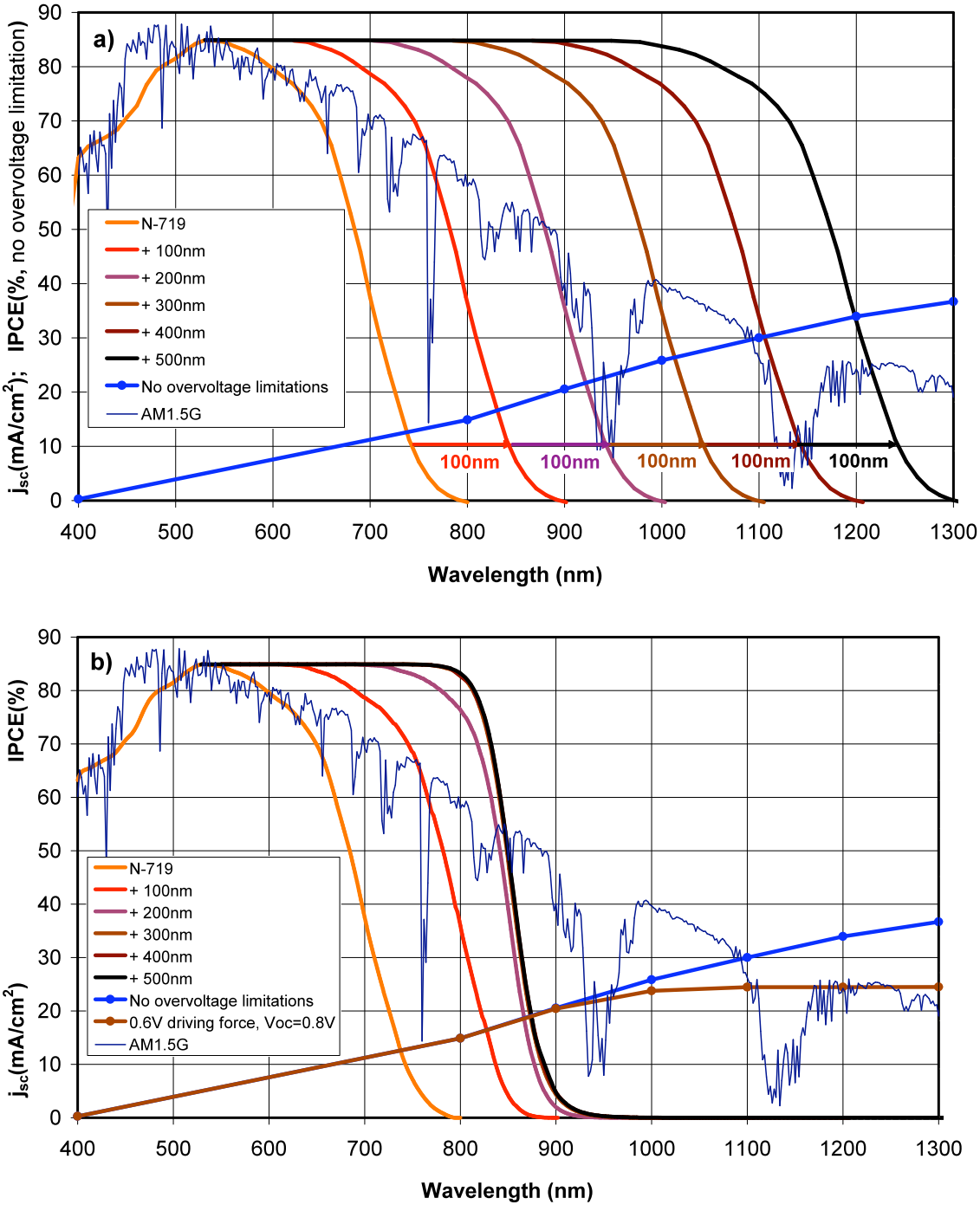

Fig. 3: Experimental IPCE for N719 (orange curve) and schematically for dyes with an absorption edge extended by 100 nm increments. (a): j_{sc} (blue points) derived for the 6 dye examples assuming no overvoltage limitations. (b) j_{sc} (brown points) derived for the 6 dye examples assuming a required driving force of 0.6 eV and V_{oc}=0.8V and the corresponding IPCE curves corrected through Eq. [2].

Using a more realistic 'overvoltage' of 0.6 V for dye regeneration and electron injection combined, virtually no light beyond 900 nm can be converted to electricity if the open circuit voltage is 0.8 V. Equation [2] was used to approximate a more realistic long wavelength cut-off than a sharp step according to Eq. [1]. Under such conditions, j_{sc} plateaus at 25 mA/cm^2 and Fig. 3b shows that dyes absorbing beyond 1000 nm cannot contribute to photocurrent increase and thus device efficiency anymore.

$$IPCE-correction-factor = \frac{\exp\left(\frac{E_{light}-E_{dr.force}-V_{oc}-0.05}{kT}\right)}{\left(1+\exp\left(\frac{E_{light}-E_{dr.force}-V_{oc}-0.05}{kT}\right)\right)} \quad [2]$$

Therefore it is important to carefully tune and optimise the semiconductor conduction band and the dye and redox couple energy levels in relation to each other and in combination with V_{oc}. Before undertaking such an optimisation exercise, the third key contributor to efficiency, i.e. fill factor shall be discussed.

ff limits

Fill factors depend on many materials and cell design parameters as well as light intensity (Desilvestro 2008). For estimating ff, the diode equation [3] (I_{gen} = photo generated current, generally corresponding to I_{sc}, I_{sat} = reverse saturation current, F= Faraday constant, n = diode ideality factor, R = universal gas constant, T = absolute temperature) can be used.

$$I_{ph} = I_{gen} - I_{sat}\left(e^{\frac{FV}{nRT}} - 1\right) \quad [3]$$

In addition, the following assumptions were made:

- laboratory strip cells with 3 mm TiO_2 width vs industrial-type strip cells with 8 mm TiO_2width, Z-connected (see Desilvestro 2008)
- 0.5 mm seal width on each side of the active area, corresponding to 1mm effective cell-to-cell separation
- 7 Ohm/square sheet resistance
- n=1.3
- a fast counter electrode with a charge transfer resistance $R_{ct} \leq 0.3$ Ohm cm^2
- low, i.e. practically negligible, concentration polarisation in a thin cell arrangement

Through such an analysis, a current density of 30 mA/cm^2 results in ff=0.80 for a 3mm active area width cell and ff=0.66 for a TiO_2 width of 8 mm.

Optimum efficiencies for realistically achievable DSC configurations

Combining limits for minimum required dye excitation energy in combination with V_{oc}, as well as j_{sc} and ff limits discussed above, DSC efficiency can be estimated in dependence of dye onset wavelength for absorption and V_{oc}. Figures 4a) and 4b) show DSC efficiencies for a hole transport system with an energy loss of 0.6 eV at the semiconductor/dye interface for a narrow laboratory cell (a) and a wider cell with 8 mm TiO_2 width (b). For the former case, a relatively flat maximum of 15.8% (Fig. 4a) is

estimated for V_{oc} = 0.8 V and a dye with an absorption tail up to ~1100 nm. Dyes absorbing further into the IR region are not expected to additionally increase cell efficiency. On the other hand, wider, industrially feasible cells display, because of overall lower fill factors, a maximum of 13.8% at V_{oc} = 0.9 V for dyes with an absorption tail of 1100-1200 nm (Fig. 4b). This analysis shows that different strategies will be required for maximising device efficiencies for very small cells and for industrially viable products. In the specific case of $E_{dr.force}$ = 0.6 eV, increasing V_{oc} beyond 0.8 V is more important for commercially relevant applications than for laboratory cells.

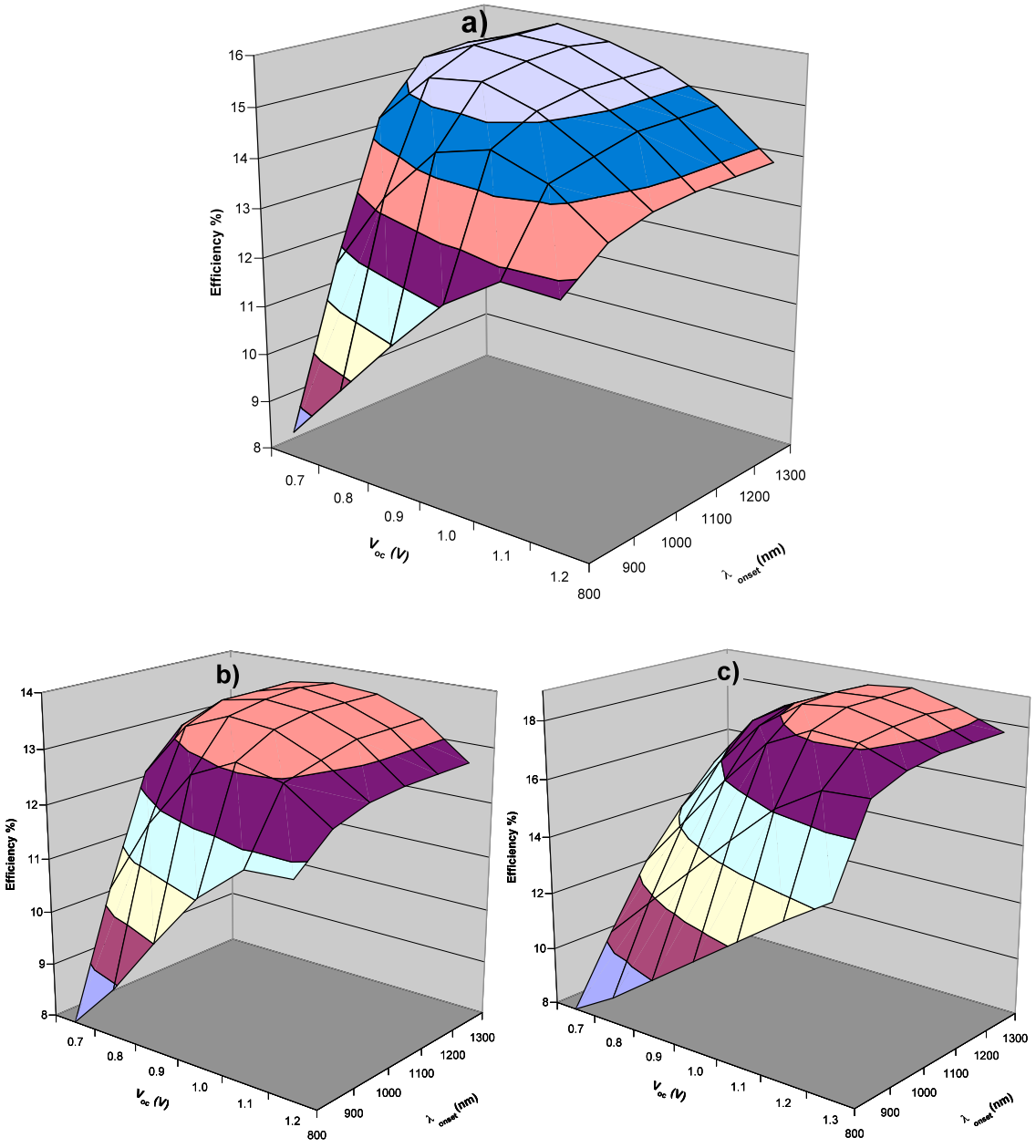

Fig. 4: Calculated cell efficiencies, based on active area as a function of V_{oc} and onset wavelength λ_{onset} for dye absorption. Strip cell with TiO_2 width of 3mm and $E_{dr.force}$ = 0.6 eV (a); TiO_2 width of 8mm and $E_{dr.force}$ = 0.6 eV (b); TiO_2 width of 8mm and $E_{dr.force}$ = 0.3 eV (c).

If suitable alternatives to the presently used I_3^-/I^- redox system can be found, which require a lower driving force only, substantial efficiency gains will be possible. Fig. 4c) shows that for a cell with active area width of 8 mm and a driving force of 0.3 eV, maximum efficiencies of 18.7% are reached for V_{oc} =1.1 V and a dyes with an absorption tail up to at least 1100 nm.

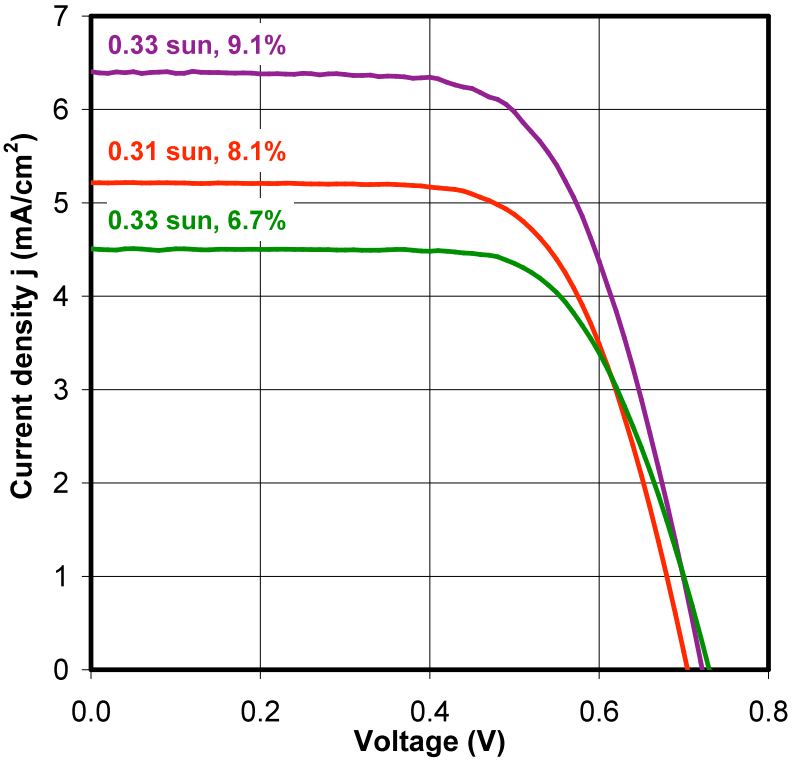

Fig. 5: Photocurrent-voltage curves at 0.31-0.33 sun for dyes C106 (purple), N719 (red), Z907 (green) using standard Dyesol materials and cell components Active area = 8×11mm active area.

CONCLUSIONS

The present analysis revealed that still substantial performance gains are possible for DSC beyond the present laboratory benchmark of 12.2% (Fig. 1). Even for cells based on industrially viable materials and designs, which offer long product life, a significant efficiency increase from 8-9% today (Fig. 5) towards almost 14% ($E_{dr.force}$ = 0.6 eV, i.e. based on I_3^-/I^-) and close to 19% ($E_{dr.force}$ = 0.3 eV) are feasible if dye, semiconductor and hole conductor system can optimally be matched to each other. These are demanding, but ultimately rewarding challenges to materials science. With an aperture area of 80%, DSC panel efficiencies of 11% are estimated to become realistically achievable even with the I_3^-/I^- couple, making DSC highly competitive with other thin film technologies and even with standard Si PV in many applications. If more effective hole conductor systems can be deployed DSC panel efficiencies of >16% are expected for the future. This would definitely propel DSC to the top of any of the commercially viable technologies for most applications.

REFERENCES

Boschloo, G., Lindström, H.; Magnusson, E.; Holmberg, A.; Hagfeldt, A., 2002. Optimization of dye-sensitized solar cells prepared by compression method. J. Photochem. Photobiol. A: Chem. 148, 11-15.

Desilvestro, H, 2008. http://www.dyesol.com/index.php?element=What_Physical_Factors_Do_Affect_Current-Voltage_Characteristics_of_Dye_Solar_Cells

Desilvestro, H., 2010. Dye Solar Cells – Towards Commercialisation. 4th International Conference on the Industrialisation of DSC, Colorado Springs, 1-4 November. Presentation accessible on http://www.dyesol.com/download/DSCIC10/HDesilvestro.pdf

Grätzel, M., 2009. Historical development of the DSC, from its inception to its current state. 3rd International Conference on the Industrialisation of DSC, Nara, Japan, 22-24 April. Presentation accessible on http://www.dyesol.com/download/DSCIC09/22Apr09Graetzel.pdf.

Hagfeldt, A. Boschloo, B., Sun, L, Kloo, L., Pettersson, H., 2010. Dye-Sensitized Solar Cells. Chem. Rev. 110, 6595–6663.

Hamann, T.W., Jensen, R.A., Martinson, A.B.F., Van Ryswyk, H., Hupp, J.T., 2008. Advancing beyond current generation dye-sensitized solar cells. Energy Environ. Sci 1, 66-78.

O'Regan, B. & Grätzel, M. 1991. A low-cost, high-efficiency solar cell based on dye-sensitized colloidal TiO_2 films. Nature 353, 737-740.

BRIEF BIOGRAPHY OF PRESENTER

Dr Hans Desilvestro has close to 30 years of hands-on experience and thorough theoretical understanding of electrochemical energy storage and energy conversion systems. He gained his PhD from the Swiss Institute of Technology based on his work on photoelectrochemistry and dye sensitisation under the direction of Prof. Michael Grätzel. After many years of R&D and technical management within the battery technology industry, including nickel metal hydride, supercapacitors and high power Li-ion batteries, he returned to the world of dye solar cells in 2005 as Dyesol's Chief Scientist. Hans is the author or co-author of more than 50 scientific-technical publications, 2 book chapters and 7 patents or patent applications.

Financial Solution To A Technical Problem: How To Open The Energy Market For Solar Generation

Authors

Robert Enemuwe[1], Igor Skryabin[2], Joe Maisano[3] and Dr. Alex Radchik[4]

[1]University of Sydney, [2]Australian National University, [3]TTA Pty Ltd, [4]EnergyOne Ltd.

Dr. Alex Radchik, Email: aradchik@aksong.com, Phone: +61 417 224 800

It is general consensus that solar power is one of the cleanest energy technologies available. Nevertheless, investment in the development of large-scale solar power generation (SPG) is mostly impeded by the current National Electricity Market (NEM) setup rather than lack of progress in design of efficient photovoltaic panels. According to existing NEM Registration Guidelines, any generation facility with total capacity greater than 30MW in one connection point are required to register either as Market Scheduled or Market Semi-Scheduled Generator [1]. Due to highly intermittent nature of solar generation it is not possible to supply electricity power 24×7 without interruptions.

At present the work around this problem is to build supplementary alternative-fuel generating or energy storage facility connected to the grid at the same connection point. This solution is not always feasible and often requires significant additional infrastructure investment.

We propose an inexpensive, financial approach which requires no additional infrastructure investment. It will link physically separated but complimentary SPG and Gas-fired or/and other rapid ramping generator by a set of specific financial contracts, compensating each party for the intermittence in supply due to exogenous events. The parties will submit their bids to a Virtual Generator which in turn bids into the NEM as a single entity. We have successfully constructed these set of contracts and have demonstrated their profitability for both the SPG and Gas-Fired generator. The model was prototyped using real market data and shows the benefits to implementing the proposed alternative approach.

References

[1] NEM GENERATOR REGISTRATION GUIDE, available from www.aemo.com.au

IEA SHC Task 41 - Solar Energy and Architecture Survey of architects to identify barriers and needs for building integration of Solar Thermal and Photovoltaics

Klaudia Farkas[1], M.C. Munari Probst[2], Miljana Horvat[3] and Mark Snow[4]

[1] Dep. of Architectural Design, History and Technology, NTNU, Trondheim, Alfred Getz vei 3, NO-7491, Trondheim, Norway

2 EPFL ENAC IIC LESO-PB, LE 004, Station 18, CH-1015 Lausanne, Switzerland

3 Dep. of Architectural Science, Ryerson University, 350 Victoria St., Toronto, Ontario, M5B 2K3, Canada

4 Faculty of the Built Environment, University of NSW, Sydney, NSW 2052, Australia

ABSTRACT

The International Energy Agency (IEA) Solar Heating and Cooling (SHC) Task 41 – Solar Energy and Architecture is aimed at helping to achieve high quality architecture for buildings integrating solar energy systems, as well as improving the qualifications of the architects, their communications and interactions with engineers, manufactures and clients.

Increased user acceptance of solar designs and technologies will accelerate the market penetration. The overall benefit will be an increased use of solar energy in buildings, thus reducing the non-renewable energy demand and greenhouse gas emissions.

To achieve these goals, Task 41 focuses on three main topics:

A. Architectural quality criteria; guidelines for architects and product developers by technology and application for new products development.

B. Guidelines for tool developers, focusing on tools for early stage evaluations and balancing of various solar technologies integration.

C. Integration concepts and examples, and derived guidelines for architects.

This paper describes the sub task activities being undertaken but specifically an international survey concerning the integration of solar energy systems and architecture in order to identify barriers that architects are facing in incorporating active solar technologies in their design. The survey investigates the possible barriers of solar thermal and photovoltaics, to understand why there is still a resistance among architects for using these elements in their architectural design.

Moreover, it asks about the needs of architects and what should be developed for a wider use of solar active systems in the building skin. The survey also provides valuable information towards a comparative study of the two solar technologies from the perspective of architectural integration potential. As the survey is conducted in 14 countries around the world (EU, Canada, South Korea, Australia), it presents an opportunity to identify possible regional differences in the understanding and acceptance of active solar technologies.